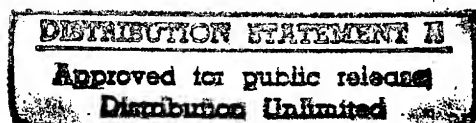


UNIVERSITY OF THE WEST
TIMIȘOARA

EUROPEAN OFFICE OF
AEROSPACE RESEARCH AND
DEVELOPMENT OF US AIR-FORCE



PROCEEDINGS **OF THE** **INTERNATIONAL CONFERENCE**

Analysis and Numerical Computation of Solutions of
Nonlinear Systems Modelling Physical Phenomena,
Especially: Nonlinear Optics, Inverse Problems,
Mathematical Material Sciences and
Theoretical Fluid Mechanics

DTIC QUALITY INSPECTED 3

UNIVERSITY OF THE WEST TIMIȘOARA,
ROMANIA

19 - 21 May, 1997

19970619 018

REPORT DOCUMENTATION PAGE

Form Approved OMB No. 0704-0188

Public reporting burden for this collection of information is estimated to average 1 hour per response, including the time for reviewing instructions, searching existing data sources, gathering and maintaining the data needed, and completing and reviewing the collection of information. Send comments regarding this burden estimate or any other aspect of this collection of information, including suggestions for reducing this burden to Washington Headquarters Services, Directorate for Information Operations and Reports, 1215 Jefferson Davis Highway, Suite 1204, Arlington, VA 22202-4302, and to the Office of Management and Budget, Paperwork Reduction Project (0704-0188), Washington, DC 20503.

1. AGENCY USE ONLY (Leave blank)		2. REPORT DATE 2 June 1997		3. REPORT TYPE AND DATES COVERED Conference Proceedings	
4. TITLE AND SUBTITLE Analysis and numerical computation of solutions of nonlinear systems of partial differential equations modelling physical phenomena. Systems arising in the areas of nonlinear optics, mathematical material science, and theoretical fluid mechanics				5. FUNDING NUMBERS F6170897W0174	
6. AUTHOR(S) Conference Committee					
7. PERFORMING ORGANIZATION NAME(S) AND ADDRESS(ES) West University of Timisoara Bd. Vasile Parvan no. 4 Timisoara 1900 Romania				8. PERFORMING ORGANIZATION REPORT NUMBER N/A	
9. SPONSORING/MONITORING AGENCY NAME(S) AND ADDRESS(ES) EOARD PSC 802 BOX 14 FPO 09499-0200				10. SPONSORING/MONITORING AGENCY REPORT NUMBER CSP 97-1049	
11. SUPPLEMENTARY NOTES					
12a. DISTRIBUTION/AVAILABILITY STATEMENT Approved for public release; distribution is unlimited.				12b. DISTRIBUTION CODE A	
13. ABSTRACT (Maximum 200 words) The Final Proceedings for Analysis and Numerical Solution of Nonlinear Models of Physical Phenomena, 19 May 1997 - 21 May 1997 The Topics covered include: Analysis and numerical computation of solutions of nonlinear systems of partial differential equations modelling physical phenomena. Systems arising in the areas of nonlinear optics, mathematical material science, and theoretical fluid mechanics will be addressed.					
14. SUBJECT TERMS Mathematics, Non-linear Optics, Materials, Fluid Mechanics				15. NUMBER OF PAGES 594	
				16. PRICE CODE N/A	
17. SECURITY CLASSIFICATION OF REPORT UNCLASSIFIED	18. SECURITY CLASSIFICATION OF THIS PAGE UNCLASSIFIED	19. SECURITY CLASSIFICATION OF ABSTRACT UNCLASSIFIED	20. LIMITATION OF ABSTRACT UL		

NSN 7540-01-280-5500

Standard Form 298 (Rev. 2-89)
Prescribed by ANSI Std. Z39-18
298-102

**PROCEEDINGS
of the
INTERNATIONAL CONFERENCE**

*Analysis and Numerical Computation of Solutions of
Nonlinear Systems Modelling Physical Phenomena,
Especially : Nonlinear Optics, Inverse Problems,
Mathematical Material Science and Theoretical Fluid
Mechanics*

19-21 May 1997

UNIVERSITY OF THE WEST TIMIȘOARA

TIMIȘOARA, ROMANIA

DTIC QUALITY INSPECTED 3

We wish to thank the following for their contribution to the success of the conference: United States Air Force European Office of Aerospace Research and Development; United States Office of Naval Research, Europe; the Soros Foundation Timișoara; the French Cultural Center Timișoara.

Finally, I thank to my colleagues for their efforts and carefullness over several months that will culminate, I hope, in a successfull and enjoyable Conference

Timișoara, Romania

Șt. Balint

Contents

<i>D. Drăgulescu, M. Toth-Tascău</i> - Method to Study the Dynamical Behaviour of a Complex Mechanical Structure	1
<i>D. Dincă Baran</i> - Lyapunov Exponents and Strange Attractors in the Dynamic the Buckled Beam	1
<i>O. Trifu</i> - Lift Enhancement by Aerodynamic MultiParametric Optimization of a Wing-Strake Configuration	2
<i>A. Ioniță</i> - Some Qualitative Aspects about Pilot Induced Oscillation Phenomena	3
<i>G.W. Bao, M. Pascal</i> - Stability of a Spinning Liquid-Filled Spacecraft	3
<i>D. Cioranescu, J.S.J. Paulin</i> - Study of Reticulaires Structures of Thin Width. Grillages and Tower	5
<i>C. Mitrovic, D. Cvetkovic, D. Bekric, A. Bengin</i> - Unsteady Motion of Two Dimensional Airfoil in Incompressible Inviscid Flow	8
<i>V.A.J. Butoescu</i> - A Second-Order Analysis of an Oscillating Body in a Subsonic Flow	9
<i>H. Dumitrescu, A. Dumitrache</i> - An Inverse Formulation For Separated Turbulent Boundary Layer	107
<i>A. Șerbănescu, P. Ciotirnae, V. Eugen</i> - Iterative Aspects in Nonlinear Dynamic Systems with Chaotic Behaviour	123
<i>I. Copae, L. Matei</i> - The Integration of the Nonlinear Differential Equations that Describe Straight Motion of the Automotives	132
<i>A. Soloi</i> - On a problem of Evolution Magnetic Field in a Given Flow	138
<i>L. Răduțu</i> - Consideration Regarding NonLinear Structural Components Influence on Rocket Rudder Actuator Stability	156
<i>V. Zeljkovic, S. Maksimovic</i> - Numerical Simulation of Nonlinear Transient Aircraft Response During Ground Motion	163
<i>M. Olariu</i> - The Numerical Integration of a System of Differential Equations through the Method of the Norm Minimization of the Error Matrix	164
<i>C. Mitrovic, D. Cvetkovic, D. Bekric, A. Bengin</i> - Effectivity of Hypergeometric Function Application in Helicopter Rotor Blades Theory Numerical Simulation	170
<i>V. Zeljkovic, S. Maksimovic</i> - Strength Analysis of Aircraft Structures Using Elastoplastic Finite Element Analysis and Probabilistic Approach	176
<i>G. Karolyi, A. Pentek, T. Tel, Z. Toroczai</i> - Chemical Reactions in Open Chaotic Flows	177
<i>R. Precup, E. Kirr</i> - Analysis of a Nonlinear Integral Equation Modelling Infection Diseases	178
<i>C. Dumache, I. Nicoară</i> - The Calculus of the Energetic Illumination Produced by an Infrared Radiation Source in a Space Point	196
<i>D. Trif</i> - Sinc Method for the Two-Dimensional Navier-Stokes Equations	210
<i>Th. Lévy</i> - Nonlinear Acoustics in Rigid Porous Media	216
<i>St. Balint, A. Balint, D. Bălțean, A. Neculai</i> - The Dopant Transport by Convection and Diffusion During Melt Growth of Semiconductor Crystals in the context of the Bridgman-Stockbarger Crystal Growth Configuration	225
<i>H. Ene</i> - On Heat Transfer in Porous Media	240
<i>F. Moraru, D. Safta</i> - Regarding on the Integration of the NonLinear Differential Equations for the Rocket Incidence During the Flight	248
<i>I.A. Rus</i> - An Abstract Point of View for some Integral Equations from Applied Mathematics	256
<i>C. Avramescu, O. Musîafa</i> - Approximation Methods and Existence Problems for Nonlinear Equations in Banach Spaces	271
<i>S. Birăuș, St. Balint, A.M. Balint</i> - Weak solutions for the Non-Linear One Dimensional Wave Equation in Adiabatic Case	285
<i>V. Iordan, St. Balint, A.M. Balint</i> - Weak solution and Hydrodynamical Shock Generation by NonLinear Oscillations in the Case of One Dimensional Non-Linear Wave Equation	286
<i>St. Balint, A.M. Balint, D. Bălțean, A. Neculai</i> - The Heat and Mass Transport by Convection and Diffusion During Quartz Crystal Growth by Hydrothermal System	298

<i>R. Stavre</i> - A Theoretical and Numerical Approach of a Distributed Control Model for a Free Boundary Problem	311
<i>V. Marinca</i> - The Exact Solution in the Case of Certain Non-Linear Cauchy Problem	332
<i>P. Găvruta</i> - On the Minimally Supported Frequency Wavelets and Scaling Functions	343
<i>N. Szirbik, St. Holban</i> - Some Complexity Issues Concerning a Nonlinear Dynamical System	354
<i>N. Vlăsceanu, M. Saitoc</i> - Influența rotațiilor elicopterului în tangaj și ruliu asupra distribuției vitezei induse pe rotor	366
<i>N. Vlăsceanu, V. Popescu, D. Simota</i> - Bătaia liberă a palei în zborul curbiliniu al elicopterului	369
<i>R. Selescu</i> - The General Properties of the Canonical motions	373
<i>R. Selescu</i> - Determining the liquid (Water) Depth for Satisfying the Gas/Hydrodynamic Analogy	383
<i>E. Tulcan, St. Balint</i> - The Effects of a Longitudinal Magnetic Field on the Flow Velocity of a Magnetic Fluid in a Circular Pipe	389
<i>Gh. D. Stoicescu</i> - Mathematical Peculiarities in Model Issues of Aggregation Process of Trivalent Impurities in Cubic Symmetry Monocrystals NaCl Type	394
<i>M. Pascal, D. Comănescu</i> - Uniform Rotation of a Liquid-Filled Spacecraft about a Fixed Point in a Constant Force Field	400
<i>B. Rasuo</i> - On Numerical Modelling of Wall Boundary Conditions in Solving Wind Tunnel Wall Interference Problem	415
<i>C. Timofie</i> - Application of Central Limit Theorems to Macrotransport Processes	416
<i>D. Ruzic, N. Anđeljc</i> - Nonlinear Approach to the Behaviour of Thin Walled Turbine Blade Shaped Elements	426
<i>D. Vizman, I. Nicoară, J. Friedrich</i> - 3D Numerical Simulation of Melt Flow in the Presence of Magnetic Fields	432
<i>D. Hărăguș</i> - Statistical Solutions for Bioconvective Flow	441
<i>D. Bălțean, Th. Lévy, St. Balint</i> - Dispersion of a Solute in Periodic Porous Media	451
<i>J. M. Jankovic</i> - Computer Analysis and Simulation of Transient State and Pressure Recovering in Fast Cyclic Hydraulic Actuators	466
<i>O. Manole, D. Pantazopol</i> - Numerical Simulation of Euler Flows with Mach Effect	471
<i>V. Sofonea</i> - Lattice Boltzmann Models for Complex Fluids Subjected to Terrestrial or Space Conditions	477
<i>M. Puta, F. Creț</i> - Some Remarks on the Witten Laplacian	489
<i>A. De Sabata</i> - Sampling Expansions for General Bandpass Signals	494
<i>E. Petrisor</i> - Cascade of Creation and Annihilation of Symmetric Periodic Orbits in Reversible Flow	501
<i>D. Siposean, I. Lancrânjean</i> - A Numerical Solution of Equations Describing the three Photons Interaction in Nonlinear Optical Materials	517
<i>I. Lancrânjean, D. Siposean</i> - Computer Symulation of Passive Optical Q-Switches Laser Operation Thermal Loading	518
<i>Z. Dumitru, A. Stefan</i> - Modelling of the Thermic Phenomena in Diffusive Burning of Gaseous Combustion	519
<i>S. Sterie, I. A. Goleanu, P. Poradici</i> - Some Considerations Concerning the Eulerian-Lagrangean Probability Model	525
<i>S. Sterie, C. Curea, C. Avadanei</i> - Some Considerations Concerning Molecular Diffusion in Gases	533
<i>S. Sterie, D. Vasiu, N. Marin, M. Bunea</i> - Algebraic Invariants Used in the Modelling of Explosive Phenomena	539
<i>Z. Neufeld</i> - Advection in Chaotically Time-Dependent Open Flows	545
<i>E. Barvinschi, I. Nicoară, O. Bunoiu, D. Nicoară</i> - Global Heat Transfer Modelling on Bridgman Crystal Growth	562
<i>I. Nicoară, M. Nicolov, A. Pusztai, D. Vizman</i> - On the Solidification Particularities of the Opaque and SemiTransparent Crystals obtained by Bridgman Method	570
<i>S. Petricevici, I. Elazar</i> - Fourier Approach to Numerical Laser Resonator Calculations	589

METHOD TO STUDY THE DYNAMICAL BEHAVIOUR OF A COMPLEX MECHANICAL STRUCTURE

D.Drăgulescu and M.Toth-Taşcău

*"Politehnica" University of Timișoara, Faculty of Mechanical Engineering, Mechanical Department,
Bd.Mihai Viteazul No.1, 1900 Timișoara, Romania, Tel: +40 56 204333, Fax:+40 56 192062*

Abstract

The paper presents a serial robot, treated as a mechanical structure made of flexible links, capable to accomplish some task in a three-dimensional working space. The method used for deformations calculus adjusts and applies the general approaches developed in the theory of structures dynamics to the usual methods for the robot modelling. The force-displacement relationship is obtained using the robot's stiffness matrix and the forces system acting on the end effector of the robot. Each link of the mechanical structure, modelled as a beam, is considered as a single flexible finit element. The stiffness matrix for an element is a square 12×12 one. So for a robot with n degrees of freedom, the stiffness matrix is $12n \times 12n$. Using the displacement's method and the geometric modelling of the robot, that is to say the transfer matrices between the links, a osft package was developed to compute the deformation matrix for each element as function of the torques acting on its joints. The exposed method is irrespective of the robot's architecture and number of its degrees of freedom. It can be used for any type of mechanical systems

1. Introduction

The paper approach is related to the direct influence of flexibility on accuracy of positioning. Like any other mechanism, a robot arm will deform under the action of a load. The robot's mechanical structure deformations cause a decrease in the real accuracy of the end effector positioning.

The robots with flexible links are continuous dynamical systems having n degrees of freedom, whose motion is illustrated by a system of non-linear coupled differential equations, with variable coefficients, whose exact solution is almost impossible to derive. Hence, it is necessary that these continuous systems are idealized and discretized. In the present paper, a modified rigid finite element method is proposed to discretize flexible systems [1], [2], [7], [8], [9], [10]. A systematic modelling procedure for spatial flexible manipulators, with revolute and prismatic joints, using a modification of the finite element method is presented. The robot links are considered as beams, and each robot link is a flexible finite element. The structure nodes are the robot joints.

2. Force-displacement relationship for the robot structure in local reference frames

In order to study the flexibility of a serial robot, its kinematic chain and attached reference frames S_i , are considered. In order to derive the torque-displacement relationship, the techniques and methods already developed in theory of structures dynamics, were used

While the robot task is accomplished, a forces system reduced at a torque τ_{EF}^0 with respect to the fixed S_0 reference frame, acts on the end effector. The equivalent torque acting on each joint i , expressed in its own reference frame S_i is obtained with:

$$\tau_i^i = \left[(J_i^0)^{-1} \right]^T \cdot \tau_{EF}^0 \quad (1)$$

where J_i^0 is the S_i reference frame Jacobian. In the figure 1, the reference frames attached to each link i of the robot in the joint $i-1$ are represented.

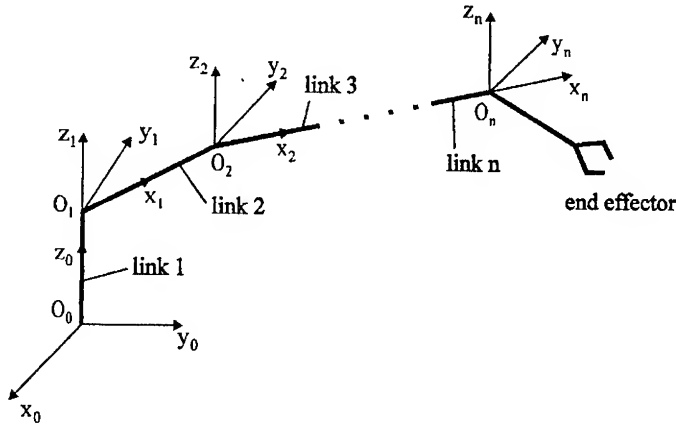


Fig.1. Kinematic chain and reference frames attached to the robot links

Let us consider a certain link i of the robot (fig2). Using the relationship (1), the torques τ_i^i with respect to S_i , and τ_{i+1}^{i+1} with respect to S_{i+1} , respectively, can be computed. But, the torque acting on the joint $i+1$ can be expressed with respect to S_i reference frame using J_{i+1}^i , the S_{i+1} reference frame Jacobian with respect to S_i :

$$\tau_{i+1}^i = J_{i+1}^i \tau_{i+1}^{i+1} \quad (2)$$

Thus, the torque $\underline{\tau}_i$ acting on the link of the robot, may be expressed by a 12×1 matrix:

$$\underline{\tau}_i = \left[\tau_i^i \quad \tau_{i+1}^i \right]^T \quad (3)$$

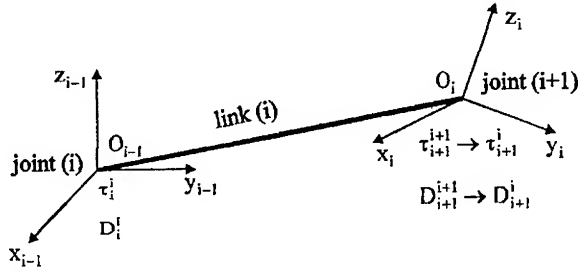


Fig.2. Torques acting on the link i of the robot

The matrix (3) was obtained by putting together the torques acting on the joints i and $i+1$, expressed with respect to the S_i reference frame.

The torque, acting on the whole mechanical system, is than:

$$\underline{\tau} = [\underline{\tau}_1 \dots \underline{\tau}_i \dots \underline{\tau}_n]^T \quad (4)$$

each of the torques $\underline{\tau}_i$ being expressed with respect to its own S_i reference frame.

For each link i of the robot, with respect to its own S_i reference frame, a differential vector of displacement can be considered and expressed as a 6×1 matrix:

$$\underline{D}_i^i = [d_i^i \ \delta_i^i]^T \quad (5)$$

As in the torque case, the vectors \underline{D}_i , and \underline{D} , the last for the entire robot, can be draw:

$$\underline{D}_i = [\underline{D}_i^i \ \underline{D}_{i+1}^i]^T \quad (6)$$

$$\underline{D} = [\underline{D}_1 \dots \underline{D}_i \dots \underline{D}_n]^T \quad (7)$$

If it is considered that the variations of the position and orientation of each robot link are due to the links flexibility, the vectors $\underline{\tau}$ and \underline{D} are related to each other using the system stiffness matrix \underline{K} :

$$\underline{\tau} = \underline{K} \underline{D} \quad (8)$$

where \underline{K} is a quadratic symmetric matrix $12n \times 12n$, whose inverse generally exists and is called the system flexibility matrix $\underline{f} = \underline{K}^{-1}$. Thus, the links deformations can be obtained from:

$$\underline{D} = \underline{K}^{-1} \underline{\tau} = \underline{f} \underline{\tau} \quad (9)$$

If the robot deformations vector is known, the deviations vector \underline{D}_{EF} from the imposed position and orientation of the robot end effector can be obtained using the Jacobian robot matrix \underline{J} , [3].

The system's stiffness matrix is a diagonal matrix, whose elements are the stiffness matrices \underline{K}_i (note that every \underline{K}_i is expressed with respect to its own reference frame).

$$\underline{K} = \begin{bmatrix} \underline{K}_1 & & & \\ & \underline{K}_2 & & \\ & & \ddots & \\ & & & \underline{K}_n \end{bmatrix} \quad (10)$$

3. Force-displacement relationship for the robot structure with respect to the fixed reference frame

The problem is to express the factors of the relation (8) with respect to the fixed global system S_0 :

$$\tau = \underline{K} \underline{D} \quad (11)$$

because the end effector motion, on which the displacements due to the links flexibility are reflected, is expressed with respect to the fixed system S_0 , too.

As concerne $\underline{\tau}$, each element $\underline{\tau}_i$ can be easily transformed with respect to the fixed system, using the general matrix $\underline{G}_i^0 = \prod_{j=1}^i \underline{T}_j^{i-1}$ with which the S_i reference frame is positioned and orientated

[3]. The elements of the \underline{G}_i^0 matrix are used to compute the Jacobian matrix \underline{J}_i^0 of the S_i reference frame with respect to S_0 . In the same way, using the same Jacobian matrix \underline{J}_i^0 , the elements \underline{D}_i of the matrix \underline{D} will be computed with respect to the fixed system S_0 .

The problem is much more complicated in order to express the stiffness \underline{K} matrix with respect to the fixed S_0 system. For this, each \underline{K}_i matrix must be transformed using a so-called geometric compatibility matrix \underline{C} , with which the corresponding matrix with respect to the fixed S_0 system is:

$$\underline{K}_i = \underline{C}^T \underline{K}_i \underline{C} \quad (12)$$

where the \underline{C} matrix is a 12×12 diagonal one:

$$\underline{C} = \begin{bmatrix} \underline{G}_1^0 & & \\ & \underline{G}_2^0 & \\ & & \ddots \\ & & & \underline{G}_n^0 \end{bmatrix} \quad (13)$$

So, the system stiffness matrix with respect to the fixed S_0 system is:

$$K = \begin{bmatrix} K_1 & & & \\ & K_2 & & \\ & & \ddots & \\ & & & K_n \end{bmatrix} \quad (14)$$

All the factors of the relation (11) are now known with respect to the fixed S_0 system, and the problem is solved.

4. Applications

For the study of the links deformations of serial robots some soft packages were developed. The applications were made for two robots: KLOOS with 6 degrees of freedom and SCORBOT-ER III with 5 degrees of freedom.

The required inputs are:

- number of structure elements n (robot's links);
- length of each link ℓ_i ;
- cross-section shape of each link;
- dimensions of the link's cross-section;
- longitudinal and transversal elasticity modulus E_i , respectively G_i of each link;
- Hartenberg-Denavit parameters: a_i , α_i , d_i , θ_i and expressions of transfert matrices T_i^{i-1} ;
- general matrix G_n^0 , at the considered moment;
- torque τ_{EF}^0 acting on the end effector.

The computational sequences followed the exposed theory.

5. Conclusions

In the presented study, the serial robot is treated as an open kinematic chain, with flexible links, capable to accomplish some task in a tri-dimensional space. The method for deformations calculus adjusts and applies the general approaches developed in the theory of structures dynamics, to the usual methods for the robot modelling and dynamics.

The proposed method can be applied to any open mechanical structure, having any degree of freedom, with both revolute and prismatic joints. Each robot link is considered as a single flexible finite element. The computational complexity is modest compared with other proposed algorithms.

The stiffness matrix for a robot element in 3-D is a 12×12 one and for the robot's structure with n elements is $12n \times 12n$, respectively. Based on the proposed method, some soft packages were developed in order to determine the torques matrix, the stiffness matrix and finally, the deformations (displacements) matrix.

The mechanical structure deformations can be used to correct the position and orientation errors of the end effector, therefore, to obtain an improved accuracy.

References

- [1] I. Adamiec-Wojcik and S. Wojciech *Application of a rigid finite element method in dynamic analysis of plane manipulators*, Mechanism and Machine Theory, Vol.28, No.3, (1995).
- [2] R.H. Cannon and E. Schmitz, *Initial experiments on the end-point control of a flexible one-link robot*, International Journal of Robotics Research, 3, No.3, (1984).
- [3] D. Drăgulescu and M. Toth-Tașcău, *Elemente de inginerie mecanică. Introducere în cinematica roboților. Introducere în dinamica roboților*, (Lito UTT, Timișoara, 1993).
- [4] D. Drăgulescu and M. Toth-Tașcău, *Torque elements variation with respect to the reference system change*, (Buletinul Științific al UTT, Seria Mecanică, Tom 40 (54), Fascicola 1, 1995).
- [5] D. Drăgulescu and M. Toth-Tașcău, *Modelarea vibrațiilor unui manipulator prin metoda elementelor finite*, (A VII-a Conferință de Vibrații mecanice, Timișoara, 1993).
- [6] Ch. Massonnet, G. Deprez, R. Maquoi, R. Muller and G. Fonder, *Calculul structurilor la calculatoare electronice*, (Editura Tehnică, București, 1974).
- [7] A. Meghdari and M. Shahinpoor, *Elastic deformation characteristics of a PUMA 560 robot manipulator*, International Journal of Robotics and Automation, 2, No.1, (1987).
- [8] A. Meghdari and M. Shahinpoor, *Three-dimensional flexural-joint stiffness analysis of flexible manipulator arms*, Robotica, Vol.6, (1988).
- [9] A. Meghdari and M. Shahinpoor, *Combined flexural-joint stiffness matrix and the elastic deformation of a servo-controlled two-link robot manipulator*, Robotica Vol. 4, (1986).
- [10] R.I. Theodore and A. Ghosal, *Comparison of the assumed modes and finite element models for flexible multilink manipulators*, International Journal of Robotics Research, Vol.14, No.2, (1995).

LYAPUNOV EXPONENTS AND STRANGE ATTRACTORS IN THE DYNAMICS OF THE BUCKLED BEAM

Daniela Dincă Baran

National Institute for Aerospace Research " Elie Carafoli"-INCAS,
Bucharest, Romania,
220, Bd. Pacii, Sect. 6, Email: dbaran@aero.incas.ro

Abstract In this paper we analyze and compare some results concerning the chaotic motions of the buckled beam (using three mathematical models Bernoulli-Euler, Rayleigh and Timoshenko) by means of three different methods: maximum Lyapunov exponent, portraits in the phase plane, and the Melnikov function.

1. INTRODUCTION

The great developing of the numerical analysis of the dynamic systems emphasizes the following facts:

The existence of a strong dependence of the initial conditions, described in the phase plane by attractors with a complicated geometrical structure (see for example in [1,2]). The strong dependence is usually proved by the help of the Lyapunov exponents [3,4,5], and the complexity of the geometrical structure of the attractors leads to the notion of *strange attractor*. Strange attractors are defined in many ways, but here we adopt the definition of Holmes and Guckenheimer [2]: an attractor is a strange attractor if it contains a homoclinical transverse orbit.

The transversal vibration of a buckled beam is a well-known problem which leads to chaotic motion. Usually, to study this problem, the Bernoulli -Euler beam model was used. In this paper we adopt two more elaborated models: the Rayleigh model, which includes the rotatio inertia effect, and the Timoshenko model that includes both the rotatio inertia effect and the shear force effect, and remark the effects of these models.

2. EQUATION OF MOTION

Consider a buckled beam of length l , simply supported, acted upon by an axial force P and a lateral load $F \cos \alpha_1$. The equation of motion in

the Bernolli-Euler model including the membrane effect using non dimensional variables, is:

$$\frac{\partial^2 v}{\partial t^2} + \frac{\partial^4 v}{\partial t^4} + (\Gamma - k \int_0^1 (v'(\xi))^2 d\xi) \frac{\partial^2 v}{\partial x^2} + c \frac{\partial v}{\partial t} = f \cos \omega t. \quad (1)$$

Introducing the rotatio inertia effect equation (1) becomes (Rayleigh model):

$$\frac{\partial^2 v}{\partial t^2} - b_0 \frac{\partial^4 v}{\partial x^2 \partial t^2} + \frac{\partial^4 v}{\partial t^4} + (\Gamma - k \int_0^1 (v'(\xi))^2 d\xi) \frac{\partial^2 v}{\partial x^2} + c \frac{\partial v}{\partial t} = f \cos \omega t. \quad (2)$$

Introducing the shear force effect (2) becomes (Timoshenko model):

$$\frac{\partial^2 v}{\partial t^2} - (b_0 + b_1) \frac{\partial^4 v}{\partial x^2 \partial t^2} + \frac{\partial^4 v}{\partial t^4} + (\Gamma - k \int_0^1 (v'(\xi))^2 d\xi) \frac{\partial^2 v}{\partial x^2} + c \frac{\partial v}{\partial t} +$$

$$b_2 \frac{\partial^3 v}{\partial t^3} - b_3 \frac{\partial^3 v}{\partial x^2 \partial t} + b_4 \frac{\partial^4 v}{\partial t^4} = f \cos \omega t \quad (3)$$

where:

$$\begin{aligned} \Gamma &= \frac{Pl^2}{EI}, \quad k = \frac{\kappa l^2}{EI}, \quad c = \frac{Cl^2}{\sqrt{\rho} AEI}, \quad f = \frac{Fl^2}{EI} \\ b_0 &= \frac{I}{l^2 A}, \quad b_1 = \frac{EI}{k' GI^2 A}, \quad b_2 = \frac{IC}{k' A^2 GI} \sqrt{\frac{EI}{\rho A}} \\ b_3 &= \left(\frac{EI}{\rho A}\right)^{1/2} ck' AG, \quad b_4 = \frac{(EI)^2}{k' GI^4}, \quad b_5 = \frac{I}{k' AG} \end{aligned}$$

The chaotic vibrations of the simply supported buckled beam are analyzed using the first approximation in the Galerkin method, developing the transversal displacement $u(x, t) = h(t) \sin \pi x$, with the following nonlinear equation of Duffing type:

$$\begin{aligned} h - \beta^i h + \alpha^i h^3 &= \varepsilon(\gamma^i \cos \omega t - \delta^i h), \quad i = 1, 2, 3 \\ h(0) &= h_0, \quad \dot{h}(0) = \dot{h}_0 \end{aligned} \quad (4)$$

where the coefficients $\alpha^i, \beta^i, \gamma^i, \delta^i$ have slightly different values for the three mathematical models considered.

2. ANALYSIS AND RESULTS

2.1 Obtaining the Bifurcation Values with the Melnikov method

Equation (4) has, for $\varepsilon=0$ a hyperbolic saddle point and a homoclinical orbit. For $\varepsilon>0$ one associates to such an equation a real valued function, called the Melnikov function. One shows that if the Melnikov function is independent of ε and has simple zeroes, then for $\varepsilon>0$ sufficiently small, the motion described by (4) becomes chaotic [2].

The Melnikov function for (4) is:

$$M_i(t_0) = \sqrt{\frac{2}{\alpha_i}} \gamma_i \frac{\pi \omega_i \sin \omega t_0}{\cosh(\pi \omega / 2 \sqrt{\beta_i})} - 4 \frac{\delta \beta_i^{3/2}}{3 \alpha_i} \quad (5)$$

Introducing the notation:

$$R_i(\omega) = 4 \beta_i^{3/2} \cosh\left(\frac{\omega \pi}{2 \sqrt{\beta_i}}\right) / (3 \pi \omega \sqrt{2 \alpha_i}) \quad (6)$$

the condition for homoclinical transverse intersection is:

$$\frac{\gamma_i}{\delta_i} > R_i, i = 1, 2, 3. \quad (7)$$

Taking into account the form of the coefficients of the equation (4) for $\omega=1$ one obtains the following inequality:

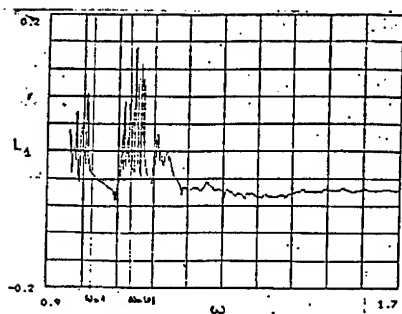
$$R_1 > R_2 > R_3. \quad (8)$$

This inequality reflects the different way in which the three models can perform chaotic motions: it is possible that under the same initial conditions and external loads some of the beams perform periodic motions and others perform chaotic ones.

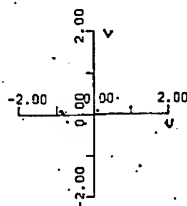
2.2. Lyapunov exponents

The Lyapunov exponents are a sort of "measure" of the separation of a reference solution from a perturbed one. The principal information offered by these coefficients are:

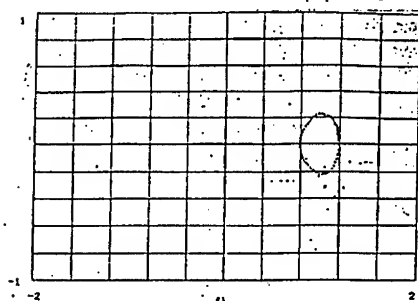
1. There is at least a positive exponent if the system has a chaotic evolution.
2. All the Lyapunov coefficients are negative if the system has not a chaotic evolution.



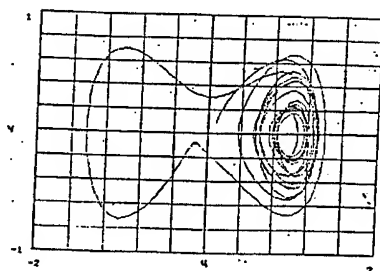
a) $L_1, \gamma_1/\delta_1=1.$



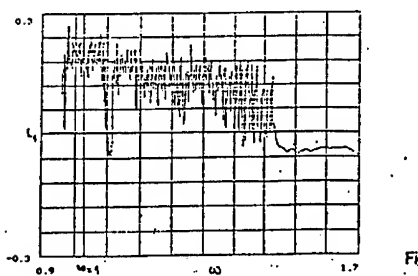
b) Poincaré map; $\gamma_1/\delta_1=1, \omega=1.$



c) Poincaré map; $\gamma_1/\delta_1=1, \omega=1.08.$



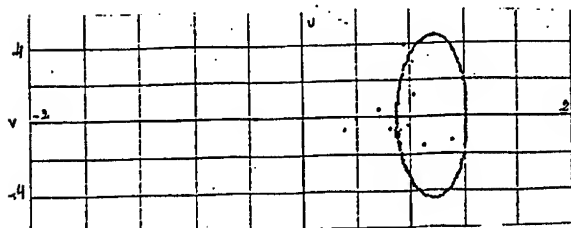
d) Phase plane portrait, $\gamma_1/\delta_1=1, \omega=1.08.$



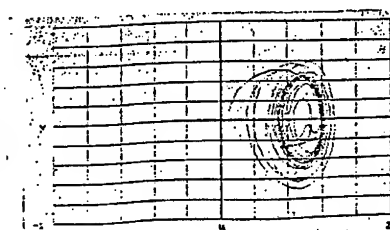
a') $L_1, \gamma_1/\delta_1=2.$



b') Poincaré map; $\gamma_1/\delta_1=2, \omega=1.$

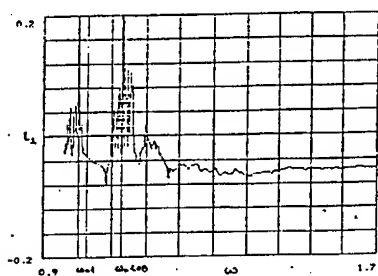


c') Poincaré map; $\gamma_1/\delta_1=2, \omega=1.7.$

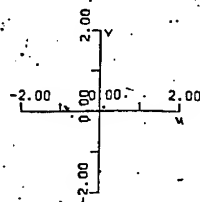


d') Phase plane portrait, $\gamma_1/\delta_1=2, \omega=1.08.$

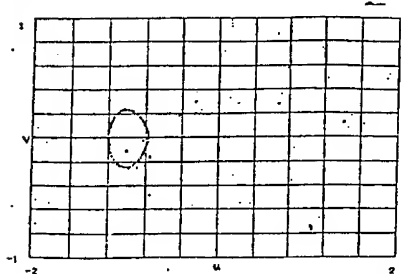
Fig. 1 Bernoulli-Euler beam.



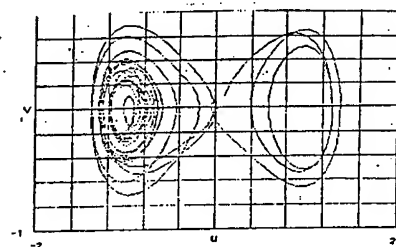
a) $L_2, \gamma_2/\delta_2=1.$



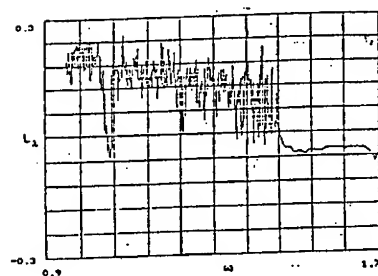
b) Poincaré map; $\gamma_2/\delta_2=1, \omega=1.$



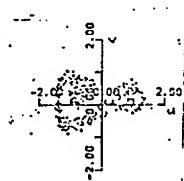
c) Poincaré map; $\gamma_2/\delta_2=1, \omega=1.08.$



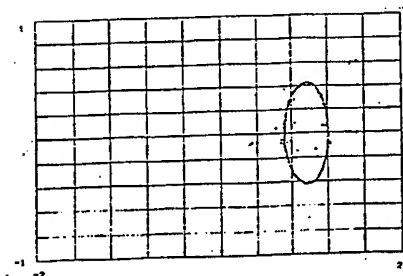
d) Phase plane portrait, $\gamma_2/\delta_2=1, \omega=1.08.$



a') $L_2, \gamma_2/\delta_2=2.$



b') Poincaré map; $\gamma_2/\delta_2=2, \omega=1.$

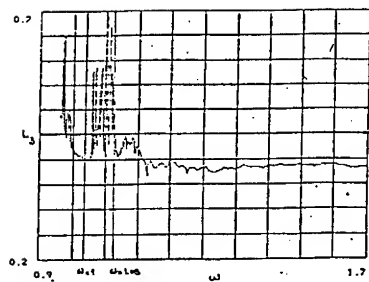


c') Poincaré map; $\gamma_2/\delta_2=2, \omega=1.7.$

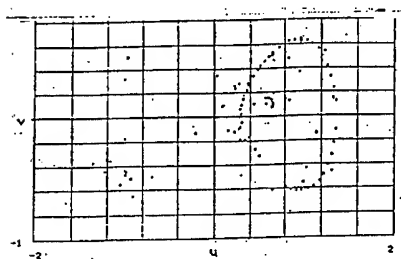


d') Phase plane portrait, $\gamma_2/\delta_2=2, \omega=1.08.$

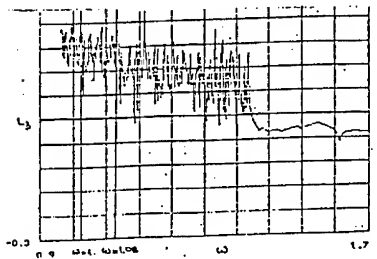
Fig.2 Rayleigh beam.



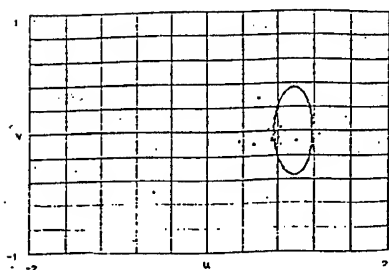
a) $L_3, \gamma_3/\delta_3=1.$



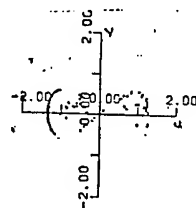
c) Poincaré map; $\gamma_3/\delta_3=1, \omega=1.08.$



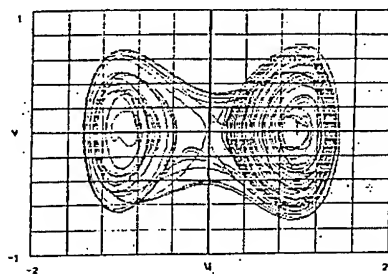
a') $L_3, \gamma_3/\delta_3=2.$



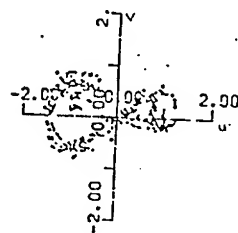
c') Poincaré map; $\gamma_3/\delta_3=2, \omega=1.7.$



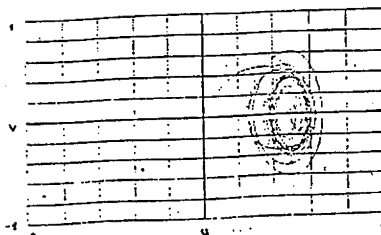
b) Poincaré map; $\gamma_3/\delta_3=1, \omega=1.$



d) Phase plane portrait, $\gamma_3/\delta_3=1, \omega=1.08.$



b') Poincaré map; $\gamma_3/\delta_3=2, \omega=1.$



d') Phase plane portrait, $\gamma_3/\delta_3=1, \omega=1.08.$

Fig.3 Timoshenko beam.

We note that to draw the two conclusions below are sufficient to determine the greatest Lyapunov exponent, which is easier to calculate and many authors use this method to evaluate the strong dependence of the initial conditions [3], [10, 11, 12, 13, 14].

The expression of the maximum Lyapunov exponent is [3]:

$$L_N = \frac{1}{N\Delta t} \sum_{j=1}^N \ln \frac{d_j}{d} \quad (9)$$

where Δt is the time step considered in the evaluation of the solution (and it is also the numerical integration time step), N is the number of such time steps considered, d_j is the distance between the perturbed solution and the unperturbed one at the j -th time moment, and d is the distance between the two solutions at the initial moment.

We perform our analysis with the initial conditions $h_{i0} = h_{i\infty} = 0.1$, which are in a small neighborhood of the homoclinical saddle point of (4) when $\varepsilon=0$. The evolution is analyzed using the maximum Lyapunov exponents L_i , ($i = 1, 2, 3$), Poincaré maps and portraits in the phase planes.

2.4. Conclusions

1. When the maximum Lyapunov exponent is negative the evolution is periodic or quasi-periodic.
2. When the maximum Lyapunov exponent is positive the evolution is rather complex, we may say it is chaotic.
3. There are cases in which for the same initial conditions and external loads we obtain periodic quasi periodic motions for the Bernoulli and Rayleigh models and chaotic for the Timoshenko model. As a final remark, in these cases the Timoshenko beam is more sensible to chaotic motions than the other two models.

REFERENCES

1. David Ruelle, *Hasard et chaos*, Edition Odile Jacob, Paris 1990.
2. John Guckenheimer, Philip Holmes, *Nonlinear Oscillation Dynamical Systems and Bifurcation of Vector Fields*, Springer Verlag, New York, Berlin, Heidelberg, Tokyo, 1988.
3. Radu Voinea, Ion Stroe, *Sisteme dinamice*, Universitatea Politehnica Bucurest, 1993.
4. Alan Wolf, Jack B. Swift, Harry L. Swiney, John A. Vastano, *Determining Liapunov Exponents from a time series*, *Physica 16D* (1985) 285-317, North Holland, Amsterdam.

5. J. Wright, Method for Calculating a Lyapunov Exponent, Physics Review A29(1984) 2923.

6. Emilia Petrisor, Sisteme dinamice, Editura Universitatii Timisoara, Timisoara, 1992.

7. Earl Dowell, Chaotic Oscillations in Mechanical Systems, Computers and Structures, vol 30, No. 1/2, 1988.

8. S. H. Chen S. S. Chen, Chaotic Vibration in Fluid Elastic Instability of a tube Row in Crossflow, PVP -vol 258, Flow-Induced Vibration and Fluid-Structure Interaction, ASME, 1993.

9. Daniela Baran, Vibratiile aleatoare si haotice ale structurilor mecanice cu aplicatii in aviatie si energetica nucleara, teza de doctorat, Universitatea Bucuresti, 1995.

10. J. P. Gallub, E. J. Romer, J. E. Socolor, Trajectory divergence for coupled relation oscillators: measurements and models, J. Stat. Phys. 74 (1981) 6171.

11. J. L. Hudson, J. C. Mankin, Chaos in the Belousov - Zhabotinskii Reaction, J. Phys. Soc. Japon (1982) 21.

12. H. Nagashima, Experiment on Chaotic Response of Forced Belousov-Zhabotinskii Reaction, J. Phys. Soc. Jap (1982) 21.

13. A. Wolf, J. Swift, Progress in Computing Lyapunov Exponent from Experimental Data, in Stat. Phys. and Chaos in Fusion Plasmas, Wiley, New-York, 1984.

14. J. Wright, Method for Calculating a Lyapunov Exponent, Phys. Rev. A29 (1984) 2923.

Lift Enhancement by Aerodynamic Multiparametric Optimization of a Wing-Strake Configuration

Octavian Trifu*

National Institute of Aerospace Research "Elie Carafoli"
Bd. Păcii 220, 77538, Bucharest

An aerodynamic multiparametric optimization procedure, for the strakes optimum planform design, is presented. Its purpose is to define, through a numerical optimization process, the geometrical characteristics of these elements, in order to obtain a maximum lift increase for the complex aircraft configuration (fuselage+wing+tails) on which they are installed. Since its aerodynamic analysis module is based on approximate methods, the procedure is fast and may be useful especially in the initial stages of an aerodynamic design project. For a generic configuration strakes of larger and smaller area were optimized. Lift increases of about 14-18% were obtained accompanied by alterations of the longitudinal stability characteristics. Therefore the strakes optimization problem requires a careful attention and a multidisciplinary - aerodynamic and stability- treatment seems to be, as finally suggested, its adequate solution.

Nomenclature

A	= area of a panel
ΔC_p	= difference between the upper and lower surface pressure coefficients
CL	= lift coefficient
CD	= drag coefficient
Cm	= pitching moment coefficient
\vec{F}	= aerodynamic force on a panel
M	= Mach number; number of chordwise panels
p	= optimization parameter
Δp	= pressure difference (constant) applied on panel
N	= normal force on a lifting surface
\vec{n}	= unit normal vector
N	= normal force (component)
S	= potential flow leading-edge suction force; area of a lifting surface
S_R	= reference area
s	= segment on the horseshoe vortex associated to a panel
S_{wred}	= planform area of the reduced wing (out of the fuselage)
T	= potential flow leading edge thrust force (component)
\vec{V}	= velocity
α	= angle of incidence
γ	= strength of a horseshoe vortex
ϕ	= disturbance potential of the analyzed flow
Λ	= leading edge sweepback angle
μ	= setting angle
ρ	= density

Subscripts

∞	= freestream conditions
i	= optimization parameter index
j	= panel chordwise index
k	= strip on wing's inner zone
LE	= leading-edge
p	= potential flow
S	= strake
V	= due to the rolled-up vortices

Introduction

For the "classical" aerodynamic designer, one of the main concerns is to avoid, as much as possible, the separation of the flow over the airplane's surface. However, since some beneficial effects, related to certain types of controlled separations were experimentally revealed¹, numerous experimental and theoretical studies²⁻¹⁴ were dedicated to this subject. Physical explanations were formulated and successful attempts to elaborate theoretical methods for a quantitative evaluation of the aerodynamic effects were made.

Among other, the *strakes* are an outcome of these studies. They are small aspect ratio lifting surfaces, having sharp leading edges with large sweep angles, used in the modern aerodynamic design practice as *vortex lift generators*. When placed ahead of the leading edge of a wing with a smaller sweep angle and a larger aspect ratio (Fig. 1) the rolled-up (spiral) vortices, created by the separation of the flow at their sharp leading edges followed by a reattachment on the wing's upper side, produce nonlinear lift as a consequence of the depression acting on the strakes and also on a certain region of the wing (the augmentation effect).

*Senior Scientist, Aerodynamics Department

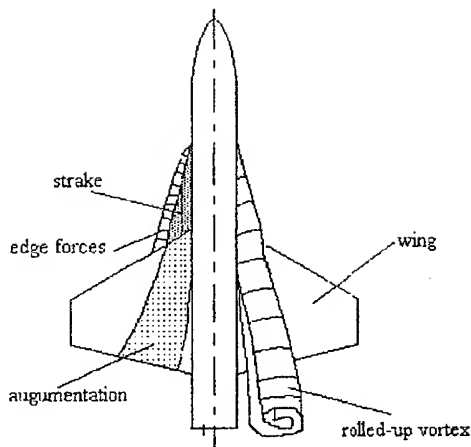


Fig. 1 The rolled-up vortices associated with a strake-wing configuration

Thus, as a result of an aerodynamic synergistic effect, the lift of the wing+strakes combination is greater than the sum of the lifts produced separately by each of these components (Fig. 2).

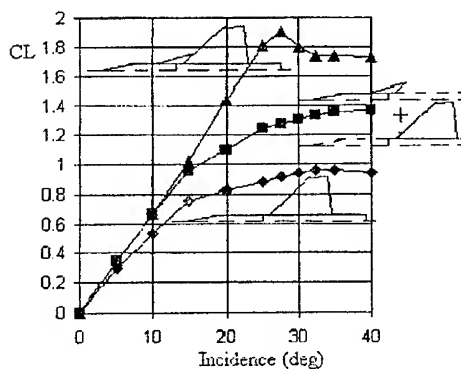


Fig. 2 Synergistic effect in the case of a strake-wing configuration

Parametric studies¹¹⁻¹³ revealed the influence of both: surface and shape of the nonlinear lift generators on the lift augmentation of various fuselage+wing configurations. Therefore, defining the geometrical details of the strakes, through an aerodynamic optimization process, will certainly maximize the benefits expected when such elements are installed on a given airplane.

The relation that links the strake's shape with the aerodynamic characteristics of the whole configuration is implicit (nonlinear). Accordingly, the optimization procedure presented in this paper, is a numerical one.

The Principle of the Optimization Procedure

The purpose of the procedure for the optimum definition of the strakes¹⁵ is to find a planform for these elements that provides, for certain given flight conditions, the maximum lift for the airplane on which they are installed. Since an airplane's lift depends, among other, on the shape of its wing, that can be expressed with a number of geometrical parameters, it is possible to define a function including CL, thus having as variables those parameters. For the optimization process, this is the *objective function* and its variables are the *optimization parameters*. In the optimization process the search of one extreme (usually the minimum) of the objective function is performed, namely one looks for the values of the parameters for which that extreme value is reached. In the real situations, the domain where the optimization parameters are allowed to take their values is limited by a number of *restrictions* that are meant to ensure the necessary physical consistency for the optimum solution.

For an airplane having a complex configuration (fuselage+wing+tails) it is practically impossible to deduce an exact analytical relation between CL and the geometrical parameters that define its shape. Therefore, in such situations, numerical methods are used to determine the aerodynamic characteristics. Hence the nonlinear function that links the lift coefficient to the geometrical parameters is an implicit one. Accordingly, the optimization procedure of the configuration (in this case only a part of it - the strakes) must be also numerical. In principle (Fig. 3), such a procedure is based upon an algorithm (of iterative nature) for the searching of the given objective function's minimum, in which an aerodynamic analysis module is included. This module calculates the aerodynamic characteristics of the configuration, corresponding to its current shape as defined by the optimization parameters, and provides them to the optimization algorithm.

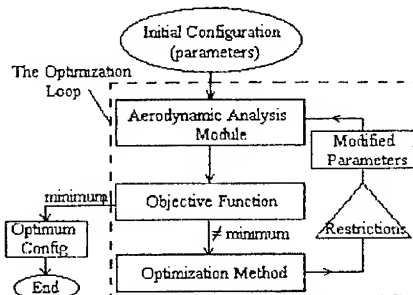


Fig. 3 The optimization procedure

For a given set of flight conditions (altitude, speed, incidence, deflection angles of the

aerodynamic controls), the aerodynamic analysis module determines the characteristics of the *initial configuration*, so that an initial value of the objective function can be computed. Then, using an optimization method, the parameters are changed (within the limits of the imposed restrictions) and the modified configuration is aerodynamically analyzed, so that a new value is determined for the objective function. During the *search for the optimum* process only those variations of the parameters that produce a decrease of the objective function are accepted. When at two successive optimization steps the variation of the objective function becomes smaller than a certain error level, the search for the optimum is ceased. The corresponding values of the parameters are those who define the optimum configuration.

Since the procedure discussed here is conceived to determine the optimum planform of the strakes, the wing of the analyzed airplane is divided into two: an inner zone at the junction with the fuselage, corresponding to that region of the leading edge where the strakes are placed, and an outer zone (Fig. 4).

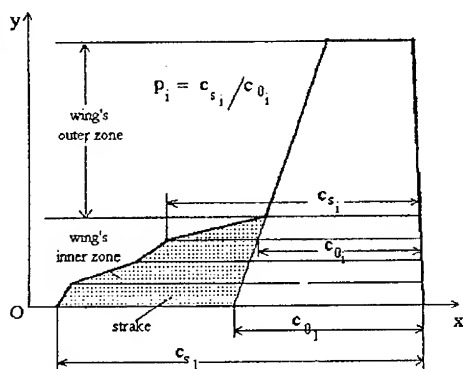


Fig. 4. Definition of the parameters for the strake's planform optimization

The inner zone is divided spanwise in equally wide strips Δy_k , and thus on its leading edge a number of intervals are defined by points that are initially equally spaced. During the optimization process these points are moved in a such manner that a strake "grows" on the leading edge of the wing's inner zone. The ratios between the chord of the wing with strakes (c_{s1}) and the chord of the initial wing (without strakes - c_{01}) in the given i sections, are used as optimization parameters. The search of the strake's optimum planform is performed in two stages:

- first, p_1 is increased and the other parameters p_i determined from the condition that the strake's leading edge remains straight;
- then, by modifying individually, in a sequential manner, all the parameters (p_i included) the final shape of the leading edge, in this wing's zone, is obtained.

As mentioned, the initial and the modified values of the optimization parameters must satisfy certain restrictions. These are related to the lowest/highest allowable values for p_i and to the limits that restrict the variation of the leading-edge's sweep angle on the Δy_k divisions of the inner zone.

The value of each parameter is modified by the module which does the search for the objective function's minimum and the strake's configuration is updated, at each step, in the lifting surface geometry section of the aerodynamic analysis module. The geometrical characteristics of the fuselage, wing's outer zone and tails remain unchanged during the optimization process. This is also true for the relative position of the configuration's main parts (fuselage-wing-tail).

The Aerodynamic Analysis Module

The aerodynamic analysis module is derived from a program that calculates the air-flow characteristics around an airplane configuration: fuselage+lifting surfaces (wing, horizontal and vertical tails, etc.) at subsonic, subcritical speeds developed at NIAR^{16,17} upon the algorithm published by Hua¹⁸. It has two main sections:

- One in which are determined, on the basis of the input data, the geometrical characteristics for the elements of the analyzed configuration. In this section are also made the modifications of the wing's inner zone, according to the current values of the parameters at a certain moment during the optimization process;
- The main section where the characteristics of the flow and the aerodynamic characteristics are computed.

The analyzed flow is supposed to be inviscid, steady, subsonic, subcritical, with small perturbations. The configuration's basic parts are treated in a simplified manner:

- The fuselage is approximated by an axisymmetric body, closed at both ends, defined by the values of the circular section radius r_i given at a number of stations x_i ;
- The lifting surfaces: supposed to be thin (without thickness), and defined by the root chord, an aspect ratio, a taper ratio, a sweep angle (at 25% chord), a setting angle and a dihedral angle. Each lifting surface may have a certain camber and/or twist and a pair of control

surfaces (deflected or not). The data for the lifting surfaces must correspond to their "reduced" form (only the parts which are outside the fuselage)

The configuration may include only one fuselage (or equivalents - a store's body, for example) and an unlimited (in principle) number of lifting surfaces.

The flow defined by the above stated hypothesis is governed by the potential small disturbance equation:

$$(1-M_\infty^2) \frac{\partial^2 \phi}{\partial x^2} + \frac{\partial^2 \phi}{\partial y^2} + \frac{\partial^2 \phi}{\partial z^2} = 0. \quad (1)$$

The modeling of the flow is based on the summation of the effects produced by a distribution of point sources and doublets (for the fuselage) and horseshoe vortices (for the lifting surfaces) placed in the undisturbed U_∞ incident flow (Fig. 5). The sum of the potentials of these elementary singularities is the solution ϕ of equation (1).

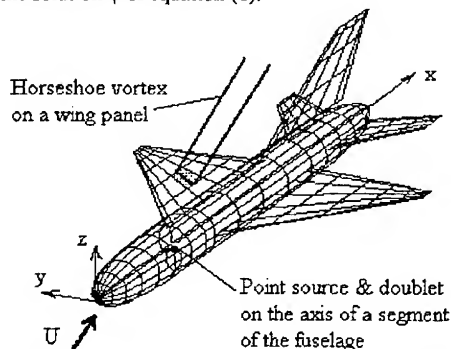


Fig. 5 The modelling of the perturbed flow around a discretized airplane configuration

The boundary condition, assumes that at any point on the external surface S of the analyzed configuration, the normal component of the local velocity \vec{V} is zero:

$$\vec{V} \cdot \vec{n} = 0 \quad (2)$$

\vec{n} - being the outward normal unit vector

When \vec{V} is substituted in equation (2) with the sum of the contributions (induced velocities) of all the singularities (sources, doublets, vortices), an integral equation is obtained, whose unknowns are their strength. The method of solution uses a technique which replaces the integral equation by a set of linear algebraic nonhomogenous equations. This is accomplished by dividing the body in tronconic segments (each associated with a point source and a point doublet) and the lifting surfaces in quadrilateral panels (each associated with a

horseshoe vortex). Therefore the method belongs to the "first order Panel Methods" category.

The coefficients of the algebraic nonhomogenous linear equations are calculated as functions of the configuration's geometrical characteristics and of the parameters that define the incident flow (M_∞ , α , β). The linear equation system is solved by a *Gauss elimination with complete pivoting* technique.

Once the solution (the strengths of the elementary singularities), is obtained, the calculation of the velocity and pressure distributions is straightforward. The determination of the local and global aerodynamic forces and moments and of the corresponding aerodynamic coefficients is then immediate.

Another possibility to simulate the perturbations produced by the presence of the fuselage, consists in replacing it by a lifting surface of very low aspect ratio, whose planform is, as much as possible, close to the xOy projection of the real item (*the Belotserkovski model*¹³). Having certain advantages, as far as the accuracy of the calculated lift and the speed of the computations are concerned, this approximation was used in the present study.

Due to the iterative nature of the optimization procedure, the low computer memory and time required to perform the aerodynamic analysis of the analyzed configuration was, in fact, one of the main arguments towards the decision to include this panel method in the aerodynamic module. Another strong argument was offered by the ability of this method to analyze configurations having a quite high degree of complexity.

In the above described form, the method (and the corresponding computing module) was unable to evaluate the lift produced by the rolled-up vortices generated by the separation of the flow at the sharp leading and/or side edges of the lifting surfaces (*the vortex lift*). Therefore, to meet the necessities of the strakes optimization process, the aerodynamic analysis algorithm was completed with the vortex lift quantitative evaluation capabilities¹⁵.

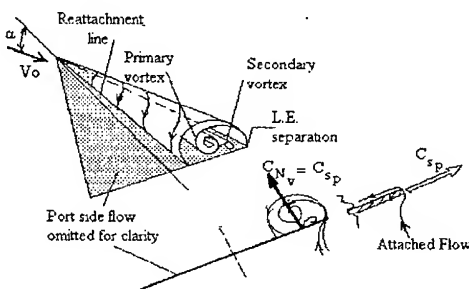


Fig. 6 Principle of the leading-edge suction analogy

Due to its qualities (very good precision/computing time factor) the suction analogy method due to Polhamus³ was chosen to calculate this lift component. This method, despite its rather intuitive foundations, was remarkably validated by many experimental data, especially at subsonic speeds, and was largely adopted by the applied aerodynamics community.

Polhamus assumed that: the normal (perpendicular) force on the upper side of a wing required to maintain a flow with reattachment about the rolled up vortices formed at its swept and sharp leading edges (Fig.6) is the same as the leading-edge suction force required to maintain the attached flow about the leading edge in the potential flow case, hence:

$$N_v = S_p = \frac{T_p}{\cos \Lambda_{LE}} \quad (3)$$

For the purposes of this study, the method of Lan and Mehrotra¹⁰ was adopted to calculate, in a potential flow, the local suction force S_{pk} acting on the leading edge of the strip k , obtained by the spanwise division of a thin lifting surface. This method uses the development in a Fourier series of the chordwise pressure distribution corresponding to that strip.

On a panel j (belonging to the strip k) to which is associated the elementary horseshoe vortex with the strength γ_{kj} , the difference between the upper and the lower surface pressure coefficients is given by:

$$\Delta C_{p_{kj}} = \frac{\Delta p_{kj}}{\frac{\rho_\infty}{2} V_\infty^2} = \frac{F_{kj} \cdot \rho_{kj}}{\frac{\rho_\infty}{2} V_\infty^2 A_{kj}} \quad (4)$$

where:

$$F_{kj} = \rho_\infty \int_{l_{kj}} \vec{V}_{kj} \times \gamma_{kj} \cdot d\vec{s}_{kj} \quad (5)$$

The $\Delta C_{p_{kj}}$ values distribution on each k strip is developed in a cosine Fourier series:

$$f(\theta) = \frac{1}{2} \Delta C_p \sin \theta = a_0 + \sum_{j=1}^m a_j \cos \left(\frac{j\pi\theta_j}{\theta_M - \theta_1} \right) \quad (6)$$

the angle θ_j , being defined by (Fig. 7):

$$\theta_j = \arccos(1 - 2 \cdot \bar{x}_j) \quad (7)$$

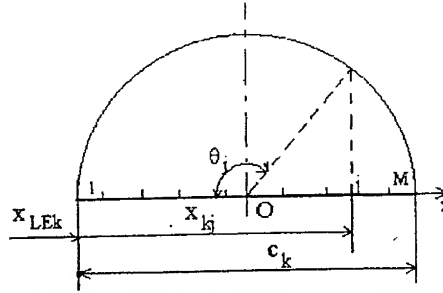


Fig. 7 The chordwise division of the k -th strip on a lifting surface

M = the number of chordwise divisions of the strip k

with:

$$\bar{x}_j = \frac{x_{kj} - x_{LEk}}{c_k} \quad (8)$$

The use of a simple numerical integration rule (trapeze) for the calculation of the Fourier series coefficients proved to be satisfactory.

$$a_0 = \frac{1}{\Theta} \int_0^\Theta f(\theta) \cdot d\theta = \frac{1}{2m} \sum_{j=1}^m (f_j + f_{j+1}) \quad (9)$$

and:

$$a_j = \frac{2}{\Theta} \int_0^\Theta f(\theta) \cdot \cos \frac{j\pi\theta}{\Theta} \cdot d\theta = \frac{1}{m} \sum_{i=1}^m \left[f_j \cdot \cos \left(j \frac{i-1}{m} \pi \right) + f_{j+1} \cdot \cos \left(j \frac{i}{m} \pi \right) \right] \quad (10)$$

where:

$$\Theta = \theta_M - \theta_1 \quad (11)$$

m = a number ($> M$) of equal divisions of the $[\theta_1 - \theta_M]$ domain; ($m = 20$ was used)

$f_j = m+1$ values obtained by the interpolation of the M values calculated for the function $f(\theta_j) = \frac{1}{2} \Delta C_{p_{kj}} \sin \theta_j$, on the k -th strip of the thin lifting surface.

Near the leading edge, the variation of ΔC_p is similar to that of the function:

$$\Delta C_p \equiv C \sqrt{\frac{1-x}{x}} \quad (12)$$

and therefore:

$$\lim_{x \rightarrow 0} \frac{1}{2} \Delta C_p \sin \theta = C = a_0 + \sum_{j=1}^m a_j \quad (13)$$

C being the *leading-edge suction parameter*. As a function of its value, the coefficient of the suction force on the k -th strip will be¹⁰:

$$c_{sk} = \frac{\pi}{8} C_k^2 \sqrt{1 - (M_{\infty} \cos \Lambda_{LEk})^2} / \cos^2 \Lambda_{LEk} \quad (14)$$

Thus, according to Polhamus's model, the contribution of the rolled-up vortices to the normal aerodynamic force on the k -th strip of the lifting surface is:

$$P_{NVk} = c_{sk} \cdot \rho_{\infty} \frac{V_{\infty}^2}{2} \cdot A_k \quad (15)$$

and to the thrust (axial) force (see relation 3):

$$P_{TVk} = P_{NVk} \cos \Lambda_{LEk} \quad (16)$$

These forces are added to the *normal* and *axial* components, determined with the above described potential method, on the first panel (near the leading-edge) of each strip k :

$$P_{z1k}^* = P_{z1k}^p + P_{NVk} \quad (17)$$

$$P_{x1k}^* = P_{x1k}^p - P_{TVk} \quad (18)$$

Relation (18), that corrects the drag with the contribution of the leading edge suction, may not be applied on those lifting surfaces (or portions of their leading edge) where the flow separates and rolled-up vortices are formed, hence where relation (17) is applied. Relation (17) introduces also the influence of the vortex lift over the airplane's pitching moment.

In the case of an airplane with strakes, the vortices generated at their leading-edges travel downstream, exerting an influence in the flowfield. To take into account these effects, to the "ensemble" of singularities used to calculate the potential flow around the analyzed configuration, two symmetrical, free, semiinfinite line vortices were added, having the strength Γ_s , the origins at R, L (Fig. 8) and passing (when $\alpha > 0^\circ$) above the wing. Their influence (perturbation velocities) was considered here only on the outer zone of the wing and on the airplane's tail.

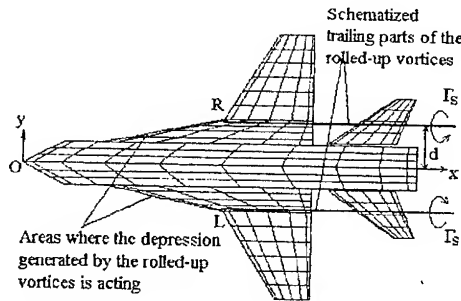


Fig. 8 Elements of the model used in the vortex-lift calculations

The coordinates of R, L and the strength Γ_s are calculated according to the indications given by Mendenhall et al.²⁰, by using the *vortex-lift* spanwise distribution. Thus, the strength of the two free vortices, which will be referred here as *supplementary vortices*, can be determined using the relations:

$$\Gamma_s = \frac{S_R V_{\infty}}{4 \cdot d} C_{NV} \cos(\alpha + \mu_0) \quad (19)$$

where:

$$C_{NV} = \frac{2}{S_R} \int_0^{b_1} (c \cdot c_s) \cdot dy \quad (20)$$

and the distance d , gives the spanwise location:

$$d = \frac{\int_0^{b_1} (c \cdot c_s) \cdot y \cdot dy}{\int_0^{b_1} (c \cdot c_s) \cdot dy} \quad (21)$$

A simple numerical integration is used to evaluate the integrals of (20, 21) on the semispan b_1 of the wing's inner zone, divided in the k strips. In the expressions of the integrands, c_s is the suction force coefficient (relation 14) and c is the local chord (strake included). The points R and L, are placed near the intersection point of the strake's and the wing's leading-edges (for details, on the calculation of their coordinates, see Ref. 15).

As seen, for the calculation of the position and the strength of the supplementary vortices, the suction force distribution on the strake's leading-edge must be known. Hence, an iterative method of solution must be applied. In a first approximation, the flow around the airplane's configuration (with strakes) is calculated without taking into consideration the influence of the supplementary

vortices. After the suction force distribution and, based on it (relations 19-21) the characteristics of these vortices, are determined, their influence can also be considered, in a new computational cycle. The iterations are stopped when two successive values determined for Γ_s satisfy an imposed relative error level (2% was used).

All the elements related to the calculation of the *vortex-lift* generated by the strakes (including the influences over the rest of the airplane's configuration) were introduced in the algorithm of the aerodynamic analysis module. To validate the accuracy and the efficiency of these modifications, several numerical tests were performed on a number of straight or delta wings and on a complete airplane configuration (without and with strakes).

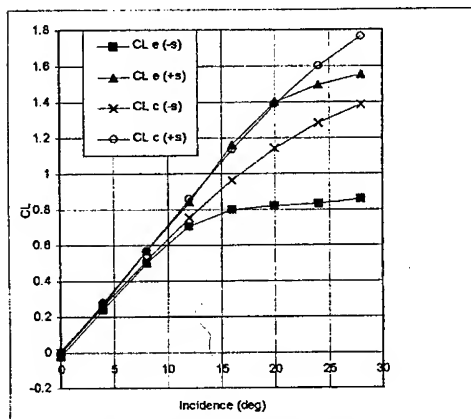


Fig.9 Lift coefficient variation with incidence for the configuration of Fig.8, without (-s) and with (+s) strakes. Comparison of computed (c) and experimental (e) data

For instance, in the case of the generic fighter of Ref.13 (Fig. 8), the results given by the aerodynamic analysis module, for the configurations without and with strakes, are represented in Fig. 9. The agreement of the calculated and the experimental CL data is good up to $\alpha = 12^\circ$ for the basic configuration, and up to $\alpha = 20^\circ$ for the configuration with strakes. In the first situation, the experimental lift becomes almost constant for $\alpha > 12^\circ$, due to the enlargement of the separation regions on the wing's upper side and in the second situation the occurrence, at $\alpha > 16-18^\circ$, of the *vortex breakdown* causes, due to a reduced vortex-lift contribution, a decrease in the experimental lift curve slope. Although the above described flow model is unable to evaluate separation or vortex breakdown effects, the numerical tests confirmed that the updated version of the aerodynamic analysis module has the capacity to determine, with

reasonable accuracy, up to the *breakdown* incidence, the contribution of the strakes to the aerodynamic characteristics of an airplane on which such elements are installed.

The Optimization Method

As specified in section 2, besides the *aerodynamic analysis module*, a very important component of the optimization procedure is the *optimization module*, in which the former is repeatedly called during the process of searching the minimum of the objective function

Since the planform of the strakes can be defined with a relatively small number of parameters, an optimization algorithm, based on the *One Dimensional Searching (ODS)* method²¹ was adopted to perform the present study. Although is usually slower than the *gradient* methods, it is quite satisfactory for the problems with few parameters because it does not require the calculation of the objective function derivatives and provides an easy way to impose the necessary restrictions. Its straightforward principle is illustrated in Fig. 10 for the two parameter case.

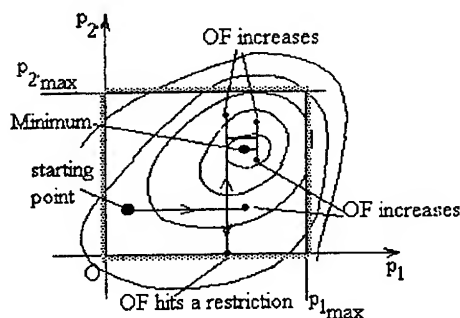


Fig. 10 The principle of the *One Dimensional Searching* optimization method

- For the strakes planform optimization, 4 parameters ($p_1 - 4$), as defined in figure 4, are used here. On the starboard wing, their index increases in the positive sense of the Oy axis. At the beginning of the optimization process, the value of all the four parameters is 1.0, and at the end, their values are greater than 1.0, but do not exceed the domain bounded by the imposed restrictions. As already mentioned, the restrictions are set on:
- the minimum allowed values for p_i . Thus, without exception, during the whole optimization process, the parameters must satisfy:

$$p_i \geq 1.0 \quad (i = 1, 4) \quad (22)$$

- the maximum value of the parameter p_1 which cannot exceed a given limit. In this study, this way, a maximum attainable limit of 80° was set for the value of the mean sweep angle of the optimized strake's leading-edge.
- the lower/upper limits for the local sweep angle of the leading-edge (Λ_{LEk}) on the four Δy_k strips in which each strake is divided. The values indicated in Table 1 were used to perform the optimizations presented in section 5.

Table 1 The limits imposed on the local sweep angle of the strake's leading edge

Strip	1	2	3	4
$\Lambda_{LEk}(^\circ)$	5 ± 90	10 ± 90	15 ± 90	20 ± 90

A simple relation links the coordinates x_i of the points that define the segments on strake's leading-edge and the local sweep angle Λ_{LEk} . Also, x_i and p_i are directly related. Therefore, the restrictions of Table 1 are applied, in fact, on the values of the optimization parameters

Since the purpose of this procedure is to enhance the lift of an airplane with strakes by optimizing their planform, the following expression of the objective function was considered suitable:

$$OF = k_1 \cdot \frac{1}{CL} + k_2 \cdot |Cm| + \sum_{i=1}^5 g_i \quad (23)$$

where:

g_i - penalty function, defined by:

$$g_i = \begin{cases} 0 \dots \text{when } p_i \text{ is inside the restricted domain} \\ 1.03 \cdot OF_v \dots \text{when } p_i \text{ is outside the domain} \end{cases} \quad (24)$$

OF_v - the value of the objective function at the previous optimization step

k_1, k_2 = weight coefficients (≥ 0)

During the optimization process the minimum of the objective function OF is searched, thus, given the relation (23), the optimum configuration must have a higher CL . The term containing the absolute value of Cm was included to reduce, as far as possible, the variation of the pitching moment caused by the addition of the strakes to the initial configuration.

Results

Based on the presented optimization procedure, the computer code SAO (Strakes Aerodynamic Optimization) was written (in FORTRAN). The code was used to analyze the advantages / disadvantages

of matching optimum shaped strakes on some existent configurations. To illustrate the capabilities and the limits of the optimization procedure, in this section are presented several results obtained with the jet-fighter type generic configuration of Ref. 13. The subsonic version, without strakes, was used as the initial configuration in these calculations.

As specified in section 3, in the present study Belotserkovski's method¹⁹ was adopted to approximate the influence of the fuselage over the flow around the airplane's fuselage, so that the entire equivalent configuration is composed only of lifting surfaces. The two zones of the wing (Fig.4) were considered as two adjacent lifting surfaces. A xOy plane view of the initial configuration, showing its division into panels, is presented in Fig. 11. The geometrical data, required as input by the SAO code, were measured directly on the figures of Ref.13 with an inherent degree of approximation.

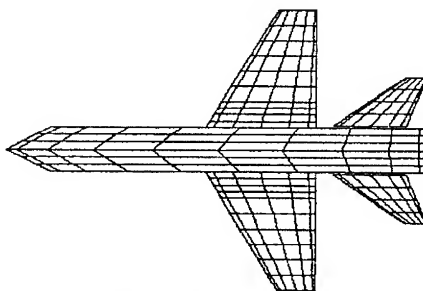


Fig. 11. The initial configuration

All the strakes planform optimizations with this initial configuration were performed for the same symmetrical flight conditions: $M_\infty = 0.40$, $\alpha = 16^\circ$, all aerodynamic controls at zero deflection. Strakes with larger dimensions ($S_s = 16.8\% S_{Wred}$) and of reduced dimensions ($S_s = 5.6\% S_{Wred}$) were studied, for several values of the weight coefficient k_2 (relation 23). Since the semispan of the larger strake is 22.56% of the reduced wing semispan, for an average leading -edge sweep angle of 80° , the restriction on the upper value of p_1 is 2.01. With the same average leading-edge sweep angle, the semispan of the small strake must be 13.03% of the reduced wing semispan and $p_{1max} = 1.58$. In Table 2 are given the characteristics of the cases selected to be presented in this section.

Table 2 Characteristics of the test cases

No.	Config.	S_s/S_{Wred}	k_2	P_{1max}
1	1.1	0.168	0.00	2.01
2	1.2	0.168	0.30	2.01
3	2.1	0.056	0.00	1.58
4	2.2	0.056	1.00	1.58

The values of the parameters ($p_1 - p_4$), the aircraft's aerodynamic coefficients CL, CD, Cm for the initial and the optimized configurations, along with the reductions of the objective function are given in Tables 3a, 3b.

Table 3a Optimization results for the large strakes

Param.	Configuration		
	Initial	1.1	1.2
p_1	1.0000	1.9992	2.0076
p_2	1.0000	1.8341	1.5141
p_3	1.0000	1.8817	1.5628
p_4	1.0000	1.3726	1.3367
CL	0.9972	1.1772	1.1828
CD	0.2992	0.3531	0.3534
Cm	-0.0878	0.1746	0.1533
$\Delta OF(\%)$	-	15.28	15.56

Table 3b Optimization results for the small strakes

Param.	Configuration		
	Initial	2.1	2.2
p_1	1.0000	1.5788	1.4578
p_2	1.0000	1.1551	1.4839
p_3	1.0000	0.3421	1.1547
p_4	1.0000	0.8729	1.1710
CL	1.0030	1.1456	1.1000
CD	0.3008	0.3421	0.3318
Cm	-0.0910	0.0401	0.0002
$\Delta OF(\%)$	-	12.45	17.18

For all the cases, in the optimization module (ODS method) the parameter's variation step and its decrease ratio (for a new cycle) were set to 0.08, respectively 0.7. In these conditions, to reach the 10^{-3} limit (for the step's value) at which the minimum search process was ended, 140 - 160 steps (according to each case) were necessary. The procedure proved itself to be quite fast since, on a Pentium/100MHz, 16MB RAM system, one execution of the SAO code required 166 to 253 CPU seconds. Figure 12 shows the variation of the objective function during the optimization process in which the configuration 1.2 was defined. The decreasing evolution is interrupted by peaks which mark the steps where a parameter exits the restricted domain inside which the minimum may be searched. In this case the process ended after 160 steps, the minimum being found at the step 153.

The results of Tables 3a, 3b indicate that through optimization, the objective function was reduced by 12 - 17%, and consequently increases of 9 - 18% were obtained for CL. The small differences in the data given in Tables 3a, 3b for the initial configuration are due to the different ways in which the wing was approximated for the large / small strakes. The greater lift increases (around 18%) were

obtained with the large strakes, but, even if the drag penalty is reasonable (also 18%) in these cases, the variation of the pitching moment coefficient is too large (almost 300%), reaching high positive (unacceptable) values. In the case of the configuration 1.2, obtained for $k_2=0.3$, the variation of Cm is somewhat smaller (near 275%), but still much too large. With $k_2 > 0.3$ in the objective function used for the large strakes optimization, the Cm variation could have been reduced, but the obtainable lift increase would have been only around 10% or even less. Thus, in the case of the large strakes, the lift enhancement, obtained as a result of the optimization, is accompanied by important modifications of the pitching moment which cause unacceptable alterations of the airplane's stability.

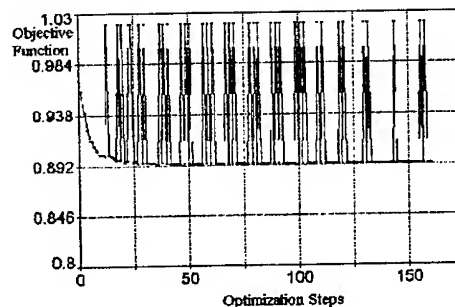


Fig. 12. Variation of the Objective Function during the optimization of the configuration 1.2

Although their surface is three times smaller, the optimum strakes with reduced dimensions (Table 3b) produce however a 9-14% increase of the lift, with a 10-13% drag penalty and only a 100-144% variation of the pitching moment. For instance, in the case of the configuration 2.2, obtained with $k_2=1.0$, the optimum strakes produce a 9% lift increase and reduce to zero the pitching moment (in the conditions in which the optimization was performed).

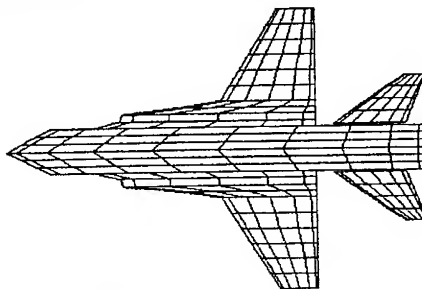


Fig. 13 Plane view of the optimum configuration 1.1

Plane projections of the optimum configurations of Table 2 are shown in Fig.13 - 16. It may be noticed that, in general, the optimum strakes have a S shaped leading-edge. The obvious difference between the dimensions of the large and small strakes as well as the effect produced on their shape by the different k_2 values, are also evident.

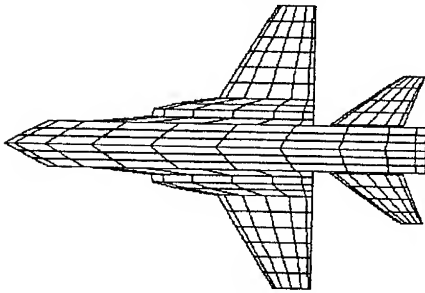


Fig. 14 Plane view of the optimum configuration 1.2

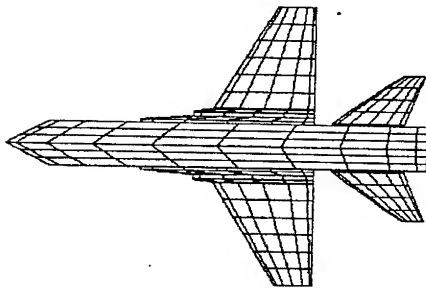


Fig. 15 Plane view of the optimum configuration 2.1

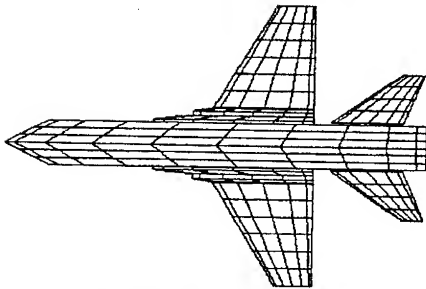


Fig. 16 Plane view of the optimum configuration 2.2

Since the optimizations were done at a given angle of incidence ($\alpha=16^\circ$), the aerodynamic coefficients of the optimum configurations were also computed in a larger incidence domain ($0.01^\circ \leq \alpha \leq 28^\circ$), to enable the necessary evaluation of their *off design* behaviour. The results are those represented in Fig. 17 - 19.

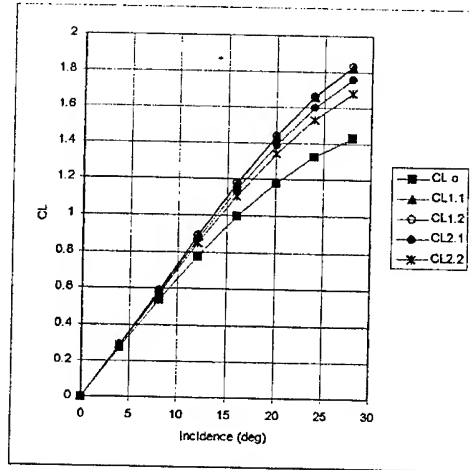


Fig. 17 Variation of CL with incidence, calculated for the initial (o) and the optimized configurations of Table 2

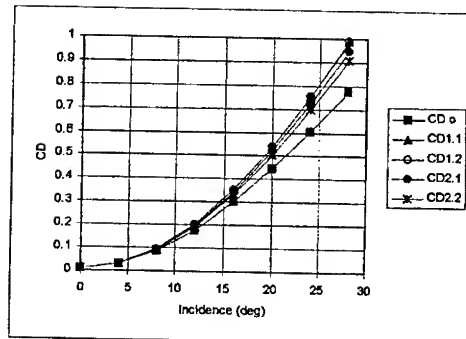


Fig. 18 Variation of CD with incidence, calculated for the initial (o) and the optimized configurations of Table 2

According to these theoretical results, on the whole analyzed range of incidences, all the configurations with optimum strakes have a better lift than the initial configuration (Fig.17). The above discussed influences of k_2 and of the strakes area over the lift increase are proportionally maintained at all incidences. The drag penalties are reasonable (Fig.18) and are also different as a consequence of the higher lift effects on the induced drag.

The variation of C_m (Fig.19) indicates that both configurations having large strakes (1.1, 1.2) are unstable at any of the analyzed incidences. Even in the case of the configurations with small strakes, the unstable behaviour is present, especially for $\alpha > 8^\circ$. But, for instance, if the moment reference point (the airplane's gravity center) is changed from the previously considered position at 15%MAC, to 10%MAC, the C_m variation, calculated for the configuration 2.2 (Fig. 20) shows an improvement,

with a stable behaviour up to $\alpha \approx 16^\circ$. This may be a possible solution to preserve/improve the longitudinal static stability of an airplane with strakes.

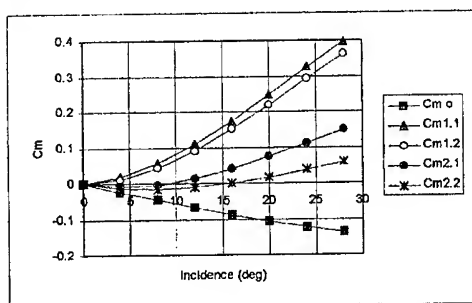


Fig.19 Variation of C_D with incidence, calculated for the initial (o) and the optimized configurations of Table 2

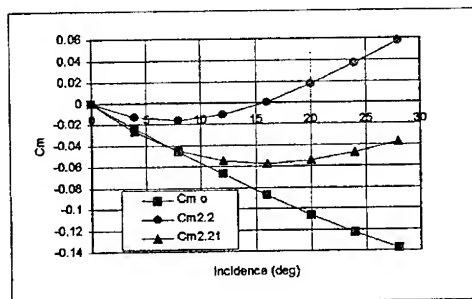


Fig. 20 Variation of C_m with incidence, calculated for the initial (o) and the optimized configuration 2.2. The $C_{m2.2.1}$ values were obtained with the moment reference point at 10%MAC

Conclusions

The presented numerical procedure, performing a lift enhancing aerodynamic optimization of the strakes placed at the leading edge of an airplane's wing, is operational. Its aerodynamic analysis module uses a first order panel method to compute the potential flow around the airplane's configuration and the suction analogy method to evaluate the effects of the rolled-up vortices generated by the strakes. Therefore, the procedure is fast, and may be useful especially in the initial stages of an aerodynamic design process.

An optimum found with this procedure is not necessarily a *global optimum*, but rather is a *local* one. However, the optimum configuration has a smaller value for the objective function, so that is better than the initial configuration. The planform of the optimum strakes and consequently their contribution to the modifications of the aerodynamic characteristics of the analyzed airplane, depend upon

the initial configuration, the objective function, the number and nature of the considered optimization parameters and the restrictions that are imposed upon them. Also, when the ODS method is used to perform the optimization, the values of the parameter's variation step and of its decrease ratio exert an influence upon the searching process, and certainly may lead to another local minimum.

In the studied cases, the lift increases, obtained by optimizing the strakes, were as high as 18%, at the price of reasonable drag penalties and, especially, of unacceptable large variations of the airplane's pitching moment. Theoretically, it was demonstrated that reducing by a factor of 3 the area of the strakes, for the same value of the average leading-edge sweep angle, the lift increase is only 4% lower, but the pitching moment (i.e. stability) problems are much closer to a solution if, for instance, a shift of the gravity center is feasible. Thus, to perform a realistic optimization of the strakes planform, a multidisciplinary (aerodynamic + stability) approach seems to be necessary.

For a better handling of the C_m limitations, it will, perhaps, be useful to introduce the semispan of the strakes in the set of optimization parameters. Also, for a more accurate description of the strake's leading-edge shape, it may be worth-while to increase the number of segments into which this is divided, hence the number of parameters. In this case, a gradient type optimization method would probably be mandatory.

References

- ¹Peake, D.J., "Controlled and Uncontrolled Flow Separation in Three Dimensions", National Aeronautical Establishment, Aeronautical Report LR-591, Ottawa, July 1976
- ²Belotserkovski, S.M., "Calculation of the Flow About Wings of Arbitrary Planform at a Wide Range of Angles of Attack", R.A.E. Library Translation 1433, 1970.
- ³Polhamus, E.C., "Predictions of Vortex-Lift Characteristics by a Leading-Edge Suction Analogy", *Journal of Aircraft*, Vol. 8, No. 4, 1971, pp.193-199.
- ⁴Lan, C.T., Roskam, J., "Leading-Edge Force Features of the Aerodynamic Finite Element Method", *Journal of Aircraft*, Vol. 9, No. 12, 1972, pp.864-867
- ⁵Bradley, R.G., Smith, C.W., Bhateley, I.C., "Vortex-Lift Prediction for Complex Wing Planforms", *Journal of Aircraft*, Vol. 10, No. 6, 1973, pp.379-381
- ⁶Rehbach, C. "Calcul d'écoulements autour d'ailes sans épaisseur avec nappes tourbillonnaires évolutives", *La Recherche Aérospatiale*, No. 2 (Mars-Avril) 1973 pp 53-61

⁷Mook, D.T., Maddox, S.A., "Extension of a Vortex-Lattice Method to Include the Effects of Leading-Edge Separation", *Journal of Aircraft*, Vol. 11, No. 2, 1974, pp. 127-128.

⁸Zorea, C., Rom, J., "Vortex Rollup Over and Behind Wings Related to Nonlinear Aerodynamic Characteristics", *Journal of Aircraft*, Vol. 15, No. 4, 1978, pp. 193-194.

⁹Lamar, J.E., "Subsonic Vortex-Flow Design Study for Slender Wings", *Journal of Aircraft*, Vol. 15, No. 9, 1978, pp. 617.

¹⁰Lan, C.E., Mehrotra, S.C., "Improved Woodward's Panel Method for Calculating Edge Suction Forces", *Journal of Aircraft*, Vol. 16, No. 9, 1979, pp. 632-635.

¹¹Lukring, J.M., "Aerodynamics of Strake-Wing Interactions", *Journal of Aircraft*, Vol. 16, No. 11, 1979, pp. 756-762.

¹²Lamar, J.E., "Analysis and Design of Strake-Wing Configurations", *Journal of Aircraft*, Vol. 17, No. 1, 1980, pp. 20-27.

¹³Liu, M.J., Lu, Z.Y., Qiu, W.H., Su, W.H., Gao, X.K., Deng, X.Y., Xiong, S.W., "Flow Patterns and Aerodynamic Characteristics of a Wing-Strake Configuration", *Journal of Aircraft*, Vol. 17, No. 5, 1980, pp. 332-338.

¹⁴Kern, S.B., "Vortex Flow Control Using Fillets on a Double-Delta Wing", *Journal of Aircraft*, Vol. 30, No. 6, 1993, pp. 818-825.

¹⁵Trifu, O., "An Aerodynamic Optimization Procedure for Configurations with Nonlinear Lift Generators" (in Romanian), National Institute of Aerospace Research "Elie Carafoli", C-573, Bucharest, 1996.

¹⁶Trifu, O., "A Computer Code for the Calculation of the Aerodynamic Characteristics of a Subsonic Airplane" (in Romanian), INCREST, Computer Code Library, Bucharest, 1979.

¹⁷Trifu, O., "Calculation of the Optimum Configuration of a Subsonic Jet-Trainer's Wing for the Improvement of its Aerodynamic Characteristics (in Romanian)", National Institute of Aerospace Research "Elie Carafoli", P-1604, Bucharest, 1995.

¹⁸Hua, H.M., "A Finite Element Method for Calculating Aerodynamic Coefficients of a Subsonic Airplane", *Journal of Aircraft*, Vol. 10, No. 7, 1973, pp. 422-426.

¹⁹Belotserkovski, S.M., Skripach, B.K., "Aerodynamic Derivatives of the Flying Machines", (in Russian), Nauka Publishing House, Moscow, 1975.

²⁰Mendenhall, M.R., Nielsen, J.N., "Effect of Symmetrical Vortex Shedding on the Longitudinal Aerodynamic Characteristics of the Wing-Body-Tail Combinations", NASA-CR-2473, January 1975.

²¹Dancea, I., "Optimization Methods" (in Romanian), Dacia Publishing House, Cluj-Napoca, 1976.

SOME QUALITATIVE ASPECTS ABOUT PILOT INDUCED OSCILLATION PHENOMENA

by
Achim Ionita

National Institute for Aerospace Research "Elie Carafoli"
Bucharest, Romania
Bd. Iuliu Maniu, 220, Sect. 6, Code 77538
Phone (401) 7453732; Fax : (401) 3125341 ; Email : ionita @ aero.incas.ro

Abstract

In the precision tracking tasks (landing, aerial refuelling, bombing, etc.) can appear the Pilot Induced Oscillations (PIO) which currently are associated with the control time-delay.

Referring to Mc Ruer paper /1/, into the pilot-vehicle closed-loop systems PIO's can be divided into three convenient categories (essentially linear, quasi-linear and non-linear/nonstationary). They can be results of excessive lags from high pilot gain or path gain shaping, rate and surface position limits and non-linear effects due to aerodynamic configurations.

This paper considers an qualitative treatment of PIO's phenomena and outlines cumulative effects of the control time-delay (τ_p -the pilot effective lag and / or τ_m - the control time-delay in the resulting low-order models /4/), separately or together with non-linear saturating actuators effect or nonlinear effect given by the instantaneous loss of lift.

To analyse validity of our predictions take the example of the landing task with two distinct phases (approach and flare).

Consider a dynamical system containing time-delay and other effects described by the following equations :

$$\dot{x}(t) = Ax(t) + bf(u)$$

$$y(t) = Cx(t)$$

$$x(s) = \Phi(s), s \in [-\tau_0, 0], \tau_0 = \max(\tau_p, \tau_m)$$

where state vector contains velocity, pitch attitude, incidence and pitch rate :

$x = [V, \theta, \alpha, q]^T$ or $x = [V, \gamma, \alpha, q]^T$ with γ flight-path angle. The control vector contains elevator angle $u = [\delta_e]$.

Three cases are employed to treat PIO's phenomena.

Case 1 - cumulative effect of the pilot lag (τ_p), and control time-delay (τ_m), where :

$$f(u) = u_1(t - \tau_m) + u_2(t)$$

with :

$$u_1 = \delta_e(t) = k_\alpha \alpha(t) + k_q q(t)$$

u_2 different for each landing phase :

- approach $u_2(t) = k_p \theta(t - \tau_p)$

- flare $u_2(t) = k_p \gamma(t - \tau_p)$

(see / 4 / , / 5 /).

Case 2 - control time-delay and effect of surface position limits with :

$$f(u) = g(u(t - \tau_p))$$

and

$$f(u) = \begin{cases} u & |u| \leq u_0 \\ \text{sgn } u & |u| > u_0 \end{cases}$$

(see / 2 /).

Case 3 - control time-delay (τ_p or τ_m), and loss of lift modelled by introduction of a hypothetical relay

where :

$$f(u) = u(t - \tau)$$

and

$$a_{ij} = h(L), L = L_\alpha \alpha + L_q q + L_0 \text{sgn}(\alpha - \alpha_c)$$

(see / 3 /).

Reference

1. D. Mc Ruer, D. H. Klyde, T. T. Myers - Development of a Comprehensive PIO Theory, AIAA-96-3433-CP, Atmospheric Flight Conference, San Diego, U.S., 1996 ;
2. J. C. Shen, F. C. Kung - Stabilisation of Input Delay Systems with Saturating Actuator, Int. J. Control, 1989, vol. 50, No.5 ;
3. A. I. Schoenstadt - Non-linear relay model for Post-Stall Oscillation, J. Aircraft, July 1975 ;
4. A. Ionita - Input Delay Investigation in the Short Period Flying Qualities Criteria, AIAA-96-3424 -CP, Atmospheric Flight Conference, San Diego, U.S., 1996 ;
5. A. Halanay, A. Ionita - Delay Induced Oscillation (to be published) .

Stability of a Spinning Liquid-Filled Spacecraft

G.W. Bao

Shanghai Jiao Tong University

M. Pascal

Université Pierre et Marie Curie

July 19, 1995

Abstract

The stability of a spinning liquid-filled spacecraft is investigated in the present paper. Using Ritz modal superposition method, the attitude dynamic equations were given and thus the Liapunov direct method was employed to obtain a sufficient condition for stability. Three kinds of characteristic modals, modals of free motion of inviscid fluid, modals of slosh motion, modals of non-slosh motion, have been investigated and all characteristic problems can be solved numerically by FEM or BEM. It was demonstrated that the viscosity of fluid plays a dissipative effect for large Reynolds number, the slosh motion plays a destabilizing role and the non-slosh model of fluid takes no effect on the stability criterion.

Keywords: Dynamics of spacecraft, liquid sloshing, stability of motion

1 Introduction

It is known that liquid slosh in a spin-stabilized spacecraft is a dynamically unstable source which will cause the vehicle in nutational instability under certain parameterized conditions. LEASAT, a geosynchronous spacecraft with liquid apogee motor, launched in September 1984, experienced attitude control motion instability during the pre-apogee injection phase. It was found that the instability is due to the interaction between the liquid motion and the attitude control. This experience demonstrated that the analysis of dynamic interaction between liquid motion and the attitude control is important in the attitude control design of these spacecraft.

For a non-spinning system, or say liquid slosh in a three-axis stabilized spacecraft, theory and solution methods have been well developed^[1]. The characteristic problem of liquid sloshing in tanks can be solved numerically either by finite element method or by boundary element method^[2, 3]. Liquid sloshing in the coupled system can be represented accurately by an equivalent mechanical model. It was found that there exists a "stability center"^[4, 5] which indicates the stability condition of the fluid-spacecraft and also demonstrates the instability effect of liquid slosh.

Study of liquid motion in rotating containers is more complex than that in motionless containers due to the effect of Coriolis force. Mathematically, the kinds of the characteristic equations of liquid motions are different. The former is of elliptic or hyperbolic one depending on a parameter but the latter is of Laplacian^[6]. Analytic solution seems only available to the liquid motion in a cylindric

container with coaxially cylindric free surface in steady state [7, 8]. Pfeiffer^[9] introduced the concept of homogeneous vorticity to the problem of partially filled containers and Ebert^[10] modified the theory, thus the problem is governed by the Laplace equation, which can be solved numerically similar to the non-spinning problem. However, it should be noted that using Pfeiffer's method will lead to a result of fictitious instability of liquid motion in certain parameterized conditions due to the introduction of homogeneous vorticity assumption^[2, 11, 12]. This means that the homogeneous vorticity assumption is not valid in all the parameterized space. McIntyre and Tanner^[13] developed a finite element method to the characteristic problem of liquid motion without any assumption for the vortex flow. This model has been extensively used to study the effects of liquid motion on the attitude dynamics and control of INTELSAT VI, a dual-spin spacecraft with a liquid apogee motor^[14, 15]. To study the nutational frequency, the nutation time constant and the attitude stability of a spinning spacecraft with a viscous fluid, a boundary-layer model has been suggested^[15] and the solution is obtained by solving three boundary-value problems: an inviscid fluid problem, a boundary-layer problem, and a viscous correction problem, which can be established by using multi-time-scale method. However, the solution process is tedious and the solution is so complex that it is hard to find the effect of liquid motion, especially on spacecraft stability.

To investigate the attitude stability of spacecraft under the effect of liquid motion, Liapunov's direct method can be employed which is more simpler but more powerful to study the effect of liquid motion on stability. The establishment of Liapunov function might exclude the effect of the gyroscopic term in dynamic equations because it is well known that its stabilizing effect will vanish when damping is introduced in the system^[16]. This exclusion undoubtedly simplifies the stability analysis. The boundary-layer model, in fact, includes not only the slosh motion, but also the vortex motion and further the viscous modification. Therefore, the model leads the problem to be very complicated.

The stability of a spinning spacecraft with fluid was investigated in this paper. It was demonstrated that the viscous term in Navier-Stokes equation only plays a dissipative role when using Liapunov's direct method. A stability criterion was obtained, which is a sufficient condition for stability and the effect of gyroscopic term is disregarded. When we decomposed the fluid motion into slosh part and non-slosh part, it was demonstrated that the non-slosh motion has no effect on the stability. Despite that the stability criterion given here is a sufficient condition, it is concise indeed and shows the effect of slosh on stability very clear.

2 General Modal Superposition

An analytical model is developed for the spacecraft configuration shown in Figure 1. The tank is onset on the spin axis and is partially filled with liquid. The tank is of rotational symmetry but its contour may be of arbitrary shape. Two coordinate systems, the space-fixed coordinate system XYZ and the body-fixed coordinate system xyz are set up respectively with origin at the point o .

Assume that the steady state motion of the system is that both the rigid body and the liquid rotate about z axis (coaxial to Z axis in steady state) with constant angular velocity ω_0 . The perturbational motion of the rigid body is assumed to be in nutation about point o . Therefore, the linearized Navier-Stokes equation, incompressibility, kinematic and dynamic conditions on free surface, no-slip condition on cavity wall, compose a boundary value problem:

$$\frac{\partial \mathbf{u}}{\partial t} + 2\boldsymbol{\Omega}_0 \times \mathbf{u} + \nabla \frac{p}{\rho} = \mathbf{G} + \nu \Delta \mathbf{u}, \quad \nabla \cdot \mathbf{u} = 0, \quad \text{in } V$$

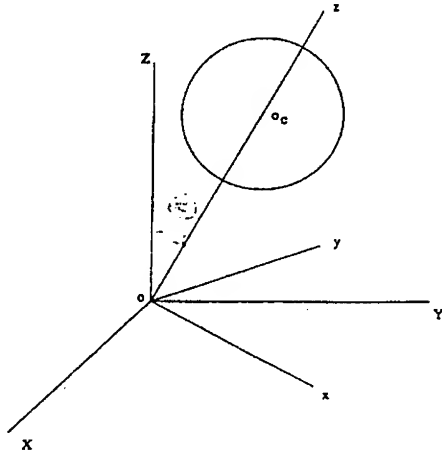


Figure 1: Coordinate systems

$$\begin{aligned} \mathbf{u} &= 0, & \text{on } \partial V_w \\ \mathbf{u} \cdot \mathbf{n} &= \frac{\partial \xi}{\partial t}, \quad p/\rho = B\xi, & \text{on } \partial V_f \end{aligned} \quad (1)$$

$$\begin{aligned} \mathbf{G} &= -\dot{\Omega} \times \mathbf{r} - \nabla \{g\mathbf{k} \times \Theta \cdot \mathbf{r} - (\Omega_0 \times \mathbf{r}) \cdot (\Omega' \times \mathbf{r})\} \\ B &= \sqrt{\omega_0^4 r^2 + g^2} \end{aligned}$$

where \mathbf{u} is the relative velocity of the liquid with respect to the tank, \mathbf{r} the position vector of liquid particle, $\Omega_0 = \omega_0 \mathbf{k}$ the constant angular velocity where \mathbf{k} is the unit vector of Z -axis, $\Omega = \Omega_0 + \Omega'$ the angular velocity of rigid body in motion, ρ the liquid density, p the liquid pressure disturbance, ν the kinematic viscosity, ξ the wave-height along the outer normal direction \mathbf{n} of the free surface ∂V_f , V the liquid domain, ∂V_w the liquid boundary on cavity wall, g the thrust acceleration, and Θ the nutation angle vector, related with the angular velocity by $\Omega' = \dot{\Theta} + \omega_0 \mathbf{k} \times \Theta$, $(\dot{})$ derivative about time t with reference to $o-xyz$.

When we use Liapunov's direct method to analyze the stability problem, the construction of Liapunov function may be arbitrary, leading to different sufficient conditions for stability, which will undoubtedly enlarge the stability domain in parameterized space for good choice of function, the better the larger, tending to the domain whose boundary indicates the necessary and sufficient conditions for stability. In our problem, since the construction of Liapunov function does not need to know the exact solution of the fluid motion, the fluid motion in Liapunov function may be described by any physical characters, e.g., the perturbed angular momentum of the fluid, the fluid vorticity^[17], etc..

Let the fluid motion in Liapunov function be expressed by Ritz expression as

$$\mathbf{u} = \sum_{i=1}^n \mathbf{U}_i(x, y, z) \dot{q}_i(t), \quad p = \sum_{i=1}^n P_i(x, y, z) q_i(t), \quad \xi = \sum_{i=1}^n H_i(x, y, z) q_i(t) \quad (2)$$

with modals satisfying

$$\begin{aligned}
\nabla \cdot \mathbf{U}_i &= 0, & \text{in } V \\
\mathbf{U}_i &= 0, & \text{on } \partial V_w \quad i = 1, 2, \dots, n \\
\mathbf{U}_i \cdot \mathbf{n} &= H_i, \quad P_i/\rho = BH_i, & \text{on } \partial V_f
\end{aligned} \tag{3}$$

which indicates that the solutions (2) satisfy the incompressible condition ($\nabla \cdot \mathbf{u} = 0$), the kinematic and dynamic conditions on free surface ($\mathbf{u} \cdot \mathbf{n} = \partial \xi / \partial t$, $p/\rho = B\xi$), and the no-slip condition on cavity wall ($\mathbf{u} = 0$).

Substitute the expression (2) of \mathbf{u} , p , and ξ into the linearized Navier-Stokes equation (the first of (1)), and scalar-product the equation by $\rho \mathbf{U}_i$ and then integrate the equation over the volume V , we have

$$\begin{aligned}
\sum_{j=1}^n (m_{ij} \ddot{q}_j - 2\omega_0 d_{ij} \dot{q}_j + k_{ij} q_j) + \mathbf{c}_i \cdot \ddot{\Theta} \\
-\omega_0 (\mathbf{b}_i + \mathbf{k} \times \mathbf{c}_i) \cdot \dot{\Theta} + \mathbf{k} \times (\omega_0^2 \mathbf{b}_i - g \mathbf{a}_i) \cdot \Theta = \mu \int_V \mathbf{U}_i \cdot \Delta \mathbf{u} dv \quad i = 1, 2, \dots, n
\end{aligned} \tag{4}$$

where $\mu = \rho\nu$ is the dynamic viscosity and the coefficients have the following integral expressions:

$$\begin{aligned}
m_{ij} &= \rho \int_V \mathbf{U}_i \cdot \mathbf{U}_j dv, \quad d_{ij} = \mathbf{k} \cdot \rho \int_V \mathbf{U}_i \times \mathbf{U}_j dv, \quad k_{ij} = \rho \int_{\partial V_f} BH_i H_j dS, \\
\mathbf{a}_i &= \rho \int_{\partial V_f} H_i \mathbf{r} dS, \quad \mathbf{b}_i = \mathbf{k} \cdot \rho \int_{\partial V_f} H_i (r^2 \mathbf{I} - \mathbf{r} \mathbf{r}) dS, \quad \mathbf{c}_i = \rho \int_V \mathbf{r} \times \mathbf{U}_i dv
\end{aligned} \tag{5}$$

The angular momentum equation of the total system with respect to point o , yields

$$\begin{aligned}
\mathbf{J} \cdot \ddot{\Theta} - \omega_0 (C\mathbf{I} \times \mathbf{k} - \mathbf{J} \times \mathbf{k} - \mathbf{k} \times \mathbf{J}) \cdot \dot{\Theta} + [\omega_0^2 (C\mathbf{I} + \mathbf{k} \times \mathbf{J} \times \mathbf{k}) - mgz_{CG}\mathbf{I}] \cdot \Theta \\
+ \sum_{i=1}^n \{ \mathbf{c}_i \ddot{q}_i + \omega_0 (\mathbf{b}_i + \mathbf{k} \times \mathbf{c}_i) \dot{q}_i + \mathbf{k} \times (\omega_0^2 \mathbf{b}_i - g \mathbf{a}_i) q_i \} = 0
\end{aligned} \tag{6}$$

where $\mathbf{J} = A\mathbf{i}\mathbf{i} + B\mathbf{j}\mathbf{j} + C\mathbf{k}\mathbf{k}$ is the inertia tensor of the total system with respect to o , \mathbf{i} , \mathbf{j} the unit vectors of x -, y -axis respectively, \mathbf{I} the unit tensor, m the total mass, z_{CG} the z -coordinate of the mass center of the total system when neglecting the surface wave ($\xi = 0$).

Introduce variable $\mathbf{w} = (\theta_x, \theta_y, \mathbf{q}^T)^T$, in which $\Theta = \theta_x \mathbf{i} + \theta_y \mathbf{j}$, and $\mathbf{q} = (q_1 \dots q_n)^T$, equations (4) and (6) can be rewritten in a matrix form,

$$\mathbf{M}_s \ddot{\mathbf{w}} - \omega_0 \mathbf{D}_s \dot{\mathbf{w}} + \mathbf{K}_s \mathbf{w} = \mathbf{f}_s \tag{7}$$

where

$$\begin{aligned}
M_s &= \begin{bmatrix} A & 0 & c_x^T \\ 0 & B & c_y^T \\ c_x & c_y & M \end{bmatrix} \\
D_s &= \begin{bmatrix} 0 & -(C-A-B) & -(b_x - c_y)^T \\ (C-A-B) & 0 & -(b_y + c_x)^T \\ (b_x - c_y) & (b_y + c_x) & 2D \end{bmatrix} \\
K_s &= \begin{bmatrix} \omega_0^2(C-B) - mgz_{CG} & 0 & -(\omega_0^2 b_y - ga_y)^T \\ 0 & \omega_0^2(C-A) - mgz_{CG} & (\omega_0^2 b_x - ga_x)^T \\ -(\omega_0^2 b_y - ga_y) & \omega_0^2 b_x - ga_x & K \end{bmatrix} \\
f_s &= (0, 0, \mu \int_V U_1 \cdot \Delta u dv, \dots, \mu \int_V U_n \cdot \Delta u dv)^T
\end{aligned} \tag{8}$$

where $a_x = (a_{1,x}, \dots, a_{n,x})^T$, and the same definition to a_y, b_x, b_y, c_x and c_y , $M = [m_{ij}]$, $D = [d_{ij}]$ and $K = [k_{ij}]$ denote $n \times n$ matrices respectively.

Since matrices M_s, K_s are symmetric and D_s skew-symmetric, left-multiply the Eq. (7) by \dot{w}^T , and thus we construct function \mathcal{V} as follows

$$\mathcal{V} = \frac{1}{2}(\dot{w}^T M_s \dot{w} + w^T K_s w) \tag{9}$$

then we have the derivative of Liapunov function with respect to time t ,

$$\frac{d\mathcal{V}}{dt} = \mu \int_V u \cdot \Delta u \tag{10}$$

in which the fluid motion is governed by Navier-Stokes equation.

For large Reynolds number, $Re > O(10^5)$, the boundary-layer approximation is appropriate. For INTELSAT VI parameters, the Reynolds number is greater than 10^6 . In this case, the viscosity of fluid only affects in the boundary layer with very thin width. While in the interior liquid domain, the fluid motion can be seen as inviscid one. So we can choose modals which are characteristic solutions of the free motion of inviscid and incompressible fluid in spinning container as the Ritz modals in expression (2).

The damping term on the right-hand side of Eq. (10) can be analyzed in dimensionless form, in which the damping term becomes

$$\frac{1}{Re} \int_V u \cdot \Delta u dv = \frac{1}{Re} \int_{\partial V} u \cdot \frac{\partial u}{\partial n} dS - \frac{1}{Re} \int_V \sum_{i=1}^3 \frac{\partial u}{\partial x_i} \cdot \frac{\partial u}{\partial x_i} dv \tag{11}$$

where Reynolds number $Re = a^2/\nu T$, a, T the characteristic units of length and time respectively. For large Reynolds number, $Re > O(10^5)$, the boundary-layer approximation can be applied. The width of the boundary-layer is in the order of $Re^{-1/2}$. Thus the first term on the right-hand side of Eq. (11) is in the order of Re^{-1} while the second is in the order of $Re^{-1/2}$. Therefore, the effect of the first term can be neglected in expression (11), the damping term is then a dissipative one, i.e., we may conclude from (10) and (11) that the following inequality holds for large Reynolds,

$$\frac{d\mathcal{V}}{dt} \leq 0 \tag{12}$$

So, if both M_s and K_s are positive definite, then \mathcal{V} is positive and from inequality (12), \mathcal{V} is a Liapunov function and thus the statement of stability for w and \dot{w} is that if both M_s and K_s are positive definite, the system is stable for perturbation (w, \dot{w}) .

One can prove that M_s is positive definite when one establishes a positive function \mathcal{T}' ,

$$\mathcal{T}' = \frac{1}{2} \int (\dot{\Theta} \times r + u)^2 dm = \frac{1}{2} \dot{w}^T M_s \dot{w} \quad (13)$$

Hence, $\mathcal{T}' \geq 0$. The case that $\mathcal{T}' = 0$ but $\dot{w} \neq 0$ only exists when $\dot{\Theta} \times r + u = 0$ in liquid domain, which indicates that the liquid keeps rotating like a rigid body around Z -axis with angular velocity ω_0 , not affected by the nutation of the container. In physical view, this case only exists for an inviscid fluid (no drag effect) contained in a spherical cavity with which the center is just located at the point o (no variation of container configuration due to nutation). In general, \mathcal{T}' is equal to zero if and only if $\dot{w} = 0$ holds except the mentioned case. So, M_s is a positive definite matrix and therefore, the sufficient condition of stability for w and \dot{w} becomes that K_s is a positive definite matrix.

3 Complex Modal Superposition

In practice, it is known that if one takes the eigenfunctions of the characteristic motion of spinning liquid as Ritz's modals, then complex modals could be chosen due to mathematical simplicity. Employing complex modals, the fluid motion can be expressed as follows:

$$u = \sum_{i=1}^n \frac{1}{2} (U_i \dot{q}_i + U_i^* \dot{q}_i^*), \quad p = \sum_{i=1}^n \frac{1}{2} (P_i \dot{q}_i + P_i^* \dot{q}_i^*), \quad \xi = \sum_{i=1}^n \frac{1}{2} (H_i \dot{q}_i + H_i^* \dot{q}_i^*) \quad (14)$$

where $(\cdot)^*$ denotes the conjugate of (\cdot) .

Similarly, substitute the expression (14) of u , p and ξ into the linearized Navier-Stokes equation and scalar-left-product the equation by ρU_i^* and then integrate the equation over the volume V , we have

$$\sum_{j=1}^n (m_{ij} \ddot{q}_j - 2\omega_0 d_{ij} \dot{q}_j + k_{ij} q_j + \bar{m}_{ij} \ddot{q}_j^* - 2\omega_0 \bar{d}_{ij} \dot{q}_j^* + \bar{k}_{ij} q_j^*) + c_i^* \cdot \dot{\Theta} - \omega_0 (b_i^* + k \times c_i^*) \cdot \dot{\Theta} + k \times (\omega_0^2 b_i^* - g a_i^*) \cdot \Theta = \mu \int_V U_i^* \cdot \Delta u \quad i = 1, 2, \dots, n \quad (15)$$

where the coefficients have the following integral expression:

$$m_{ij} = \frac{1}{2} \rho \int_V U_i^* \cdot U_j dv, \quad d_{ij} = \frac{1}{2} k \cdot \rho \int_V U_i^* \times U_j dv, \quad k_{ij} = \frac{1}{2} \rho \int_{\partial V_i} B H_i^* H_j dS \\ \bar{m}_{ij} = \frac{1}{2} \rho \int_V U_i \cdot U_j dv, \quad \bar{d}_{ij} = \frac{1}{2} k \cdot \rho \int_V U_i \times U_j dv, \quad \bar{k}_{ij} = \frac{1}{2} \rho \int_{\partial V_i} B H_i H_j dS \quad (16)$$

and the expression of a_i , b_i , c_i are in the same form as those in (5) despite the modals in the integral kernels are complex in the present case.

The angular momentum equation of the total system then becomes

$$\begin{aligned}
& \mathbf{J} \cdot \ddot{\Theta} - \omega_0(\mathbf{CI} \times \mathbf{k} - \mathbf{J} \times \mathbf{k} - \mathbf{k} \times \mathbf{J}) \cdot \ddot{\Theta} + \{\omega_0^2(\mathbf{CI} + \mathbf{k} \times \mathbf{J} \times \mathbf{k}) - mgz_{CG}\mathbf{I}\} \cdot \ddot{\Theta} \\
& + \frac{1}{2} \sum_{i=1}^n \{ \mathbf{c}_i \ddot{q}_i + \omega_0(\mathbf{b}_i + \mathbf{k} \times \mathbf{c}_i) \dot{q}_i + \mathbf{k} \times (\omega_0^2 \mathbf{b}_i - g\mathbf{a}_i) q_i \} \\
& + \frac{1}{2} \sum_{i=1}^n \{ \mathbf{c}_i^* \ddot{q}_i^* + \omega_0(\mathbf{b}_i^* + \mathbf{k} \times \mathbf{c}_i^*) \dot{q}_i^* + \mathbf{k} \times (\omega_0^2 \mathbf{b}_i^* - g\mathbf{a}_i^*) q_i^* \} = 0
\end{aligned} \quad (17)$$

Decompose Eq. (15) and (17) into two parts, the real part and the imaginary part, respectively, and introduce variable $\mathbf{w} = (\theta_x, \theta_y, \mathbf{q}_R^T, \mathbf{q}_I^T)^T$, in which $\mathbf{q}_R = \text{Re}\{\mathbf{q}\}$, $\mathbf{q}_I = \text{Im}\{\mathbf{q}\}$, we can take Eq. (15) and (17) in a matrix form (7) with coefficient matrice,

$$\begin{aligned}
\mathbf{M}_s &= \begin{bmatrix} A & 0 & \mathbf{c}_{R,x}^T & -\mathbf{c}_{I,x}^T \\ 0 & B & \mathbf{c}_{R,y}^T & -\mathbf{c}_{I,y}^T \\ \mathbf{c}_{R,x} & \mathbf{c}_{R,y} & \mathbf{M}_R + \tilde{\mathbf{M}}_R & -\mathbf{M}_I - \tilde{\mathbf{M}}_I \\ -\mathbf{c}_{I,x} & -\mathbf{c}_{I,y} & \mathbf{M}_I - \tilde{\mathbf{M}}_I & \mathbf{M}_R - \tilde{\mathbf{M}}_R \end{bmatrix} \\
\mathbf{D}_s &= \begin{bmatrix} 0 & -(C - A - B) & -(\mathbf{b}_x - \mathbf{c}_y)_R^T & (\mathbf{b}_x - \mathbf{c}_y)_I^T \\ (C - A - B) & 0 & -(\mathbf{b}_y + \mathbf{c}_x)_R^T & (\mathbf{b}_y + \mathbf{c}_x)_I^T \\ (\mathbf{b}_x - \mathbf{c}_y)_R & (\mathbf{b}_y + \mathbf{c}_x)_R & 2\mathbf{D}_R + 2\tilde{\mathbf{D}}_R & -2\mathbf{D}_I - 2\tilde{\mathbf{D}}_I \\ -(\mathbf{b}_x - \mathbf{c}_y)_I & -(\mathbf{b}_y + \mathbf{c}_x)_I & 2\mathbf{D}_I - 2\tilde{\mathbf{D}}_I & 2\mathbf{D}_R - 2\tilde{\mathbf{D}}_R \end{bmatrix} \\
\mathbf{K}_s &= \begin{bmatrix} \omega_0^2(C - B) - mgz_{CG} & 0 & -(\omega_0^2 \mathbf{b}_y - g\mathbf{a}_y)_R^T & (\omega_0^2 \mathbf{b}_y - g\mathbf{a}_y)_I^T \\ 0 & \omega_0^2(C - A) - mgz_{CG} & (\omega_0^2 \mathbf{b}_x - g\mathbf{a}_x)_R^T & -(\omega_0^2 \mathbf{b}_x - g\mathbf{a}_x)_I^T \\ -(\omega_0^2 \mathbf{b}_y - g\mathbf{a}_y)_R & (\omega_0^2 \mathbf{b}_x - g\mathbf{a}_x)_R & \mathbf{K}_R + \tilde{\mathbf{K}}_R & -\mathbf{K}_I - \tilde{\mathbf{K}}_I \\ (\omega_0^2 \mathbf{b}_y - g\mathbf{a}_y)_I & -(\omega_0^2 \mathbf{b}_x - g\mathbf{a}_x)_I & \mathbf{K}_I - \tilde{\mathbf{K}}_I & \mathbf{K}_R - \tilde{\mathbf{K}}_R \end{bmatrix}
\end{aligned} \quad (18)$$

where $(\cdot)_R = \text{Re}\{\cdot\}$, $(\cdot)_I = \text{Im}\{\cdot\}$.

Also, \mathbf{M}_s , \mathbf{K}_s are symmetric and \mathbf{D}_s is skew-symmetric. It can be proved that \mathbf{M}_s is positive definite, too. Left-multiply the Eq. (7) by $\dot{\mathbf{w}}^T$, yields Eq. (10) and function \mathcal{V} has the expression (9). Therefore, we obtain a sufficient condition of stability for \mathbf{w} and $\dot{\mathbf{w}}$ which states that if \mathbf{K}_s expressed in (18) is positive definite, the system is stable for perturbation $(\mathbf{w}, \dot{\mathbf{w}})$.

4 Characteristic Motion of Fluid

Consider a free motion of inviscid fluid in container, $\mathbf{G} = 0$, we have the boundary-value problem as follows,

$$\begin{aligned}
\frac{\partial \mathbf{u}}{\partial t} + 2\Omega_0 \times \mathbf{u} + \nabla \frac{p}{\rho} &= 0, \quad \nabla \cdot \mathbf{u} = 0, \quad \text{in } V \\
\mathbf{u} \cdot \mathbf{n} &= 0, \quad \text{on } \partial V_w \\
\mathbf{u} \cdot \mathbf{n} &= \frac{\partial \xi}{\partial t}, \quad p/\rho = B\xi, \quad \text{on } \partial V_f
\end{aligned} \quad (19)$$

There are two ways to get the characteristic solution: (i) From (19) to get the characteristic problem directly; (ii) decompose the free motion into two parts, slosh motion and non-slosh motion, get two corresponding boundary-value problems respectively and then establish the characteristic problems respectively.

4.1 Method 1. Direct Derivation

Let $u = i\sigma U e^{i\sigma t}$, $p = P e^{i\sigma t}$, $\xi = H e^{i\sigma t}$, the characteristic problem of (19) becomes

$$\begin{aligned} -\sigma^2 U + 2i\sigma \Omega_0 \times U + \nabla \frac{P}{\rho} &= 0, \quad \nabla \cdot U = 0, \quad \text{in } V \\ U \cdot n &= 0, \quad \text{on } \partial V_w \\ U \cdot n &= H, \quad P/\rho = BH, \quad \text{on } \partial V_f \end{aligned} \quad (20)$$

The eigenvalues σ_i and the corresponding eigenfunctions (U_i, P_i, H_i) have the following properties:

- (i) All eigenvalues σ_i are real.
- (ii) If (σ, U, P, H) is a characteristic solution of (20), so is $(-\sigma, U^*, P^*, H^*)$.
- (iii) Orthogonality of the characteristic solutions:

$$\begin{aligned} \sigma_i \sigma_j \int_V U_i^* \cdot U_j dv + \int_{\partial V_f} B H_i^* H_j dS &= 0, \quad i \neq j, \quad i, j \in Z^+ \\ -\sigma_i \sigma_j \int_V U_i \cdot U_j dv + \int_{\partial V_f} B H_i H_j dS &= 0, \quad \forall i, j \in Z^+ \end{aligned}$$

Numerical methods will depend on the establishment of a variational formula. Since the linear Euler's equation (first of (19)) can be derived into the following form:

$$\mathcal{E}u + \mathcal{D} \nabla \frac{P}{\rho} = 0 \quad (21)$$

where operators \mathcal{E} , \mathcal{D} denote

$$\mathcal{E} = \frac{\partial^3}{\partial t^3} + 4\omega_0^2 \frac{\partial}{\partial t}, \quad \mathcal{D}(f) = \frac{\partial^2 f}{\partial t^2} - 2\Omega_0 \times \frac{\partial f}{\partial t} + 4\Omega_0(\Omega_0 \cdot f) \quad (22)$$

respectively, the characteristic problem (20) becomes

$$\begin{aligned} \nabla \cdot \mathcal{D}_\sigma \nabla \Phi &= 0, \quad \text{in } V \\ n \cdot \mathcal{D}_\sigma \nabla \Phi &= 0, \quad \text{on } \partial V_w \\ n \cdot \mathcal{D}_\sigma \nabla \Phi + \frac{1}{B} \mathcal{E}'_\sigma \Phi &= 0, \quad \text{on } \partial V_f \end{aligned} \quad (23)$$

where Φ is introduced as

$$i\sigma U = \mathcal{D}_\sigma \nabla \Phi, \quad \frac{P}{\rho} = -\mathcal{E}_\sigma \Phi, \quad H = -\frac{1}{B} \mathcal{E}_\sigma \Phi \quad (24)$$

and \mathcal{D}_σ , \mathcal{E}_σ , \mathcal{E}'_σ denote

$$\begin{aligned} \mathcal{D}_\sigma(f) &= -\sigma^2 f - 2i\sigma \Omega_0 \times f + 4\Omega_0(\Omega_0 \cdot f) \\ \mathcal{E}_\sigma &= -i\sigma(\sigma^2 - 4\omega_0^2) \\ \mathcal{E}'_\sigma &= \sigma^2(\sigma^2 - 4\omega_0^2) = i\sigma \mathcal{E}_\sigma \end{aligned} \quad (25)$$

respectively. Characteristic problem (23) can be converted into an extreme-value problem with a variational formula,

$$\begin{aligned} \mathcal{L}_3 = & \int_V \{ \sigma^2 \nabla \Phi^* \cdot \nabla \Phi - 2i\sigma\Omega_0 \cdot \nabla \Phi^* \times \nabla \Phi - 4(\Omega_0 \cdot \nabla \Phi^*)(\Omega_0 \cdot \nabla \Phi) \} dv \\ & - \sigma^2(\sigma^2 - 4\omega_0^2) \int_{\partial V_f} \frac{\Phi^* \Phi}{B} dS \end{aligned} \quad (26)$$

In expanding Φ we have chosen the azimuthal wave number to be one. Although other azimuthal modes may exist in the fluid, they can have no effect on the spacecraft motion since the forces due to the pressure and the drag at the cavity wall integrate to zero. Let $\Phi = \phi(r, z)e^{i\theta}$, a straightforward calculation shows (26) have the form

$$\mathcal{L}_2 = \int_S r \{ \tau^2 [(\frac{\partial \phi}{\partial r})^2 + (\frac{\phi}{r})^2 + (\frac{\partial \phi}{\partial z})^2] - (\frac{\partial \phi}{\partial z})^2 \} dS + \tau \int_{\partial S} n_r \phi^2 ds - 4\tau^2(\tau^2 - 1) \int_{\partial S_f} \frac{r\phi^2}{B'} ds \quad (27)$$

where $\tau = \sigma/2\omega_0$, $B' = \sqrt{r^2 + (g/\omega_0)^2}$, $n_r = \mathbf{n} \cdot \mathbf{r}^0$, $\mathcal{L}_3 = 8\pi\omega_0^2\mathcal{L}_2$, S , ∂S , ∂S_f are liquid domain, boundary and free surface on the longitudinal section, corresponding to V , ∂V , and ∂V_f , respectively. Using finite element method and setting the first variation of (27) to be zero, the problem (23) is reduced to determine the eigenvalues of a matrix polynomial

$$(\tau^4 \mathbf{A} + \tau^2 \mathbf{B} + \tau \mathbf{C} + \mathbf{D}) \Phi = 0 \quad (28)$$

where Φ denotes an array of nodal variables of $\phi(r, z)$.

4.2 Method 2. Decomposition into Slosh Motion and Non-Slosh Motion

Decompose the fluid motion (19) into two parts, the slosh motion and the non-slosh motion,

$$\mathbf{u} = \mathbf{u}^{(s)} + \mathbf{u}^{(n)}, p = p^{(s)} + p^{(n)}, \xi = \xi^{(s)}, \xi^{(n)} = 0 \quad (29)$$

both motions are governed by the following boundary-value problems respectively:

$$\begin{aligned} \frac{\partial \mathbf{u}^{(s)}}{\partial t} + \nabla \frac{p^{(s)}}{\rho} &= 0, \quad \nabla \cdot \mathbf{u}^{(s)} = 0, \quad \text{in } V \\ \mathbf{u}^{(s)} \cdot \mathbf{n} &= 0, \quad \text{on } \partial V_w \\ \mathbf{u}^{(s)} \cdot \mathbf{n} &= \frac{\partial \xi}{\partial t}, \quad p^{(s)}/\rho = B\xi, \quad \text{on } \partial V_f \end{aligned} \quad (30)$$

$$\begin{aligned} \frac{\partial \mathbf{u}^{(n)}}{\partial t} + 2\Omega_0 \times \mathbf{u}^{(n)} + \nabla \frac{p^{(n)}}{\rho} &= 0, \quad \nabla \cdot \mathbf{u}^{(n)} = 0, \quad \text{in } V \\ \mathbf{u}^{(n)} \cdot \mathbf{n} &= 0, \quad \text{on } \partial V_w \\ \mathbf{u}^{(n)} \cdot \mathbf{n} &= 0, \quad p^{(n)} = 0, \quad \text{on } \partial V_f \end{aligned} \quad (31)$$

Let $\mathbf{u} = i\sigma \mathbf{U} e^{i\sigma t}$, $p = P e^{i\sigma t}$, $\xi = H e^{i\sigma t}$, the characteristic problem of (30) becomes

$$\begin{aligned}
-\sigma^2 \mathbf{U}^{(s)} + \nabla \frac{P^{(s)}}{\rho} &= 0, \quad \nabla \cdot \mathbf{U}^{(s)} = 0, \quad \text{in } V \\
\mathbf{U}^{(s)} \cdot \mathbf{n} &= 0, \quad \text{on } \partial V_w \\
\mathbf{U}^{(s)} \cdot \mathbf{n} &= H, \quad P^{(s)}/\rho = BH, \quad \text{on } \partial V_f
\end{aligned} \tag{32}$$

while the characteristic problem of (31) becomes

$$\begin{aligned}
-\sigma^2 \mathbf{U}^{(n)} + 2i\sigma\Omega_0 \times \mathbf{U}^{(n)} + \nabla \frac{P^{(n)}}{\rho} &= 0, \quad \nabla \cdot \mathbf{U}^{(n)} = 0, \quad \text{in } V \\
\mathbf{U}^{(n)} \cdot \mathbf{n} &= 0, \quad \text{on } \partial V_w \\
\mathbf{U}^{(n)} \cdot \mathbf{n} &= 0, \quad P^{(n)} = 0, \quad \text{on } \partial V_f
\end{aligned} \tag{33}$$

The eigenvalues $\sigma_i^{(s)}$ and the corresponding eigenfunctions $(\mathbf{U}, P, H)_i^{(s)}$ have the following properties:

- (i) All eigenvalues $\sigma_i^{(s)}$ are real.
- (ii) If $(\sigma^2, \mathbf{U}, P, H)^{(s)}$ is a characteristic solution of (32), so is $(\sigma^2, \mathbf{U}^*, P^*, H^*)^{(s)}$.
- (iii) Orthogonality:

$$\begin{aligned}
\int_V (\mathbf{U}_i^* \cdot \mathbf{U}_j)^{(s)} dv &= 0, \quad i \neq j, \quad \int_{\partial V_f} BH_i^* H_j dS = \sigma_j^2 \int_V (\mathbf{U}_i^* \cdot \mathbf{U}_j)^{(s)} dv, \quad \forall i, j \\
\int_V (\mathbf{U}_i \cdot \mathbf{U}_j)^{(s)} dv &= 0, \quad i \neq j, \quad \int_{\partial V_f} BH_i H_j dS = \sigma_j^2 \int_V (\mathbf{U}_i \cdot \mathbf{U}_j)^{(s)} dv, \quad \forall i, j
\end{aligned}$$

For the non-slosh characteristic motion, the properties are

- (i) All eigenvalues $\sigma_i^{(n)}$ are real and $|\sigma_i^{(n)}| \leq 2\omega_0$.
- (ii) If $(\sigma, \mathbf{U}, P)^{(n)}$ is a characteristic solution of (33), so is $(-\sigma, \mathbf{U}^*, P^*)^{(n)}$.
- (iii) Orthogonality:

$$\int_V (\mathbf{U}_i^* \cdot \mathbf{U}_j)^{(n)} dv = 0, \quad i \neq j, \quad \int_V (\mathbf{U}_i \cdot \mathbf{U}_j)^{(n)} dv = 0, \quad \forall i, j, \quad i, j \in \mathbb{Z}^+$$

For numerical solution, since $\mathbf{U}^{(s)}$ can be assumed to be potential, $\mathbf{U}^{(s)} = \nabla \Phi$, then $P^{(s)}/\rho = \sigma^2 \Phi$, (32) is reduced to have

$$\begin{aligned}
\Delta \Phi &= 0, \quad \text{in } V \\
\frac{\partial \Phi}{\partial n} &= 0, \quad \text{on } \partial V_w \\
\frac{\partial \Phi}{\partial n} &= H, \quad \sigma^2 \Phi = BH, \quad \text{on } \partial V_f
\end{aligned} \tag{34}$$

which can be solved either by finite element method or by boundary element method due to Φ is a Laplacian.

Also, employing the variational formula (27) where the last integral on free surface is omitted, (33) can be solved by finite element method.

5 Stability of Spacecraft Motion

In stability analysis, we employ both slosh and non-slosh modes to express the fluid motion,

$$\begin{aligned} \mathbf{u} &= \sum_{i=1}^{n_s} \frac{1}{2} (\mathbf{U}_i \dot{q}_i + \mathbf{U}_i^* \dot{q}_i^*)^{(s)} + \sum_{i=1}^{n_s} \frac{1}{2} (\mathbf{U}_i \dot{q}_i + \mathbf{U}_i^* \dot{q}_i^*)^{(n)} \\ p &= \sum_{i=1}^{n_s} \frac{1}{2} (P_i q_i + P_i^* q_i^*)^{(s)} + \sum_{i=1}^{n_s} \frac{1}{2} (P_i q_i + P_i^* q_i^*)^{(n)} \\ \xi &= \sum_{i=1}^{n_s} \frac{1}{2} (H_i q_i + H_i^* q_i^*) \end{aligned} \quad (35)$$

Then in derivation of Eq. (7), introduce $\mathbf{w} = (\theta_x, \theta_y, \mathbf{q}_R^{(s)T}, \mathbf{q}_I^{(s)T}, \mathbf{q}_R^{(n)T}, \mathbf{q}_I^{(n)T})^T$ and the stiffness matrix \mathbf{K} , becomes

$$\mathbf{K}_s = \begin{bmatrix} \omega_0^2(C-B) - mgz_{CG} & 0 & 0 & -(\omega_0^2\nu + g\lambda)^T & 0 & 0 \\ 0 & \omega_0^2(C-A) - mgz_{CG} & -(\omega_0^2\nu + g\lambda)^T & 0 & 0 & 0 \\ 0 & -(\omega_0^2\nu + g\lambda) & \mathbf{K} & 0 & 0 & 0 \\ -(\omega_0^2\nu + g\lambda) & 0 & 0 & \mathbf{K} & 0 & 0 \\ 0 & 0 & 0 & 0 & 0 & 0 \\ 0 & 0 & 0 & 0 & 0 & 0 \end{bmatrix} \quad (36)$$

where $\mathbf{K} = \text{diag}(k_1, \dots, k_{n_s})$, $\lambda = (\lambda_1, \dots, \lambda_{n_s})^T$, $\nu = (\nu_1, \dots, \nu_{n_s})^T$ and

$$k_i = \rho\pi \int_{\partial S_f} r B H_i^2 ds, \quad \lambda_i = \rho\pi \int_{\partial S_f} r^2 H_i ds, \quad \nu_i = \rho\pi \int_{\partial S_f} r^2 z H_i ds \quad (37)$$

The Liapunow function \mathcal{V} , if we introduce two variables $\mathbf{y} = \dot{\mathbf{w}}$, $\mathbf{z} = (\theta_x, \theta_y, \mathbf{q}_R^{(s)}, \mathbf{q}_I^{(s)})^T$, becomes

$$\mathcal{V} = \frac{1}{2} (\mathbf{y}^T \mathbf{M}_s \mathbf{y} + \mathbf{z}^T \mathbf{K}'_s \mathbf{z}) \quad (38)$$

and thus we obtain a sufficient condition of stability for variables \mathbf{y} and \mathbf{z} which states that if

$$\mathbf{K}'_s = \begin{bmatrix} \omega_0^2(C-B) - mgz_{CG} & 0 & 0 & -(\omega_0^2\nu + g\lambda)^T \\ 0 & \omega_0^2(C-A) - mgz_{CG} & -(\omega_0^2\nu + g\lambda)^T & 0 \\ 0 & -(\omega_0^2\nu + g\lambda) & \mathbf{K} & 0 \\ -(\omega_0^2\nu + g\lambda) & 0 & 0 & \mathbf{K} \end{bmatrix} \quad (39)$$

is definite positive, the system is stable for partial variables (\mathbf{y}, \mathbf{z}) . The stability criterion can be derived as

$$\omega_0^2(C-B) - mgz_{CG} - \sum_{i=1}^{n_s} \frac{1}{k_i} (\omega_0^2\nu_i + g\lambda_i)^2 > 0 \quad (40)$$

$$\omega_0^2(C-A) - mgz_{CG} - \sum_{i=1}^{n_s} \frac{1}{k_i} (\omega_0^2\nu_i + g\lambda_i)^2 > 0$$

Here, the stability criterion (40) shows that the effect of non-slosh motion of liquid can be disregarded. The slosh motion of liquid only plays a destabilizing role. The stability criterion (40) also can be seen as an extension of the corresponding three-axis stabilized spacecraft problem because if we let $\omega_0 = 0$, (40) becomes the necessary and sufficient condition of stability^[5].

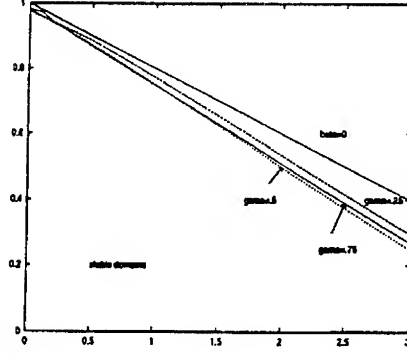


Figure 2: Stability on A/C vs $g/\omega_0^2 a$ ($a = b$)

6 Numerical Results

For simplicity, two cases are considered.

6.1 Destabilization Effect of Fluid Slosh

Stability criterion (40) shows that the last term representing the effect of liquid slosh plays a destabilizing role since the first two terms in inequality (40) demonstrate the stability statement without fluid slosh. Assume that $A = B$, the dimensionless of (40) becomes

$$1 - \frac{A}{C} - \alpha \frac{g}{\omega_0^2 a} - \beta \sum_{i=1}^{n_s} \left(\nu_i + \frac{g}{\omega_0^2 a} \lambda_i \right)^2 > 0 \quad (41)$$

where $\alpha = m z_{CG} a / C$, $\beta = \rho \pi a^5 / C$ and

$$\lambda_i = \int_{\partial S_f} r^2 H_i ds, \quad \nu_i = \int_{\partial S_f} r^2 z H_i ds \quad (42)$$

with normalization

$$\int_{\partial S_f} r \sqrt{r^2 + (g/\omega_0^2 a)^2} H_i^2 ds = 1 \quad (43)$$

Let the container be spheroid with horizontal and vertical semi-axis a , b , respectively, filling ratio γ , container position from point o to container center o_c , h_0 , Fig. 2 shows that the stability domains (below the critic curves) in parameterized plane $(g/\omega_0^2 a, A/C)$ when the effect of liquid slosh is excluded ($\beta = 0$) and included respectively. It is assumed in Fig. 2 that both α and β are independent of parameters A/C and $g/\omega_0^2 a$.

6.2 Neglecting the Effect of Rigid Body

Assume that the shell of the rigid container is thin enough to neglect its mass and inertia momenta. Fig. 3 give the stability domains in parameterized plane $(g/\omega_0^2 a, h_0)$, showing the destabilizing effect of slosh.

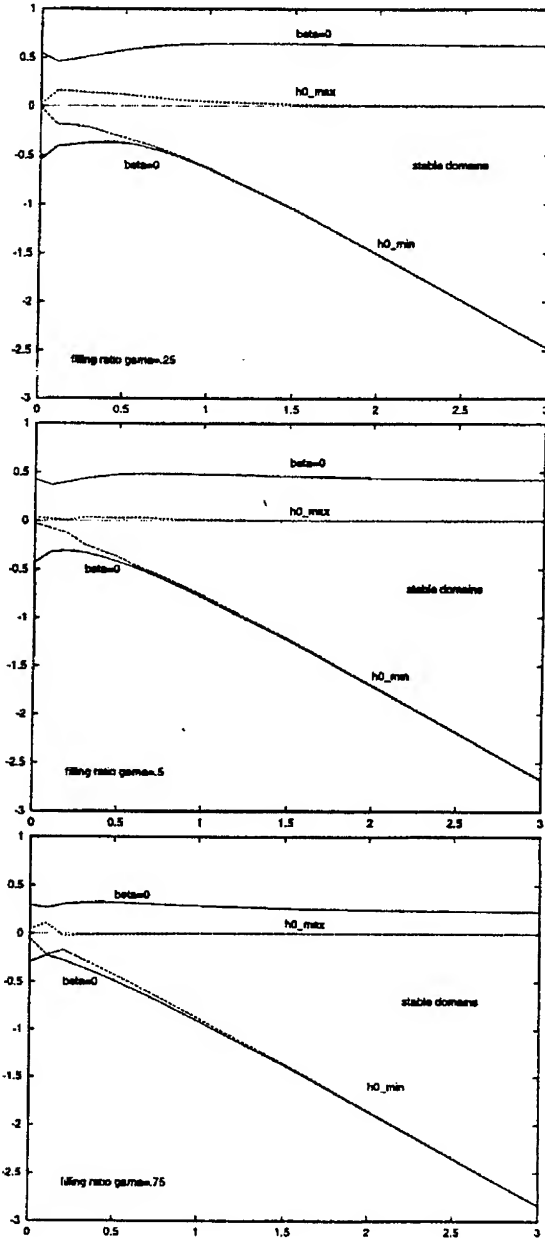


Figure 3: Stability on h_0/a vs $g/\omega_0^2 a$ ($a = b$)

Fig. 4 demonstrate the stability criteria for z_{CG} and $z_{CS} = z_{CG} + \sum \lambda_i^2 g / \omega_0^2 a m$, the stability center defined in three-axis stabilized problem, in which $z_{CG} (\beta = 0)$ indicates the extreme value of total mass center position for stability when slosh effect is excluded. It shows that the maximum z -coordinate of z_{CS} for stability tends to zero as $g / \omega_0^2 a$ tends larger, in agreement with the result from the three-axis problem^[5].

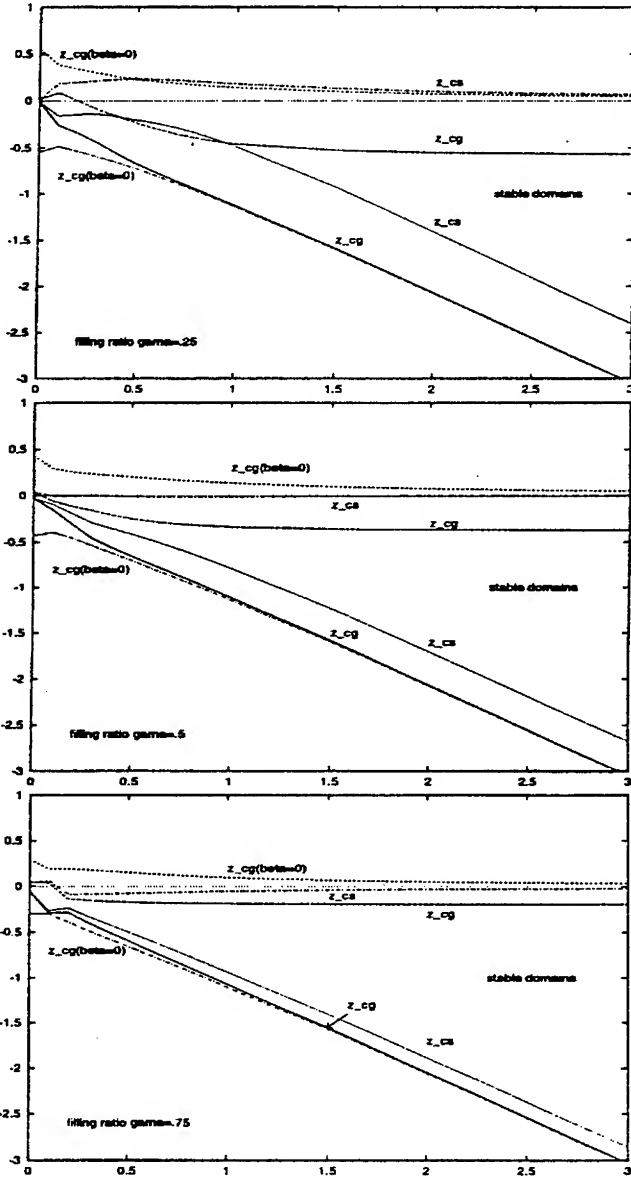


Figure 4: Stability on z_{CG}/a and z_{CS}/a vs $g/\omega_0^2 a$ ($a = b$)

References

- [1] Abramson, H.N.(ed.) : The dynamic behavior of liquids in moving containers. NASA-SP-106, 1966
- [2] El-Raheb, M. ; Wagner, P. : Vibration of a liquid with a free surface in a spinning spherical tank. J. of Sound and Vib. 76 (1981) 83-93
- [3] Schilling, U. ; Sickmann, J. : Numerical calculation of the natural frequencies of a sloshing liquid in an axial symmetrical tanks under strong capillary and weak gravity conditions. Israel J. of Tech. 19 (1981) 44-50
- [4] Mikishev, G. N. : Experimental methods of spacecraft dynamics (in Russian). Mechanical Maunfacture, Moscow, 1978
- [5] Bao, G. W. : The attitude stability of three-axis liquid filled satellite (in Chinese). Chinese J. of Space Science 13, 1 (1993) 31-38
- [6] Greenspan, H. P. : The theory of rotating fluids. London, Cambridge Univ. Press, 1968
- [7] Miles, J. W. ; Troesch, B. A. : Surface oscillations of a rotating liquid. ASME J. of Appl. Mech. 83, 4 (1961) 491-496
- [8] Stewartson, K. : On the stability of a spinning top containing liquid. J. Fluid Mech. 5 (1959) 577-592
- [9] Pfeiffer, F. : Ein Näherungsverfahren für Flüssigkeitsgefüllte Kreisel. Ingenier-Archiv 43 (1974) 306-316
- [10] Ebert, K. : Fluid slosh studies, vol. 2 - Study of slosh dynamics of fluid filled containers on slowly rotating spacecraft. NASA N86-14550, ESA-CR(P)-2077-Vol 2, 1986
- [11] Bao, G. W. : Dynamic equations of spin spacecraft partially containing fluid in the presence of thrust. Archiv of Appl. Mech. 64 (1994) 111-118
- [12] Bao, G. W. : Study on slosh of spinning liquid (in Chinese). Acta Mech. Sinica 27, 1 (1995) 104-109
- [13] McIntyre, J. E. ; Tanner, T. M. : Fuel slosh in a spinning on-axis propellant tank : an eigenmode approach. Space Communication and Broadcasting 5 (1987) 229-251
- [14] Pohl, A. : Dynamic effects of liquid on spinning spacecraft. Proceedings of the First INTELSAT/ESA Symposium on Dynamic Effects of Liquids on Spacecraft Attitude Control, INTELSAT, Washington, DC, April 1984, pp. 121-147
- [15] Agrawal, N. A. : Dynamic characteristics of liquid motion in partially filled tanks of a spinning spacecraft, J. Guidance, Control and Dynamics 16, 4 (1993) 636-640
- [16] Meirovitch, L. : Methods of analytical dynamics. New York, McGraw-Hill, 1970
- [17] Moiseyev, N. N. ; Rumyantsev, V. V. : Dynamic stability of bodies containing fluid. New York, Springer-Verlag, 1968

Towers and Cranes in Linearized Elasticity,
An asymptotic Study

D. Cioranescu(*) and J. Saint Jean Paulin(**)

(*) Université P. & M. Curie, Analyse numérique, LA 189, 4 place Jussieu, 75252 Paris Cedex 05, France.
e-mail: cioran@ann.jussieu.fr

(**) Université de Metz, Département de Mathématiques, URA 399, Ile du Saulcy, 57045 Metz cedex 01.
France. e-mail: sjpaulin@poncelet.univ-metz.fr

TOWERS AND CRANES IN LINEARIZED ELASTICITY : AN ASYMPTOTIC STUDY

D. CIORANESCU - J. SAINT JEAN PAULIN

Towers and cranes are spatial structures where one global dimension is large compared with the others. The material is periodically distributed along bars or layers with a very small thickness.

We study here the linearized elasticity system and the dependence of the displacement on the three small parameters characterizing these structures : their width, the size of the period and the thickness of their constitutive elements (bars or layers). The same structures have already been studied for thermal problems in [7].

The technics used to pass to the limit are close to those used to study networks, see [5]. It is interesting to point out the kind of duality which relates these two types of structures. Towers and cranes involve a beam aspect (material concentrated in one dimension) whereas a network involves a plate aspect (material concentrated in a two dimensional domain).

§1 - STATEMENT OF THE PROBLEM

1.1. Notations

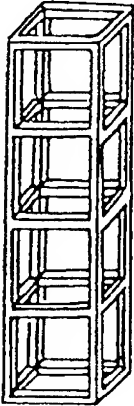


Figure 1

We consider the domain

$$Q^e = \left(-\frac{e}{2}, \frac{e}{2} \right) \times \left(-\frac{e}{2}, \frac{e}{2} \right) \times (0, L)$$

The structure we study here is contained in Q^e , it is formed by four vertical bars of thickness $e\delta/2$ and length L and by horizontal bars periodically distributed along $(0, L)$ with period ε . A period is the cube

$$Y_\varepsilon^e = \omega_\varepsilon \times (0, \varepsilon)$$

where

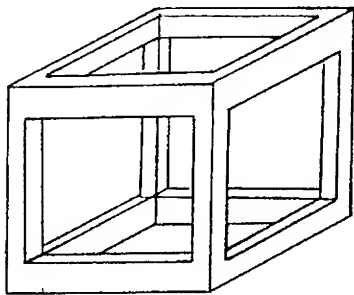


Figure 2

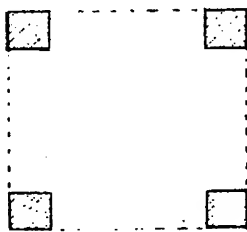
$$\omega_e = \left(-\frac{e}{2}, \frac{e}{2}\right) \times \left(-\frac{e}{2}, \frac{e}{2}\right).$$

In this cube the material is concentrated in bars located along the edges. We denote the material by $Y_{\delta\epsilon}^e$, the cross-section of the horizontal bars is $(e\delta/2) \times (e\delta/2)$ and that of the vertical bars in $(e\delta/2) \times (e\delta/2)$. We can characterize our structure by pointing out that in a period we have very few material and a big hole which is denoted $T_{\delta\epsilon}^e$.

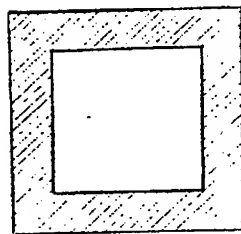
The crane (or the tall structure) $\Omega_{\delta\epsilon}^e \subset Q^e$ is henceforth obtained as the union of translates of $Y_{\delta\epsilon}^e$ in the directions Ox_3 (see fig. 1). There are $N_\epsilon = L/\epsilon$ such periods in $\Omega_{\delta\epsilon}^e$. Of course we choose ϵ such that N_ϵ is an integer.

Denote

$$S_{\delta\epsilon}^e(z_3) = \left\{x = (x_1, x_2) / (x_1, x_2, z_3) \in Y_{\delta\epsilon}^e\right\}$$



a.



b.

Figure 3

As it can be seen from fig. 2, $S_{\delta\epsilon}^e(z_3)$ is the union of the four shaded squares if $e\delta/2 < z_3 < \epsilon(1 - \delta/2)$ (fig. 3.a.) and $S_{\delta\epsilon}^e(z_3)$ is the shaded area in fig. 3.b. if $0 < z_3 < e\delta/2$ or $\epsilon(1 - \delta/2) < z_3 < \epsilon$. In the sequel we shall use the following result which is a simple consequence of the definition of $S_{\delta\epsilon}^e(z_3)$:

Proposition 1.1. We have :

$$\int_{S_{\delta\epsilon}^e(z_3)} z_1 dz_1 dz_2 = \int_{S_{\delta\epsilon}^e(z_3)} z_2 dz_1 dz_2 = \int_{S_{\delta\epsilon}^e(z_3)} z_1 z_2 dz_1 dz_2 = 0$$

$$\int_{S_{\delta\epsilon}^e(z_3)} z_1^2 dz_1 dz_2 = \int_{S_{\delta\epsilon}^e(z_3)} z_2^2 dz_1 dz_2$$

We can extend $S_{\delta\epsilon}^e(z_3)$ by periodicity on $(0,L)$. We shall use the notation :

$$\Gamma_{\delta}^e = S_{\delta\epsilon}^e(0) = S_{\delta\epsilon}^e(\epsilon)$$

which is independent of ϵ .

In the following we make use of the convention of summation on repeated indices. As a rule greek indices take the values 1 and 2 and latin indices the values 1, 2 and 3. Also whenever a geometric domain has $e = 1$, we drop the index 1 to simplify the notations (ex : $\Omega_{\delta\epsilon}^1 = \Omega_{\delta\epsilon}$, $Q^1 = Q...$).

1.2. Variational formulation of the problem

Consider the system of linearized elasticity on $\Omega_{\delta\epsilon}^e$:

$$(1.1.) \quad \left\{ \begin{array}{l} -\frac{\partial}{\partial x_j} (a_{ijkh} \frac{\partial u_{\delta,k}^{e\epsilon}}{\partial x_h}) = F_i^e \text{ in } \Omega_{\delta\epsilon}^e \\ u_{\delta}^{e\epsilon} = 0 \text{ on } \Gamma_{\delta}^e \times \{0\} \text{ - bottom of the crane} \\ a_{i3kh} \frac{\partial u_{\delta,k}^{e\epsilon}}{\partial x_h} n_3 = 0 \text{ on } \Gamma_{\delta}^e \times \{L\} \text{ - top of the crane} \\ a_{i\alpha kh} \frac{\partial u_{\delta,k}^{e\epsilon}}{\partial x_h} n_{\alpha} = G_i^{e\epsilon} \text{ on } \partial T_{\delta\epsilon}^e \text{ (boundary of the crane} \\ \text{except the top and bottom bases)} \end{array} \right.$$

Here $u_{\delta}^{e\epsilon}$ is the displacement. F^e is the applied body force, $G^{e\epsilon}$ is the surface force.

Introduce the stress tensor

$$(1.2) \quad \sigma_{\delta,ij}^{e\epsilon} = a_{ijkh} \gamma_{kh}^{e\epsilon}(u_{\delta}^{e\epsilon})$$

where

$$\gamma_{kh}(v) = \frac{1}{2} \left(\frac{\partial v_k}{\partial x_h} + \frac{\partial v_h}{\partial x_k} \right)$$

is the linearized strain tensor.

Then system (1.1.) can be written as :

$$(1.3) \quad \begin{cases} \frac{\partial}{\partial x_i} \sigma_{\delta,ij}^{e\epsilon} + F_i^e = 0 & \text{in } \Omega_{\delta\epsilon}^e \\ \sigma_{\delta,ij}^{e\epsilon} n_j = G_i^{e\epsilon} & \text{on } \partial T_{\delta\epsilon}^e \\ u_{\delta}^{e\epsilon} = 0 & \text{on } \Gamma_{\delta}^e \times \{0\} \\ \sigma_{\delta,ij}^{e\epsilon} n_j = 0 & \text{on } \Gamma_{\delta}^e \times \{L\} \end{cases}$$

We also give a weak formulation of problem (1.1.).

For this purpose, let us introduce the space

$$V_{\delta\epsilon}^e = \{ \varphi \in H^1(\Omega_{\delta\epsilon}^e), \varphi = 0 \text{ on } \Gamma_{\delta}^e \times \{0\} \}$$

which is a Hilbert space for the H^1 norm.

Then the weak equivalent form of system (1.1) is :

$$(1.4) \quad \begin{cases} u_{\delta}^{e\epsilon} \in V_{\delta\epsilon}^e \\ \int_{\Omega_{\delta\epsilon}^e} a_{ijkh} \gamma_{kh}(u_{\delta}^{e\epsilon}) \gamma_{ij}(v) dx = \int_{\Omega_{\delta\epsilon}^e} F^e v dx + \int_{\partial T_{\delta\epsilon}^e} G^e v dx \quad \forall v \in V_{\delta\epsilon}^e \end{cases}$$

We make the following assumptions :

- i) $F^e \in L^2(Q^e)$
- ii) $G^{ee} \in L^2(\partial T_{\delta\epsilon}^e)$
- iii) a_{ijkh} are the elasticity coefficients and satisfy the symmetry and coercivity conditions :

$$(1.5) \quad a_{ijkh} = a_{jikh} = a_{khij} \quad \forall i,j,k,h$$

$$(1.6) \quad \begin{cases} \text{there exists } C_0 > 0 \text{ such that} \\ C_0 v_{ij} v_{ij} \leq a_{ijkh} v_{ij} v_{kh} \end{cases} \quad \text{for all } v = \{v_{ij}\} \text{ such that } v_{ij} = v_{ji}.$$

Under these hypotheses by the Lax-Milgram theorem, there exists $u_{\delta}^{e\epsilon}$ solution of system (1.4), this solution is unique.

We are interested in the dependence of $u_{\delta}^{e\epsilon}$ on e (the length of the horizontal bars), ϵ (the period in the x_3 direction) and δ (which measures the thickness of the bars in the unit cell).

First we fix ϵ and δ and let $e \rightarrow 0$. Then with δ fixed, we let $\epsilon \rightarrow 0$ (this is the homogenization step). Finally we give the limit for $\delta \rightarrow 0$.

§2 - LIMIT FOR $e \rightarrow 0$

With ϵ and δ fixed, we let $e \rightarrow 0$. This is a technique which is similar to those used for plates (Caillerie [2], Ciarlet - Destuynder [3]) and for beams (Cimetière - Geymonat - Le Dret - Raoult - Tutek [4], Trabucho - Viano [7]). It consists in the transformation of the domain $\Omega_{\delta\epsilon}^e$ into $\Omega_{\delta\epsilon}^1 = \Omega_{\delta\epsilon}$, a fixed domain independent of e , by a dilatation in the x_1 and x_2 directions.

Introduce the new variables

$$\begin{cases} z_\alpha = x_\alpha / e \\ z_3 = x_3 \end{cases}$$

and transform any vector function Φ^e defined on $\Omega_{\delta e}^e$ into a vector function Φ defined on $\Omega_{\delta e}$ by

$$\begin{cases} \Phi_\alpha(z_1, z_2, z_3) = e^{-1} \Phi_\alpha^e(ez_1, ez_2, z_3) \\ \Phi_3(z_1, z_2, z_3) = e^{-2} \Phi_3^e(ez_1, ez_2, z_3) \end{cases}$$

With these transformations, equation (1.1.) becomes :

$$(2.1.) \quad \begin{cases} - \left(e^{-1} \frac{\partial}{\partial z_\beta} \left[a_{i\beta\tau\alpha} \gamma_{\tau\alpha}(u_\delta^\epsilon) + \frac{\partial}{\partial z_3} \left[a_{i3\delta\alpha} \gamma_{\tau\alpha}(u_\delta^\epsilon) \right] \right] \right) - \\ - \left(e^{-1} \frac{\partial}{\partial z_\beta} \left[2e a_{i\beta 3\alpha} \gamma_{3\alpha}(u_\delta^\epsilon) + \frac{\partial}{\partial z_3} \left[2e a_{i33\alpha} \gamma_{3\alpha}(u_\delta^\epsilon) \right] \right] \right) - \\ - \left(e^{-1} \frac{\partial}{\partial z_\beta} \left[e^2 a_{i\beta 33} \gamma_{33}(u_\delta^\epsilon) + \frac{\partial}{\partial z_3} \left[e^2 a_{i333} \gamma_{33}(u_\delta^\epsilon) \right] \right] \right) = f_i \end{cases}$$

where

$$(2.2.) \quad \begin{cases} f_\alpha = e F_\alpha \\ f_3 = e^2 F_3 \end{cases}$$

Define now

$$(2.3.) \quad \sigma_{\delta,ij}^\epsilon = a_{ij\tau\alpha} \gamma_{\tau\alpha}(u_\delta^\epsilon) + 2e a_{ij3\alpha} \gamma_{3\alpha}(u_\delta^\epsilon) + e^2 a_{ij33} \gamma_{33}(u_\delta^\epsilon).$$

With this notation, (2.1) is written as :

$$(2.4.) \quad - \left(e^{-1} \frac{\partial}{\partial z_\beta} \sigma_{\delta,i\beta}^\epsilon + \frac{\partial}{\partial z_3} \sigma_{\delta,i3}^\epsilon \right) = f_i \text{ in } \Omega_{\delta e}$$

The boundary conditions derived from (1.1) are :

$$(2.5.) \quad \begin{cases} -e^{-1} \sigma_{\delta, i\beta}^\epsilon n_\beta = g_i^\epsilon & \text{on } \partial T_{\delta\epsilon} \\ u_\delta^\epsilon = 0 & \text{on } \Gamma_\delta \times \{0\} \\ \sigma_{\delta, i3}^\epsilon = 0 & \text{on } \Gamma_\delta \times \{1\} \end{cases}$$

where

$$\begin{cases} g_\alpha^\epsilon = G_\alpha^\epsilon \\ g_3^\epsilon = e G_3^\epsilon \end{cases}$$

Theorem 2.1.

Let us assume that for $e \rightarrow 0$ we have

$$(2.6.) \quad \begin{cases} f_\alpha \rightarrow f_\alpha^* & \text{in } L^2(Q) \text{ weak} \\ ef_3 \rightarrow f_3^* & \text{in } L^2(Q) \text{ weak} \\ g_\alpha^\epsilon \rightarrow g_\alpha^* & \text{in } L^2(\partial T_{\delta\epsilon}) \text{ weak} \\ eg_3^\epsilon \rightarrow g_3^* & \text{in } L^2(\partial T_{\delta\epsilon}) \text{ weak.} \end{cases}$$

Then

$$e^3 u_\delta^\epsilon \rightarrow u_\delta^* \text{ in } H^1(\Omega_{\delta\epsilon}) \text{ weak}$$

with

$$\begin{cases} u_{\delta, \alpha}^* = V_\alpha(z_3) & \text{in } \Omega_{\delta\epsilon} \\ u_{\delta, 3}^* = -z_1 \frac{\partial V_1}{\partial z_3}(z_3) - z_2 \frac{\partial V_2}{\partial z_3}(z_3) + V_3(z_3) & \text{in } \Omega_{\delta\epsilon} \end{cases}$$

The functions V_i satisfy respectively

$$(2.8) \quad \begin{cases} V_\alpha \in H^2(O, L), V_\alpha(O) = \frac{\partial V_\alpha}{\partial z_3}(O) = 0 \\ \int_0^L \left[\iint_{S(z_3)} z_1^2 dz_1 dz_2 \right] \frac{\partial^2 V_\alpha}{\partial z_3^2} \frac{\partial^2 \varphi}{\partial z_3^2} dz_3 = - \frac{\lambda + \mu}{\mu(3\lambda + 2\mu)} \left[\int_0^L \mathcal{F}_\alpha \varphi dz_3 + \right. \\ \left. + \int_0^L \mathcal{G}_\alpha \frac{\partial \varphi}{\partial z_3} dz_3 \right] \\ \forall \varphi \in H^2(O, L), \varphi(O) = \frac{\partial \varphi}{\partial z_3}(O) = 0 \end{cases}$$

$$(2.9) \quad \begin{cases} V_3 \in H^1(O, L), V_3(O) = 0 \\ \int_0^L \text{mes } S(z_3) \frac{\partial V_3}{\partial z_3} \frac{\partial \psi}{\partial z_3} dz_3 = \frac{\lambda + \mu}{\mu(3\lambda + 2\mu)} \int_0^L \mathcal{F}_3 \psi dz_3 \\ \forall \psi \in H^1(O, L), \psi(O) = 0 \end{cases}$$

where

$$\mathcal{F}_\alpha(z_3) = \iint_{S(z_3)} f_\alpha^* dz_1 dz_2 + \int_{\partial S(z_3)} g_\alpha^* ds, \quad \mathcal{F}_3(z_3) = \iint_{S(z_3)} f_3^* dz_1 dz_2$$

$$\mathcal{G}_\alpha(z_3) = \iint_{S(z_3)} z_\alpha f_3^* dz_1 dz_2 + \int_{\partial S(z_3)} z_\alpha g_3^* ds$$

Remark 2.2 Hypothesis (2.6) implies that

$$F_\alpha^e = O(1), F_3^e = e^{-1} O(1), G_\alpha^{e\varepsilon} = e O(1), G_3^{e\varepsilon} = O(1)$$

Remark 2.3 Note that the initial problem is given on a domain $\Omega_{\delta\epsilon}^e$ where the material is concentrated along bars, in fact $\Omega_{\delta\epsilon}^e$ is a kind of perforated domain with big holes. Nevertheless the limit equations for $e \rightarrow 0$ are given on a non perforated domain, ie on the interval $]0, L[$. But the holes are still present in the coefficients of the equations (2.8) (2.9) because $S(z_3)$ depends on ϵ . As we saw in §1 (fig. 3) the shape $S(z_3)$ depends on the value of z_3 in the cell of height ϵ . Moreover $S(z_3)$ also depends on δ (which gives the thickness of the bars). For the sake of simplicity in the present section we drop the indices ϵ and δ .

Proof of theorem 2.1

The proof consists in several steps. We begin by establishing a priori estimates on u_δ^ϵ and $\gamma_{ij}(u_\delta^\epsilon)$. Then we study the displacements and prove formula (2.7). In order to obtain the limit systems (2.8), (2.9) we introduce the moments, give their limit equations as $e \rightarrow 0$ and express them in terms of limit stresses. Finally by using the geometry of the cross-section $S(z_3)$ and particular test functions, we derive systems (2.8) and (2.9).

1. A priori estimates

Let us take $\varphi = (e^{-1} u_{\delta,1}^\epsilon, e^{-1} u_{\delta,2}^\epsilon, u_{\delta,3}^\epsilon)$ as a test function in system (2.3) - (2.6). Using the coercivity of the tensor (a_{ijkh}) and Korn's inequality, it follows

$$(2.12) \quad \left\{ \begin{array}{l} |u_\delta^\epsilon|_{H^1(\Omega_{\delta\epsilon})} \leq c e^{-3} \\ |\gamma_{\alpha\beta}(u_\delta^\epsilon)|_{L^2(\Omega_{\delta\epsilon})} \leq c e^{-1} \\ |\gamma_{\alpha 3}(u_\delta^\epsilon)|_{L^2(\Omega_{\delta\epsilon})} \leq c e^{-2} \\ |\gamma_{33}(u_\delta^\epsilon)|_{L^2(\Omega_{\delta\epsilon})} \leq c e^{-3} \end{array} \right.$$

which implies successively

$$(2.13) \quad \begin{cases} \vartheta^3 u_\delta^\varepsilon \xrightarrow[\varepsilon \rightarrow 0]{} u_\delta^{\varepsilon^*} \text{ in } H^1(\Omega_{\delta\varepsilon}) \text{ weak} \\ \text{with } u_\delta^{\varepsilon^*} = 0 \text{ on } \Gamma_\delta \times \{0\} \\ \gamma_{\alpha\beta}(u_\delta^{\varepsilon^*}) = 0 \\ \gamma_{\alpha 3}(u_\delta^{\varepsilon^*}) = 0 \end{cases}$$

2. Limit of displacements

From (2.13) it follows :

$$(2.14) \quad \frac{\partial u_{\delta,\alpha}^{\varepsilon^*}}{\partial z_j} + \frac{\partial u_{\delta,j}^{\varepsilon^*}}{\partial z_\alpha} = 0 \quad \forall j = 1,2,3 \quad \forall \alpha = 1,2$$

i) Take first $j = \alpha = 1$, and then $j = \alpha = 2$. We get :

$$\begin{aligned} u_{\delta,1}^{\varepsilon^*}(z) &= u_{\delta,1}^{\varepsilon^*}(z_2, z_3) && \text{independent of } z_1 \\ u_{\delta,2}^{\varepsilon^*}(z) &= u_{\delta,2}^{\varepsilon^*}(z_1, z_3) && \text{independent of } z_2 \end{aligned}$$

ii) Now with $\alpha = 1, j = 2$ we have :

$$\frac{\partial u_{\delta,1}^{\varepsilon^*}}{\partial z_2}(z_2, z_3) = - \frac{\partial u_{\delta,2}^{\varepsilon^*}}{\partial z_1}(z_1, z_3)$$

But the left handside is independent of z_1 and the right handside is independent of z_2 , hence both terms depend only on z_3 . So $u_{\delta,1}^{\varepsilon^*}$ and $u_{\delta,2}^{\varepsilon^*}$ have the form :

$$(2.15) \quad \begin{cases} u_{\delta,1}^{\varepsilon^*}(z_2, z_3) = -z_2 U(z_3) + V_1(z_3) \\ u_{\delta,2}^{\varepsilon^*}(z_1, z_3) = +z_1 U(z_3) + V_2(z_3) \end{cases}$$

iii) Finally take $j = 3$ and successively $\alpha = 1$ and $\alpha = 2$ in (2.14). Using (2.15) we get

$$(2.16) \quad \begin{cases} -z_2 \frac{dU}{dz_3} + \frac{dV_1}{dz_3} + \frac{\partial u_{\delta,3}^{\varepsilon^*}}{\partial z_1} = 0 \\ z_1 \frac{dU}{dz_3} + \frac{dV_2}{dz_3} + \frac{\partial u_{\delta,3}^{\varepsilon^*}}{\partial z_2} = 0 \end{cases}$$

Differentiate now the first equation in z_2 , the second one in z_1 and add :

$$\frac{\partial^2 u_{\delta,3}^{\varepsilon^*}}{\partial z_1 \partial z_2} = 0$$

hence $\frac{\partial u_{\delta,3}^{\varepsilon^*}}{\partial z_1}$ is independent of z_2 and from (2.16) :

$$\frac{\partial u_{\delta,3}^{\varepsilon^*}}{\partial z_1} = \phi(z_1, z_3) = z_2 \frac{dU}{dz_3} - \frac{dV_1}{dz_3}$$

Since ϕ and V_1 do not depend on z_2 , we obtain

$$\frac{dU}{dz_3} = 0$$

that is

$$u_{\delta,1}^{\varepsilon^*} = -z_2 U(0) + V_1(z_3)$$

Now using the boundary condition satisfied by $u_{\delta,1}^{\varepsilon^*}$, i.e. $u_{\delta,1}^{\varepsilon^*} = 0$ on $\Gamma_\delta \times \{0\}$, it follows that

$$U(0) = 0 = V_1(0)$$

so

$$u_{\delta,1}^{\varepsilon^*}(z_1, z_2, z_3) = V_1(z_3)$$

and

$$u_{\delta,2}^{\varepsilon^*}(z_1, z_2, z_3) = V_2(z_3)$$

with

$$V_\alpha \in H^1(O, L) \text{ and } V_\alpha(O) = 0$$

Coming back to (2.16) we have :

$$\frac{\partial u_{\delta,3}^{\varepsilon^*}}{\partial z_1} = - \frac{dV_1}{dz_3} \quad \frac{\partial u_{\delta,3}^{\varepsilon^*}}{\partial z_2} = - \frac{dV_2}{dz_3}$$

which implies that

$$u_{\delta,3}^{\varepsilon^*}(z_1, z_2, z_3) = -z_1 \frac{dV_1}{dz_3}(z_3) - z_2 \frac{dV_2}{dz_3}(z_3) + V_3(z_3).$$

Now by standard arguments, used in plate theory (see Ciarlet - Destuynder [3]) we get that V_α can be identified with a function of $H^2(O, L)$ such that :

$$V_\alpha(0) = 0, \quad \frac{\partial V_\alpha}{\partial z_3}(0) = 0$$

which ends the proof of statement (2.7) of the theorem.

3. Study of moments

First from (2.12) and the definition (2.3) of $\sigma_\delta^\varepsilon$, we have the a priori estimate :

$$(2.17) \quad |\sigma_{\delta,ij}^\varepsilon|_{L^2(\Omega_{\delta\varepsilon})} \leq C\varepsilon^{-1}$$

so :

$$e \sigma_{\delta,ij}^\varepsilon \xrightarrow{\varepsilon \rightarrow 0} \sigma_{\delta,ij}^{\varepsilon^*} \text{ in } L^2(\Omega_{\delta\varepsilon}) \text{ weak.}$$

Introduce

$$(2.18) \quad \begin{cases} M_{\delta,\alpha} = \iint_{S(z_3)} z_\alpha \sigma_{\delta,33}^\varepsilon dz_1 dz_2 \\ N_\delta = \iint_{S(z_3)} \sigma_{\delta,33}^\varepsilon dz_1 dz_2 \\ Q_{\delta,\alpha} = e^{-1} \iint_{S(z_3)} \sigma_{\delta,\alpha 3}^\varepsilon dz_1 dz_2 \end{cases}$$

A consequence of the a priori estimate is that :

$$(2.19) \quad \begin{cases} eM_{\delta,\alpha} \rightarrow M_{\delta,\alpha}^* & \text{in } L^2(O,L) \text{ weak} \\ eN_\delta \rightarrow N_\delta^* & \text{in } L^2(O,L) \text{ weak} \end{cases}$$

We shall prove a convergence result for $eQ_{\delta,\alpha}$ and establish relations between the limits of $eM_{\delta,\alpha}$, eN_δ and $eQ_{\delta,\alpha}$. For doing so, we use here a method derived from Caillerie's technique for plates (see [2] for details).

However the asymptotic study of plates leads to equations in a $(n-1)$ - dimensional manifold whereas in our study we get equations in a 1 - dimensional manifold. Thus there is a kind of duality between the two methods. Limit equations are obtained by an appropriate choice of test functions.

i). Let us take the test function $(0, 0, ez_\alpha \varphi(z_3))$ with $\varphi \in \mathcal{V}$ in (2.4) where

$$\mathcal{V} = \{ \psi \in H^1(O,L), \psi(0) = 0 \}$$

By integrating by parts we get:

$$\int_0^L e Q_{\delta,\alpha} \varphi dz_3 + \int_0^L e M_{\delta,\alpha} \frac{\partial \varphi}{\partial z_3} dz_3 = \int_0^L \left[\iint_{S(z_3)} z_\alpha (e f_3) dz_1 dz_2 \right] \varphi dz_3 + \int_0^L \left[\int_{\partial S(z_3)} z_\alpha (e g_3) ds \right] \varphi dz_3$$

where $\partial S(z_3) = \partial \Gamma_\delta \times \{z_3\}$. Using the assumption (2.6) and the convergence (2.19) we get from (2.20) :

$$e Q_{\delta,\alpha} \rightarrow Q_{\delta,\alpha}^* \text{ in } \mathcal{V}'$$

and

$$(2.21) \quad - \frac{\partial}{\partial z_3} (M_{\delta,\alpha}^*) + Q_{\delta,\alpha}^* = \iint_{S(z_3)} z_\alpha f_3^* dz_2 + \int_{\partial S(z_3)} z_\alpha g_3^* ds \text{ on } (0,L)$$

ii) Choose now $(\varphi_1(z_3), \varphi_2(z_3), 0)$ as a test function :

$$\int_0^L e Q_{\delta,\alpha} \frac{\partial \varphi_\alpha}{\partial z_3} dz_3 = \int_0^L \left[\iint_{S(z_3)} f_\alpha dz_1 dz_2 \right] \varphi_\alpha dz_3 + \int_0^L \left[\int_{\partial S(z_3)} g_\alpha ds \right] \varphi_\alpha dz_3$$

We pass to the limit and take successively $\varphi_1 = 0$ and $\varphi_2 = 0$. Finally we have :

$$(2.22.) \quad \begin{cases} - \frac{\partial}{\partial z_3} (Q_{\delta,\alpha}^*) = \iint_{S(z_3)} f_\alpha^* dz_1 dz_2 + \int_{\partial S(z_3)} g_\alpha^* ds \text{ on } (0,L) \\ Q_{\delta,\alpha}^*(L) = 0 \end{cases}$$

iii) Multiply now equation (2.4) by the test function $(0, 0, \varphi(z_3))$, $\varphi \in \mathcal{V}$:

$$\int_0^L e N_\delta \frac{\partial \varphi}{\partial z_3} dz_3 = \int_0^L \left[\iint_{S(z_3)} e f_3 dz_1 dz_2 \right] \varphi dz_3$$

and hence :

$$(2.23) \quad \begin{cases} -\frac{\partial}{\partial z_3} (N_\delta) = \iint_{S(z_3)} f_3^* dz_1 dz_2 & \text{on } (0,L) \\ N_\delta(L) = 0 \end{cases}$$

iv) Multiply equation (2.4) by $(e^2 z_1 \varphi(z_3), 0, 0)$, $\varphi \in \mathcal{V}$ and pass to the limit for $\epsilon \rightarrow 0$:

$$\int_0^L \iint_{S(z_3)} \sigma_{\delta,11}^{\epsilon^*} \varphi(z_3) dz = 0$$

so that

$$\iint_{S(z_3)} \sigma_{\delta,11}^{\epsilon^*} dz_1 dz_2 = 0$$

The same calculation made with $(0, e^2 z_2 \varphi(z_3), 0)$ leads finally to :

$$(2.24) \quad \iint_{S(z_3)} \sigma_{\delta,i\alpha}^{\epsilon^*} dz_1 dz_2 = 0 \quad \forall \alpha$$

v) Take now $(e^2 z_\alpha^2 \varphi(z_3), 0, 0)$, $\varphi \in \mathcal{V}$. We get for $\alpha = 1, 2$ successively :

$$\iint_{S(z_3)} z_\alpha \sigma_{\delta,1\alpha}^{\epsilon^*} dz_1 dz_2 = 0 \quad (\text{no summation on } \alpha)$$

Similarly with $(0, e^2 z_\alpha^2 \varphi(z_3), 0)$, $\varphi \in \mathcal{V}$ we have :

$$(2.25) \quad \iint_{S(z_3)} z_\alpha \sigma_{\delta,2\alpha}^{\epsilon^*} dz_1 dz_2 = 0 \quad (\text{no summation on } \alpha)$$

If we choose $(\epsilon^2 z_1 z_2 \varphi(z_3), 0, 0)$, $\varphi \in \mathcal{V}$ as a test function we obtain :

$$\int_0^L \left[\iint_{S(z_3)} (z_2 \sigma_{\delta,11}^{\epsilon^*} + z_1 \sigma_{\delta,12}^{\epsilon^*}) \varphi(z_3) dz = 0 \right.$$

so that :

$$\iint_{S(z_3)} (z_2 \sigma_{\delta,11}^{\epsilon^*} + z_1 \sigma_{\delta,12}^{\epsilon^*}) dz_1 dz_2 = 0$$

hence by using (2.25) and the symmetry of $\sigma_{\delta}^{\epsilon^*}$, we get :

$$\iint_{S(z_3)} z_2 \sigma_{\delta,11}^{\epsilon^*} dz_1 dz_2 = 0$$

The same calculation made by interchanging the roles of indices 1 et 2 in the preceding argument gives :

$$\iint_{S(z_3)} z_1 \sigma_{\delta,22}^{\epsilon^*} dz_1 dz_2 = 0$$

All the results established in this step can be summarized in the following formula :

$$(2.26) \quad \iint_{S(z_3)} z_{\alpha} \sigma_{\delta,\beta\beta}^{\epsilon^*} dz_1 dz_2 = 0$$

4 . Limit of stresses

Our aim is to obtain the limit equations satisfied by $u_{\delta}^{\epsilon^*}$. To do this, we use the equations satisfied by $M_{\delta,\alpha}^*$, $Q_{\delta,\alpha}^*$ and N_{δ}^* . As can be seen from their definitions, we need to express $\sigma_{\delta,33}^{\epsilon^*}$ in terms of $u_{\delta}^{\epsilon^*}$.

Actually we shall prove that :

$$(2.27) \quad \sigma_{\delta,33}^{\varepsilon^*} = a_{33j\alpha} b_{\alpha j p i} \sigma_{\delta,ip}^{\varepsilon^*} + [a_{3333} - a_{33j\alpha} b_{\alpha j p i} a_{ip33}] \gamma_{33} \left(u_{\delta}^{\varepsilon^*} \right)$$

where $(b_{\alpha j p i})$ is the inverse tensor of the tensor $(a_{\alpha j p i})$.
Indeed, from (2.3) we have :

$$(2.28) \quad \sigma_{\delta,ip}^{\varepsilon} - e^2 a_{ip33} \gamma_{33} (u_{\delta}^{\varepsilon}) = a_{ipj\alpha} \psi_{\alpha j}$$

with

$$(2.29) \quad \begin{cases} \psi_{\alpha\beta} = \gamma_{\alpha\beta} (u_{\delta}^{\varepsilon}) \\ \psi_{\alpha 3} = 2e \gamma_{\alpha 3} (u_{\delta}^{\varepsilon}) \end{cases}$$

The coercivity of the tensor (a_{ijkh}) implies that the tensor $(a_{ipj\alpha})$ is coercive too, therefore we can take the inverse in (2.28) i.e.

$$(2.30) \quad \psi_{\alpha j} = b_{\alpha j p i} \left(\sigma_{\delta,ip}^{\varepsilon} - e^2 a_{ip33} \gamma_{33} (u_{\delta}^{\varepsilon}) \right)$$

Using again the definition (2.3) of $\sigma_{\delta,33}^{\varepsilon}$ and formulas (2.29) (2.30), the identity (2.27) follows easily.

5 . Limit equations

Let $v \in H^2(O,L)$, $v(O) = 0$, $\frac{\partial v}{\partial z_3}(O) = 0$ and multiply equation (2.21) by $\frac{\partial v}{\partial z_3}$.

Using the equation satisfied by $Q_{\delta,\alpha}^*$, we have :

$$(2.31) \quad \int_0^L M_{\delta,\alpha} \frac{\partial^2 v}{\partial z_3^2} dz_3 = \int_0^L \mathcal{F}_{\alpha} v dz_3 + \int_0^L \mathcal{G}_{\alpha} \frac{\partial v}{\partial z_3} dz_3$$

where \mathcal{F}_{α} and \mathcal{G}_{α} are given by (2.10).

But using (2.27) and the definition (2.18) of $M_{\delta, \alpha}$:

$$\begin{aligned} \int_0^L M_{\delta, \alpha}^* \frac{\partial^2 v}{\partial z_3^2} dz_3 &= a_{33j\beta} b_{\beta j p i} \int_0^L \left[\iint_{S(z_3)} z_\alpha \sigma_{\delta, ip}^{\epsilon^*} dz_1 dz_2 \right] \frac{\partial^2 v}{\partial z_3^2} dz_3 + \\ &+ [a_{3333} - a_{33j\beta} b_{\beta j p i} a_{ip33}] \int_0^L \iint_{S(z_3)} z_\alpha \gamma_{33} (u_\delta^{\epsilon^*}) \frac{\partial^2 v}{\partial z_3^2} dz. \end{aligned}$$

Note that the first right handside term vanishes. This is a consequence of (2.26) and of the explicit values of $b_{\alpha j p i}$. Indeed as a_{jjkh} are Lamé constants we have

$$b_{11p3} = b_{22p3} = 0$$

This result is contained in Annex 1 which also gives all the values of the tensor $b_{\alpha j p i}$.

We also have :

$$(2.32) \quad A_3 = a_{3333} - a_{33j\beta} b_{\beta j p i} a_{ip33} = \frac{\mu(3\lambda + 2\mu)}{\lambda + \mu}$$

Recalling now formula (2.27) giving $u_{\delta, 3}^{\epsilon^*}$ in terms of V_1 we get :

$$\begin{aligned} (2.33) \quad \int_0^L M_{\delta, \alpha}^* \frac{\partial^2 v}{\partial z_3^2} dz_3 &= -A_3 \int_0^L \left\{ \iint_{S(z_3)} z_\alpha z_\beta dz_1 dz_2 \right\} \frac{\partial^2 V_\beta}{\partial z_3^2} \frac{\partial^2 v}{\partial z_3^2} dz_3 + \\ &+ A_3 \int_0^L \left\{ \iint_{S(z_3)} z_\alpha dz_1 dz_2 \right\} \frac{\partial V_3}{\partial z_3} \frac{\partial^2 v}{\partial z_3^2} dz_3. \end{aligned}$$

From (2.31) (2.32) and Proposition 1.1, we obtain the limit equation (2.8).

The second limit equation (2.9) is derived from the equation (2.23) satisfied by N_δ^* , by an analogous argument using (2.24) and again Proposition 1.1.

As a conclusion, remark that each V_α is solution of a fourth order equation and V_3 of a second order equation. These three equations are uncoupled. Existence and uniqueness of V_i are straightforward by Lax-Milgram theorem.

§3 - LIMIT FOR $\epsilon \rightarrow 0$

In this section we study the behaviour of $u_{\delta,i}^\epsilon$ (in fact of V_i) as $\epsilon \rightarrow 0$. This is a homogenization process in a quite simple case, the equation verified by V_i being one-dimensional.

Recalling Remark 2.3, we introduce the notations

$$V_i = V_{\delta i}^\epsilon, \quad \mathcal{F}_\alpha = \mathcal{F}_{\delta\alpha}^\epsilon, \quad \mathcal{G}_\alpha = \mathcal{G}_{\delta\alpha}^\epsilon, \quad S(z_3) = S_\delta^\epsilon(z_3).$$

We prove :

Theorem 3.1 Let $\epsilon \rightarrow 0$. Then :

$$V_{\delta,\alpha}^\epsilon \rightarrow V_{\delta,\alpha} \text{ in } H^2(O,L) \text{ weak}$$

$$V_{\delta,3}^\epsilon \rightarrow V_{\delta,3} \text{ in } H^1(O,L) \text{ weak}$$

and $V_{\delta,i}$ are characterized by the homogenized equations :

$$(3.1) \quad \begin{cases} q_\delta \frac{\partial^4 V_{\delta,\alpha}}{\partial z_3^4} = \frac{\lambda + \mu}{\mu (3\lambda + 2\mu)} \left[- \mathcal{F}_{\delta\alpha}^\cdot + \frac{\partial}{\partial z_3} \mathcal{G}_{\delta\alpha}^\cdot \right] \\ V_{\delta,\alpha}(0) = \frac{\partial V_{\delta,\alpha}}{\partial z_3}(0) = 0 ; \quad \frac{\partial^3 V_{\delta,\alpha}}{\partial z_3^3}(L) = \frac{\partial^2 V_{\delta,\alpha}}{\partial z_3^2}(L) = 0 \end{cases}$$

respectively

$$(3.2) \quad \begin{cases} \tilde{q}_\delta \frac{\partial^2 V_{\delta,3}}{\partial z_3^2} = -\frac{\lambda + \mu}{\mu(3\lambda + 2\mu)} \mathcal{F}_{\delta 3}^* \\ V_{\delta 3}(0) = 0 \quad ; \quad \frac{\partial V_{\delta 3}}{\partial z_3}(L) = 0 \end{cases}$$

where

$$(3.3) \quad \begin{cases} \mathcal{F}_{\delta\alpha}^* = \int_0^1 \left[\int \int_{\Sigma_\delta(y)} \dot{f}_\alpha dz_1 dz_2 \right] dy + \int_0^1 \left[\int_{\partial \Sigma_\delta(y)} \dot{g}_\alpha ds \right] dy \\ \mathcal{F}_{\delta 3}^* = \int_0^1 \left[\int \int_{\Sigma_\delta(y)} \dot{f}_3 dz_1 dz_2 \right] dy \\ \mathcal{G}_{\delta\alpha}^* = \int_0^1 \left[\int \int_{\Sigma_\delta(y)} z_\alpha \dot{f}_3 dz_1 dz_2 \right] dy + \int_0^1 \left[\int_{\partial \Sigma_\delta(y)} z_\alpha \dot{g}_3 ds \right] dy \end{cases}$$

where $\Sigma_\delta(y) = S_\delta^e(y/\epsilon)$. The homogenized coefficients are defined by :

$$(3.4) \quad q_\delta = \int_0^1 \left[\int \int_{\Sigma_\delta(y)} y_1^2 dy_1 dy_2 \right] \frac{\partial^2 \mathcal{W}_\delta}{\partial y^2}(y) dy$$

$$(3.5) \quad [\tilde{q}_\delta]^{-1} = \int_0^1 \frac{dy}{\text{mes } \Sigma_\delta(y)}$$

and \mathcal{W}_δ is defined by :

$$(3.6) \quad \begin{cases} \frac{\partial^2}{\partial y^2} \left[\left(\iint_{\Sigma_\delta(y)} y_1^2 dy_1 dy_2 \right) \frac{\partial^2 w_\delta}{\partial y^2} \right] = 0 & \text{in } (0,1) \\ w_\delta - \frac{1}{2} y^2 \text{ periodic in } (0,1) \text{ and } \int_0^1 \left(w_\delta - \frac{1}{2} y^2 \right) dy = 0 \end{cases}$$

Proof : concerning the second order system (2.9), the equation (3.2) (3.4) is a simple consequence of a now classical case.

Let us consider the fourth order system (2.8). It is obvious that it implies the a priori estimate

$$(3.7) \quad \left[\frac{\partial^2 V_{\delta,\alpha}^\epsilon}{\partial z_3^2} \right]_{L^2(0,L)} \leq C$$

where C is a constant independent of ϵ . Therefore, up to a subsequence

$$V_{\delta,\alpha}^\epsilon \rightarrow V_{\delta,\alpha} \text{ in } H^2(0,L)$$

and

$$V_{\delta,\alpha}(0) = \frac{\partial V_{\delta,\alpha}}{\partial z_3}(0) = 0$$

To obtain the equation satisfied by $V_{\delta,\alpha}^*$ we follow the usual variational method of Tartar in homogenization theory. Set

$$\xi_{\delta,\alpha}^\epsilon = \left[\iint_{S_\delta^\epsilon(z_3)} z_1^2 dz_1 dz_2 \right] \frac{\partial^2 V_{\delta,\alpha}^\epsilon}{\partial z_3^2}$$

which satisfies the equation

$$(3.8) \quad \left\{ \begin{aligned} \int_0^L \xi_{\delta,\alpha}^\varepsilon \frac{\partial^2 \varphi}{\partial z_3^2} dz_3 &= - \frac{\lambda + \mu}{\mu(3\lambda + 2\mu)} \left[\int_0^L \mathcal{F}_{\delta,\alpha}^\varepsilon \varphi dz_3 + \right. \\ &\quad \left. + \int_0^L \mathcal{G}_{\delta,\alpha}^\varepsilon \frac{\partial \varphi}{\partial z_3} dz_3 \right] \\ \forall \varphi \in H^2(O,L), \quad \varphi(0) &= \frac{\partial \varphi}{\partial z_3}(0) = 0. \end{aligned} \right.$$

As

$$\iint_{S_\delta(z_3)} z_1^2 dz_1 \leq \iint_{(0,1) \times (0,1)} z_1^2 dz_1 dz_2$$

we have from (3.7) :

$$(3.9) \quad \xi_{\delta,\alpha}^\varepsilon \rightarrow \dot{\xi}_{\delta,\alpha} \text{ in } L^2(O,L).$$

On the other hand

$$(3.10) \quad \left\{ \begin{aligned} \mathcal{F}_{\delta,\alpha}^\varepsilon &\rightarrow \dot{\mathcal{F}}_{\delta,\alpha} \text{ in } L^2(O,L) \text{ weak} \\ \mathcal{G}_{\delta,\alpha}^\varepsilon &\rightarrow \dot{\mathcal{G}}_{\delta,\alpha} \text{ in } L^\infty(O,L) \text{ weak star} \end{aligned} \right.$$

and thus from system (2.8) we have in the limit :

$$(3.11) \quad \int_0^L \dot{\xi}_{\delta,\alpha} \frac{\partial^2 \varphi}{\partial z_3^2} dz_3 = - \frac{\lambda + \mu}{\mu(3\lambda + 2\mu)} \left[\int_0^L \dot{\mathcal{F}}_{\delta,\alpha} \varphi dz_3 + \int_0^L \dot{\mathcal{G}}_{\delta,\alpha} \frac{\partial \varphi}{\partial z_3} dz_3 \right].$$

Let us consider the function \mathcal{W}_δ defined by system (3.6) and introduce the functions

$$\eta_\delta^\varepsilon(z_3) = \varepsilon^2 \mathcal{W}_\delta\left(\frac{z_3}{\varepsilon}\right)$$

$$\eta_\delta(y) = \left(\iint_{\Sigma_\delta(y)} z_1^2 dz_1 dz_2 \right) \frac{\partial^2 \mathcal{W}_\delta}{\partial y^2}$$

$$\eta_\delta^\varepsilon(z_3) = \eta_\delta(z_3/\varepsilon)$$

It follows from (3.6) that :

$$(3.12) \quad \frac{\partial^2 \eta_\delta^\varepsilon}{\partial z_3^2} = 0$$

and as $\varepsilon \rightarrow 0$ we have the convergences (due to the periodicity) :

$$(3.13) \quad \begin{cases} \mathcal{W}_\delta^\varepsilon \rightarrow \frac{1}{2} z_3^2 & \text{in } H^2(O,L) \text{ weak} \\ \frac{\partial \mathcal{W}_\delta^\varepsilon}{\partial z_3} \rightarrow z_3 & \text{in } H^1(O,L) \text{ weak} \\ \frac{\partial^2 \mathcal{W}_\delta^\varepsilon}{\partial z_3^2} \rightarrow 1 & \text{in } L^2(O,L) \text{ weak} \\ \eta_\delta^\varepsilon \rightarrow q_\delta & \text{in } L^\infty(O,L) \text{ weak star} \end{cases}$$

where q_δ is defined by (3.4).

Let now $\varphi \in \mathfrak{D}(O,L)$. Multiply equation (3.8) by $\varphi \mathcal{W}_\delta^\varepsilon$ and equation (3.12) by $\varphi V_{\delta,\alpha}^\varepsilon$, integrating by parts we have :

$$\begin{aligned}
& \int_0^L \xi_{\delta,\alpha}^\varepsilon \left(2 \frac{\partial \varphi}{\partial z_3} \frac{\partial \mathcal{W}_\delta^\varepsilon}{\partial z_3} + \frac{\partial^2 \varphi}{\partial z_3^2} \mathcal{W}_\delta^\varepsilon \right) dz_3 - \\
& - \int_0^L \eta_\delta^\varepsilon \left(2 \frac{\partial \varphi}{\partial z_3} \frac{\partial V_{\delta,\alpha}^\varepsilon}{\partial z_3} + \frac{\partial^2 \varphi}{\partial z_3^2} V_{\delta,\alpha}^\varepsilon \right) dz_3 = \\
& = - \frac{\lambda + \mu}{\mu(3\lambda + 2\mu)} \int_0^L \left\{ \mathcal{F}_{\delta,\alpha}^\varepsilon \varphi \mathcal{W}_\delta^\varepsilon + \mathcal{G}_{\delta,\alpha}^\varepsilon \frac{\partial}{\partial z_3} (\varphi \mathcal{W}_\delta^\varepsilon) \right\} dz_3
\end{aligned}$$

We pass to the limit for $\varepsilon \rightarrow 0$. Using convergences (3.9) (3.10) (3.11) we get :

$$\begin{aligned}
& \int_0^L \xi_{\delta,\alpha}^\varepsilon \left(2 \frac{\partial \varphi}{\partial z_3} z_3 + \frac{1}{2} \frac{\partial^2 \varphi}{\partial z_3^2} z_3^2 \right) dz_3 - \\
& - \int_0^L \eta_\delta^\varepsilon \left(2 \frac{\partial \varphi}{\partial z_3} \frac{\partial V_{\delta,\alpha}^\varepsilon}{\partial z_3} + \frac{\partial^2 \varphi}{\partial z_3^2} V_{\delta,\alpha}^\varepsilon \right) dz_3 = \\
& = - \frac{\lambda + \mu}{\mu(3\lambda + 2\mu)} \int_0^L \left[\frac{1}{2} \mathcal{F}_{\delta,\alpha}^\varepsilon \varphi z_3^2 + \mathcal{G}_{\delta,\alpha}^\varepsilon \frac{\partial}{\partial z_3} \left(\frac{1}{2} \varphi z_3^2 \right) \right] dz_3
\end{aligned}$$

Integrating again by parts and taking into account equation (3.11) we have finally equation (3.1) and thus Theorem 3.1 is proved.

The following result concerns the displacement u_δ^ε . The formula (2.1) giving this displacement permits to construct the extension $\tilde{u}_\delta^\varepsilon$ on the whole $Q = (0,1) \times (0,1) \times (0,L)$ defined by :

$$\begin{cases} \tilde{u}_{\delta,\alpha}^{\varepsilon*} = V_\alpha(z_3) & \text{in } Q \\ \tilde{u}_{\delta,3}^{\varepsilon*} = -z_1 \frac{\partial V_1}{\partial z_3} - z_2 \frac{\partial V_2}{\partial z_3} + V_3 & \text{in } Q. \end{cases}$$

A consequence of Theorem 3.1 is :

Corollary 3.2 Let $\varepsilon \rightarrow 0$. Then :

$$\tilde{u}_{\delta,\alpha}^{\varepsilon*} \rightarrow \dot{u}_{\delta,\alpha} \quad \text{in } H^2(Q).$$

$$\tilde{u}_{\delta,\alpha}^{\varepsilon*} \rightarrow \dot{u}_{\delta,3} \quad \text{in } H^1(Q)$$

with

$$\dot{u}_{\delta,\alpha} = V_{\delta,\alpha} \quad \text{in } Q$$

$$\dot{u}_{\delta,\alpha} = -z_1 \frac{\partial V_{\delta,1}}{\partial z_3} - z_2 \frac{\partial V_{\delta,2}}{\partial z_3} + V_{\delta,3} \quad \text{in } Q$$

where V_δ is given by (3.1) (3.6).

§4 - LIMIT FOR $\delta \rightarrow 0$

The last step in our asymptotic study of crane-like structures is the dependence on the thickness δ . We have :

Theorem 4.1.

Suppose that f_i^* and g_i^* are smooth enough. Then if $\delta \rightarrow 0$:

$$(4.1) \quad V_{\delta,\alpha} \rightarrow \dot{V}_\alpha \quad \text{in } H^2(O,L) \quad \text{weak}$$

$$(4.2) \quad V_{\delta,3} \rightarrow \dot{V}_3 \quad \text{in } H^1(O,L) \quad \text{Weak}$$

where \dot{V}^* is characterized by the equations :

$$(4.3) \quad \begin{cases} \frac{\mu(3\lambda + 2\mu)}{4(\lambda + \mu)} \frac{\partial^4 \dot{V}_\alpha}{\partial z_3^4} = - \dot{\mathcal{F}}_\alpha + \frac{\partial}{\partial z_3} \dot{\mathcal{G}}_\alpha \quad \text{in } (O,L) \\ \dot{V}_\alpha(O) = \frac{\partial \dot{V}_\alpha}{\partial z_3}(O) = 0 ; \quad \frac{\partial^3 \dot{V}_\alpha}{\partial z_3^3}(L) = \frac{\partial^2 \dot{V}_\alpha}{\partial z_3^2}(L) = 0 \end{cases}$$

$$(4.4) \quad \begin{cases} \frac{\mu(3\lambda + 2\mu)}{(\lambda + \mu)} \frac{\partial^2 \dot{V}_3}{\partial^2 z_3} = \dot{\mathcal{F}}_3 \text{ in } (0, L) \\ \dot{V}_3(0) = 0 ; \frac{\partial \dot{V}_3}{\partial z_3}(L) = 0 \end{cases}$$

and

$$(4.5) \quad \begin{cases} \dot{\mathcal{F}}_i = \lim_{\delta \rightarrow 0} \delta^{-2} \dot{\mathcal{F}}_{\delta, i} \\ \dot{\mathcal{G}}_\alpha = \lim_{\delta \rightarrow 0} \delta^{-2} \dot{\mathcal{G}}_{\delta, \alpha} \end{cases}$$

Corollary 3.2

Under the hypotheses of Theorem 4.1 :

$$\dot{u}_{\delta, \alpha} \rightarrow \dot{u}_\alpha \text{ in } H^2(Q)$$

$$\dot{u}_{\delta, 3} \rightarrow \dot{u}_3 \text{ in } H^1(Q)$$

with

$$\dot{u}_\alpha = \dot{V}_\alpha \text{ in } Q$$

$$\dot{u}_3 = -z_1 \frac{\partial \dot{V}_1}{\partial z_3} - z_2 \frac{\partial \dot{V}_2}{\partial z_3} + \dot{V}_3 \text{ in } Q$$

Proof of theorem 4.1

Let us begin with the second order equation (3.2). An easy calculation shows that :

$$[\tilde{q}_\delta]^{-1} = \frac{2 - 3\delta + 2\delta^2}{\delta^2 (2 - \delta)}$$

hence

$$\delta^{-2} \tilde{q}_\delta \rightarrow 1$$

and so (4.2) and (4.4) are proved.

We consider now the fourth order system (3.1). We shall estimate q_δ . In order to do that we calculate first the integral of y_1^2 over $\Sigma_\delta(y)$. We obtain :

$$(4.6) \quad a(y) = \iint_{\Sigma_\delta(y)} y_1^2 dy_1 dy_2 = \begin{cases} \frac{\delta^2}{4} (1 - \delta + \frac{\delta^2}{3}) & \text{if } \frac{\delta}{2} < y < 1 - \frac{\delta}{2} \\ \delta (1 - \frac{3\delta}{2} + \delta^2 - \frac{\delta^3}{4}) & \text{if } 0 < y < \frac{\delta}{2} \text{ or } 1 - \frac{\delta}{2} < y < 1 \end{cases}$$

Then we solve system (3.6) explicitly to get the value of $\frac{\partial^2 \mathcal{W}_\delta}{\partial y^2}$ which is present in the formula (3.4) of q_δ .

Set

$$\chi_\delta = -\mathcal{W}_\delta + \frac{1}{2} y^2$$

Then (3.6) can be rewritten as :

$$(4.7) \quad \begin{cases} \frac{\partial^2}{\partial y^2} \left[a(y) \frac{\partial^2 (\chi_\delta - \frac{1}{2} y^2)}{\partial y^2} \right] = 0 \\ \chi_\delta \text{ periodic in } (0,1) \end{cases}$$

and (3.4) becomes :

$$(4.8) \quad q_\delta = \int_0^1 a(y) \frac{\partial^2}{\partial y^2} \left(\frac{1}{2} y^2 - \chi_\delta \right) dy$$

Integrate twice system (4.7) :

$$(4.9) \quad a(y) \frac{\partial^2 \left(\chi_\delta - \frac{1}{2} y^2 \right)}{\partial y^2} = k_1 y + k_2$$

and the periodicity requires $k_1 = 0$. Thus from (4.8) we have :

$$q_\delta = -k_2$$

Integrate once more (4.9) :

$$\frac{\partial}{\partial y} \left(\chi_\delta - \frac{1}{2} y^2 \right) = k_2 \int_0^y \frac{1}{a(y)} dy + k_3$$

and the periodicity requires

$$k_2 = - \frac{1}{\int_0^1 \frac{1}{a(y)} dy}$$

and using (4.6) :

$$- \frac{1}{k_2} = \frac{1 - \delta}{\frac{\delta^2}{4} \left(1 - \delta + \frac{\delta^2}{6} \right)} + \frac{\delta}{\delta \left(1 - \frac{3\delta}{2} + \delta^2 - \frac{\delta^3}{4} \right)}$$

hence

$$\delta^{-2} q_\delta = -\delta^{-2} k_2 \rightarrow \frac{1}{4}$$

The proof is achieved if we use (4.5).

Comments on hypothesis (4.5)

As f_i^* and g_i^* are sufficiently smooth we can calculate $\mathcal{F}_{\delta,i}^*$ and $\mathcal{G}_{\delta,\alpha}^*$ using formulas (3.3). As an example we obtain, if f_i^* is supposed independant of δ :

$$\begin{aligned} \lim_{\delta \rightarrow 0} \delta^{-2} \int_0^1 \left[\iint_{\Sigma_\delta(y)} \dot{f}_i \, dz_1 \, dz_2 \right] dy &= \frac{1}{4} \int_{-1/2}^{1/2} \left[\dot{f}_i \left(-\frac{1}{2}, y_2, 0 \right) + \dot{f}_i \left(\frac{1}{2}, y_2, 0 \right) \right. \\ &+ \dot{f}_i \left(-\frac{1}{2}, y_2, 1 \right) + \dot{f}_i \left(\frac{1}{2}, y_2, 1 \right) \Big] dy_2 + \frac{1}{4} \int_{-1/2}^{1/2} \left[\dot{f}_i \left(y_1, -\frac{1}{2}, 0 \right) + \right. \\ &+ \dot{f}_i \left(y_1, \frac{1}{2}, 0 \right) + \dot{f}_i \left(y_1, -\frac{1}{2}, 1 \right) + \dot{f}_i \left(y_1, \frac{1}{2}, 1 \right) \Big] dy_1 + \\ &+ \int_0^1 \left[\dot{f}_i \left(-\frac{1}{2}, -\frac{1}{2}, y_3 \right) + \dot{f}_i \left(-\frac{1}{2}, \frac{1}{2}, y_3 \right) + \dot{f}_i \left(\frac{1}{2}, -\frac{1}{2}, y_3 \right) + \right. \\ &+ \left. \dot{f}_i \left(\frac{1}{2}, \frac{1}{2}, y_3 \right) \right] dy_3. \end{aligned}$$

Similary, if g_i^* is independent of δ , we have :

$$\begin{aligned} \lim_{\delta \rightarrow 0} \delta^{-1} \int_0^1 \left[\iint_{\partial \Sigma_\delta(y)} \dot{g}_i \, ds \right] dy &= \frac{1}{2} \int_{-1/2}^{1/2} \left[\dot{g}_i \left(z_1, -\frac{1}{2}, 0 \right) + \dot{g}_i \left(z_1, \frac{1}{2}, 0 \right) + \right. \\ &+ \dot{g}_i \left(z_1, -\frac{1}{2}, 1 \right) + \dot{g}_i \left(z_1, \frac{1}{2}, 1 \right) \Big] dz_1 + \frac{1}{2} \int_{-1/2}^{1/2} \left[\dot{g}_i \left(-\frac{1}{2}, z_2, 0 \right) + \right. \\ &+ \dot{g}_i \left(\frac{1}{2}, z_2, 0 \right) + \dot{g}_i \left(-\frac{1}{2}, z_2, 1 \right) + \dot{g}_i \left(\frac{1}{2}, z_2, 1 \right) \Big] dz_2 + \\ &+ \int_0^1 \left[\dot{g}_i \left(-\frac{1}{2}, -\frac{1}{2}, y_3 \right) + \dot{g}_i \left(-\frac{1}{2}, \frac{1}{2}, y_3 \right) + \dot{g}_i \left(\frac{1}{2}, -\frac{1}{2}, y_3 \right) + \dot{g}_i \left(\frac{1}{2}, \frac{1}{2}, y_3 \right) \right] dy_3 \end{aligned}$$

Formulas (3.3) giving $\mathcal{F}_{\delta,\alpha}^*$ and $\mathcal{G}_{\delta,\alpha}^*$ both contain two terms. If f_i^* and g_i^* are supposed independent of δ , these two terms do not have the same order in δ . As shown by the preceding relations, the first term is $\delta^2 O(1)$ and the second one is $\delta O(1)$. It follows that hypotheses (4.5) contain automatically a relative dependence between the δ - order of f_i^* and g_i^* . In particular it implies that $g_i^* \sim \delta$.

If g_i^* is of order 1, hypotheses (4.5) have to be modified, for instance :

$$(4.5)' \quad \begin{cases} \mathcal{F}_{\alpha}^* = \lim_{\delta \rightarrow 0} \delta^{-1} \mathcal{F}_{\delta,\alpha}^* & , & \mathcal{F}_3^* = \lim_{\delta \rightarrow 0} \delta^{-2} \mathcal{F}_{\delta,3}^* \\ \mathcal{G}_{\alpha}^* = \lim_{\delta \rightarrow 0} \delta^{-1} \mathcal{G}_{\delta,\alpha}^* & & \end{cases}$$

which will change (4.1) into

$$(4.1)' \quad \delta v_{\delta} \rightarrow \bar{V}_{\alpha}^* \text{ in } H^2(O,L) \text{ weak}$$

but (4.2) and (4.3) remain unchanged. Moreover, in the limit equation (4.3), the right handside term no longer contains any limit of f_i^* .

Of course the result of Corollary 3.2 changes too :

$$\delta u_{\delta,\alpha}^* \rightarrow \bar{u}_{\alpha}^* \text{ in } H^2(Q)$$

$$\delta u_{\delta,3}^* \rightarrow \bar{u}_3^* \text{ in } H^1(Q)$$

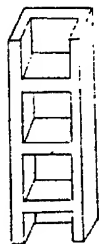
with

$$\begin{cases} \bar{u}_{\alpha}^* = \bar{V}_{\alpha}^* & \text{in } Q \\ \bar{u}_3^* = -z_1 \frac{\partial \bar{V}_1^*}{\partial z_3} - z_2 \frac{\partial \bar{V}_2^*}{\partial z_3} & \text{in } Q \end{cases}$$

§5 - APPLICATIONS TO OTHER STRUCTURES

5.1 - Towers

Now the material is concentrated along layers on all the faces of the period (which in this case is an empty box).



Passing to the limit with $e \rightarrow 0$, $\varepsilon \rightarrow 0$ and $\delta \rightarrow 0$ we get the following result (the equivalent of Theorem 4.1) :

Theorem 5.1

Let us assume the hypotheses of Theorem 4.1. Then if $\delta \rightarrow 0$, the limit problems are :

$$\left\{ \begin{array}{l} \frac{\mu (3\lambda + 2\mu)}{(\lambda + \mu)} \frac{\partial^4 \dot{V}_\alpha}{\partial z_3^4} = - \mathcal{F}_\alpha + \frac{\partial}{\partial z_3} \mathcal{G}_\alpha \text{ in } (0, L) \\ \dot{V}_\alpha(0) = \frac{\partial \dot{V}_\alpha}{\partial z_3}(0) = 0 \end{array} \right.$$

and

$$\left\{ \begin{array}{l} \frac{2\mu (3\lambda + 2\mu)}{(\lambda + \mu)} \frac{\partial^2 \dot{V}_3}{\partial z_3^2} = \mathcal{F}_3 \text{ in } (0, L) \\ \dot{V}_3(0) = 0 \end{array} \right.$$

where :

$$\begin{cases} \mathcal{F}_i^* = \lim \delta^{-1} \mathcal{F}_{\delta,i}^* \\ \mathcal{G}_\alpha^* = \lim \delta^{-1} \mathcal{G}_{\delta,\alpha}^* \end{cases}$$

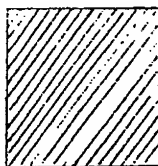
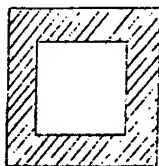
Proof

The proof is the same as that of Theorem 4.1, the only difference being that

$$\delta^{-1} \tilde{q}_\delta \rightarrow 2$$

$$\delta^{-1} q_\delta \rightarrow 1$$

which come from the explicit calculation with the new $\Sigma_\delta(y)$. In this case $S(z)$ is of the form

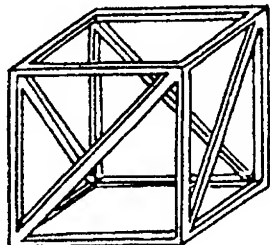


$$\varepsilon\delta/2 < z_3 < \varepsilon(1 - \delta/2) \quad 0 < z_3 < \varepsilon\delta/2 \text{ or } \varepsilon(1 - \delta/2) < z_3 < \varepsilon$$

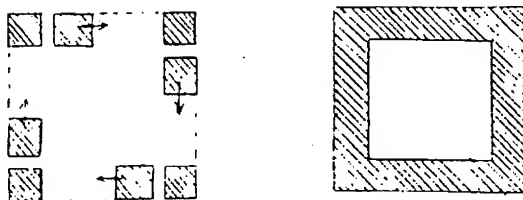
and it can be shown that Proposition 1.1 still holds

5.2 - Cranes with oblique bars

We consider the case when the period has the form



Here on each lateral face there are two diagonal oblique bars and the cross section $S(z_3)$ is of the form



One checks that Proposition 1.1 still holds and the equivalent of Theorem 4.1 is now :

Theorem 5.2

The limit problem is :

$$\left\{ \begin{array}{l} q \cdot \frac{\mu (3\lambda + 2\mu)}{\lambda + \mu} \frac{\partial^4 \dot{V}_\alpha}{\partial z_3^4} = - \mathcal{F}_\alpha + \frac{\partial}{\partial z_3} \mathcal{G}_\alpha \quad \text{in } (0, L) \\ \dot{V}_\alpha(0) = \frac{\partial \dot{V}_\alpha}{\partial z_3}(0) = 0 ; \quad \frac{\partial^3 \dot{V}_\alpha}{\partial z_3^3}(L) = \frac{\partial^2 \dot{V}_\alpha}{\partial z_3^2}(L) = 0 \end{array} \right.$$

and

$$\left\{ \begin{array}{l} (1 + 2\sqrt{2}) \frac{\mu (3\lambda + 2\mu)}{(\lambda + \mu)} \frac{\partial^2 \dot{V}_3}{\partial z_3^2} = \mathcal{F}_3 \quad \text{in } (0, L) \\ \dot{V}_3(0) = 0 ; \quad \frac{\partial \dot{V}_3}{\partial z_3}(L) = 0 \end{array} \right.$$

with

$$\mathcal{F}_i = \lim \delta^{-2} \mathcal{F}_{\delta,i}$$

$$\mathcal{G}_\alpha = \lim \delta^{-2} \mathcal{G}_{\delta,\alpha}$$

and

$$q = \frac{\sqrt{2}}{\sqrt{2 - \sqrt{2}} \arctan \sqrt{2 - \sqrt{2}}}$$

ANNEX 1

Lemma : Suppose that

$$a_{ijkh} = \lambda \delta_{ij} \delta_{kh} + \mu (\delta_{ik} \delta_{jh} + \delta_{ih} \delta_{jk}).$$

Then the tensor $(b_{\alpha j \rho i})$ - the inverse of the tensor $(a_{\alpha j \rho i})$ - satisfies :

$$(A.1) \quad \begin{cases} b_{1111} = b_{2222} = \frac{\lambda + 2\mu}{4\mu (\lambda + \mu)} \\ b_{1122} = b_{2211} = -\frac{\lambda}{4\mu (\lambda + \mu)} \\ b_{1212} = \frac{1}{2\mu} \\ b_{1313} = \frac{1}{\mu} \\ \text{all the others} = 0 \end{cases}$$

Proof

The tensor $b_{\alpha j \rho i}$ is defined by the formulas :

$$a_{ipj\alpha} \psi_{\alpha j} = \phi_{ip} \Leftrightarrow \psi_{\alpha j} = b_{\alpha j \rho i} \phi_{ip}$$

with : $\psi_{\alpha\beta} = \psi_{\beta\alpha}$.

Let us calculate for instance $b_{11\rho i}$. As a_{ijkh} are Lamé constants we have:

$$\begin{cases} \phi_{11} = (\lambda + 2\mu) \psi_{11} + \lambda \psi_{22} \\ \phi_{22} = \lambda \psi_{11} + (\lambda + 2\mu) \psi_{22} \end{cases}$$

which gives

$$\psi_{11} = \frac{\lambda + 2\mu}{4\mu(\lambda + \mu)} \phi_{11} - \frac{\lambda}{4\mu(\lambda + \mu)} \phi_{22}$$

hence $b_{11\theta i} = 0$ if $p \neq i$ and b_{1111}, b_{1122} have the values given by (A1).

Analogous calculations give the other values.

REFERENCES

- [1] N.S. BAKHAVALOV - G.P. PANASENKO - *Averaged processes in periodic media*, Moscow, Nauka 1984 (in Russian).
- [2] D. CAILLERIE - Etude de quelques problèmes de perturbation en théorie de l'élasticité et de la conduction thermique, Thèse d'Etat, Université P. et M. CURIE, Paris 1982.
- [3] P.G. CIARLET - P. DESTUYNDER - A justification of the two-dimensional linear plate model, *J. Méca.* 18 (1978), 315-344.
- [4] A. CIMETIERE - G. GEYMONAT - H. LE DRET - A. RAOULT - Z. TUTEK - Asymptotic theory and analysis for displacements and stress distribution in non linear elastic straight slender rods, *J. Elasticity* 19 (1988), 111-161.
- [5] D. CIORANESCU - J. SAINT JEAN PAULIN - Tall structures, problem of towers and cranes in *Proceedings of Int. Conf. on the Appl. of Multiple scaling in Mechanics*, RMA n°4, Masson, Paris (1987), 77-92.
- [6] D. CIORANESCU - J. SAINT JEAN PAULIN - Overall behaviour of elastic wireworks (to appear).
- [7] L. TRABUCHO - J.M. VIANO - Existence and characterization of higher order terms in an asymptotic expansion method for linearized elastic beams (to appear).

Unsteady Motion of Two Dimensional Airfoil in Incompressible Inviscid Flow

Časlav Mitrović, MSc, Dragan Cvetković, MSc,
Dragoljub Bekrić, BSc, Aleksandar Bengin, MSc

Faculty of Mechanical Engineering, University of Belgrade
Aeronautical Engineering Department, 27. marta St. 80
11000 Belgrade, F.R. of Yugoslavia

Abstract

This paper presents a numerical method for the calculation of the pressure distribution, forces and moments on an airfoils in unsteady inviscid incompressible flow. The method involve vortex-shed model. The method is applied to an airfoil harmonically oscillating at high frequency with an amplitude. The flow characteristics have been calculated at successive time intervals.

Introduction

Numerical method for solution of unsteady flow over airfoil oscillating in compressible, inviscid flow field is dominated in this paper. The model is based on well known panel method in form developed for steady flow by Hess and Smith. Due to unsteadiness in addition to boundary conditions, additional conditions are necessary (Kelvin theorem) and Kutta condition is to be applied in unsteady form. This results with a nonlinear problem.

Formulation of Problem and Boundary Conditions

Inviscid incompressible fluid flow is described by one partial differential equation which satisfy law of fluid continuity (Laplace equation):

$$\frac{\partial^2 \Phi}{\partial x^2} + \frac{\partial^2 \Phi}{\partial y^2} = 0$$

Equation is the same for steady and unsteady flow. Hence, methods for steady flow can be applied in a solution procedure for unsteady flow. When is the panel method applied, direct calculation of the potential is not necessary. The problem is reduced on determination of the velocity field which must satisfy boundary condition of zero normal flow at the surface of airfoil.

When the airfoil is moving relative to a steady undisturbed flow, this kinematics boundary condition must be expressed in form:

$$[\vec{V}_F(t) - \vec{V}_S(t)] \cdot \vec{n}(t) = 0$$

where \vec{V}_F is the fluid velocity, \vec{V}_S is the surface velocity and \vec{n} is normal at the surface.

When the airfoil is moving relative to a steady incompressible inviscid flow, circulation $\Gamma(t)$ around airfoil varying with time t . Total circulation around airfoil and vortex wake must be zero (conservation of total circulation – Kelvin theorem), which is possible to achieve only if the circulation

with intensity $(\partial\Gamma/\partial t)\delta t$ is separated from trailing edge of airfoil in interval δt . This separate vorticity is carried out in downstream direction.

Although not easily noticeable, direct relationship between this and Kutta condition for trailing edge still exist. Kutta condition can be expressed as equality of airfoil upper and lower side pressures on the trailing edge.

$$\Delta p(t)|_{TE} = p_U - p_L = 0$$

where U and L denote upper and lower side of trailing edge, respectively ($x/l \rightarrow 1$). On the basis of unsteady Bernoulli equation this equation can be transformed into:

$$2 \frac{\partial}{\partial t} (\Phi_U - \Phi_L) - (V_U^2 - V_L^2) = 0$$

or

$$\frac{\partial \Gamma}{\partial t} = -\frac{1}{2} (V_U^2 - V_L^2) = -\frac{(V_U + V_L)}{2} (V_U - V_L)$$

Therefore, above mentioned consistence of Kutta condition and vortex shedding model can be clearly seen. Namely, during time above mentioned circulation $\Gamma(t)$ around airfoil is balanced by vortex shedding with intensity $(V_U - V_L)$, with mean velocity $(V_U + V_L)/2$.

Therefore, unsteadiness of the problem is taken into consideration through unsteady form of kinematics boundary condition, Kelvin theorem, unsteady Bernoulli equation, and unsteady form of Kutta condition for trailing edge.

Discretization and Numerical Solution Procedure

Solution of flow over airfoil (moving arbitrary), depending on time and starting from time $t=0$ is calculated in successive time intervals t_k ($t_0=0, k=1,2,3\dots$). Method is based on Hess-Smith method for steady flow. Fig. 1 shows model for the time t_k .

Airfoil contour in time t_k is replaced by N linear elements. $(\sigma_i)_k$ and γ_k are uniform source and circulation distributions on i -th element ($i=1,2,\dots,N$), where $(\sigma_i)_k$ varies from one element to another, γ_k is the same for each element on airfoil and k denotes time t_k . Total circulation Γ_k is given as $\gamma_k \times$ (airfoil perimeter).

An elementary vortex wake with length of Δ_k and pitch angle of θ_k in regard to the x -axis (to the free stream direction) is attached to the trailing edge. Length Δ_k and angle θ_k are arbitrary in first iteration. Their values will be determined as the part of the solution. Circulation in trailing edge vortex wake element is $(\gamma_w)_k$, where:

$$\Delta_k (\gamma_w)_k = \Gamma_k - \Gamma_{k-1} \quad (1)$$

Hence, circulation on the element is equal to the difference between circulations around airfoil in times t_{k-1} and t_k , assuming that Γ_{k-1} has been already determined. Vortex wake consist of concentrated vortices formed by vorticity shed at earlier times, which is assumed to be transformed into discrete vortices. Concentrated vortices is moving with resulting velocity calculated in the center of each vortex at each successive time interval. Therefore, strength and positions of discrete vortices are regarded as known at time t_k .

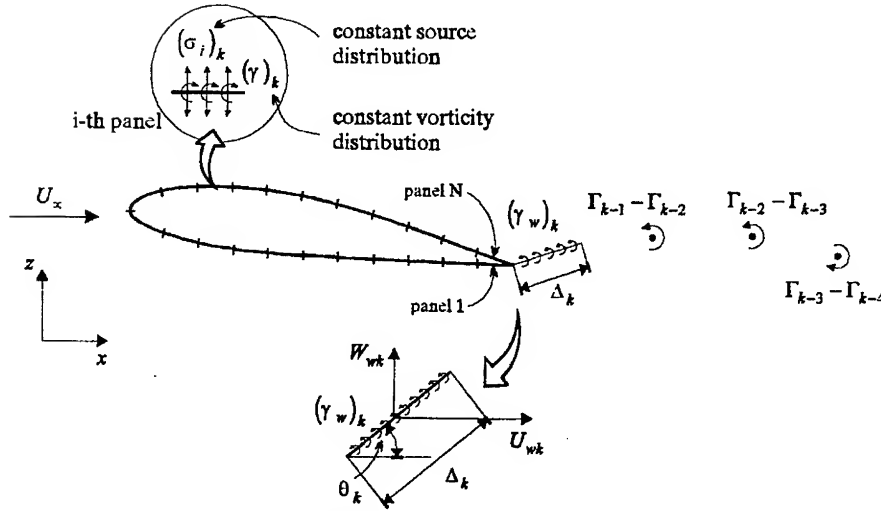


Figure 1. Solution at time t_k

Therefore in time t_k there are $N+3$ unknowns $(\sigma_i)_k$ ($i=1,2,\dots,N$), γ_k , Δ_k and θ_k . They are determined by satisfying following conditions:

- N conditions of zero normal velocity component in external middle point at each segment of airfoil:

$$(V_n)_k = 0 \quad (3)$$

where $(V_n)_k$ is total normal velocity component at the external middle point of j -th. element in time t_k .

- condition of equal pressures in middle points of two elements on an airfoil on both sides of trailing edge (unsteady Kutta condition):

$$(V_n)_k^2 = (V_n)_{k-1}^2 + 2(\Gamma_k - \Gamma_{k-1}) / (t_k - t_{k-1}) \quad (4)$$

where $(V_n)_k$ is total tangent velocity component at middle point of first element and $(V_n)_{k-1}$ is total tangent velocity component at middle point of N -th element in time t_k .

- trailing edge vortex wake element length and direction (Δ_k and θ_k) are determined from condition that the element is tangent to the local resultant velocity and that its velocity is proportional to the local resulting velocity. If $(U_w)_k$ and $(W_w)_k$ are components of total velocity at middle point of trailing edge vortex wake element, excluding influence of the element on itself, then:

$$\begin{aligned} \tan \theta_k &= (W_w)_k / (U_w)_k \\ \Delta_k &= \left[(U_w)_k^2 + (W_w)_k^2 \right]^{1/2} [t_k - t_{k-1}] \end{aligned} \quad (5)$$

By taking into the consideration that the problem considers incompressible flow, formulas for velocities induced from source and vorticity distributions are the same as these for the steady case. Thus, steady Hess & Smith method can be modified for unsteady problem.

If $(\sigma_i)_k$ and γ_k are normalized with respect to the l and U_∞ , normalized disturbance velocities in the external surface middle point of j -th element induced by distributed sources and vortices on the airfoil can be expressed in form:

$$\begin{aligned}(u_j)_k &= \sum_{i=1}^N A_{ji}(\sigma_i)_k + \gamma_k \sum_{i=1}^N B_{ji} \\ (w_j)_k &= \sum_{i=1}^N B_{ji}(\sigma_i)_k - \gamma_k \sum_{i=1}^N A_{ji}\end{aligned}\quad (6)$$

where A_{ji} and B_{ji} corresponding influence coefficients depending on instantaneous coordinates of i -th and j -th element.

Normalized disturbing velocity components induced in the middle point of j -th element by linear trailing edge vortex wake element can be expressed in form:

$$(w_{wj})_k = -(\gamma_w)_k A_{jN-1} \quad (7)$$

Normalized disturbing velocity components induced in the middle point of j -th element by concentrated wake vortices $\bar{\Gamma}_m (= \Gamma_m / U_\infty t)$ induced in previous times can be expressed in form:

$$(u_{vj})_k = \sum_{m=1}^{k-1} C_{jm} \bar{\Gamma}_m \quad (w_{vj})_k = \sum_{m=1}^{k-1} D_{jm} \bar{\Gamma}_m \quad (8)$$

where C_{jm} and D_{jm} are corresponding influence coefficients.

Total normalized disturbing velocity components are the sum of components given in equations (6) – (8). These total normalized disturbing velocity components are added to undisturbed flow components and replaced into basic equations (2) – (5). Basic set of equations is nonlinear therefore iterative procedure for its solution is accepted.

Since Δ_k and θ_k are assumed it leaves N linear equations from (3) and square equation from (4). N linear equations are solved to give $(\sigma_i)_k$ ($i=1,2,\dots,N$) relatively to the γ_k . Then γ_k is determined from square equation (4). Once known $(\sigma_i)_k$ ($i=1,2,\dots,N$) and γ_k , $(U_w)_k$ and $(W_w)_k$ can be determined and replaced into (5) to obtain new values of Δ_k and θ_k . Procedure is repeated until Δ_k and θ_k are of requested accuracy.

When intensities are determined, source and vortex distribution is known from (6) – (8). Pressure coefficient follows from unsteady form of Bernoulli equation:

$$c_p = 1 - \frac{V^2}{U_\infty^2} - \frac{2}{U_\infty^2} \frac{\partial \Phi}{\partial t} \quad (9)$$

where V is total velocity on external side of airfoil, and Φ is velocity potential. Forces and moment coefficients are obtained by direct integration of pressure distribution.

In pressure coefficient computation $\partial \Phi / \partial t$ must be determined. In the numerical method value of $\partial \Phi / \partial t$ in the middle point of j -th element in time t_k is approximately equal to:

$$\left(\frac{\partial \Phi}{\partial t} \right)_k = \frac{\{(\Phi_j)_k - (\Phi_j)_{k-1}\}}{t_k - t_{k-1}}$$

Velocity potential Φ is obtained by integrating velocity field along x -axis from infinity upstream of the airfoil and then over airfoil surface.

Since solution in time t_k is determined, model is applied for the time t_{k+1} in the same way as this for time t_k , with vortex value computed in time t_k . Distributed vorticity in trailing edge vortex wake element in time t_k is now considered as concentrated in vortex with strength $(\gamma_w)_k \Delta_k$ at the position in time t_{k+1} determined by coordinates:

$$x = (x_{TE})_k + \frac{1}{2} \Delta_k \cos \theta_k + (U_w)_k (t_{k+1} - t_k)$$

$$z = (z_{TE})_k + \frac{1}{2} \Delta_k \sin \theta_k + (W_w)_k (t_{k+1} - t_k)$$

Resultant velocity in the center of each next concentrated vortex in vortex wake is calculated by solution at time t_k , and their position in time t_{k+1} directly follows.

In this paper this numerical method is applied on an airfoil starting to oscillate about an angle of incidence at high frequency.

Discussion of Results

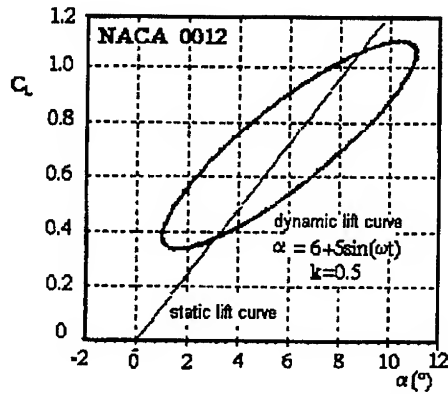


Figure 2. Static and dynamic lift curve

Computer program was developed from formulated numerical method. Flow over NACA 0012 airfoil was modeled by using 20 linear elements. Airfoil oscillating at high frequency through certain angle of attack is considered flow characteristics are computed in time interval from 0 to 30 sec.

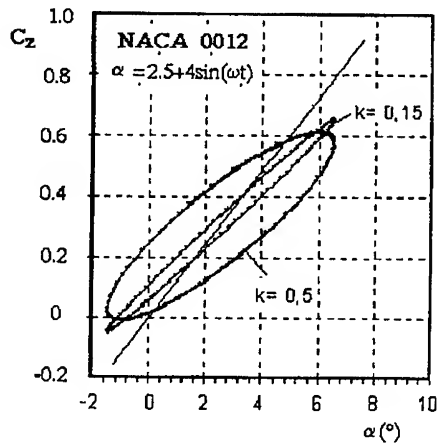


Figure 3. Influence of reduced frequency on unsteady lift curve

Fig. 2 shows static and dynamic lift curve resulting from the application of this numerical method. Dynamic lift curve is obtained by airfoil oscillating through angle of attack of 6° , with amplitude 5° and reduced frequency $k=0.5$.

Dynamics lift curves for two reduced frequencies $k=0.5$ and $k=0.15$ based on obtained results are also shown (Fig. 3). In this case, airfoil oscillating through angle of attack of 2.5° , with amplitude of 4° . Dynamic lift curve shape depending on reduced frequency can be seen from the figure.

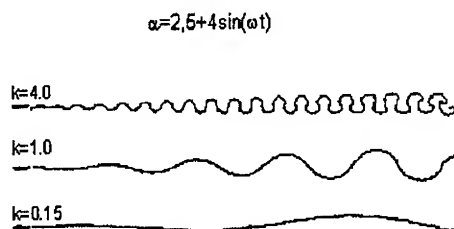


Figure 4. Computed vortex traces as a function of the reduced frequency k

Vortex wake shape of airfoil oscillating through same angle of attack, with same amplitude, but with different reduced frequency obtained by this method is shown at Fig. 4. It is similar with one obtained by methods of visualization in tunnels.

Conclusions

Numerical method presented in this paper leads to inviscid flow field calculation over airfoil moving arbitrary in time if it is supposed that flow stays attached and that it is separated at trailing edge. Method is completely general although only results of oscillating at high frequencies are presented.

References

1. Basu, B. C. and Hancock, G. J. "Two dimensional aerofoils and control surface in simple harmonic motion in incompressible inviscid flow". *Aero. Res. Coun. Current Paper*, 1978.
2. Hess, J. L. and Smith, A. M., "Calculation of potential flow about arbitrary bodies", *Prog. Aero. Sci.*
3. Saffman, P.G. and Sheffield, J.S., "Flow over a Wing with an Attached Free Vortex", *Studies in Applied Mathematics*, Vol.57, 1977.
4. Rossow, V. J., "Lift Enhancement by an Externally Trapped Vortex", *Journal of Aircraft*, Vol.15, 1978.
5. Saffman, P. G. and Tanveer, S., "Vortex Induced Lift on Two Dimensional Low Speed Wings" *Studies in Applied Mathematics*, 1984
6. Theodorsen, T., "Theory of Wing Sections of Arbitrary Shape", NACA TR 411, 1932

**A SECOND - ORDER ANALYSIS
OF AN OSCILLATING BODY IN A SUBSONIC FLOW**

V. A.-J. Butoescu

National Institute for Aerospace Research "Elie Carafoli" INCAS

Bucharest, Romania

Bd. Pacii, No.220, Sect.6, Code 77538

Abstract

A method for calculating of the velocity field about a panel covered with constant oscillatory sources is briefly presented.

The coupling formulæ relating the steady and unsteady flows, available for bodies of revolution, is extended to the general case.

A new method for calculating the oscillatory flow about a body or a combination of bodies is developed. It is based on the panel method and has the advantage of a good geometry approximation, but avoids the occurrence of large influence coefficients matrices.

1. Introduction

The problem of predicting the unsteady aerodynamic forces on an aircraft is of great importance, both for design and estimating the performances.

The usual way of investigating such problems is the Munk's slender body theory (Ref. 1). This method is based on the assumption that the flow is two dimensional in planes normal to the stream direction. Laitone (Ref. 2) and Stewartson (e. g., Ref. 3) also presented slender body theories.

All these methods have the major drawback that they are valid only in the neighborhood of the body. Consequently, they cannot be used for calculating the interference problems. To this must be added the fact that the thickness effects are completely neglected.

Recently, Wu, Garcia-Fogeda and Liu (Ref. 4) gave a method for calculating the flow about oscillating bodies of revolution in incompressible flow. In their theory, the authors take into account that the steady flow influences both the boundary condition and the pressure coefficient.

In 1992, Butoescu presented in Ref. 5 a method of calculating the induced potential and velocity about a panel of pulsating sources. In Ref. 6, the same author gave some numerical applications of the method, illustrating the potential and the velocity fields in the neighborhood of panels of different shapes, in steady and oscillatory regimes. Later, this method was successfully applied to isolated bodies (Ref. 7).

Chen, Lee and Liu (Ref. 8) applied a panel method for calculating the aerodynamic characteristics of a combination of wings and bodies oscillating harmonically in subsonic flow, including the body wake effect.

The efforts of the present author towards the study of the aerodynamic interference in unsteady flow were made difficult because of the computer limits. Then our attention was concerned to a step by step approach. The objective of the present study is the interference of twin bodies performing oscillations in subsonic flow. Thus we applied the panel method previously developed to the interference problem in order to see the main features of the flow. So we presented a method to avoid the increasing of the number of unknowns by assuming that the strength of the sources can be approximated by a trigonometric polynomial on every "slice" of the body. The developing of this method has not been finished yet, but the first results are encouraging.

2. General Equations

2.1 Wind-Fixed Coordinates

Let us consider the coordinate system $Oxyz$, with x axis along the undisturbed flow. The total potential,

$$\Phi(\bar{x}, \bar{y}, \bar{z}) = U_{\infty} l \times [\bar{x} + \phi_0(\bar{x}, \bar{y}, \bar{z}) + \delta \times \phi_1(\bar{x}, \bar{y}, \bar{z}) \times e^{i\omega t}] \quad (1)$$

where,

$$x = l \cdot \bar{x}, \quad y = l \cdot \bar{y}, \quad z = l \cdot \bar{z} \quad (2)$$

Here l denotes the reference length, δ is the non-dimensional amplitude and ω is the angular frequency.

If $\delta \ll 1$, the full potential equation splits into two equations,

$$(1 - M_{\infty}^2) \frac{\partial^2 \phi_0}{\partial \bar{x}^2} + \frac{\partial^2 \phi_0}{\partial \bar{y}^2} + \frac{\partial^2 \phi_0}{\partial \bar{z}^2} = F_0(\phi_{0x}, \phi_{0y}, \dots, M_{\infty}) \quad (3a)$$

$$(1 - M_{\infty}^2) \frac{\partial^2 \phi_1}{\partial \bar{x}^2} + \frac{\partial^2 \phi_1}{\partial \bar{y}^2} + \frac{\partial^2 \phi_1}{\partial \bar{z}^2} - 2ikM_{\infty}^2 \frac{\partial \phi_1}{\partial \bar{x}} + k^2 M_{\infty}^2 \phi_1 = F_1(\phi_{0x}, \phi_{0y}, \dots) \quad (3b)$$

where,

$$k = \frac{\omega \cdot l}{U_{\infty}}, \quad M_{\infty} = \frac{U_{\infty}}{a_{\infty}}$$

The expressions of F_0 and F_1 are not simple and they are not given herein.

The pressure coefficient reads. for $\delta \ll 1$.

$$C_p = C_{p0} + \delta \cdot C_{p1} \cdot e^{i\omega t} \quad (4)$$

where,

$$C_{p0} = \frac{2}{\gamma M_\infty^2} \left\{ \left[1 - \frac{\gamma-1}{2} M_\infty^2 (2u_0 + \bar{v}_0^2) \right]^{\frac{\gamma}{\gamma-1}} - 1 \right\}$$

$$C_{p1} = -2 \left[1 - \frac{\gamma-1}{2} M_\infty^2 (2u_0 + \bar{v}_0^2) \right]^{\frac{1}{\gamma-1}} (u_1 + i \cdot k \phi_1 + \bar{v}_0 \bar{v}_1)$$

$$\bar{v}_0 = u_0 \bar{i} + v_0 \bar{j} + w_0 \bar{k} = \text{grad } \phi_0$$

$$\bar{v}_1 = u_1 \bar{i} + v_1 \bar{j} + w_1 \bar{k} = \text{grad } \phi_1$$

This expression of C_p is available at a given, fixed point in space.

Let us now consider an elastic body oscillating harmonically and let \bar{P} be a point on its surface, (B). Then this surface can be written,

$$\bar{P} = 1 \cdot [\bar{P}_0(\lambda, \mu) + \delta \cdot \bar{P}_1(\lambda, \mu) \cdot e^{i\omega t}] \quad (5)$$

The surface described by (5) with $\delta = 0$ will be referred to as the *rest surface*, (B_0). Now a normal to (B) reads,

$$\bar{n} = \bar{n}_0(\lambda, \mu) + \delta \cdot \bar{n}_1(\lambda, \mu) \cdot e^{i\omega t}$$

where $\bar{n}_0(\lambda, \mu)$ is the unit normal to (B_0).

Following Ref. 9 we can derive the boundary condition taking into account the actual position of \bar{P} rather than its mean position on (B_0). This is usually done by considering a Taylor expansion of \bar{v}_F about the mean position of \bar{P} . We obtain finally,

$$\bar{v}_{0F_0} \cdot \bar{n}_0 + n_{0x} = 0$$

$$\bar{v}_{1F_0} \cdot \bar{n}_0 + n_{1x} - ik \bar{P}_1 \cdot \bar{n}_0 = \Delta \quad (6)$$

where

$$\Delta = -[(\bar{P}_1 \nabla) \bar{v}_0] \cdot \bar{n}_0 - \bar{v}_{0F_0} \cdot \bar{n}_1 \quad (7)$$

Similarly, we get the pressure coefficient on (B) as,

$$C_{pF} = C_{p0F_0} + \delta \cdot C_{p1F_0} \cdot e^{i\omega t} \quad (8)$$

where

$$C_{p0F_0} = \frac{2}{\gamma M_\infty^2} \left\{ \left[1 - \frac{\gamma-1}{2} M_\infty^2 (2u_0 + \bar{v}_0^2) \right]^{\frac{\gamma}{\gamma-1}} - 1 \right\}_{F_0}$$

$$C_{p1F_0} = -2 \left[1 - \frac{\gamma-1}{2} M_\infty^2 (2u_0 + \bar{v}_0^2) \right]_{F_0}^{\frac{1}{\gamma-1}} [u_1 + i \cdot k \varphi_1 + \bar{v}_0 \bar{v}_1 + \bar{P}_1 (\nabla u_0) + \bar{P}_1 \nabla (\frac{1}{2} \bar{v}_0^2)]_{F_0} \quad (9)$$

As pointed out firstly by Hoffman and Platzer (Ref. 9), the formulae (6) to (9) will not reduce to the well-known slender body equations as $\delta \rightarrow 0$.

Similar equations were obtained by Garcia-Fogeda and Liu (Ref. 10), but they are available only for bodies of revolution. These authors note that both (7) and (9) have singular terms at the body apices if $\bar{P}_1 \neq 0$ there. This situation also occurs when the body surface is not smooth. Then the Taylor expansion previously used does not hold any more. To prevent this, the above mentioned authors propose to use the *body-fixed coordinates*.

2.2 Body-Fixed Coordinates

Following Garcia -Fogeda and Liu, a curvilinear coordinate system is introduced instead of the aerodynamic system : The x axis is taken along the mean body axis. Then all the above equations will become more complicated, but Δ and C_{p1} will not contain singular terms.

The authors also proposed an alternative system, the *pseudo-wind fixed coordinates*, where x axis remains linear, but always attached to the body apex. The equations are then simpler, but the method is not valid when the body slope is discontinuous.

3. Analysis

3.1 The Integral Solution

In the linearized form, F_0 and F_1 are neglected. However, when using a body fixed system or a pseudo-body fixed system, the equation of the unsteady flow becomes again inhomogeneous, but, in principle, the solution can be obtained using a Green-function method.

Then, we can write,

$$\varphi_1(x, y, z) = -\frac{1}{4\pi} \int_{(F_0)} \frac{\exp[i\kappa(Mx_0 - R)]}{R} q_1(\xi, \eta, \zeta) dS \quad (10)$$

where,

$$x_0 = x - \xi, \quad y_0 = y - \eta, \quad z_0 = z - \zeta; \quad (\xi, \eta, \zeta) \in (F_0)$$

$$R = \sqrt{x_0^2 + \beta^2 \cdot r^2}, \quad r^2 = y_0^2 + z_0^2, \quad \kappa = k \frac{M}{\beta^2}$$

In the above equations and henceforward, the $-$ symbol on x, y, z is dropped.

Equation (10) expresses the oscillatory flow in terms of a simple layer potential. In what follows, it will be called *oscillatory -source potential*.

On the other hand, equation (10) becomes, for $k=0$, the well-known steady flow equation satisfied by ϕ_0 and the oscillatory source turns itself into a source distribution.

The potential (10) steady or unsteady and the corresponding boundary condition (6) lead us to a Neumann problem, with q_0 or q_1 unknowns.

3.2 Potential and Velocities Induced by a Planar Quadrilateral Panel

In order to solve the integral equation relating the normalwash and the strength of the source sheet, we shall discretize the body surface into a number of planar quadrilateral panels. On these panels the strength of the source layer is assumed to be constant.

It is necessary to calculate the potential and the velocity field induced by a planar quadrilateral on which the oscillating sources are constantly distributed.

The potential and the velocity field can be expressed as,

$$\begin{aligned}\phi(Q) &= \frac{1}{4\pi} \cdot q \cdot I_{01} \\ u(Q) &= \frac{1}{4\pi} \cdot q \cdot (I_{x3} + i \cdot \kappa \cdot I_{x2} - i \cdot \kappa \cdot M_{\omega} I_{01}) \\ v(Q) &= \frac{\beta^2}{4\pi} \cdot q \cdot (I_{y3} + i \cdot \kappa \cdot I_{y2}) \\ w(Q) &= \frac{\beta^2}{4\pi} \cdot q \cdot (I_{z3} + i \cdot \kappa \cdot I_{z2})\end{aligned}\tag{11}$$

where Q stands for (x,y,z) and

$$\begin{aligned}I_{01} &= \int_{(P)} \frac{1}{R} \exp[i\kappa(Mx_0 - R)] dS \\ I_{xm} &= \int_{(P)} \frac{x_0}{R^m} \exp[i\kappa(Mx_0 - R)] dS \\ I_{ym} &= \int_{(P)} \frac{y_0}{R^m} \exp[i\kappa(Mx_0 - R)] dS \\ I_{zm} &= \int_{(P)} \frac{z_0}{R^m} \exp[i\kappa(Mx_0 - R)] dS\end{aligned}\tag{12}$$

Here, $m=2,3$ and (P) is a planar domain.

The above integrals cannot be expressed by means of usual functions.

In Ref. 5 we dealt with the evaluation of ϕ and \vec{v} . In that paper, we considered two cases, depending on the distance between Q and the panel:

- 1) For large or moderate distances, a Gaussian quadrature will give good results.
- 2) For small distances, a more elaborated analysis was performed. Finally, we obtained expressions for ϕ, u, v, w which can be evaluated numerically even when Q is located at an infinitely small distance to the panel. These formulae are not given here because they are too complex, but they reveal some important characteristics as:

(a) the "steady effect" can be de coupled, so that for $\omega = 0$, the method is exact;
 (b) the "steady effect" generates a jump of the normal velocity across the panel, which is a function of its incidence and Mach number; but on the other hand, the incidence influence is small, if $|\alpha| \leq 30^\circ$;

(c) a singular behaviour occurs along the panel sides, but it is not only because of the "steady effect", but also because of a non-steady singular term.

The method proposed in Ref. 5 was analysed in Ref. 6, to establish:

- the convergence and precision of the approximate methods with respect to the Gaussian integration points number;
- the effect of panel incidence on the induced field;
- the field pattern about a panel;
- the effects of the panel shape on the flow field;
- the Mach no. and reduced frequency effects on the flow field.

3.3 The Panel Solution of the Problem

After paneling of the (F_0) surface, we can write,

$$\varphi_1(Q) = -\frac{1}{4\pi} \cdot \sum_j q_{1j} \cdot \int_{(F_j)} \frac{\exp[i\kappa \cdot (M_\infty x_0 - R)]}{R} dS$$

$$\bar{v}_1(Q) = -\frac{1}{4\pi} \cdot \sum_j q_{1j} \cdot \int_{(F_j)} \text{grad} \frac{\exp[i\kappa \cdot (M_\infty x_0 - R)]}{R} dS$$

If we have a combination of NB bodies, the potential reads,

$$\varphi_{1\text{tot}}(Q) = \sum_{m=1}^{NB} \varphi_{1m}(Q)$$

and a similar equation for $\bar{v}_{1\text{tot}}(Q)$. We can write now the boundary condition (6) and so we obtain a system of linear equations with q_{1j} unknowns.

3.4. The Modified Panel Method

As we can see, the number of unknowns increases when there are more than one body. In order to avoid the large number of equations, a new method is proposed.

Suppose we have just one body. The extension to the more general case of the interference of NB bodies is very easy to apply as we have already shown in the other paragraph.

The body is divided into NS "slices" with the exception of the two body apices which are usually excluded.

For the sake of simplicity, the body is supposed to be symmetrical with respect to the $y=0$ plane and the (un)steady flow also symmetrical with respect to the same plane.

The source distribution will be written as,

$$q_1(P) = \sum_{j=1}^{NF} a_{(i-1)NF+j} \cos(j-1)\theta, \quad P \in (B_i) \quad (14)$$

where (B_i) is the i -th "slice", and ϑ is the shown in fig. 1.

Then equation (10) becomes,

$$\varphi(M) = -\frac{1}{4\pi} \sum_{i=1}^{NS} \sum_{j=1}^{NF} a_{(i-1)NS+j} \int_{(B_i)} K(M-P) \cdot \cos(j-1) \vartheta dS_p$$

Here M is a point in space and

$$K = \frac{\exp[ik \cdot (M - x_0 - R)]}{R}$$

Let us put,

$$\begin{aligned} \Phi_m &= -\frac{1}{4\pi} \int_{(B_i)} K(M-P) \cos(j-1) \vartheta dS_p \\ m &= (i-1)NS + j \quad ; \quad NT = NS \cdot NF \end{aligned} \quad (15)$$

Similar relations can be written for \bar{v} so that we finally obtain,

$$\begin{aligned} \varphi(M) &= \sum_{m=1}^{NT} a_m \cdot \Phi_m(M) \\ \bar{v}(M) &= \sum_{m=1}^{NT} a_m \cdot \bar{V}_m(M) \end{aligned} \quad (16)$$

Now the functions Φ_m and \bar{V}_m can be evaluated numerically. Consider that the "slice" (B_i) is divided into N domains (fig. 2),

$$(B_i) = (b_{i1}) \cup (b_{i2}) \cup \dots \cup (b_{iN})$$

so that on each interval (b_{ij}) , the sign of $\cos(j-1)\vartheta$ is unchanged. Then,

$$\begin{aligned} \Phi_m(M) &= \sum_{n=1}^N \left(-\frac{1}{4\pi} \right) \cdot \int_{(b_{in})} K(M-P) \cos(j-1) \vartheta dS_p \approx \\ &\approx \sum_{n=1}^N \cos(j-1) \vartheta_n^* \left[-\frac{1}{4\pi} \right] \cdot \int_{(b_{in})} K(M-P) dS_p \end{aligned} \quad (16)$$

where (\bar{b}_{in}) is a planar panel approximating (b_{in}) . In (16) ϑ_n^* is a mean value of ϑ in (b_{in}) . But the factor in the brackets (i. e. [...]) can be evaluated using the procedure given at paragraph 3.2. Of course, \bar{V}_m can be estimated in a similar way.

The coefficients a_m remain still unknown. To find them, we must apply the boundary condition. For this purpose we take NF points as collocation points on each "slice". Let's put.

$$l = (n-1) \cdot NF + m, \quad n = 1, 2, \dots, NS, \quad m = 1, 2, \dots, NF$$

Then we will define,

$$C_{m1} = \vec{V}_m \cdot \vec{n}_1$$

where \vec{n}_1 is the unit normal vector on (B) at each NT collocation point.

We have obtained a linear system,

$$\sum_{m=1}^{NT} a_m \cdot C_{m1} = w_l \quad (17)$$

$$l = 1, 2, \dots, NT$$

where w_l is the unknown normalwash.

This system can be solved using an available procedure. So, the source distribution (14) is determined. Then we can find the potential and the velocity using equation (16). The pressure coefficient is given by equation (8).

4. Results

The results presented herein are the first ones obtained with the proposed method, so that a further verification and validation are necessary.

The method was tested on both isolated bodies and the configuration shown in fig. 1, for $l=1$ and $d=0.1$

The basic body geometry presented here was very simple, i. e. a parabolic spindle (Ref. 4), described by

$$R(x) = 2 \cdot \tau \cdot x \cdot (1-x), \quad 0 \leq x \leq 1, \quad \tau = 0.1.$$

The steady flow corresponds to $\alpha = 0$ and the unsteady flow is described by the rigid modes,

$$\bar{P}'_1 = \pm \bar{P}''_1 = \bar{k} \cdot e^{i\omega t}$$

$$\bar{P}'_1 = \pm \bar{P}''_1 = \bar{j} \cdot e^{i\omega t}$$

where \bar{P}'_1 stands for lower body movement, while \bar{P}''_1 stands for the upper body movement.

In fig. 3 is shown the unsteady pressure distribution on the isolated paraboloid for $M = 0$ and for $k = 0.5$. The continuous line represents the present method and the dotted line shows the values obtained by applying the Stewartson's method.

Figs. 4 and 5 refer to the configuration with $d=0.1$, in steady and unsteady flows. All the curves refer to the lower body.

5. Conclusions

A method for calculating the velocity field induced by a constant strength oscillatory sources distributed over a planar panel was briefly presented.

The coupling formulæ relating the steady and unsteady flows, available only for axisymmetric bodies, was extended to the general geometry.

A modified panel method for calculating the oscillatory flow about a body and a body combination was presented. It has the advantage of a good paneling of the bodies, without being necessary to store large matrices. The method can be extended to the wing body combination as well. In this case, the method could be improved, to render the jump of the velocity at the wing root. Therefore, one more term added to the Fourier-like source strength distribution is desirable. It could be represented by a combination of Heaviside step functions.

All the numerical results now available are the first ones obtained, so that a further systematic investigation and validation should be made.

References

1. Munk, M.M. *The Aerodynamic Forces on Airship Hulls*, NACA Rpt. 184 (1924)
2. Laitone, E.V. *The Subsonic Flow About a Body of Revolution*, *Quarterly of Applied Mathematics*, Vol. 5, No. 2, 1947.
3. Carafoli, E. *High Speeds Aerodynamics (compressible fluids)*, Ed. Academiei, 1957, Bucharest.
4. Wu, M.Sh., Garcia-Fogeda, P., Liu, D.D. *Potential Flow Over Bodies of Revolution in Unsteady Motion*, *AIAA Journal*, Vol. 27, No. 6, June, 1989.
5. Butoescu, V. *A Harmonically Pulsating Source Panel Method For Subsonic Flow, I. Mathematical Background*, *Rev. Roum. Sci. Tech.-Mec. Appl.* Vol. 36, No. 6, (1992).
6. Butoescu, V. *A Harmonically Pulsating Source Panel Method For Subsonic Flow, II. Some numerical results*, *Rev. Roum. Sci. Tech.-Mec. Appl.* Vol. 38, No. 1, (1993).
7. Butoescu, V. *Pressure Distribution on Oscillating Bodies in Subsonic Flow*, *Rev. Roum. Sci. Tech.-Mec. Appl.* Vol. 39, No. 6, (1994).
8. Chen, P.C., Lee, H.W., Liu, D.D. *Unsteady Subsonic Aerodynamics for Bodies and Wings With External Stores Including Wake Effect*, *J. Aircraft*, Vol. 30, No. 5, Sept.-Oct., 1993.
9. Hoffman, G.H., Platzler, M.F., *On Supersonic Flow Past Oscillating Bodies of Revolution*, *AIAA Journal*, Vol. 4, No. 2, Feb. 1966.

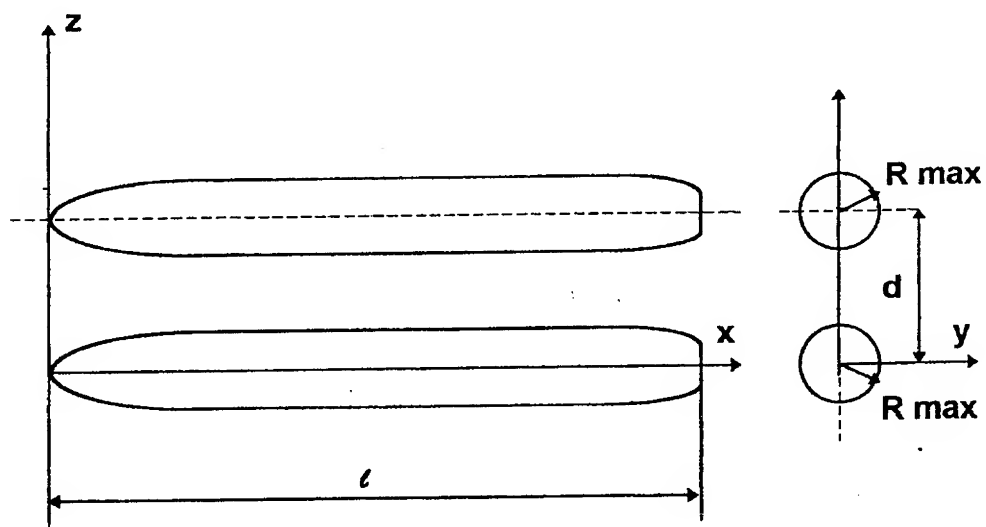


Fig.1 Twin bodies arrangement

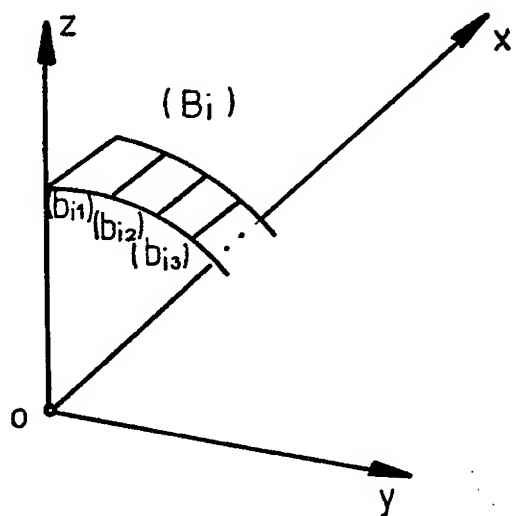


Fig.2 A body slice

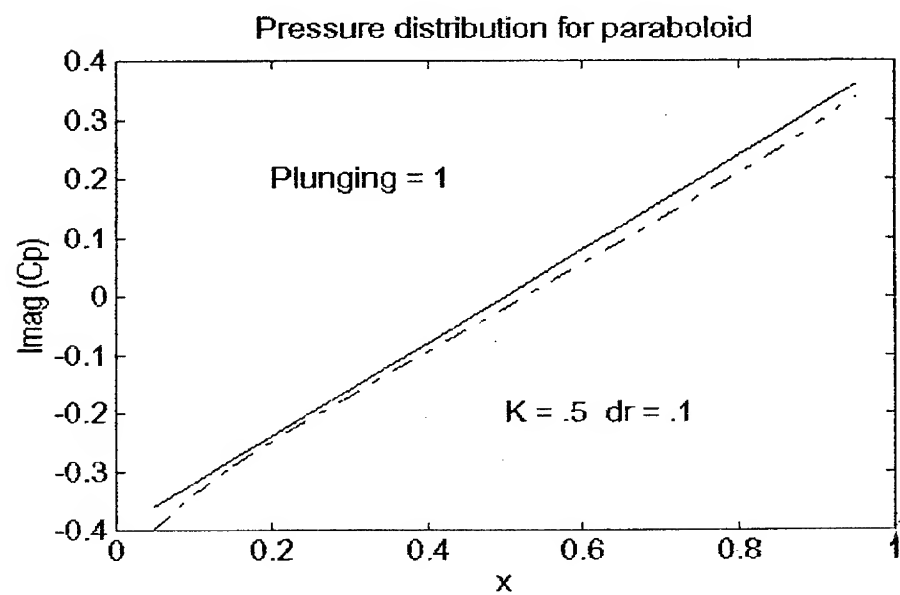
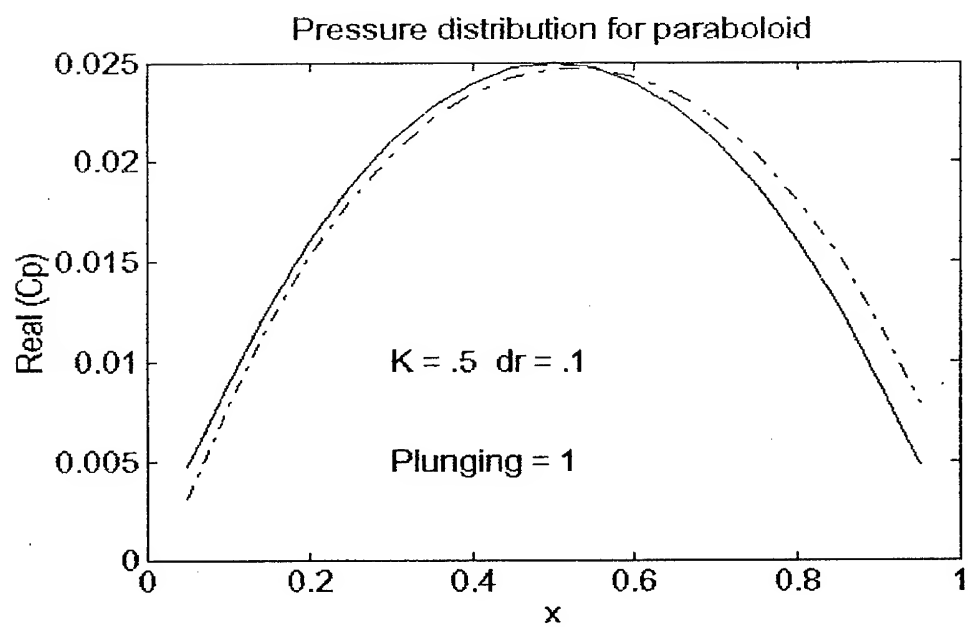


Fig.3 One parabolic spindle.

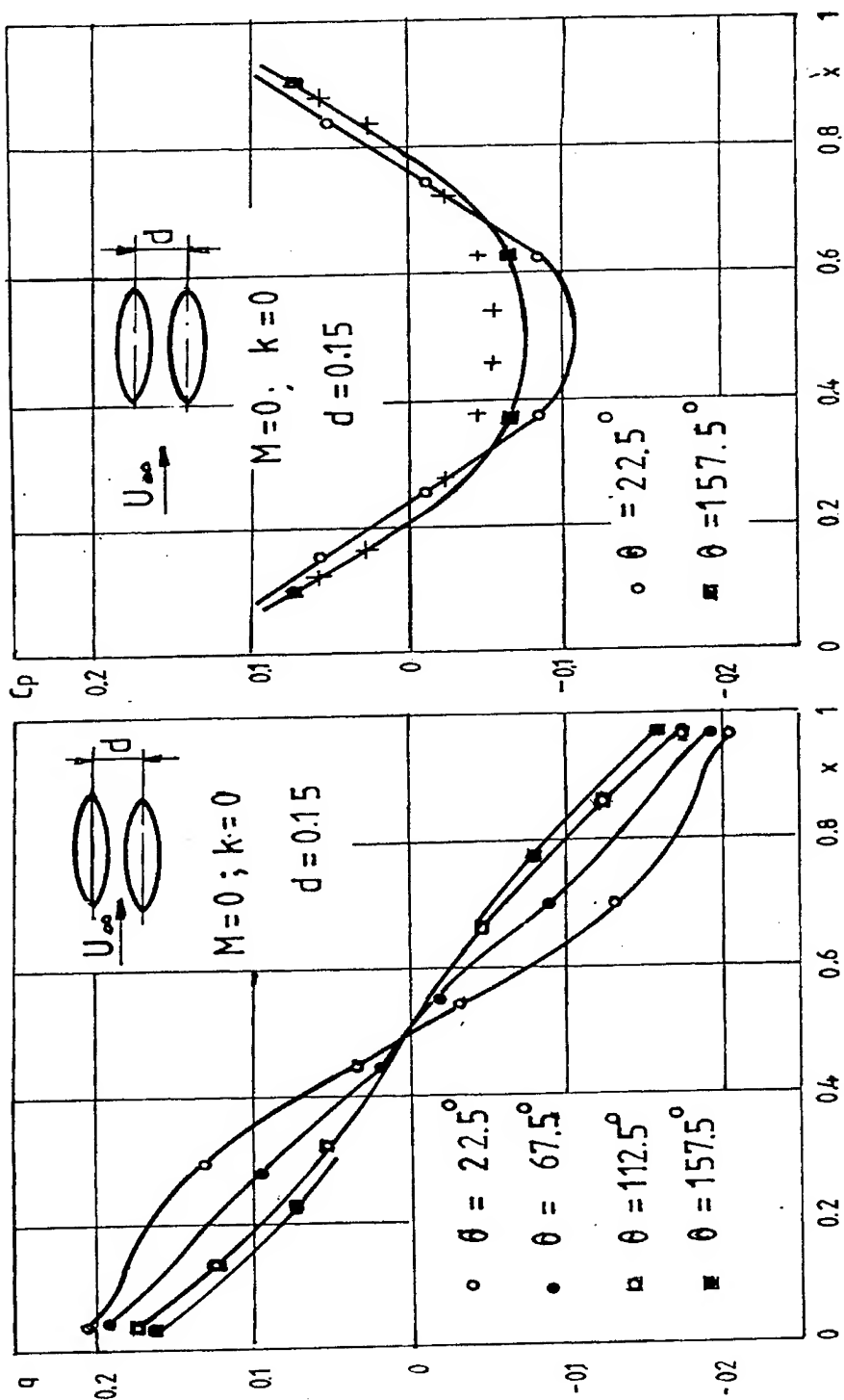


Fig. 4 Twoparabolic spindles, $\alpha=0.1$ Lower spindle distributions

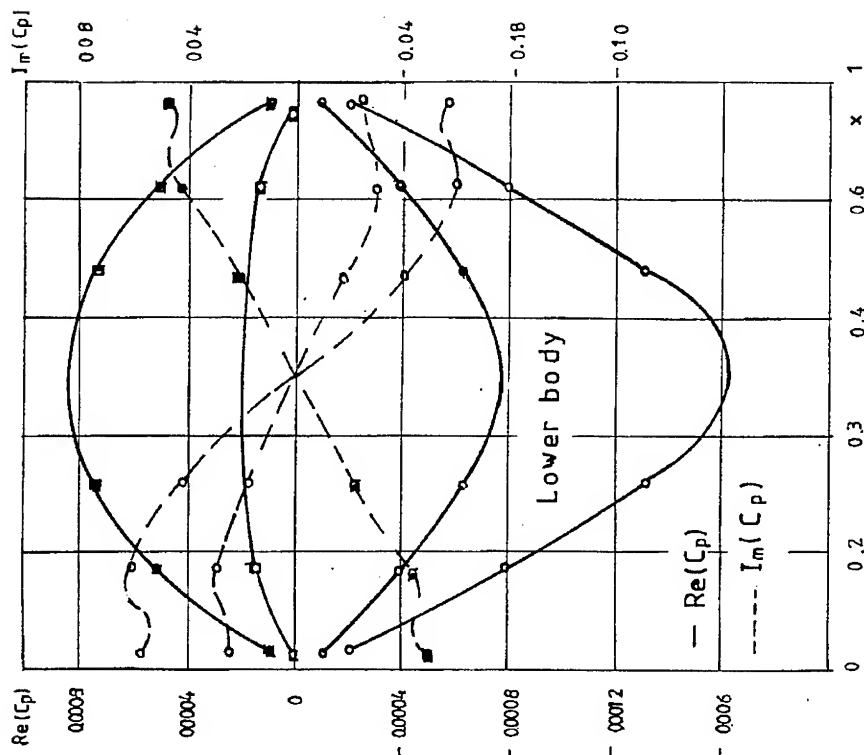
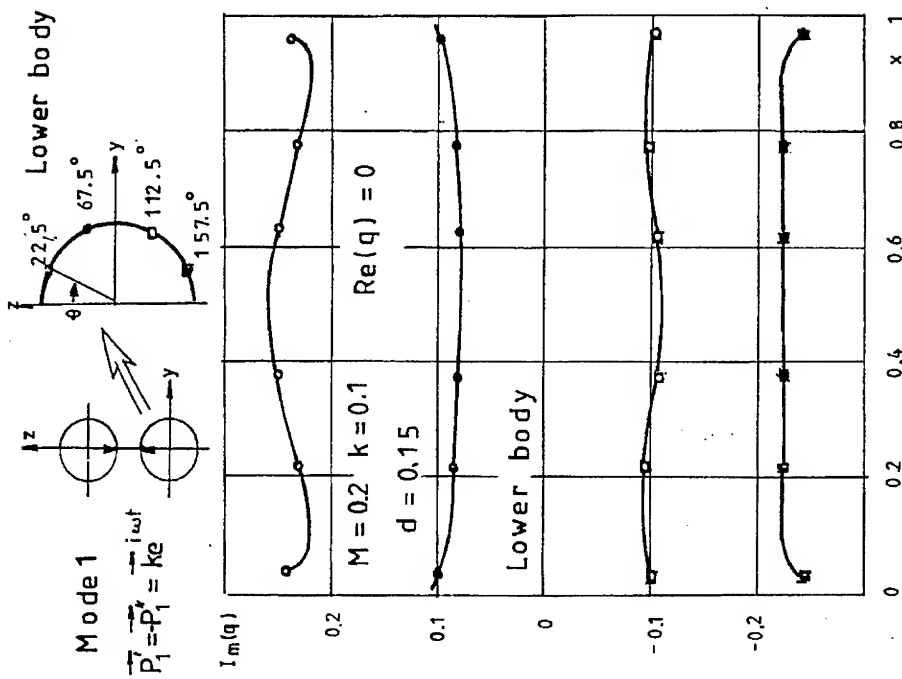


Fig. 5 Twoparabolic spindles, $\alpha = 0.1$ plunging symmetrically in $y=0$ plane

AN INVERSE INTEGRAL METHOD FOR SEPARATED TURBULENT BOUNDARY LAYERS

by H. Dumitrescu^{*}, Al. Dumitrache^{**}

ABSTRACT

A method designed to calculate incompressible turbulent boundary layers with strong adverse pressure gradients, attendant separation and reattachment is presented. The boundary-layer method is a two-dimensional planar inverse integral technique based on a pressure gradient-velocity defect correlation and the extended Coles analytical description of attached and separated boundary-layer velocity profiles. Predictions by this method for boundary-layer properties and separation, and reattachment locations agree well with experimental data.

1. INTRODUCTION

So far significant progress has been made in the solution of time-dependent, ensemble-averaged Navier-Stokes equations for turbulent flow. The Navier-Stokes approach, however, is presently too expensive for much of the technical community and, although complex flows can be solved, further advances in numerical techniques and computer, technology are needed before this approach can be used routinely.

In the meantime, problems involving viscous-inviscid interaction with and without separation are commonplace and must be confronted. One approach to solve these problems is to use an inviscid solution for the region away from the body, a viscous solution near the body, and match the two of some location and in some fashion. Besides the problem of where and how to match these solutions is the problem of dealing with the singularity in the boundary-layer equations at the point of separation if the pressure is prescribed as a boundary condition in the usual direct method of calculation. Catherall and Mangler [1] demonstrated that these singularities at the separation and possible reattachment points can be removed by prescribing the displacement thickness or the wall shear-stress distribution in place of the pressure distribution. This is the so-called inverse boundary-layer method. It is obvious that massive separated regions (occurring, for example, on circular cylinders or on configurations with a blunt base) cannot be handled. Separated flows which still fit within the

^{*} National Institute for Aerospace Research "Elie Carafoli" - Bucharest

^{**} Institute of Applied Mathematics "Caius Iacob" - Bucharest

boundary - layer concept can, however, be dealt with. Here the term boundary-layer concept means that the normal pressure gradients are negligible and that the dividing streamline, which separates the reverse flow from the downstream direction moving flow, is reasonably close to the body surface.

Inverse methods for two-dimensional flows using integral approaches have been developed in the past, from 1973 onwards [2], [3], [4], [5], [6], [7], [8]. These methods have been classified into three categories [5]. All three use the standard Kármán momentum integral equation; it is the choice of the second integral equation that distinguishes one method from the other. Thus, the second equation can be : a moment of momentum equation [2] - [10], a kinetic energy equation [6], [7], [11] or an entrainment equation [12], [13]. The boundary - layer method described in this paper differs from the integral method previously cited in that it uses the well-known correlation between the Clauser (pressure-gradient) parameter β and the velocity-defect parameter G , as closure equation. This closure type is similar to that used in Das method [14].

The main advantage of the proposed method is the fact that it needs a minimal amount of computer storage and time, being suitable for practical design computations. The use of that approach in association with a calculation procedure for the inviscid flow is straight forward.

The details of this method will be described and compared with the test cases including both separating and reattaching flows.

2. CALCULATION METHOD

The turbulent boundary-layer calculation method presented herein is an inverse method for separated flow. The key feature of this method is the use of a new closure equation as the desired third relation. The method also uses an extension of the Coles' velocity profile family to include velocity profiles in separated flow. This allows for the development of auxiliary relations necessary for calculating turbulent boundary layers with separation.

2.1 VELOCITY PROFILE FAMILY AND AUXILIARY EQUATIONS

As velocity profile family, Coles family has been used for the present work. The Coles velocity are employed in an extended form [2] to describe unseparated and separated velocity profiles. The Coles profiles in the defect form including reversed flows are given by

$$\frac{U_e - U}{U_e} = 2V_B \cos^2\left(\frac{\pi}{2} \frac{y}{\delta}\right) - V_T \ln \frac{y}{\delta} \quad (1)$$

where $V_T = U_\tau / (kU_e) = |C_f| / (kC_f) \left(|C_f| / 2 \right)^{1/2}$,

$$V_B = U_\tau \Pi / (kU_e) = V_T \Pi, \quad k = 0.4$$

and Π is Coles' wake parameter.

Approaching separation, the quantity V_T tends to zero ($V_T \rightarrow 0$) at the same time, the wake parameter Π achieves infinite large values ($\Pi \rightarrow \infty$). In order to avoid numerical problems in this region, a new variable V_B has been defined, which stays finite even at separation ($V_B = 1/2$). A precise meaning can now be given to the terms separation and reattachment. They will be taken to be the points where the variable V_B is exactly 0.5. This improvement results in stable computations in the vicinity of separation.

The Coles velocity profiles provide the relationship for the skin friction by considering them for $y = \delta$,

$$\frac{1}{V_T} - \ln|V_T| = \ln\left(\frac{\delta U_e}{\nu}\right) + 2\frac{V_B}{V_T} + \text{const.} \quad (2)$$

Differentiation of the above equation with respect to the coordinate parallel to the wall, x , gives one wall-friction equation for V_T

$$\frac{d\delta}{dx} + \frac{2\delta}{V_T} \frac{dV_B}{dx} + \delta \left(\frac{1}{V_T^2} + \frac{1}{V_T} - 2\frac{V_B}{V_T^2} \right) \frac{dV_T}{dx} + \frac{\delta}{U_e} \frac{dU_e}{dx} = 0 \quad (3)$$

Using the definition of displacement thickness and integrating the velocity profile, Eq. (1), we obtain

$$\Lambda = \frac{\delta^*}{\delta} = V_T + V_B \quad (4)$$

Differentiating Eq. (4) and rearranging results in

$$\Lambda \frac{d\delta}{dx} + \delta \frac{dV_B}{dx} + \delta \frac{dV_T}{dx} = \frac{d\delta^*}{dx} \quad (5)$$

Now, the traditional momentum integral equation is converted to the variables V_T and V_B via the velocity profiles, Eq. (1). The resulting equation is

$$(\Lambda - D) \frac{d\delta}{dx} + (1 - D_P) \delta \frac{dV_B}{dx} + (1 - D_\sigma) \delta \frac{dV_T}{dx} + (3\Lambda - 2D) \frac{\delta}{U_e} \frac{dU_e}{dx} = k^2 V_T |V_T| \quad (6)$$

where

$$\begin{aligned}\Lambda &= V_T + V_B \\ D &= 1.5V_B^2 + 3.179V_B V_T + 2V_T^2 \\ D_p &= 3V_B + 3.179V_T \\ D_\sigma &= 4V_T + 3.179V_B\end{aligned}$$

2.2 PRESSURE GRADIENT - VELOCITY FORM FACTOR CORRELATION

Several empirical correlations to relate the velocity form factor

$$G = \left(\frac{\int_0^\delta [(U_e - U) / U_\tau]^2 dy}{\int_0^\delta [(U_e - U) / U_\tau] dy} = \frac{H-1}{H} \sqrt{\frac{2}{C_f}} \right) \quad \text{to Clauser's pressure gradient parameter}$$

$\beta \left(= \frac{\delta^*}{\tau_w} \frac{dp}{dx} \right)$ have appeared in the literature. Two $\beta - G$ relations are comparatively well known, one given by Mellor and Gibson [15] in tabular form, and the other given by Nash [16] explicitly as

$$G = 6.1(\beta + 1.81)^{1/2} - 1.7 \quad (7)$$

For the present work Mellor and Gibson's relation was approximated by an expression similar to Nash's but with different values of the numerical constants, namely

$$G = 5.8824(\beta + 0.8802)^{1/2} + 1.1108 \quad (8)$$

Initially Nash's expression was used, as it had proved very satisfactory in earlier work, but it became apparent that it did not agree with Cole's data for zero pressure gradient, nor did it give the best possible fit to what seemed the most reliable sets of measurements, namely those of Bradshaw [17] and Herring and Norbury [18].

Reference to Coles's paper [19] and Smith and Walker's experimental data [20] indicated that Nash's value of G ($= 6.5$) for zero pressure gradient was rather too low and Head and Galbraith [21] modified his $\beta - G$ relation so that it gave the best fit to measurements of Bradshaw and Herring and Norbury. This procedure gave the following expression

$$G = 4.8285(\beta + 1.0717)^{1/2} + 1.8438 \quad (9)$$

Comparison between three $\beta - G$ correlations and experimental values is shown in Fig. 1. Near separation β and G go to infinity and their inverse values $1/\beta$ and $1/G$ were plotted in the $(1/\beta, 1/G)$ - plane in Fig. 2. Fig. 2 suggests that the same curve can be used in the vicinity of separation, both before and after flow detaching. In the present work the expression of Nash, which gives values located between the other two curves, is used to relate the absolute values of β and G .

With $\beta - G$ relation established, the third equation can now be derived, which provides closure to our inverse method. From the definitions of the pressure gradient parameter and the velocity form factor we have

$$\beta = \frac{\delta^*}{|\tau_w|} \frac{dp}{dx} = - \frac{\delta^*}{|V_T| |V_T| k^2} \frac{1}{U_e} \frac{dU_e}{dx} \quad (10)$$

$$G = \frac{H-1}{H} \sqrt{\frac{2}{|C_f|}} = \frac{h}{k|V_T|}$$

where $h = 1.5\Lambda + 0.179V_T + 0.321V_T^2/\Lambda$

Note that the sign of β is governed by the sign of the pressure or velocity gradient. The absolute values of τ_w and C_f are used in Eqs. (10) so that the signs of β and G are not affected when separation occurs and τ_w , respectively C_f , changes sign.

Eliminating δ^* from Eq. (10) through Eq. (4) and substituting for β from the experimental correlation (7), one obtains

$$\frac{1}{U_e} \frac{dU_e}{dx} = -0.026974(G^2 + 3.4G - 64.46) \frac{V_T^2}{\delta\Lambda} \quad (11)$$

Equations (3), (5), (6) and (11) can be solved simultaneously for $\frac{d\delta}{dx}$, $\frac{dV_B}{dx}$, $\frac{dV_T}{dx}$ and $\frac{dU_e}{dx}$. The derivatives of δ , V_T and U_e are retained for the following reasons. Solving a differential equation in V_T will produce better results for wall shear or skin friction; a differential equation in δ will give better results for integral thickness and shape factor; and a differential equation in U_e will predict the boundary layer edge velocity correctly as necessary in an inverse method. Therefore, $\frac{dV_B}{dx}$ is eliminated in favor of the other derivatives using Eq. (3). Following this elimination, Eqs. (5) and (6) simplify to:

$$A_1 \frac{dV_T}{dx} + A_2 \frac{d\delta}{dx} + A_3 \frac{dU_e}{dx} = A_4 \quad (12)$$

$$B_1 \frac{dV_T}{dx} + B_2 \frac{d\delta}{dx} + B_3 \frac{dU_e}{dx} = B_4 \quad (13)$$

Equation (11) can be viewed in the same form as Eqs. (12) and (13), where the first two coefficients are zero and the right side of Eq. (11) can be denoted as C_4 .

There are now three ordinary differential equation Eqs. - (11), (12), and (13) - which can be solved simultaneously for three variables - V_T , δ and U_e - after applying Cramer's rule.

The origin of these three relations are:

- momentum equation, displacement thickness equation and $\beta - G$ equation.

$$\begin{bmatrix} A_1 & A_2 & A_3 \\ B_1 & B_2 & B_3 \\ 0 & 0 & 1 \end{bmatrix} \begin{bmatrix} \frac{dV_T}{dx} \\ \frac{d\delta}{dx} \\ \frac{dU_e}{dx} \end{bmatrix} = \begin{bmatrix} A_4 \\ B_4 \\ C_4 \end{bmatrix} \quad (14)$$

After solving them at each spatial step in the streamwise direction, the fourth variables V_B is obtained from the displacement thickness relation Eq. (4),

$$V_B = \delta^* / \delta - V_T \quad (15)$$

and the skin friction coefficient follows from

$$C_f = 2k^2 V_T |V_T|.$$

Once V_T , δ , U_e and V_B are computed at any streamwise location, computing the momentum thickness θ and then the shape factor is straightforward. Integration of the velocity profile (1) yields

$$\theta = \delta^* - \delta (2V_T^2 + 3.1786V_TV_B + 1.5V_B^2) \quad (16)$$

2.3 COMPUTATIONAL SCHEME

It is convenient to nondimensionalize the final working equations before applying them to a set of experiments. This transformation helps free the computations from dependence of any particular unit. For this, the following dimensionless variables have been selected

$$\bar{X} = \frac{X}{L}, \bar{V} = \frac{U_e}{U_0}, \bar{\delta} = \frac{\delta}{L}, \bar{\delta}^* = \frac{\delta^*}{L}, \bar{\theta} = \frac{\theta}{L} \quad (17)$$

where L is reference length, usually length of the body, and U_0 is a reference velocity, usually the velocity at entrance.

The three first-order nonlinear ordinary differential equations (ODE) can be solved using any ODE solver to obtain V_T , $\bar{\delta}$ and \bar{V} . Notice that a direct output of this solution is V_T , the skin friction parameter that determines the skin friction coefficient via $C_f = 2k^2 V_T |V_T|$. Thus, our method yields separation and reattachment points directly where the skin friction vanishes, while the Karman-type integral methods must resort to correlations of shape factor and momentum thickness to infer separation.

3. COMPARISONS WITH EXPERIMENTS

The parameters that are important for comparison with experimental data are: velocity V , skin friction C_f , and momentum thickness $\bar{\theta}$. The distribution of displacement thickness $\bar{\delta}^*$, which is the input to our method, will also be shown for each test case.

A Separated Flow: Figure 3 presents the results for the separated flow of Simpson et al. [22]. The overall predictions for all parameters are quite good. There are slight deviations in the momentum thickness curve, after separation, being not an outcome of the solution of our ODEs, but rather, it is calculated as a byproduct from the algebraic Eq. (16).

Flow Separation on a Cylinder: Figure 4 presents results for the boundary layer separation on a cylinder in axially symmetric flow conducted by Moses [23]. Since the flow is axisymmetric, and our theory is two-dimensional, slight deviations in skin friction and pressure coefficient curves are observed in the beginning. However, all other parameters show quite good agreement with experimental data. Pressure measurements had been reported well into the separation region, and the pressure coefficient prediction looks excellent in the separated region.

Flow with Separation Bubble: Figures 5 and 6 present results for two flows (different Reynolds number) with separation bubble [24]. These two flows differ from the other cases in that they entail boundary layer separation and subsequent reattachment on a curved surface. Simulations of these two flows are much more complex than the ones already discussed, because the theory should be able to handle both the separation and the reattachment regions. The computation must be carried through the separation bubble into the reattachment region. The experimental data are presented as surface shear stress τ_w instead of skin friction C_f . We compared our theory against this parameter. Our prediction of τ_w is good in the increasing region, but it somewhat overpredicts the data in the

decreasing region due to inadequate input of the distribution of displacement thickness. Very few data are available for displacement thickness in that region, even though the flow is undergoing transformation from acceleration to deceleration in that region. There are seven τ_w data points available before $\bar{X} = 0.1$, but only three δ^+ data points are available from the experiment in the same region. One must input sufficient points to accurately capture the sharp rise and fall of τ_w that occurs in this very narrow region. However, the overall trend of τ_w computation matches with the experiment. Separation and reattachment (denoted as S and R in figures) agree very closely with the experimental results. The experimental separation points for these two flows are at $X = 0.4978\ m$ and $X = 0.447\ m$ respectively, and our computed separation points are at $X = 0.504\ m$ and $X = 0.468\ m$, respectively. Similarly, the experimental reattachment points are at $X = 1.006\ m$ and $X = 0.986\ m$, respectively, whereas our method computes reattachment at $X = 1.086\ m$ and $X = 1.022\ m$, respectively. The overall prediction for \bar{V} and $\bar{\theta}$ are very good. In addition to the test cases just discussed, we have tested the method against a variety of separated and reattached flows. All results have shown good agreement with experimental data.

4. CONCLUSIONS

A practical integral method has been presented for computing separated and reattached turbulent boundary layer flows. Relative to earlier methods, the new inverse formulation has the advantages that it is based on an improved pressure gradient. Velocity defect friction correlation valid for attached and separated flows, replaces the unstable wake parameter Π with the stable parameter V_B and is simpler to apply. The method may be attractive due to its low computing time and costs.

REFERENCES

1. D.CATHERALL, K.W.MANGLER, *The integration of the two-dimensional laminar boundary-layer equations past the point of vanishing skin friction*, Journal of Fluid Mechanics, **26** (1966).
2. G.D.KUHN, J.N.NIELSEN, *Prediction of turbulent separated boundary layers*, AIAA Journal, **12**, 7(1974).
3. J.C. LE BALLEUR, J. MIRANDE, *Étude expérimentale et théorique du recollement bidimensionnel turbulent incompressible*, ONERA TP 1975-16(1975).
4. J.E. CARTER, S.F. WORNOM, *Solution for incompressible separated boundary layers including viscous-inviscid interaction*, NASA SP-347, 1975.
5. T. CEBECI, *An inverse boundary-layer method for compressible laminar and turbulent boundary layers*, Journal of Aircraft, **13**(1976).

6. G.M.ASSASSA, K.D. PAPAILIOU, *An integral method for calculating turbulent boundary layer with separation*, Journal of Fluids Engineering, **110**, 3(1979).
7. D.L. WHITFIELD, T.W. SWAFFORD, J.L. JACOBS, *Calculation of turbulent boundary layers with separation and viscous-inviscid interaction*, AIAA Journal, **19**(1981).
8. D.K. DAS, F.M. WHITE, *Integral skin friction prediction for turbulent separated flows*, Journal of Fluids Engineering, **108**, 4(1986).
9. S.J. KLINE, B.J. CANTWELL, G.M. LILLEY (eds.), *Proceedings of the 1980-81, AFOSR-HTTM-Stanford Conference on Complex Turbulent Flows: Comparison of Computation and Experiment*, Stanford University, CA(1981).
10. P.M. GERHART, *An integral method for predicting subsonic turbulent separating boundary layers with specified free stream input*, Turbulent Boundary Layers, ASME Fluids Engineering Conference (1970).
11. H.L. MOSES, S.B. THOMASON, R.R. JONES, *Simultaneous solution of the inviscid flow and boundary layers for compressor cascades*, AIAA Journal, **20**, 10(1982).
12. J. BARDINA, A. LYRIO, S.J. KLINE, J.H. FERZIGER, J.P. JOHNSTON, *A prediction method for planar diffuser flows*, Journal of Fluids Engineering, **103**, 3(1981).
13. H.W. STOCK, *An inverse boundary-layer method for turbulent flows on infinite swept wings*, Zeitschrift für Flugwissenschaften und Weltraumforschung, **2**, 1(1988).
14. D.K. DAS, *An inverse inner-variable theory for separated turbulent boundary layers*, Journal of Fluids Engineering, **114**, 4(1992).
15. G.L. MELLOR, D.M. GIBSON, *Equilibrium turbulent boundary layers*, Journal of Fluid Mechanics, **24**(1966).
16. J.F. NASH, *Turbulent boundary layer behaviour and the auxiliary equation*, ARC Current Paper 835 (1965).
17. P. BRADSHAW, *The turbulent structure of equilibrium turbulent boundary layers*, Journal of Fluid Mechanics, **29**(1967).
18. H.J. HERRING, J.F. NORBURY, *Some experiments on equilibrium turbulent boundary layers in favorable pressure gradients*, Journal of Fluid Mechanics, **27**(1967).
19. D. COLES, *The law of the wake in the turbulent boundary layer*, Journal of Fluid Mechanics, **1**(1956).
20. D.W. SMITH, J.H. WALKER, *Skin friction measurements in incompressible flow*, NASA TR R-26 (1959).
21. M.R. HEAD, R.A. McD. GALBRAITH, *Eddy viscosity and entrainment in equilibrium boundary layers*, Aeronautical Quarterly **26**, 4(1975).

-
22. R.L. SIMPSON, Y.T. CHEW, B.G. SHIVAPRASAD, *The structure of a separating turbulent boundary layer, Part I. Mean flow and Reynolds stresses*, Journal of Fluid Mechanics, **113**(1981).
23. D.E. COLES, E.A. HIRST, *Computation of turbulent boundary layers - 1968 AFOSR-IFP-Stanford Conference*, Vol.II, Stanford University (1968).
24. J.M. SERPA, R.C. LESSMANN, W.M. HAGIST, *Turbulent separated and reattached flow over a curved surface*, Journal of Fluids Engineering, **109**, 4(1987).

Fig.1 Comparison between three $\beta - G$ correlations and experimental values.

Fig. 2 $\beta - G$ correlations near separation.

Fig.3 Comparison between theoretical and experimental results for the flow of Simpson et al. [22].

Fig.4 Comparison between theoretical and experimental results for the flow of Moses [23].

Fig.5 Comparison between theoretical and experimental results for the flow of Serpa et al. [24],

Flow 1.

Fig.6 Comparison between theoretical and experimental results for the flow of Serpa et al. [24],

Flow 2.

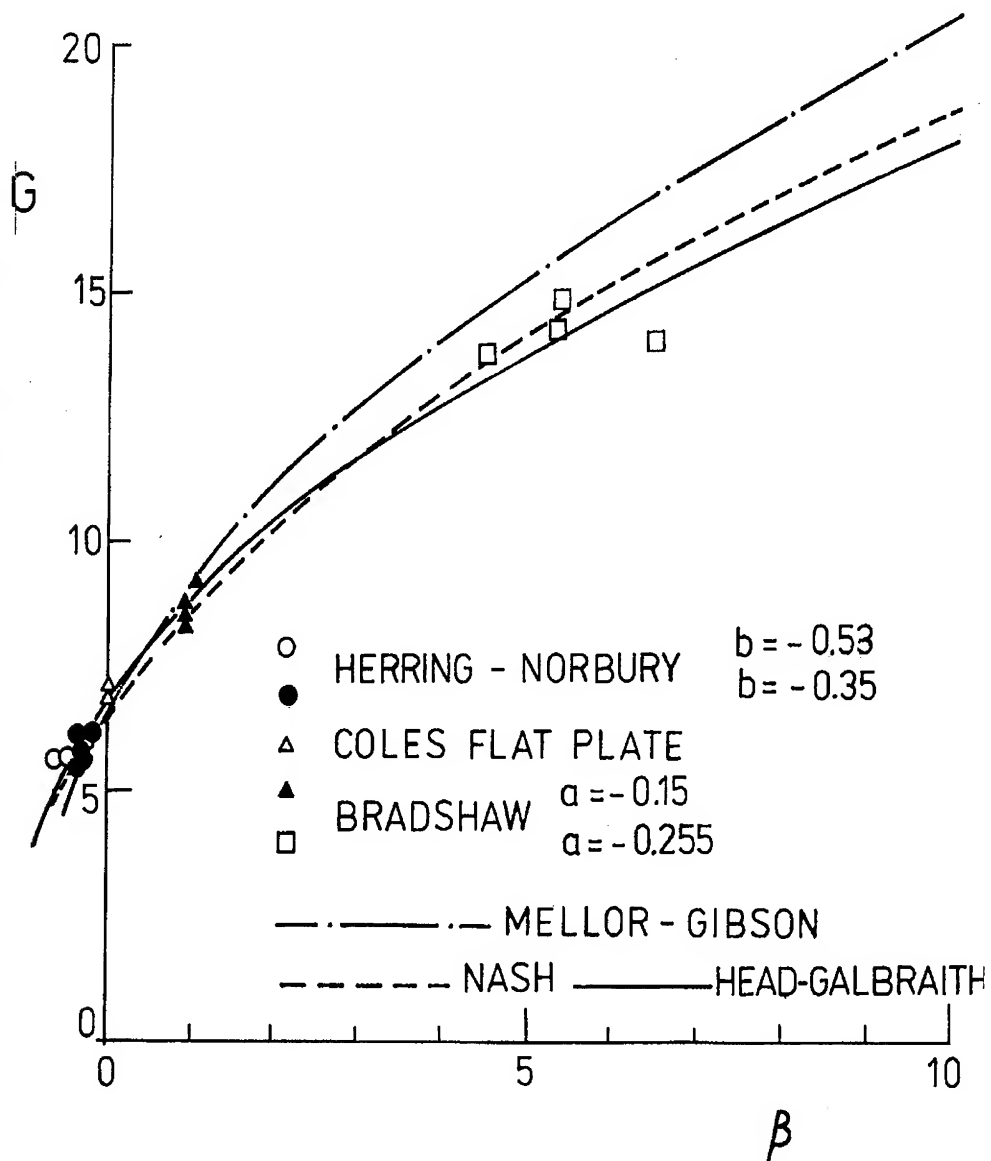


Fig. 1

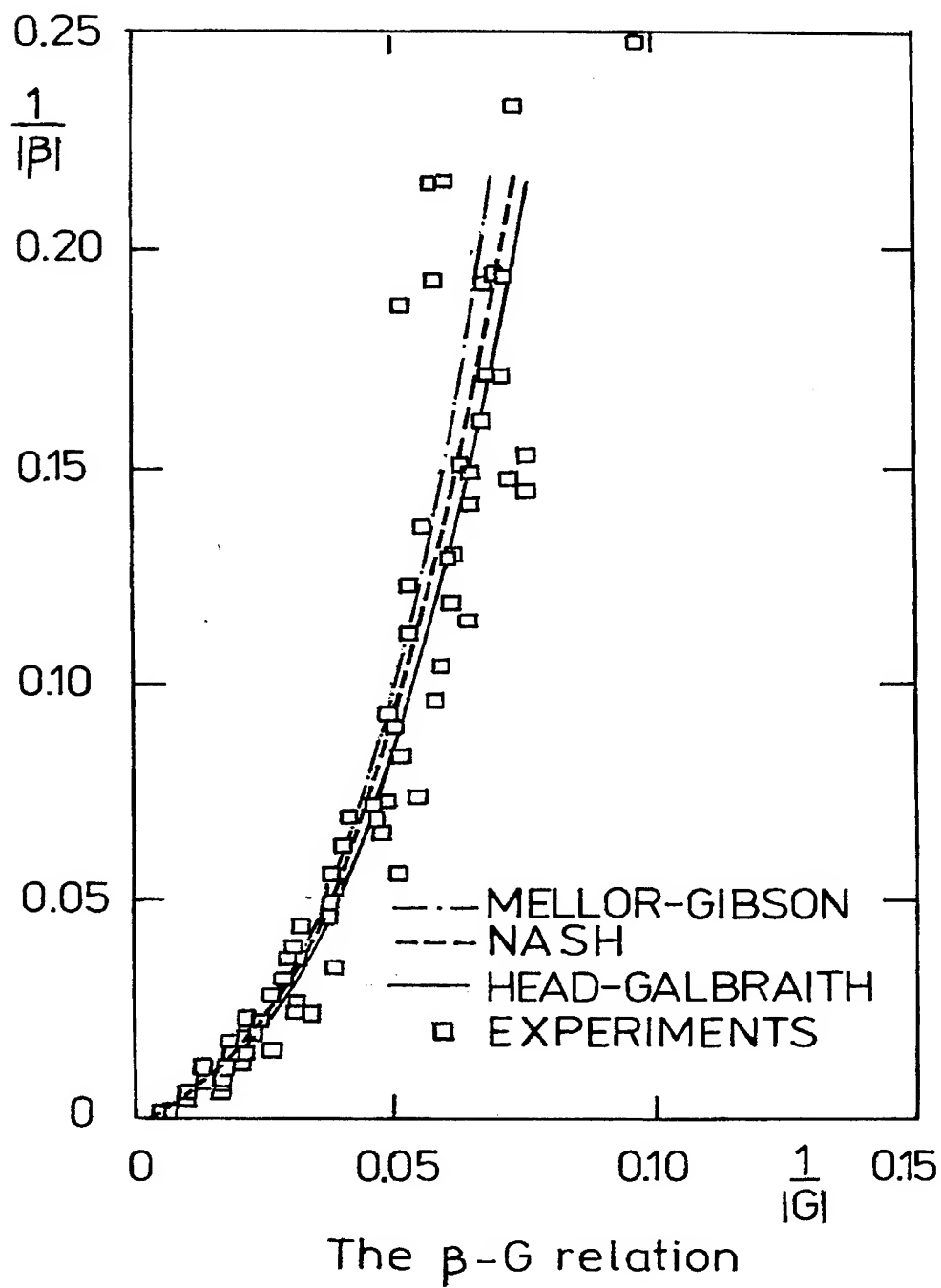
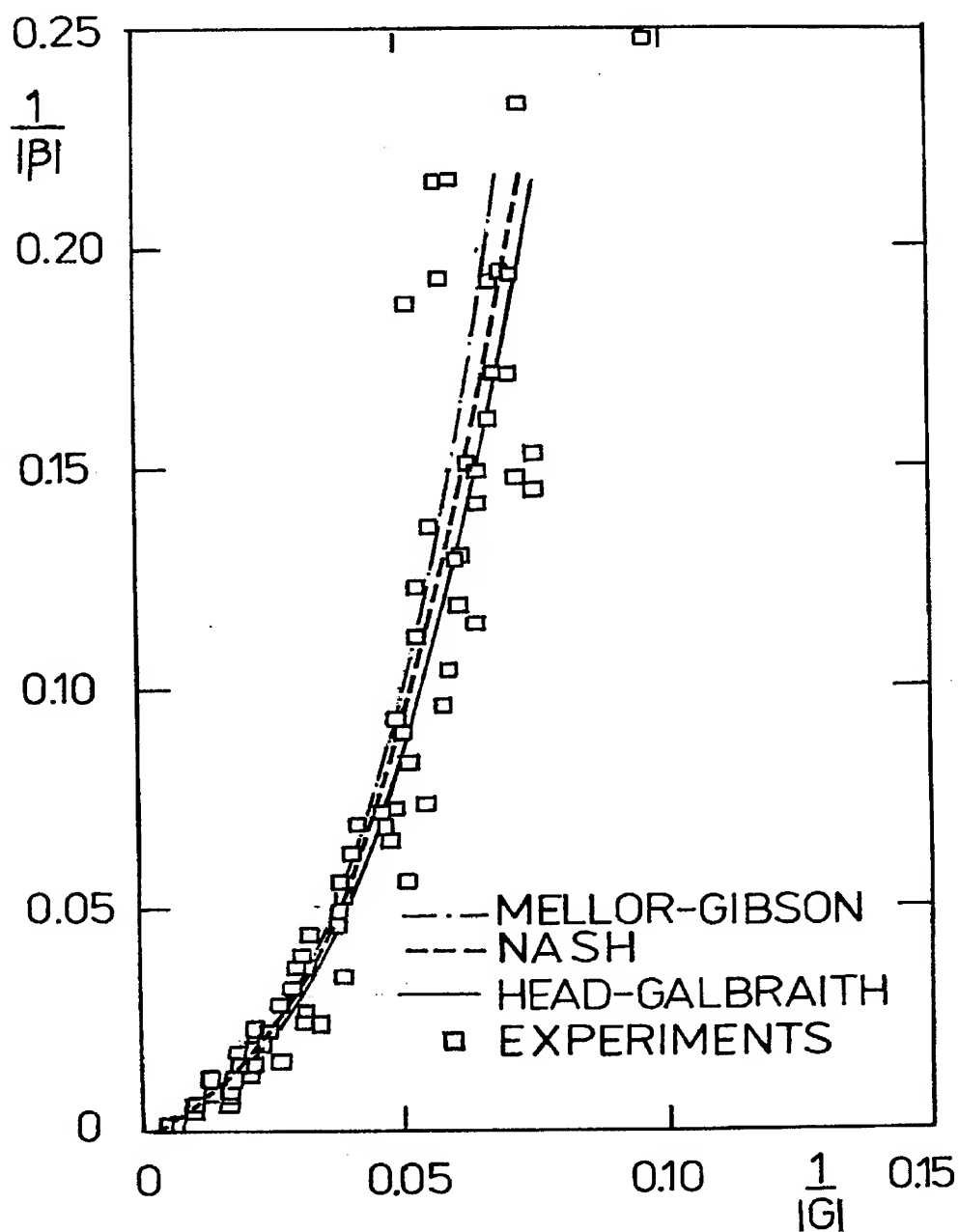


Fig. 2



The β -G relation

Fig. 2

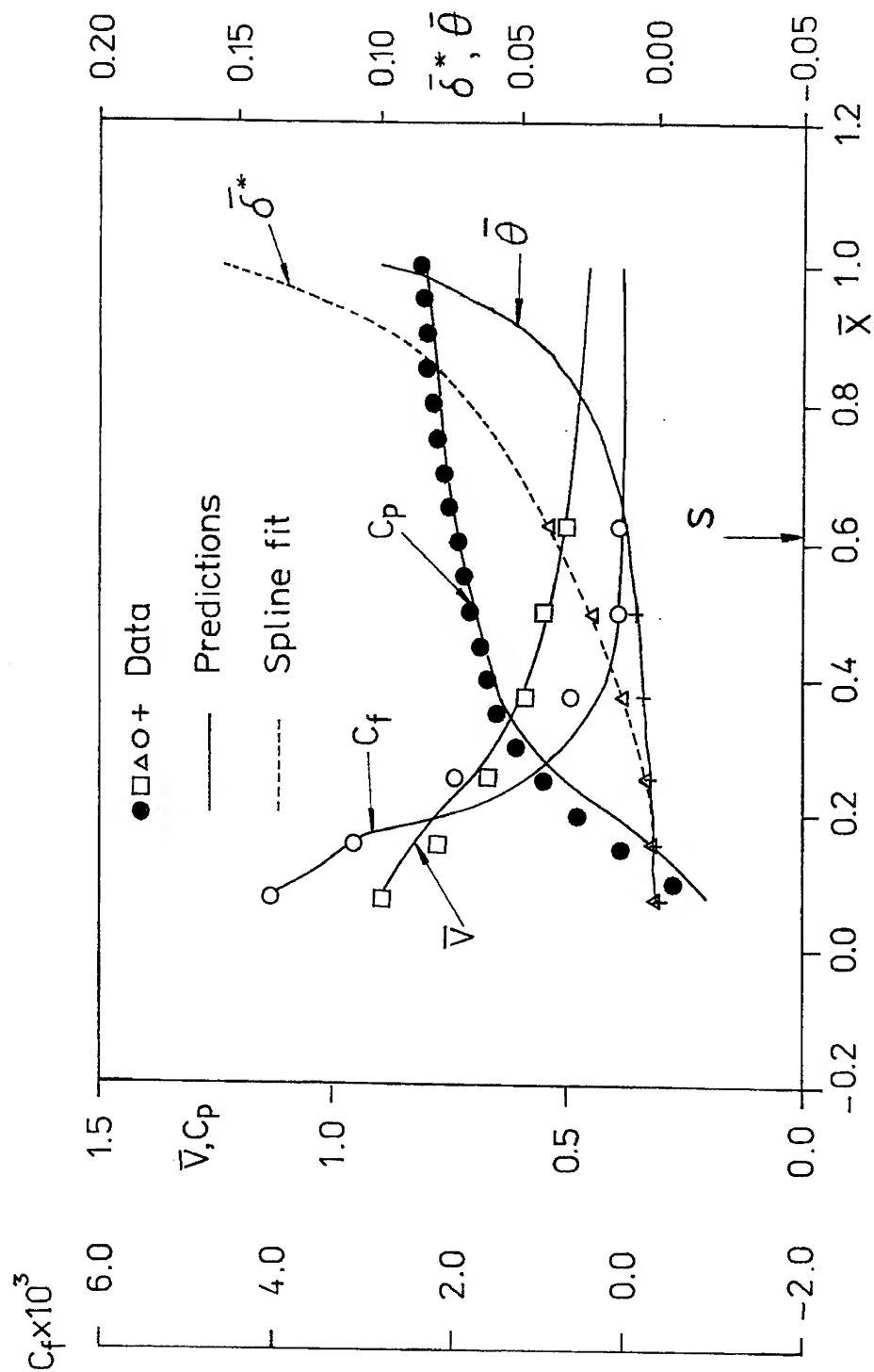


Fig. 4

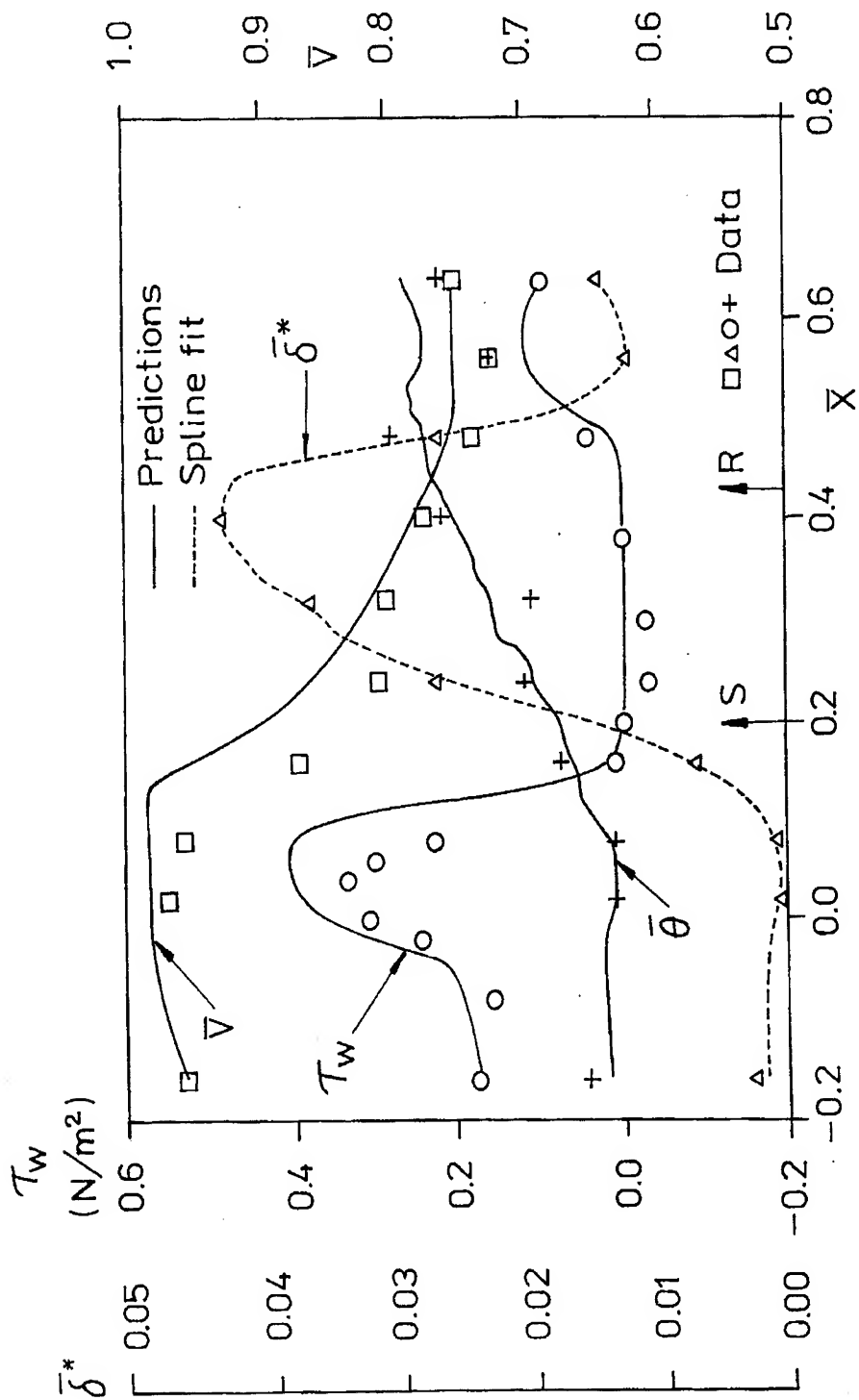


Fig. 5

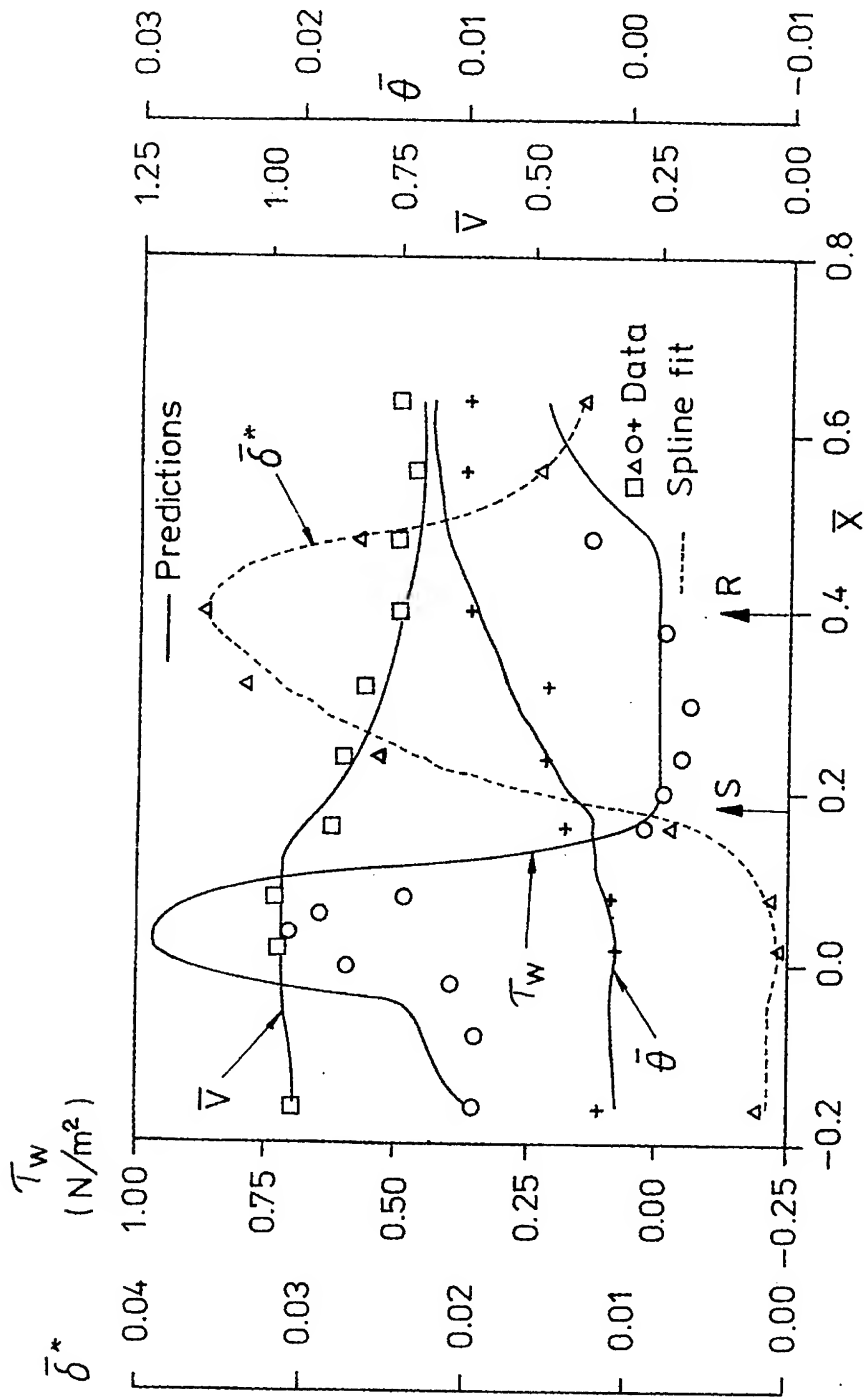


Fig 6

ITERATIVE ASPECTS in NONLINEAR DYNAMICAL SYSTEMS with CHAOTIC BEHAVIOUR

prof. Alexandru Serbanescu*
lt. eng. Petrica Ciotirnae*
eng. Vasile Eugen**

*) Military Technical Academy, Bd. Regina Maria, 81-83, Bucharest, Romania
**) Research and Development National Institute of Microtechnology

Abstract - The first purpose of this paper is to present our experience in non-linear dynamical systems with chaotic behaviour approach according to a system conception. In the second part, the main problems that appear in transmission on chaotic carrier are reported. The dead-beat synchronization, or exact synchronization in finite time is presented. We propose control methods for chaotic synchronization in uniformly connected systems. In the last part of the paper some chaotical behaviour in semiconductor devices are reported.

1. Introduction in Nonlinear Dynamical Systems

In the electrical engineering community, in recent years, much interest has been devoted to the study of the dynamics of circuits and systems that exhibit a chaotic behaviour.

A **dynamical system** is one which changes with time; what change is the state of the system. Mathematically, a dynamical system consists of a space of states (called the state space or phase space) and a rule, called the dynamic for determining which state corresponds at a given future time to a given present state. A deterministic dynamical system is one whose state at any time is completely determined by its initial state and dynamic. It may have a continuous or discrete state space and a continuous-time or discrete-time dynamic [1].

A **continuous-time dynamical system** can be defined by a system of ordinary differential equations of the form:

$$\dot{\mathbf{X}}(t) = \mathbf{F}(\mathbf{X}(t), t) \quad (1.1)$$

where $\mathbf{X}(t) \in \mathbb{R}^n$ is called the state, $\mathbf{X}(t_0) = \mathbf{X}_0$ denotes the initial condition and the map $\mathbf{F}(\cdot, \cdot): \mathbb{R}^n \times \mathbb{R}_+ \rightarrow \mathbb{R}^n$ is continuous almost everywhere on $\mathbb{R}^n \times \mathbb{R}_+$ and globally Lipschitz. Then, for each $(\mathbf{X}_0, t_0) \in \mathbb{R}^n \times \mathbb{R}_+$, there exists a continuous function $\varphi(\cdot; \mathbf{X}_0, t_0): \mathbb{R}_+ \rightarrow \mathbb{R}^n$ such that $\varphi(t_0; \mathbf{X}_0, t_0) = \mathbf{X}_0$ and

$\dot{\varphi}(t; \mathbf{X}_0, t_0) = \mathbf{F}(\varphi(t; \mathbf{X}_0, t_0), t)$. The function $\varphi(\cdot; \mathbf{X}_0, t_0)$ is called the solution or trajectory through (\mathbf{X}_0, t_0) of the differential equation (1.1).

The vector field \mathbf{F} of a dynamical system generates a flow that maps a point in the state space to its image after t seconds. If the vector field \mathbf{F} of a continuous-time deterministic dynamical system depends only on the state and is independent of time t , then the system is said to be autonomous and may be written as: $\dot{\mathbf{X}}(t) = \mathbf{F}(\mathbf{X}(t))$ or, simply: $\dot{\mathbf{X}} = \mathbf{F}(\mathbf{X})$.

A **discrete-time dynamical system** is defined by a system of difference equations of the form:

$$\mathbf{X}(k+1) = \mathbf{G}(\mathbf{X}(k), k) \quad (1.2)$$

where $\mathbf{X}(k) \in \mathbb{R}^n$ is called the state, $\mathbf{X}(k_0) = \mathbf{X}_0$ is the initial condition, and $\mathbf{G}(\cdot, \cdot): \mathbb{R}^n \times \mathbb{Z}_+ \rightarrow \mathbb{R}^n$ maps the current state $\mathbf{X}(k)$ into the next state $\mathbf{X}(k+1)$, where $k_0 \in \mathbb{Z}_+$. By analogy with the continuous-time case, the function $\varphi(\cdot; \mathbf{X}_0, t_0): \mathbb{Z}_+ \rightarrow \mathbb{R}^n$ such that $\varphi(k_0; \mathbf{X}_0, k_0) = \mathbf{X}_0$ and $\varphi(k+1; \mathbf{X}_0, k_0) = \mathbf{G}(\varphi(k; \mathbf{X}_0, k_0), k)$ is called the solution or the trajectory through (\mathbf{X}_0, k_0) of difference equation (1.2). The image $\{\varphi(k; \mathbf{X}_0, k_0) \in \mathbb{R}^n | k \in \mathbb{Z}_+\}$ in \mathbb{R}^n of the trajectory through (\mathbf{X}_0, k_0) is called an orbit through (\mathbf{X}_0, k_0) . If the map of the discrete-time dynamical system depends only on the state $\mathbf{X}(k)$, and is independent of k , then the system is said to be autonomous and may be written more simply as:

$$\mathbf{X}(k+1) = \mathbf{G}(\mathbf{X}(k)) \text{ where: } \mathbf{G}(\cdot): \mathbb{R}^n \rightarrow \mathbb{R}^n.$$

A trajectory of a dynamical system from an initial state \mathbf{X}_0 settles, possibly after some transient, onto a set of points called a limit set. The limit set corresponds to the asymptotic behaviour of the system as $t \rightarrow +\infty$ and is called the steady state response. From an experimentalist's point of view chaos may be defined as a bounded steady-state behaviour which is not an equilibrium point, not periodic and not quasiperiodic. The local behaviour of the vector field along a trajectory $\varphi_t(\mathbf{X}_0)$ of an autonomous continuous-time dynamical system is governed by the linearized dynamics: $\dot{\mathbf{x}} = \mathbf{D}_x \mathbf{F}(\varphi_t(\mathbf{X}_0))\mathbf{x}$. This is a linear time-varying system whose state transition matrix $\Phi_t(\mathbf{X}_0)$ maps a point \mathbf{x}_0 into $\mathbf{x}(t) = \Phi_t(\mathbf{X}_0)\mathbf{x}_0$. Note that Φ_t is a linear operator. The singular values $\sigma_1(t) > \sigma_2(t) > \dots > \sigma_n(t)$ of Φ_t are defined as the square roots of the eigenvalues of $\Phi_t^H \Phi_t$, where Φ_t^H is the complex conjugate transpose of Φ_t . The stability of a steady-state orbit is governed by the average local rates

of expansion and contraction of volumes of the state-space close to the orbit. The Liapunov (LE) exponents λ_i are defined by $\lambda_i = \lim_{t \rightarrow \infty} \frac{1}{t} \ln \sigma_i(t)$, whenever this limit exists. The LEs are a property of a steady-state trajectory. The set $\{\lambda_i, i = 1, 2, \dots, n\}$ is called the Liapunov spectrum. The Liapunov spectrum may be used to identify attractors, as summarized in Table 1.

Table 1.

Steady state	Limit set	Spectrum	LEs	Dimension
DC	fixed point	spike at DC	$0 > \lambda_1 \geq \dots \geq \lambda_n$	0
Periodic	closed curve	fundamental plus integer harmonics	$\lambda_1 = 0$ $0 > \lambda_2 \geq \dots \geq \lambda_n$	1
Quasiperiodic	K-torus	incommensurate frequencies	$\lambda_1 = \dots \lambda_K = 0$ $0 > \lambda_{K+1} \geq \dots \geq \lambda_n$	K
Chaotic	fractal	broad spectrum	$\lambda_1 > 0$ $\sum_{i=1}^n \lambda_i < 0$	non-integer

Many non-linear dynamical systems in various fields have been clarified to exhibit chaotic oscillations and recently applications of chaos to engineering systems attract many researchers' attentions.

There are at least two reasons for studding unstable and chaotic circuits. Taking the traditional view that instability is unacceptable, it is important to know if this sort of behaviour can be present in an experimental situation in order to avoid it. From a more optimistic view, if a mode of operation is well understood and clarified, it can be of engineering use. The understanding of a chaotic behaviour opens new possibilities of operating regimes that can help to optimise design.

Electronic circuits exhibiting chaotic behaviour can be exploited as a basic components of emerging classes of complex dynamic electronic networks and systems, including cellular networks and secure communication systems based on chaos synchronization.

Cellular neural networks (CNN) are non-linear continous computing-array structures well suited for non-linear signal processing. A CNN is a high dimensional dynamic non-linear system having a local interconnection of simple circuits units called cells, or artificial neurones.

2. COMMUNICATION ON CHAOTIC CARRIER

We try to use chaotic signals to transmit information on a chaotic carrier. The motivation for this is the privacy of the communication and the advantages to transmit a broadband signal. The purposes of this procedure are to broaden the spectrum of the transmitted signal (to protect against electro-magnetical perturbations) and to hide the information in the chaotic signal. To assure all of these we use a master-slave configuration adapted to communication systems. In order to receive the transmitted signal, it is necessary to synchronize the sender and the receiver. We consider a set-up where a master system drives a slave system in order to impose its wave forms. This situation is depicted schematically in Fig. 2.1.

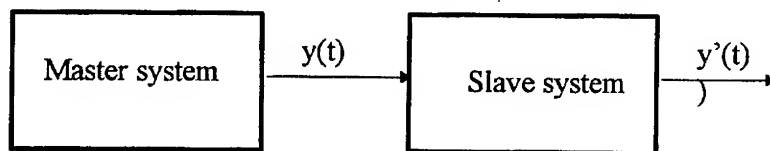


Fig. 2.1. Master-slave configuration adapted to communication systems.

Both systems should be thought of as being dynamical and non-linear. In general, the slave system closely resembles the master system. The transmitted signal $y(t)$ may have the effect to force the output $y'(t)$ of the slave system to copy its wave form [5]. The signal $y(t)$ represents the only interaction between the two systems and the initial state of the two systems is not co-ordinated. The time evolution of dynamic system depends on its initial state, so we cannot expect $y'(t)$ to be identical to $y(t)$. If the time $t \rightarrow \infty$ the influence of the initial state can be expected to fade away. So we can construct the follow definition for synchronization between our two systems:

The slave system synchronizes with the master system if $|y'(t) - y(t)| \rightarrow 0$ when $t \rightarrow \infty$, for any combination of initial states of the master and slave system. Usually, the notion of **synchronization** is used for periodic signals, in our case it means that, asymptotically, $y'(t)$ copies the irregular behaviour of $y(t)$. A chaotic system has sensitive dependence on initial conditions [4]. This means that even if the two system in Fig. 2.1 are perfectly identical, and if they are started at almost identical states, after some time, the two time evolution become completely uncorrelated and definition is far from being satisfied. This is the case as long as the two systems do not interact. But if the interaction between master and slave exist, the interaction may be able to force synchronization.

2.1 Discrete-Time Synchronization

Consider a second order chaotic system, represented by the following equations [3]:

$$x_1(k+1) = 1 - \alpha x_1^2(k) + x_2(k) \quad (2.1.a)$$

$$x_2(k+1) = \beta x_1(k) \quad (2.1.b)$$

System exhibit chaotic behaviour in a large neighbourhood of the parameter values $\alpha = 1.4$ and $\beta = 0.3$.

We assume the system (2.1) to be the transmitter and we select its output as:

$$y(k) = 1 - \alpha x_1^2(k) \quad (2.2)$$

The receiver is then defined by:

$$\hat{x}_1(k+1) = \hat{x}_2(k) + y(k) \quad (2.3.a)$$

$$\hat{x}_2(k+1) = \beta \hat{x}_1(k) \quad (2.3.b)$$

From (2.1)-(2.3), the synchronization error $\Delta x_i(k) = \hat{x}_i(k) - x_i(k)$ is governed by:

$$\Delta x_1(k+1) = \Delta x_2(k) \quad (2.4.a)$$

$$\Delta x_2(k+1) = \beta \Delta x_1(k) \quad (2.4.b)$$

so tending to zero for $|\beta| < 1$.

2.2 Synchronization in Composite Chaotic Systems

Many secure communication methods using chaotic synchronization are developed now. Composite systems and non-linear networks exhibit various non-linear phenomena such bifurcation and chaotic behaviour. It is impossible to synthesis a composite system such that some specified subsystems are synchronized and other subsystems are not, and for solving this problem feedback control is very useful [2].

We consider uniformly connected discrete-time composite systems with additive interactions; N is the number of subsystems, we assume that all have same dynamically characteristics and each subsystem S_i ($i=1,2,\dots,N$) is described as follows:

$$x_i(k+1) = f[x_i(k)] + g[x_1(k), x_2(k), \dots, x_N(k)] + bu_i(k) \quad (2.5)$$

where $x_i(k)$ is the local state of S_i , f represent non-linear characteristic of each subsystems and g represent the effect of interaction.

A control objective is to synchronize subsystems $S_{j1}, S_{j2}, \dots, S_{jm}$ chaotically in (2.5).

2.3 Application to Secure Communications Systems

This section deals a synthesis of a secure communication between subsystems S_1 and S_2 using chaotically synchronizing control. Each subsystem consists a synchronization part, a modulation part and a demodulation part as shown in Fig. 2.2.

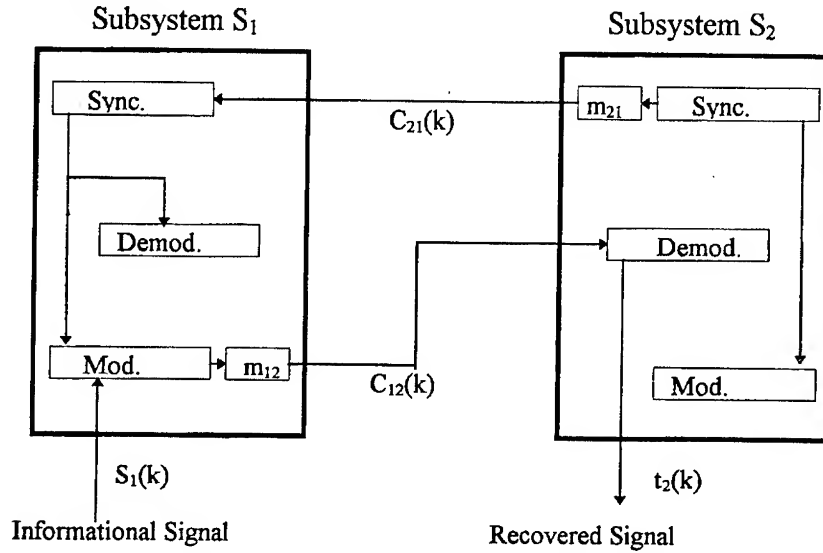


Fig. 2.2. Secure communication system.

Each part is described as follows:

- Synchronization part:

$$x_i(k+1) = f[x_i(k)] + bu_i(k)$$

- Modulation part:

$$z_i(K+1) = g[x_i(k), z_i(k), w_i(k)] + \varepsilon s_i(k+1)$$

$$w_i(k+1) = p[x_i(k), w_i(k)] + \eta z_i(k)$$

- Demodulation part:

$$t_i(k) = \frac{v_i(k) - p[x_i(k-1), v_i(k-1)]}{\eta}$$

$$r_i(k) = \frac{t_i(k) - g[x_i(k-2), t_i(k-1), v_i(k-2)]}{\varepsilon}$$

Since the transmitted signals $c_{12}(k)$ and $c_{21}(k)$ may be observed by someone, it is very important that the informational signal $s_i(k)$ can not be recovered from them.

3 CHAOS in SEMICONDUCTOR DEVICES

3.1 A dynamical system analysis for a photoconductor

Taking into account the transport and relaxation (i.e. generation-recombination) phenomena in an extrinsic P-type semiconductor photoresistor, assuming the spatial uniformity conditions (in the simplest case of a bar with the length L) [6], two differential equations are describing the dynamics of both (local) the p hole concentration and the E electrical field strength; in any given spatial position in the device we have:

$$\begin{aligned} dp/dt &= \gamma \cdot N_{A0} + p \cdot (k \cdot N_{A0} - r \cdot N_{A*}) \\ dE/dt &= (1/\epsilon) \cdot (J - p \cdot q_0 \cdot v_d) \end{aligned}$$

where:

N_A = the acceptor concentration	γ = the optical irradiation coefficient
N_D = the donor concentration	k = the impact ionisation coefficient
N_{A0} = the neutral acceptor concentration	r = the recombination coefficient
N_{A*} = the ionised acceptor concentration	ϵ = the dielectric constant
$N_{A*} = N_A - N_{A0}$	q_0 = the elementary charge
$v_d = \mu_p \cdot E$ = the drift velocity of holes with μ_p mobility	

J is the electrical current density considered here as a drive quantity in order to avoid the electrical external circuit relations. Assuming the local electric charge neutrality we have: $N_D + p - N_{A*} = 0$.

The equations determine both the steady-state response and the dynamic response of the extrinsic photoconductor. In accordance with the dynamical system theory we shall consider the state vector $\mathbf{X} = (p, E)$ and we have the associated dynamical system $d\mathbf{X}/dt = \mathbf{g}(\mathbf{X}, t)$, that is bidimensional and non-autonomous because by modulated light it has $\gamma = \gamma(t)$. At the end the system is:

$$\begin{aligned} dp/dt &= -[A(E) \cdot p^2 + B(E) \cdot p + C(E)] \\ dE/dt &= (1/\epsilon) \cdot [J - q_0 \cdot \mu_p(E) \cdot E \cdot p] \\ A &= k(E) + r(E) \\ B &= \gamma(t) + r(E) \cdot N_D + k(E) \cdot N; \quad N = N_D - N_A \\ C &= \gamma(t) \cdot N \end{aligned}$$

The dependences of the ionisation, recombination and mobility coefficients on the electric field have been mentioned. One can neglect these dependencies at weak electric fields.

The numerical simulation by time discretisation shows how fast the system goes towards the steady state by a step type drive function $\gamma(t)$, when the system becomes autonomous. In other specific drive conditions a chaotic behaviour might appear. In each case the evolution, after an iteration number

T , is appreciated by the variation of the informational entropy regarding the system state:

$$\Delta S = (T / \ln 2) \lambda(\mathbf{X}_0)$$

where $\lambda(\mathbf{X}_0)$ is the Liapunov index calculated for the initial state \mathbf{X}_0

$$\lambda(\mathbf{X}_0) = (1/T) \cdot \sum_{n=0, T} \ln |J(\mathbf{X}_n)|$$

where J is the Jacobian of the transformation: $\mathbf{X}_{n+1} = F(\mathbf{X}_n)$ resulted by temporal discretisation.

A big complication appears when the photoconductor is not spatially uniform (as it is in the case of junction devices); in this case: $p = p(x)$, $E = E(x)$, $0 < x < L$ and the dynamical system is infinite-dimensional with great numerical calculus difficulties.

3.2 Nonlinearities in semiconductor diodes

Detailed measurements have been performed [7] in the RLC series oscillator circuit having as non-linear element the semiconductor diode. The differential equation of this problem is:

$$L d^2 q / dt^2 + R \cdot dq / dt + V = A \cdot \sin \omega t$$

where q is the electrical charge and $V = q/C(V)$ is the voltage across the diode capacitance $C = C_d + C_b$, including both the diffusion C_d and the barrier C_b capacitance.

At forward bias, the diffusion capacitance $C_d(V, \tau) = C_{d0}(\tau) \cdot \exp(V/V_T)$ dominates; τ is the minority carriers life time and V_T is the thermal voltage.

At reverse bias the barrier capacitance C_b dominates.

$$C_b(V) = C_{b0} \cdot (1 - V/\Phi)^{-1/(m+2)} \quad \begin{array}{l} m = 1 \text{ for linearly graded junction,} \\ m = 0 \text{ for abrupt junction} \end{array}$$

$$-2 < m < 0 \text{ for hyperabrupt junction (varicap)}$$

The associated dynamical system has as state vector $\mathbf{X} = [q, dq/dt]$. The above mentioned experiment has been repeated with the varicap diode BB-125 manufactured by Baneasa S.A., in a circuit with $R = 47 \Omega / 10 \Omega$ and $L = 0.9 \text{ mH}$; the first bifurcation phenomena of the diode voltage amplitude could be noticed around the frequency of 750 kHz. The different level amplitudes have a double period (subharmonics). The control parameter was $A = 0.1 \dots 5 \text{ V}$.

The frequency domain at which one can notice the bifurcations corresponds to a period of the driving signal $T = 2\pi/\omega \cong t_r / (0.1 \dots 0.6)$ where t_r is the recovery time from the forward to reverse conduction. This time is conditioned by the storage time of the mobile charge at the forward-reverse switching and creates the delay "necessary" for the apparition of multiple bifurcations and of chaos. This scenery could be an experimental method to evaluate the life and storage time, otherwise determined by classical non-chaotically methods.

CONCLUSION

In order to understand chaotic circuits theory, it is important to consider the following problems: theoretical evidence for chaos, classifications of chaos and route to chaos.

We introduced the problem of discrete-time chaos synchronization. A first significant feature of numerical chaos synchronization concerns the fact that it can be applied to numerical secure communications. We proposed methods for synchronizing composite chaotically systems. Many patterns can be realised by changing a feedback structure.

In the last part of the paper we reports existence of chaotical behaviour in semiconductor devices due non-linearities of the material parameters.

References

- [1] Kenedy M. P., "Basic Concepts of Non-linear Dynamics and Chaos", *Proc. of ISCAS'95*, IEEE Press.
- [2] Toshimitsu Ushio, "Control of Chaotic Synchronization in Composite Systems with Applications to Secure Communications Systems", *IEEE Transactions on Circuits and Systems-I: Fundamental Theory and Applications*, Vol. 43, No. 6, June 1996.
- [3] Tesi A., De Angeli A., Genesio R., "Dead-Beat Chaos Synchronization in Discrete-Time Systems", *IEEE Transactions on Circuits and Systems-I: Fundamental Theory and Applications*, Vol. 42, No. 1, January 1995.
- [4] L. M. Pecora, T. L. Carroll, "Synchronization in Chaotic Systems", *Phys. Rev. Letters*, Vol. 64, pp 821-824, 1990.
- [5] M. Hasler, "Synchronization principles and applications" *Circuit and Systems Tutorials* C. Toumazou, N. Battersby, S. Porta Eds., pp. 314-327, IEEE Press, New York, 1994.
- [6] R. Westerwelt, S. W. Teitworth, "Non-linear transient response of extrinsic Ge far-infrared photoconductors", *J. Appl. Phys* 57 (12), 15 June 1985, pp 5457-5469
- [7] Chua L.O., Tanaka S., Matsumoto T., "A chaotic Attractor from a 2-segment Piecewise-Linear Capacitor Circuit", *The Theory of Dynamical Systems and Its Applications to Nonlinear Problems* World Scientific Publishing Co Pte Ltd.

THE INTEGRATION OF THE NONLINEAR DIFFERENTIAL EQUATIONS THAT DESCRIBE STRAIGHT MOTION OF THE AUTOMOTIVES

Col.prof.univ.dr.ing. ION COPAE
Cpt.asist.univ.drd.ing. LUCIAN MATEI
Military Technical Academy, București

The experimental research [1] show that the automotive's work is accompanied by some static nonlinearities (due to the driver's action upon the throttle, and by tracks irregularities) as well as by some dynamic nonlinearities (if one takes into account the aerodynamic resistance, and/or estimating the rolling resistance coefficient as to be dependent upon the square of the motion speed). The example given in fig.1 represents the position of the throttle v. time, and one can see the nonlinearities input by the driver.

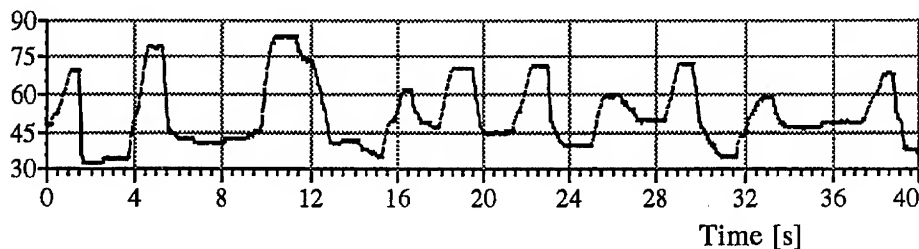


Fig.1

Both of the types of static nonlinearities above mentioned are treated using the methods of the automatic system theory. Considering the study methodology to be unique, this paper intends to deal only with nonlinearities input by the driver. Some experimental researches shown that the driver acts the throttle in some specific ways (requested by the needs of the motion), but always the throttle position is varying between a minimum and a maximum value. So, one can say that the static nonlinearities input by the driver have different forms, some of them being presented in fig.2.

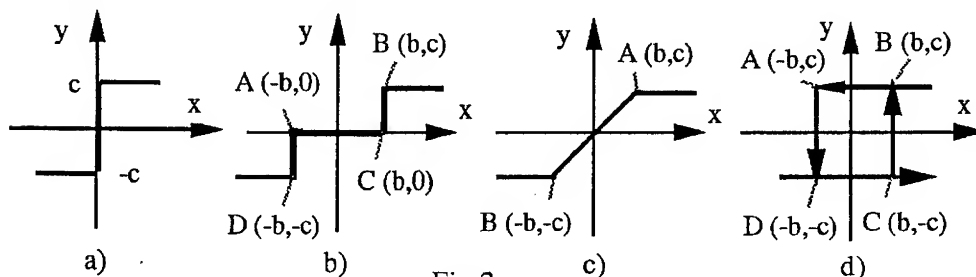


Fig.2

According to automatic system theory the static nonlinearities presented in fig.2 are some relay type nonlinearities. Thus, in fig.2,a is represented the ideal relay type function; it corresponds to a sudden press of the throttle by the driver starting from the minimum position (-c) and ending to the maximum position (c); as a matter of fact, the maximum displacement of the throttle is 2c, but the automatic system theory methodology asks for a middlepoint. This characteristic neglects the inertia in acting the throttle (actually, the answer of the command lever of the injection pump), and the constant positioning of it in the neighborhood of the origin; so it can be concluded in to dealing with an ideal relay-type characteristic (without sensitiveness and histeresis characteristic).

In fig.2,b there is presented a relay-type characteristic, but also having sensitiveness and without histeresis behavior. This shows that the driver doesn't act the throttle along the area of 2b -length in the neighborhood of the origin. Actually this gives the sensitiveness property of the function. Also, is considered the sudden press of the throttle, neglecting the inertia.

In fig.2,c is represented a relay-type static nonlinearity without sensitiveness and without histeresis, but taking into account the inertia of the throttle' mechanism; the same characteristic is used to represent a smooth press of the throttle.

In fig.2,d is represented a relay-type static nonlinearity, having histeresis and a sensitiveness area. This illustrates the next behavior of the driver: on DC area he keeps the throttle constant, then he presses it suddenly CB (neglecting inertia), then he keeps it constant on BA and finally he releases the throttle on AD (also neglecting inertia). Obviously, there are a lot of some other ways in acting the throttle, so there are a lot of other static nonlinearities. In fig.2, the input value $x(t)$ could represent the fluctuation of the speed in car motion, that the driver would like to keep constant, and the output value $y(t)$ represents the throttle position. The relay-type static characteristics in fig.2 are mathematically described by analytic expressions, eg. static nonlinearities of the fig.2,a and fig.2,d are:

$$y(t) = c \cdot \text{sgn}[x(t)] \quad (1)$$

respectively

$$y(t) = \begin{cases} -c, \text{ pentru } \begin{cases} x(t) < -b \\ |x(t)| \leq b \end{cases} & \text{si } \frac{dx(t)}{dt} > 0 \\ c, \text{ pentru } \begin{cases} x(t) > b \\ |x(t)| \leq b \end{cases} & \text{si } \frac{dx(t)}{dt} < 0 \end{cases} \quad (2)$$

Considering the dynamic system made of engine, automotive, terrain and

driver as an automatic system of engine speed regulation (actually, the vehicle's speed), the dynamic nonlinearities are included in the differential equation of vehicle' motion written as:

$$\frac{dv}{dt} = \frac{g}{\delta G_a} \left[F_t - (G_a \psi + k S v^2) \right] \quad (3)$$

where: v -vehicle's speed, g -gravity, δ -coefficient of angular motion of the masses, F_t -tractive force, G_a -vehicle's weight, δ -global resistance coefficient, k -aerodynamic resistance coefficient, S -frontal section of the vehicle, t -time.

The global resistance coefficient is:

$$\psi = f \cos \alpha \pm \sin \alpha = (f_p + f_t) \cos \alpha \pm \sin \alpha \quad (4)$$

where f_p and f_t are the resistance coefficient due to the propeller and due to the soil respectively.

Generally f_p is given by:

$$f_p = a + bv + cv^2 \quad (5)$$

where a , b , c belong to propeller's type.

Considering (4)+(5), equation (3) becomes:

$$\frac{dv}{dt} = \frac{g}{\delta G_a} \left\{ F_t - \left[G_a (a + bv + cv^2 + f_t) \cos \alpha \pm \sin \alpha - k S v^2 \right] \right\} \quad (6)$$

A nonlinear system's functioning analysis could be made using several methods; the most used is the harmonic signal developed on Fourier trigonometric serial, supposed to be an input. In practice, only the first term of Fourier serial is considered. Also, could be used a computer numerical methods or some exact analytical calculus (where possible). Suppose the driver should keep a constant speed. So he is to follow the speed fluctuations Δv regarding an imposed speed v_0 (so the engine's speed fluctuates with $\Delta \omega$ reported to ω_0). If he doesn't shift the gears, then:

$$\frac{\Delta v}{v_0} = \frac{\Delta(\omega_r \cdot r_r)}{\omega_{r0} \cdot r_r} = \frac{\Delta \left(\frac{\omega}{i_t} r_r \right)}{\frac{\omega_0}{i_t} r_r} = \frac{\Delta \omega}{\omega_0} = \varphi \quad (7)$$

where ω_r , r_r are the wheel's angular speed and the tire radius respectively. Consequently, i_t is the transmission ratio and φ is the relative angular speed of the engine. Suppose the driver is acting the throttle like in fig.2,c. So, $y(t)$ is the function that describes the throttle motion and $x(t)$ is the engine's angular speed variation. The equation that describes above mentioned nonlinearity is:

$$\tau(t) = \frac{c}{b} \varphi(t) = k_1 \varphi(t) \quad (8)$$

where c/b represents the tangent of the angle made by AB with the positive axis Ox ($c/b = k_1$).

Considering a noninertial angular speed regulator, the dynamic system made of the engine (non-overcharged), vehicle, terrain and driver is described [2], [3] by:

$$\begin{cases} \frac{d\varphi(t)}{dt} = \frac{\theta_3 - k_m k_c}{k_c t_m} \varphi(t) - \frac{k}{k_c t_m} \eta(t) - \frac{\theta_1}{t_m} \sigma(t) \\ \frac{d\eta(t)}{dt} = \frac{1 - \theta_2 k_1}{t_f} \varphi(t) - \frac{g_n}{t_f} \eta(t) \end{cases} \quad (9)$$

where: $t_{(.)}$ -time constants, $k_{(.)}$ -self-levelling coefficients, g_n -irregularity degree of the angular speed regulator (ASR), η -relative stroke of the speed regulator coupling, φ -relative angular speed of the engine, $\theta_{(.)}$ -amplifying coefficients, k -ASR's lever ratio, τ -relative position of the throttle; σ -terrain's reaction.

In fig.3...5 are presented the results obtained for engine speed decrease of 100 RPM relative to stationary speed of 1719 RPM (wich corresponding to 15.2 kph). The driver wants to keep constant speed, so he presses the throttle. As a result, the tension of ASR's resort increases, disrupting the counterweights former equilibrium. As a fact, the displacement z of the ASR's coupling decreases, creating an increase of the rack stroke h .

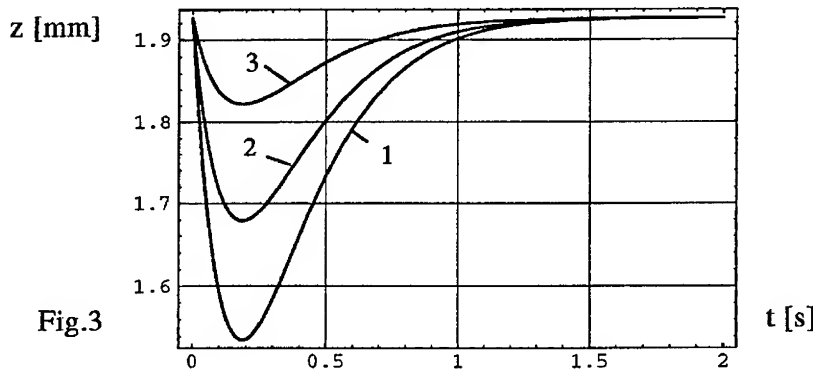
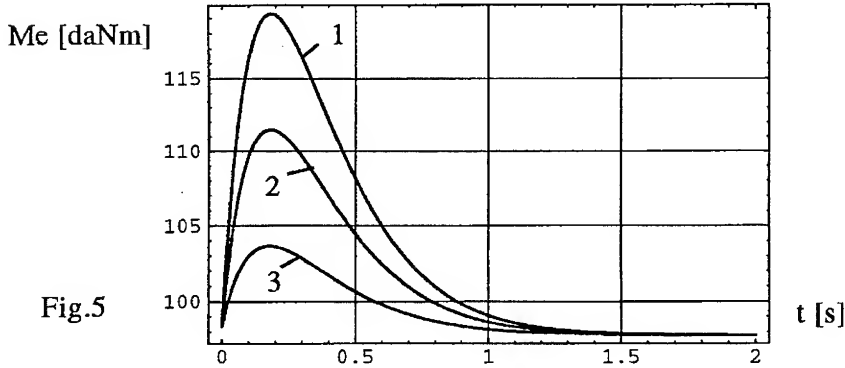
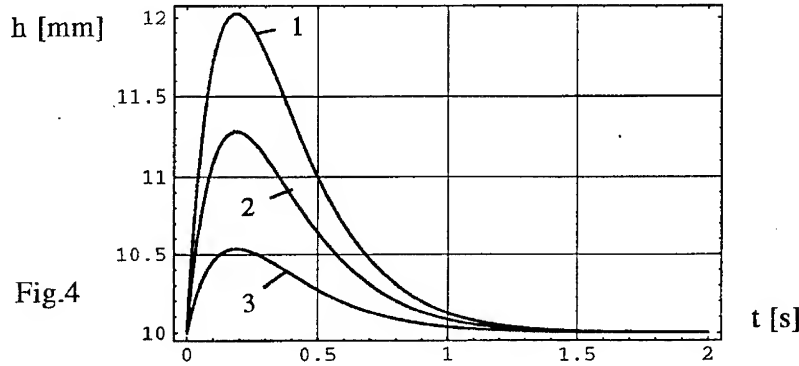


Fig.3

Thus, the engine's torque M_e (fig.5) and its speed (consequently -the car's speed) increases. As soon as is no more inertia in coupling's motion (that was previously pulled out of its equilibrium status), after about 0.2s it trends to restore itself to the former position (maintain force is higher than restore force), so its displacement begins to raise (fig.3). As a fact, the phenomenon are similar but the fluctuations are opposite: rack's stroke and engine's torque

start to decrease (fig.4 and fig.5 respectively). In the end of the transient process all the functions involved reach the initial values and the driver assures 15.2 *kph*.



For the presented figures, the calculus was made for 3 different values of k_1 (curve 1 is for $k=1$, curve 2 is for $k=1.5$ and curve 3 for $k=2$); the higher is k the more sudden is pressed the throttle.

Both given example and eq. (6) could be solved using a numeric method. For instance eq. (6) can be written:

$$\frac{dv(t)}{dt} = -A_1v(t) - A_2v^2(t) + A_3 \Rightarrow \frac{dv(t)}{dt} = f(t) \quad (10)$$

Using Runge-Kutta-Merson method, the transient process represents, generally speaking, the solution of a vectorial differential equations.

$$\mathbf{x}'(t) = \mathbf{f}(\mathbf{x}, t) \quad (11)$$

having $\mathbf{x}(t)$ vector as unknown and $\mathbf{f}(\mathbf{x}, t)$ as field vector.

The recurrence relations of the method are:

$$\mathbf{x}_{k+1} = \mathbf{x}_k + 0,5(\mathbf{k}_1 + 4\mathbf{k}_4 + \mathbf{k}_5) \quad ; k = 0, 1, 2, \dots \quad (12)$$

where the vectors k_1, \dots, k_5 are:

$$k_1 = \frac{1}{3}hf(x_k, t_k); k_2 = \frac{1}{3}hf(x_k + k_1, t_k + \frac{1}{3}h) \quad (13)$$

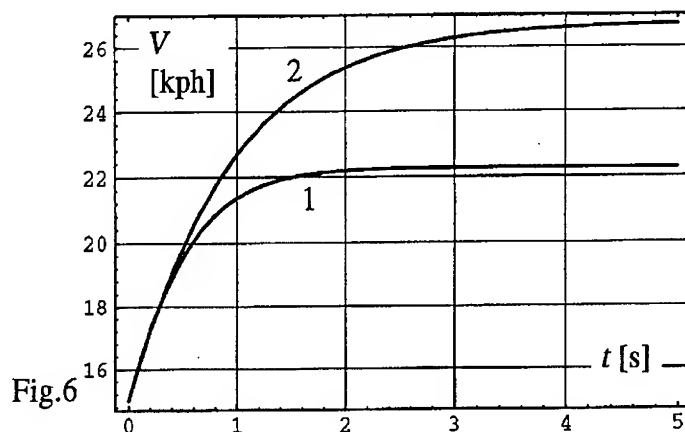
$$k_3 = \frac{1}{3}hf(x_k + \frac{1}{2}k_1 + \frac{1}{2}k_2, t_k + \frac{1}{3}h) \quad (14)$$

$$k_4 = \frac{1}{3}hf(x_k + \frac{3}{8}k_1 + \frac{9}{8}k_3, t_k + \frac{1}{2}h) \quad (15)$$

$$k_5 = \frac{1}{3}hf(x_k + \frac{3}{2}k_1 - \frac{9}{2}k_3 + 6k_4, t_k + h) \quad (16)$$

where h is the integration step and $x_0 = x(0)$ is the initial condition given for $t=0$.

Fig.6 presents differential equation's solution, when considering the dynamic nonlinearities (curve 1) or neglecting them (curve 2).



BIBLIOGRAPHY

- 1.Copae-I."Contribuții privind regimurile funcționale ale autovehiculelor militare cu șenile", Teză de doctorat, Academia Tehnică Militară, 1995.
- 2.Copae-I."Aspecte privind automatica motoarelor Diesel utilizate pe autovehicule", Revista Academiei Tehnice Militare, nr.1, 1991, pag. 142-151.
- 3.Copae I., Matei-L."Sisteme automate de blindate. Automatica motorului", Editura Academiei Tehnice Militare, 1994.

On a problem of evolution magnetic field in a given flow

Anton Soloi

Department of Mathematics, Technical Military Academy,
Bucharest, Regina Maria Bvd., No.81-83, P.O. Code 75275, Romania

Abstract

This work presents the approximations of solutions of stochastic Cauchy problem for the magnetic field in a generalised random velocity field.

Introduction

The problem is to describe the evolution of the initial magnetic field $(H_0(x))_{x \in \mathbb{R}^3}$ in a given flow $(v(t, x))_{(t, x) \in \mathbb{R}_+ \times \mathbb{R}^3}$ of conducting fluid. Many physicists are interested in describing the magnetic field in a turbulent flow. (see [1], [2])

It is been know that initial intensity of magnetic field $(H_0(x))_{x \in \mathbb{R}^3}$ in a given flow $(v(t, x))_{(t, x) \in \mathbb{R}_+ \times \mathbb{R}^3}$ with magnetically permeability μ , in the absence a external perturbation, is change in accordance with the following evolution equation; this equation of evolution can be directly obtained from the Maxwell equations, and it can be written as follows:

$$\frac{\partial}{\partial t} H^i = \frac{1}{2} \mu \Delta H^i + v_{xj}^i H^j - v_j^i H_{xj}^i; \quad i=1,2,3. \quad (1)$$

$$\operatorname{div} H = 0 \quad (2)$$

$$H(0, x) = H_0(x) \quad (3)$$

where $H^i := H^i(t, x)$ is the i -th coordinate of the magnetic field H ; t and $x := (x^1, x^2, x^3)$ are time and space variables; $v(t, x) := (v^1(t, x), v^2(t, x), v^3(t, x))$ is the velocity of the fluid and μ is magnetically permeability constant.

The fluid is assumed to be incompressible, i.e. $\nabla v(t, x) = 0$.

We use the notations $\nabla v := v_{x1}^1 + v_{x2}^2 + v_{x3}^3$; $f_{xi} := \frac{\partial}{\partial x^i} f$; and Δ for the Laplacian in the space variable.

Many physicists are interested in describing the magnetic field in a turbulent flow (see e.g. [1], [2] and the reference there). In order to give a mathematical model of the phenomenon, they write a random field in place of the vector-field $v(t, x)$ in Eq. 1, and hence they derive an equation for the mean (and sometimes for the second and higher moments) of the random magnetic field they obtain.

Instead of a generalised random field $v(t, \omega, x)$, physicists usually take a "short correlated" random field $v_\delta(t, \omega, x)$, that is $v_\delta(t, \omega, x)$ - Wiener standard process, which is considered for small $\delta > 0$ as a good interpretation (approximation) of the turbulent velocity flow. Taking simple "short correlated" random fields (as approximations of a white noise) the system (1)-(3) can be solved for the magnetic field H_δ (or for its mean) approximately explicitly. In this hypothesis equations (1)-(3) is transformed in a system of stochastic partial differential equations, but the problem of existence and uniqueness of solution of this system is not solved. In some works (see e.g. [10] and the references there) the limit (as $\delta \rightarrow 0$) of the mean and the second moment of the magnetic field are studied and the equations for them

are derived. Almost interesting results of this theory is Steinbach-Krause-Rodler equation for mean.

It turned out that these equations contain surprising new second order terms, which were not expected by Eq. 1. Using the theory of stochastic partial differential equations build up by Pardoux and Krylov and Rozovskii, one can study problems like (1)-(3) not only with short correlated random field v_δ , having nice sample paths, but with generalised random fields $v(t, \omega, x)$ as well. A stochastic Cauchy problem for the magnetic field in a generalised random velocity field is considered by Rozovskii in [10].

An existence and uniqueness theorem and estimates for the solutions are presented, without formulating any connection with the earlier results with short correlated random fields v_δ . There is such a gap in both the physical and the mathematical literature of the field.

Namely, though the analogy with Wong-Zakai type approximations for stochastic differential equations is obvious, up till now it has not been proved that $H_\delta(t, \omega, x) \rightarrow H(t, \omega, x)$ in some reasonable topology, as $v_\delta \rightarrow v$.

Our aim is now to fill this gap.

We consider here the case when:

$$v^j(t, \omega, x) := \int_0^t b^{jk}(s, x) dW^k(s, \omega), \quad j = 1, 2, 3 \quad (4)$$

$$v_\delta^j(t, \omega, x) := \int_0^t b_\delta^{jk}(s, x) dW_\delta^k(s, \omega), \quad j = 1, 2, 3 \quad (5)$$

where $W := (W^1, \dots, W^{d_1})$ is a d_1 -dimensional Wiener process, W_δ is a symmetric good approximation for W , and b^{jk}, b_δ^{jk} are measurable real functions for every $j = 1, 2, 3; k = \overline{1, d_1}; \delta > 0$.

If in equation (1) with $v^i(t, \omega, x)$, satisfying (4), formally differentiate in sense Ito and use the solenoid propriety of field H and its coefficients, we obtained:

$$\begin{aligned} dH^i = & \left\{ \frac{1}{2} \mu^2 \Delta H^i + \frac{1}{2} (bb^*)^{jk} H_{x^j x^k}^i \right\} dt + \\ & + \left\{ -\frac{1}{2} (bb^*)_{x^k}^{jk} H_{x^j}^i - b_{x^j}^{ik} b^{lk} H_{x^l}^i + \frac{1}{2} b^{jk} b_{x^j}^{lk} H_{x^l}^i - b^{jk} b_{x^l x^j}^{ik} H^l + \frac{1}{2} b_{x^j}^{ik} b_{x^l}^{jk} H^l \right\} dt + \\ & + \left(b_{x^j}^{ik} H^j - b^{jk} H_{x^j}^i \right) dW^k; \quad i = 1, 2, 3 \end{aligned}$$

For $v_\delta^i(t, \omega, x)$ we obtained:

$$dH_\delta^i = \frac{1}{2} \mu^2 \Delta H_\delta^i dt + \left(b_{\delta x^j}^{ik} H_\delta^j - b_\delta^{jk} H_{\delta x^j}^i \right) dW_\delta^k; \quad i = 1, 2, 3$$

1. Notions, Notations and Definitions.

Definition 1.1. Let $\Theta := (\Omega, \mathcal{F}, \{\mathcal{F}_t\}_{t \geq 0}, P)$ be a complete probability space equipped with a complete right-continuous filtration $\{\mathcal{F}_t\}_{t \geq 0}$ such that \mathcal{F} and \mathcal{F}_0 contain the P -null subsets of Ω , and $\mathcal{F}_t := \bigcap_{s \geq t} \mathcal{F}_s, \forall t \geq 0$.

Then Θ is called a stochastic basis.

We use a stochastic basis $\Theta_\delta := (\Omega_\delta, \mathcal{F}_\delta, \{\mathcal{F}_{\delta t}\}_{t \geq 0}, P_\delta)$ for every $\delta > 0$, and the random elements indexed by δ are defined on Θ_δ throughout the paper.

Definition 1.2. We say that a stochastic process $(v(t, \omega))_{t \geq 0}$, taking values in Banach space V , is a bounded variation process if:

$$\forall t > 0, \quad \|v\|(t) := \sup_{\substack{n \\ t_{i+1}^n \leq t}} \left| v(t_{i+1}^n, \omega) - v(t_i^n, \omega) \right|_V < \infty \quad (\text{a.s.})$$

where supremum is taken over all $\{0 = t_0^n \leq t_1^n \leq \dots \leq t_N^n = t\}$ of interval $[0, t]$.

Definition 1.3. We say that stochastic process $(A(t, \omega))_{t \geq 0}$ is a progressive measurable process (or well-measurable process) in $L(U, V)$ if:

- ◆ $\forall (t, \omega) \in [0, \infty) \times \Omega, A(t, \omega) \in L(U, V)$
- ◆ the process $(A(t, \omega)u)_{t \geq 0}$ is a progressive measurable process in V .

Let H be a Hilbert space and V, V' two Banach space such that V is continuously and dense embedding in H while H is continuously and dense embedding in V' . We suppose that:

$$\forall v \in V, \forall h \in H, \exists k > 0 \quad |(v, h)| \leq k|v|_V|h|_{V'}.$$

Definition 1.4.

In this conditions we may unique defined a linear bounded functional over V by:

$$\forall v' \in V', v \in V, \exists h_n \in H : |h_n - v'|_{V'} \rightarrow 0 \text{ and } (v, v') := \lim_{n \rightarrow \infty} (v, h_n)$$

We suppose that linear bounded operator $T : V' \rightarrow V^*$ is bijective. Then T have a bounded inverse $T^{-1} : V^* \rightarrow V'$ and we may identify the space V' with space V by T .

Definition 1.5. The triple (V, H, V') with above propriety, together with scalar product in H and with the duality between V and V' is called the normal triple.

Remark 1.6. If V is a Banach space continuously and dense embedding in Hilbert space H we may identify (through scalar product in H) with its dual H^* . We write:

$$V \hookrightarrow H \equiv H^* \hookrightarrow V^*$$

where $H^* \hookrightarrow V^*$ is adjunct of $V \hookrightarrow H$.

If V is a reflexive space then (1) is a normal triple.

Notation 1.7. We denote by $\mathcal{F}(V)$ the set of \mathcal{F} -adapted strongly continuous stochastic processes, with bounded variation in Banach space V .

We denote by $\mathcal{F}_+(V)$ the set of increasing \mathcal{F} -adapted strongly continuous stochastic processes, with bounded variation in Banach space V .

Let T be a finite stopping time and $V \in \mathcal{F}_+^c(\mathbb{R})$.

Definition 1.8. We say that stochastic process $v \in C([0, T]; H_0) \cap \mathcal{F}_2(dV, H_1)$ if:

- ◆ v is a \mathcal{F} -adapted process,
- ◆ v is strongly continuous in H_0
- ◆ $\int_0^T |v(t)|_{V_1}^2 dV(t) < \infty$ (a.s.)

Notation 1.9. We denote by $\mathcal{M}(E)$ the set of strong continuous locale martingale $(M(t), \mathcal{F}_t)_{t \geq 0}$ taking values in separable Hilbert space E and $M(0) = 0 \in E$.

Notation 1.10. If $M := \{M(t, \omega)\}_{t \geq 0}$ is a continuous semimartingale in the d -dimensional Euclidean space \mathbb{R}^d , then $M(t) \equiv \tilde{M}(t) + \bar{M}(t)$ where we denote by \tilde{M} and by \bar{M} its locale martingale part starting from 0 and its bounded variation part, respectively.

By $\langle M \rangle(t)$ we denote quadratic variation of semimartingale M over the interval $[0, t]$.

We denote by $S\mathcal{M}(E)$ the set of continuous semimartingales, taking values in E .

For every $M \in S\mathcal{M}(E)$ its locale martingale part \tilde{M} and its bounded variation part \bar{M} is uniqueness determined.

Notation 1.11. The total variation of martingale part \tilde{M} over the interval $[0, t]$ is denoted by $\|\tilde{M}\|(t)$.

Notation 1.12. We denote by \mathcal{H} the σ -algebra of optional subsets of $[0, \infty) \times \Omega$ and by $\mathcal{B}(\mathbb{R}^d)$ the σ -algebra of Borel sets of the d -dimensional Euclidean space \mathbb{R}^d .

Notation 1.13. We fix an orthonormal basis in \mathbb{R}^d , and x_1, \dots, x_d are the coordinates and $|x|$ is the norm of $x \in \mathbb{R}^d$. We use the notation $D_p := \frac{\partial}{\partial x_p}$ if $p = \overline{1, d}$ and for the identity if $p := 0$, where the derivatives are understood in the generalised sense. We also use the notation:

$$D^\gamma := \frac{\partial |\gamma|}{\partial x_1^{i_1} \partial x_2^{i_2} \dots \partial x_d^{i_d}} \quad \text{where } \gamma := (i_1, \dots, i_d) \text{ and } |\gamma| := i_1 + i_2 + \dots + i_d.$$

Notation 1.14. Let V be a Banach space.

Then $C([0, T]; V)$ denotes the Banach space of strongly continuous functions $f: [0, T] \rightarrow V$ with the supremum norm. Space $L_p([0, T]; V)$ denotes (for $p \geq 1$) the Banach space of strongly Lebesgue measurable functions $g: [0, T] \rightarrow V$ with

$$\|g\| := \left(\int_0^T \|g(t)\|_V^p dt \right)^{\frac{1}{p}} < \infty \quad \text{where } \|u\|_V \text{ is the norm of } u \text{ in } V.$$

The class of strongly continuous stochastic processes $(u(t, \omega))_{t \in [0, T]}$ taking values in V is denoted by \mathcal{SV} .

Notation 1.15. Let U be a Banach space which is continuously and densely embedded into Banach space V , and $(h(t, \omega))_{t \in [0, T]}$ is an increasing \mathcal{F}_t -adapted continuous random process.

If $(u(t, \omega))_{t \in [0, T]}$ is an \mathcal{F}_t -adapted strongly continuous process in V such that:

$$\int_0^T \|u(t)\|_U^2 dh(t) < \infty \quad (\text{a.s.})$$

we denote that $u \in \mathcal{SV} \cap \mathcal{S}_2(dh)U$, and when $h(t) \equiv t$ we write $\mathcal{SV} \cap \mathcal{S}_2 U$.

Definition 1.16. Let A_δ and a_δ be random elements in a metric space (X, ρ) for every $\delta > 0$. We say that $A_\delta \sim a_\delta$ in (X, ρ) (w.r. to P_δ) if:

$$\forall \varepsilon > 0, \quad \lim_{\delta \rightarrow 0} P_\delta(\rho(A_\delta, a_\delta) \geq \varepsilon) = 0$$

where ρ is metric in space X .

Definition 1.17. We say that A_δ is tight in X , uniformly in $\delta > 0$, if A_δ is a random element in X and:

$$\forall \varepsilon > 0, \quad \forall \delta > 0, \quad \text{there exists a compact } K_\varepsilon \text{ in } X \text{ such that: } P_\varepsilon(A_\delta \notin K_\varepsilon) < \varepsilon$$

Definition 1.19. Let A_δ be a random element in normed space $(X, \|\cdot\|_X)$ for $\forall \delta > 0$.

We say that A_δ is P_δ -bounded for $\delta > 0$ if:

$$\lim_{L \rightarrow \infty} \sup_{\delta > 0} P_\delta(\|A_\delta\|_X \geq L) = 0.$$

Definition 1.20. Let $(F_\delta(t, \omega))_{t \in [0, T]}$, $(f_\delta(t, \omega))_{t \in [0, T]}$ be random processes in Banach space V for every $\delta > 0$. We say that $F_\delta \sim f_\delta$ in \mathcal{SV} (w.r. to P_δ) if:

$$\forall \varepsilon > 0, \quad \lim_{\delta \rightarrow 0} P_\delta \left(\sup_{t \leq T} \|F_\delta(t) - f_\delta(t)\|_V \geq \varepsilon \right) = 0.$$

Definition 1.21. Let $(A_\delta(t, \omega))_{t \in [0, T]}$, $(a_\delta(t, \omega))_{t \in [0, T]}$ be random processes in $L(U, V)$, where U, V are Banach spaces and $L(U, V)$ is the locally convex vector space of bounded linear operator mapping U into V with the topology of strong pointwise convergence; that means:

$\forall u \in U$, $A_n u \rightarrow A u$ strongly convergent in V , we say $A_n \rightarrow A$ strongly convergent in $L(u, V)$

We say that $A_\delta \sim a_\delta$ in $\mathcal{SL}(U, V)$, if: $\forall u \in U$, $A_\delta u \sim a_\delta u$ in \mathcal{SV} .

Definition 1.22. Let $(h_\delta(t, \omega))_{t \in [0, T]}$ be an \mathcal{F}_t -adapted increasing cadlag process, and

$(F_\delta(t, \omega))_{t \in [0, T]}$, $(f_\delta(t, \omega))_{t \in [0, T]}$ random processes in Banach space V for every $\delta > 0$.

We say that $F_\delta \sim f_\delta$ in $\mathcal{S}_p(dh_\delta)V$, if:

$$\forall \varepsilon > 0, \quad \lim_{\delta \rightarrow 0} P_\delta \left(\int_0^T \|F_\delta - f_\delta\|_V^p dh_\delta(s) \geq \varepsilon \right) = 0$$

Definition 1.23. Let $(A_\delta(t, \omega))_{t \in [0, T]}$, $(a_\delta(t, \omega))_{t \in [0, T]}$ be random processes in $L(U, V)$.

We say that $A_\delta \sim a_\delta$ in $\mathcal{S}_p(dh_\delta)L(U, V)$, if: $\forall u \in U$, $A_\delta u \sim a_\delta u$ in $\mathcal{S}_p(dh_\delta)V$.

If $h_8(t, \omega) \equiv t$ we write $\mathcal{L}_p V$ and $\mathcal{L}_p L(U, V)$ in place of $\mathcal{L}_p(dh_8)V$ and $\mathcal{L}_p(dh_8)L(U, V)$

Notation 1.24. Let $m \geq 0$ be an integer. Then $L_p^m(r, \rho)$ denotes the subspace of locally p -integrable real functions $f: R^d \rightarrow R$ whose derivatives up to the order m are locally p -integrable such that:

$$\|f\|_{m,p,r,\rho} := \left(\sum_{|\gamma| \leq m} \int_{R^d} C_\gamma^m |r(x)\rho^{|\gamma|}(x)|^\gamma |f(x)|^p dx \right)^{\frac{1}{p}} < \infty,$$

where $C_\gamma^m := \frac{m!}{i_1! \dots i_d! (m-|\gamma|)!}$, $p \in N^*$.

By $W_p^m(r, \rho)$ we denote the closure in norm $\|\cdot\|_{m,p,r,\rho}$ of the space $L_p^m(r, \rho)$.

We know that the space $W_p^m(r, \rho)$ is a Banach space with the above norm. (for $p=2$ it is a separable Hilbert space) For $m=0$ and $p=2$ this is the Hilbert space of those measurable functions on R^d which are square-integrable with respect to the measure $r^2(x)dx$. For this space we use the notation $L_2(r)$. It is not difficult to show that the operator:

$$\mathcal{A} := 1 - \frac{1}{r^2} \frac{\partial}{\partial x_i} \left(r^2 \rho^2 \frac{\partial}{\partial x_i} \right)$$

is positive and self-adjoint in $L_2(r)$. $\forall f \in L_2(r)$, $(f, \mathcal{A}f) = (f, f) + \left(\frac{\partial}{\partial x_i} f, \rho^2 \frac{\partial}{\partial x_i} f \right) = (\mathcal{A}f, f) \geq 0$.

Let $\{H^\alpha\}_{\alpha \in R}$ be the scale of Hilbert space constructed from $L_2(r)$ by the operator $\mathcal{A}^{\frac{1}{2}}$.

We know ([17]) that in some hypothesis (I_1) the space $C_0^\infty(R^d)$ is dense in $W_2^m(r, \rho)$, for every integer m . Moreover for $k \leq m+4$ we have $W_2^n(r, \rho) \equiv H^n$ as set, and norms in $W_2^n(r, \rho)$ and H^n are equivalent. By this we identify the Banach space $W_2^n(r, \rho)$ and H^n for all integer $n \in [0, m+4]$. For $n < 0$ we set $W_2^n(r, \rho) := H^n$.

Notation 1.25. For an integer $n \in N$, let $C^{0,n} := C^{0,n}([0, T] \times R^d)$ denote the space of continuous real functions $f: [0, T] \times R^d \rightarrow R$ whose partial derivatives in x up to the order n are continuous in $(t, x) \in [0, T] \times R^d$. The topology on $C^{0,n}$ is induced by the family of seminorms $r \geq 0$, $p_{n,r}(f) := \sup_{t \in [0, t]} \sup_{|x| \leq r} \sum_{|\gamma| \leq n} |D^\gamma f(t, x)|$.

Let $C^{0,\infty} := C^{0,\infty}([0, T] \times R^d) = \bigcap_{n=1}^\infty C^{0,n}$ with the topology induced by the family of seminorms $p_{n,r}$ for all positive integers n, r .

Note that $C^{0,n}$ and $C^{0,\infty}$ are Frechet spaces with the metrics:

$$\rho_T^{(n)}(u, v) := \sum_{r=1}^\infty \frac{1}{2^r} \frac{p_{n,r}(u-v)}{1+p_{n,r}(u-v)} \text{ in } C^{0,n}$$

and, respectively: $\rho_T^{(\infty)}(u, v) := \sum_{n=1}^\infty \frac{1}{2^n} \rho_T^{(n)}(u, v) \text{ in } C^{0,\infty}$.

The following generalisation of Ito's formula plays a very important role in the theory of stochastic differential equations. ([5])

Let $(y_i(t, \omega))_{t \geq 0}$, $i = 1, 2$ be two progressive measurable stochastic processes taking values in V^* such that:

$$i = 1, 2 \quad y_i(t) := \int_0^t v_i^*(s) dV(s) + h_i(s)$$

where $(v_i^*(t, \omega))_{t \geq 0}$ is a progressive measurable stochastic processes, taking values in V^* , $h_i \in S_{\mathcal{A}}(H)$ and $V \in \mathcal{V}_+^c(R)$.

Let $(v_i(t, \omega))_{t \geq 0}$, $i = 1, 2$ be two progressive measurable stochastic processes taking values in V such that $v_i(t) = y_i(t) - dV \times dP$ a.p.t. $(t, \omega) \in [0, \tau(\omega)] \times \Omega$ and

$|v_i|_V, |v_i^*|_{V^*}, |v_i|_V \cdot |v_j|_{V^*}$ are (a.s) locally integrable (w.r with $dV(t)$) where τ be a stopping time. Then exist a subset $\Omega' \subset \Omega$, such that $P(\Omega') \neq 0$ and $\chi_{\Omega'}/y_i(t)$ is a strongly continuous process taking values in H and: $\forall \omega \in \Omega', \forall t \in [0, \tau(\omega)]$

$$\begin{aligned} (y_1(t), y_2(t)) &= (y_1(0), y_2(0)) + \int_0^t (v_1(s), v_2^*(s)) dV(s) + \int_0^t (v_2(s), v_1^*(s)) dV(s) + \\ &+ \int_0^t (y_1(s), dh_2(s)) + \int_0^t (y_2(s), dh_1(s)) + \langle h_1, h_2 \rangle(t) \end{aligned}$$

This formula may be obtained by Ito's formula ([5]) using relation:

$$(y_1, y_2) = \frac{1}{4} \left(|y_1 + y_2|^2 - |y_1 - y_2|^2 \right)$$

Definition 1.26. The family $\{y_\delta(t) : \delta > 0\}$ of d_1 -dimensional stochastic processes is called a good approximation (with accompanying process S) of the continuous semimartingale $y(t)$ if:

1) the process $(y_\delta(t))_{t \geq 0}$ is an \mathcal{F}_t -adapted stochastic process with absolutely continuous trajectories for every $\delta > 0$, such that:

- ♦ $\int_0^T \left| \frac{d}{dt} y_\delta \right|^2(t) dt < \infty$,
- ♦ $\limsup_{\delta \rightarrow \infty, t \leq T} |y_\delta^i(t) - y^i(t)| = 0$ in probability,
- ♦ $\limsup_{\delta \rightarrow \infty, t \leq T} |S_\delta^{ij}(t) - S^{ij}(t)| = 0$ in probability

for every $i, j := 1, \dots, d_1$, where $S = (S^{ij})$ is a stochastic process with absolutely trajectory and:

$$S_\delta^{ij}(t) := \int_0^t (y^i(s) - y_\delta^i(s)) dy_\delta^j(s) - \frac{1}{2} \langle y^i, y^j \rangle(t)$$

2) The family of random variables:

$$\left\{ \int_0^T |y^i(t) - y_\delta^i(t)| \left| \frac{d}{dt} y_\delta^j(t) \right| dt : \delta > 0 \right\}$$

is bounded in probability for every $i, j := 1, \dots, d_1$

3) $\forall (t, \omega) \in [0, T] \times \Omega; i, j = \overline{1, d_1}, \exists K > 0, \left| \frac{d}{dt} S^{ij}(t) \right| \leq K$

Notation 1.27. We write $f \sim g$ in \mathbb{R}^d if the Lebesgue integrals of the real functions f and g are the same. We take $v \in W_2^{m+2}(r, \rho)$ and use the notation $f \angle g$ if $\exists h$ Lebesgue integrable function such that: $f \sim g + h$ and

$$\forall x \in \mathbb{R}^d, |h(x)| \leq K \sum_{|\gamma| \leq m+1} r^2(x) |\rho(x)|^2 |\gamma| |D^\gamma v(x)|^2$$

where K is a constant called relation constant.

2. Preliminaries. Stochastic Partial Differential Equations -Unbounded Coefficients.

In this section we quote some important notions and results from [7] and [5] which we need in the sequel. (cf. with [4], [5], [7])

In the next sections we deal with stochastic Cauchy problems of the form:

$$\begin{aligned} du(t, \omega, x) &= (D_p(a^{pq}(t, \omega, x) D^q u(t, \omega, x)) + f(t, \omega, x)) dV(t, \omega) + \\ &+ (b_1^p(t, \omega, x) D_p u(t, \omega, x) + g_i(t, \omega, x)) dM^i(t, \omega) \end{aligned} \quad (2.1)$$

$$u(0, \omega, x) = u_0(\omega, x) \quad (2.2)$$

given on a stochastic basis Θ , where V is an increasing \mathcal{F}_t -adapted continuous process, M^i is a continuous \mathcal{F}_t -semimartingale, u_0 is an $\mathcal{F}_0 \otimes \mathcal{B}(\mathbb{R}^d)$ measurable real function on $\Omega \times \mathbb{R}^d$,

a^{pq}, b_i^p, f and g_i are $\mathcal{O} \times \mathcal{B}(R^d)$ measurable functions on $[0, T] \times \Omega \times R^d$ for every $p, q = 0, \dots, d$ $i = 1, \dots, d_1$. We denote by \mathcal{O} the σ -algebra of well measurable sets.

Considering such equations, assume that $d\langle M \rangle(t) \leq K dV(t)$ and $d\|\bar{M}\|(t) \ll dV(t)$, where K be a constant, and that $\int_0^T \left(\frac{d\|\bar{M}\|}{dV} \right)^2 dV(s) < \infty$.

Definition 2.1. The stochastic process $(u(t))_{t \in [0, T]}$ is called a generalised solution to the problem (1)-(2) if:

- ◆ $u \in \mathcal{E}L_2(r) \cap \mathcal{E}_2(dV)W_2^1(r, \rho)$
- ◆ $\forall t \in [0, T], \eta \in C_0^\infty, (u(t), \eta)_0 = (u_0, \eta) + \int_0^t \left\{ (-1)^{\hat{p}} (a^{pq} D_p u(s), D_p \eta)_0 + (f(s), \eta)_0 \right\} dV(s) + \int_0^t \left\{ (b_i^p D_p u(s), \eta)_0 + (g_i, \eta)_0 \right\} dM^i(s) \quad (\text{a.s.})$

where $(\cdot, \cdot)_0$ is the scalar product in $L_2(R^d)$. We use the notation: $\hat{p} := \chi_{\{1, +\infty\}}(p)$.

In order to formulate an existence and uniqueness theorem for the problem (1)-(2) we assume the following:

- (J₁) $|r^{-1} \rho^{|\gamma|} D^\gamma r| \leq K; |\rho^{|\gamma|-1} D^\gamma \rho| \leq K, \forall |\gamma| \leq n+1$, on R^d
 $\exists \varepsilon > 0 : \sup_{|x-y| \leq \varepsilon} \left(\frac{r(x)}{r(y)} + \frac{\rho(x)}{\rho(y)} \right) < \infty$
- (J₂) For all $(t, \omega, x) \in [0, T] \times \Omega \times R^d, p, q = 0, \dots, d; i = 1, \dots, d_1$ we have:
 $\forall |\gamma| \leq n, \forall |\beta| \leq n+1, |D^\gamma a^{pq}(t, \omega, x)| \leq K |\rho(x)|^{\hat{p} + \hat{q} - |\gamma|}, |D^\beta b_i^p(t, \omega, x)| \leq K |\rho(x)|^{\hat{p} - |\beta|}$
- (J₃) $\forall (t, \omega, x) \in [0, T] \times \Omega \times R^d, \exists \lambda > 0$ such that:
 $\sum_{k,l=1}^d \left(2a^{kl}(t, \omega, x) - b_i^k(t, \omega, x) b_j^l(t, \omega, x) Q^{ij}(t, \omega) \right) \theta_k \theta_l \geq \lambda \rho^2(x) \sum_{k=1}^d \theta_k^2$

where $Q^{ij}(t)$ is a predictable stochastic process such that:

for all $t \in [0, T]$ and P -almost $\omega \in \Omega$: $\langle M^i, M^j \rangle(t) = Q^{ij} V(t)$

Theorem 2.2 Assume (J₁)-(J₃). Then the Cauchy problem (2.1)-(2.2) has a unique generalised solution u . Moreover $u \in \mathcal{E}W_2^n(r, \rho) \cap \mathcal{E}_2(dV)W_2^{n+1}(r, \rho)$.

This theorem is proved in [7] in the special case when $V(t) = t$ and $M(t)$ is a Wiener process. In [5] is proved the general case when $V(t)$ and $M(t)$ is driving processes.

In the last of section we quote the main result from [5].

Let θ_δ for $\forall \delta > 0$, be a stochastic basis.

Let $A_\delta^{pq}, B_{\delta i}^p, B_{\delta i}^{p(k)}, F_\delta, G_{\delta i}, G_{\delta i}^{(k)}$ and $a_\delta^{pq}, b_{\delta i}^p, b_{\delta i}^{p(k)}, f_\delta, g_{\delta i}, g_{\delta i}^{(k)}, b_{\delta i}^{(k)}$ $\mathcal{O}_\delta \times \mathcal{B}(R^d)$ -measurable functions on $[0, T] \times \Omega_\delta \times R^d$ for every $\forall \delta > 0, i = 1, d_1; k = 1, d_2; p, q = 0, d$

Assume that for $\forall \eta \in C_0^\infty(R^d)$ the processes

$(B_{\delta i}^p(t), \eta)_0, (b_{\delta i}^p(t), \eta)_0, (G_{\delta i}(t), \eta)_0, (g_{\delta i}(t), \eta)_0$ admit the stochastic differentials:

$$\begin{aligned} d(B_{\delta i}^p(t), \eta)_0 &= (B_{\delta i}^{(k)}(t), \eta)_0 dN_\delta^k(t) \\ d(b_{\delta i}^p(t), \eta)_0 &= (b_{\delta i}^{(k)}(t), \eta)_0 d\bar{n}_\delta^k(t) \\ d(G_{\delta i}(t), \eta)_0 &= (G_{\delta i}^{(k)}(t), \eta)_0 dN_\delta^k(t) \\ d(g_{\delta i}(t), \eta)_0 &= (g_{\delta i}^{(k)}(t), \eta)_0 d\bar{n}_\delta^k(t) \end{aligned}$$

$\forall t \in [0, T], i = \overline{1, d}$, where $(\cdot, \cdot)_0$ denotes the scalar product in $L_2(R^d)$ and $N_\delta^k(t), n_\delta^k(t)$ are continuous $\mathcal{F}_{\delta t}$ -semimartingale for $\forall \delta > 0, k = \overline{1, d_2}$

We are given $\mathcal{F}_{\delta t}$ -adapted continuous increasing processes $H_\delta(t), h_\delta(t)$, continuous $\mathcal{F}_{\delta t}$ -semimartingales $M_\delta^i(t), m_\delta^i(t)$ and continuous $\mathcal{F}_{\delta t}$ -adapted processes $c_\delta^{ij}(t), r_\delta^{ij}(t)$ of bounded variation for $\forall \delta > 0; i, j = \overline{1, d_1}; k = \overline{1, d_2}$.

For $\forall \delta > 0$ we consider the Cauchy problems:

$$\begin{aligned} du_\delta(t, x) = & \left(D_p \left(A_\delta^{pq}(t, x) D_q u_\delta(t, x) \right) + F_\delta(t, x) \right) dH_\delta(t) + \\ & + \left(B_{\delta i}^p(t, x) D_p u_\delta(t, x) + G_{\delta i}(t, x) \right) \circ dM_\delta^i(t) \end{aligned} \quad (2.3)$$

$$u_\delta(0, x) = u_{\delta 0}(x) \quad (2.4)$$

$$\begin{aligned} dv_\delta(t, x) = & \left(D_p \left(a_\delta^{pq}(t, x) D_q v_\delta(t, x) \right) + f_\delta(t, x) \right) dh_\delta(t) + \left(b_{\delta i}^p(t, x) D_p v_\delta(t, x) + g_{\delta i}(t, x) \right) \circ dm_\delta^i(t) + \\ & + \frac{1}{2} \left([b_{\delta i}, b_{\delta j}]^p(t, x) D_p v_\delta(t, x) + b_{\delta i}^{p(k)}(t, x) D_p g_{\delta i}(t, x) - b_{\delta j}^p(t, x) D_p g_{\delta i}(t, x) \right) dc_\delta^{ij}(t) + \\ & + \left(b_{\delta i}^{p(k)}(t, x) D_p v_\delta(t, x) + g_{\delta i}^{(k)}(t, x) \right) dr_\delta^{ik}(t) \end{aligned} \quad (2.5)$$

$$v_\delta(0, x) = v_{\delta 0}(x) \quad (2.6)$$

with $\mathcal{F}_{\delta 0}$ -measurable random variables $u_{\delta 0}, v_{\delta 0}$ in $L_2(r)$, where:

$$\begin{aligned} [b_{\delta i}, b_{\delta j}]^p(t, x) = & \left(b_{\delta i}^k \frac{\partial}{\partial x_k} b_{\delta j}^p - b_{\delta j}^k \frac{\partial}{\partial x_k} b_{\delta i}^p \right)(t, x), \quad p = \overline{0, d} \\ \left(B_{\delta i}^p(t, x) D_p u_\delta(t, x) + G_{\delta i}(t, x) \right) \circ dM_\delta^i(t) = & \left(B_{\delta i}^p(t, x) D_p u_\delta(t, x) + G_{\delta i}(t, x) \right) dM_\delta^i(t) + \\ & + \frac{1}{2} \left(B_{\delta i}^p(t, x) D_p \left(B_{\delta j}^q(t, x) D_q u_\delta(t, x) \right) + B_{\delta i}^p(t, x) D_p G_{\delta j}(t, x) \right) d\langle M_\delta^i, M_\delta^j \rangle(t) + \\ & + \frac{1}{2} \left(B_{\delta i}^{p(k)}(t, x) D_p u_\delta(t, x) + G_{\delta j}^{(k)}(t, x) \right) d\langle M_\delta^i, N_\delta^k \rangle(t) \\ \left(b_{\delta i}^p(t, x) D_p v_\delta(t, x) + g_{\delta i}(t, x) \right) \circ dm_\delta^i(t) = & \left(b_{\delta i}^p(t, x) D_p v_\delta(t, x) + g_{\delta i}(t, x) \right) dm_\delta^i(t) + \\ & + \frac{1}{2} \left(b_{\delta i}^p(t, x) D_p \left(b_{\delta j}^q(t, x) D_q v_\delta(t, x) \right) + b_{\delta i}^p(t, x) D_p g_{\delta j}(t, x) \right) d\langle m_\delta^i, m_\delta^j \rangle(t) + \\ & + \frac{1}{2} \left(b_{\delta i}^{p(k)}(t, x) D_p v_\delta(t, x) + g_{\delta j}^{(k)}(t, x) \right) d\langle m_\delta^i, n_\delta^k \rangle(t) \end{aligned}$$

Further, $c_\delta^{ij} = -c_\delta^{ji}$ for $\forall t, \omega_\delta, \delta, i, j$.

From the assumptions below it follows, in particular, that the problems (2.3)-(2.4) and (2.5)-(2.6) are meaningful in the sense of Definition 2.1.

Let $m \in N^*$. We assume that the following conditions are satisfied:

I₁) For $\forall \delta > 0$ we have:

$$\begin{aligned} |D^\gamma A_\delta^{pq}(t, \omega_\delta, x)| & \leq K |\rho(x)|^{\hat{p} + \hat{q} - |\gamma|} \\ |D^{\gamma_1} A_\delta^{pq}(t, \omega_\delta, x)| & \leq K_\delta |\rho(x)|^{\hat{p} + \hat{q} - |\gamma_1|} \\ |D^\beta B_{\delta i}^q(t, \omega_\delta, x)| & \leq K |\rho(x)|^{\hat{p} - |\beta|} \\ |D^\gamma B_{\delta i}^{p(k)}(t, \omega_\delta, x)| & \leq K |\rho(x)|^{\hat{p} - |\gamma|} \\ |D^{\gamma_2} a_\delta^{pq}(t, \omega_\delta, x)| & \leq K |\rho(x)|^{\hat{p} + \hat{q} - |\gamma_2|} \\ |D^{\gamma_2} b_{\delta i}^p(t, \omega_\delta, x)| & \leq K |\rho(x)|^{\hat{p} - |\gamma_2|} \end{aligned}$$

$$\left| D^{\gamma_2} b_{\delta i}^{p(k)}(t, \omega_\delta, x) \right| \leq K |\rho(x)|^{\hat{p} - |\gamma_2|}$$

$$p, q = \overline{0, d}; i = \overline{1, d_1}; k = \overline{1, d_2}; (t, \omega_\delta, x) \in [0, T] \times \Omega_\delta \times \mathbb{R}^d;$$

$$|\gamma| \leq m; |\gamma_1| \leq m+1; |\gamma_2| \leq m+2; |\beta| \leq \max(m+1, 2); \hat{p} = \chi_{[1, +\infty)}(p); \hat{q} = \chi_{[1, +\infty)}(q);$$
 where K_δ and K are constants.

Moreover

$$\begin{aligned}
 & u_{\delta 0} \in W_2^{m+1}(r, \rho); \text{ and } u_{\delta 0} \in W_2^{m+1}(r, \rho); \text{ (a.s)} \\
 & |F_\delta|_{m, r, \rho} \leq K; |G_{\delta i}|_{m+1, r, \rho} \leq K; \left| G_{\delta i}^{(k)} \right|_{m, r, \rho} \leq K; |f_\delta|_{m+1, r, \rho} \leq K; |g_{\delta i}|_{m+2, r, \rho} \leq K; \\
 & \left| g_{\delta i}^{(k)} \right|_{m+1, r, \rho} \leq K, i = \overline{1, d_1}; k = \overline{1, d_2}; (t, \omega_\delta) \in [0, T] \times \Omega_\delta
 \end{aligned}$$

$$\begin{aligned}
 I_2) \quad & D^\gamma A_\delta^{pq}(t, x) \sim D^\gamma a_\delta^{pq}(t, x) \text{ in } L_2(dH_\delta)R \quad \text{w.r. to } P_\delta \\
 & D^{\gamma_1} B_{\delta i}^p(t, x) \sim D^{\gamma_1} b_{\delta i}^p(t, x) \text{ in } \mathcal{R} \quad \text{w.r. to } P_\delta \\
 & D^{\gamma} B_{\delta i}^{p(k)}(t, x) \sim D^{\gamma} b_{\delta i}^{p(k)}(t, x) \text{ in } \mathcal{R} \quad \text{w.r. to } P_\delta
 \end{aligned}$$

for all : $|\gamma| \leq m; |\gamma_1| \leq m+1$; and $p, q = \overline{0, d}; i = \overline{1, d_1}; k = \overline{1, d_2}$.

Moreover:

$$\begin{aligned}
 & F_\delta(t) \sim f_\delta(t) \text{ in } \mathcal{L}_2(dH_\delta)W_2^m(r, \rho) \quad \text{w.r. to } P_\delta \\
 & G_{\delta i}(t) \sim g_{\delta i}(t) \text{ in } \mathcal{R}W_2^m(r, \rho) \text{ w.r. to } P_\delta \\
 & G_{\delta i}^{(k)}(t) \sim g_{\delta i}^{(k)}(t) \text{ in } \mathcal{R}W_2^m(r, \rho) \text{ w.r. to } P_\delta \\
 & u_{\delta 0} \sim v_{\delta 0} \text{ in } W_2^m(r, \rho) \text{ w.r. to } P_\delta, \quad i = \overline{1, d_1}; k = \overline{1, d_2}
 \end{aligned}$$

I_3) If we defined following operators:

$$\begin{aligned}
 L_\delta(t)u_2 &:= D^p \left(a_\delta^{pq}(t) D^q u_2 \right) \\
 M_{\delta i}(t)u_1 &:= b_{\delta i}^p(t) D^p u_1 \\
 M_{\delta i}^{(k)}(t)u_1 &:= b_{\delta i}^{p(k)}(t) D^p u_1
 \end{aligned}$$

for $u_1 \in W_2^{m+1}(r, \rho)$ and $u_2 \in W_2^{m+2}(r, \rho)$, and the operator $M_{\delta i}^{(m^*)}(t)$ is the adjoint of $M_{\delta i}(t)$ with respect to the duality defined by the scalar product in $W_2^m(r, \rho)$; then stochastic processes:

$L_\delta(t)u_2; M_{\delta i}(t)u_1; M_{\delta i}^{(m^*)}(t)u_1; M_{\delta i}^{(k)}(t)u_1; f_\delta(t); g_{\delta i}^{(k)}(t);$
 are tight in $C\left([0, T]; W_2^m(r, \rho)\right)$ uniformly in $\delta > 0; i = \overline{1, d_1}; k = \overline{1, d_2}$ and the stochastic processes: $M_{\delta i}(t)u_2; g_{\delta i}(t)$ are tight in $C\left([0, T]; W_2^{m+1}(r, \rho)\right)$ uniformly in $\delta > 0; i = \overline{1, d_1}$.

I_4) There exist a constant $\lambda > 0$ such that:

$$\forall (t, \omega_\delta, x) \in [0, T] \times \Omega_\delta \times \mathbb{R}^d; \forall (\theta_1, \dots, \theta_d) \in \mathbb{R}^d \Rightarrow \sum_{j,l=1}^d A_\delta^{jl}(t, \omega_\delta, x) \theta_j \theta_l \geq \lambda \rho^2(x) \sum_{l=1}^d \theta_l^2$$

I_5) The problem (2.5)-(2.6) has a generalised solution $v_\delta, \forall \delta > 0$ such that:

$$\begin{aligned}
 & v_\delta \text{ is tight in } C\left([0, T]; W_2^{m+2}(r, \rho)\right) \text{ uniformly in } \delta > 0; \\
 & \int_0^T |v_\delta|_{m+3, r, \rho}^2 dh_\delta(s) \text{ is } P_\delta\text{-bounded in } W_2^{m+3}(r, \rho).
 \end{aligned}$$

I_6) $H_\delta(t) \sim h_\delta(t); M_\delta^i(t) \sim m_\delta^i(t); N_\delta^i(t) \sim n_\delta^i(t); C_\delta^{ij}(t) \sim c_\delta^{ij}(t); R_\delta^{ik}(t) \sim r_\delta^{ik}(t)$ in \mathcal{R}
 w.r. to $P_\delta; i, j = \overline{1, d_1}; k = \overline{1, d_2}$ where stochastic processes $C_\delta^{ij}(t), R_\delta^{ik}(t)$ are defined by:

$$C_{\delta}^{ij}(t) := (m_{\delta}^i - M_{\delta}^i) \bar{M}_{\delta}^j(t) + \langle m_{\delta}^i - M_{\delta}^i, M_{\delta}^j \rangle(t) + \frac{1}{2} \left(\langle M_{\delta}^i, M_{\delta}^j \rangle(t) - \langle m_{\delta}^i, m_{\delta}^j \rangle(t) \right)$$

$$R_{\delta}^{ik}(t) := (m_{\delta}^i - M_{\delta}^i) \bar{N}_{\delta}^k(t) + \langle m_{\delta}^i - M_{\delta}^i, N_{\delta}^k \rangle(t) + \frac{1}{2} \left(\langle M_{\delta}^i, N_{\delta}^k \rangle(t) - \langle m_{\delta}^i, n_{\delta}^k \rangle(t) \right)$$

I_7) The random variables:

$$|m_{\delta}^i - M_{\delta}^i| \cdot \|M_{\delta}^i\|(T); \langle M_{\delta}^i \rangle(T); \|c_{\delta}^{ij}\|(T); \|r_{\delta}^{ik}\|(T); \|\bar{m}_{\delta}^i\|(T); |m_{\delta}^i - M_{\delta}^i| \cdot \|\bar{N}_{\delta}^k\|(T); \\ \langle N_{\delta}^k \rangle(T); \langle n_{\delta}^k \rangle(T); \|\bar{n}_{\delta}^k\|(T); H_{\delta}(T); h_{\delta}(T)$$

are P_{δ} -bounded, $\forall \delta > 0$; $i, j=1, d_1$; $k=1, d_2$

I_8) Let $\zeta_{\delta}, \xi_{\delta}$ are two P_{δ} -bounded random variables: $\forall \delta > 0$

$$d\langle M_{\delta}^i \rangle(t) \leq \zeta_{\delta} dH_{\delta}(t); d\|\bar{M}_{\delta}^i\|(t) \leq \xi_{\delta} dH_{\delta}(t); d\langle N_{\delta}^k \rangle(t) \leq \zeta_{\delta} dH(t);$$

$$d\langle m_{\delta}^i \rangle(t) \leq \xi_{\delta} dh_{\delta}(t); d\langle n_{\delta}^k \rangle(t) \leq \xi_{\delta} dh_{\delta}(t); \int_0^T \left(\frac{d\|\bar{M}_{\delta}^i\|}{dH_{\delta}} \right)^2 dH_{\delta}(s) < \infty.$$

Theorem 2.3. ([5]) Assume (J_1) , $(I_1 - I_8)$. Then there exists a unique generalised solution $(u_{\delta}(t, \omega))_{(t, \omega) \in [0, T] \times \Omega}$ of the problem (2.3)-(2.4) for every $\delta > 0$ with following properties:

- 1) $u_{\delta} \in \mathcal{E}W_2^m(r, \rho) \cap \mathcal{E}_2(dH_{\delta})W_2^{m+1}(r, \rho)$
- 2) $\forall \varepsilon > 0 \Rightarrow \lim_{\delta \rightarrow \infty} P_{\delta} \left(\sup_{t \leq T} |u_{\delta}(t) - v_{\delta}(t)|_{m, r, \rho} \geq \varepsilon \right) = 0$
- 3) $\forall \varepsilon > 0 \Rightarrow \lim_{\delta \rightarrow 0} P_{\delta} \left(\int_0^T |u_{\delta} - v_{\delta}|_{m+1, r, \rho}^2 dH_{\delta}(s) \geq \varepsilon \right) = 0$

3. The Formulation of the Result

To formulate the result of this section let $m \in \mathbb{N}^*$ and let r, ρ be positive weight functions. We suppose the following:

(I_1) The weight functions r and ρ satisfies the conditions :

$$|r^{-1} \rho^{|\gamma|} D^{\gamma} r| \leq K; | \rho^{|\gamma|-1} D^{\gamma} \rho | \leq K, \forall |\gamma| \leq m+4, \text{ on } R^d$$

$$\exists \varepsilon > 0 : \sup_{|x-y| \leq \varepsilon} \left(\frac{r(x)}{r(y)} + \frac{\rho(x)}{\rho(y)} \right) < \infty$$

(I_2) The partial derivatives in x of $b_{\delta}^{ij}(x)$, $b^{jk}(t, x)$ up to the order $m+4$ are functions,

such that $\forall T \geq 0; \forall (t, x) \in [0, T] \times R^d; \forall |\gamma| \leq m+4; \forall \delta > 0$ we have:

$$|D^{\gamma} b_{\delta}^{ij}(t, x)| \leq K_T |\rho(x)|^{1-|\gamma|}; |D^{\gamma} b^{ij}(t, x)| \leq K_T |\rho(x)|^{1-|\gamma|}; j=1, 2, 3; i=\overline{1, d_1}$$

(I_3) For every $\delta > 0$, for almost every $(t, x) \in [0, \infty) \times R^3$: (w.r to Lebesgue measure)

$$b_{\delta x^1}^{1i}(t, x) + b_{\delta x^2}^{2i}(t, x) + b_{\delta x^3}^{3i}(t, x) = 0; i=1, 2, 3$$

(I_4) $\forall x \in R^3; \forall |\gamma| \leq m+2; \forall T \geq 0 \Rightarrow$

$$\limsup_{\delta \rightarrow 0} |D^{\gamma} b^{ij}(t, x) - D^{\gamma} b_{\delta}^{ij}(t, x)| = 0; j=1, 2, 3; i=\overline{1, d_1} \text{ in probability.}$$

We consider the following Cauchy problems:

$$dH_{\delta}^i = \frac{1}{2}\mu^2 \Delta H_{\delta}^i dt + \left(b_{\delta xj}^{ik} H_{\delta}^j - b_{\delta}^{ik} H_{\delta xj}^j \right) dW_{\delta}^k; \quad i=1,2,3 \quad (3.1)$$

$$\operatorname{div} H_{\delta}^i = 0; \quad i=1,2,3 \quad (3.2)$$

$$H_{\delta}(0, x) = H_{\delta 0}(x), \quad (3.3)$$

$$dH^i = \left\{ \frac{1}{2}\mu^2 \Delta H^i + \frac{1}{2}(bb^*)^{jk} H_{xj xk}^i - b_{xj}^{ik} b^{lk} H_{x1}^j + \frac{1}{2} b^{jk} b_{xj}^{lk} H_{x1}^i - b^{jk} b_{x1 xj}^{lk} H^1 + \frac{1}{2} b_{xj}^{ik} b_{x1}^{jk} H^1 \right\} dt +$$

$$+ \left(b_{xj}^{ik} H^j - b^{jk} H_{xj}^i \right) dW^k; \quad i=1,2,3 \quad (3.4)$$

$$\operatorname{div} H^i = 0; \quad i=1,2,3 \quad (3.5)$$

$$H(0, x) = H_0(x) \quad (3.6)$$

where $H_{\delta 0}, H_0$ are \mathcal{F}_0 measurable random variables in $W_2^{m+3}(r, \rho)$ for every $\delta > 0, i=1,2,3$.

Moreover we assume:

(I₅) $\operatorname{div} H_{\delta 0}^i(x) = 0$ for almost every $x \in \mathbb{R}^3$ (w.r to the Lebesgue measure in \mathbb{R}^3) and

$$\lim_{\delta \rightarrow 0} \|H_{\delta 0}^i - H_0^i\|_{m, r, \rho} = 0 \text{ in probability, for } i=1,2,3$$

Definition 3.1 (cf.[5])

The random functions $H_{\delta}(t, x) = (H_{\delta}^1(t, x), H_{\delta}^2(t, x), H_{\delta}^3(t, x))$ and

$H(t, x) = (H^1(t, x), H^2(t, x), H^3(t, x))$ are called generalised solutions of the problems

(3.1)-(3.3) and (3.4)-(3.6), respectively, if:

- ◆ $\left(H_{\delta}^i(t) \right)_{t \in [0, T]}, \left(H^i(t) \right)_{t \in [0, T]} \in \mathcal{L}_2(r) \cap \mathcal{L}_2 W_2^1(r, \rho)$ for every $T \geq 0, i=1,2,3$ and
- ◆ for P-almost $\omega \in \Omega$:

$$\left(H_{\delta}^i(t, \eta) \right)_0 = \left(H_{\delta 0}^i, \eta \right)_0 - \int_0^t \frac{1}{2} \mu^2 \left(H_{\delta xj}^i(s), \eta_{xj} \right)_0 ds +$$

$$+ \int_0^t \left(b_{\delta xj}^{ik}(s) H_{\delta}^j(s) - b_{\delta}^{ik}(s) H_{\delta xj}^j(s), \eta \right)_0 dW_{\delta}^k(s), \quad i=1,2,3 \quad (3.7)$$

$$\sum_{j=1}^3 \left(H_{\delta xj}^i(t, \eta) \right)_0 = 0, \quad i=1,2,3 \quad (3.8)$$

and:

$$\left(H^i(t, \eta) \right)_0 = - \int_0^t \frac{1}{2} \left(\mu^2 H_{xk}^i(s) + (bb^*)^{jk}(s) H_{xj xk}^i(s), \eta_{xk} \right)_0 ds +$$

$$+ \int_0^t \left(-\frac{1}{2} (bb^*)^{jk}(s) H_{xj xk}^i(s) - b_{xj}^{ik}(s) b^{lk} H_{x1}^j(s) + \frac{1}{2} b^{jk}(s) b_{xj}^{lk}(s) H_{x1}^i(s), \eta \right)_0 ds +$$

$$+ \int_0^t \left(-b^{jk}(s) b_{x1 xj}^{lk}(s) H^1(s) + \frac{1}{2} b_{xj}^{ik}(s) b_{x1}^{jk}(s) H^1(s), \eta \right)_0 ds +$$

$$+ \int_0^t \left(b_{xj}^{ik}(s) H^j(s) - b^{jk}(s) H_{xj}^i(s), \eta \right)_0 dW^k(s); \quad i=1,2,3 \quad (3.9)$$

$$\sum_{j=1}^3 \left(H_{xj}^i(t, \eta) \right)_0 = 0; \quad i=1,2,3 \quad (3.10)$$

hold for all $t \geq 0$ and every $\eta \in C_0^{\infty}(\mathbb{R}^3)$, where $(\cdot, \cdot)_0$ denotes the scalar product in $L_2(\mathbb{R}^3)$, the last integral in the right side of the equality (3.7) is a Lebesgue-Stieltjes integral for every $\omega \in \Omega$, and the last integral in the right side of equality (3.9) is understood in Ito's sense.

Remark 3.1. By the assumptions (I₁)-(I₅) it is not difficult to show that if

$H_{\delta} = (H_{\delta}^1, H_{\delta}^2, H_{\delta}^3)$ is a function on $[0, \infty) \times \Omega \times \mathbb{R}^3$ such that

$$\left(H_{\delta}^i(t) \right)_{t \in [0, T]} \in \mathcal{L}_2(r) \cap \mathcal{L}_2 W_2^1(r, \rho), \quad \forall T \geq 0$$

and almost surely (3.1) holds for all t , then almost surely (3.2) also holds for all $t \geq 0$.

Theorem 3.2. Let $(W_{\delta}(t))_{t \geq 0}$ be a symmetric good approximation (i.e. with accompanying process $S := 0$) of the Wiener process $(W(t))_{t \geq 0}$. Assume (I_1) – (I_3) .

Then the problem (3.1)–(3.3) has a unique generalised solution $(H_{\delta}(t))_{t \in [0, T]}$ for every $\delta > 0$ and the problem (3.4)–(3.6) has a unique generalised solution $(H(t))_{t \in [0, T]}$.

The coordinate processes:

$$\left(H_{\delta}^i(t) \right)_{t \in [0, T]}, \left(H^i(t) \right)_{t \in [0, T]} \in \mathcal{W}_2^{m+3}(r, \rho) \cap \mathcal{L}_2 W_2^{m+4}(r, \rho), \quad \forall T > 0$$

and:

$$\forall T \geq 0, i = 1, 2, 3 \quad \lim_{\delta \rightarrow 0} \sup_{t \leq T} |H_{\delta}^i(t) - H^i(t)|_{m, r, \rho} = 0 \text{ in probability.}$$

4. The Proof of Theorem 3.2.

The existence and the uniqueness of the generalised solution $(H_{\delta}(t))_{t \in [0, T]}$ of the problem (3.7)–(3.9) follows from the assumption (I_1) – (I_3) by virtue of Theorem 2.2. Moreover, by Theorem 2.2 $H_{\delta}, H_{\delta} \in \mathcal{W}_2^{m+3}(r, \rho) \cap \mathcal{L}_2 W_2^{m+4}(r, \rho)$.

It is not difficult to show that first two conditions of the Theorem 2.2 are verified.

For the last condition we note: $\lambda := \mu^{-2} \sup \rho^2(x)$ and by (I_3) we have:

$$\mu^2 + b_{\delta}^{ik} \left(b_{\delta x_1}^{li} + b_{\delta x_2}^{2i} + b_{\delta x_3}^{3i} \right) Q^{ij} - \lambda \rho^2 = v^2 - \lambda \rho^2 \geq 0$$

Similarly we may verify the conditions of theorem 2.3 for the problem (3.7)–(3.9).

By the definition of the generalised solution, for P_{δ} -almost every $\omega_{\delta} \in \Omega_{\delta}$ we write the relations (3.7) and (3.9). With the following notation:

$$\begin{aligned} L_{\delta} &:= \frac{\mu^2}{2} D_p D_p, \quad M_{\delta k}(t) := (-1)^p b_{\delta}^{ik(p)} D_p = (-1)^p b_{\delta x p}^{ik} D_p, \\ \check{L}_{\delta} &:= \frac{1}{2} D_p [\mu^2 D_p + (bb^*) D_q], \quad \check{M}_{\delta k}(t) := (-1)^p b_{\delta}^{ik(p)} D_p. \end{aligned}$$

and with the notation in Section 2 we have:

$$\begin{aligned} (H_{\delta}(t), \eta)_0 &= (H_{\delta 0}, \eta)_0 + \int_0^t (L_{\delta} H_{\delta}(s), \eta)_0 ds + \int_0^t (M_{\delta i}(s) H_{\delta}(s), \eta)_0 dW_{\delta}^i(s) + \\ &+ \frac{1}{2} \int_0^t \left(M_{\delta i} M_{\delta j}(s) H_{\delta}(s), \eta \right)_0 d \left(W_{\delta}^i, W_{\delta}^j \right)(s) + \frac{1}{2} \int_0^t \left(M_{\delta i}^{(k)}(s) H_{\delta}(s), \eta \right)_0 d \left(W_{\delta}^i, N_{\delta}^k \right)(s) \quad (4.1) \end{aligned}$$

$$\begin{aligned} (H(t), \eta)_0 &= (H_0, \eta)_0 + \int_0^t (\check{L}_{\delta} H(s), \eta)_0 ds + \int_0^t (\check{M}_{\delta i}(s) H(s), \eta)_0 dW_{\delta}^i(s) + \\ &+ \int_0^t (\check{M}_{\delta i} \check{M}_{\delta j}(s) H(s), \eta)_0 d \left(\frac{1}{2} \left(W_{\delta}^i, W_{\delta}^j \right)(s) + c_{\delta}^{ij}(s) \right) + \\ &+ \int_0^t (\check{M}_{\delta i}^{(k)}(s) H(s), \eta)_0 d \left(\frac{1}{2} \left(W_{\delta}^i, N_{\delta}^k \right)(s) + r_{\delta}^{ik}(s) \right) \quad (4.2) \end{aligned}$$

hold for all $t \in [0, T]$, $\eta \in C_0^{\infty}(R^d)$.

For $\eta \in C_0^{\infty}(R^d)$ we define: $\Lambda_m \eta := \sum_{|\gamma| \leq m} (-1)^{|\gamma|} C_{\gamma}^m D^{\gamma} (r^2 \rho^{2|\gamma|} D^{\gamma} \eta)$

Note that: $\Lambda_m \eta \in C_0^{\infty}(R^d)$ and $\forall u \in W_2^m(r, \rho)$, $(u, \Lambda_m \eta)_0 = (u, \eta)_m$.

Consequently, replacing η in the above equalities by $\Lambda_m \eta$ we get that P_δ -almost every $\omega_\delta \in \Omega_\delta$ equalities (4.1) and (4.2) are true with all the scalar product $(\cdot, \cdot)_0$ are replaced by scalar product $(\cdot, \cdot)_m$, we note this equation by (4.1)' and (4.2)'.

For every $u, v \in C_0^\infty(\mathbb{R}^d)$ we have $(L_\delta(t)u, v)_m = (L_\delta(t)u, \Lambda_m v)_0$.

By integration by parts and using the derivation rule for products we get the estimate:

$$\begin{aligned} (L_\delta(t)u, v)_m &\leq K \sum_{|\gamma| \leq m} \sum_{\gamma_1 + \gamma_2 = \gamma} \left| \left(D^{\gamma_1} D_p D^{\gamma_2} u, D_p \left(r^2 \rho^2 |\gamma| D^\gamma v \right) \right)_0 \right| \leq \\ &\leq K \sum_{|\gamma| \leq m} \sum_{\gamma_1 + \gamma_2 = \gamma} \left| \left(r^{-1} \rho^{|\gamma| - \hat{p}} D^{\gamma_1} u, \rho^{-|\gamma| + \hat{p}} D_p \left(r^2 \rho^2 |\gamma| D^\gamma v \right) \right)_0 \right| \end{aligned}$$

where K is a constant which does not depend on δ .

Hence making use of the hypotheses (I_1) of the weight functions r and ρ we get:

$$(L_\delta(t)u, v)_m \leq K' |u|_{m+1, r, \rho} |v|_{m+1, r, \rho} \quad (4.3)$$

Set $H_\alpha := W_2^{m+\alpha}(r, \rho)$, for $\alpha := 0, 1, 2, 3$. Then, identifying H_0 with its dual H_0^* , by the help of scalar product in H_0 , we have:

$$H_3 \hookrightarrow H_2 \hookrightarrow H_1 \hookrightarrow H_0 \equiv H_0^* \hookrightarrow H_1^* \hookrightarrow H_2^* \hookrightarrow H_3^*$$

where $H_\alpha^* \hookrightarrow H_{\alpha+1}^*$ is the adjoint of the continuous and dense injection $H_{\alpha+1} \hookrightarrow H_\alpha$. We use the notation (\cdot, \cdot) for the scalar product in H_0 and also for the duality between H_α and H_α^* .

By (3.14) the linear operator $A_\delta(t) : H_1 \rightarrow H_1^*$ defined by:

$$\forall \delta > 0, \forall (t, \omega_\delta) \in [0, T] \times \Omega_\delta, \quad (A_\delta(t)u, v) := (L_\delta(t)u, v)_m$$

is a bounded linear operator, and its operator norm is bounded by the constant K (uniformly in t, ω_δ, δ) In the same way as we get (4.3), we obtain from (I_1) and (I_2) that:

$$\begin{aligned} (a_\delta(t)u, v) &:= \left(\tilde{L}_\delta(t)u, v \right)_m \leq K |u|_{m+1, r, \rho} |v|_{m+1, r, \rho} \\ (B_{\delta i}(t)u, v) &:= (M_{\delta i}(t)u, v)_m \leq K |u|_{m+1, r, \rho} |v|_{m, r, \rho} \\ (b_{\delta i}(t)u, v) &:= \left(\check{M}_{\delta i}(t)u, v \right)_m \leq K |u|_{m+1, r, \rho} |v|_{m, r, \rho} \\ (B_{\delta}^{(k)}(t)u, v) &:= \left(M_{\delta}^{(k)}(t)u, v \right)_m \leq K |u|_{m+1, r, \rho} |v|_{m, r, \rho} \\ (b_{\delta}^{(k)}(t)u, v) &:= \left(\check{M}_{\delta}^{(k)}(t)u, v \right)_m \leq K |u|_{m+1, r, \rho} |v|_{m, r, \rho} \\ (B_{\delta i(j)}(t)u, v) &:= \left(M_{\delta i} M_{\delta j}(t)u, v \right)_m \leq K |u|_{m+1, r, \rho} |v|_{m+1, r, \rho} \\ (b_{\delta i(j)}(t)u, v) &:= \left(\check{M}_{\delta i} \check{M}_{\delta j}(t)u, v \right)_m \leq K |u|_{m+1, r, \rho} |v|_{m+1, r, \rho} \\ (C_{\delta ij}(t)u, v) &:= \left(M_{\delta i} M_{\delta j}(t)u - M_{\delta j} M_{\delta i}(t)u, v \right)_m \leq K |u|_{m+1, r, \rho} |v|_{m, r, \rho} \\ (c_{\delta ij}(t)u, v) &:= \left(\check{M}_{\delta i} \check{M}_{\delta j}(t)u - \check{M}_{\delta j} \check{M}_{\delta i}(t)u, v \right)_m \leq K |u|_{m+1, r, \rho} |v|_{m, r, \rho} \quad (4.4) \end{aligned}$$

for all $t \in [0, T]$, $\omega_\delta \in \Omega_\delta$, $u, v \in C_0^\infty(\mathbb{R}^d)$, $i, j = \overline{1, d_1}$, $k = \overline{1, d_2}$, $\delta > 0$.

Consequently $a_\delta(t)$, $B_{\delta i(j)}(t)$, $b_{\delta i(j)}(t)$ are bounded linear operators from H_1 into H_1^* and $B_{\delta i}(t)$, $b_{\delta i}(t)$, $B_{\delta}^{(k)}(t)$, $b_{\delta}^{(k)}(t)$, $C_{\delta ij}(t)$, $c_{\delta ij}(t)$ are bounded linear operators from H_1 into H_0 for every $t \in [0, T]$, $\omega_\delta \in \Omega_\delta$, $\delta > 0$ and their operator norms are bounded by K , uniformly in t, ω_δ, δ .

In the same way we get also that for all $u, v \in C_0^\infty(\mathbb{R}^d)$

$$(M_{\delta i}(t)u, v)_m \leq K |u|_{m, r, \rho} |v|_{m+1, r, \rho}$$

$$\left(\check{M}_{\delta i}(t)u, v \right)_m \leq K|u|_{m, r, p}|v|_{m+1, r, p}$$

for all $t \in [0, T]$, $\omega_\delta \in \Omega_\delta$, $u, v \in C_0^\infty(\mathbb{R}^d)$, $i, j = \overline{1, d_1}$, $\delta > 0$.

Consequently the operators $B_{\delta i}(t)$ and $b_{\delta i}(t)$ are bounded linear operators also from H_0 into H_1^* and their operator norms are bounded by K , uniformly in t, ω_δ, δ .

Note that $B_{\delta i(j)}(t) : H_1 \rightarrow H_1^*$ is the composition of the operators $B_{\delta j}(t) : H_1 \rightarrow H_0$ and $B_{\delta i}(t) : H_0 \rightarrow H_1^*$, that means: $B_{\delta i(j)}(t) := B_{\delta i}(t)B_{\delta j}(t)$.

Note also that $C_{\delta ij}(t) = B_{\delta i}(t)B_{\delta j}(t) - B_{\delta j}(t)B_{\delta i}(t) := [B_{\delta i}(t), B_{\delta j}(t)]$.

Similarly $B_{\delta i(j)}(t) := B_{\delta i}(t)B_{\delta j}(t)$ and $c_{\delta ij}(t) = [b_{\delta i}(t), b_{\delta j}(t)]$.

Hence, by the equations (4.1)' and (4.2)' we can see that H_δ and H are solutions on $[0, T]$ of the stochastic evolution equations:

$$H_\delta(t) = H_{\delta 0} + \int_0^t A_\delta H_\delta(s) ds + \int_0^t B_{\delta i}(s) H_\delta(s) dW_\delta^i(s) + \frac{1}{2} \int_0^t B_{\delta i(j)}(s) H_\delta(s) d\langle W_\delta^i, W_\delta^j \rangle(s) + \frac{1}{2} \int_0^t B_{\delta i}^{(k)}(s) H_\delta(s) d\langle W_\delta^i, N_\delta^k \rangle(s) \quad (4.5)$$

$$H(t) := H_0 + \int_0^t a_\delta(s) H(s) ds + \int_0^t b_{\delta i}(s) H(s) dW^i(s) + \frac{1}{2} \int_0^t b_{\delta i(j)} H(s) d\langle W^i, W^j \rangle(s) + \frac{1}{2} \int_0^t c_{\delta ij} H(s) d\langle W^i, W^j \rangle(s) + \frac{1}{2} \int_0^t b_{\delta i}^{(k)}(s) H(s) d\left(\frac{1}{2} \langle W^i, N^k \rangle + I_\delta^{ik}(s)\right) \quad (4.6)$$

considered in the normal triple $H_1 \hookrightarrow H_0 \equiv H_0^* \hookrightarrow H_1^*$.

By stochastic differential of $B_{\delta i}^p := (-1)^p b_{\delta i}^{ik(p)}$ we have, for P_δ -almost every $\omega_\delta \in \Omega_\delta$

$$\int_{\mathbb{R}^d} B_{\delta i}^p(t, x) \eta(x) dx = \int_{\mathbb{R}^d} B_{\delta i}^p(0, x) \eta(x) dx + \int_0^t \left(\int_{\mathbb{R}^d} B_{\delta i}^{p(k)}(s, x) \eta(x) dx \right) dN_\delta^k(s)$$

for all $t \in [0, T]$ and for every $\eta \in C_0^\infty(\mathbb{R}^d)$. Substituting $D_p H A_m \eta$ in place of η we get:

$$(M_{\delta i}(t)v, \eta)_m = (M_{\delta i}(0)v, \eta)_m + \int_0^t \left(M_{\delta i}^{(k)}(s)v, \eta \right)_m dN_\delta^k(s)$$

i.e., we have: $(B_{\delta i}(t)v, \eta) = (B_{\delta i}(0)v, \eta) + \int_0^t (B_{\delta i}^{(k)}(s)v, \eta) dN_\delta^k(s)$

for every $v, \eta \in C_0^\infty \subset H_1$ and hence for every $v, \eta \in H_1$ by (3.15). In the same way we can show that $(b_{\delta i}(t)v, \eta)$ have the stochastic differentials:

$$\forall v, \eta \in H_1, d(b_{\delta i}(t)v, \eta) = (b_{\delta i}^{(k)}(t)v, \eta) dN_\delta^k(t)$$

We can verify the conditions of Theorem 2.3 by using the following lemmas.

$|v|_\alpha$ denotes the norm of v in H_α and $|v|_{-\alpha}$ is the norm of v in H_α^* . Recall that (\cdot, \cdot) denotes the scalar product in H_0 and the duality between H_α and H_α^* .

Lemma 4.1 Let L, M, N be differential operators of the form:

$L := D_p(a^{pq}(x)D_q)$, $M := b^p(x)D_p$, $N := c^p(x)D_p$, where a^{pq}, b^p, c^p are real functions on \mathbb{R}^d ($p, q := 0, \dots, d$)

1) Let $v := 0, 1, 2$. Suppose that:

$$\forall x \in \mathbb{R}^d, \forall |\gamma| \leq m+v, |D^\gamma a^{pq}(x)| \leq K|\rho(x)|^{\hat{p}+\hat{q}-|\gamma|}, |D^\gamma b^p(x)| \leq K|\rho(x)|^{\hat{p}-|\gamma|}$$

$$\text{Then: } \forall v, \Phi \in C_0^\infty(\mathbb{R}^d), |L v, \Phi| \leq K' |v|_{1+v} |\Phi|_{1-v}, |M v, \Phi| \leq K' |v|_{1+v} |\Phi|_{-v}.$$

2) Suppose that: $\forall x \in \mathbb{R}^d, \forall |\gamma| \leq \max(m, 2), \forall |\beta| \leq \max(m, 1)$

$$|D^\beta c^j(x)| \leq K|\rho(x)|^{1-|\beta|}, |D^\gamma c^0(x)| \leq K|\rho(x)|^{-|\gamma|}$$

$$\text{Then: } \forall v, \Phi \in C_0^\infty(\mathbb{R}^d), \forall \alpha = 0, \pm 1, |(N v, \Phi)| \leq K' |v|_\alpha |\Phi|_{1-\alpha}.$$

The constant K' in the above statements depends only on v, m, k , on the weight functions r, ρ and on the dimension d .

Proof

$$1) \quad |(D_p(a^{pq}D_q v), \Phi)| \leq |(-1)^{\hat{p}}(a^{pq}D_q v, D_p \Phi)| \leq |(D_v(a^{pq}D_q v), D_{-v}D_p \Phi)| \leq \\ \leq |D_v(a^{pq}D_q v)| \cdot |D_{-v} \Phi| \leq K' |v|_{1+v} |\Phi|_{1-v}, \\ |(b^p D_p v, \Phi)| \leq |(D_v b^p D_p v, D_{-v} \Phi)| \leq |D_v b^p D_p v| \cdot |D_{-v} \Phi| \leq K' |v|_{1+v} |\Phi|_{-v}$$

2) Let us prove only the case $\alpha := -1$. The rest of Lemma is obvious.

Let v be an arbitrary generalised function from H_{-1} . Then $v = (I - \Delta)u$ and

$\exists u \in H_1 : |u|_1 = |v|_{-1}$, where I is the identity and Δ is the Laplace operator.

Therefore:

$$(c^k D_k v, \Phi) = -((I - \Delta)u, D_k(c^k \Phi)) = -(D_p u, D_p D_k(c^k \Phi)) \leq K' |u|_1 |\Phi|_2 = K' |v|_{-1} |\Phi|_2$$

Remark 4.2 Note that under the conditions of statement 2) of the above lemma, M is a bounded linear operator from H_α into $H_{\alpha-1}$ for $\alpha = 0, \pm 1$.

Lemma 4.3 Let $L_\delta(t), M_\delta(t), N_\delta(t)$ be differential operators of the form

$$L_\delta(t) := D_p(a_\delta^{pq}(x)D_q), \quad M_\delta(t) := b_\delta^p(x)D_p, \quad N_\delta(t) := c_\delta^p(x)D_p$$

for every $\delta > 0$, where $a_\delta^{pq}, b_\delta^p, c_\delta^p$ are measurable functions on $[0, T] \times \Omega_\delta \times \mathbb{R}^d$.

Suppose that for all $(t, \omega_\delta, x) \in [0, T] \times \Omega_\delta \times \mathbb{R}^d$ and $\delta > 0$:

$$\forall |\gamma| \leq m, \quad |D^\gamma a_\delta^{pq}(t, \omega_\delta, x)| \leq K |\rho(x)|^{\hat{p} + \hat{q} - |\gamma|} \\ \forall |\gamma_1| \leq m+1, \quad |D^{\gamma_1} b_\delta^p(t, \omega_\delta, x)| \leq K |\rho(x)|^{\hat{p} - |\gamma_1|}$$

For $H_\delta(t)$ be an increasing continuous random process for every $\delta > 0$.

1) If $D^\gamma a_\delta^{pq}(t, x) \sim 0$ in $\mathcal{L}_2(dH_\delta)R$ (w.r. to P_δ) for all $|\gamma| \leq m$, then:

$$\forall v \in W_2^{m+1}(r, \rho), \quad \forall \delta > 0, \quad L_\delta v \sim 0 \text{ in } \mathcal{L}_2(dH_\delta)W_2^{m-1}(r, \rho) \text{ (w.r. to } P_\delta)$$

2) If: $\forall x \in \mathbb{R}^d, \forall |\gamma_1| \leq m+1, p=0, \dots, d \quad D^{\gamma_1} b_\delta^p(t, x) \sim 0$ in $\mathcal{L}R$ (w.r. to P_δ)

then: a) $\forall u_1 \in W_2^{m+1}(r, \rho), \quad M_\delta(t)u_1 \sim 0$ and $M_\delta^{(m*)}(t)u_1 \sim 0$ in $\mathcal{L}W_2^m(r, \rho)$,

b) $\forall u_2 \in W_2^{m+2}(r, \rho), \quad M_\delta(t)u_2 \sim 0$ in $\mathcal{L}W_2^{m+1}(r, \rho)$ (w.r. to P_δ),

where $M_\delta^{(m*)}(t)$ is the adjoint of $M_\delta(t)$ in the duality determined by the scalar product in $W_2^m(r, \rho)$.

Proof We only prove that $\forall u_1 \in W_2^{m+1}(r, \rho), \quad M_\delta^{(m*)}(t)u_1 \sim 0$ in $\mathcal{L}W_2^m(r, \rho)$.

The rest of Lemma is similarly proved. Obviously,

$$I_\delta := \sup_{t \leq T} |M_\delta^{(m*)}(t)u_1|_0^2 = \sup_{t \leq T} \sup_{|v|_0 \leq 1} \left| (M_\delta^{(m*)}(t)u_1, v) \right|^2 = \sup_{t \leq T} \sup_{|v|_0 \leq 1} |(u_1, M_\delta(t)v)|^2.$$

Hence, by integration by parts and by using property (I_1) of the weight functions r and

$$\rho \text{ we get: } I_\delta \leq k \int_{\mathbb{R}^d} \sup_{t \leq T} g_\delta(t, x) f(x) dx, \quad (4.7)$$

$$\text{where: } g_\delta(t, x) := \sum_{|\gamma_1| \leq \max(m, 1)} \sum_{p=0}^d |\rho(x)|^2 |\gamma_1|^{-2\hat{p}} |D^{\gamma_1} b_\delta^p(t, x)|^2$$

$$f(x) := \sum_{|\gamma_2| \leq m+1} r^2(x) |\rho(x)|^2 |\gamma_2| |D^{\gamma_2} u_1(x)|^2$$

By the assumption of the lemma we have $\forall x \in \mathbb{R}^d, \quad g_\delta(t, x) \sim 0$ in $\mathcal{L}R$ (w.r. to P_δ) and

$$\forall(t, \omega_\delta, x) \in [0, T] \times \Omega_\delta \times \mathbb{R}^d, \forall \delta > 0, \quad g_\delta(t, x) \leq K$$

Therefore: $\forall x \in \mathbb{R}^d, \forall \delta > 0, \quad \lim_{\delta \rightarrow 0} E_\delta \sup_{t \leq T} g_\delta(t, x) = 0$ and $E_\delta \sup_{t \leq T} g_\delta(t, x) \leq K$, where

E_δ denotes the expectation with respect to P_δ . Thus from (4.7) we have, by Lebesgue's theorem on dominated convergence:

$$\limsup_{\delta \rightarrow 0} E_\delta I_\delta \leq K \limsup_{\delta \rightarrow 0} \int_{\mathbb{R}^d} \left(E_\delta \sup_{t \leq T} g_\delta(t, x) \right) f(x) dx = 0$$

Hence, by Chebyshev's inequality we have: $\forall u_1 \in W_2^{m+1}(r, \rho), \quad M_\delta^{(m^*)}(t)u_1 \rightarrow 0$ in $W_2^m(r, \rho)$ (w.r. to P_δ). \square

Lemma 4.4 Let L be a differential operator of the form $L := D_p(a^{pq}(x)D_q)$, where a^{pq} is a measurable function on \mathbb{R}^d for every $p, q := \overline{0, d}$. Assume that:

$$\forall x \in \mathbb{R}^d, \forall |\gamma| \leq m, \quad |D^\gamma a^{pq}(x)| \leq K|\rho(x)|^{\hat{p}+\hat{q}-|\gamma|}$$

$$\forall x \in \mathbb{R}^d, \forall \theta := (\theta_1, \dots, \theta_d) \in \mathbb{R}^d, \exists \lambda > 0, \quad \sum_{p,q=1}^d a^{pq}(x)\theta_p\theta_q \geq \lambda \rho^2(x) \sum_{j=1}^d \theta_j^2 \quad (4.8)$$

$$\text{Then:} \quad \forall v \in H_1 := W_2^{m+1}(r, \rho), \exists K' > 0 : (Lv, v) + \frac{\lambda}{2}|v|_1^2 \leq K'|v|_0^2$$

where K' is a constant which depends only on d, λ, m, r, ρ and on the constant K above.

Proof By the definition of the scalar product in $W_2^m(r, \rho)$ (which is extended by continuity to the duality between $W_2^{m+1}(r, \rho)$ and $W_2^{m-1}(r, \rho) \equiv W_2^{(m+1)^*}$) and by using the property (I₁) of the weight functions r and ρ we have:

$$\begin{aligned} (Lv, v) &= \sum_{|\gamma| \leq m} C_\gamma^m (-1)^{\hat{p}} \int_{\mathbb{R}^d} \left\{ D^\gamma a^{pq}(x) D_q v(x) D_p \left(r^2(x) \rho^2(x) D^\gamma v(x) \right) \right\} dx \leq \\ &\leq \sum_{|\gamma| \leq m} C_\gamma^m \int_{\mathbb{R}^d} r^2(x) |\rho(x)|^{2|\gamma|} a^{jl}(x) (D_l D^\gamma v(x)) (D_j D^\gamma v(x)) dx + k|v|_0|v|_1 = \\ &= \sum_{|\gamma| \leq m} C_\gamma^m \int_{\mathbb{R}^d} \rho^{-2}(x) a^{jl}(x) \left(r(x) |\rho(x)|^{|\gamma|+1} D_l D^\gamma v(x) \right) \left(r(x) |\rho(x)|^{|\gamma|+1} D_j D^\gamma v(x) \right) dx + k|v|_0|v|_1 \end{aligned}$$

where k is a constant, depending on d, m, K and on the weight functions r and ρ . Hence by

(3.19) and by the inequality: $k|v|_0|v|_1 \leq \frac{\lambda}{2}|v|_1^2 + \frac{k^2}{2\lambda}|v|_0^2$ we have:

$$\begin{aligned} (Lv, v) &\leq -\lambda \sum_{|\gamma| \leq m} C_\gamma^m \int_{\mathbb{R}^d} \sum_{j=1}^d r^2(x) |\rho(x)|^{2|\gamma|+1} |D_j D^\gamma v(x)|^2 dx + k|v|_0|v|_1 \leq \\ &\leq -\lambda|v|_1^2 + k_0|v|_0^2 + \frac{\lambda}{2}|v|_1^2 + \frac{k^2}{2\lambda}|v|_0^2 \leq \frac{\lambda}{2}|v|_1^2 + K'|v|_0^2, \end{aligned}$$

with $K' := k_0 + \frac{k^2}{2\lambda}$, where k_0 is a constant depending on λ, d, m . \square

Lemma 4.5 Let L, M, N be differential operators of the form:

$L := D_p(a^{pq}(x)D_q), \quad M := b^p(x)D_p, \quad N := c^p(x)D_p$, where a^{pq}, b^p, c^p are measurable real functions on \mathbb{R}^d for $p, q := \overline{0, \dots, d}$.

1) Assume that:

$$\forall x \in \mathbb{R}^d, \forall |\gamma| \leq m, |\beta| \leq \max(m, 1), \quad |D^\beta c^j(x)| \leq K|\rho(x)|^{1-|\beta|}, \quad |D^\gamma c^0(x)| \leq K|\rho(x)|^{-|\gamma|}$$

$$\text{Then:} \quad \forall v \in H_1 := W_2^{m+1}(r, \rho), \exists K' > 0, \quad |(Nv, v)| \leq K'|v|_0^2$$

2) Assume that:

$$\forall x \in \mathbb{R}^d, \forall |\beta| \leq \max(m+1, 2), \quad |D^\beta b^j(x)| \leq K|\rho(x)|^{1-|\beta|}, \quad |D^\beta c^j(x)| \leq K|\rho(x)|^{1-|\beta|}$$

$$\forall x \in \mathbb{R}^d, \forall |\gamma| \leq m+1, \quad |D^\gamma b^0(x)| \leq K|\rho(x)|^{-|\gamma|}, \quad |D^\gamma c^0(x)| \leq K|\rho(x)|^{-|\gamma|} \quad (4.9)$$

$$\text{Then:} \quad \forall v \in H_1, \quad |(Mv, Nv) + (v, MNv)| \leq K'|v|$$

3) Suppose the assumptions of 2). Assume moreover that:

$$\forall x \in \mathbb{R}^d, \forall |\gamma| \leq m, |D^\gamma a^{pq}(x)| \leq K|\rho(x)|^{\hat{p}+\hat{q}-|\gamma|} \quad (4.10)$$

$$\text{Then: } \forall v \in H_2, |(Lv, Mv) + (v, MLv)| \leq K'|v|_1^2, \quad (4.11)$$

where constant K' in the statements depends only on K, m, d and on the weight functions r, ρ .

Proof

We prove only 3). The statements 1) and 2) can be proved in the same fashion.

Assume first that $\forall p, q := \overline{0, d}, a^{pq} \in C_0^\infty(\mathbb{R}^d)$. We use the notations:

$$f_{i_1, \dots, i_n} := \frac{\partial}{\partial x_{i_1}} \dots \frac{\partial}{\partial x_{i_n}} f, \quad f_{i_1, \dots, i_k, \dots, i_n} := \frac{\partial}{\partial x_{i_1}} \dots \frac{\partial}{\partial x_{i_{k-1}}} \frac{\partial}{\partial x_{i_{k+1}}} \dots \frac{\partial}{\partial x_{i_n}} f$$

Note that to prove 3) it suffices to show that for every integer $n = 0, m$

$$\forall v \in C_0^\infty(\mathbb{R}^d), r^2 \rho^{2n} (a^{jl} v)_{j i_1 \dots i_n} \dots (b^k v_k)_{i_1 \dots i_n} + r^2 \rho^{2n} v_{i_1 \dots i_n} \left(b^k (a^{jl} v_l)_{jk} \right)_{i_1 \dots i_n} < 0$$

with a relation constant K depending only on K, m and d .

Obviously:

$$I_1 := r^2 \rho^{2n} (a^{jl} v)_{j i_1 \dots i_n} \dots (b^k v_k)_{i_1 \dots i_n} = r^2 \rho^{2n} (a^{jl} v_l)_{j i_1 \dots i_n} b^k v_{i_1 \dots i_k} + r^2 \rho^{2n} (a^{jl} v_l)_{j i_1 \dots i_n} g$$

where $g := (b^k v_k)_{i_1 \dots i_n} - b^k v_{k i_1 \dots i_n}$. By integration by parts:

$$r^2 \rho^{2n} (a^{jl} v_l)_{j i_1 \dots i_n} g \sim - (a^{jl} v_l)_{i_1 \dots i_n} (r^2 \rho^{2n} g)_j = \left(-r \rho^{n-1} (a^{jl} v_l)_{i_1 \dots i_n} \right) r^{-1} \rho^{1-n} (r^2 \rho^{2n} g)_j$$

Taking into account property (I_1) of the weight functions and the assumptions (3.20)-(3.21) we have:

$$\forall x \in \mathbb{R}^d, \left| r \rho^{n-1} (a^{jl} v_l)_{i_1 \dots i_n} \right| \leq K' \sum_{|\gamma| \leq m+1} r \rho^{|\gamma|} |D^\gamma v|$$

$$\forall x \in \mathbb{R}^d, \left| r^{-1} \rho^{1-n} (r^2 \rho^{2n} g)_j \right| \leq K' \sum_{|\gamma| \leq m+1} r \rho^{|\gamma|} |D^\gamma v|$$

where K' is a constant, depending only on K, m, d, r, ρ . Hence: $r^2 \rho^{2n} (a^{jl} v_l)_{j i_1 \dots i_n} g < 0$ and

consequently: $I_1 < r^2 \rho^{2n} (a^{jl} v_l)_{j i_1 \dots i_n} b^k v_{i_1 \dots i_k}$

Using property (I_1) and the assumptions (4.9)-(4.10) again, we have:

$$I_2 := r^2 \rho^{2n} v_{i_1 \dots i_n} \left(b^k (a^{jl} v_l)_{jk} \right)_{i_1 \dots i_n} < I_{21} + I_{22}$$

where: $I_{21} := r^2 \rho^{2n} v_{i_1 \dots i_n} b_{ip}^k (a^{jl} v_l)_{j k i_1 \dots i_p \dots i_n}$ and $I_{22} := r^2 \rho^{2n} v_{i_1 \dots i_n} b^k (a^{jl} v_l)_{j k i_1 \dots i_n}$

By integration by parts, we have:

$$I_{21} \sim - (r^2 \rho^{2n} v_{i_1 \dots i_n} b_{ip}^k)_{i_1 \dots i_n} (a^{jl} v_l)_{j i_1 \dots i_p \dots i_n} = I_{22} \sim - (r^2 \rho^{2n} v_{i_1 \dots i_n} b^k)_{i_1 \dots i_n} (a^{jl} v_l)_{j i_1 \dots i_n} =$$

$$= -r^2 \rho^{2n} b^k v_{i_1 \dots i_n k} (a^{jl} v_l)_{j i_1 \dots i_n} + Q$$

where $Q := - (r^2 \rho^{2n} b^k)_{i_1 \dots i_n} v_{i_1 \dots i_n} (a^{jl} v_l)_{j i_1 \dots i_n}$. By condition (I_1) and (4.9)-(4.10) we can

show that $I_{21} < 0, Q < 0$. Therefore: $I_2 < I_{22} < -r^2 \rho^{2n} b^k v_{i_1 \dots i_n k} (a^{jl} v_l)_{j i_1 \dots i_n}$.

Hence $I = I_1 + I_2 < 0$ by (4.10). In the general case of coefficients a^{pq} we take a non-negative kernel $\eta \in C_0^\infty(\mathbb{R}^d)$ such that $\int_{\mathbb{R}^d} \eta(x) dx = 1$ and define:

$$\forall \varepsilon > 0, a_\varepsilon^{ij} := \int_{\mathbb{R}^d} a^{ij}(x - \varepsilon y) \eta(y) dy, a_\varepsilon^p(x) := \int_{\mathbb{R}^d} a^p(x - \varepsilon y) \eta(y) dy, L_\varepsilon := D_p(a_\varepsilon^{pq} D_q)$$

Obviously $a_\varepsilon^{pq} \in C_0^\infty(\mathbb{R}^d)$ and by using the property (I_1) we can see that a_ε^{pq} satisfy the assumption (4.10) for every $\varepsilon > 0$, with some constant K which does not depend on ε .

Consequently, by virtue of what we have proved above:

$$\forall \varepsilon > 0, \forall v \in C_0^\infty(\mathbb{R}^d), |(L_\varepsilon v, Mv) + (v, M L_\varepsilon v)| \leq K' |v|_1^2$$

Letting here $\varepsilon \rightarrow 0$ we get (4.11) for every $v \in C_0^\infty(\mathbb{R}^d)$, and hence we can get (4.11) for every $v \in W_2^{m+2}(r, \rho)$. \square

Using now Lemmas 4.1 and 4.2 we can see that Equations (3.7) and (3.9) satisfy the assumptions (I_1) and (I_2) of Theorem 2.3. Moreover by lemmas 4.4 and 4.5 we can verify the assumption (I_4) . The assumption (I_3) and $(I_5)-(I_8)$ of Theorem 2.3 are obviously satisfied.

Hence we can finish the proof of Theorem 3.2 by applying Theorem 2.3. \square

5. References

- [1] Zeldovich Ya.B., Ruzmaikin A.A., Sokoloff D.D., Magnetic fields in astrophysics. N.Y.: Gordon and Breach, 1984, p.365
- [2] Molchanov S.A., Ruzmaikin A.A., Sokoloff D.D., Geophysics, Astrophysics, Fluid Dynamics, 1984, vol. 30, p. 242-259.
- [3] J.S. Baras, G. L. Blankenship and W. E. Hopkins; Existence, Uniqueness and Asymptotic Behaviour of Solutions to a Class of Zakai Equations with Unbounded Coefficients; IEEE Trans.A.C.28 (1986), p.203-214.
- [4] I.Gyongy, On the Approximation of Stochastic Partial Differential Equations, *Stochastics and Stochastics Reports* 25,26 (1988-1989), p.59-85,p.129-164.
- [5] I.Gyongy, The Stability of Stochastic Partial Differential Equations and Applications *Stochastics and Stochastics Reports* 27 (1989), p.129-150, p.189-232.
- [6] N.Ikeda and S.Watanabe, *Stochastic Differential Equations and Diffusion Processes*, North-Holland Publishing Co., Amsterdam-Oxford-New York (1981).
- [7] O.G.Purtukhia, Innovation problem for degenerate diffusion processes (unbounded coefficients), *Uspekhi Math. Nauk* 39 (238), No.4 (1984), p.177-178.
- [8] O.G.Purtukhia, On the Cauchy problem for linear stochastic partial differential equations (unbounded coefficients), in *Stochastic Analysis and Asymptotic Problems of Probability Theory and Mathematical Statistics*, Tibilisi (1984), p.57-71.
- [9] O.G.Purtukhia, On the Equations of filtering of Multidimensional diffusions Processes (unbounded coefficients), Thesis, Moscow, Lomonosow University 1984.
- [10] B.L.Rozovkii, to the Mathematical Theory of Hydromagnetic Dynamo in random Flow. *Doklady Akademik Nauk USSR*, No.6 (1987) p.1311-1314.
- [11] S.J.Shen, Solutions of certain parabolic equations with unbounded coefficients and its applications to non-linear filtering, *Stochastics* 10 (1983), p.31-46.

CONSIDERATIONS REGARDING NON-LINEAR STRUCTURAL COMPONENTS INFLUENCE ON ROCKET RUDDER ACTUATOR STABILITY

**Lecturer Eng. Luca Radutu
Military Technical Academy, Bucharest,
81-83 Regina Maria Boulevard, code 75275, Romania**

Abstract. In the specific literature, the rocket rudder actuators are mathematically treated as linear systems. Reality strongly infirm the linear character of these systems, whose structural elements generally have a non-linear behaviour.

The paper concerns with the evaluation of the pneumatic amplifier non-linear characteristics on the stability of the rudder actuator of an air-air rocket. Giving up the simplifying hypotheses which are usually adopted at rocket rudder actuators modelling, a non-linear mathematical model is elaborated, which takes into account the real variation of the working agent pressures inside the pneumatic cylinder chambers. On the basis of this mathematical model, using the description function method, the existence and the nature of the periodic solutions is analysed, for the equation of harmonic equilibrium.

The harmonic equilibrium equation solving is realised by numeric, graphic and analytic methods, in the specific conditions of some significant flying regimes.

1. Introduction

The specific literature treating the analysis and synthesis of rocket rudder actuators[2], [3] is based on a series of ideal, simple or approximate models for the physical processes which characterise these systems dynamics. In these conditions, the dynamic behaviour of the rocket rudder actuator is described, from the mathematical point view, by stationary linear differential equations system.. The analysis of actuator stability, under the hypothesis of small angular displacement of rocket rudder, in the proximity of the equilibrium position, is performed on the basis of this linear model. Mainly, the results obtained in such conditions could be satisfactory regarding a reasonable concordance between theory and experiment. It is also possible the occurrence of the situation in which the hypotheses adopted for the linear model could be unacceptable, leading to great differences with respect to the results obtained on the basis of the non-linear model.

Further, giving up the simplifying hypotheses adopted on pneumatic amplifier modelling, a non-linear mathematical model will be adopted, which consist the basis of the rocket rudder actuator stability analysis.

2. Mathematical modelling of rocket rudder actuator

The actuator consists in a electronic amplifier (A), a non-linear pressure amplifier (AP), a pneumatic cylinder (CP), a mechanical transmission (TM) and a linear displacement transducer (TP), connected as in the block schema represented in fig. 1.

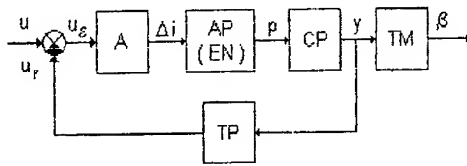


Fig.1. Block schema of non-linear actuator

The mathematical modelling on the physical processes consisting the functional basis of rocket rudder actuator structural elements, lead on the non-linear differential equations system

$$\left. \begin{aligned} \Delta i &= k_a (u - u_r); \\ T_c^2 \frac{d^2 \bar{x}_t}{dt^2} + 2 \xi_c T_c \frac{d \bar{x}_t}{dt} + \bar{x}_t &= k_c \Delta i; \\ \frac{dy}{dt} &= \frac{1}{S_p} \left\{ Q_0 \left[(1 + \varepsilon) \bar{x}_t - \frac{\varepsilon^2}{2 p_k} p \right] - \frac{\varepsilon V_0}{2 k p_k} \frac{dp}{dt} \right\}; \\ m_p \frac{d^2 y}{dt^2} + k_{fv} \frac{dy}{dt} + a_s y &= p S_p; \\ u_r &= k_p y; \\ \beta &= r y, \end{aligned} \right\} \quad (1)$$

where

$$p = p_1 - p_2;$$

$$p_1 = \begin{cases} \frac{1 + \bar{x}_t}{\varepsilon - \bar{x}_t} p_k, & p_1 \leq p_k B; \\ \left\{ \frac{1}{2} \left[1 + \frac{1}{K} \sqrt{K^2 + 4 \left(\frac{\varepsilon - \bar{x}_t}{1 + \bar{x}_t} \right)^2} \right] \right\}^{-\frac{k}{k-1}} p_k, & p_1 > p_k B; \end{cases}$$

$$p_2 = \begin{cases} \frac{1 - \bar{x}_t}{\varepsilon + \bar{x}_t} p_k, & p_2 \leq p_k B; \\ \left\{ \frac{1}{2} \bar{p}_a^{-\frac{1}{k}} \left[\bar{p}_a + \sqrt{K^2 \bar{p}_a^2 + 4 \left(\frac{1 - \bar{x}_t}{\varepsilon + \bar{x}_t} \right)^2} \right] \right\}^{\frac{k}{k-1}} p_k, & p_2 > p_k B, \end{cases} \quad (2)$$

and

$$B = \left(\frac{2}{k+1} \right)^k; \quad K = \sqrt{\frac{2}{k-1} \left(\frac{k+1}{2} \right)^{\frac{k+1}{k-1}}}; \quad \bar{p}_a = \frac{p_a}{p_k}. \quad (3)$$

The non-linear feature of equations system (1) is given by the relations (2) which express the real variations of working agent pressures inside the pneumatic cylinder chambers, function of jet tube relative displacement. On the basis of relations (2), taking into account the second equation of system (1), in fig.2 we represented the pressure loss on pneumatic cylinder piston, versus command electric current differential.

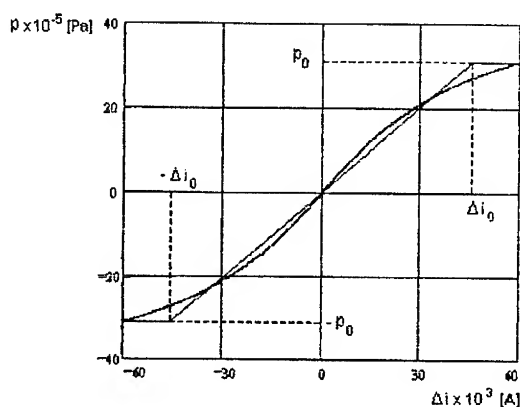


Fig.2. Non-linear characteristic on the pneumatic amplifier

The non-linear characteristic of the pneumatic amplifier may be taken as linear on intervals and assimilated with the characteristic of a non-linear element with saturation.

3. Formulation of harmonic linearisation problem of rocket rudder actuator

In order to study the rocket rudder actuator stability when the non-linear pneumatic amplifier is considered, the method of description function [1], [4], [5] will be used. This method is based on the hypothesis of separability, which consists in the possibility of performing system structural splitting into a linear subsystem and a non-linear subsystem.

Structural splitting of rocket rudder actuator is performed on the basis of block schema given in fig.1, of the equations system (1) and the non-linear characteristic showed in fig.2. Thus, the equivalent structural schema of the non-linear actuator takes the form showed in fig.3.

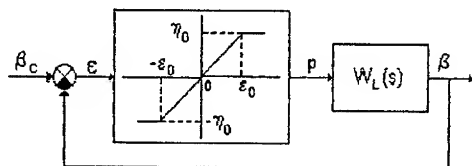


Fig.3. The equivalent structural schema of the non-linear actuator

The operator $W_L(s)$ represents the linear part transfer function of the non-linear actuator. This transfer function takes the form

$$W_L(s) = \frac{k_L}{(T_c^2 s^2 + 2 \xi_c T_c s + 1)(As^3 + Bs^2 + Cs + D)}, \quad (4)$$

where

$$\begin{aligned} k_L &= 2 k_r p_k S_p k_c Q_0 (1 + \varepsilon); \quad A = \varepsilon V_0 m_p; \quad B = \varepsilon (k_{fv} V_0 + k Q_0 m_p \varepsilon); \\ C &= \varepsilon V_0 a_s + k (2 p_k S_p^2 + k_{fv} Q_0 \varepsilon^2); \quad D = k Q_0 a_s \varepsilon^2. \end{aligned} \quad (5)$$

The relations between parameters of the non-linear characteristics represented in fig.2 and 3, are

$$\varepsilon_0 = \frac{\Delta_{i0}}{k_a k_p} r; \quad \eta_0 = p_0; \quad \beta_c = \frac{r}{k_p} u \quad (6)$$

At the equivalent structural schema, represented in fig.3, the functional relation input-output which characterises the non-linear pneumatic amplifier, is $p = f(\varepsilon)$, where f is a continuous and monotonous function on intervals, also, univalent and symmetric with respect to the plane (ε, p) .

The complex characteristic equation ($s = j\omega$) of the non-linear rocket rudder actuator (harmonic equilibrium equation) takes the form

$$1 + \bar{S}(\bar{A}) W_L(j\omega) = 0, \quad (7)$$

where \bar{A} represents the relative amplitude of non-linear element input signal, and $\bar{S}(\bar{A})$ is the harmonic complex relative operator (description function), which can be expressed with the relation

$$\bar{S}(\bar{A}) = \bar{a}(\bar{A}) + j \bar{b}(\bar{A}). \quad (8)$$

In (8), $\bar{a}(\bar{A})$ and $\bar{b}(\bar{A})$ represent the description function coefficients, which can be determined [1] by the help of the expressions

$$\bar{a}(\bar{A}) = \frac{2}{\pi} \left[\arcsin \frac{1}{\bar{A}} + \frac{1}{\bar{A}} \sqrt{1 - \left(\frac{1}{\bar{A}} \right)^2} \right], \quad \bar{A} \geq 1; \quad \bar{b}(\bar{A}) = 0. \quad (9)$$

Taking account of (8), the harmonic equilibrium equation (7) is equivalent with the non-linear real equations system

$$\begin{cases} \bar{a}(\bar{A}) = - \operatorname{Re} [W_L^{-1}(j\omega)]; \\ \bar{b}(\bar{A}) = - \operatorname{Im} [W_L^{-1}(j\omega)]. \end{cases} \quad (10)$$

Whether the non-linear equations system (10) have solutions, then the non-linear actuator is excited oscillating with pulsation ω_k and amplitude \bar{A}_k .

4. Analysis of existence and nature of periodic solutions of harmonic equilibrium equation

As the expressions of the description function relative coefficients, and these of the real and imaginary parts of the reversed transfer operator of the linear subsystem, are intricate, the analytical determination of non-linear equations system (10) solutions, is not possible. Therefore, in order to find these solutions, numeric or graphic methods could be used. The analysis of equations system (10) periodic solutions existence, lays on the basis

of the pneumatic mechanism functional and constructive features, for an air-air rocket which flies in some significant regime.

The numeric solving of non-linear equations system (10) by Newton-Raphson method, lead to the solutions showed in table 1.

Table 1

Excited oscillations parameters	Rocket flight regime			
	H=15 km		H=20 km	
	M=0,5	M=2,5	M=0,5	M=2,5
\bar{A}_k	2,85	2,01	2,82	2,40
A_k [rad]	0,005	0,003	0,005	0,004
ω_k [rad / s]	353,4	408,9	354,6	381,1

Note: $A_k = \bar{A}_k \varepsilon_0$.

The periodic solutions existence shows the fact that an oscillating working regime is induced in the non-linear actuator.

From the analysis on the values presented in table 1 results that for the same flight height, the excited oscillations pulsation increases and their amplitude decreases in supersonic regime, compared to the values obtained for the subsonic regime. In subsonic regime, when rocket flight height increases, the excited oscillations pulsation increases very slow, almost not significant, while their amplitude remains at the same level. On other hand, in supersonic regime, while rocket flight height increases, the excited oscillations pulsation decreases while their amplitude increases very slow.

In conformity with Loeb first rule [4], the excited oscillations characterised by the pairs of values (\bar{A}_k, ω_k) , are stable if the following condition is satisfied

$$S_0 = - \left(\frac{d \operatorname{Im}[W_L(j\omega)]}{d\omega} \right)_{\omega_k} \left(\frac{d \operatorname{Re}[\bar{S}_i(\bar{A})]}{d\bar{A}} \right)_{\bar{A}_k} > 0, \quad (11)$$

where

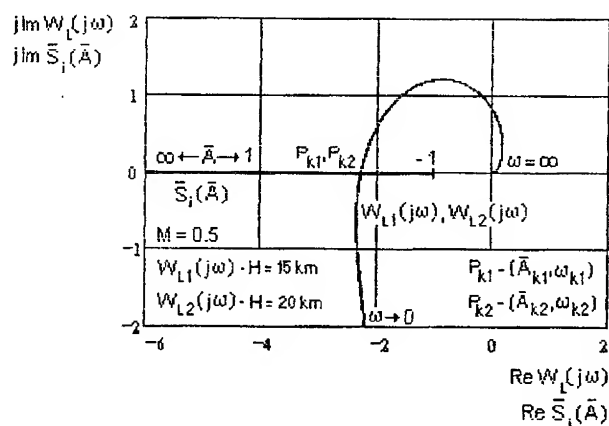
$$\bar{S}_i(\bar{A}) = -[\bar{S}(\bar{A})]^{-1} = -\frac{\bar{a}(\bar{A})}{\bar{a}(\bar{A})^2 + \bar{b}(\bar{A})^2} + j \frac{\bar{b}(\bar{A})}{\bar{a}(\bar{A})^2 + \bar{b}(\bar{A})^2}. \quad (12)$$

The $\bar{S}_i(\bar{A})$ operator, represents the relative reversed negative description function of the non-linear pneumatic amplifier.

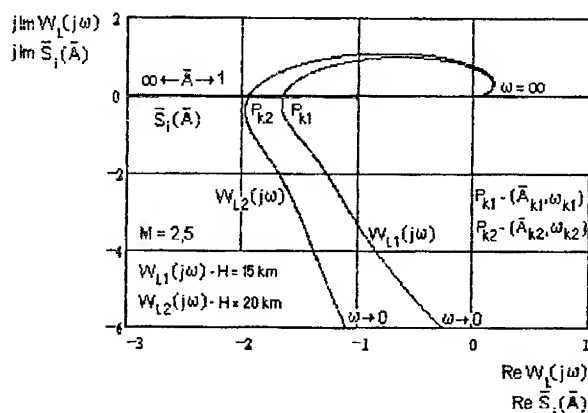
The validation of condition (11) is a difficult problem because of the intricate form of the expressions implied into the derivation procedure. One of the possibilities of avoiding the derivative computation, consists in graphic an analytic solving of equation (7), which, taking consideration of (12), can be expressed under the equivalent form

$$W_L(j\omega) = \bar{S}_i(\bar{A}). \quad (13)$$

The graphic and analytic solving of equation (13) is performed by Nyquist method with variable critic point [1], [4], and consists in a harmonic balance variant (Goldfarb) in the direct Nyquist plane. The transfer places $W_L(j\omega)$, $\omega \geq 0$ and $\bar{S}_i(\bar{A})$, $\bar{A} \geq 1$ are represented in fig.4, corresponding to the flight regimes indicated on the diagrams.



a)



b)

Fig. 4. The transfer places $W_L(j\omega)$ and $\bar{S}_i(\bar{A})$

a) - subsonic regime; b) - supersonic regime

Analysing the figure 4,a) results that in subsonic regime, near the origin of the complex plane, the transfer places $W_{L1}(j\omega)$ and $W_{L2}(j\omega)$, corresponding to the two flight height of the rocket, are practically the same. This observation confirms the fact that there are no significant differences in subsonic regime between the excited oscillations parameters, which appear in the non-linear actuator. Also, there are no significant differences between the excited oscillations parameters values, corresponding to the intersection points P_{k1} and P_{k2} and the values obtained by numerical method used.

The evaluation of the periodic oscillations nature, on the basis of the represented transfer places (fig.4), is done by the help of Lobe second rule [4]. In conformity with this rule, the excited oscillation characterised by the pair of values (\bar{A}_k, ω_k) is stable if starting from the intersection point of the two places on $W_L(j\omega)$ transfer place for increasing ω , the $\bar{S}_i(\bar{A})$ transfer place for \bar{A} ascending remains at the left. The analysis of the diagrams

presented in fig.4, considering this rule, indicates the fact that for the two flight regimes, the excited oscillations which appear in non-linear actuator are stable (self excited oscillations).

5. Conclusions

The stability analysis based on the linear mathematical model, shows that for a properly choose of the functional and constructive parameters, the rocket rudder actuator is structural stable. The pneumatic amplifier non-linear characteristic induces a excited oscillation regime in rocket rudder actuator, which, in this case, is no longer global asymptotic stable. In spite of this fact, for the flight regimes of the rocket analysed in the paper, the excited oscillations are stable, their parameters taking values whose short time perturbation does not lead to their unbounded increase in time.

List of symbols

- u - command signal;
- u_r - reaction signal;
- u_e - error signal;
- k_a - electronic amplifier transfer coefficient;
- Δi - electric current difference in electromagnetic converter coils;
- k_e - electromagnetic converter transfer coefficient;
- T_e - electromagnetic converter time constant;
- ξ_e - electromagnetic converter damping factor;
- k_p - displacement transducer transfer coefficient;
- p_k - working agent pressure;
- p_1, p_2 - pressures inside the pneumatic cylinder chambers;
- p - pressure differential on the pneumatic cylinder piston;
- p_a - atmospheric pressure;
- k_{rv} - viscous friction coefficient for the pneumatic cylinder;
- k - adiabatic exponent;
- \bar{x}_t - jet tube relative displacement;
- m_p - piston reduced mass;
- S_p - piston effective section area;
- V_0 - pneumatic cylinder chambers volume;
- y - piston displacement;
- r - mechanical transmission transfer coefficient;
- β - rudder braking angle;
- a_a - aerodynamic load coefficient;
- ε, Q_0 - actuator constructive parameters.

References

1. Belea, C. - Teoria sistemelor. Sisteme neliniare - Editura Didactică și Pedagogică, București, 1985.
2. Grigoriev, V.G. - Aviațione upravliaemae raketī - Izd. VVIA N. Jukovski, Moskva, 1985.
3. Kostin, S.V. - Rulevāe privodī - Izd. Mašinostroenie, Moskva, 1974.
4. Voicu, M. - Tehnici de analiză a stabilității sistemelor automate - Editura Tehnică, București, 1986.
5. Voronov, A.A. - Teoria nelineināh i spețialināh sistem upravlenia - Izd. Vāšaia Škola, Moskva, 1986.

Numerical Simulation of Nonlinear Transient Aircraft Response During Ground Motion

Vladimir ZELJKOVIC* & Stevan MAKSIMOVIC**

* Lola institute, Kneza Višeslava 70a, Belgrade

** Aeronautical Institute, Niška bb, 11133 Zarkovu, Belgrade

Abstract

In this paper, the aircraft motion and stability during taxiing and take-off were analyzed. The equations for aircraft yawing, including nose wheel was derived. Certain terms in these equations of motion have nonlinear character. Nonlinear equation for aircraft yawing, including nose wheel motion are derived. Suitable numerical techniques are used to solve this nonlinear problem. Linearization of nonlinear elements is performed to analyze the stability condition. The effect of main parameters (castering nose wheels, centering spring and damper) to the aircraft motion (natural frequency and damping) was analyzed. Presented coupled (aircraft and nose wheel) equation and parameters variation are illustrated by calculation and the numerical simulation of aircraft motion on the light trainer aircraft. The various types of rider input are applied for time response simulations.

*The numerical integration in a given domain of a system of
differential equations through the method of the norm
minimization of the error matrix*

Author: cpt. cdor. eng. Mihai Olariu
The Military Tehnical Academy,
No. 81-83, Regina Maria Bvd.P.O.Code 75275,
Sector 5, Bucharest.

This work presents some methods of integration for systems of differential equations with variable coefficients like: the method of the matricial polinomial expression, the method of developement in Taylor series or the method of the norm minimization of the error matrix. The obtained results and the conclusion drawn by using the three methods are analysed on a concrete exemple.

In most of the orientation problems, for example in the position determination of a body reported to an inertial referential system of axes, starting from the measurement of the angular velocities, a matricial system of differential equations must be integrated as follows:

$$\dot{C}(t) = C(t) \cdot \bar{\omega}(t), \quad (1)$$

where: $-C(t) \in M_3(C_R^1(T))$ is the director cosines matrix;

$-\bar{\omega}(t) \in M_3(C_R^1(T))$ is the matrix associated the momentary angular velocity vector.

$-C_R^1(T)$ is the set of real functions with a continue derivative on the T interval.

The theorem of existance and singleness for a system of differential equations with initial conditions given assures us that this system admits a unique solution on an interval. The no. (1) system admits an analytic solution only in certain conditions that are showed in the passages below. The numerical integration of the system can be done in two ways:

1)- analytic methods that give the approximation of the solution under the form of an analytic expression on an interval;

2)- numerical methods, that give the solution under the form of a succession of values, starting from an initial value of the solution.

Further on we will show in what conditions the no. 1 system admits an analytic solution.

The method of the matricial polynomial expression

The no. (1) system admits an analytic solution only if we have the equality of the matrices product:

$$\bar{\omega}(t) \cdot \int_0^t \bar{\omega}(s) ds = \left(\int_0^t \bar{\omega}(s) ds \right) \bar{\omega}(t), \quad (2)$$

The solution of the no. (1) system can be generalized because the rank of the matrix doesn't interfere in the demonstration that we will give below. But because third rank matrices interfere in solving this problem, we assume that the matrix

$C(t) \in M_3(C_R^1(T))$. We will demonstrate that the $C(t)$ matrix, having the form below, is a solution of the given system:

$$C(t) = C(0) \left[I_3 + \int_0^t \bar{\omega}(s) ds + \frac{1}{2!} \left(\int_0^t \bar{\omega}(s) ds \right)^2 + \frac{1}{3!} \left(\int_0^t \bar{\omega}(s) ds \right)^3 + \dots + \frac{1}{m!} \left(\int_0^t \bar{\omega}(s) ds \right)^m \right] \quad (3)$$

We called this relation a matricial polynomial expression because the forms of the terms in the development of the $C(t)$ matrix are matrices of different ranks.

Calculating the derivative (the derived function) of the no. (3) relation we have:

$$\begin{aligned} \dot{C}(t) = C(0) & \left[\bar{\omega}(t) + \frac{1}{2!} \bar{\omega}(t) \left(\int_0^t \bar{\omega}(s) ds \right) + \left(\int_0^t \bar{\omega}(s) ds \right) \bar{\omega}(t) \right] + \\ & + C(0) \left\{ \frac{1}{3!} \left[\bar{\omega}(t) \left(\int_0^t \bar{\omega}(s) ds \right)^2 + \left(\int_0^t \bar{\omega}(s) ds \right) \bar{\omega}(t) \left(\int_0^t \bar{\omega}(s) ds \right) + \right. \right. \\ & \left. \left. + \left(\int_0^t \bar{\omega}(s) ds \right)^2 \bar{\omega}(t) \right] + \dots \right\} \quad (4) \end{aligned}$$

By replacing the relations no. (3) and (4) in the no. (1) system of differential equations and making the necessary reckonings, we obtain:

$$\begin{aligned} \dot{C}(t) - C(t) \bar{\omega}(t) = \\ = C(0) \left[(\bar{\omega}(t) - \bar{\omega}(t)) + \left[\frac{1}{2} \bar{\omega}(t) \left(\int_0^t \bar{\omega}(s) ds \right) - \frac{1}{2} \left(\int_0^t \bar{\omega}(s) ds \right) \bar{\omega}(t) \right] + \right. \end{aligned}$$

$$+C(0)\left\{\frac{1}{3!}\left[\tilde{\omega}(t)\int_0^t\tilde{\omega}(s)ds\right]^2+\left(\int_0^t\tilde{\omega}(s)ds\right)\tilde{\omega}(t)\left(\int_0^t\tilde{\omega}(s)ds\right)+\right. \\ \left.-\frac{2}{6}\left(\int_0^t\tilde{\omega}(s)ds\right)^2\tilde{\omega}(t)+\dots\right\}. \quad (5)$$

If condition no. (2) respected, the differences from the right member of the no.5 relation are equal to zero. The demonstration backwards is easy to find. Meantime, from relation no. (3) can be noticed that for an effective estimation of the $C(t)$ matrix we must limit to the calculation of a certain number of terms of its development. Usually, the matrix associated to the angular velocity vector does not respect relation (2) and that is why the following types of errors result:

-errors due to the not interchangeable matrices $\tilde{\omega}(t)$ și $\int_0^t \tilde{\omega}(s)ds$;

-errors due to the truncation, because the fact the we limit to a certain number of terms, the first terms of relation (3).

If the angular velocity vector is fixed, the error due to the fact that the no. (2) product is not interchangeable is zero as it will be shown further on;

$$\omega_x(t) = \omega_{x0}f(t), \omega_y(t) = \omega_{y0}f(t), \omega_z(t) = \omega_{z0}f(t), \quad (6)$$

are the director cosines of the support of the $\vec{\omega}(t)$ vector. In this case the matrix associated to the angular velocity vector has the expression:

$$\tilde{\omega}(t) = \tilde{\omega}_0 f(t) \quad (7)$$

$$\text{where: } \tilde{\omega}_0 \in M_3(R). \text{ So: } \int_0^t \tilde{\omega}(s)ds = \tilde{\omega}_0 \int_0^t f(s)ds. \quad (8)$$

Considering the no. relation (8), relation (2) becomes:

$$\tilde{\omega}_0 f(t) \int_0^t \tilde{\omega}_0 f(s)ds = \tilde{\omega}_0^2 f(t) \int_0^t f(s)ds = \left(\int_0^t \tilde{\omega}_0 f(s)ds \right) \tilde{\omega}_0 f(t) = \tilde{\omega}_0^2 \left(\int_0^t f(s)ds \right) f(t). \quad (9)$$

Relation no. (9) confirms the justness of the previous statement. This method of integration justifies its implementation on a system of calculus of a navigator from the following reason: at every interval of calculus these integrals are used:

$$\theta_x = \int_0^T \omega_x(t)dt, \theta_y = \int_0^T \omega_y(t)dt, \theta_z = \int_0^T \omega_z(t)dt. \quad (10)$$

They are natural information from an integrating speed gyroscope or from a laser speed gyroscope.

The method of development in Taylor series

We intend to find a solution for the no. (1) system of differential equations, that approximates the exact one on a given interval with a certain error. If we acknowledge the $C(t)$ solution can be developed in Taylor series around the point t_0 under the form of a matricial polynomial expression, we have:

$$C(t) = C^{(0)}(t_0) + C^{(1)}(t_0) \frac{t-t_0}{1!} + C^{(2)}(t_0) \frac{(t-t_0)^2}{2!} + \dots + C^{(p)}(t_0) \frac{(t-t_0)^p}{p!}, \quad (11)$$

If we note with $C(t_i)$ the approximate form of the real solution, for $t=t_i$ and $t_i-t_0=h$, we have:

$$C(t_i) = C^{(0)}(t_0) + C^{(1)}(t_0) \frac{h}{1!} + C^{(2)}(t_0) \frac{h^2}{2!} + \dots + C^{(p)}(t_0) \frac{h^p}{p!}. \quad (12)$$

As it can be seen in relation no. (12), for establishing the $C(t_i)$ solution, we must find the constant matrices, symbolically noted : $C^{(0)}(t_0)$, $C^{(1)}(t_0)$, ..., $C^{(p)}(t_0)$; h being constant. Using the given system of differential equations it can be written:

$C^{(1)}(t_0) = C(t_0) \bar{\omega}(t_0)$. Further on the matrices of superior rank are calculated using the following relations:

$$C^{(2)}(t) = C^{(1)}(t) \bar{\omega}(t) + C(t) \bar{\omega}^{(1)}(t) = C(t) \bar{\omega}^2(t) + C(t) \bar{\omega}^{(1)}(t), \quad (13)$$

In relation no. (13) if $t=t_0$ we have:

$$C^{(2)}(t_0) = C(t_0) \left[\bar{\omega}^2(t_0) + \bar{\omega}^{(1)}(t_0) \right], \quad (14)$$

For the third rank derivative, we derive relation (14) and obtain:

$$C^{(3)}(t) = C(t) \left[\bar{\omega}^3(t) + 2 \bar{\omega}(t) \bar{\omega}^{(1)}(t) + \bar{\omega}^{(1)}(t) \bar{\omega}(t) + \bar{\omega}^{(2)}(t) \right], \quad (15)$$

respectively:

$$C^{(3)}(t_0) = C(t_0) \left[\bar{\omega}^3(t_0) + 2 \bar{\omega}(t_0) \bar{\omega}^{(1)}(t_0) + \bar{\omega}^{(1)}(t_0) \bar{\omega}(t_0) + \bar{\omega}^{(2)}(t_0) \right]$$

The proceeding can go on and other terms of higher rank can be taken from relation (12) according to the precision we want to provide to the calculus, but the expressions will be more complicated because of these derivations. The parameters „precision“ and „calculus duration“ are contradictory, the minimization of the error of approximation as much as possible leads to an increase of the time of calculus and backwards, so we are forced to take from relation (11) such a number of terms so that we can obtain maximum of efficiency. Because of this cause we won't obtain the real value $C(t_i)$, but an approximation determined, the C_2 approximation of the true $C(t_2)$ value can be found, using the same method. Finally, a table of values for the $C(t)$ solution is obtained, in which, besides $C(t_0)$ all the values are approximated.

The method of the norm minimization of the error matrix

Now, the problem of the integration of system no. (1) arises, but this time a solution of the following form is estimated:

$$\bar{C}(t) = C^{(0)} + C^{(1)} \frac{t}{1!} + C^{(2)} \frac{t^2}{2!} + \dots + C^{(s)} \frac{t^s}{s!}, \quad (16)$$

whose coefficients $C^{(0)}, C^{(1)}, \dots, C^{(s)}$ will be determined in conditions in which the error between the exact $C(t)$ solution and its estimation is minimum. We take into consideration the fact that the matrix will have to be an orthogonal matrix, and the relations between its elements constitute the bands for determining the extreme. Taking into account the orthogonality of the $C(t)$ matrix the following relations can be written:

$$r_p = \sum_{j=1}^3 \bar{c}_{kj}(t) \bar{c}_{ij}(t) - \delta_{ki} = 0, \quad p=1, 6, \quad \text{for } k=i=1, k=i=2, k=i=3, k=1 \text{ and } i=2, k=1 \text{ and } i=3, k=2 \text{ and } i=3. \quad (17)$$

So, for a certain estimation of the $C(t)$ matrix, we note the norm of the error matrix through the relation:

$$\varepsilon(\bar{c}_{ij}) = \int_0^t \sum_{i,j} \left\| \frac{d \bar{c}_{ij}(s)}{ds} - \sum_{k=1}^3 \bar{c}_{ik}(s) \omega_{kj}(s) \right\| ds, \quad (18)$$

With the aid of relation no. (17) and r_p restrictions the Lagrange function attached to this problem can be built:

$$L(\varepsilon, r) = \int_0^t \sum_{i,j} \left\| \frac{d \bar{c}_{ij}(s)}{ds} - \sum_{k=1}^3 \bar{c}_{ik}(s) \omega_{kj}(s) \right\| ds - \sum_{p=1}^6 \lambda_p r_p \quad (19)$$

which depends on the $\bar{c}_{ij}(t)$ elements of the $C(t)$ matrix and on the λ_p Lagrange's multipliers. Its points of local minimum must be sought among the critical points of $L(\varepsilon, r)$. These points are given by the solutions of the system:

$$\begin{aligned} \frac{\partial L(\varepsilon, r)}{\partial \bar{c}_{ij}} &= \frac{\partial \varepsilon(\bar{c}_{ij})}{\partial \bar{c}_{ij}} - \sum_{p=1}^6 \frac{\partial r_p(\bar{c}_{ij})}{\partial \bar{c}_{ij}} = 0 \\ \frac{\partial L(\varepsilon, r)}{\partial \lambda_p} &= -r_p(\bar{c}_{ij}) = 0, \quad i, j=1, 2, 3. \end{aligned} \quad (20)$$

Solving the no. (20) system we find the solution of no. (16) estimation.

Further on we consider that a vehicle is simultaneously rolled with the following angular velocities:

Conclusions

For the first two methods, the errors in the determination of the solution to the no. (1) system increase with the growth of the interval of integration.

In the case of the method of development in Taylor series, the solution of the system diverts far away from the real solution if the interval of integration increases.

The lowest error is obtained in the case of the third method. An improvement of the calculus process, from the point of view of the error in determining the solution, can be done considering more terms in relations no. (3), (12), and (16) with the inconvenience of increasing the time of calculus. In a given situation a compromise can be done between the time of obtaining the solution and the number of terms considered in the approximate solution.

References

1) Şabac, Gh. Ion, Special Mathematics, The Didactic and Pedagogic Publishing House, Bucharest, 1981.

2) Marusciuc, I., Methods of Solving the Problems of Non Linier Programation, „Dacia” Publishing House, Cluj-Napoca, 1973.

3) Udrişte, C., Tănăsescu, E., Minimums and Maximums for real functions of real variables, The Technical Publishing House, Bucharest.

4) Stăicu, St., Applications of the Matriceal Calculus in Solid Mechanics, The Academy of R.S.R Publishing House, 1986.

Roşculeţ, M., Mathematical Analysis, The Didactic and Pedagogic Publishing House, Bucharest, 1979.

Effectivity of hypergeometric function application in helicopter rotor blades theory numerical simulation

Časlav Mitrović, MSc, Dragan Cvetković, MSc,
Dragoljub Bekrić, B.Sc., Aleksandar Bengin, MSc

Faculty of Mechanical Engineering, University of Belgrade
Aeronautical Engineering Department, 27. marta St. 80
11000 Belgrade, F.R. of Yugoslavia

Abstract

Efficiency and justification of hypergeometric functions application in achieving simple formulas used in numerical simulation of helicopter rotor blades theory are presented in this paper.

First of all, basic equations of stream field over helicopter rotor are formulated, their decomposition is made and mean induced velocity harmonics are integrally presented. Theoretical basis of hypergeometric function application in transformation of integral equations of k - bladed rotor average induced velocity into special functions then follows. All necessary conditions for transformation hypergeometric functions into special functions are defined.

Various variants of integral transformation of expressions obtained in that way are presented here by numerical simulation and convenient solutions are found among them. This approach to effectivity of hypergeometric function application in helicopter rotor blades theory by numerical simulation allows achieving of synthetic method which can be used to define helicopter k - bladed main rotor optimal characteristics.

Basic assumptions and mutual relations

In practical rotor calculations based on disc theory it can be assumed that circulation along supporting line is constant over blade azimuth angle. This assumption does not cause large differences in induced velocity computation at small values of μ , and it significantly simplifies the computation.

This assumption is applied only for induced velocities calculation which represents the basis for further determination of actual values of angles of attack blade section and variable circulation $\bar{\Gamma}(\bar{\rho}, \theta)$ which are necessary for rotor characteristics calculation.

Let the k -bladed rotor with diameter $2R$ and center in origin of Cartesian system $Oxyz$ be placed in undisturbed flow field with velocity V . Rotor is rotating around y -axis with angular velocity ω . Direction of velocity V forms with xz plane arbitrary angle α . Rotor blade is presented by radial segment of supporting line with circulation varying with radius ρ ($0 \leq \rho \leq R$) and with constant circulation over azimuth angle θ .

It is assumed that free vortex elements separating from supporting line are moving in space $Oxyz$ along with particles of undisturbed flow field forming vortex shade in form of pitched spiral surface. Induced velocity V is calculated in arbitrary point of xz plane. That point is defined by polar coordinates: radius r and azimuth angle ψ .

In order to simplify the calculation dimensions coefficients defined by following expressions will be used:

$$\bar{V} = \frac{V}{\omega R}; \quad \bar{\Gamma} = \frac{\Gamma}{\omega R^2}; \quad \bar{\rho} = \frac{\rho}{R}; \quad \bar{\rho} = \frac{\rho}{r}; \quad \bar{r} = \frac{r}{R}$$

Induced velocity can be presented in following integral form [1]:

$$\bar{V} = \bar{V}_r + \frac{k}{4\pi\bar{V}} \int_0^1 \frac{\partial \bar{\Gamma}}{\partial \bar{\rho}} \Phi_p d\bar{\rho} + \frac{k}{4\pi\bar{r}} \int_0^1 \frac{\partial \bar{\Gamma}}{\partial \bar{\rho}} \Phi_q d\bar{\rho} \quad (1)$$

where

$$\bar{V}_r = -\frac{k \bar{\Gamma}(\bar{r})}{4\pi\bar{V}} \quad (2)$$

$$\Phi_p = \frac{1}{2\pi} \int_0^{2\pi} \frac{L_z \bar{\rho} \sin \theta \cos \alpha}{L^2 (L + L_x \cos \alpha)} d\theta \quad (3)$$

$$\Phi_q = \frac{1}{2\pi} \int_0^{2\pi} \frac{L_z \cos \alpha}{L (L + L_x \cos \alpha)} d\theta \quad (4)$$

and

$$L_x = (\bar{\rho} \cos \theta - 1) \cos \psi - \bar{\rho} \sin \theta \sin \psi;$$

$$L_z = (\bar{\rho} \cos \theta - 1) \sin \psi + \bar{\rho} \sin \theta \cos \psi; \quad L = \sqrt{1 + \bar{\rho}^2 - 2\bar{\rho} \cos \theta}$$

Periodic functions (3) and (4) with period 2 have following characteristics

$$\Phi_p(-\psi) = \Phi_p(\psi); \quad \Phi_q(-\psi) = -\Phi_q(\psi) \quad (5)$$

and consequently

$$\int_0^{2\pi} \Phi_p d\psi = \int_0^{2\pi} \Phi_q d\psi = 0$$

Therefore second term in expression (1) presents velocity field component symmetrical in regard to x-axis, and third term presents velocity field component asymmetrical in regard to x-axis. Let the velocity \bar{v} be presented in form of Fourier series progression:

$$\bar{v} = \bar{v}_r + \sum_{n=1}^{\infty} (\bar{v}_{cn} \cos n\psi - \bar{v}_{sn} \sin n\psi)$$

and coefficients determined as

$$\bar{v}_{cn} = \frac{1}{\pi} \int_0^{2\pi} \bar{v} \cos n\psi d\psi; \quad \bar{v}_{sn} = \frac{1}{\pi} \int_0^{2\pi} \bar{v} \sin n\psi d\psi \quad (6)$$

by use of formula (1). By replacing $t = \psi + \varphi$ expression (1) is transformed on basis of (5) and (6) into

$$\bar{v}_{cn} = -\frac{k k_{an}}{4\pi \bar{V}} \int_0^1 \frac{\partial \bar{\Gamma}}{\partial \bar{\rho}} C_n d\bar{\rho} \quad (7)$$

$$\bar{v}_{sn} = -\frac{k k_{an}}{4\pi \bar{r}} \int_0^1 \frac{\partial \bar{\Gamma}}{\partial \bar{\rho}} S_n d\bar{\rho} \quad (8)$$

where

$$k_{an} = -\frac{1}{2\pi} \int_0^{2\pi} \frac{\sin t \sin nt \cos \alpha}{1 + \cos t \cos \alpha} dt \quad (9)$$

$$C_n = \frac{1}{\pi} \int_0^{2\pi} \frac{1}{L} \sin \varphi \sin n\varphi d\theta; \quad S_n = \frac{1}{\pi} \int_0^{2\pi} \frac{1}{L} \cos n\varphi d\theta \quad (10)$$

Integral (9) is calculated elementarily and integrals (10) are presented in form

$$C_n = \frac{1}{\pi} \int_0^{\pi} \frac{1}{L} [T_n(\cos \varphi) - T_{n+1}(\cos \varphi)] d\theta; \quad (11)$$

$$S_n = \frac{2}{\pi} \int_0^{\pi} \frac{1}{L} T_n(\cos \varphi) d\theta \quad (12)$$

In expression (12) $T_n(\cos \varphi) = \cos n\varphi$ is first order Chebyshev polynomial. Polynomials Chebyshev are convenient because second equation from (8) is excluded. From (1) and (12) consequently follows:

$$C_n = \frac{1}{2} (S_{n-1} - S_{n+1}) \quad (13)$$

which correlates coefficients (7) and (8)

$$\bar{v}_{cn} = \frac{\bar{r}}{2\bar{V}} \left(k_{a1} \bar{v}_{sn-1} - \frac{1}{k_{a1}} \bar{v}_{sn+1} \right)$$

where k_{a1} is value k_{an} for $n = 1$.

From equations (11) and (12) follows that nuclei C_n and S_n of integrals (9) and (10) are not dependent of parameters characterizing rotor working order. Integral (12) allows transformation into hypergeometric function. It can be shown that integral (12) represents solution of Gauss differential equation:

$$\xi(1-\xi)\eta'' + [\gamma - (\alpha + \beta + 1)\xi]\eta' - \alpha\beta\eta = 0$$

with boundary conditions defined by nucleus (12) in form:

$$\begin{aligned} \eta(0) &= -2 \\ \eta'(0) &= 2m(m+1) \end{aligned} \quad (14)$$

if

$$\xi = \hat{\rho}^2; \quad \alpha = -m; \quad \beta = m+1; \quad \gamma = 1$$

It consequently follows that integral (12) represents hypergeometric function in form

$$S_{2m+1} = \begin{cases} -2F(-m, m+1, 1; \hat{\rho}^2); & \hat{\rho} < 1 \\ 0 & ; \hat{\rho} > 1 \end{cases} \quad (15)$$

Hypergeometric function F in expression (17) is Legendre polynomial P_m for $x = 1 - 2\hat{\rho}^2$. Calculation of nucleus (14) by using Legendre polynomial has following form

$$S_{2m+1} = \begin{cases} -2P_m(1 - 2\hat{\rho}^2); & \hat{\rho} < 1 \\ 0 & ; \hat{\rho} > 1 \end{cases} \quad (16)$$

For smaller values of index m equation (18) gives elementary expressions of requested nuclei

$$\begin{aligned} S_1 &= -2; \\ S_3 &= -2 + 4\hat{\rho}^2; \\ S_5 &= -2 + 12\hat{\rho}^2 - 12\hat{\rho}^4; \\ S_7 &= -2 + 24\hat{\rho}^2 - 60\hat{\rho}^4 + 40\hat{\rho}^6 \end{aligned} \quad (17)$$

Expression (16) can be rewritten in form

$$S_{2m+1} = -2 - \sum_{\mu=1}^m \alpha_{m\mu} \hat{\rho}^{2\mu} \quad (18)$$

where

$$\alpha_{m\mu} = \frac{(-1)^\mu (2\mu-1)!!}{2^\mu \mu! (2\mu)!} \left[(2m+1)^2 - 1^2 \right] \left[(2m+1)^2 - 3^2 \right] \dots \left[(2m+1)^2 - (2\mu-1)^2 \right]$$

where $(2\mu-1)!! = 1 \cdot 3 \cdot 5 \dots (2\mu-1)$.

For nuclei calculation for large values of index m it is convenient to use recurrence formula

$$S_{2m+3} = \frac{2m+1}{m+1} (1 - 2\hat{\rho}^2) S_{2m+1} - \frac{m}{m+1} S_{2m-1} \quad (19)$$

Graphic representation of function S_{2m+1} for different m are shown at Fig 1.

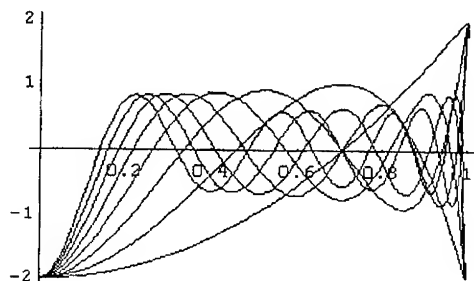


Fig. 1

In addition to convenient practical results (17), (18), (19), transformation of nucleus S_{2m-1} in form (16) gives following integral representation of Legendre polynomial which contains Chebyshev polynomial in form

$$P_m(\cos \theta) = -\frac{1}{\pi} \int_0^\pi T_{2m+1}(\rho) \frac{d\theta}{l}$$

where

$$\rho = \frac{1}{l} \left(\sin \frac{\theta}{2} \cos \theta - 1 \right); \quad l = \sqrt{1 + \sin^2 \frac{\theta}{2} - 2 \sin \frac{\theta}{2} \cos \theta}; \quad 0 \leq \theta \leq \pi, \quad m = 0, 1, 2, \dots$$

Since for $\bar{\rho} > 1$ according to (18) nuclei S_{2m+1} are zero, formula (10) can be transformed in form:

$$\bar{v}_{s2m+1} = \frac{k}{4\pi\bar{r}} \left(\frac{\cos \alpha}{1 + |\sin \alpha|} \right)^{2m+1} \int_0^{\partial \bar{\Gamma}} \frac{\partial \bar{\Gamma}}{\partial \bar{\rho}} S_{2m+1} d\bar{\rho} \quad (20)$$

For analytical solution expression (20) can be rewritten in form

$$\bar{v}_{s2m+1} = \frac{k}{4\pi\bar{r}} \left(\frac{\cos \alpha}{1 + |\sin \alpha|} \right)^{2m+1} \int_{-1}^{\partial \bar{\Gamma}} \frac{\partial \bar{\Gamma}}{\partial x} P_m(x) d\bar{\rho} \quad (21)$$

where $x = 1 - 2\bar{\rho}^2$ and partial derivative of circulation can be expressed in Legendre progression.

$$\frac{\partial \bar{\Gamma}}{\partial x} = \sum_{\mu=0}^{\infty} h_\mu P_\mu(x) \quad (22)$$

and taking into consideration that Legendre polynomial is orthogonal on basis of equation (21) analytical expression is obtained:

$$\bar{v}_{s2m+1} = \frac{k}{\pi\bar{r}} \frac{h_m}{2m+1} \left(\frac{\cos \alpha}{1 + |\sin \alpha|} \right)^{2m+1} \quad (23)$$

which shows that coefficient \bar{v}_{s2m+1} is dependent only on one coefficient from expression (22), that with index $\mu = m$. It can be shown by using Gauss hypergeometric equations, in a similar way to transformation of equation (16), that integral (10) can be expressed by following hypergeometric function

$$S_{2m} = \begin{cases} 2F\left(-m + \frac{1}{2}, m + \frac{1}{2}, 1; \bar{\rho}^2\right) & ; \quad \bar{\rho} < 1 \\ \frac{(-1)^m (2m-1)!!}{2^{3m-1} m!} \bar{\rho}^{-2m-1} F\left(m - \frac{1}{2}, m + \frac{1}{2}, 2m+1; \frac{1}{\bar{\rho}^2}\right) & ; \quad \bar{\rho} > 1 \end{cases} \quad (24)$$

which can be transformed into first and second order of Legendre functions.

$$S_{2m} = \begin{cases} 2P_{m-\frac{1}{2}}(1-2\bar{\rho}^2) & ; \quad \bar{\rho} < 1 \\ \frac{(-1)^m 4}{\pi} Q_{m-\frac{1}{2}}(2\bar{\rho}^2-1) & ; \quad \bar{\rho} > 1 \end{cases} \quad (25)$$

On basis of expression (25) it is possible to achieve following recurrence formula

$$S_{2m+2} = \frac{4m}{2m+1} (1-2\bar{\rho}^2) S_{2m} - \frac{2m-1}{2m+1} S_{2m-2} \quad (26)$$

For practical application of calculation function in expression (24) can be transformed into first and second order elliptic integrals by taking into consideration that they can be rewritten in following form:

$$K(x) = \frac{\pi}{2} F\left(\frac{1}{2}, \frac{1}{2}, 1; x^2\right); \quad E(x) = \frac{\pi}{2} F\left(-\frac{1}{2}, \frac{1}{2}, 1; x^2\right) \quad (27)$$

By replacing (27) into $m = 0$ and $m = 1$, following equations are obtained:

$$S_0 = \begin{cases} \frac{4}{\pi} K(\bar{\rho}) & ; \quad \bar{\rho} < 1 \\ \frac{4}{\pi \bar{\rho}} K\left(\frac{1}{\bar{\rho}}\right) & ; \quad \bar{\rho} > 1 \end{cases} \quad (28)$$

and

$$S_2 = \begin{cases} \frac{4}{\pi} [2E(\bar{\rho}) - K(\bar{\rho})] & ; \quad \bar{\rho} < 1 \\ \frac{4}{\pi \bar{\rho}} \left[2\bar{\rho}^2 E\left(\frac{1}{\bar{\rho}}\right) - (2\bar{\rho} - 1) K\left(\frac{1}{\bar{\rho}}\right) \right] & ; \quad \bar{\rho} > 1 \end{cases} \quad (29)$$

Recurrence formula (26) with equations (28) and (29) allows easy determination of nuclei S_{2m} for every m greater than zero. Transformation of (12) into (25) allows achieving of following integral representation of first and second order of Legendre function:

$$P_{m-\frac{1}{2}}(1-2x^2) = I_{2m}(x) ; \quad 0 \leq x < 1; \quad (30)$$

$$Q_{m-\frac{1}{2}}(2x^2-1) = (-1)^m \frac{\pi}{2} I_{2m}(x) ; \quad x > 1 \quad (31)$$

where

$$I_{2m} = \frac{1}{\pi} \int_0^\pi T_{2m}(\rho) \frac{d\theta}{l} ; \quad (m = 0, 1, 2, \dots)$$

and $T_{2m}(\rho)$ is first order Chedyshev polynomial with $\rho = \frac{1}{l}(x \cos \theta - 1)$ and $l = \sqrt{1+x^2-2x \cos \theta}$.

When nuclei S_n and coefficients \bar{v}_{sn} are once determined by using expression (9) it is possible to express nuclei C_n for even indices $n = 2m$ on basis of expressions (13) and (16) through Legendre polynomial

$$C_{2m} = \begin{cases} P_m(1-2\bar{\rho}^2) - P_{m-1}(1-2\bar{\rho}^2) & ; \quad \bar{\rho} < 1 \\ 0 & ; \quad \bar{\rho} > 1 \end{cases} \quad (32)$$

Nuclei C_{2m} can be expressed as hypergeometric functions by using assumptions (30):

$$C_{2m} = -2m \bar{\rho}^2 F(-m+1, m+1, 2; \bar{\rho}^2) \quad (33)$$

For smaller values of index m elementary formulas are achieved:

$$C_2 = -2\bar{\rho}^2 ;$$

$$C_4 = -4\bar{\rho}^2 + 6\bar{\rho}^2 ;$$

$$C_6 = -6\bar{\rho}^2 + 24\bar{\rho}^4 - 20\bar{\rho}^6 ;$$

$$C_8 = -8\bar{\rho}^2 + 60\bar{\rho}^4 - 120\bar{\rho}^6 + 70\bar{\rho}^8$$

Nuclei C_n for odd indices $n = 2m+1$ can be transformed by using expressions (13) and (25) into first and second order Jacobi functions which allows representation in form of elliptic integrals. For smaller m follows:

$$C_1 = \begin{cases} \frac{4}{\pi} [K(\bar{\rho}) - E(\bar{\rho})] & ; \quad \bar{\rho} < 1 \\ \frac{4}{\pi \bar{\rho}} \left[K\left(\frac{1}{\bar{\rho}}\right) - E\left(\frac{1}{\bar{\rho}}\right) \right] & ; \quad \bar{\rho} > 1 \end{cases} \quad (34)$$

$$C_3 = \begin{cases} \frac{4}{3\pi} [(1-4\bar{\rho}^2)K(\bar{\rho}) - (1-8\bar{\rho}^2)E(\bar{\rho})] & ; \quad \bar{\rho} < 1 \\ \frac{4}{3\pi \bar{\rho}} \left[(5-8\bar{\rho}^2)K\left(\frac{1}{\bar{\rho}}\right) - (1-8\bar{\rho}^2)E\left(\frac{1}{\bar{\rho}}\right) \right] & ; \quad \bar{\rho} > 1 \end{cases} \quad (35)$$

Conclusion

Efficiency of application of theory of hypergeometric function in rotor theory is reflected in achieving simple formulas representing velocity harmonics and representing basis for further numerical analyses of unsteady flow over helicopter rotor blades. Use of analytical presentation of induced velocity components significantly reduces working time and increases accuracy of calculation. Efficiency of applied method is shown by example and presented method shows great advantage in regard to classic approach to the problem solution because working time is shortened. Results achieved by this method are given by examples (Fig. 2-5)



Fig. 2



Fig. 3



References

1. Martinov, A.K., "Teoria nesuscevo vinta", *Masinstroenie*, 1973
2. Betchelor, G.K., "An introduction to Fluid Dynamics", *Cambridge University Press*, 1983
3. White, F.M., "Viscous Fluid Flow", 1974
4. Chia-Shun Y., "Fluid Mechanics", *The University of Mich.*, 1979
5. Rand O., "Extension of the Circle Theorems by Source Distribution", *JFE Vol 11* 1989.
6. Saffman P.G. and Sheffield, J.S., "Flow over a Wing with an Attached Free Vortex", *Studies in Applied Mathematics*, Vol. 57, No 2, 1977, pp. 107-117
7. Higuchi, H. and Park, O.W., "Computations of the Flow Past Solid and Slotted Two-Dimensional Bluff Bodies with Vortex Tracing Method", *AIAA Paper 89-0929*.
8. NASA TM 100068, Vortex Methods for Separated Flows & NASA TM 84328, Numerical Simulation of Separated Flows
9. Stepniewski W.Z., "Rotary-Wing Aerodynamics" New York, 1984
10. Fishelov, D., "A New Vortex Scheme for Viscous Flows", *Journal of Computational Physics*, Vol. 27, 1990, pp 211-224.

STRENGTH ANALYSIS OF AIRCRAFT STRUCTURES USING ELASTOPLASTIC FINITE ELEMENT ANALYSIS AND PROBABILISTIC APPROACH

Stevan MAKSIMOVIC

Aeronautical Institute, Niska bb, 11133 Zarkovo, Belgrade, Yugoslavia

&

Vladimir ZELJKOVIC

Lola Institute, Kneza Viseslava 70a, 11000, Belgrade

ABSTRACT

This paper presents a numerical method for evaluating the structural reliability of the aircraft structural components when the nonlinear finite element method (FEM) is used for the stress analysis. Reliability-based analysis and design describe the load, load effects and the strength as random variables so that safety is related to some measure of the probability that strength capacity exceeds loading. Possible errors in elastic-plastic stress-strain analysis at notches are resulting from the use of approximate, but relative simple, analysis techniques instead of more accurate, but more complex finite element technique. In order to evaluate the accuracy the stresses at the complex structural components, both elastic and elastic-plastic finite element analyses are used. For this purpose 4-node shell finite element, based on third order shear deformation theory, is used. As illustrative examples different kinds of aircraft structural elements are analyzed by reliability-based design procedures. For these examples very satisfactory results are obtained. This confirms the effectiveness of the proposed procedure.

Chemical reactions in open chaotic flows

G. Károlyi¹, Á. Péntek², T. Tél³ and Z. Toroczkai⁴

¹ Research Group for Computational Mechanics of the Hungarian Academy of Sciences, Műegyetem rkp. 3, H-1521 Budapest, Hungary

² Institute for Pure and Applied Physical Sciences, University of California, San Diego, La Jolla, CA 92093-0075 USA

³ Institute for Theoretical Physics, Eötvös University, Puskin u. 5-7, H-1088 Budapest, Hungary

⁴ Department of Physics, Virginia Polytechnic Institute and State University, Blacksburg, VA 24061, USA

Simple chemical processes due to an underlying chaotic hydrodynamical flow are considered. In such flows the non-turbulent, but time dependent velocity field leads to chaotic tracer dynamics, i.e., to Lagrangian chaos. Chemical reactions in such flows will act along the unstable manifold of the nonattracting chaotic saddle governing the dynamics. Thus it is natural to expect that fractal properties and chaos characteristics of the flow appear in the reaction equations, in fact the fractal dimension and the escape rate influence the concentration of the constituents.

The flow chosen to illustrate these phenomena is an example of a two-dimensional time-periodic fluid motion, the case of the von Karman vortex street in the wake of a cylinder. We consider simple *kinetic* reaction models where two particles of different kind undergo a reaction if and only if they come within a given distance, which can be called the interaction range. We shall consider an autocatalytic process $A + B \rightarrow 2B$ and a collisional reaction $A + B \rightarrow 2C$.

ANALYSIS OF A NONLINEAR INTEGRAL EQUATION MODELLING INFECTION DISEASES

Radu PRECUP and Eduard KIRR

Faculty of Mathematics and Informatics
University "Babeş-Bolyai", 3400 Cluj, Romania

Abstract

To describe the spread of virus diseases with contact rate that varies seasonally, the following delay integral equation has been proposed by K.L. Cooke and J.L. Kaplan

$$x(t) = \int_{t-\tau}^t f(s, x(s)) ds.$$

This model can also be interpreted as an evolution equation of a single species population. The purpose of this paper is to describe and improve recent results on this equation, obtained by the authors in the last decade. Our analysis is concerned with the existence, uniqueness, approximation and continuous dependence on data of the positive solutions of the initial-value problem, and of the periodic solutions. We use topological methods (fixed point theorems, continuation principle) and monotone iterative techniques.

Keywords: nonlinear integral equation, positive solutions, periodic solutions, fixed point, continuation principle, monotone iterations, continuous dependence, population dynamics.

AMS subject classification: 45G10, 45M15, 47H15.

1 Introduction

In this paper we are concerned with the following nonlinear delay integral equation

$$x(t) = \int_{t-\tau}^t f(s, x(s)) ds. \quad (1)$$

This equation and similar others appear when investigating the spread of virus diseases or, more generally, the growth of single species populations. Delay equations also arise from the study of materials with thermal- or shape-memory (see [28]).

Several results regarding various mathematical aspects of Eq.(1), or of equations of type (1), have been obtained by K.L. Cooke and J.L. Kaplan [1], H.L. Smith [2],[8], R.D. Nussbaum [3], J. Kaplan, M. Sorg and J. Yorke [4], S. Busenberg and K. Cooke [5], R.W. Leggett and L.R. Williams [7],[9], A. Cañada [11], D. Guo and V. Lakshmikantham [12], I.A. Rus [13], S.G. Hristova and D.D. Bainov [14], N.G. Kazakova and D.D. Bainov [15], A.M. Fink and J.A. Gatica [16], R. Precup [17],[20],[24], R. Torrejón [19], E. Kirr [21],[25], A. Cañada and A. Zertiti [22],[23], Ait Dads, K. Ezzinbi and O. Arino [26]. Eq.(1) also appears in the monographs [6],[10, Example 20.1] and [18].

Let us first describe the meaning of Eq.(1) in terms of epidemics. In this case, it is assumed that the total number of population members is constant; $x(t)$ represents the proportion of infectives in population at time t , regarded as a continuous quantity; τ is the length of time an individual remains infectious (duration of infectivity); $f(t, x(t))$ means the proportion of new infectives per unit time (instantaneous contact rate). Then, $f(t, x(t)) dt$ represents the proportion of individuals infected within the period $t, t + dt$. In consequence, the number of infectious individuals at time t equals the sum of all individuals infected between $t - \tau$ and t .

Let us now interpret Eq.(1) as a growth equation of a single species population when the birth rate varies seasonally. In this case, $x(t)$ is the number of individuals of a single species population at time t , $f(t, x(t))$ is the number of new births per unit time, and τ is the lifetime. It is assumed that each individual lives to the age τ exactly and then dies.

In this paper we report on two distinct problems on Eq.(1). In both cases, because of the biological interpretation, we shall be interested in positive solutions.

(I) *The initial-values problem (IVP)*

We look for positive continuous solutions $x(t)$ of Eq.(1), for $-\tau \leq t \leq T$, when it is known the proportion $\varphi(t)$ of infectives for $-\tau \leq t \leq 0$, i.e.,

$$x(t) = \varphi(t) \quad \text{for } -\tau \leq t \leq 0. \quad (2)$$

Obviously, we have to assume that $\varphi(t)$ is a positive continuous function on $[-\tau, 0]$ and satisfies

$$\varphi(0) = \int_{-\tau}^0 f(s, \varphi(s)) ds. \quad (3)$$

It is easy to see that, under assumption (3), problem (1)-(2) is equivalent with the following initial-values problem

$$\begin{cases} x'(t) = f(t, x(t)) - f(t - \tau, x(t - \tau)) & \text{for } 0 \leq t \leq T \\ x(t) = \varphi(t) & \text{for } -\tau \leq t \leq 0. \end{cases} \quad (4)$$

(II) *The periodic problem (PP)*

Because of seasonal factors, the rate $f(t, x)$ may be a ω -periodic function of t and, in such situations, one is interested in ω -periodic solutions of Eq.(1).

I. THE INITIAL-VALUES PROBLEM

2 Existence results

A. *Positive solutions in space.*

We are looking for solutions of (1)-(2) in the space C of all continuous functions $x(t)$ satisfying $x(t) \geq a$ for $-\tau \leq t \leq T$, where $a \geq 0$ is a given number.

Let us list our assumptions:

(a1) $f(t, x)$ is nonnegative and continuous for $-\tau \leq t \leq T$ and $x \geq a$.

(a2) $\varphi(t)$ is continuous, satisfies (3) and $\varphi(t) \geq a$ for $-\tau \leq t \leq 0$.

(a3) There exists a continuous function $g(t)$ such that

$$f(t, x) \geq g(t) \quad \text{for } -\tau \leq t \leq T \text{ and } x \geq a$$

and

$$\int_{t-\tau}^t g(s) ds \geq a \quad \text{for } 0 \leq t \leq T.$$

(a4) There exists a positive continuous function $h(x)$ on $[a, \infty)$ such that

$$f(t, x) \leq h(x) \quad \text{for } 0 \leq t \leq T \text{ and } x \geq a$$

and

$$T < \int_{\varphi(0)}^{\infty} (1/h(x)) dx.$$

Denote $b = \varphi(0)$ and let R_0 be given by

$$T = \int_b^{R_0} (1/h(x)) dx. \quad (5)$$

Theorem 2.1 ([17]). *Suppose (a1)-(a4) are satisfied. Then the problem (1)-(2) has at least one solution $x(t) \in C$. Moreover, any solution in C satisfies*

$$x(t) \leq R_0 \quad \text{for } 0 \leq t \leq T. \quad (6)$$

Proof. Let E be the Banach space of all continuous functions $x(t)$ defined on $[0, T]$, endowed with the uniform norm. Consider the closed convex set of E , $K = \{x \in E; x(t) \geq a \text{ for } 0 \leq t \leq T\}$, and let

$$X = \{x \in E; x(0) = b \text{ and } x(t) \geq a \text{ for } 0 \leq t \leq T\}.$$

Also consider the homotopy

$$H : K \times [0, 1] \rightarrow X,$$

$$H(x, \lambda)(t) = (1 - \lambda)b + \lambda \int_{t-\tau}^t f(s, \tilde{x}(s)) ds,$$

where $\tilde{x}(t) = x(t)$ for $0 < t \leq T$ and $\tilde{x}(t) = \varphi(t)$ for $-\tau \leq t \leq 0$. By (a3) and $b \geq a$, H is well-defined, i.e., $H(K \times [0, 1]) \subset X$, while by means of Ascoli-Arzelà theorem, it is completely continuous.

Next we establish the *a priori* boundedness of the set of all solutions of equations $H(x, \lambda) = x$, $\lambda \in [0, 1]$. Let x be such a solution. Then, for each $t \in [0, T]$, we have

$$x'(t) = \lambda f(t, x(t)) - \lambda f(t - \tau, x(t - \tau)).$$

Since f is nonnegative, we get

$$x'(t) \leq \lambda f(t, x(t)).$$

Further, by (a4),

$$x'(t) \leq \lambda h(x(t)).$$

It follows that

$$\int_0^t (x'(s)/h(x(s))) ds \leq \lambda t \leq \lambda T \leq T,$$

for all $t \in [0, T]$. Hence

$$\int_b^{x(t)} (1/h(u)) du \leq T \text{ for } 0 \leq t \leq T$$

whence, by (5), we see that x satisfies (6).

Therefore, if we choose any $R > R_0$, we have that H is an admissible (fixed point free on boundary) homotopy on the closure of the open bounded set of X ,

$$U = \{x \in X; x(t) < R \text{ for } 0 \leq t \leq T\}.$$

On the other hand, the constant map $H(., 0) = b$ is essential (see [27, Theorem 2.2]). Consequently, by the topological transversality theorem ([27, Theorem 2.5]), the map $A = H(., 1)$ is essential too. It follows that A has at least one fixed point $x \in U$. Clearly, x is a solution of (1)-(2). \square

Remark 2.1. Let us assume that instead of (a4) one has

(a4') $\lim_{x \rightarrow \infty} \sup f(t, x)/x = \mu(t)$ uniformly in $t \in [0, T]$ and $\mu = \sup_{0 \leq t \leq T} \mu(t) < \infty$.

Then, choosing $\alpha > \mu$, we get $\beta \geq 0$ such that

$$f(t, x) \leq \alpha x + \beta \text{ for } 0 \leq t \leq T \text{ and } x \geq a. \quad (7)$$

Hence (a4) is fulfilled by $h(x) = \alpha x + \beta$, and

$$\int_b^\infty (1/h(u)) du = \infty.$$

If in addition, in (a4'), we suppose $\mu < 1/\tau$ (this is assumption (H5) in [12]), then taking $\mu < \alpha < 1/\tau$ we can choose $R > b$ such that

$$\alpha R + \beta \leq R/\tau, \quad (8)$$

in order that A maps \bar{U} into itself and so, in this situation, Theorem 2.1 follows directly by Schauder's fixed point theorem. Next we show that this is also true for an arbitrary value of μ .

Indeed, let us use an equivalent norm on E , namely

$$\|x\|_\theta = \max_{0 \leq t \leq T} (|x(t)| \exp(-\theta t))$$

with a suitable positive number θ . By (8), we get

$$A(x)(t) \leq \tau\gamma + \int_0^t (\alpha x(s) + \beta) ds =$$

$$\tau\gamma + \beta t + \alpha \int_0^t x(s) \exp(-\theta s) \exp(\theta s) ds \leq \tau\gamma + \beta T + \alpha \|x\|_\theta \int_0^t \exp(\theta s) ds \leq$$

$$\tau\gamma + \beta T + (\alpha/\theta) \|x\|_\theta \exp(\theta t),$$

where $\gamma = \max_{-\tau \leq t \leq 0} f(t, \varphi(t))$. Thus

$$A(x)(t) \exp(-\theta t) \leq (\alpha/\theta) \|x\|_\theta + \tau\gamma + \beta T.$$

Now, if we choose $\theta > \alpha$ and $R > b$ such that

$$(\alpha/\theta) R + \tau\gamma + \beta T \leq R,$$

we see that A maps $\{x \in X; \|x\|_\theta \leq R\}$ into itself and so Schauder's fixed point theorem applies.

Let us now consider instead of (a4) a more restrictive condition than (a4'), namely

(a4'') There exists $L > 0$ such that

$$|f(t, x) - f(t, y)| \leq L|x - y| \quad (9)$$

for all $t \in [-\tau, T]$ and $x, y \in [a, \infty)$.

Theorem 2.2 ([17]). Suppose (a1)-(a3) and (a4'') are satisfied. Then the problem (1)-(2) has a unique solution $x(t) \in C$. Moreover,

$$x_n(t) \rightarrow x(t) \text{ as } n \rightarrow \infty, \text{ uniformly in } t \in [0, T],$$

where $x_0(t) = b$ and $x_n(t) = A(x_{n-1})(t)$ for $n = 1, 2, \dots$

Proof. Similar arguments as in Remark 2.1 yield to the conclusion that the map $A : X \rightarrow X$ is a contraction with respect to a suitable norm $\|\cdot\|_\theta$. Thus, Banach's fixed point theorem is applicable. \square

B. Positive solutions in a ball.

Suppose we are interested in solutions $x(t) \in C$ of (1)-(2), in a given ball of E , say of ray R . Obviously, in this situation, the contact rate $f(t, x)$ may be known only for $a \leq x \leq R$.

Let us list the hypotheses corresponding to this case.

(h1) $f(t, x)$ is nonnegative and continuous for $-\tau \leq t \leq T$ and $a \leq x \leq R$.

(h2) $\varphi(t)$ is continuous, satisfies (3) and $a \leq \varphi(t) \leq R$ for $-\tau \leq t \leq 0$.

(h3) There exists a continuous function $g(t)$ such that

$$f(t, x) \geq g(t) \text{ for } -\tau \leq t \leq T \text{ and } a \leq x \leq R$$

and

$$\int_{t-\tau}^t g(s) ds \geq a \text{ for } 0 \leq t \leq T. \quad (10)$$

(h4) There exists a positive continuous function $h(x)$ on $[a, R]$ such that

$$f(t, x) \leq h(x) \text{ for } 0 \leq t \leq T \text{ and } a \leq x \leq R \quad (11)$$

and

$$T < \int_{\varphi(0)}^R (1/h(x)) dx. \quad (12)$$

Theorem 2.3. Suppose (h1)-(h4) are satisfied. Then the problem (1)-(2) has at least one continuous solution $x(t)$ such that $a \leq x(t) \leq R$ for $-\tau \leq t \leq T$. In addition, any such solution satisfies (6).

Proof. The proof is the same as for Theorem 2.1. There is only one difference, the fact that the homotopy H can be defined only on $\bar{U} \times [0, 1]$. \square

Let us now suppose that instead of (h4) the following condition is satisfied:

(h4*) There exists $L > 0$ such that (9) holds for all $t \in [-\tau, T]$ and $x, y \in [a, R]$.

Theorem 2.4. Suppose (h1)-(h3) and (h4*) are satisfied. Then there exists T_0 , $0 < T_0 \leq T$, such that (1)-(2) has a unique continuous solution $x(t)$ on $[-\tau, T_0]$ satisfying $a \leq x(t) \leq R$ for $-\tau \leq t \leq T_0$.

Proof. By (9), we obtain

$$f(t, x) \leq L(x - a) + \max_{0 \leq t \leq T} f(t, a) =: h(x) \quad \text{for } a \leq x \leq R.$$

So (11) holds. Now we choose $T_0 \leq T$ such that

$$T_0 < \int_{\varphi(0)}^R (1/h(x)) dx,$$

and we apply Theorem 2.3 with T_0 instead of T . Thus the existence of solutions is proved. To show the uniqueness, suppose $x_1(t)$ and $x_2(t)$ are two solutions on $[-\tau, T_0]$. Then, by (9), we have

$$|x_1(t) - x_2(t)| \leq \int_{t-\tau}^t |f(s, \tilde{x}_1(s)) - f(s, \tilde{x}_2(s))| ds \leq$$

$$L \int_{t-\tau}^t |\tilde{x}_1(s) - \tilde{x}_2(s)| ds \leq L \int_0^t |x_1(s) - x_2(s)| ds,$$

for $0 \leq t \leq T_0$. This, by Gronwall's inequality, implies $x_1(t) = x_2(t)$. \square

3 Continuous dependence on data

Suppose the data f , φ and τ satisfy (h1)-(h4) and that the corresponding IVP, (1)-(2), has a unique continuous solution $x(t)$ satisfying $a \leq x(t) \leq R$ for $-\tau \leq t \leq T$.

Let (τ_n) be a nonincreasing sequence of positive numbers and let (φ_n) and (f_n) be two sequences of nonnegative continuous functions defined on $[-\tau_n, 0]$ and $[-\tau_n, T] \times [a, R]$, respectively. We suppose that

$$a \leq \varphi_n \leq R, \quad \varphi_n(0) = \int_{-\tau_n}^0 f_n(s, \varphi_n(s)) ds, \quad \tau_n \rightarrow \tau, \quad (13)$$

$$\varphi_n \rightarrow \varphi \quad \text{and} \quad f_n \rightarrow f \quad \text{uniformly,}$$

i.e., for each $\varepsilon > 0$ there is $n_\varepsilon \geq 1$ such that, for every $n \geq n_\varepsilon$, one has

$$|\tau_n - \tau| < \varepsilon, \quad |\varphi_n(t) - \varphi(t)| < \varepsilon \quad \text{for } -\tau_n \leq t \leq 0$$

and

$$|f_n(t, x) - f(t, x)| < \varepsilon \quad \text{for } -\tau_n \leq t \leq T \text{ and } a \leq x \leq R.$$

Finally, let us consider the IVP corresponding to f_n , φ_n and τ_n :

$$x_n(t) = \int_{t-\tau_n}^t f_n(s, x_n(s)) ds \quad \text{for } 0 \leq t \leq T,$$

$$x_n(t) = \varphi_n(t) \quad \text{for } -\tau_n \leq t \leq 0,$$

denoted by (1n)-(2n).

If inequality in (10) is strict, by Theorem 2.3, it follows that for sufficiently large n , say $n \geq n_0$, (1n)-(2n) has at least one continuous solution $x_n(t)$ satisfying

$$a \leq x_n(t) \leq R \text{ for } -\tau_n \leq t \leq T. \quad (14)$$

The question is: if for each n we choose an arbitrary continuous solution $x_n(t)$ of (1n)-(2n) satisfying (14), does the sequence $(x_n(t))$ converge to $x(t)$ uniformly in $t \in [0, T]$? The answer is positive as shows the following theorem essentially established in [25].

Theorem 3.1. *Suppose (h1)-(h4) are satisfied and that (1)-(2) has a unique continuous solution $x(t)$ such that $a \leq x(t) \leq R$ on $[-\tau, T]$. If the sequences (τ_n) , (φ_n) and (f_n) satisfy (13), and $(x_n(t))$ is any sequence of continuous solutions of (1n)-(2n) satisfying (14), then*

$$x_n(t) \rightarrow x(t) \text{ as } n \rightarrow \infty, \text{ uniformly in } t \in [0, T].$$

Proof. From (14) we have that $(x_n(t))$ is bounded in $C[0, T]$. On the other hand, by (13) and

$$x'_n(t) = f_n(t, x_n(t)) - f_n(t - \tau, x_n(t - \tau)) \text{ for } 0 \leq t \leq T,$$

we easily see that the sequence $(x'_n(t))$ is also bounded in $C[0, T]$. Thus, the sequence $(x_n(t))$ is equibounded and equicontinuous on $[0, T]$. By Ascoli-Arzelà theorem, there is a convergent subsequence $(x_{k_n}(t))$ of $(x_n(t))$. Suppose $x_{k_n}(t) \rightarrow \bar{x}(t)$ as $n \rightarrow \infty$, uniformly in $t \in [0, T]$. Now taking the limit as $n \rightarrow \infty$ in $(1k_n) - (2k_n)$, we obtain that $\bar{x}(t)$ is solution of (1)-(2). Finally, the uniqueness of the solution implies $\bar{x}(t) = x(t)$ and that the entire sequence $(x_n(t))$ converges uniformly to $x(t)$. \square

4 Minimal and maximal solutions

Theorem 4.1 ([24]). *Suppose (a1)-(a4) are satisfied. In addition assume that $f(t, x)$ is nondecreasing in x for $a \leq x \leq R_0$. Denote*

$$u_0(t) = a, \quad u_n(t) = A(u_{n-1})(t) \text{ for } 0 \leq t \leq T, \quad n = 1, 2, \dots$$

Then, $u_n(t) \rightarrow x_(t)$ as $n \rightarrow \infty$, uniformly in $t \in [0, T]$, $x_*(t)$ is the minimal solution of (1)-(2) in C , and*

$$a \leq u_1(t) \leq \dots \leq u_n(t) \leq \dots \leq x_*(t) \leq R_0 \text{ for } 0 \leq t \leq T.$$

Proof. By Theorem 2.1, there exists in C at least one solution of (1)-(2). Moreover, any such solution $x(t)$ satisfies $a \leq x(t) \leq R_0$ for $0 \leq t \leq T$. Let $x_1(t) \in C$ be an arbitrary solution. Then, $a = u_0(t) \leq x_1(t) \leq R_0$ for $0 \leq t \leq T$. Since $f(t, x)$ is nondecreasing in x for $a \leq x \leq R_0$, it follows that the map A is nondecreasing on the interval $[a, R_0]$ of E . Thus, $u_1(t) = A(u_0)(t) \leq A(x_1)(t) = x_1(t)$. On the other hand, since $A(K) \subset X$, we have $u_1(t) = A(u_0)(t) \geq a = u_0(t)$. Hence $u_0(t) \leq u_1(t) \leq x_1(t)$ for $0 \leq t \leq T$. Further, we inductively find

$$a \leq u_1(t) \leq u_2(t) \leq \dots \leq u_n(t) \leq \dots \leq x_1(t) \quad \text{for } 0 \leq t \leq T.$$

Since A is completely continuous, the sequence $(u_n)_{n \geq 1} = A((u_n)_{n \geq 0})$ must contain a subsequence, say (u_{k_n}) , convergent to some $x_* \in X$. Now taking into account the monotonicity of $(u_n(t))$, we easily see that the entire sequence (u_n) converges to x_* , uniformly on $[0, T]$, and

$$u_n(t) \leq x_*(t) \leq x_1(t) \quad \text{for } 0 \leq t \leq T, \quad n = 0, 1, \dots$$

Letting $n \rightarrow \infty$ in $A(u_n)(t) = u_{n+1}(t)$, we get $A(x_*)(t) = x_*(t)$, i.e., $x_*(t)$ is a solution of (1)-(2). Finally, since inequality $x_*(t) \leq x_1(t)$ holds for any solution $x_1(t) \in C$, we see that $x_*(t)$ is the minimal solution in C of (1)-(2). \square

The next result deals with the existence and approximation of the maximal solution in C of (1)-(2).

Theorem 4.2 ([24]). *Suppose (a1)-(a4) are satisfied. In addition assume that there is $R \geq R_0$ such that*

$$f(t, \tilde{R}) \leq R/\tau \quad \text{for } -\tau \leq t \leq T \quad (15)$$

(i.e., $f(t, \varphi(t)) \leq R/\tau$ for $-\tau \leq t \leq 0$ and $f(t, R) \leq R/\tau$ for $0 < t \leq T$), and $f(t, x)$ is nondecreasing in x for $a \leq x \leq R$. Denote

$$v_0(t) = R, \quad v_n(t) = A(v_{n-1})(t) \quad \text{for } 0 \leq t \leq T, \quad n = 1, 2, \dots$$

Then, $v_n(t) \rightarrow x^*(t)$ as $n \rightarrow \infty$, uniformly in $t \in [0, T]$, $x^*(t)$ is the maximal solution in C of (1)-(2), and

$$a \leq x^*(t) \leq \dots \leq v_n(t) \leq \dots \leq v_1(t) \leq R \quad \text{for } 0 \leq t \leq T.$$

Proof. By (15), we have $v_1(t) \leq v_0(t) = R$ for $0 \leq t \leq T$. Further the proof is analog with that of Theorem 4.1. \square

Theorem 4.3. *Suppose the assumptions of Theorem 4.1 are satisfied. In addition assume $a > 0$ and that there is a function $\chi : [a/R_0, 1) \rightarrow \mathbf{R}$ such that for all $\rho \in [a/R_0, 1)$, $t \in [0, T]$ and $x \in [a, R_0]$ with $\rho x \geq a$, one has*

$$1 \geq \chi(\rho) > \rho \quad \text{and} \quad f(t, \rho x) \geq \chi(\rho) f(t, x). \quad (16)$$

Then (1)-(2) has a unique solution in C .

Proof. Let $x_1(t) \in C$ be any solution of (1)-(2). We will show that $x_1(t) = x_*(t)$. Let $\rho_0 = \min_{0 \leq t \leq T} (x_*(t)/x_1(t))$. Since $a \leq x_*(t) \leq x_1(t) \leq R_0$, we then have $a/R_0 \leq \rho_0 \leq 1$. Now we show that $\rho_0 = 1$. Suppose $\rho_0 < 1$. Since $x_*(t) \geq \max\{a, \rho_0 x_1(t)\} = \rho_0 \max\{a/\rho_0, x_1(t)\} \geq a$ for $0 \leq t \leq T$, by (16), we get

$$x_*(t) = A(x_*)(t) \geq A(\rho_0 \max\{a/\rho_0, x_1(t)\}) \geq$$

$$\chi(\rho_0) A(\max\{a/\rho_0, x_1(t)\}) \geq \chi(\rho_0) A(x_1)(t) = \chi(\rho_0) x_1(t).$$

It follows $\rho_0 \geq \chi(\rho_0)$, a contradiction. Therefore $\rho_0 = 1$ and so $x_*(t) = x_1(t)$. \square

Remark 4.1. For $\chi(\rho) = \rho^\alpha$, $\alpha \in (0, 1)$, Theorem 4.3 becomes Theorem 4 in [24]. An other example of function χ satisfying (16), is $\chi(\rho) = \log(1 + a\rho) / \log(1 + a)$, for $f(t, x)$ of the form $q(t) \log(1 + x)$ (see [26, Example 17]).

Corollary 4.1. Suppose the assumptions of Theorems 4.2 and 4.3 are satisfied. Then, (1)-(2) has a unique solution $x_*(t)$ in C , and for any $x_0(t) \in E$ with $a \leq x_0(t) \leq R$ for $0 \leq t \leq T$, one has $x_n(t) \rightarrow x_*(t)$ as $n \rightarrow \infty$, uniformly in $t \in [0, T]$, where $x_n(t) = A(x_{n-1})(t)$, $n = 1, 2, \dots$

Proof. From $a = u_0(t) \leq x_0(t) \leq v_0(t) = R$, one gets $u_n(t) \leq x_n(t) \leq v_n(t)$ for $n = 1, 2, \dots$. On the other hand, Theorems 4.2 and 4.3 imply that $u_n(t) \rightarrow x_*(t)$ and $v_n(t) \rightarrow x_*(t)$ as $n \rightarrow \infty$, uniformly in $t \in [0, T]$. \square

The last result of this section refers to functions $f(t, x)$ which are nonincreasing in x .

Theorem 4.5. Suppose (a1)-(a4) are satisfied. Denote

$$R = \max \left\{ R_0, \max_{0 \leq t \leq T} |u_1(t)| \right\}$$

and suppose $f(t, x)$ is nonincreasing in x for $0 < a \leq x \leq R$. Also suppose that there is a function $\chi: [a/R, 1) \rightarrow \mathbf{R}$ such that for all $\rho \in [a/R, 1)$, $t \in [0, T]$ and $x \in [a, R]$ with $\rho x \geq a$, one has

$$1 \leq \chi(\rho) < 1/\rho \text{ and } f(t, \rho x) \leq \chi(\rho) f(t, x). \quad (17)$$

Then (1)-(2) has a unique solution $x_*(t)$ in C ,

$$a = u_0(t) \leq v_1(t) \leq \dots \leq u_{2n}(t) \leq v_{2n+1}(t) \leq \dots \leq x_*(t) \leq \dots$$

$$\leq u_{2n+1}(t) \leq v_{2n}(t) \leq \dots \leq u_1(t) \leq v_0(t) = R \text{ for } 0 \leq t \leq T,$$

and $u_n(t) \rightarrow x_*(t)$, $v_n(t) \rightarrow x_*(t)$ as $n \rightarrow \infty$, uniformly in $t \in [0, T]$.

Proof. By Theorem 4.1, there is in C at least one solution $x_1(t)$ of (1)-(2), and $a \leq x_1(t) \leq R_0$ for $0 \leq t \leq T$. We have $a = u_0(t) \leq x_1(t) \leq v_0(t) = R$, whence $v_1(t) \leq x_1(t) \leq u_1(t)$. By (a3), $a \leq v_1(t)$. Also $u_1(t) \leq \max_{0 \leq t \leq T} |u_1(t)| \leq R$. Hence

$$u_0(t) \leq v_1(t) \leq x_1(t) \leq u_1(t) \leq v_0(t).$$

We then have successively,

$$\begin{aligned} a = u_0(t) &\leq v_1(t) \leq \dots \leq u_{2n}(t) \leq v_{2n+1}(t) \leq \dots \leq x_1(t) \leq \dots \\ &\leq u_{2n+1}(t) \leq v_{2n}(t) \leq \dots \leq u_1(t) \leq v_0(t) = R. \end{aligned} \quad (18)$$

Since A is completely continuous, there are two subsequences of $(A(u_{2n-1}))$ and $(A(v_{2n-1}))$, convergent to some $y_*(t) \in X$ and $y^*(t) \in X$, respectively. Then, by (18), it follows that

$$\begin{aligned} u_{2n}(t) &\rightarrow y_*(t), \quad v_{2n+1}(t) \rightarrow y_*(t), \\ u_{2n+1}(t) &\rightarrow y^*(t), \quad v_{2n}(t) \rightarrow y^*(t), \end{aligned} \quad (19)$$

uniformly in $t \in [0, T]$, and

$$y_*(t) \leq x_1(t) \leq y^*(t).$$

By (19), we obtain

$$y^*(t) = A(y_*)(t) \quad \text{and} \quad y_*(t) = A(y^*)(t).$$

Next we show that (17) implies $y_*(t) = y^*(t)$. To do this, let

$$\rho_0 = \min_{0 \leq t \leq T} (y_*(t) / y^*(t)).$$

Obviously, $a/R \leq \rho_0 \leq 1$. We will show that $\rho_0 = 1$. Suppose $\rho_0 < 1$. Then (17) yields

$$y^* = A(y_*) \leq A(\rho_0 \max \{a/\rho_0, y^*\}) \leq$$

$$\chi(\rho_0) A(\max \{a/\rho_0, y^*\}) \leq \chi(\rho_0) A(y^*) = \chi(\rho_0) y_.*$$

Thus, $\chi(\rho_0) \geq 1/\rho_0$, a contradiction. Therefore, $\rho_0 = 1$ as claimed. \square

Remark 4.2. For $\chi(\rho) = \rho^\alpha$, $\alpha \in (-1, 0)$, Theorem 4.5 becomes Theorem 6 in [24].

II. THE PERIODIC PROBLEM

5 Existence of periodic solutions

We are interested in periodic continuous solutions $x(t)$ of Eq.(1), such that $0 \leq a \leq x(t) \leq R$ for all $t \in \mathbf{R}$. Our hypotheses are as follows:

- (H1) $f(t, x)$ is nonnegative and continuous for $t \in \mathbf{R}$ and $a \leq x \leq R$.
- (H2) There is $\omega > 0$ such that $f(t + \omega, x) = f(t, x)$ for $t \in \mathbf{R}$ and $a \leq x \leq R$.
- (H3) There exists a continuous function $g(t)$ with period ω such that

$$f(t, x) \geq g(t) \quad \text{for } 0 \leq t \leq \omega \text{ and } a \leq x \leq R,$$

and

$$\int_{t-\tau}^t g(s) ds \geq a \quad \text{for } 0 \leq t \leq \omega.$$

- (H4) There is a positive continuous function $h(x)$ for $a \leq x \leq R$, and a number b such that $a < b < R$,

$$f(t, x) \leq h(x) \quad \text{for } 0 \leq t \leq \omega \text{ and } a \leq x \leq R,$$

$$\int_a^R (1/h(x)) dx \geq \omega$$

and

$$f(t, x) < b/\tau \quad \text{for } 0 \leq t \leq \omega \text{ and } b \leq x \leq R. \quad (20)$$

Theorem 5.1 ([20]). *Suppose (H1)-(H4) are satisfied. Then (1) has at least one continuous solution $x(t)$ with period ω satisfying*

$$a \leq \min_{0 \leq t \leq \omega} x(t) < b \quad \text{and} \quad \max_{0 \leq t \leq \omega} x(t) < R.$$

Proof. Let E be the Banach space of all continuous ω -periodic functions $x(t)$ on \mathbf{R} , endowed with the uniform norm $\|x\| = \max_{0 \leq t \leq \omega} |x(t)|$. Let

$$K = \{x \in E; a \leq x(t) \text{ for } 0 \leq t \leq \omega\}$$

and

$$U = \left\{ x \in K; \min_{0 \leq t \leq \omega} x(t) < b \text{ and } \|x\| < R \right\}.$$

Obviously, K is a closed convex set of E , and U is bounded and open in K . We consider the homotopy

$$H : \bar{U} \times [0, 1] \rightarrow K, \quad H(x, \lambda)(t) = (1 - \lambda)a + \lambda \int_{t-\tau}^t f(s, x(s)) ds.$$

By (H1)-(H3), H is well-defined and completely continuous. We claim that, for each λ , $H(\cdot, \lambda)$ is fixed point free on the boundary ∂U of U with respect to K . Assume, by contradiction, that there would exist $\lambda \in (0, 1]$ and $x \in \partial U$ such that $H(x, \lambda) = x$, that is

$$x(t) = (1 - \lambda)a + \lambda \int_{t-\tau}^t f(s, x(s)) ds \quad \text{for } t \in \mathbf{R}. \quad (21)$$

Since x is on ∂U , we have either

$$\|x\| = R \quad \text{and} \quad \min_{0 \leq t \leq \omega} x(t) < b, \quad (22)$$

or

$$\|x\| \leq R \quad \text{and} \quad \min_{0 \leq t \leq \omega} x(t) = b. \quad (23)$$

First, suppose (22). Then, by differentiating (21), we get

$$x'(t) = \lambda f(t, x(t)) - \lambda f(t - \tau, x(t - \tau)).$$

It follows

$$x'(t) \leq \lambda f(t, x(t)) \leq \lambda h(x(t)) \leq h(x(t)).$$

Let $t_0 \in [0, \omega]$ be such that $x(t_0) = \min_{0 \leq t \leq \omega} x(t)$. Integration from t_0 to t yields

$$\int_{t_0}^t (x'(s)/h(x(s))) ds \leq t - t_0 \leq \omega \quad \text{for } t_0 \leq t \leq t_0 + \omega.$$

Thus,

$$\int_{x(t_0)}^{x(t)} (1/h(u)) du \leq \omega \quad \text{for } t_0 \leq t \leq t_0 + \omega.$$

Since $x(t_0) < b$, by (H4), we deduce that $x(t) < R$ for $t_0 \leq t \leq t_0 + \omega$, equivalently for all $t \in \mathbf{R}$. Therefore, $\|x\| < R$, a contradiction. Next, suppose (23). Let $0 \leq t_0 \leq \omega$ be such that $x(t_0) = \min_{0 \leq t \leq \omega} x(t) = b$. Then, by (21) and (20), we obtain

$$b = x(t_0) = (1 - \lambda)a + \lambda \int_{t_0-\tau}^{t_0} f(s, x(s)) ds <$$

$$(1 - \lambda)b + \lambda b = b,$$

again a contradiction. Thus, H is an admissible homotopy on \bar{U} . On the other hand, the constant map $H(\cdot, 0) \equiv a$ is essential because $a \in U$. Consequently, by the topological transversality theorem, $H(\cdot, 1)$ is essential too. \square

6 Monotone iterative approximation

Under the assumptions of Theorem 5.1, denote by A the completely continuous map from $P = \{x \in E; a \leq x(t) \leq R \text{ for } 0 \leq t \leq \omega\}$ into K ,

$$A(x)(t) = \int_{t-\tau}^t f(s, x(s)) ds, \quad t \in \mathbf{R}, x \in P.$$

Theorem 6.1. *Suppose (H1)-(H4) are satisfied. In addition suppose that $a > 0$, $f(t, x)$ is nonincreasing in x for $a \leq x \leq R$ and there exists a function $\chi : [a/R, 1) \rightarrow \mathbf{R}$ satisfying (17) for all $t \in [0, \omega]$, $\rho \in [a/R, 1)$ and $x \in [a, R]$ with $\rho x \geq a$. If*

$$A^2(R)(t) \leq R \text{ for } 0 \leq t \leq \omega, \quad (24)$$

then (1) has a unique solution $x^(t) \in P$. Moreover, the sequence $v_0(t) = R$, $v_n(t) = A(v_{n-1}(t))$, $n = 1, 2, \dots$, converges to $x^*(t)$, uniformly in $t \in [0, \omega]$, and*

$$a \leq v_1(t) \leq v_3(t) \leq \dots \leq v_{2n+1}(t) \leq \dots \leq x^*(t) \leq \dots$$

$$\leq v_{2n}(t) \leq \dots \leq v_4(t) \leq v_2(t) \leq v_0(t) = R.$$

Proof. By Theorem 5.1, there exists at least one solution in P . Let $x(t) \in P$ be any solution of (1). Since $f(t, x)$ is nonincreasing in x for $a \leq x \leq R$, from $a \leq x(t) \leq R = v_0(t)$, we get $a \leq A(R)(t) \leq A(x)(t) = x(t)$. Then,

$$a \leq A(R)(t) \leq x(t) \leq A^2(R)(t).$$

This, by (24), yields

$$a \leq A(R)(t) \leq A^3(R)(t) \leq x(t) \leq A^2(R)(t) \leq R.$$

We successively obtain

$$\begin{aligned} a \leq v_1(t) \leq v_3(t) \leq \dots \leq v_{2n+1}(t) \leq \dots \leq x(t) \leq \dots \\ \leq v_{2n}(t) \leq \dots \leq v_4(t) \leq v_2(t) \leq v_0(t) = R. \end{aligned} \quad (25)$$

Since A is completely continuous, there are two subsequences of (v_{2n+1}) and (v_{2n}) uniformly convergent to some $x_* \in P$ and $x^* \in P$, respectively. By (25) we see that the entire sequences (v_{2n+1}) and (v_{2n}) converge uniformly to x_* and x^* , respectively, and

$$a \leq x_*(t) \leq x(t) \leq x^*(t) \leq R.$$

Obviously,

$$x_*(t) = A(x^*)(t) \text{ and } x^*(t) = A(x_*)(t).$$

Now we prove that (17) implies $x_*(t) = x^*(t)$ for all $t \in \mathbf{R}$. To this end, let $\rho_0 = \min_{0 \leq t \leq \omega} (x_*(t)/x^*(t))$. Clearly, $0 < a/R \leq \rho_0 \leq 1$. We have to show that $\rho_0 = 1$. Suppose $\rho_0 < 1$. Since $x_*(t) \geq \max\{a, \rho_0 x^*(t)\} = \rho_0 \max\{a/\rho_0, x^*(t)\} \geq a$, by (17), we get

$$x^* = A(x_*) \leq A(\rho_0 \max\{a/\rho_0, x^*\}) \leq \chi(\rho_0) A(\max\{a/\rho_0, x^*\}) \leq \chi(\rho_0) A(x^*) = \chi(\rho_0) x^*.$$

It follows that $\chi(\rho_0) \geq 1/\rho_0$, a contradiction. Thus $\rho_0 = 1$ as claimed. Consequently, $x_*(t) = x(t) = x^*(t)$ and the proof is complete. \square

Corollary 6.1. *Suppose the assumptions of Theorem 6.1 hold with*

$$A(a)(t) \leq R \text{ for } 0 \leq t \leq \omega \quad (26)$$

instead of (24). Then (1) has a unique solution $x^(t) \in P$ and $A^n(x_0)(t) \rightarrow x^*(t)$ as $n \rightarrow \infty$, uniformly in $t \in [0, \omega]$, for any $x_0(t) \in P$.*

Proof. Let us remark that (26) implies (24). Indeed, from $a \leq A(R)(t) \leq A(a)(t)$, we get

$$A^2(a)(t) \leq A^2(R)(t) \leq A(a)(t) \leq R,$$

whence (24). Thus, Theorem 6.1 applies.

Further, if $x_0(t)$ is any function in P , then from $a \leq x_0(t) \leq R$, we obtain

$$a \leq v_1(t) \leq A(x_0)(t) \leq A(a)(t) \leq R = v_0(t).$$

This yields

$$a \leq v_1(t) \leq A^2(x_0)(t) \leq v_2(t) \leq A(a)(t) \leq R,$$

and, in general,

$$a \leq v_1(t) \leq v_3(t) \leq \dots \leq v_{2[(n-1)/2]+1}(t) \leq$$

$$A^n(x_0)(t) \leq v_{2[n/2]}(t) \leq \dots \leq v_2(t) \leq v_0(t) = R,$$

for $n = 1, 2, \dots$. Since $v_n(t) \rightarrow x^*(t)$, it follows that $A^n(x_0)(t) \rightarrow x^*(t)$, as claimed. \square

Remark 6.1. A sufficient condition for (26) is that $f(t, a) \leq R/\tau$ for all $t \in \mathbf{R}$.

For the next results, let us replace (H4) by the following assumption used in [12]:

(H4') $f(t, x) \leq R/\tau$ for $0 \leq t \leq \omega$ and $a \leq x \leq R$.

The following theorems complement the results in [12].

Theorem 6.2. Suppose (H1)-(H3) and (H4') are satisfied. In addition suppose $a > 0$, $f(t, x)$ is nonincreasing in x for $a \leq x \leq R$, and there is a function $\chi : [a/R, 1) \rightarrow \mathbf{R}$ satisfying (17) for all $t \in [0, \omega]$, $\rho \in [a/R, 1)$ and $x \in [a, R]$ with $\rho x \geq a$. Then (1) has a unique solution $x^*(t) \in P$ and $A^n(x_0)(t) \rightarrow x^*(t)$ as $n \rightarrow \infty$, uniformly in $t \in [0, \omega]$, for any $x_0(t) \in P$.

Theorem 6.3. Suppose (H1)-(H3) and (H4') are satisfied. In addition suppose $a > 0$, $f(t, x)$ is nondecreasing in x for $a \leq x \leq R$, and there is a function $\chi : [a/R, 1) \rightarrow \mathbf{R}$ satisfying (16) for all $t \in [0, \omega]$, $\rho \in [a/R, 1)$ and $x \in [a, R]$ with $\rho x \geq a$. Then (1) has a unique solution $x^*(t) \in P$ and $A^n(x_0)(t) \rightarrow x^*(t)$ as $n \rightarrow \infty$, uniformly in $t \in [0, \omega]$, for any $x_0(t) \in P$.

The proofs of Theorems 6.2 and 6.3 are similar with that of Theorem 6.1, so we omit the details.

Remark 6.2. For $\chi(\rho) = \rho^\alpha$, $\alpha \in (-1, 0)$, Theorems 6.1 and 6.2 have been established in [20]. Also, in [20], several examples can be found.

The monotone iterative approximation of periodic solutions of Eq.(1), for the case when $f(t, x)$ is nondecreasing in x , was discussed in [12].

Finally, for similar results by means of more subtle conditions than (a4) and (H4), we send to [21] and [25].

References

- [1] K.L. Cooke, J.L. Kaplan, *A periodicity threshold theorem for epidemics and population growth*, Math. Biosci. **31** (1976), 87-104.
- [2] H.L. Smith, *On periodic solutions of a delay integral equation modelling epidemics*, J. Math. Biol. **4** (1977), 69-80.
- [3] R.D. Nussbaum, *A periodicity threshold theorem for some nonlinear integral equations*, SIAM J. Math. Anal. **9** (1978), 356-367.
- [4] J. Kaplan, M. Sorg, J. Yorke, *Asymptotic behavior for epidemic equations*, Nonlinear Analysis (1978).
- [5] S. Busenberg, K. Cooke, *Periodic solutions of delay differential equations arising in some models of epidemics*, in "Applied Nonlinear Analysis" (Proc. Third Internat. Conf., Univ. Texas, Arlington, Texas, 1978), Academic Press, New York, 1979, 67-78.
- [6] I.A. Rus, *Principii și aplicații ale teoriei punctului fix*, Dacia, Cluj, 1979.

-
- [7] R.W. Leggett, L.R. Williams, *A fixed point theorem with application to an infectious disease model*, J. Math. Anal. Appl. **76** (1980), 91-97.
 - [8] H.L. Smith, *An abstract threshold theorem for one parameter families of positive noncompact operators*, Funkcial Ekvac. **24** (1981), 141-152.
 - [9] L.R. Williams, R.W. Leggett, *Nonzero solutions of nonlinear integral equations modeling infectious disease*, SIAM J. Math. Anal. **13** (1982), 112-121.
 - [10] K. Deimling, *Nonlinear Functional Analysis*, Springer, Berlin, 1985.
 - [11] A. Cañada, *Method of upper and lower solutions for nonlinear integral equations and an application to an infectious disease model*, in "Dynamics of Infinite Dimensional Systems", S.N. Chow and J.K. Hale eds., Springer, Berlin, 1987, 39-44.
 - [12] D. Guo, V. Lakshmikantham, *Positive solutions of nonlinear integral equations arising in infectious diseases*, J. Math. Anal. Appl. **134** (1988), 1-8.
 - [13] I.A. Rus, *A delay integral equation from biomathematics*, in "Seminar on Differential Equations: Preprint Nr. 3, 1989", I.A. Rus ed., University "Babeş-Bolyai", Cluj, 1989, 87-90.
 - [14] S.G. Hristova, D.D. Bainov, *Method for solving the periodic problem for integro-differential equations*, Matematiche (Catania) **44** (1989), 149-157.
 - [15] N.G. Kazakova, D.D. Bainov, *An approximate solution of the initial value problem for integro-differential equations with a deviating argument*, Math. J. Toyama Univ. **13** (1990), 9-27.
 - [16] A.M. Fink, J.A. Gatica, *Positive almost periodic solutions of some delay integral equations*, J. Diff. Eqns. **83** (1990), 166-178.
 - [17] R. Precup, *Positive solutions of the initial value problem for an integral equation modeling infectious disease*, in "Seminar on Differential Equations: Preprint Nr. 3, 1991", I.A. Rus ed., University "Babeş-Bolyai", Cluj, 1991, 25-30.
 - [18] R. Precup, *Ecuatii integrale neliniare*, Univ. "Babeş-Bolyai", Cluj, 1993.
 - [19] R. Torrejón, *Positive almost periodic solutions of a state-dependent delay nonlinear integral equation*, Nonlinear Analysis **20** (1993), 1383-1416.
 - [20] R. Precup, *Periodic solutions for an integral equation from biomathematics via Leray-Schauder principle*, Studia Univ. Babeş-Bolyai, Mathematica **39**, No. 1 (1994), 47-58.

- [21] E. Kirr, *Existence of periodic solutions for some integral equations arising in infectious diseases*, Studia Univ. Babeş-Bolyai, Mathematica **39**, No. 2 (1994), 107-119.
- [22] A. Cañada, A. Zertiti, *Method of upper and lower solutions for nonlinear delay integral equations modelling epidemics and population growth*, Math. Models and Methods in Applied Sciences **4** (1994), 107-120.
- [23] A. Cañada, A. Zertiti, *Systems of nonlinear delay integral equations modelling population growth in a periodic environment*, Comment. Math. Univ. Carolinae **35**, No. 4 (1994), 633-644.
- [24] R. Precup, *Monotone technique to the initial values problem for a delay integral equation from biomathematics*, Studia Univ. Babeş-Bolyai, Mathematica **40**, No. 2 (1995), 63-73.
- [25] E. Kirr, *Existence and continuous dependence on data of the positive solutions of an integral equation from biomathematics*, Studia Univ. Babeş-Bolyai, Mathematica **41**, No. 2 (1996).
- [26] Aid Dads, K. Ezzinbi, O. Arino, *Positive almost periodic solution for some nonlinear delay integral equation*, Nonlinear Studies **3** (1996), 85-101.
- [27] A. Granas, R. Guenther, J. Lee, *Nonlinear Boundary Value Problems for Ordinary Differential Equations*, Dissertationes Mathematicae, Vol. 244, Warszawa, 1985.
- [28] V. Kolmanovskii, A. Myshkis, *Applied Theory of Functional Differential Equations*, Kluwer, Dordrecht, 1992.

The Calculus of the Energetic Illumination

Produced by an Infrared Radiation Source in a Space Point

Micoară Ioan, Professor Doctor Engineer
Politechnical University of Timișoara

Dumache Constantin, M.E, Quality Assurance
Director, S.C. OPTICA - S.A. Timișoara
Abstract

The energetic illumination E_c produced by an infrared radiation source of a certain geometrical configuration and temperature T in a point P of the (H) plane is calculated taking into account the contribution of each surface element ds (fig.1).

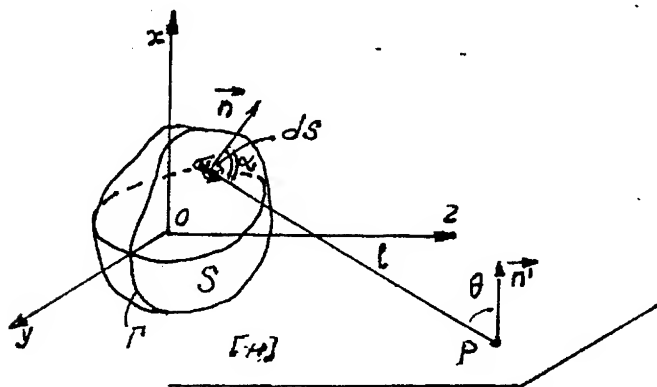


fig.1

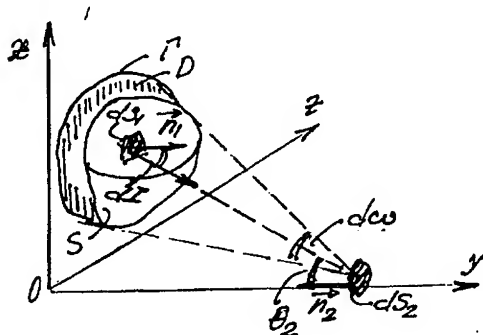
$$dE_p = \frac{B \cdot \cos \alpha \cdot \cos \theta \cdot \mathcal{E}(l) \cdot ds}{l^2} \quad (1)$$

$$E_p = B \cdot \iint_{S_p} \frac{\cos \alpha \cdot \cos \theta \cdot \mathcal{E}(l) \cdot dx dy}{l^2} \quad (2)$$

- b) the detector is illuminated by a finite surface thermal source

The energetic illumination produced in P (fig.2) by an element ds is :

$$dE_p = \frac{dI_{\theta_1}}{r^2} \cos \theta_2 \quad (2)$$



As the source has finite dimensions we may write:

$$dI_{\theta_1} = B \cdot ds_1 \cdot \cos \theta_1$$

where: B is the energetic brightness of the surface S_1

fig.2

The solid angle in which the surface ds_1 is seen from the point P is:

$$d\omega = \frac{\cos \theta_1 ds_1}{r^2}$$

The relationship (2) may be written as:

$$dE_p = \frac{B \cdot ds_1 \cos \theta_1 \cos \theta_2}{r^2} \quad (3)$$

$$\text{or } dE_p = B \cos \theta_2 \cdot d\omega \quad (4)$$

The total energetic illumination in P is:

$$E_p = \iint \frac{B \cos \theta_1 \cos \theta_2}{r^2} ds_1 = \iint B \cos \theta_2 d\omega \quad (5)$$

If B is constant over the entire surface, condition fulfilled by the thermal source for which the temperature is the same in every point of the surface we may write:

$$E_p = B \cdot \Sigma \quad (6)$$

$$\text{where } \Sigma = \iint \frac{\cos \theta_1 \cos \theta_2}{r^2} ds_1 = \iint \cos \theta_2 d\omega \quad (7)$$

The Calculs of the Energetic Illumination

Produced by an Infrared Radiation Source in a Space Point

Nicoară Ioan, Professor Doctor Engineer
Politechnical University of Timișoara

Dumache Constantin, M.E, Quality Assurance
Director, S.C. OPTICA - S.A. Timișoara

1. Introduction

In order to know the fraction of the radiated energy of a thermal source that reaches a radiation detector, the energetic illumination produced by the source in a space point where the detector is has to be calculated.

In the solving of the problem, two cases may occur :

a) the detector is illuminated by thermal point source:

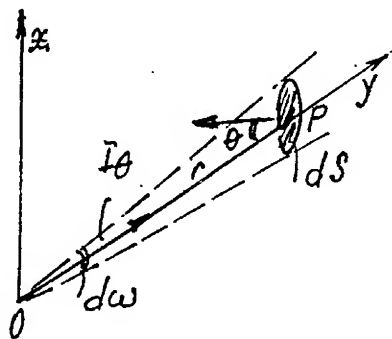


fig.1

$$E_P = \frac{d\phi}{dS} = \frac{I_e \cdot d\omega}{dS}$$

$$\text{and } d\omega = \frac{dS}{r^2} \cos \theta$$

we obtain:

$$E_P = \frac{I_e \cos \theta}{r^2} \quad (1)$$

where: E_P - the energetic illumination of the point P (fig1)

I_e - the energetic intensity of the point source.

with $\tau(l) = e^{-kl}$ - the absorption coefficient.

The function $f(x,y)$ to be integrated is defined as continuous in the domain S and the calculus of E_p can be performed only by using the numerical calculus formula.

$$\iint_S f(x,y) dx dy = \sum_{i=1}^N A_i f(x_i, y_i)$$

If the integrating domain is limited by curves defined by : $x = \varphi(y)$, $x = \psi(y)$ with $\varphi(y) < \psi(y)$ and the vertical lines : $y = a$, $y = b$ the double integral becomes :

$$\iint_{S_p} f(x,y) dx dy = \int_a^b dy \int_{\varphi(y)}^{\psi(y)} f(x,y) dx = \int_a^b F(y) dy$$

or

$$\iint_{S_p} f(x,y) dx dy = \sum_{i=1}^N C_i \cdot F(y_i)$$

where the summ calculus is performed by known methods.

Conclusion : The ascertainment of the energetic illumination produced by an infrared radiating body is a difficult or even almost impossible operation. In the paper two methods of solving the integral (1) for radiation sources of any geometrical shape by using numerical calculus methods are presented.

An analysis is also performed on the situations when a thermal source of finite dimensions can be considered a point source and the error that occurs in the calculus in this case.

The expression (7) shows that the energetic illumination produced by the surface S, of brightness B, is a point P, is equal with the illumination produced by an equivalent surface S, of the same brightness and which is seen from under the same solid angle. Therefore, S may be replaced with a plane surface, analytically expressed by the function: $y=f(x,z)$ (in a rectangular system of coordinates) or $y=\varphi(\rho,\theta)$ (in a polar system of coordinates); the functions are defined and continuous in a domain D limited by the curve Γ , generated in the plane $y=0$ by the cone with the point in P and the basis the surface S of the thermal body as it is seen from P (fig.2). The relationship (6) establishes a link between the energetic characteristics of the thermal source and those of the radiation detector. In the way rel.(6) was presented, we have not taken into account the undesired effects produced by the environment (phenomena such as absorption, dispersion, reflection, refraction and others). The energetic brightness of the body surface was defined as:

$$B = \frac{\sigma}{\pi} \cdot \epsilon \cdot T^4$$

where ϵ is the total emission coefficient;
 T is the absolute temperature of the body.

In many cases found in practice, the equivalent surface of the thermal source has not a regular shape; therefore the solving of the integral (7) by mathematical methods is almost impossible. In these cases, the solving may be done only by using numerical methods:

$$\iint f(x,z) \cdot dx \cdot dz \cong \sum_{i=1}^n A_i \cdot f(x_i, z_i) \quad (3)$$

or

$$\iint F(\rho, \theta) \cdot d\rho \cdot d\theta \cong \sum_{i=1}^n B_i \cdot F(\rho_i, \theta_i) \quad (9)$$

If the integrating domain is limited by curves expressed by $x=\varphi(z)$ $x=\psi(z)$ or $\rho=\rho_1(\theta)$, $\rho=\rho_2(\theta)$ with $\varphi(z) \geq \psi(z)$ or $\rho_2(\theta) \geq \rho_1(\theta)$ and the vertical lines $z=a, z=b$ or the radii $\theta=\alpha$ and $\theta=\beta$ the integrals (3) and (9) become:

$$\iint_S f(x,z) \cdot dx \cdot dz = \int_a^b dz \int_{\varphi(z)}^{\psi(z)} f(x,z) \cdot dx = \int_a^b F(z) \cdot dz \quad (10)$$

$$\iint F(\rho, \theta) d\rho \cdot d\theta = \int_{\alpha}^{\beta} d\theta \int_{\varphi(\theta)}^{\psi(\theta)} F(\rho, \theta) d\rho = \int_{\alpha}^{\beta} F(\theta) \cdot d\theta \quad (11)$$

$$\Delta z_i = z_i - z_{i-1}; \quad \Delta \theta_i = \theta_i - \theta_{i-1} \quad (12)$$

with

$$\int_a^b F(z) \cdot dz \cong \sum_{i=1}^n F(z_i) \cdot \Delta z_i \quad (13)$$

and

$$\int_{\alpha}^{\beta} F(\theta) d\theta \cong \sum_{i=1}^n F(\theta_i) \cdot \Delta \theta_i \quad (14)$$

From (13) and (14) one may see that the numerical solving of the integrals is possible only if the values of $F(z_i)$ or $F(\theta_i)$ in the points z_i or θ_i ($i=1, 2, \dots, n$) are known.

The analytic expressions of the functions $F(z_i)$ and $F(\theta_i)$ may be easily calculated for the cases in which the surface ds represents a rectangle with the width much smaller than the length or a triangle with one side much smaller than the other two. In this way, by dividing the equivalent surface of the thermal body in elementary surfaces the calculus of the energetic illumination in P may be performed by using (13) or (14).

2. Thermal source of rectangular shape

The rectangular source with a dimension much bigger than the others are considered linear (fig.3)

An element of length dx has in a certain direction an energetic intensity $dI_\theta = dI_{\max} \cos \theta$ where $dI_{\max} = B \cdot \delta \cdot dx = I_0 \cdot dx$ and I_0 is the energetic intensity in a direction rectangular with the surface of the source.

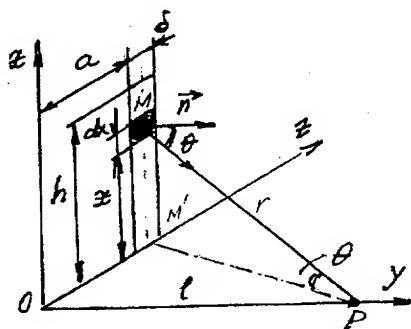


fig.3

The energetic illumination produced in P is:

$$E_P = \int_0^l \frac{B \cdot \delta \cdot \cos^2 \theta \cdot dx}{r^2} \quad (15)$$

where, $\cos \theta = \frac{h}{r} = \frac{h^2}{\sqrt{a^2 + h^2 + z^2}}$ and $r = \sqrt{a^2 + h^2 + z^2}$

By integrating the relationship (15), we have:

$$E_P = \frac{I_0 l^2}{2(a^2 + l^2)} \left[\frac{h}{a^2 + l^2 + h^2} + \frac{1}{\sqrt{a^2 + l^2}} \operatorname{arctg} \frac{h}{\sqrt{a^2 + l^2}} \right] \quad (16)$$

which represents the energetic illumination produced by a thermal source of height h and width δ , $h > \delta$ in a point P , situated at the distance $\sqrt{a^2 + l^2}$

3. Triangle thermal source

Let us consider a triangular source ABC . We shall calculate the energetic illumination E_P produced in a point P situated at the distance l on the perpendicular line considered in the point A at the source plane (fig.4)

For this, an infinite small triangle shall be considered with the angle in A equal to $d\theta$ and the length of the median line ρ . This triangle may be considered a circle sector of radius ρ , belonging to a circular disk centred in A . The contribution of the circle sector at the illumination in P is proportional to its area by respect to an imaginary disk of radius ρ :

$$2\pi \rho^2 dE_P = E_P' \rho^2 d\theta \quad (17)$$

fig.4

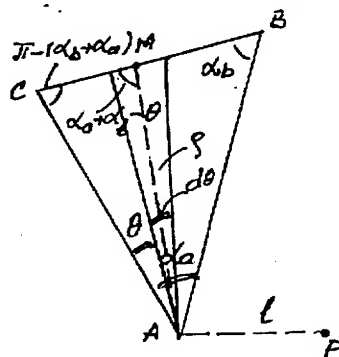
where $E_P' = \pi B \rho^2 (\rho^2 + l^2)^{-\frac{1}{2}}$ is the illumination produced by the disk source of radius ρ .

With E_P' in (17), we obtain:

$$dE_P = \frac{B}{2} \cdot \frac{\rho^2}{\rho^2 + l^2} \cdot d\theta \quad (13)$$

From fig.4, we have:

$$\rho = \frac{b \cdot \sin(\alpha_a + \alpha_b)}{\sin(\alpha_a + \alpha_b - \theta)} = \frac{b_0}{\sin(\theta_0 - \theta)}$$



By making the final calculus, we obtain:

$$E_P = \frac{B}{2} \int_{\theta=0}^{\theta=\alpha_0} \frac{d[\operatorname{ctg}(\beta_0 - \theta)]}{1 + \frac{l^2}{b_0^2} + \operatorname{ctg}^2(\beta_0 - \theta)} \quad (19)$$

4. The Numeric Calculus of the Illumination Produced by Plane Thermal Source of No Particular Shape

In the case when the radiant surface has no regular shape, numerical methods of calculus shall be used.

4.1. The Equivalent Surface of the Source in Rectangular Coordinates

In order to obtain this, the radiant surface (fig.5) will be divided in rectangular portions of as small a width as possible, for which the expression of the illumination produced in P is given by (16)

The energetic illumination in P is the sum of the illuminations produced by each portion:

$$E_P = \int_a^b \left(\int_{\varphi_1(z)}^{\varphi_2(z)} \frac{I_0 \cdot h \cdot dz}{(z^2 + x^2 + h^2)^{3/2}} \right) dz = \int_a^b \psi(z) \cdot dz \quad (20)$$

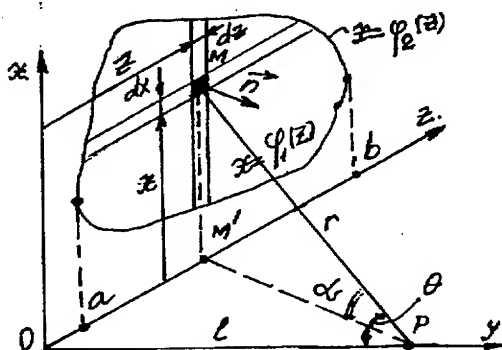


fig.5

In order to calculate (13), the interval (a,b) will be divided in n equal parts, of length δ , so that:

$$\delta = \frac{b-a}{n} \quad \text{with} \quad z_i = a + i\delta$$

and, for $i = 0, z_0 = a$

$$i = n, z_n = a + n\delta = b$$

Let ψ_i be the value of the function $\psi = \psi(z)$ in the points

$$z = z_i : \psi_i = \psi(a + i\delta)$$

The values of ψ_i , with $i=0,1,2,\dots,n$ are known from (16)

The integral (20) may be written as:

$$\int_a^b \psi(z) dz = \lim_{n \rightarrow \infty} \sum \psi(\xi_i) (z_i - z_{i-1}) \quad (21)$$

where $\xi_i = z_i$ or $\xi_i = z_{i-1}$ and $\psi(\xi_i) = \psi_i$

From (21), two calculus formulae are obtained:

$$\int_a^b \psi(z) dz \cong \sum_{i=1}^n \psi(z_{i-1}) \cdot \delta = \frac{b-a}{n} [\psi_0 + \psi_1 + \dots + \psi_{n-1}] \quad (22)$$

$$\int_a^b \psi(z) dz \cong \sum_{i=1}^n \psi(z_i) \cdot \delta = \frac{b-a}{n} [\psi_1 + \psi_2 + \dots + \psi_n] \quad (23)$$

As n grows, the formulae (22) and (23) are more precise. If $n \rightarrow \infty$, therefore $\delta \rightarrow 0$, from (21) we may see that they give the exact value of the integral (20).

From fig. 5 we may see that the surface defined by the curves $\psi_1(z)$ and $\psi_2(z)$ is replaced with the sum of the rectangular surfaces of basis $\delta = z_i - z_{i-1}$, and height ψ_i or ψ_{i-1} . The calculus errors that occur by using the formulae (22) or (23) are:

$$\sqrt{1} = \int_a^b \psi(z) dz - \frac{b-a}{n} [\psi_0 + \psi_1 + \dots + \psi_{n-1}] \quad (24)$$

and

$$\sqrt{2} = \frac{b-a}{n} [\psi_1 + \psi_2 + \dots + \psi_n] - \int_a^b \psi(z) dz \quad (25)$$

Adding (24) and (25), we obtain:

$$\sqrt{1} + \sqrt{2} = \frac{b-a}{n} [\psi_n - \psi_0] \quad (26)$$

As $\psi(z)$ is a monotone function, the sum of the errors is equal with the area of a rectangle of width $\delta = \frac{b-a}{n}$ and height $\psi_n - \psi_0$. In this case, the error given by (22) or (23) will not be bigger than the one given by (26).

The formulae (22) and (23) may be used if $l \leq h$. For $l > h$ from (10) one may see that the numerical value of the expression in brackets is very small and the illumination in P may be calculated with the relation (1) - point source.

The following problem may be considered: to define a relationship between l and h so that by using relation (1) in the calculus of the illumination, the error produced to remain smaller than an imposed value.

For this, let us consider a point source placed in O, with energetic characteristics similar to those of a rectangular source, that is:

$$I_{max} = B h \delta$$

The illumination produced in P is:

$$E_p = \frac{I_{max}}{L^2} = \frac{B h \delta}{L^2} \quad (27)$$

If the surface is rectangular (fig.6), the illumination produced in P is:

$$E = \frac{B \delta}{2} \left[\frac{h}{h^2 + L^2} + \frac{1}{L} \operatorname{arctg} \frac{h}{L} \right] \quad (28)$$

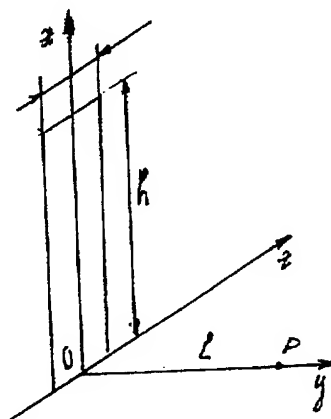


fig.6

Let $x = h/L$ and (28) becomes:

$$E = \frac{B \delta h}{2 L^2} \left[\frac{1}{1+x^2} + \frac{1}{x} \operatorname{arctg} x \right] \quad (29)$$

As $x < 1$, the expressions in brackets from (29) may be approximated by their Taylor series and from (29).

$$E = \frac{B h \delta}{2 L^2} \left[1 - \frac{2}{3} x^2 + \frac{3}{5} x^4 - \frac{4}{7} x^6 + \dots \right] \quad (30)$$

The relative error that appears by using (27) instead of (28) is:

$$\varepsilon[\%] = \frac{E' - E}{E} 100\% \quad (31)$$

With (27) and (30) in relation (31), we have:

$$\varepsilon[\%] = \frac{\frac{2}{3} x^2 - \frac{3}{5} x^4 + \frac{4}{7} x^6 + \dots}{1 - \frac{2}{3} x^2 + \frac{3}{5} x^4 - \frac{4}{7} x^6 + \dots} \cdot 100\% \quad (32)$$

If $x = h/L = 0,1$ we notice that $\frac{3}{5} x^4 < 10^{-4}$ and all the series terms, beginning with $\frac{3}{5} x^4$ may be neglected (their sum is smaller than the imposed error). The error given by (32) is defined only by the first term:

$$\varepsilon[\%] = \frac{\frac{2}{3} 10^{-2}}{1 - \frac{2}{3} 10^{-2}} 100\% = \frac{2 \cdot 10^{-2}}{3 - 2 \cdot 10^{-2}} \cdot 100\% \quad (33)$$

From (33) we obtain $0.66\% \leq \epsilon < 1\%$ for $l \geq 10 h$ (the distance from source to the illuminated point is at least 10 times the height of the source). The error produced by using the formula of the point sources in the calculus of the illumination produced by sources of finite dimensions is less than 1% .

4.2. The Surface of the Source in Polar Coordinates

Let us suppose that the area of the radiant surface limited by a curve with equation in polar coordinates is $\rho = f(\theta)$ and by the radianes $\theta_1 = \alpha$ and $\theta_2 = \beta$ taken from the pole under the angles α , respectively β with the polar axis (fig.7).

The calculus of the energetic illumination in the point P is performed by using relation (18).

In this purpose, the surface considered is divided in n parts with the point angle

$$\Delta\theta = \frac{\beta - \alpha}{n} \quad (34)$$

We point out that:

$$\theta_i = \alpha + i \Delta\theta$$

and from $i = 0$, $\theta_0 = \alpha$

$$i = n, \theta_n = \alpha + n \Delta\theta = \beta$$

The triangle OMN gives in P energetic illumination given by:

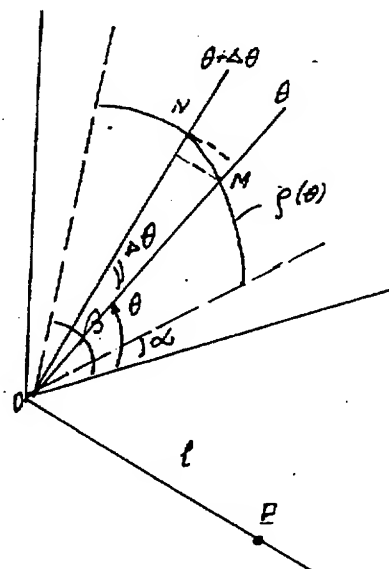


fig.7

$$dE_P = \frac{B}{2} \cdot \frac{\rho^2}{\rho^2 + l^2} d\theta \quad (35)$$

or

$$E_P = \frac{B}{2} \int_{\alpha}^{\beta} \frac{\rho^2}{\rho^2 + l^2} d\theta \quad (36)$$

Let $\psi(\rho)$ be the function to be integrated and, as $\rho = \rho(\theta)$ we obtain:

$$\psi_i = \psi(\theta_i) = \frac{\rho^2(\theta_i)}{\rho^2(\theta_i) + l^2} \quad (37)$$

Where $\psi_i = \psi(\alpha + i \cdot \Delta\theta)$

The values ψ_i , with $i=0, 1, 2, \dots, n$ are known from (37) for $\theta_i = \alpha + i \cdot \Delta\theta$

The total illumination in P is:

$$E_P = \sum_{i=1}^n \Delta E_P = \frac{B}{2} \sum_{i=1}^n \frac{\rho^2(\theta_i)}{\rho^2(\theta_i) + l^2} \Delta\theta$$

Two cases may be discussed: when ψ_i is calculated in the point M or N of the curve $\rho = \rho(\theta)$

Therefore, the integral (36) becomes:

$$\frac{B}{2} \int_{\alpha}^{\beta} \frac{\rho^2}{\rho^2 + l^2} d\theta \cong \frac{B}{2} \sum_{i=1}^n \psi(\xi_i) \cdot \Delta\theta$$

Where $\xi_i = \rho_i$ or $\xi_i = \rho_{i-1}$ and $\psi(\xi_i) = \psi_i$

With the notations made above two approximation formulae may be obtained:

$$\frac{B}{2} \int_{\alpha}^{\beta} \psi(\rho) d\theta \cong \frac{B}{2} \sum_{i=1}^n \psi(\rho_{i-1}) \Delta\theta = \frac{B}{2} \frac{\beta - \alpha}{n} [\psi_0 + \psi_1 + \dots + \psi_{n-1}] \quad (38)$$

and

$$\frac{B}{2} \int_{\alpha}^{\beta} \psi(\rho) d\theta \cong \frac{B}{2} \sum_{i=1}^n \psi(\rho_i) \Delta\theta = \frac{B}{2} \frac{\beta - \alpha}{n} [\psi_1 + \psi_2 + \dots + \psi_n] \quad (39)$$

The maximum error that occurs when using (38) or (39) is:

$$\eta_1 + \eta_2 = \frac{B}{2} \frac{\beta - \alpha}{n} [\psi_n - \psi_0] \quad (40)$$

One may see that (40) is the area of triangle with the width $(\beta - \alpha)/n \cdot R$, where $R=1$ and the height $\psi_n - \psi_0$

No matter what formula we use, (38) or (39), the error is smaller the one given by (40).

In the case of circular shape plane sources, the energetic illumination may also be calculated with the relation (1) if $l \geq \rho$ where ρ represents a medium radius of the equivalent surface.

If the source is a disk with finite dimensions, the illumination produced in the point P situated at the distance l from the source is:

$$E_p = \pi \cdot B \frac{d^2}{d^2 + 4l^2} \quad (41)$$

Where d is the source diameter.

By using for the calculus relation (1), where:

$$I = B \cdot S = \pi/4 \cdot B \cdot d^2$$

We obtain:

$$E_p' = \frac{\pi}{4} \frac{B \cdot d^2}{l^2} \quad (42)$$

The relative error produced by calculating is:

$$\varepsilon[\%] = \frac{\Delta E}{E} 100\% \quad (43)$$

were

$$\Delta E = E' - E = \frac{\pi \cdot B \cdot d^4}{4l^2(d^2 + 4l^2)} \quad (44)$$

By replacing (41) and (44) in (43) we have:

$$\varepsilon[\%] = \frac{1}{4} \left(\frac{d}{l} \right)^2 \cdot 100\% \quad (45)$$

If $d/l \leq 1/10$ or $l \geq 10d$ (the distance from the source to the illuminated point is at least 10 times the source diameter), the error produced by using the point source formula is $\varepsilon \leq 0.25\%$

5. Conclusions

In the paper we have presented two numerical methods of calculating the energetic illumination produced by a thermal source, in a certain point, by using coordinates system.

We have also analysed the condition in which finite dimensions sources may be considered point sources, in order to use less complicated relations in the calculus.

The ascertainment of the energetic illumination produced by a thermal source in a certain point in space is essential in picking up a reliable detector, which may assure a maximum detection and positioning distance.

6. References

- Piskunov S. Calculul diferențial și integral
vol. I și II, Moscova 1970.
- Fihttenholt G. Curs de calcul diferențial și integral
vol. II și III, Ed. tehnică,
București 1965.
- Demidovici B. Elemente de calcul numeric
Editura Mir, Moscova 1973.
- Zeldovici I. Elemente de matematică aplicată
Editura Mir, Moscova 1974.
- Paul Sterian Fizica
Editura didactică și pedagogică,
București 1985.
- Popescu I. Optica
Editura științifică și enciclopedică,
București 1989.

SINC METHOD FOR THE TWO-DIMENSIONAL NAVIER-STOKES EQUATIONS

Damian TRIF

Faculty of Mathematics and Informatics
"Babes-Bolyai" University, Cluj-Napoca
Str. M. Kogalniceanu nr. 1, 3400 Cluj-Napoca, ROMANIA
e-mail: dtrif@math.ubbcluj.ro

Abstract. The paper is devoted to the *sinc* approximation for the two-dimensional unsteady Navier-Stokes equations. To avoid the difficulty of choosing the trial function space satisfying the incompressible condition, we can consider the representation (12) of Navier-Stokes system.

1 Introduction

Sinc methods, originally introduced and analyzed by Stenger [3], have been used on a variety of differential equations. They can be used to solve problems with boundary singularities, while maintaining their exponential convergence rate. The sinc coefficient matrices are easy to assemble, requiring none of numerical integrations.

This paper illustrates the application of a sinc method to the approximate solution of Navier-Stokes equations on a rectangle. To avoid the difficulty of choosing the trial function space satisfying the incompressible condition, we can consider a representation of Navier-Stokes equations as in [1]. The pressure is evaluated by solving a Poisson equation with an artificial boundary condition.

We give a brief overview of sinc methods, after [3], in the first section and present the Navier-Stokes equations in the second section. In the last section, we consider the numerical scheme, illustrated by numerical experiments with the regularized lid driven cavity flow problem.

2 Sinc methods

Corresponding to a function f defined on \mathbb{R} , the Whittaker's cardinal function $C(f, h)$ is defined by

$$C(f, h)(x) = \sum_{k=-\infty}^{\infty} f(kh)S(k, h)(x) \quad (1)$$

whenever this series converges, where $h > 0$ is the stepsize and where

$$S(k, h)(x) = \frac{\sin[(\pi/h)(x - kh)]}{(\pi/h)(x - kh)} \quad (2)$$

In the case of the interval $[0, 1]$, instead of the basis functions (2) we now have

$$S(k, h) \circ \Phi(x) = \frac{\sin[(\pi/h)(\Phi(x) - kh)]}{(\pi/h)(\Phi(x) - kh)} \quad (3)$$

where $\Phi(z) = \log\left(\frac{z}{1-z}\right)$. If F is analytic and bounded in the domain

$$\mathcal{D} = \left\{ z : \left| \arg\left(\frac{z}{1-z}\right) \right| < d \right\} \quad (4)$$

and

$$|F(x)| \leq Cx^\alpha(1-x)^\alpha \quad \text{on } [0, 1]$$

where $\alpha > 0, C > 0$, then if we take $h = [\pi d/(\alpha N)]^{1/2}$ and $x_k = \frac{e^{kh}}{1+e^{kh}}$ we have

$$\left| F(x) - \frac{h}{\pi} \sin\left\{ \frac{\pi}{h} \log\left(\frac{x}{1-x}\right) \right\} \sum_{k=-N}^N \frac{(-1)^k F(x_k)}{\log(x/(1-x)) - kh} \right| \leq C_1 N^{1/2} e^{-(\pi d \alpha N)^{1/2}}$$

If F does not vanish at 0 or at 1, the function

$$G(x) = F(x) - (1-x)F(0) - xF(1) \quad (5)$$

may.

In addition, if F is analytic in the region \mathcal{D} , if $F \in C^2[0, 1]$ and if $F'' \in Lip_\alpha[0, 1]$, then

$$F(x) \simeq F_N(x) = c_{-N-3}(1-x) + c_{-N-2}x(1-x) + c_{-N-1}x^2(1-x)^3 + \quad (6)$$

$$+ x^2(1-x)^2 \sum_{k=-N}^N c_k S(k, h) \circ \Phi(x) + c_{N+1}x^3(1-x)^2 + c_{N+2}x^2(1-x) + c_{N+3}x$$

in which the c_k are linear combinations of F and its first and second derivatives at $(0, 1)$ and $x_k, k = -N..N$. Then taking h as above yields an approximation F_N of F on $[0, 1]$ for which all three of $F(x) - F_N(x)$, $F'(x) - F'_N(x)$ and $F''(x) - F''_N(x)$ are bounded by

$$|\text{error}| \leq C e^{-cN^{1/2}} \quad (7)$$

where C and c are positive constants.

In the case of Dirichlet or Neumann problems, the sinc approximation procedures are particularly powerful. As an example, let us consider the Dirichlet problem

$$(Lu)(x) \equiv u''(x) - f = 0, \quad x \in (0, 1) \quad (8)$$

$$u(0) = u(1) = 0$$

We may use the approximation u_N given by (6), in which we set $c_{-N-3} = c_{N+3} = 0$ in order that u_N satisfies the boundary conditions. The remaining $c_j, j = -N-2, \dots, N+2$ are determined by solving the linear system of equations

$$\int_0^1 (Lu_N)(x) \Psi_k(x) dx = 0, \quad k = -N-2, \dots, N+2$$

where Ψ_k are the coefficients of c_k in (6). By means of the quadrature formula

$$\int_0^1 g(x) dx \simeq h \sum_{k=-N-2}^{N+2} x_k(1-x_k)g(x_k)$$

of order (7), we get the linear system of $2N+5$ equations

$$(Lu_N)(x_k) = 0, \quad k = -N-2, \dots, N+2 \quad (9)$$

for the $2N+5$ coefficients c_k . The resulting approximation (6) may be used to accurately approximate u on $[0, 1]$, and by differentiating u_N once resp. twice, we get an accurate approximation to u' resp. u'' on $[0, 1]$. The errors satisfy

$$\begin{aligned} |u(x) - u_N(x)| &\leq C_1 N^{3/2} e^{-(\pi d \alpha N)^{1/2}} \\ |u'(x) - u'_N(x)| &\leq C_2 N^2 e^{-(\pi d \alpha N)^{1/2}} \\ |u''(x) - u''_N(x)| &\leq C_3 N^{5/2} e^{-(\pi d \alpha N)^{1/2}} \end{aligned}$$

If u does not vanish at 0 or 1 we consider u_N as in (5).

In the case of a Neumann problem, as an example

$$(Lu)(x) \equiv u''(x) - f = 0, \quad x \in (0, 1) \quad (10)$$

$$u'(0) = u'(1) = 0$$

where $\int_0^1 f(x) dx = 0$ and $\int_0^1 u(x) dx = 0$ to fixing the value of u , (6) becomes

$$\begin{aligned} u_N(x) = & c_{-N-2} + c_{-N-1}x^2(1-x)^3 + x^2(1-x)^2 \sum_{k=-N}^N c_k S(k, h) \circ \Phi(x) + \\ & + c_{N+1}x^3(1-x)^2 + c_{N+2}x^2(3-2x) \end{aligned} \quad (11)$$

As above, we get the linear system of $2N+5$ equations

$$(Lu_N)(x_k) = 0, \quad k = -N-2, \dots, N+1$$

$$\sum_{k=-N-2}^{N+2} x_k(1-x_k)u_N(x_k) = 0$$

for the $2N+5$ coefficients c_k .

In the above equations we have for $S(k, h, x) = S(k, h) \circ \Phi(x)$

$$S(k, h, x_n) = \delta_{kn}, \quad \frac{d}{dx} S(k, h, x_n) = \begin{cases} \frac{(-1)^{n-k}}{(n-k)hx_n(1-x_n)} & n \neq k \\ 0 & n = k \end{cases}$$

$$\frac{d^2}{dx^2} S(k, h, x_n) = \begin{cases} \frac{(-1)^{n-k}(2x_n-1)}{(n-k)hx_n^2(1-x_n)^2} - \frac{2(-1)^{n-k}}{h^2x_n^2(1-x_n)^2(n-k)^2} & n \neq k \\ -\frac{2}{3h^2x_n^2(1-x_n)^2} & n = k \end{cases}$$

3 Navier-Stokes equations

The two-dimensional unsteady Navier-Stokes equations, in the representation analyzed by [1] for Fourier-Chebyshev spectral method are as follows

$$\begin{aligned} \partial_t U + (U \cdot \nabla) U - \nu \nabla^2 U + \nabla P &= f & \text{in } \Omega \times (0, T] \\ \nabla^2 P + \Theta(U) &= \nabla \cdot f & \text{in } \Omega \times (0, T] \\ U(x, 0) &= U_0(x) & \text{in } \bar{\Omega} \\ \text{Dirichlet conditions} & & \text{on } \partial\Omega \end{aligned} \quad (12)$$

where $\Omega = (0, 1) \times (0, 1)$, $U = (U_1, U_2)^T$ is the speed vector and P is the pressure, $\partial_t = \frac{\partial}{\partial t}$, $\partial_i = \frac{\partial}{\partial x_i}$, $i = 1, 2$, and $\Theta(U) = 2(\partial_2 U_1 \partial_1 U_2 - \partial_1 U_1 \partial_2 U_2)$.

The main advantage of this method is that the incompressibility condition does not appear explicitly in the first equation. Thus we avoid the difficult job of choosing in Galerkin's method the trial function space in which the divergence of every element vanishes everywhere.

We have also to solve a Poisson equation for the pressure. Generally, there is no boundary condition for it. Thus we need an artificial boundary condition, as in our example where we adopt $\frac{\partial P}{\partial n} = 0$ on $\partial\Omega$. In addition to fixing the value of P , we require that $\int_{\Omega} P(x, t) dx = 0$, $\forall t \in [0, T]$.

4 The numerical results

We approximate U and P of (12) by the *sinc* method:

$$w_N(x_1, x_2, t) = \sum_{i=-N-2}^{N+2} \sum_{j=-N-2}^{N+2} w_{i,j}(t) \Psi_i(x_1) \Psi_j(x_2)$$

where w_N is $U_{1,N}$, $U_{2,N}$ or P , Ψ_i , Ψ_j are the coefficients of c_i , c_j in (6) or (11), and $h = 0.75/N^{1/2}$.

We can use the values of the speed $U_N^n \simeq U(x, t^n)$ and the pressure $P_N^n \simeq P(x, t^n)$ at the time level n (and $n-1$ for U) to evaluate the speed at the next time level, $U_N^{n+1} \simeq U(x, t^n + \Delta t)$ by a semi-implicit scheme

$$\frac{U_N^{n+1} - U_N^n}{\Delta t} - \nu \nabla^2 U_N^{n+1} + \frac{3}{2} (U_N^n \cdot \nabla) U_N^n - \frac{1}{2} (U_N^{n-1} \cdot \nabla) U_N^{n-1} + \nabla P_N^n = f_N^n$$

i.e. by systems

$$M_1 w + w M_2 = F \quad (13)$$

Here $w = (w_{i,j})_{i,j=-N-2..N+2}$ and M_1 , M_2 are matrices of (9) with homogeneous or nonhomogeneous Dirichlet conditions.

Next, we can evaluate the value of the pressure $P^{n+1} \simeq P(x, t^n + \Delta t)$ separately by the second formula of (12), which is a Neumann problem for P^{n+1} at each time, from a system of the type (13) too.

We take as test problem the regularized lid driven cavity flow problem, that is the homogeneous problem (12) with the only non-homogeneous Dirichlet condition $U_1(x_1, 1, t) = (1 - (2x_1 - 1)^{64})^{64}$, $x_1 \in [0, 1]$. In this case the Neumann problem for P is consistent and our algorithm gives for $N = 32$, $\nu = 0.001$, $\Delta t = 0.005$ and $t^{n+1} = 5$ the picture in fig. 1.

Our result preserves qualitatively the dynamical properties of the flow and it is in good concordance with [2], where the speed on the upper lid of the cavity was $16x^2(1-x)^2$.

The method is only conditionally stable due to the explicit treatment of the nonlinear terms, but the experiments show that the critical time step is not very restrictive with respect to ν and N .

About the accuracy, a comparison with the Chebyshev collocation method shows for the upper lid of the cavity a 10^{-3} error for Chebyshev while a 10^{-7} error for sinc method.

References

- [1] Guo Ben-Yu, Li Jian, *Fourier-Chebyshev spectral method for the two-dimensional Navier-Stokes equations*, SIAM J. Numer. Anal., 33, 3, pp. 1169-1187, 1996.
- [2] Jie Shen, *Hopf bifurcation of the unsteady regularized driven cavity flow*, J. Comp. Phys., 95, pp. 228-245, 1991.
- [3] Frank Stenger, *Numerical methods based on Whittaker cardinal, or sinc functions*, SIAM Review, 23, 2, pp. 165-224, 1981.

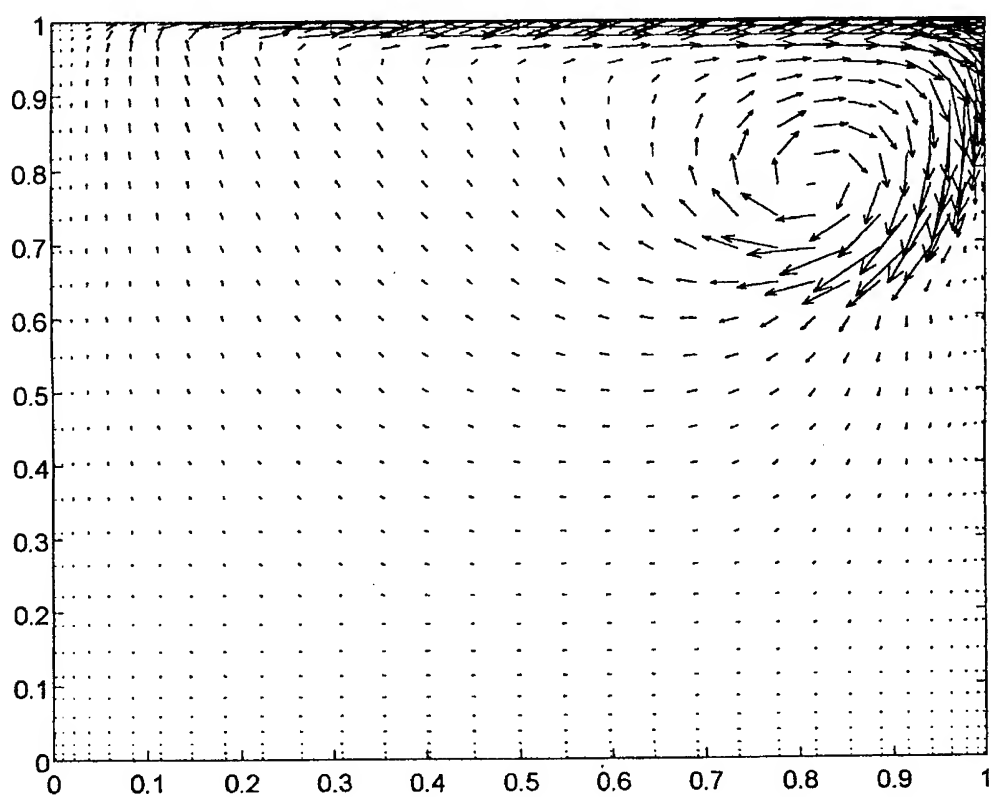


Figure 1: Speed vectors at $t=5$

Nonlinear acoustics in rigid porous media

Thérèse LÉVY

Laboratoire de Modélisation en Mécanique

associé au CNRS, n° 229

Université Pierre et Marie Curie

4 place Jussieu - 75252 Paris Cedex 05 - France

Abstract.

The homogenization method is applied to describe how a fluid behaves acoustically in a porous material. The linear theory leads to a Darcy's law involving a complex permeability tensor. The first order nonlinear correction of this law is performed. It is proved that it is quadratic with respect to the mean pressure gradient (or with respect to the bulk velocity) and cancels out if the material is macroscopically isotropic.

1. - INTRODUCTION

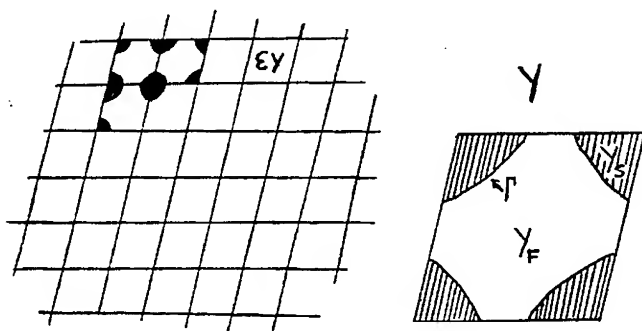
The nonlinear wave propagation through rigid porous materials has been the aim of many studies (Wilson 1988, McIntosh 1990, Norris 1995). The source of nonlinearity may originate from the constitutive equation of the fluid or from the conservation equations of mass, momentum... We are interested in the second problem. We consider a rigid porous structure saturated with a viscous compressible isothermic fluid. It is known that in many cases of practical concern, the pores are sufficiently small and the frequencies are sufficiently low so that the thermal process in the pores is nearly isothermal (Wilson 1988). These assumptions are precisely used in the homogenization technique which is employed in this paper. Otherwise a rigid frame implies that the porous matrix of the material does not vibrate as the fluid in the material is being acoustically excited. It is assumed that the wavelength of the sound perturbation is much larger than the pores dimensions, so the material may be treated as a homogeneous one with bulk properties. We employ the two-scale technique of homogenization for heterogeneous media with disparate length scales. Our objective is the nonlinear correction, for low velocities, to the linear Darcy's acoustic law.

In first, section 2 deals with the statement of the problem. The equations of nonlinear acoustics in a viscous isothermic fluid are recalled. The basic idea of the homogenization and its implementation in the problem are given in section 3. Section 4 is devoted to the theory of linear acoustics, with $\exp(i\omega t)$ time dependence, in a rigid porous periodic medium using the homogenization method. Then the linear Darcy's law for the bulk acoustic filtration involves a complex permeability tensor depending on the frequency ω . The nonlinear correction of this law for low velocities is the subject of section 5. It

is proved that the first order correction originates exclusively from the convection in the pores. The "apparent permeability" tensor of the relationship existing between the mean velocity and the macroscopic pressure gradient varies linearly with the mean fluid velocity if the bulk medium is anisotropic but in the case of bulk isotropy this correction cancels out.

2. - STATEMENT OF THE PROBLEM

We consider an infinite periodic rigid porous medium. The period of which is a parallelepiped cell homothetic with the ratio $\varepsilon \ll 1$ of a basic period Y in which the fluid domain Y_F and the solid one Y_S have a smooth boundary Γ . The pores εY_F of the structure are interconnected so as to allow fluid flow through the material. The medium is saturated by a compressible fluid and we suppose that thermal effects may be neglected.



We are interested in the small perturbations of the porous material in which the fluid is at rest. We denote by ρ_0 the constant density, p_0 the constant pressure and $c_0 = (dp/d\rho)_0^{1/2}$ the constant sound velocity of the fluid at rest. The magnitude order of the acoustic perturbation is measured by the acoustic Mach number M , which is the ratio of the characteristic velocity chosen by the observer to the sound velocity c_0 . We assume that the Mach number is very small compared to unity : $M \ll 1$. The velocity \vec{V}^ε , the density ρ^ε and the pressure p^ε in the fluid are of the form :

$$\vec{V}^\varepsilon = M \vec{V}_a, \quad \rho^\varepsilon = \rho_0 + M \rho_a, \quad p^\varepsilon = p_0 + M p_a$$

by assuming that the fluctuations are of order M . They satisfy the fluid mass and momentum conservation laws :

$$\begin{aligned}\frac{\partial \rho^\varepsilon}{\partial t} + \operatorname{div} \rho^\varepsilon \vec{V}^\varepsilon &= 0 \\ \rho^\varepsilon \left(\frac{\partial V_i^\varepsilon}{\partial t} + V_j^\varepsilon \frac{\partial V_i^\varepsilon}{\partial x_j} \right) &= -\frac{\partial p^\varepsilon}{\partial x_i} + (\bar{\lambda} + \bar{\mu}) \frac{\partial}{\partial x_i} \left(\frac{\partial V_j^\varepsilon}{\partial x_j} \right) + \bar{\mu} \frac{\partial^2 V_i}{\partial x_j \partial x_j}\end{aligned}$$

where $\bar{\lambda}$ and $\bar{\mu}$ are the fluid viscosity coefficients, and using the Einstein summation convention, the constitutive law :

$$p^\varepsilon = p(\rho^\varepsilon)$$

and the non-slip condition on the solid surfaces :

$$\vec{V}^\varepsilon = 0$$

Thus the acoustic perturbation is governed in the fluid by :

$$(1) \quad \frac{\partial \rho_a}{\partial t} + \rho_0 \operatorname{div} \vec{V}_a + M \operatorname{div}(\rho_a \vec{V}_a) = 0$$

$$(2) \quad \begin{aligned}\rho_0 \frac{\partial V_{ai}}{\partial t} + \frac{\partial p_a}{\partial x_i} - \bar{\mu} \frac{\partial^2 V_{ai}}{\partial x_j \partial x_j} - (\bar{\lambda} + \bar{\mu}) \frac{\partial}{\partial x_i} \left(\frac{\partial V_{aj}}{\partial x_j} \right) \\ + M \rho_a \frac{\partial V_{ai}}{\partial t} + M \rho_0 V_{aj} \frac{\partial V_{ai}}{\partial x_j} + M^2 \rho_a V_{aj} \frac{\partial V_{ai}}{\partial x_j} = 0\end{aligned}$$

$$(3) \quad p_a = c_0^2 \rho_a + \frac{1}{2} M \left(\frac{d^2 p}{d \rho^2} \right)_0 \rho_a^2 + O(M^2)$$

and the non-slip condition on the pores boundaries :

$$(4) \quad \vec{V}_a = 0.$$

3. - HOMOGENIZATION PROCEDURE

The homogenization (Sanchez-Palencia 1980, Lévy 1987) is an asymptotic two-scale method for studying physical processes in a finely heterogeneous medium in order to obtain an equivalent macroscopic description. It is based on the existence of two well separated length scales, ℓ and L , the characteristic lengths of the microstructure and the macroprocess respectively. In this problem, ℓ characterizes the dimensions of the physical period of the medium and L the wavelength of the sound propagation in the porous medium. It is assumed that ℓ is much smaller than L and the asymptotic process is associated with the small parameter $\varepsilon = \ell/L$. Under the hypothesis of a periodic geometry of the medium the homogenization furnishes a rigorous procedure for obtaining the macroscopic equations of the limit phenomenon as ε tends to zero. Two space variables are introduced, the standard macroscopic one $x = (x_1, x_2, x_3)$ and the microscopic one $y = x/\varepsilon$. The solution of the considered problem is searched in the form

of a double scale asymptotic expansion with the same periodicity as the medium, that means :

$$\begin{aligned} (5) \quad & \bar{V}_a = \bar{V}^0(t, x, y) + \varepsilon \bar{V}^1(t, x, y) + \dots \\ (6) \quad & p_a = p^0(t, x, y) + \varepsilon p^1(t, x, y) + \dots \\ (7) \quad & \rho_a = \rho^{0*}(t, x, y) + \varepsilon \rho^{1*}(t, x, y) + \dots \end{aligned}$$

with $\bar{V}^i, p^i, \rho^{i*}$ Y -periodic with respect to the local stretched variable y , and $\|V^i\| / \|V^{i-1}\|, p^i/p^{i-1}, \rho^{i*}/\rho^{(i-1)*}$ bounded functions in the whole medium. Whereas dissipation is generally negligible in acoustics, on the contrary in a porous material the fluid viscosity cannot be neglected on account of the very small dimensions of the cavities. In order to take it into account at the pore level, the viscosity coefficients are assumed to be of order ε^2 ($\bar{\mu} = \varepsilon^2 \mu, \bar{\lambda} = \varepsilon^2 \lambda$). The usual homogenization procedure (Sanchez-Palencia 1980, Lévy 1987) is to insert expansions (5)-(7) in equations (1)-(4) taking care that, when applied to a function $f(x, y)$, $\partial/\partial x_i$ becomes $\partial/\partial x_i + \varepsilon^{-1} \partial/\partial y_i$. In the following, index x (or y) specifies partial derivative, for example $\Delta_y = \partial^2/\partial y_i \partial y_i$. By identifying like powers of ε , we obtain successive differential problems with respect to the local variable y (at this stage x is considered as a parameter). Let us remark that according to the condition of Y -periodicity, we may consider that y varies in the basic period Y , then the periodicity of a function means that it takes equal values on the opposite faces of ∂Y . The solution of these local problems gives the local variations of \bar{V}_a, p_a, ρ_a and equations that relate them. The required homogenized equations that eliminate the explicit dependence on y , leaving us with equations in x , are obtained by averaging these relations on the period.

4. - LINEAR THEORY

The homogenization of equations (1)-(4) with $M = 0$ leads to the theory of linear acoustics in a rigid porous medium (Lévy 1977, 1987, M. Firdaouss 1996). The first approximation of (2) is $\text{grad}_y p^0 = 0$, so we obtain, using also the first approximation of (3) :

$$p^0(t, x, y) = p^0(t, x), \quad \rho^{0*}(t, x, y) = \rho^{0*}(t, x) = p^0(t, x)/c_0^2.$$

Then, the $O(\varepsilon^{-1})$ approximation of (1), the $O(\varepsilon^0)$ approximation of (2) and the $O(\varepsilon^0)$ approximation of (4) lead to the following differential problem which is to be solved in the basic period Y :

$$(8) \quad \text{div}_y \bar{V}^0 = 0 \quad \text{in } Y_F$$

$$(9) \quad \rho_0 \frac{\partial \bar{V}^0}{\partial t} = -\text{grad}_x p^0 - \text{grad}_y p^1 + \mu \Delta_y \bar{V}^0 \quad \text{in } Y_F$$

$$(10) \quad \bar{V}^0 = 0 \quad \text{on } \Gamma.$$

We consider now time dependence of the form $e^{i\omega t}$, we write :

$$\vec{V}^0 = \vec{V}(x, y)e^{i\omega t}, \quad p^0 = P^0(x, y)e^{i\omega t}, \quad p^1 = P^1(x, y)e^{i\omega t}, \\ \rho^{0*} = \rho^0(x, y)e^{i\omega t}, \dots$$

In order to obtain a variational formulation of the problem, we define the Hilbert space F of complex vectorial functions :

$$F = \left\{ \vec{W}, \vec{W} \in [H^1(Y_F)]^3, \vec{W} \text{ } Y\text{-periodic}, \vec{W} = 0 \text{ on } \Gamma, \operatorname{div}_y \vec{W} = 0 \right\}$$

with the scalar product

$$(\vec{W}, \vec{U})_F = \int_{Y_F} \left(\frac{\partial W_k}{\partial y_j} \frac{\partial \bar{U}_k}{\partial y_j} + W_k \bar{U}_k \right) dy$$

(where $\bar{}$ is for the complex conjugate).

The variational formulation of equations (8)-(10) is easily found by multiplying (9) by a test function $\vec{W} \in F$, integrating in Y_F , and using the Y -periodicity of the functions, it is :

$$\left\{ \begin{array}{l} \text{Find } \vec{V} \in W \text{ such that} \\ \int_{Y_F} i\omega \rho_0 V_k \bar{W}_k dy + \mu \int_{Y_F} \frac{\partial V_k}{\partial y_j} \frac{\partial \bar{W}_k}{\partial y_j} dy = - \frac{\partial P^0}{\partial x_k} \int_{Y_F} \bar{W}_k dy, \quad \forall \vec{W} \in F. \end{array} \right.$$

The existence and uniqueness of \vec{V} are proved using the Lax-Milgram lemma, and on account of the linearity property, we can write

$$(11) \quad \vec{V} = - \frac{\partial P^0}{\partial x_i} \vec{v}^i(y, \omega)$$

where \vec{v}^i is the unique solution of :

$$(12) \quad \left\{ \begin{array}{l} \text{Find } \vec{v}^i \in F \text{ such that} \\ \int_{Y_F} i\omega \rho_0 v_k^i \bar{W}_k dy + \mu \int_{Y_F} \frac{\partial v_k^i}{\partial y_j} \frac{\partial \bar{W}_k}{\partial y_j} dy = \int_{Y_F} \bar{W}_i dy, \quad \forall \vec{W} \in F. \end{array} \right.$$

Let us define the mean value $\tilde{f}(x)$ in Y_F of $f(x, y)$:

$$\tilde{f}(x) = \frac{1}{|Y|} \int_{Y_F} f(x, y) dy,$$

then we obtain, taking the mean value of (11)

$$(13) \quad \vec{V} = -K(\omega) \operatorname{grad} P^0.$$

this is a linear Darcy's law, with the complex permeability tensor defined by :

$$K_{ij} = \tilde{v}_i^j$$

The permeability tensor \mathbb{K} depends on the frequency ω and is completely defined by the microstructure. It is easy to prove the symmetry of the tensor \mathbb{K} , as a matter of fact writing (12) with $\tilde{\bar{W}} = \tilde{v}^j$ and the variational formulation of the \tilde{v}^j determination with $\tilde{\bar{W}} = \tilde{v}^i$, we conclude that $K_{ij} = K_{ji}$.

In order to emphasize the physical origin of the real and imaginary parts of the permeability, let us suppose the isotropy of the medium, then the permeability is a scalar. Denoting by k_1 and k_2 its real and imaginary part respectively, (13) may be written

$$\tilde{\bar{V}} = -[k_1(\omega) + ik_2(\omega)] \text{grad } P^0 = -(\tilde{\epsilon} \cdot \tilde{v}) \text{grad } P^0$$

with $\tilde{\epsilon} = -\text{grad } P^0 / |\text{grad } P^0|$, and $\tilde{v}(y, \omega) \in F$, verifying (12), that is to say (Firdaouss 1996)

$$\int_{Y_F} i\omega\rho_0 v_k \bar{W}_k dy + \mu \int_{Y_F} \frac{\partial v_k}{\partial y_j} \frac{\partial \bar{W}_k}{\partial y_j} dy = \int_{Y_F} e_k \bar{W}_k dy, \quad \forall \bar{W} \in F.$$

By taking $\tilde{\bar{W}} = \tilde{v}$ in this relation, we obtain the real part k_1 and the imaginary part k_2 in the form

$$k_1(\omega) = \frac{1}{|Y|} \int_{Y_F} \mu \frac{\partial v_k}{\partial y_j} \frac{\partial \bar{v}_k}{\partial y_j} dy$$

$$k_2(\omega) = -\frac{\omega\rho_0}{|Y|} \int_{Y_F} v_k \bar{v}_k dy$$

Then the real part of the permeability may be associated with the viscous dissipation and the imaginary part with the inertia. Similar considerations are displayed in (Wilson 1988). Though the subject of the study is the Darcy's law, let us note the second macroscopic law. Integrating in Y_F the $O(\epsilon^0)$ approximation of (1), we obtain

$$i\omega \frac{\pi}{c_0^2} P^0 + \rho_0 \text{div } \tilde{\bar{V}} = 0$$

with $\pi = |Y_F| / |Y|$, the porosity of the medium. This equation and (13) lead to Helmholtz-like equation in porous media

$$i\omega \frac{\pi}{c_0^2} P^0 - \rho_0 \frac{\partial}{\partial x_i} \left[K_{ij}(\omega) \frac{\partial P^0}{\partial x_j} \right] = 0.$$

5. - NONLINEAR CORRECTION OF THE DARCY'S LAW

We wish to find corrections to the linear theory of section 4, which will include the nonlinear properties of the fluid in the material. As a matter of fact the homogenization method is used to predict the nonlinear correction of the Darcy's law. A similar study has been performed for the stationary filtration (Wodé 1991) in order to discuss the Forchheimer equation.

We now deal with the homogenization of equations (1)-(4), neglecting the terms smaller than M . The $O(M)$ nonlinear terms lead to the first order correction of the asymptotic expansions (5)-(7). In order to take into account the nonlinearities at the pore level, we assume $\varepsilon^2 \ll M \ll \varepsilon$ and asymptotic expansions of the form

$$\begin{aligned}\vec{V}_a &= \left[\vec{V}^0(t, x, y) + \frac{M}{\varepsilon} \vec{u}^0(t, x, y) + \dots \right] + O(\varepsilon) \\ p_a &= p^0(t, x) + \varepsilon \left[p^1(t, x, y) + \frac{M}{\varepsilon} q^1(t, x, y) + \dots \right] + O(\varepsilon^2) \\ \rho_a &= \rho^{0*}(t, x) + \varepsilon \left[\rho^{1*}(t, x, y) + \frac{M}{\varepsilon} r^{1*}(t, x, y) + \dots \right] + O(\varepsilon^2)\end{aligned}$$

Substituting these expansions into the governing system (1)-(4) yields to the next set of equations :

$$(14) \quad \operatorname{div}_y \vec{u}^0 = 0 \quad \text{in } Y_F$$

$$(15) \quad \rho_0 \left(\frac{\partial u_i^0}{\partial t} + V_j^0 \frac{\partial V_i^0}{\partial y_j} \right) = - \frac{\partial q^1}{\partial y_i} + \mu \Delta_y u_i^0 \quad \text{in } Y_F$$

$$(16) \quad q^1 = c_0^2 r^{1*} + \frac{1}{2} \left(\frac{d^2 p}{d \rho^2} \right)_0 \rho^{0*2} \quad \text{in } Y_F$$

$$(17) \quad \vec{u}^0 = 0 \quad \text{on } \Gamma.$$

When \vec{V}^0 , p^0 and ρ^{0*} are harmonic function of t , the perturbation implies a time dependence of the form $e^{2i\omega t}$, we write :

$$\vec{u}^0 = \vec{U}(x, y) e^{2i\omega t}, \quad q^1 = Q^1(x, y) e^{2i\omega t}.$$

Then, using (11) \vec{U} and Q^1 are solutions of :

$$\begin{aligned}\operatorname{div}_y \vec{U} &= 0 \quad \text{in } Y_F \\ 2i\omega \rho_0 U_i + \frac{\partial Q^1}{\partial y_i} - \mu \Delta_y U_i &= -\rho_0 \frac{\partial P^0}{\partial x_m} \frac{\partial P^0}{\partial x_n} v_j^m \frac{\partial v_i^n}{\partial y_j} \quad \text{in } Y_F \\ \vec{U} &= 0 \quad \text{on } \Gamma.\end{aligned}$$

The variational formulation of this problem may be obtained as in the previous section and on account of its linearity, we can write :

$$(18) \quad \vec{U} = \rho_0 \frac{\partial P^0}{\partial x_m} \frac{\partial P^0}{\partial x_n} \vec{Z}^{mn}(y, \omega)$$

with $\vec{Z}^{mn} = \vec{Z}^{nm}$ the unique solution of

$$\left\{ \begin{array}{l} \text{Find } \vec{Z}^{mn} \in F \\ \int_{Y_F} 2i\omega\rho_0 Z_k^{mn} \bar{W}_k dy + \\ + \mu \int_{Y_F} \frac{\partial Z_k^{mn}}{\partial y_j} \frac{\partial \bar{W}_k}{\partial y_j} dy = -\frac{1}{2} \int_{Y_F} \left(v_j^m \frac{\partial v_k^n}{\partial y_j} + v_j^n \frac{\partial v_k^m}{\partial y_j} \right) \bar{W}_k dy, \quad \forall \bar{W} \in F. \end{array} \right.$$

At once, we remark in view of equations (14)-(17) that the first order correction of the linear Darcy's law is due to the only convection terms in the momentum equation. We define now the mean velocity in the porous medium :

$$\langle \vec{V} \rangle = \vec{V}^0 + \frac{M}{\varepsilon} \vec{u}^0.$$

With (13) and (18) we can write

$$(19) \quad \langle V \rangle_t = -K_{tj}(\omega) \frac{\partial P^0}{\partial x_j} e^{i\omega t} + \rho_0 T_{lmn}(\omega) \frac{\partial P^0}{\partial x_m} \frac{\partial P^0}{\partial x_n} e^{2i\omega t}.$$

The nonlinear correction of the Darcy's law looks like a Forchheimer law, it involves a third order tensor $T(\omega)$ such that

$$T_{lmn} = \frac{M}{\varepsilon} \vec{Z}_l^{mn}.$$

Like the \vec{Z}^{mn} , $T(\omega)$ depends only on the microstructure geometry. The correction is generally quadratic but it can be proved as in (Wodíé 1991) that if the medium is macroscopically isotropic the tensor $T(\omega)$ is zero and then the nonlinear correction must be re-examined. This result agrees with the description of (McIntosh 1990) for the nonlinear wave propagation through rigid porous materials for low velocities and isotropic media.

References

- M. Firdaouss, J.L. Guermond, D. Lagarge, T. Lévy, "Propagation du son dans un gaz saturant une structure poreuse : effets visco-thermiques", Congrès Français de Thermique, Valenciennes (France), mai 1996 (to appear).
- T. Lévy, "Fluid in porous media and suspensions". Lecture Notes in Physics, n° 272, Springer-Verlag, 1987.
- J.D. McIntosh and R.F. Lambert, "Nonlinear wave propagation through rigid porous materials.I", J. Acoust. Soc. Am., 88(4), 1990.
- A.N. Norris and M.A. Grinfeld, "Nonlinear poroelasticity of a layered medium", J. Acoust. Soc. Am. 98(2), 1995.
- E. Sanchez-Palencia, "Non homogeneous media and vibration theory", Lecture Notes in Physics, n° 127, Springer-Verlag, 1980.
- D.K. Wilson, J.D. McIntosh and R.F. Lambert, "Forchhermer-type nonlinearities for high intensity propagation of pure tones in air-saturated porous media", J. Acoust. Soc. Am., 84(1), 1988.
- J.C. Wodé et T. Lévy, "Correction non linéaire de la loi de Darcy", C. R. Acad. Sc. Paris, 312, série II, 1991.

The dopant transport by convection and diffusion during melt growth of semiconductor crystals in the context of the Bridgman-Stockbarger crystal growth configuration

Șt. Balint, A.M. Balint, D. Bălțean, A. Neculae
Univ. of the West Timișoara,
Blv. V. Pârvan No.4, 1900 Timișoara, Romania

Abstract

In this paper we give a short description of the physical model of the Bridgman-Stockbarger crystal growth system. This is followed by the presentation of the existing mathematical models of the system, including equations governing the processes. Because these models describe the dopant field assuming that the interface is a mathematical surface, we continue with a new dopant field analysis proposal. In order to develop this analysis, we make two kinds of hypothesis concerning the neighbourhood of the growth interface, which is a thin region, but not a mathematical surface. The first hypothesis is that in this region there is already a "periodic" structure formed by microcells like in crystal and the dispersion mechanism of the dopant is due also to convection of dopant by the microscopic velocity field in these microcells. The second hypothesis is that this region is like a bed of randomly distributed spheres and the dispersion mechanism of dopant is due also to convection of the dopant by the random velocity field generated at the microscale by the randomly distributed inclusions. In both situations we obtain a new effective convective-diffusive equation for this region. For realize this we used the method of homogenization, that is a multiple scale analysis in terms of a small ratio ϵ between the characteristic micro and macroscales.

1 The physical model of the Bridgman-Stockbarger crystal growth system

The schematic of the system is presented in fig. 1.

The system consists of two isothermal zones separated by a gradient region, which is radially adiabatic.

The growth direction is considered to be aligned with the gravitational acceleration.

The solidification front is located inside the gradient region.

The charge extends sufficiently into the hot and cold zones so that heat transfer in the charge is quasi-steady and the growth rate is equal to charge lowering rate.

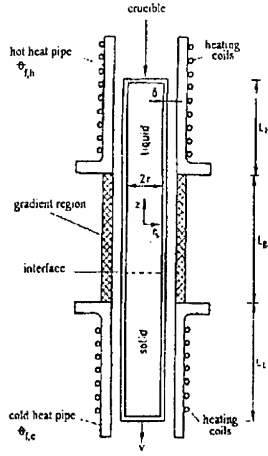


Figure 1: Schematic of the Bridgman-Stockbarger crystal growth system.

2 Mathematical models for the Bridgman-Stockbarger crystal growth system. Equations governing the process.

Calculations made by Wang, C. in [1] have been extensively used for crystal growth experiments in this system. The system has also been subject of the following modelling studies: [2],[3],[4],[5],[6].

The equations used in the above models are the following:

$$(1) \quad \frac{\partial \bar{u}}{\partial t} + (\bar{u} \nabla) \bar{u} = -\nabla p + \nabla^2 \bar{u} - \frac{R_o}{P_r} \theta e_z$$

the non-dimensional transient momentum equations in the melt

$$(2) \quad \frac{\partial \theta}{\partial t} + \bar{u} \nabla \theta = \frac{1}{P_r} \nabla^2 \theta$$

the non-dimensional energy equation in the melt

$$(3) \quad \nabla \bar{u} = 0$$

the non-dimensional mass continuity equation in the melt

$$(4) \quad \frac{\alpha_s}{\alpha_m} \frac{\partial \theta_s}{\partial t} = P e_s \frac{\partial \theta_s}{\partial z} + \nabla^2 \theta_s$$

the non-dimensional energy equation in solid (crystal)

$$(5) \quad \frac{\alpha_c}{\alpha_m} \frac{\partial \theta_c}{\partial t} = P c_c \frac{\partial \theta_c}{\partial z} + \nabla^2 \theta_c$$

the non-dimensional energy equation in crucible

$$(6) \quad \frac{\partial \theta_c}{\partial r} = Rn_h^*(\theta_{fh} - \theta_c) \quad \text{for} \quad \frac{L_G}{2} < z$$

the non-dimensional linearized radiative interaction between the crucible outer walls and the furnace in the hot zone

$$(7) \quad \frac{\partial \theta_c}{\partial r} = 0 \quad \text{for} \quad -\frac{L_G}{2} < z < \frac{L_G}{2}$$

the radially adiabatic condition in the gradient region

$$(8) \quad \frac{\partial \theta_c}{\partial r} = Rn_c^*(\theta_{fc} - \theta_c) \quad \text{for} \quad z < -\frac{L_G}{2}$$

the non-dimensional linearized radiative interaction between the crucible outer walls and the furnace in the cold zone

$$(9) \quad \frac{\partial \theta_c}{\partial z} = 0$$

the adiabatic condition on the top and bottom of the crucible

$$(10) \quad \frac{\partial \theta_m}{\partial n} + \frac{k_s}{k_m} PeSt = \frac{k_s}{k_m} \frac{\partial \theta_s}{\partial n}$$

the non-dimensional latent heat equation on the crystallization front.

The list of symbols used in these equations:

u - non-dimensional velocity vector ($= \bar{v}r_s/\nu$)

\bar{v} - velocity vector

r_s - radius of solid (crystal)

\bar{R} - position vector

$\frac{\bar{R}}{r_s}$ - non-dimensional space variable

ν - kinematic viscosity

l - non-dimensional time ($= \tau\nu/r_s^2$)

τ - time

p - non-dimensional pressure ($= \tilde{p}r_s^2/(\rho_m\nu^2)$)

\hat{p} - pressure

ρ_m - density of the melt

R_a - Rayleigh number ($= g\beta(T_h - T_m)r_s^3/\nu\alpha_m$)

g - gravitational acceleration

β - thermal expansion coefficient

T_h - hot temperature

T_m - melting point temperature of the charge

α_m - thermal diffusivity of the melt

Pr - Prandtl number ($= \nu/\alpha_m$)

θ - non-dimensional temperature in the melt ($= (T - T_m)/(T_h - T_m)$)

\bar{e}_z - unit vector parallel to gravitational acceleration

α_s - thermal diffusivity of solid (crystal)
 θ_s - non-dimensional temperature in solid (crystal) $(= (T - T_m)/(T_h - T_m))$
 $Pe_{s,c}$ - Peclet number in solid, respectively in crucible $(= Rr_s/\alpha_m)$
 R - growth rate
 α_c - thermal diffusivity in the crucible
 θ_c - non-dimensional temperature in crucible $(= (T - T_m)/(T_h - T_m))$
 Rn_h^* - linearized radiation number in hot zone $(= 4\epsilon_c \sigma T_h^3 r_s / k_c)$
 ϵ_c - crucible emissivity
 k_c - crucible thermal conductivity
 σ - the Stefan-Boltzmann constant
 θ_{fh} - non-dimensional furnace temperature in hot zone
 L_G - gradient zone length
 Rn_c^* - linearized radiation number in cold zone $(= 4\epsilon_c \sigma T_c^3 r_s / k_c)$
 T_c - cold zone temperature
 θ_{fc} - non-dimensional furnace temperature in cold zone
 k_s - solid (crystal) thermal conductivity
 k_m - melt thermal conductivity
 n - direction normal to growth interface
 θ_m - non-dimensional melt temperature at the crystallization interface
 θ_s - non-dimensional solid temperature at the crystallization interface
 St - Stefan number
 ΔH_{s-m} - latent heat of solidification $(= k_s \frac{\partial \theta_s}{\partial n} - k_m \frac{\partial \theta_m}{\partial n})$
 c_c - heat capacity.

Solutions of equations 1 to 10 requires simultaneous calculations of the velocity field \bar{u} in the melt, the temperature fields in the melt and solid, the location and shape of the crystallization interface.

For the steady state we can use the following methodology:

Equations 6, 7, 8, 9 define boundary conditions on the outer walls of crucible.

The above boundary conditions are used in order to find a stationary solution θ_c of the equation 5 in the region defined by the outer walls of the crucible (Neumann problem).

The values of the above stationary solution θ_c on the inner walls of the crucible will be used for finding the stationary solution of the non-dimensional energy equation in solid (crystal) eq.4 and liquid eq.2. The location of the growth interface is given by the points on inner walls in which the temperature θ_c is equal to zero (the crystallization temperature) and the shape is considered plane. The temperature on the interface is equal to zero (the melting point temperature).

The above boundary conditions and equation 4 define a stationary distribution of the temperature θ_s^1 in solid (crystal). The same boundary conditions and equation 2, in which at this step we neglect \bar{u} , define a stationary distribution of the temperature in the melt $\theta^{(1)}$.

With the above obtained temperature distribution in the melt $\theta^{(1)}$ we find a stationary solution $\bar{u}^{(1)}$ of the equation 1 corresponding to the boundary condition $\bar{u}^{(1)}|_D = 0$.

Using the velocity field $\bar{u}^{(1)}$ we find a stationary solution $\theta^{(2)}$ of equation 2 and with this we find a stationary solution $\bar{u}^{(2)}$ of equation 1 corresponding to the boundary condition

$\bar{u}^{(2)}|_{\partial} = 0$. With $\bar{u}^{(2)}$ we find $\theta^{(3)}$ and with $\theta^{(3)}$ we find $\bar{u}^{(3)}$. We stop this iterative process when $\theta^{(i)}$ satisfies equation 10 with enough accuracy.

The transport equation can be solved using Nekton solver. This solver is based on a spectral element technique which decomposes the flow domain in standard finite element fashion and expands the primitive variables using high-order Chebyshev polynomials. The convective and buoyancy terms are treated explicitly using a third-order Adams-Bashforth method and the diffusive terms are treated implicitly with a second order Crank-Nicolson scheme.

Steady state temperature and velocity fields were obtained in the range of $Ra = 0.1 - 1.5 \cdot 10^5$. The results indicate the presence of two distinct convective cells for Ra numbers up to 10^4 , a lower cell close to the growth interface driven by temperature gradients associated to the solidification front and an upper cell driven by lateral heat input into the melt. The convective cells are effectively decoupled by the quiescent region separating the two. At $Ra > 10^4$ the increase in the melt velocity and the interaction of the velocity field with the top of the crucible leads to the appearance of two recirculating zones in the upper cell. This suggests that with increasing Ra the upper cell will break into two and with further increases in Ra the flow in the upper cell will become unstable. It must be noted that the presence of two distinct cells is a consequence of the choice of hot and cold zone temperatures and the crucible material. With decreasing hot and/or cold zone temperature the growth interface would move towards the hot zone and the two convective cells would interact. In such conditions, the occurrence of instability in the upper cell would be expected to directly impact the growth process.

Analysis of these results can provide the basis for extrapolation to other growth configurations where different convection patterns are present. Steady dopant field analysis in this mode is considered assuming that the interface is a mathematical surface.

3 A new dopant field analysis proposal.

An analysis of the dopant field in the context of Bridgman-Stockbarger crystal growth system is justified by the fact that the unequal repartitioning of the dopant in the melt influences the compositional uniformity of the grown material. The radial and axial dopant segregation in the crystal is determined by: convection in the melt, the value of the dopant diffusivity in molten charge, morphology of the solidification front. Crystals grown from well mixed melts exhibit a non-linear variation of dopant concentration along the growth axis (see [7]). Growth from quiescent melts results, after an initial transient, in uniform axial dopant concentration in the growing material (see [8]). During growth on earth in Bridgman Stockbarger system, the unavoidable temperature gradients in the charge generate buoyancy driving forces (convection) which result in only nearly complete mixing of the melt [1]. Reduction of the magnitude of the buoyancy forces through processing the semiconductors in low gravity environments is a way for obtaining desired uniform dopant repartitioning in the grown material [9].

Another way to obtain uniform dopant repartitioning in the growth material could be to compute the evolution in time of the dopant concentration for given growth rates and thermal conditions and to find from here how they influence the repartitioning of dopant and

in what way these conditions must be modified (generating control functions) in order to have the desired uniform repartitioning of the dopant in the melt at least in the neighbourhood of the crystallization front. In this way we hope to assure the uniform repartitioning of the dopant also in the grown material. This method requires dynamic description of the growth process from initial to final stages, inclusively dynamic description of the dopant concentration. In order to make such a description we complete the system of equations 1-10 with the convective-diffusive equation of dopant concentration:

$$(11) \quad \frac{\partial c}{\partial \tau} + \bar{v} \cdot \nabla c = D(\nabla^2 c + \frac{k_T}{T} \nabla^2 T)$$

where c is the dopant concentration, \bar{v} is the velocity field given by eq.1, D is the diffusion coefficient of dopant, $k_T D$ is the thermodiffusion coefficient, T is the temperature given by eq.2. The constant k_T is called the thermodiffusion ratio and we can neglect it for small concentrations (see [10]).

The equation 11 describes with accuracy the evolution of the dopant concentration in the upper cell and in quiescent zone, but in the lower cell, close to the growth interface, this equation must be improved because the growth interface is not really a mathematical surface. The growth interface is a thin region which has one of the following characteristics:

1. There is already a "periodic" structure, formed by microcells, like in crystal and the dispersion mechanism of the dopant is due also to convection of dopant by the microscopic velocity field in these microcells.

2. This region is like a bed of randomly distributed fixed "spheres" and the dispersion mechanism of dopant is due also to convection of the dopant by the random velocity field generated at the microscale by the randomly distributed inclusions.

In both situations we must deduce a new effective convective-diffusive equation for this region.

In order to deduce the new macroscopic convective-diffusive equation in the neighbourhood of the growth interface we use the method of homogenization, that is a multiple-scale perturbative analysis in terms of the small ratio ϵ between the characteristic micro and macro length scales. The method was first proposed in 1978 by Bensoussan, Lions and Papanicolaou in [11] and later extended in a series of books and articles [12-20].

In this method the dependent variables of the problem is assumed to be expressible as a regular expansion in terms of a small parameter ϵ equal to the ratio of the microscale to macroscale characteristic lengths. Finally the macroscopic equation, which is satisfied by the leading-order term of that expansion, is expected to arise naturally from the ensuring regular perturbation analysis.

4 The macroscopic (effective) convective-diffusive equation for small concentration when we modeling the thin region in the neighbourhood of the growth interface by a spatial periodical structure.

For small concentrations, the microscopic convective-diffusive equation of dopant is

$$(12) \quad \frac{\partial c}{\partial \tau} + \bar{v} \nabla c = D \Delta c$$

and the boundary condition

$$(13) \quad \bar{n} \nabla c = 0 \quad \text{on} \quad \partial \omega$$

Here $\bar{v} = \bar{v}(y)$ is the fluid velocity in a cell Ω and is taken periodic, D is the diffusion coefficient, ω denotes the "solid" part in a cell (the part which is already solid), $\partial \omega$ denotes the boundary of the solid part and \bar{n} indicates a unit vector normal to $\partial \omega$, $\Omega' = \Omega - \omega$.

We consider the two length scales l and L corresponding to the cell size (i.e. the period of the structure) and the size of the region in question, respectively. Assume that $\varepsilon = l/L \ll 1$. Now we introduce the following hierarchy of time scales

$$(14) \quad \tau_1 = \frac{l}{V_0}, \quad \tau_2 = \frac{l^2}{D}, \quad \tau_3 = \frac{L}{V_0}, \quad \tau_4 = \frac{L^2}{D}$$

where V_0 is the characteristic value of the velocity field.

There are two related non-dimensional numbers which appear here - the local and global Peclet numbers:

$$(15) \quad Pe_l = \frac{\tau_2}{\tau_1} = \frac{lV_0}{D}, \quad Pe_g = \frac{\tau_4}{\tau_3} = \frac{LV_0}{D} = \frac{1}{\varepsilon} Pe_l$$

representing the ratio between convection and diffusion locally and globally, respectively.

We assume that convection and diffusion balance each other at the microscale, that means $Pe_l = O(1)$. In this case, $Pe_g = O(\varepsilon^{-1})$, what means that convection dominates diffusion at the macroscale.

We note by \bar{R} the macroscopic position vector, with $|\bar{R}| = O(L)$. Scaling the space variables according to

$$(16) \quad \bar{x} = \frac{\bar{R}}{L}$$

we introduce the corresponding microscopic variables

$$(17) \quad \bar{y} = \frac{\bar{R}}{l} = \frac{\bar{x}}{\varepsilon}$$

Now we introduce the following three time scales:

$$(18) \quad t = \frac{\tau}{\tau_2}, \quad T_1 = \frac{\tau}{\tau_3}, \quad T_2 = \frac{\tau}{\tau_4}$$

Assume that the effective concentration c depends on $\varepsilon, \bar{x}, \bar{y}, t, T_1, T_2$ and can be expanded as follows:

$$(19) \quad c(\varepsilon, \bar{x}, \bar{y}, t, T_1, T_2) = \sum_{n=0}^{\infty} \varepsilon^n c_n(\bar{x}, \bar{y}, t, T_1, T_2)$$

The dependence on y will be assumed periodic and we assume that $\int_{\Omega'} c_n dy = 0$, for $n=1,2,\dots$ where $\Omega' = \Omega - \omega$.

For the time derivatives formulas 18 give:

$$(20) \quad \frac{\partial}{\partial \tau} = \frac{D}{L^2} \left(\frac{\partial}{\partial T_2} + Pe_l \varepsilon^{-1} \frac{\partial}{\partial T_1} + \varepsilon^{-2} \frac{\partial}{\partial t} \right)$$

and for the space derivatives formulas 16 and 17 give:

$$(21) \quad \nabla_R = \frac{1}{L} \left(\nabla_{\bar{x}} + \frac{1}{\varepsilon} \nabla_{\bar{y}} \right), \quad \nabla_R^2 = \frac{1}{L^2} \left(\nabla_{\bar{x}}^2 + \frac{2}{\varepsilon} \nabla_{\bar{x}} \nabla_{\bar{y}} + \frac{1}{\varepsilon^2} \nabla_{\bar{y}}^2 \right)$$

Substituting 19 in 12, using 20, 21 and collecting equal powers of ε on gets:

$$(22) \quad \begin{cases} \Delta_{\bar{y}} c_0 - \bar{u} \nabla_{\bar{y}} c_0 - \frac{\partial c_0}{\partial t} = 0 \\ \bar{n} \nabla_{\bar{y}} c_0 = 0 \end{cases} \quad \text{on } \frac{\partial \omega}{\partial \omega} \quad \text{for } O(\varepsilon^{-2})$$

$$(23) \quad \begin{cases} \Delta_{\bar{y}} c_1 - \bar{u} \nabla_{\bar{y}} c_1 - \frac{\partial c_1}{\partial t} = \bar{u} \nabla_{\bar{x}} c_0 - 2 \nabla_{\bar{x}} \nabla_{\bar{y}} c_0 + Pe_l \frac{\partial c_0}{\partial T_1} \\ \bar{n} \nabla_{\bar{y}} c_1 + \bar{n} \nabla_{\bar{x}} c_0 = 0 \end{cases} \quad \text{on } \frac{\partial \omega}{\partial \omega} \quad \text{for } O(\varepsilon^{-1})$$

$$(24) \quad \begin{cases} \Delta_{\bar{y}} c_2 - \bar{u} \nabla_{\bar{y}} c_2 - \frac{\partial c_2}{\partial t} = \bar{u} \nabla_{\bar{x}} c_1 - 2 \nabla_{\bar{x}} \nabla_{\bar{y}} c_1 + Pe_l \frac{\partial c_1}{\partial T_1} - \nabla_{\bar{x}}^2 c_0 + \frac{\partial c_0}{\partial T_2} \\ \bar{n} \nabla_{\bar{y}} c_2 + \bar{n} \nabla_{\bar{x}} c_1 = 0 \end{cases} \quad \text{on } \frac{\partial \omega}{\partial \omega} \quad \text{for } O(1)$$

where we have put

$$(25) \quad \bar{u} = Pe_l \frac{\bar{v}}{V_0}$$

A function $c_0 = c_0(\bar{x}, T_1, T_2)$ satisfies 22. For such a solution of 22 equation 23 becomes

$$(26) \quad \begin{cases} \Delta_{\bar{y}} c_1 - \bar{u} \nabla_{\bar{y}} c_1 - \frac{\partial c_1}{\partial t} = \bar{u} \nabla_{\bar{x}} c_0 + Pe_l \frac{\partial c_0}{\partial T_1} \\ \bar{n} \nabla_{\bar{y}} c_1 + \bar{n} \nabla_{\bar{x}} c_0 = 0 \end{cases} \quad \text{on } \frac{\partial \omega}{\partial \omega}$$

The solvability condition for 26 gives

$$(27) \quad Pe_l \frac{\partial c_0}{\partial T_1} = - \langle \bar{u} \rangle \nabla_{\bar{x}} c_0$$

where we have

$$(28) \quad \langle \bar{u} \rangle = \frac{1}{|\Omega'|} \int_{\Omega'} \bar{u}(\bar{y}) d\bar{y}$$

For the equation 26 we look for a solution of the form

$$(29) \quad c_1(\bar{x}, \bar{y}, t, T_1, T_2) = \chi(\bar{y}, t) \nabla_{\bar{x}} c_0(\bar{x}, T_1, T_2)$$

Substitutioning 29 in 26 we find:

$$(30) \quad \begin{cases} \frac{\partial \bar{\chi}}{\partial t} + (\bar{u} \nabla_{\bar{y}}) \bar{\chi} - \Delta_{\bar{y}} \bar{\chi} = \langle \bar{u} \rangle - \bar{u} \\ (\bar{n} \nabla_{\bar{y}}) \bar{\chi} = -\bar{n} \end{cases}$$

The problem 30 has an unique stationary solution $\bar{\chi} = \bar{\chi}(\bar{y})$ which is periodic and satisfies $\langle \bar{\chi} \rangle = \frac{1}{|\Omega'|} \int_{\Omega'} \bar{\chi}(\bar{y}) d\bar{y} = 0$. We consider this function $\bar{\chi} = \bar{\chi}(\bar{y})$ and $c_1 = \bar{\chi} \nabla_{\bar{x}} c_0$. Substituting in 24 we find

$$(31) \quad \begin{cases} \Delta_{\bar{y}} c_2 - \bar{u} \nabla_{\bar{y}} c_2 - \frac{\partial c_2}{\partial t} = \bar{u} \nabla_{\bar{x}} (\bar{\chi} \nabla_{\bar{x}} c_0) - 2 \nabla_{\bar{x}} \nabla_{\bar{y}} (\bar{\chi} \nabla_{\bar{x}} c_0) + P c_1 \frac{\partial c_1}{\partial t_1} - \Delta_{\bar{x}} c_0 + \frac{\partial c_0}{\partial t_2} \\ \bar{n} \nabla_{\bar{y}} c_2 = -\bar{n} \nabla_{\bar{x}} c_1 \end{cases}$$

The solvability condition of the equation 31 gives:

$$(32) \quad \frac{\partial c_0}{\partial T_2} = \sum_{i=1}^3 \sum_{j=1}^3 \left(\delta_{ij} - \frac{1}{|\Omega'|} \int_{\Omega'} \chi_j u_i d\bar{y} + \frac{2}{|\Omega'|} \int_{\Omega'} \frac{\partial \chi_j}{\partial y_i} d\bar{y} - \frac{1}{|\Omega'|} \int_{\partial \omega} n_i \chi_j d\sigma \right) \frac{\partial^2 c_0}{\partial x_i \partial x_j}$$

or

$$(33) \quad \frac{\partial c_0}{\partial T_2} = \left[I - \langle \bar{\chi} \bar{u} \rangle + 2 \langle \nabla \bar{\chi} \rangle - \frac{1}{|\Omega'|} \int_{\partial \omega} \bar{n} \bar{\chi} d\sigma \right] \nabla_{\bar{x}} \nabla_{\bar{x}} c_0$$

Substituting $c_0 = c_0(\bar{x}, T_1, T_2)$ in 20 and using 27, 33 we find that c_0 satisfies the equation

$$(34) \quad \frac{\partial c_0}{\partial \tau} + \langle \bar{v} \rangle \nabla_{\bar{R}} c_0 = D \left[I - \langle \bar{\chi} \bar{u} \rangle + 2 \langle \nabla \bar{\chi} \rangle - \frac{1}{|\Omega'|} \int_{\partial \omega} \bar{n} \bar{\chi} d\sigma \right] \nabla_{\bar{R}} \nabla_{\bar{R}} c_0$$

This is the macroscopic convective-diffusive equation of the dopant in the neighbourhood of the crystallization front.

The quantity defined by

$$(35) \quad D^* = D \left[I - \langle \bar{\chi} \bar{u} \rangle + 2 \langle \nabla \bar{\chi} \rangle - \frac{1}{|\Omega'|} \int_{\partial \omega} \bar{n} \bar{\chi} d\sigma \right]$$

is the diffusivity tensor in this region.

The expression of the effective diffusivity tensor for periodic porous media was subject of several papers, see for example [18],[20]. For the case of spatially periodic porous media a formula was first obtained by Brenner in [21]. Brenner considers that only the symmetric part of D^* enters in the macroscopic equation 34.

In order to find the symmetric part we consider D_{ij} from 32

$$(36) \quad D_{ij} = D \left[\delta_{ij} - \frac{1}{|\Omega'|} \int_{\Omega'} \chi_i u_j d\bar{y} + \frac{2}{|\Omega'|} \int_{\Omega'} \frac{\partial \chi_i}{\partial y_j} d\bar{y} - \frac{1}{|\Omega'|} \int_{\partial \omega} \chi_i n_j d\sigma \right]$$

and using Gauss formulas we find

$$(37) \quad D_{ij} = D \left[\delta_{ij} - \frac{1}{|\Omega'|} \int_{\Omega'} \chi_i u_j d\bar{y} + \frac{1}{|\Omega'|} \int_{\Omega'} \frac{\partial \chi_i}{\partial y_j} d\bar{y} \right]$$

The symmetric part \tilde{D}_{ij} is given by

$$(38) \quad \tilde{D}_{ij} = D \left[\delta_{ij} - \frac{1}{|\Omega'|} \frac{1}{2} \int_{\Omega'} (\chi_i u_j + \chi_j u_i) d\bar{y} + \frac{1}{|\Omega'|} \frac{1}{2} \int_{\Omega'} \left(\frac{\partial \chi_i}{\partial y_j} + \frac{\partial \chi_j}{\partial y_i} \right) d\bar{y} \right]$$

The dispersion tensor given by 37 depends on the flow in the "pores" (Ω'). To calculate the dispersion tensor one must solve the Ω cell problem defined by 30. This linear Ω cell problem defined by 30 can, in principle, be solved numerically for $\bar{\chi}$ for any Ω cell geometry and velocity field \bar{v} in the Ω cell.

For the velocity field \bar{v} in the Ω cell we have at least two choices:

1) The velocity field \bar{v} generated in Ω cell by the macroscopic convective velocity field in lower cell due to the gradient of temperature in the neighbourhood of the crystallization front. That is the Brikmann velocity field given by the equation

$$(39) \quad \begin{cases} \nabla p + \frac{\mu}{\sigma} \bar{v} - \mu \nabla^2 \bar{v} = \bar{F} \\ \nabla \bar{v} = 0 \end{cases}$$

where σ denotes the permeability of the thin region which in the dilute limit equals to the ratio between the fluid velocity and the force per unit volume exerted on the fluid by the solid ω ; μ is the dynamic viscosity; $\bar{F} = -6\pi\mu a \bar{V}$; a is the radius of the solid part and \bar{V} is the average of the convective velocity field in the neighbourhood of the crystallization front.

2) The velocity field \bar{v} of a very viscous flow past a sphere.

The arguments for a velocity field \bar{v} of an uniform very viscous flow past a sphere are: the high viscosity of the melt in the neighbourhood of the crystallization front, the constant growth rate and the fact that we can approach the solid part of the cell Ω by a sphere. The slow flow equation is

$$(40) \quad \begin{cases} 0 = -\nabla p + \mu \nabla^2 \bar{v} \\ \nabla \bar{v} = 0 \end{cases}$$

For an axisymmetric flow ($\bar{e}_z = \bar{V}/|\bar{V}|$), using appropriate spherical polar coordinates ($x = r \sin \theta \cos \varphi$, $y = r \sin \theta \sin \varphi$, $z = r \cos \theta$) we have in the plane $\varphi = \pi/2$:

$$(41) \quad \bar{v} = (v_r(r, \theta), v_\theta(r, \theta), 0)$$

We may automatically satisfy the condition $\nabla \bar{v} = 0$ by introducing Stokes stream function $\psi(r, \theta)$ such that

$$(42) \quad v_r = \frac{1}{r^2 \sin \theta} \frac{\partial \psi}{\partial \theta} \quad v_\theta = -\frac{1}{r \sin \theta} \frac{\partial \psi}{\partial r}$$

In these conditions we have:

$$(43) \quad \psi = \frac{1}{4} |\bar{V}| \left(2r^2 + \frac{a^3}{r} - 3ar \right) \sin^2 \theta$$

where for $|\bar{V}|$ we take the average of the velocity field in the lower cell.

5 The effective convective-diffusive equation for small concentration in the case when we modelling the thin region in the neighbourhood of the growth interface by a fixed bed of randomly distributed spheres.

We started again from the convective-diffusive equation for small concentrations

$$(44) \quad \frac{\partial c}{\partial \tau} + \bar{v} \nabla c = D \nabla^2 c$$

In this equation c is the concentration of dopant, τ is the time, \bar{v} is the random incompressible velocity field generated at the microscale by the randomly-distributed spheres which is statistically homogenous and infinitely extended, D is the diffusion coefficient.

Following R. Mauri's considerations from [20] for a fixed bed of randomly distributed spheres we consider the two length scales l and L , indicating a typical correlation length of the random velocity field \bar{v} generated at the microscale by the randomly-distributed spheroids and a characteristic linear dimension of the macroscale (size of the bed). We assume that $\varepsilon = l/L \ll 1$ and we introduce the time scales

$$(45) \quad \tau_1 = \frac{l}{V_0}, \quad \tau_2 = \frac{l^2}{D}, \quad \tau_3 = \frac{L}{V_0}, \quad \tau_4 = \frac{L^2}{D}$$

where V_0 is the characteristic value of the velocity field.

We consider the local and global Peclet numbers:

$$(46) \quad Pe_l = \frac{\tau_2}{\tau_1} = \frac{lV_0}{D}, \quad Pe_g = \frac{\tau_4}{\tau_3} = \frac{LV_0}{D} = \frac{1}{\varepsilon} Pe_l$$

and assume that convection and diffusion balance each other at the microscale, that means $Pe_l = O(1)$. In this case, $Pe_g = O(\varepsilon^{-1})$, what means that convection dominates diffusion at the macroscale.

We note by \bar{R} the macroscopic position vector and we scale the space variables according to

$$(47) \quad \bar{x} = \frac{\bar{R}}{L}$$

The corresponding microscopic variables \bar{y} is given by

$$(48) \quad \bar{y} = \frac{\bar{R}}{l} = \frac{\bar{x}}{\varepsilon}$$

Introducing the following three time scales:

$$(49) \quad t = \frac{\tau}{\tau_2}, \quad T_1 = \frac{\tau}{\tau_3}, \quad T_2 = \frac{\tau}{\tau_4}$$

we assume that the effective concentration c depends on $\varepsilon, \bar{x}, \bar{y}, t, T_1, T_2$ and can be expanded as follows:

$$(50) \quad c(\varepsilon, x, y, t, T_1, T_2) = \sum_{n=0}^{\infty} \varepsilon^n c_n(\bar{x}, \bar{y}, t, T_1, T_2)$$

We note that the stationary random velocity field \bar{v} depends only on y ; each term c_n in the expansion 50 is locally ergodic (expressible as a product of an ergodic y, t dependent function by an x, T_1, T_2 dependent part); the ensemble average of c_n denoted by $\langle c_n \rangle$ satisfies

$$(51) \quad \langle c_n \rangle = \bar{c} \delta_{n0}$$

and each c_n is locally random.

For the time derivatives we have:

$$(52) \quad \frac{\partial}{\partial \tau} = \frac{D}{L^2} \left(\frac{\partial}{\partial T_2} + P e_l \varepsilon^{-1} \frac{\partial}{\partial T_1} + \varepsilon^{-2} \frac{\partial}{\partial t} \right)$$

and for the space derivatives:

$$(53) \quad \nabla_{\bar{R}} = \frac{1}{L} \left(\nabla_{\bar{x}} + \frac{1}{\varepsilon} \nabla_{\bar{y}} \right), \quad \nabla_{\bar{R}}^2 = \frac{1}{L^2} \left(\nabla_{\bar{x}}^2 + \frac{2}{\varepsilon} \nabla_{\bar{x}} \nabla_{\bar{y}} + \frac{1}{\varepsilon^2} \nabla_{\bar{y}}^2 \right)$$

Considering \bar{u} defined by

$$(54) \quad \bar{u} = P e_l \frac{\bar{v}}{V_0}$$

substituting 50 in 44, using 52, 53 and collecting equal powers of ε one gets:

$$(55) \quad \Delta_{\bar{y}} c_0 - \bar{u} \nabla_{\bar{y}} c_0 - \frac{\partial c_0}{\partial t} = 0 \quad \text{for } O(\varepsilon^{-2}).$$

$$(56) \quad \Delta_{\bar{y}} c_1 - \bar{u} \nabla_{\bar{y}} c_1 - \frac{\partial c_1}{\partial t} = \bar{u} \nabla_{\bar{x}} c_0 - 2 \nabla_{\bar{x}} \nabla_{\bar{y}} c_0 + P e_l \frac{\partial c_0}{\partial T_1} \quad \text{for } O(\varepsilon^{-1})$$

$$(57) \quad \Delta_{\bar{y}} c_2 - \bar{u} \nabla_{\bar{y}} c_2 - \frac{\partial c_2}{\partial t} = \bar{u} \nabla_{\bar{x}} c_1 - 2 \nabla_{\bar{x}} \nabla_{\bar{y}} c_1 + P e_l \frac{\partial c_1}{\partial T_1} - \nabla_{\bar{x}}^2 c_0 + \frac{\partial c_0}{\partial T_2} \quad \text{for } O(1)$$

A function $c_0 = c_0(\bar{x}, T_1, T_2)$ satisfies 55. For such a function 56 becomes

$$(58) \quad \Delta_{\bar{y}} c_1 - \bar{u} \nabla_{\bar{y}} c_1 - \frac{\partial c_1}{\partial t} = \bar{u} \nabla_{\bar{x}} c_0 + P e_l \frac{\partial c_0}{\partial T_1}$$

Now we impose that equation 58 is solvable; that means that ensemble averages of its left hand side and right hand side are identically equal to each other. Using that c_1 is locally random we find:

$$(59) \quad P e_l \frac{\partial c_0}{\partial T_1} = - \langle \bar{u} \rangle \nabla_{\bar{x}} c_0$$

where $\langle \bar{u} \rangle$ is the ensemble average of \bar{u} and is the effective dopant velocity.

If we look for solution of equation 56 of the form

$$(60) \quad c_1(\bar{x}, \bar{y}, t, T_1, T_2) = \bar{\chi}(\bar{y}, t) \nabla_{\bar{x}} c_0(\bar{x}, T_1, T_2)$$

we find

$$(61) \quad \frac{\partial \bar{\chi}}{\partial t} + (\bar{u} \nabla_{\bar{y}}) \bar{\chi} - \Delta_{\bar{y}} \bar{\chi} = \langle \bar{u} \rangle - \bar{u}$$

Condition 51 for $n=1$ implies that $\bar{\chi}$ satisfies also

$$(62) \quad \langle \bar{\chi} \rangle = 0$$

If we consider $\bar{\chi}$ satisfying 61, 62 and $c_1 = \bar{\chi} \nabla_{\bar{x}} c_0$ equation 57 becomes

$$(63) \quad \Delta_{\bar{y}} c_2 - \bar{u} \nabla_{\bar{y}} c_2 - \frac{\partial c_2}{\partial t} = \bar{u} \nabla_{\bar{x}} (\bar{\chi} \nabla_{\bar{x}} c_0) - 2 \nabla_{\bar{x}} \nabla_{\bar{y}} (\bar{\chi} \nabla_{\bar{x}} c_0) + Pe_l \frac{\partial c_1}{\partial T_1} - \Delta_{\bar{x}} c_0 + \frac{\partial c_0}{\partial T_2}$$

We apply the solvability condition to this equation and considering that c_2 is locally random we obtain

$$(64) \quad \frac{\partial c_0}{\partial T_2} = \sum_{i=1}^3 \sum_{j=1}^3 \left(\delta_{ij} - \langle \chi_j u_i \rangle + 2 \langle \frac{\partial \chi_j}{\partial y_i} \rangle \right) \frac{\partial^2 c_0}{\partial x_i \partial x_j}$$

or

$$(65) \quad \frac{\partial c_0}{\partial T_2} = [I - \langle \bar{\chi} \bar{u} \rangle + 2 \langle \nabla \bar{\chi} \rangle] \nabla_{\bar{x}} \nabla_{\bar{x}} c_0$$

Substituting $c_0 = c_0(\bar{x}, T_1, T_2)$ in 52 we find that c_0 satisfies the equation

$$(66) \quad \frac{\partial c_0}{\partial \tau} + \langle \bar{v} \rangle \cdot \nabla_{\bar{R}} c_0 = D [I - \langle \bar{\chi} \bar{u} \rangle + 2 \langle \nabla \bar{\chi} \rangle] \nabla_{\bar{R}} \nabla_{\bar{R}} c_0$$

This is the macroscopic convective-diffusive equation of the dopant in the neighbourhood of the crystallization front if we assume that this is a fixed bed of randomly distributed spheres.

The quantity defined by

$$(67) \quad D^* = D [I - \langle \bar{\chi} \bar{u} \rangle + 2 \langle \nabla \bar{\chi} \rangle]$$

is the diffusivity tensor in this region.

The symmetric part of this tensor is

$$(68) \quad \tilde{D}_{ij} = D \left[\delta_{ij} - \frac{1}{2} (\langle \chi_i u_j + \chi_j u_i \rangle) + \left(\langle \frac{\partial \chi_i}{\partial y_j} + \frac{\partial \chi_j}{\partial y_i} \rangle \right) \right]$$

The dispersion tensor depends on the flow. To calculate it one must solve the problem 61, 62. This linear problem can, in principle, be solved. In the papers [20],[22] this linear problem is solved for a Birkmann velocity field given by the equations

$$(69) \quad \begin{cases} \nabla p + \frac{\mu}{\sigma} \bar{v} - \mu \nabla^2 \bar{v} = \bar{F} \delta(r) + O(\phi) \\ \nabla \cdot \bar{v} = 0 \end{cases}$$

where σ denotes the permeability of the bed which, in the dilute limit, equals to the ratio between the fluid velocity and the force per unit volume exercited on the fluid by the bed particles; $\bar{F} = -6\pi\mu a \bar{V}$; a is the radius of the solid part and \bar{V} is the average of the convective velocity field in the neighbourhood of the crystallization front.

6 A conclusion

A solution c_0 of the effective convective-diffusive equation depends on the initial value, on the boundary condition and, via the velocity field \bar{v} , on the thermal conditions (T_h, T_c) . Changing the thermal conditions at a moment τ_1 we will have other solution $c_0^{(1)}$ for which c_0 is an initial value and for which the boundary conditions are given by the values of c_0 on the boundary. In this way, changing the thermal conditions we hope to realize the desired uniform distribution of dopant.

References

- [1] Wang, C.; Ph.D. Thesis (Dept. of Materials Science and Engineering, M.I.T., Cambridge, Mass., 1984)
- [2] Chang, J.C. and Brown, R.A.: Journal of Crystal Growth vol.63 (1984) 343.
- [3] Adornato, P.M. and Brown, R.A.: Journal of Crystal Growth vol.80 (1987) 155.
- [4] Griffin, P.R.: S.M. Thesis (Dept. of Mechanical Engineering, M.I.T., Cambridge, Mass., 1989).
- [5] Griffin, P.R. and Motakef, S.: Appl. microgravity tech. II. (1989), Part I, 121-127.
- [6] Griffin, P.R. and Motakef, S.: Appl. microgravity tech. II. (1989), Part II, 128-133.
- [7] Burton, J.A. et al: Journal of Chem. Phys. vol.21 (1953) pg.1987
- [8] Tiller, W.A. et al: Acta Met. vol.1 (1953) pg.428
- [9] Hamacher, H. et al: Proceedings of the Norderney Symposium on Scientific Results of the German Spacelab Mission D1, Norderney, Germany, 1986, pg.48)
- [10] Landau, L. and Lifchitz, E.; Mecanique des fluides, ed. Mir, 1971, pg.284
- [11] Bensoussan A., Lions J.L., Papanicolau G.; Asymptotic Analysis for Periodic Structures, North-Holland, Amsterdam (1978)
- [12] E. Sanchez-Palencia, Non-homogenous Media and Vibration Theory, Springer-Verlag, Berlin (1980)
- [13] J.L. Ericksen, D. Kinderlehrer, R. Kohn and J.L. Lions, Homogenization and Effective Moduli of Materials and Media, Springer-Verlag, Berlin (1986)
- [14] E. Sanchez-Palencia and A. Zaoui, Homogenization Techniques for Composite Media, Springer-Verlag, Berlin (1987)
- [15] T. Levy and E. Sanchez-Palencia, Suspensions of solid particles in a Newtonian fluid, J. Non-Nerv. Fl. Mech. 13 (1983) 13

- [16] C.L. Winter, C.M. Neuman and S.P. Neuman, A perturbation expression for diffusion in a random velocity field. SIAM J. Appl. Math. 44 (1984) 411
- [17] T. Levy and R.K.T. Hsieh, Homogenization mechanics of a non dilute suspension of magnetic particles, Int. J. Engng. Sci. 26 (1988) 1087
- [18] J. Rubinstein and R. Mauri, Dispersion and convection in periodic porous media, SIAM J. Appl. Math. 46 (1986) 1018
- [19] R. Mauri, Dispersion, convection and reaction in porous media, Phys. Fluids A 3 (1991) 743
- [20] R. Mauri, Heat and mass transport in random velocity fields with application to dispersion in porous media, Journal of Engineering Mathematics 29 (1995) 77-89
- [21] Brenner, ; Phil. Trans. R. Soc. Lond. A297 (1980) 81.
- [22] D.L. Koch and J.F. Brady, J. Fluid Mech. vol154 (1985) 399-427

On a Heat Transfer in Porous Media

Horia I. Ene

April 7, 1997

Institute of Mathematics, Romanian Academy, P. O. Box 1-764, 70700 Bucharest, Romania

Abstract

Macroscopic heat transfer in porous media, in the presence of thermal interfacial barriers between the fluid and the solid phases, is determined by using the homogenization method. The models are shown to belong to two main types: one-temperature and two-temperature field models.

1 Introduction

Usually the heat transfer in porous media is described by a single model. This is the case if we use the continuity of temperature and of the normal fluxes as boundary conditions between the fluid and the solid, cf. [1], [2].

There exists also a two-temperature field model introduced in order to describe the case when the thermal conductivities of both phases are very different. [3], [4].

The aim of this paper is to determine the influence of the thermal interfacial barrier on the structure of the macroscopic heat transfer equations. In order to do so we use the homogenization method, [5], [6].

In section 2 we present a model problem. Such a problem represents the steady heat conduction in a binary composite. Concluding we present, in section 3, the case of heat convection in porous media.

2 The model problem

We consider a medium formed by two components, periodically distributed in space and such that the domain Ω is formed by $\Omega = \Omega_{\varepsilon 1} \cup \Omega_{\varepsilon 2}$ with:

$$\Omega_{\varepsilon \alpha} = \{x \in \Omega; x \in \varepsilon Y_\alpha\} \quad \alpha = 1, 2$$

Y being the cell of periodicity.

For fixed $\Gamma > 0$ we are looking for the function $T_\varepsilon = (T_{\varepsilon 1}, T_{\varepsilon 2})$ defined in $\Omega_{\varepsilon 1} \times \Omega_{\varepsilon 2}$, solving:

$$\begin{cases} -\frac{\partial}{\partial x_i} (k_{ij}^{\varepsilon \alpha} \frac{\partial T_{\varepsilon \alpha}}{\partial x_j}) = f & \text{in } \Omega_{\varepsilon \alpha} \\ k_{ij}^{\varepsilon \alpha} \frac{\partial T_{\varepsilon \alpha}}{\partial x_j} n_i = \varepsilon^p h^\varepsilon (T_{\varepsilon \beta} - T_{\varepsilon \alpha}) & \text{on } \Gamma_\varepsilon, \quad \alpha \neq \beta \\ T_\varepsilon = 0 & \text{on } \partial\Omega \quad \alpha = 1, 2 \end{cases} \quad (1)$$

Here Γ_ε denotes the common boundary between the two components, n_i is the outward normal to $\Omega_{\varepsilon \alpha}$, and $h^\varepsilon > 0$ is the thermal interfacial barrier. This is a so-called Newton's boundary condition [7]. The coefficients $k_{ij}^{\varepsilon \alpha} = k_{ij}^\alpha(\frac{x}{\varepsilon})$ and $h^\varepsilon = h(\frac{x}{\varepsilon})$ are Y -periodic in the variable $y = \frac{x}{\varepsilon}$.

As usual in the homogenization method we are searching for an asymptotic expansion for $T_{\varepsilon \alpha}$ of the form:

$$T_{\varepsilon \alpha}(x, y) = T_\alpha^0(x, y) + \varepsilon T_\alpha^1(x, y) + \dots \quad y = \frac{x}{\varepsilon} \quad \alpha = 1, 2 \quad (2)$$

where $T_\alpha^k(x, y)$ are Y -periodic functions in y .

The method consists of incorporating expansion (2) into (1), identifying the similar power in ε and solving a set of boundary value problems in the characteristic cell Y .

The homogenization process, $\varepsilon \rightarrow 0$, produces a set of equations satisfied by T^0 which in fact represent the macroscopic behaviour of the heat transfer.

First of all, we have at order ε^2 :

$$\begin{cases} -\frac{\partial}{\partial y_i} (k_{ij}^\alpha(y) \frac{\partial T_\alpha^0}{\partial y_j}) = 0 & \text{on } Y_\alpha \\ k_{ij}^\alpha(y) \frac{\partial T_\alpha^0}{\partial y_j} n_i = 0 & \text{on } \Gamma \\ T_\alpha^0 & Y\text{-periodic } (\alpha = 1, 2) \end{cases} \quad (3)$$

By (3) T_α^0 is a function depending only on x , namely $T_\alpha^0 = T_\alpha^0(x)$, $\alpha = 1, 2$. We obtain at order ε^{-1} :

$$\begin{cases} -\frac{\partial}{\partial y_i} (k_{ij}^\alpha(y) (\frac{\partial T_\alpha^0}{\partial x_j} + \frac{\partial T_\alpha^1}{\partial y_j})) = 0 & \text{on } Y_\alpha \\ k_{ij}^\alpha(y) (\frac{\partial T_\alpha^0}{\partial y_j} + \frac{\partial T_\alpha^1}{\partial y_j}) n_i = \begin{cases} h(y)(T_\beta^0 - T_\alpha^0) & \text{for } p = 0 \\ 0 & \text{for } p \geq 1 \end{cases} \\ T_\alpha^1 & Y\text{-periodic } \beta \neq \alpha \quad \alpha = 1, 2 \end{cases} \quad (4)$$

The problem (4) has a Y -periodic solution, for $p = 0$, if and only if [5]:

$$(T_1^0 - T_2^0) \int_{\Gamma} h(y) ds = 0 \quad (5)$$

But $h(y) > 0$ and hence $\int_{\Gamma} h(y) ds \neq 0$, it results that T_α^0 is Y -periodic if $T_1^0(x) = T_2^0(x)$.

For $p \geq 1$, the problem (4) has a Y -periodic solution, and consequently $T_1^0(x) \neq T_2^0(x)$. For this reason $p = 1$ is the critical value for the order of magnitude of the thermal interface barrier.

In the case $p = 0$ we have at order ε^0 :

$$\begin{cases} -\frac{\partial}{\partial y_i} (k_{ij}^\alpha(y) (\frac{\partial T_\alpha^1}{\partial x_j} + \frac{\partial T_\alpha^2}{\partial y_j})) - \frac{\partial}{\partial x_i} (k_{ij}^\alpha(y) (\frac{\partial T_\alpha^0}{\partial x_j} + \frac{\partial T_\alpha^1}{\partial y_j})) = f & \text{in } Y_\alpha \\ k_{ij}^\alpha(y) (\frac{\partial T_\alpha^1}{\partial x_j} + \frac{\partial T_\alpha^2}{\partial y_j}) n_i = h(T_\beta^1 - T_\alpha^1) & \text{on } \Gamma, \quad \beta \neq \alpha \\ T_\alpha^2 & Y\text{-periodic } (\alpha = 1, 2) \end{cases} \quad (6)$$

On the other hand, for $p = 0$, the solution of (4) has the following form:

$$T_\alpha^1(x, y) = w_\alpha^k \frac{\partial T_\alpha^0}{\partial x_k} \quad (\alpha = 1, 2) \quad (7)$$

where w_α^k is the solution of:

$$\begin{cases} -\frac{\partial}{\partial y_i} \left(k_{ij}^\alpha(y) \left(\delta_{kj} + \frac{\partial w_\alpha^k}{\partial y_j} \right) \right) = 0 & \text{in } Y_\alpha \\ k_{ij}^\alpha(y) \left(\delta_{kj} + \frac{\partial w_\alpha^k}{\partial y_j} \right) n_i = 0 & \text{on } \Gamma \\ w_\alpha^k & Y\text{-periodic, } (\alpha = 1, 2) \end{cases} \quad (8)$$

Using (7) in (6) yields the macroscopic equation under the classical form:

$$\begin{cases} -\frac{\partial}{\partial x_i} \left(k_{ij}^h \frac{\partial T^0}{\partial x_j} \right) = f & \text{in } \Omega \\ T^0 = 0 & \text{on } \partial\Omega \end{cases} \quad (9)$$

and the homogenized coefficients:

$$k_{ij}^h = \frac{1}{|Y|} \sum_{\alpha=1,2} \int_{Y_\alpha} k_{ij}^\alpha \left(\delta_{jl} + \frac{\partial w_\alpha^l}{\partial y_j} \right) dy \quad (10)$$

Remark 2.1 In the case $p = 0$ we obtain a one temperature model, equation (9).

In the case $p = 1$ at order ε^0 we have:

$$\begin{cases} -\frac{\partial}{\partial y_i} \left(k_{ij}^\alpha \left(\frac{\partial T_\alpha^1}{\partial x_j} + \frac{\partial T_\alpha^2}{\partial y_j} \right) \right) - \frac{\partial}{\partial x_i} \left(k_{ij}^\alpha \left(\frac{\partial T_\alpha^0}{\partial x_j} + \frac{\partial T_\alpha^1}{\partial y_j} \right) \right) = f & \text{in } Y_\alpha \\ k_{ij}^\alpha \left(\frac{\partial T_\alpha^1}{\partial x_j} + \frac{\partial T_\alpha^2}{\partial y_j} \right) n_i = h(T_\beta^0 - T_\alpha^0) & \text{on } \Gamma, \quad \beta \neq \alpha \\ T_\alpha^2 & Y\text{-periodic, } \alpha = 1, 2 \end{cases} \quad (11)$$

In this case introducing w_α^k the solution of (8), the solution of (4) is also of the form $T_\alpha^1(x, y) = w_\alpha^k \frac{\partial T_\alpha^0}{\partial x_k}$, ($\alpha = 1, 2$). With the value of T_α^1 obtained, the mean value of (11) yields two coupled macroscopic equations for the two temperature fields $T_1^0(x)$ and $T_2^0(x)$:

$$\begin{cases} -\frac{\partial}{\partial x_i}(k_{ij}^1 \frac{\partial T_1^0}{\partial x_j}) + H(T_1^0 - T_2^0) = \theta f \\ -\frac{\partial}{\partial x_i}(k_{ij}^2 \frac{\partial T_2^0}{\partial x_j}) - H(T_1^0 - T_2^0) = (1 - \theta)f \end{cases} \quad (12)$$

where $\theta = \frac{|Y_1|}{|Y|}$. The macroscopic coefficients are:

$$k_{ij}^\alpha = \frac{1}{|Y|} \int_{Y_\alpha} k_{ij}^\alpha \frac{\partial}{\partial y_j} (y_i + w_\alpha^i) dy \quad \alpha = 1, 2 \quad (13)$$

and

$$H = \frac{1}{|Y|} \int_{\Gamma} h(y) ds \quad (14)$$

Remark 2.2 In case $p = 1$ we obtain a two-temperature model. Note also, that, in this case, the two equations are coupled.

Following the same procedure, for $p \geq 2$, it is clear that we have at the macroscale:

$$\begin{cases} -\frac{\partial}{\partial x_i}(k_{ij}^1 \frac{\partial T_1^0}{\partial x_j}) = \theta f \\ -\frac{\partial}{\partial x_i}(k_{ij}^2 \frac{\partial T_2^0}{\partial x_j}) = (1 - \theta)f \end{cases} \quad (15)$$

with the homogenized coefficients given by (13).

Remark 2.3 The case $p \geq 2$ gives us a two-scale temperature model, but without any coupling term. That means that the thermal fluxes are independent in the two constituents.

Part of the results of this section can be found in [8], [9].

3 Heat convection in porous media

The problem of heat convection in porous media was extensively discussed in the case of a one temperature model, using or not using the homogenization method [1], [2], [3], [4]. For heat convection in porous media it is necessary

to scale the thermal conductivity with the same factor as the velocity [1], in order to preserve the convection term in the macroscopic equation

We suppose that all such rescalings were made. Consequently we start with our problem:

$$\begin{cases} (\rho c)_\alpha \frac{\partial T_{\varepsilon\alpha}}{\partial t} + (\rho c)_f v_k \frac{\partial T_{\varepsilon f}}{\partial x_k} = \frac{\partial}{\partial x_k} (k_\alpha^\varepsilon \frac{\partial T_{\varepsilon\alpha}}{\partial x_k}) & \text{in } \Omega_{\varepsilon\alpha} \\ k_\alpha^\varepsilon \frac{\partial T_{\varepsilon\alpha}}{\partial x_k} n_k = \varepsilon^p h^\varepsilon (T_{\varepsilon\beta} - T_{\varepsilon\alpha}) & \text{on } \Gamma_\varepsilon, \quad \alpha \neq \beta \\ T_\varepsilon = 0 & \text{on } \partial\Omega, \quad \alpha = f, s \end{cases} \quad (16)$$

where the subscript f and s denote the fluid and the solid phases, respectively.

In problem (16) v denotes the velocity vector, given for example from the Darcy's law. In fact, we are interested only in the heat transfer problem. Of course, the convective term $v \nabla T$ is zero in the solid phase, the vector field v being zero in the solid.

The results from the model problem can be applied to the present case without any difficulty. We are searching for the same asymptotic expansion (2).

At order ε^{-2} we obtain again the problem (3). This means that we have $T_\alpha^0 = T_\alpha^0(x)$, $\alpha = f, s$.

At order ε^{-1} we have the problem (4), because the ε^{-1} -term from the convective one is zero. In fact it is clear that $(\rho c)_f v_k \frac{\partial T_\alpha^0}{\partial y_k}$ is zero, from the previous conclusion.

It results that $p = 1$ is the critical value for the thermal interfacial barrier.

Consequently, for $p = 0$, we have the classical one-temperature model:

$$\begin{cases} (\hat{\rho}c) \frac{\partial T^0}{\partial t} + \theta(\rho c)_f v_k \frac{\partial T^0}{\partial x_k} = \frac{\partial}{\partial x_i} (k_{ij}^h \frac{\partial T^0}{\partial x_j}) & \text{in } \Omega \\ T^0 = 0 & \text{on } \partial\Omega \end{cases} \quad (17)$$

where the mean value is defined by

$$\tilde{\phi} = \frac{1}{|Y|} \int_Y \phi(y) dy$$

$\theta = \frac{|Y_f|}{|Y|}$ is the porosity, and the homogenized coefficients are given by (10) with k_f and k_s in the fluid and solid parts.

In the case $p = 1$ we obtained a coupled system of two temperature equations, as those proposed in [3] [4]:

$$\begin{cases} \theta(\rho c)_f \left(\frac{\partial T_f^0}{\partial t} + v_k \frac{\partial T_f^0}{\partial x_k} \right) = \frac{\partial}{\partial x_i} (k_{ij}^h \frac{\partial T_f^0}{\partial x_j}) - H(T_f^0 - T_s^0) \\ (1 - \theta)(\rho c)_s \frac{\partial T_s^0}{\partial t} = \frac{\partial}{\partial x_i} (k_{ij}^s \frac{\partial T_s^0}{\partial x_j}) + H(T_f^0 - T_s^0) \end{cases} \quad (18)$$

with H given by (14) and the conductivity coefficients (13).

For $p \geq 2$ we also have a two-temperature model, but without any interaction, as in the Section 2.

4 Conclusions

The correct model describing the heat transport in porous media is depending on the order of magnitude of the thermal interfacial barrier, or on conductance. It is clear that the macroscopic description of heat transfer in porous media strongly depends on the relative value of the barrier resistance.

The problem of a correction between the difference in the thermal conductivities of the fluid and the solid, and the thermal interfacial barrier, stands still.

References

- [1]. H. I. Ene and E. Sanchez-Palencia, "On thermal equation for flow in porous media", Int. J. Eng. Sci., 20, 5, 623-630, (1982)
- [2]. H. I. Ene and D. Polisevski, "Thermal Flow in Porous Media", D. Reidel Publ. Co., Dordrecht, Boston, Lancaster and Tokyo, (1987)
- [3]. W. Derski, "Equations of thermoconsolidation in case of temperature difference between components of medium", Bull. Acad. Pol. Sci., Ser. Tech., 26, 1035-1046, (1978)
- [4]. C. Pecker and H. Deresiewicz, "Thermal effects on wave propagation in liquid-filled porous media", Acta Mech., 16, 45-64, (1973)
- [5]. A. Bensoussan, J-L. Lions and G. Papanicolaou, "Asymptotic Analysis for Periodic Structure", North-Holland, (1978)

-
- [6]. E. Sanchez-Palencia, "*Non-homogeneous Media and Vibration Theory*", Lecture Notes in Physics, vol. 127, Springer-Verlag, Berlin, (1980)
- [7]. H. S. Carslaw and J. C. Jaeger, "*Conduction of Heat in Solids*", Oxford University Press, (1959)
- [8]. J. N. Pernin, "Homogénéisation en milieux composites", Thèse d'État, Université de Franche-Comté, (1995)
- [9]. J-L. Auriault and H. I. Ene, "Macroscopic modelling of heat transfer in composites with interfacial thermal barrier", *Int. J. Heat Mass Transfer*, 37, 18, 2885-2892, (1994)

REGARDING ON THE INTEGRATION OF THE NON-LINEAR DIFFERENTIAL EQUATIONS FOR THE ROCKET INCIDENCE VARIATION DURING THE FLIGHT

General of brigade Prof. Florentin MORARU PhD
Lieutenant Colonel Assoc.Prof.Doru SAFTA PhD
Technical Military Academy, Bucharest, ROMANIA

ABSTRACT

Our researches were developed starting from the rocket longitudinal plane motion equations system, taking into account the non-linear terms of the aerodynamical coefficients C_x, C_z, C_m .

It was obtained a differential, non-linear, non-homogenous equation, with variable coefficients, which allow to obtain the variation in time of the incidence angle.

Using two numerical integration methods, the theoretical data (in many case studies) obtained by the proposed method are enough appropriate to the results of the general motion rocket study.

It was elaborated a complex program to simulate the rocket flight in the resistant environment, which operates with a large aerodynamical, rocket, engine and launcher construction data basis.

1. DIFFERENTIAL EQUATIONS SYSTEM OF ROCKET MOVEMENT

The theoretical researches, tackled in our paper, for the flight stability evaluation and more generally to study the rocket behaviour on the trajectory are developed on the basis of the mathematical model of the rocket longitudinal movement in a resistant environment [2], [6]. It is considered the case of the rocket flight with aerodynamical stability. The rocket, like study object, is assumed with an axially symmetry configuration.

The studies were elaborated for the rocket with and without spinning movement, which has a crossed wings aerodynamical configuration.

Using intrinsic coordinates, the longitudinal movement equations of the rocket under the action of the thrust, weight, drag, lift, taking into account the principal aerodynamic moment, the damping moment of the pitching oscillations, the gas damping moment and the moment provided by the thrust gasdynamical asymmetry [6] (fig.1) may be written as:

$$\begin{aligned} m \frac{dv}{dt} &= \mathcal{F} \cos(\alpha - \alpha_T) - R - m g \sin \theta \\ m \frac{v^2}{r} &= m g \cos \theta - \mathcal{F} \sin(\alpha - \alpha_T) - P - P_\omega \\ J \frac{d\omega}{dt} &= -\mathcal{M} - \mathcal{M}_\omega - \mathcal{M}_{\text{am}}^g + \mathcal{M}_2 \end{aligned}$$

$$\frac{dy}{dt} = v \sin \theta$$

$$\varphi = \alpha + \theta.$$

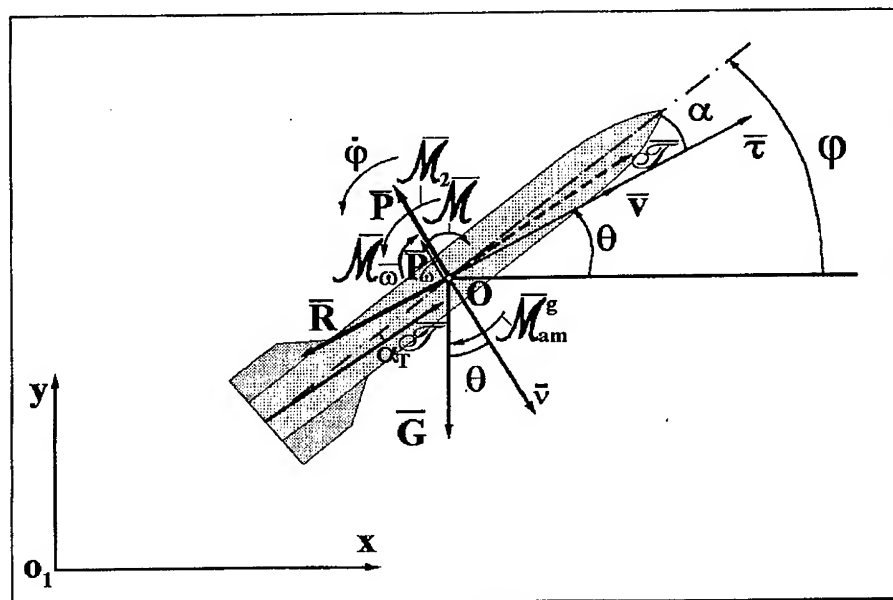
$$\varphi = \alpha + \theta.$$


Fig.1

The aerodynamical coefficients C_x , C_z , C_m are generally functions of Mach number, M and flight incidence, α .

In the case of the stable rockets, with correct flight, the incidence being sufficiently small, it is assumed that the C_z , C_m coefficients functions may be expressed as linear functions depending on incidence; the C_x coefficient is considered that practically is invariable with the incidence. Thus, usually, in the case of the rocket with blocked commands, it is accepted the approximations:

$$C_x \cong C_{x0}, \quad C_z \cong C_z^\alpha \alpha, \quad C_m \cong C_m^\alpha \alpha. \quad (3)$$

It is known that during the fly the incidence may increase at great values, in the proximity of boundary value of linearity, α_ℓ , or over this value. *In order to study the rocket behaviour at great incidence values or even in the proximity of critic flight works, it is necessary to take into account the non-linearity of the aerodynamic coefficients depending on the incidence.*

Our proposed mathematical model, developed to study the complex rocket behaviour on the trajectory at great incidences, consider for the aerodynamical coefficients the following expressions:

$$\begin{aligned} C_x &= C_{x0} + N\alpha^2, \quad N \equiv C_z^\alpha, \\ C_z &= C_z^\alpha \alpha + C_z^\omega \omega + C_z^{\dot{\alpha}} \dot{\alpha} + C_z^{\alpha^2} \alpha^2 + C_z^{\omega^2} \omega^2 + C_z^{\alpha\omega} \alpha\omega, \\ C_m &= C_m^\alpha \alpha + C_m^\omega \omega + C_m^{\dot{\alpha}} \dot{\alpha} + C_m^{\alpha^2} \alpha^2 + C_m^{\omega^2} \omega^2 + C_m^{\alpha\omega} \alpha\omega. \end{aligned} \quad (4)$$

These aerodynamical coefficients are determined by the specific known methods in aerodynamics [2], [3].

It is necessary to point out that in the lift coefficient expression the proportional term with the incidence is more important comparative the others. A smaller importance have the terms with $\dot{\alpha}$ and $\alpha\omega$ in the C_m coefficient expression. Thus, neglecting some terms that usually bring a smaller contribution in this complex study the movement equations system takes the following form:

$$\begin{aligned} \frac{dv}{dt} &= a_R \cos \alpha - \frac{\rho v^2 S}{2m} C_{x0} - \frac{\rho v^2 S}{2m} C_z^\alpha \alpha^2 - g \sin \theta \\ v \frac{d\theta}{dt} &= -g \cos \theta + a_R \sin \alpha + \frac{\rho v^2 S}{2m} C_z^\alpha \alpha + \frac{\rho v^2 S}{2m} C_z^\omega \omega^2 \\ J \frac{d\omega}{dt} &= \frac{\rho v^2 S \ell}{2} \left(C_m^\alpha \alpha + C_m^{\alpha^2} \alpha^2 \right) + \frac{\rho v^2 S \ell}{2} \left(C_m^\omega \omega + C_m^{\omega^2} \omega^2 \right) - c_j Q_e \omega \\ \frac{d\varphi}{dt} &= \omega \\ \frac{dy}{dt} &= v \sin \theta \\ \frac{dx}{dt} &= v \cos \theta. \end{aligned} \quad (5)$$

Using the following notations:

$$\begin{aligned} a_R &= \frac{\mathcal{F}}{m}, \quad K_x = \frac{\rho S C_{x0}}{2m}, \quad K_z = \frac{\rho S}{2m} C_z^\alpha, \quad K_m = \frac{\rho S \ell}{2J} C_m^\alpha, \quad K'_m = \frac{\rho S \ell}{2J} C_m^{\alpha^2}, \\ K_\omega &= \frac{\rho S \ell_c}{2J} C_m^\alpha, \quad K'_\omega = \frac{\rho S \ell_c^2}{2J} C_m^{\alpha^2}, \quad K_j = \frac{1}{J} c_j Q_e, \end{aligned} \quad (6)$$

the equations system becomes:

$$\begin{aligned}
\frac{dv}{dt} &= a_R - K_x v^2 - K_z v^2 \alpha^2 - g \sin \theta \\
\frac{d\theta}{dt} &= -\frac{g}{v} \cos \theta + \left(\frac{a_R}{v} + K_z v \right) \alpha + K_z \ell_c \omega \\
\frac{d\omega}{dt} &= K_m v^2 \alpha + K'_m v^2 \alpha^2 + K_\omega \ell v \omega + K'_\omega \ell \omega^2 - K_j \omega \\
\frac{d\phi}{dt} &= \omega \\
\frac{dy}{dt} &= v \sin \theta \\
\frac{dx}{dt} &= v \cos \theta.
\end{aligned} \tag{7}$$

This system (7) can be numeric integrated with given boundary conditions to calculate the incidence and the others flight parameters variations in time along the trajectory

2. DIFFERENTIAL NON-LINEAR EQUATION OF INCIDENCE

In order to evaluate the rocket flight stability, on the basis of the differential equations system (7), is useful to deduce a differential equation which allows to calculate the incidence variation on the trajectory.

By adequate mathematical transformations [6] (with the approximations $\cos \alpha \cong 1$, $\sin \alpha \cong \alpha$), it can be obtained the following equation :

$$\ddot{\alpha} + A_1 \dot{\alpha}^2 + A_2 v \dot{\alpha} + A_3 v \dot{\alpha} \alpha + A_4 v^2 \alpha^3 + A_5 v^2 \alpha^2 + A_6 v^2 \alpha = F v^2, \tag{8}$$

where

$$\begin{aligned}
A_1 &= \frac{K'_\omega \ell}{K_z \ell_c - 1}, \\
A_2 &= K_z + \frac{a_R}{v^2} + \frac{K_j}{v} + \frac{2K'_\omega \ell}{1 - K_z \ell_c} \frac{g}{v^2} \cos \theta - K_\omega \ell + \frac{g \sin \theta}{v^2} K_z \ell_c, \\
A_3 &= \left(K_z + \frac{a_R}{v^2} \right) \frac{2K'_\omega \ell}{K_z \ell_c - 1}, \\
A_4 &= K_z \left(\frac{a_R}{v^2} - K_z \right), \\
A_5 &= K_z \ell_c K'_m - K'_m - \left(K_z + \frac{a_R}{v^2} \right)^2 \frac{K'_\omega \ell}{1 - K_z \ell_c} - \frac{g \cos \theta}{v^2} K_z,
\end{aligned} \tag{9}$$

$$\begin{aligned}
A_6 = & K_z \ell_c K_m - K_m + \frac{\dot{a}_R}{v^3} + \left(\frac{K_z}{v^2} - \frac{a_R}{v^4} \right) \left(a_R - K_x v^2 - g \sin \theta \right) + \frac{g \sin \theta}{v^2} \left(K_z + \frac{a_R}{v^2} \right) + \\
& + \frac{K'_\omega \ell}{1 - K_z \ell_c} \frac{2g}{v^2} \left(K_z + \frac{a_R}{v^2} \right) \cos \theta - \left(K_\omega \ell v - K_j \right) \left(\frac{K_z}{v} + \frac{a_R}{v^3} \right) + \frac{g \sin \theta}{v^3} K_z \ell_c \left(K_z v + \frac{a_R}{v} \right), \\
F = & \left(K_j - K_\omega \ell v \right) \frac{g \cos \theta}{v^3} - \frac{g \cos \theta}{v^4} \left(a_R - K_x v^2 - g \sin \theta \right) + \frac{g^2 \sin \theta \cos \theta}{v^4} + \\
& + \frac{K'_\omega \ell}{1 - K_z \ell_c} \frac{1}{v^4} g^2 \cos^2 \theta + \frac{g^2 \sin \theta \cos \theta}{v^4} K_z \ell_c.
\end{aligned}$$

This differential equation (8), which permit to determine the incidence angle, is a non-linear, of second order, non-homogeneous equation with variable coefficients. The stability analyse must be done at many Mach numbers and altitudes, in the suitable range of the flight real conditions of the rocket.

The rocket flight stability studies, were also done using the linear model [6], which in a certain hypotheses, gives with a sufficient accuracy the variation of angle α on a short trajectory interval. Thus, in such case, in a more complete form, the incidence linear equation [5], [6] is

$$\frac{d^2 \alpha}{dt^2} + A_1 v \frac{d\alpha}{dt} + A_0 v^2 \alpha = F, \quad (10)$$

where the coefficients expressions are

$$\begin{aligned}
A_0 = & K_m - K_x K_z + (K_x + K_z) \frac{a_R}{v^2} + 2g \frac{a_R}{v^4} \sin \theta - \frac{a_R^2}{v^4} + \\
& + \frac{1}{1 - K_z \ell_c} \left(K_z + \frac{a_R}{v^2} \right) \left(K_\omega \ell + \frac{K_j}{v} + \frac{g \sin \theta}{v^2} K_z \ell_c + \frac{K_z^2 \ell_c^2}{v} \right), \\
A_1 = & K_z + \frac{a_R}{v^2} + \frac{K_z \ell_c}{v} + \frac{1}{1 - K_z \ell_c} \left(K_\omega \ell + \frac{K_j}{v} + \frac{g \sin \theta}{v^2} K_z \ell_c + \frac{K_z^2 \ell_c^2}{v} \right), \\
F = & g \cos \theta \left(K_x + \frac{2g \sin \theta}{v^2} - \frac{a_R}{v^2} + K_z \frac{\ell_c}{v} \right) + \alpha_T \left(K_x a_R - \frac{a_R^2}{v^2} + 2g \frac{a_R}{v^2} \sin \theta + \right. \\
& + \frac{\dot{a}_R}{v} + K_z \ell_c \frac{a_R}{v} \left. \right) + \frac{\mathcal{E}_T}{J} + \frac{a_R \alpha_T + g \cos \theta}{v(1 - K_z \ell_c)} \left(K_\omega \ell v + K_j + K_z \ell_c \frac{g \sin \theta}{v} + K_z^2 \ell_c^2 \right).
\end{aligned} \quad (11)$$

In a small time interval, hence on a short trajectory interval, the altitude and velocity have sufficient small variations as that the aerodynamic coefficients, air density, mass and the inertia moment can be substitute with constant average values. Therefore, the equation (10) becomes a constant coefficients equation, which provides an analytical solution [6]. In this way, it is possible to do a fast rocket flight stability analyse in suitable accuracy conditions.

3. RESULTS

The results, in a graphic form, of some numerical applications, which were done with a study rocket $D_R = 127$ mm (the mass and aerodynamical characteristics [5], [6]) are presented in fig.2-4, for a normal engine work.

The equations system (7) and the differential equations (8) and (10) were numerical integrated by Adams Krâlov and Runge- Kutta methods [5], [6] with the integration step 10^{-4} s (with minimum two magnitude orders smaller then incidence oscillating period).

In the same initial conditions ($\theta=30^\circ$, $\alpha=2^\circ$, $\varphi=32^\circ$, $\omega=0.7$ rad/s, $x=2.6$ m, $y=1.5$ m), more difficults from flight stability point of view, the error between the results obtained by the two numerical integration methods doesn't exceed 5%, in the case of rockets with trajectory active period duration of seconds order (fig.4).

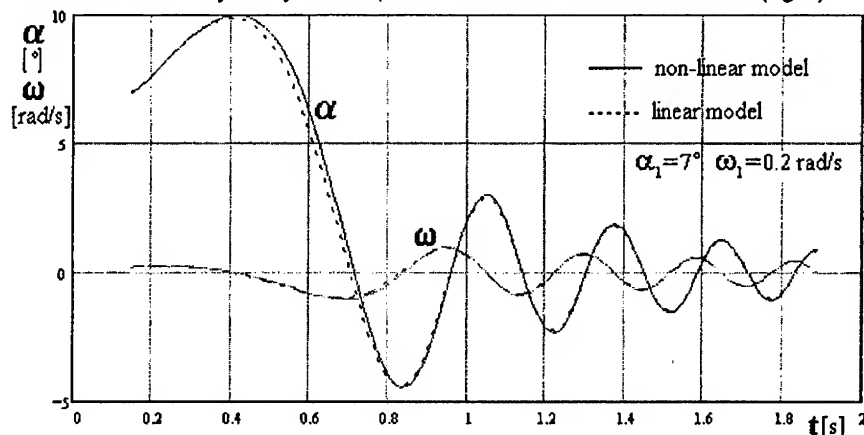


Fig.2

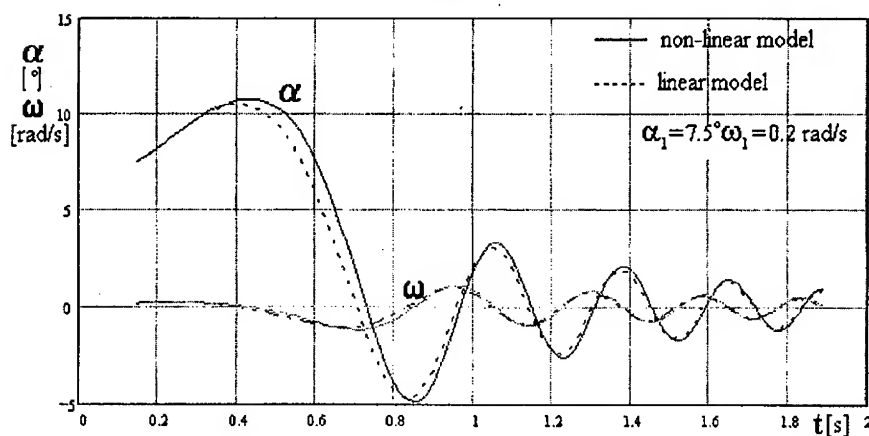
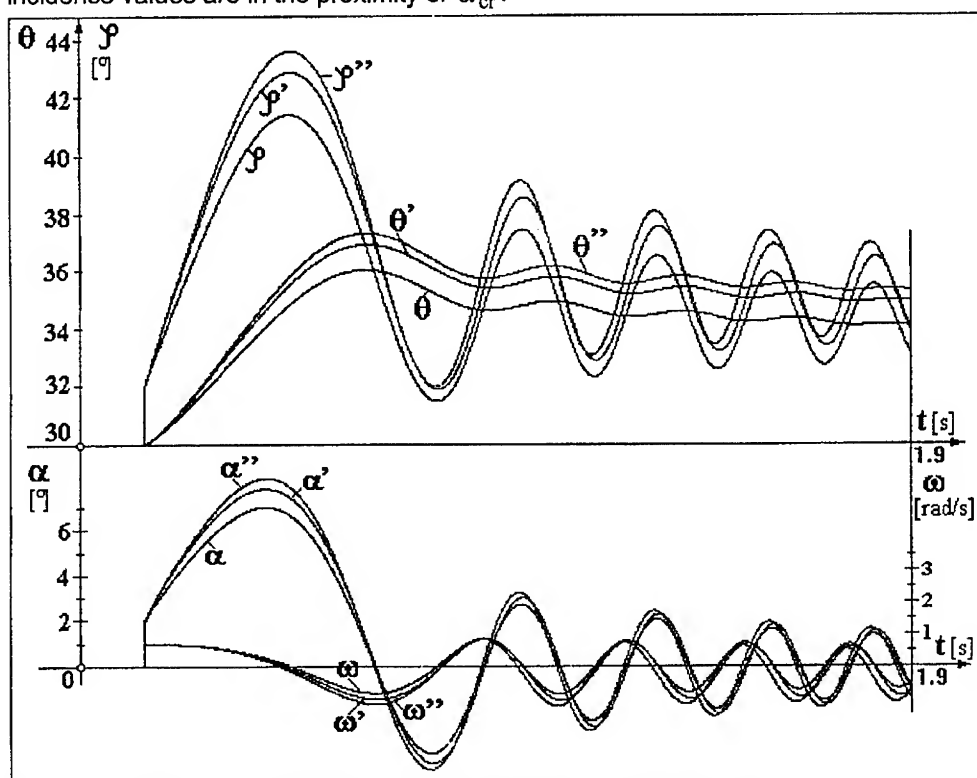


Fig.3

It is easy to observe that the linear method of incidence evaluation—differential equation (10) with constant coefficients (on a short trajectory arc), very simple to apply, gives results with a sufficient accuracy, comparative with numerical integration of the system (7), or equation (10) considered with variable coefficients [6], (fig.5). For instance, on a short time interval, 1,1÷1,4 s, when the Mach number has the average value $M=1$, and the flight altitude is about 110.8 m, the differences between these methods are sufficiently small, from practically point of view [6].

• An important conclusion is that when $\alpha < \alpha_\ell$, the non-linear and linear models give practically the same results. In this case the differential equation (10) can be useful in rocket flight stability studies. For $\alpha > \alpha_\ell$, the differences between the results obtained with these two models increase, especially when the incidence values are in the proximity of α_{cr} .

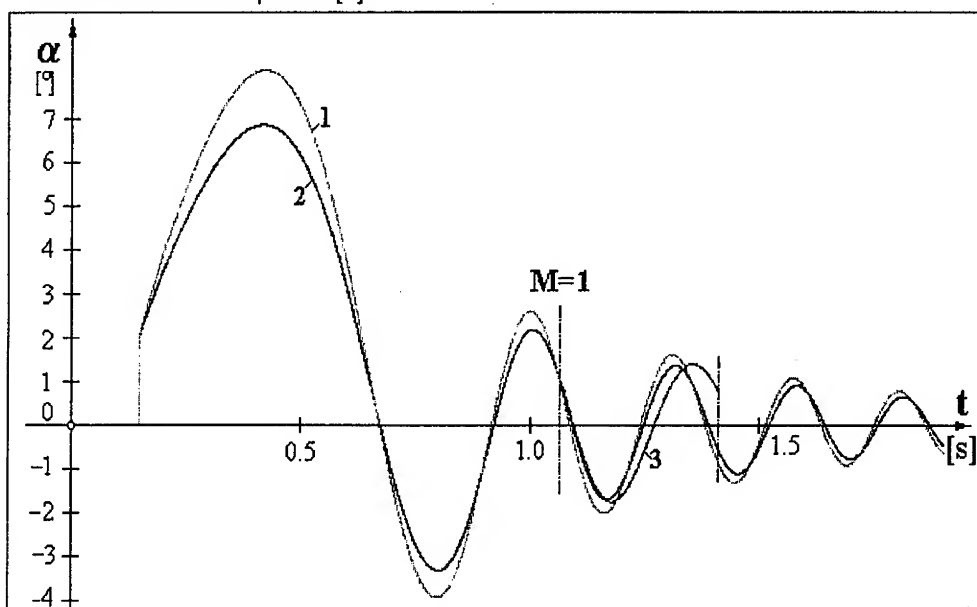


$\alpha, \theta, \dot{\theta}, \ddot{\theta}, \omega$ —plane equations system – Adams Krâlov method,
 $\alpha', \theta', \dot{\theta}', \ddot{\theta}', \omega'$ —equation (10) with variable coefficient – Adams Krâlov method,
 $\alpha'', \theta'', \dot{\theta}'', \ddot{\theta}'', \omega''$ —equation (10) with variable coefficient –Runge Kutta method.

Fig.4

It was elaborated a complex program to simulate the rocket flight in the resistant environment, which operates with a large aerodynamical, rocket, engine and launcher construction data basis, for different rocket-engine works (normal and perturbed works) [4], [5], [6].

The study pointed out also the presence of a trajectory *initial critical period*, its duration in presented diagrams being smaller then the pitching oscillations period. An important conclusion for the rocket engine is that the burning time must be longer than this initial critical period [6].



- 1.-equation (10) with variable coefficients – Runge Kutta method,
- 2-longitudinal plane movement eq. system – Adams Krâlov method,
- 3-equation (10) with constant coefficients, on a short trajectory arc.

Fig.5

References

- [1] Moraru FI.– *External ballistics and rocket flight dynamics*, III, Military Academy, Bucharest, 1973;
- [2] Moraru FI.– *Aerodynamics*, Military Academy, Bucharest, vol.I (1980), vol.II (1984);
- [3] Volker Fleck – *Balistique exterieure*, ENSIETA Brest, 1993.
- [4]. Moraru FI., Safta D., *Theoretical and experimental researches concerning the variation and the influence of the solid propellant rocket-engine thrust over the rocket motion*, CATE'95, Brno, R Ceha;
- [5]. Moraru FI., Safta D., *Regarding of the influence of the engine work over the rocket flight*, Scientific papars session of T.M.A., november 1995.
- [6]. Safta D., *Contributions to the influence study of the engine work parameters over the rocket flight parameters*, Doctor's thesis, Technical Military Academy, Bucharest, 1996.

AN ABSTRACT POINT OF VIEW FOR SOME INTEGRAL EQUATIONS FROM APPLIED MATHEMATICS

IOAN A. RUS

Babeş-Bolyai University of Cluj-Napoca
Str. Kogălniceanu Nr.1, 3400 Cluj-Napoca
Romania

AMS subject classification: 47H10, 45G, 85A25, 92D.

Key words: fibre contraction theorem, Picard operators, nonlinear integral equations,
 H -equation of Chandrasekar.

ABSTRACT. The object of this paper is to show how the fixed point principles and the theory of Picard operators are used for the study of the following integral equations:

1) an integral equation from Statistical Mechanics

$$x(t) = 1 + \lambda \int_t^1 x(s)x(s-t)ds, \quad t \in [0, 1]$$

where $\lambda \in R$;

2) Chandrasekhar equation

$$x(t) = 1 + \lambda x(t) \int_0^1 \frac{t}{t+s} x(s)ds, \quad t \in [0, 1].$$

We obtain our results on the existence and uniqueness of solutions by a fixed point principle on cartesian product and the results on data dependende by the fibre contraction theorem.

1 INTRODUCTION

The purpose of this paper is to present a unified treatment of some classes of nonlinear integral equations from Applied Mathematics. First, we give some abstract results on fixed point theory. After that, these results are applied to an integral equation from Statistical Mechanics and to the H -equation of Chandrasekhar. Some open problems are formulated.

2 BASIC NOTATIONS AND NOTIONS

Let X be a nonempty set and $A : X \rightarrow X$ an operator. In this paper we shall use the following notations:

$$P(X) := \{A \subset X \mid A \neq \emptyset\},$$

$$F_A := \{x \in X \mid A(x) = x\} - \text{the fixed point set of } A,$$

$$I(A) := \{Y \in P(X) \mid A(Y) \subset Y\}.$$

Definition 2.1 (Rus [26], [28], [30]). Let (X, d) be a metric space. An operator $A : X \rightarrow X$ is (uniformly) Picard operator if there exists $x^* \in X$ such that:

- (a) $F_A = \{x^*\}$,
- (b) $(A^n(x_0))_{n \in \mathbb{N}}$ converges (uniformly) to x^* , for all $x_0 \in X$.

Definition 2.2 (Rus [26], [28], [30]). Let (X, d) be a metric space. An operator $A : X \rightarrow X$ is (uniformly) weakly Picard operator if the sequence $(A^n(x_0))_{n \in \mathbb{N}}$ converges (uniformly) for all $x_0 \in X$ and the limit (which may depend on x_0) is a fixed point of A .

If A is weakly Picard operator, then we consider the following operator

$$A^\infty : X \rightarrow X, \quad A^\infty(x) := \lim_{n \rightarrow \infty} A^n(x).$$

3 FIXED POINT THEOREMS FOR OPERATORS ON CARTESIAN PRODUCT

Let X be a set and $A : X \times X \rightarrow X$ an operator. A point $x_0 \in X$ is a fixed point of A iff

$$x_0 = A(x_0, x_0).$$

A point $(x_0, y_0) \in X \times X$ is called a coupled fixed point of A iff

$$x_0 = A(x_0, y_0), \quad y_0 = A(y_0, x_0).$$

Remark 3.1. The fixed points of A are the fixed points of the following operator:

$$X \rightarrow X, \quad x \mapsto A(x, x).$$

Remark 3.2. If (x^*, y^*) is a fixed point of the operator

$$X \times X \rightarrow X \times X, \quad (x, y) \mapsto (f(x, y), f(x, y))$$

then $y^* = x^*$, and x^* is a fixed point of A .

Remark 3.3. The coupled fixed points of A are the fixed points of the operator

$$X \times X \rightarrow X \times X, \quad (x, y) \mapsto (A(x, y), A(y, x)).$$

Theorem 3.1. Let (X, d) be a complete metric space and $A : X \times X \rightarrow X$. We suppose that:

(i) there exists $a_1, a_2 \in [0, 1[$, $a := a_1 + a_2 < 1$ such that

$$d(A(x_1, y_1), A(x_2, y_2)) \leq a_1 d(x_1, x_2) + a_2 d(y_1, y_2),$$

for all $x_1, x_2, y_1, y_2 \in X$.

Then we have:

(a) $F_A = \{x^*\}$;

(b) for each $x_0 \in X$, the sequence

$$x_n := f(x_{n-1}, x_{n-1}), \quad n \in \mathbb{N}^*,$$

converges to x^* and

$$d(x_n, x^*) \leq \frac{a^n}{1-a} d(x_0, A(x_0, x_0));$$

(c) for all $x_0, x_1 \in X$, the sequence

$$x_{n+1} := A(x_{n-1}, x_n), \quad n \in N^*,$$

converges to x^* and

$$d(x_n, x^*) \leq \frac{a^{n-1}}{1-a} \max(d(x_0, x_1), d(x_1, x_2));$$

(d) for all $x_0, y_0 \in X$, the sequences

$$\begin{aligned} x_n &= A(x_{n-1}, y_{n-1}), \\ y_n &= A(y_{n-1}, x_{n-1}) \end{aligned} \quad n \in N^*,$$

converges to x^* and

$$\begin{pmatrix} d(x_n, x^*) \\ d(y_n, x^*) \end{pmatrix} \leq \begin{pmatrix} 1-a_1 & -a_2 \\ -a_2 & 1-a_1 \end{pmatrix}^{-1} \begin{pmatrix} a_1 & a_2 \\ a_2 & a_1 \end{pmatrix}^n \begin{pmatrix} d(x_0, x_1) \\ d(y_0, y_1) \end{pmatrix}.$$

Proof. (a)+(b). The operator

$$X \rightarrow X, \quad x \mapsto A(x, x)$$

is an α -contraction.

(c). Let $x_0, x_1, x_2 \in X$ be three elements of X . From (i) we have that

$$d(A(x_0, x_1), A(x_1, x_2)) \leq a_1 d(x_0, x_1) + a_2 d(x_1, x_2).$$

The proof follows from a theorem by Prešić (see [19]).

(d) We consider on $X \times X$ the generalized metric

$$\rho((x_1, x_2), (y_1, y_2)) := \begin{pmatrix} d(x_1, y_1) \\ d(x_2, y_2) \end{pmatrix}.$$

We consider the following operator

$$B : X \times X \rightarrow X \times X, \quad B(x_1, x_2) = (A(x_1, x_2), A(x_2, x_1)).$$

We remark that

$$B : (X \times X, \rho) \rightarrow (X \times X, \rho)$$

is a generalized contraction. The proof of (d) follows from the theorem of Perov (see [23], or [24], or [26]).

Theorem 3.2 (Fiber contraction theorem (Hirsch-Pugh ([12]))). *Let (X, d) be a metric space, (Y, ρ) a complete metric space, and $A : X \times Y \rightarrow X \times Y$. We suppose that:*

- (i) $A \in C(X \times Y, X \times Y)$;
- (ii) $A(x, y) = (B(x), C(x, y))$;
- (iii) B is a Picard operator;
- (iv) there exists $\lambda \in]0, 1[$ such that

$$\rho(C(x, y), C(x, z)) \leq \lambda \rho(y, z),$$

for all $x \in X$ and $y, z \in Y$.

In these conditions the operator A is a Picard operator.

More general, we have:

Theorem 3.3 (Fiber Picard operators theorem). *Let (X, d) be a metric space, (Y, ρ) a complete metric space and $A : X \times Y \rightarrow X \times Y$. We suppose that:*

- (i) $A \in C(X \times Y, X \times Y)$;
- (ii) $A(x, y) = (B(x), C(x, y))$;
- (iii) B is a weakly Picard operator;
- (iv) there exists $\lambda \in]0, 1[$ such that:

$$\rho(C(x, y), C(x, z)) \leq \lambda \rho(y, z)$$

for all $x \in X$ and $y, z \in Y$.

In these conditions the operator A is a weakly Picard operator. Moreover, if $C^n(B^\infty(x), \cdot)(y) \rightarrow y^*(x)$, then $A^n(x, y) \rightarrow (B^\infty(x); y^*(x))$.

Proof. Let $x \in X$ and $y \in Y$. We prove that $A^n(x, y) \rightarrow (B^\infty(x), y^*(x)) \in F_A$. Let

$$\left\{ \begin{array}{l} x_1 := B(x) \\ y_1 := C(x, y) \end{array} \right. , \dots , \left\{ \begin{array}{l} x_{n+1} := B^n(x) \\ y_{n+1} := C(B^n(x), y_n) \end{array} \right. , \dots$$

We remark that if we start with (x, z) , then

$$\left\{ \begin{array}{l} x_1 := B(x) \\ z_1 := C(x, z) \end{array} \right. , \dots , \left\{ \begin{array}{l} x_{n+1} := B^n(x) \\ z_{n+1} := C(B^n(x), z_n) \end{array} \right. , \dots$$

It is clear that

$$\pi_1 A^n(x, y) = x_n, \quad \pi_2 A^n(x, y) = y_n.$$

We have

$$\begin{aligned}\rho(\pi_2 A^n(x, y), y^*(x)) &\leq \rho(\pi_2 A^n(x, y), \pi_2 A^n(x, y^*(x))) + \rho(\pi_2 A^n(x, y^*(x)), y^*(x)) \leq \\ &\leq \lambda^n \rho(y, y^*(x)) + \rho(\pi_2 A^n(x, y^*(x)), y^*(x)).\end{aligned}$$

But

$$\sigma_n := \rho(C(B^n(x), y^*(x)), y^*(x)) \rightarrow 0 \quad \text{as } n \rightarrow \infty,$$

and

$$\begin{aligned}\rho(\pi_2 A^n(x, y^*(x)), y^*(x)) &\leq \\ &\leq \rho(\pi_2 A^n(x, y^*(x)), C(B^n(x), y^*(x))) + \rho(C(B^n(x), y^*(x)), y^*(x)) \leq \dots \leq \\ &\leq \sum_{i=0}^n \lambda^{n-i} \sigma_i = \sum_{i=0}^{n-k} \lambda^{n-i} \sigma_i + \sum_{i=n-k+1}^n \lambda^{n-i} \sigma_i \leq \\ &\leq \frac{\lambda^k}{1-\lambda} \max_{i \in \mathbb{N}} \sigma_i + \frac{1}{1-\lambda} \max\{\sigma_i \mid i \geq n-k+1\} \rightarrow 0\end{aligned}$$

as k and $n-k+1 \rightarrow \infty$.

The proof is complete.

The above consideration give rise to the following

Open problem 3.1. Let (X, d) and (Y, ρ) be two metric spaces. Let $A : X \times Y \rightarrow X \times Y$ be such that $A(x, y) = (B(x), C(x, y))$.

Are the following statements theorems?:

Conjecture 1. If B is a Picard operator and $C(x, \cdot)$ is a Picard operator for all $x \in X$, then A is a Picard operator.

Conjecture 2. If B is a weakly Picard operator and $C(x, \cdot)$ is a Picard operator for all $x \in X$, then A is a weakly Picard operator.

Conjecture 3. If B is a weakly Picard operator and $C(x, \cdot)$ is a weakly Picard operator, for all $x \in X$, then A is a weakly Picard operator.

4 AN INTEGRAL EQUATION FROM STATISTICAL MECHANICS

We begin the applications of the abstract results, given in the first part of this paper, with the following integral equation

$$x(t) = 1 + \lambda \int_t^1 x(s)x(s-t)ds, \quad t \in [0, 1], \quad (1)$$

where $\lambda \in \mathbb{R}$.

This equation is a simplified model of certain equations arising in Statistical Mechanics (see Wertheim [35], Pimbley [18] and Ramalho [21]).

The main known result for the equation (1) is the following

Theorem 4.1 (Pimbley [18]; see also Ramalho [21]). *Equation (1) has two real solutions $x^+(\cdot; \lambda)$ and $x^-(\cdot; \lambda)$ for $0 < \lambda < \frac{1}{2}$ and no real solution for $\lambda > \frac{1}{2}$. As function of t these solutions are positive, monoton decreasing, and at least twice differentiable; as functions of the real parameter λ they are continuous uniformly over $0 \leq t \leq 1$. As $\lambda \rightarrow 0$, $\lambda > 0$, $x^+(t; \lambda) \rightarrow 1$. The second solution $x^-(t; \lambda)$ joins $x^+(t; \lambda)$ at $\lambda = \frac{1}{2}$. If, for any real solution $x(\cdot; \lambda)$ of equation (1) we set*

$$I(x) := \int_0^1 x(s, \lambda) ds,$$

then $I(x)$ satisfies the equation

$$\lambda I^2(x) - 2I(x) + 2 = 0.$$

Let $X := \{x \in C([0, 1] \times [0, \lambda_0]) \mid x \geq 1 \text{ and } \int_0^1 x(s; \lambda) ds \leq M, \lambda \in [0, \lambda_0]\}$.

We have

Theorem 4.2. *There exist λ_0 and M such that:*

(a) *the equation (1) has in X a unique solution x^**

(b) *the sequence*

$$x_{n+1}(t; \lambda) := 1 + \lambda \int_t^1 x_n(s, \lambda)x_n(s-t; \lambda)ds,$$

$x_0 \in X$, $n \in \mathbb{N}$, *converges uniformly to $x^*(t; \lambda)$;*

(c) *the sequence*

$$x_{n+1}(t; \lambda) := 1 + \lambda \int_t^1 x_{n-1}(s; \lambda)x_n(s-t; \lambda)ds,$$

$x_0, x_1 \in X$, $n \in \mathbb{N}$, converges uniformly to $x^*(t; \lambda)$;

(d) the sequences

$$x_{n+1}(t; \lambda) := 1 + \lambda \int_t^1 x_n(s; \lambda) y_n(s-t; \lambda) ds,$$

$$y_{n+1}(t; \lambda) := 1 + \lambda \int_t^1 y_n(s; \lambda) x_n(s-t; \lambda) ds,$$

converges uniformly to $x^*(x; \lambda)$;

(e) $x^* \in C^1([0, 1] \times [0, \frac{3}{8}])$.

Proof. Consider the Banach space $C([0, 1] \times [0, \lambda_0])$, of continuous functions on $[0, 1] \times [0, \lambda_0]$ with the Chebyshev's norm, $\|x\| := \max\{|x(t, \lambda)| \mid t \in [0, 1], \lambda \in [0, \lambda_0]\}$. Then $X \subset C([0, 1] \times [0, \lambda_0])$ is a complete metric space. Let

$$A : X \times X \rightarrow C([0, 1] \times [0, \lambda_0])$$

be defined by

$$A(x, y)(t; \lambda) = 1 + \lambda \int_t^1 x(s) y(s-t) ds.$$

We remark that

(1) $A(X \times X) \subset X$;

(2) $\|A(x_1, y_1) - A(x_2, y_2)\| \leq \lambda M(\|x_1 - x_2\| + \|y_1 - y_2\|)$, for all $x_1, x_2, y_1, y_2 \in X$.

Now, from the Theorem 3.1, we have (a)+(b)+(c)+(d).

(c). We have that

$$x^*(t; \lambda) = 1 + \lambda \int_t^1 x^*(s; \lambda) x^*(s-t; \lambda) ds. \quad (2)$$

First we prove that $\frac{\partial x^*}{\partial t} \in C([0, 1] \times [0, \lambda_0])$.

Let $Y := C([0, 1] \times [0, \lambda_0])$.

$$B : X \rightarrow X, \quad B(x)(t, \lambda) := 1 + \lambda \int_t^1 x(s; \lambda) x(s-t; \lambda) ds,$$

$$C : X \times Y \rightarrow Y, \quad C(x, y)(t; \lambda) := -\lambda x(t; \lambda) x(0; \lambda) - \lambda \int_t^1 x(s; \lambda) y(s-t; \lambda) ds$$

and

$$A : X \times Y \rightarrow X \times Y, \quad A = (B, C).$$

If we consider on Y a Bielecki norm then we are in the condition of the Theorem 3.2. From this theorem we have that: for all $x_0 \in X$, $y_0 \in Y$ the sequences

$$x_{n+1}(t, \lambda) := 1 + \lambda \int_t^1 x_n(s; \lambda) x_n(s-t, \lambda) ds,$$

If we consider on Y a Bielecki norm then we are in the condition of the Theorem 3.2. From this theorem we have that: for all $x_0 \in X$, $y_0 \in Y$ the sequences

$$x_{n+1}(t, \lambda) := 1 + \lambda \int_t^1 x_n(s; \lambda) x_n(s-t, \lambda) ds,$$

$$y_{n+1}(t, \lambda) := -\lambda x_n(t; \lambda) x_n(0; \lambda) - \lambda \int_t^1 x_n(s; \lambda) y_n(s-t; \lambda) ds$$

converge uniformly. Moreover $(x_n)_{n \in \mathbb{N}}$ converges uniformly to the $x^* \in X$, the unique solution in X of the equation (1). Let $y^* := \lim_{n \rightarrow \infty} y_n$. We remark that if we take $y_0 = \frac{\partial x_0}{\partial t}$, then $y_n = \frac{\partial x_n}{\partial t}$, for all $n \in \mathbb{N}$. These imply that $y^* = \frac{\partial x^*}{\partial t}$.

For to prove that there exists $\frac{\partial x}{\partial \lambda}$ and $\frac{\partial x}{\partial \lambda} \in C([0, 1] \times [0, \frac{3}{8}])$ we take

$$\begin{aligned} C(x, y)(t, \lambda) &:= \int_t^1 x(s; \lambda) x(s-t; \lambda) ds + \\ &+ \int_t^1 x(s-t; \lambda) y(s; \lambda) ds + \int_t^1 x(s, \lambda) y(s-t; \lambda) ds. \end{aligned}$$

The proof is complete.

Remark 4.1. A similar results can be given for the following equation

$$x(t) = g(t) + \lambda \int_t^1 K(t, s) x(s) x(t-s) ds. \quad (3)$$

Remark 4.2. For other considerations on the equations (1) and (3) see: [18], [21] and [22].

Remark 4.3. For other applications of Theorem 3.2 see [12] and [32].

5 CHANDRASEKHAR'S EQUATION

In what follows we consider the following equation

$$x(t) = g(t) + \lambda x(t) \int_0^1 K(t, s) x(s) ds, \quad t \in [0, 1], \quad (1)$$

where $g \in C([0, 1], [m_g, M_g])$, $m_g > 0$, $K \in C([0, 1] \times [0, 1], [0, M_k])$, $\lambda \in [0, \lambda_0]$. This equation generalizes the Chandrasekhar's equation

$$x(t) = 1 + \lambda x(t) \int_0^1 \frac{t}{t+s} x(s) ds, \quad x \in [0, 1], \quad (2)$$

which is a mathematical model of certain phenomena in the transfer of radiation between stellar atmospheres (see [6], [7], [8], [1], [13], [15], [22], ...).

There exist some abstract models for the equation (2). For instance, R.W. Legget studied, in [14], the following abstract equation

$$x = x_0 + xKx \quad (3)$$

where K is a compact operator on a Banach algebra X , and $x_0 \in X$. Other abstract model for (2) is the following quadratic equation

$$x = x_0 + A(x, x) \quad (4)$$

where X is a Banach space, $A : X \times X \rightarrow X$ is a bounded bilinear operator and $x_0 \in X$ (see [2], [20]).

For the equation (1) we have

Theorem 5.1. *There exists λ_0 and $r > 0$ such that:*

- (a) *the equation (1) has in $C([0, 1], [m_g, M_g + r])$, a unique solution x^* , for all $\lambda \in [0, \lambda_0]$;*
- (b) *for all $x_0 \in C([0, 1], [m_g, M_g + r])$, the sequence*

$$x_{n+1}(t; \lambda) := g(t) + \lambda x_n(t; \lambda) \int_0^1 K(t, s) x_n(s; \lambda) ds,$$

converges uniformly to $x^(t; \lambda)$, $t \in [0, 1]$, $\lambda \in [0, \lambda_0]$;*

- (c) *for all $x_0, x_1 \in C([0, 1], [m_g, M_g + r])$, the sequence*

$$x_{n+1}(t; \lambda) := g(t) + \lambda x_{n-1}(t; \lambda) \int_0^1 K(t, s) x_n(s; \lambda) ds,$$

converges uniformly to $x^(t; \lambda)$, $t \in [0, 1]$, $\lambda \in [0, \lambda_0]$;*

- (d) *for all $x_0, y_0 \in C([0, 1], [m_g, M_g + r])$, the sequences*

$$x_{n+1}(t; \lambda) := g(t) + \lambda x_n(t; \lambda) \int_0^1 K(t, s) y_n(s; \lambda) ds,$$

$$y_{n+1}(t; \lambda) := g(t) + \lambda y_n(t; \lambda) \int_0^1 K(t, s) x_n(s; \lambda) ds,$$

converge uniformly to $x^(t; \lambda)$, $t \in [0, 1]$, $\lambda \in [0, \lambda_0]$;*

- (e) *$x^* \in C^1([0, 1] \times [0, \lambda_0])$.*

Proof. Consider the Banach space $C([0, 1] \times [0, \lambda_0])$ of continuous functions on $[0, 1] \times [0, \lambda_0]$, with the Chebyshev's norm. Then

$$X := C([0, 1] \times [0, \lambda_0], [m_g, M_g]) \subset C([0, 1] \times [0, \lambda_0])$$

is a complete metric space.

Let

$$A : X \times X \rightarrow C([0, 1] \times [0, \lambda_0]),$$

$$A(x, y)(t, \lambda) := g(t) + \lambda x(t; \lambda) \int_0^1 K(t, s) y(s; \lambda) ds.$$

We have

$$m_g \leq A(x, y)(t; \lambda) \leq M_g + \lambda(M_g + r)^2 M_k,$$

and

$$\|A(x_1, y_1) - A(x_2, y_2)\| \leq \lambda(M_g + r)M_k(\|x_1 - x_2\| + \|y_1 - y_2\|).$$

If we take λ_0 and $r > 0$ such that

$$\lambda_0(M_g + r)^2 M_k \leq r \quad (5)$$

and

$$2\lambda_0(M_g + r)M_k < 1 \quad (6)$$

then $A(X \times X) \subset X$ and A satisfies the conditions of the Theorem 3.1.

Thus we have (a)+(b)+(c)+(d).

(e) It is clear that $\frac{\partial x}{\partial t} \in C([0, 1] \times [0, \lambda_0])$. Let us prove that $\frac{\partial x}{\partial \lambda} \in C([0, 1] \times [0, \lambda_0])$.

Let

$$Y := C([0, 1] \times [0, \lambda_0]),$$

$$B : X \rightarrow X, \quad B(x)(t; \lambda) := g(t) + \lambda x(t; \lambda) \int_0^1 K(t, s) x(s; \lambda) ds,$$

$$C : X \times Y \rightarrow Y, \quad C(x, y)(t, \lambda) := x(t; \lambda) \int_0^1 K(t, s) x(s; \lambda) ds +$$

$$+ \lambda y(t; \lambda) \int_0^1 K(t, s) x(s; \lambda) ds + \lambda x(t; \lambda) \int_0^1 K(t, s) y(s; \lambda) ds,$$

and

$$A : X \times Y \rightarrow X \times Y, \quad A = (B, C).$$

From (3) and (4) we have that $C(x; \cdot)$, $x \in X$, are uniform contractions. Now we are in the conditions of the Theorem 3.2. From this theorem we have that, for all $x_0, y_0 \in Y$, the sequences

$$x_{n+1}(t; \lambda) := \pi_1 A^n(x_0, y_0),$$

$$y_{n+1}(t; \lambda) := \pi_2 A^n(x_0, y_0)$$

converges uniformly. Moreover, $x_n \rightarrow x^*$, the unique solution in X of (1). Let $y^* = \lim_{n \rightarrow \infty} y_n$. If we take $y_0 = \frac{\partial x_0}{\partial \lambda}$, then we have that $y_n = \frac{\partial x_n}{\partial \lambda}$, for all $n \in N$. These imply that $y^* = \frac{\partial x^*}{\partial \lambda}$.

The proof is complete.

6 OTHER INTEGRAL EQUATIONS FROM APPLIED MATHEMATICS

There are many other integral equations, from Applied Mathematics which can be studied by the similar way as the above equations. In what follow we mention some of them:

6.1. The equation

$$x(t) = g(t) + \lambda x(t) \int_t^1 K(t, s)x(s)ds$$

is a mathematical model in the theorie of radiativ transfer, neutron transport and in the kinetic theory of gases (see [7] and [3]).

6.2. The equation (see [34], [33])

$$x(t) = g(t) + \int_D K(t, s)f(s, x(s))ds, \quad t \in \overline{D},$$

where

$$f(t, u) = \sum_{i=0}^m a_i(t)u^{-i}, \quad t \in D, u > 0.$$

6.3. The following delay integral equation

$$x(t) = \int_{t-\tau}^t f(s, x(s))ds, \quad t \in R,$$

is a mathematical model for epidemics and population growth (see the paper by E. Kirr and Radu Precup in this Proceedings).

6.4. In the study of the spread of a disease which does not induce permanent immunity, the following equation arises

$$x(t) = \left[g(t) + \int_a^t p(s)x(s)ds \right] \left[h(t) + \int_a^t q(s)x(s)ds \right],$$

$t \geq a$ (see [9], [10], [16]).

References

- [1] P.M. Anselone (ed.), *Nonlinear integral equations*, The University of Wisconsin Press, Madison, 1964.
- [2] I.K. Argyros, *Quadratic equations and applications to Chandrasekhar's and related equations*, Bull. Austral. Math. Soc., 32(1985), 275-292.
- [3] I.K. Argyros, *On a class of nonlinear integral equations arising in neutron transport*, Aequationes Math., 36(1988), 99-111.
- [4] I.W. Busbridge, *On the H-function of Chandrasekhar*, Quart. J. Math. Oxford, 8(1957), 133-140.
- [5] I.W. Busbridge, *On solutions of Chandrasekhar's integral equation*, Trans. AMS, 105(1962), 112-117.
- [6] S. Chandrasekhar, *The transfer of radiation in stellar atmospheres*, Bull. AMS, 53(1947), 641-711.
- [7] S. Chandrasekhar, *Radiativ transfer*, Dover Publ., New York, 1960.
- [8] M.M. Crum, *On an integral equation of Chandrasekhar*, Quart. J. Math., 18(1947), 244-252.
- [9] G. Gripenberg, *Periodic solutions of an epidemic model*, J. Math. Biology, 10(1980), 271-280.
- [10] G. Gripenberg, *On some epidemic models*, Quart. of Appl. Math., 39(1981), 317-327.
- [11] S. Heikkilä, V. Lakshmikantham, *Monotone iterative techniques for discontinuous nonlinear differential equations*, Marcel Dekker, New York, 1994.
- [12] M.W. Hirsch, C.C. Pugh, *Stable manifolds and hyperbolic sets*, Proc. Symp. in Pure Math., 14(1970), 133-163.
- [13] R.W. Leggett, *A new approach to the H-equation of Chandrasekhar*, SIAM J. Math. Anal., 7(1976), 542-550.
- [14] R.W. Leggett, *On certain nonlinear integral equations*, J. Math. Anal. and Appl., 57(1977), 462-468.

- [15] R.F. Millar, *On a nonlinear integral equation occurring in diffraction theory*, Proc. Camb. Phil. Soc., 62(1966), 249-261.
- [16] B.G. Pachpatte, *On a new inequality suggested by the study of certain epidemic models*, J. Math. Anal. and Appl., 195(1995), 638-644.
- [17] I. Păvăloiu, *La resolution des systemes d'équations opérationnelles á l'aide des méthodes itérative*, Mathématica, 11(1969), 137-141.
- [18] G.H. Pimbley, *Positive solution of a quadratic integral equation*, Arch. Rat. Mech. Anal., 24(1967), 107-127.
- [19] S.B. Prešić, *Sur une classe d'inéquations aux différence finies et sur la convergence de certaines suites*, Publ. Inst. Math., 5(1965), 75-78.
- [20] L.B. Rall, *Quadratic equations in Banach spaces*, Rend. Circolo Mat. Palermo, 10(1961), 314-332.
- [21] R. Ramalho, *Existence and uniqueness theorems for a nonlinear integral equation*, Univ. Federal de Pernambuco, Notas e Comun. Nr. 40, 1972.
- [22] R. Ramalho, *Positive solutions for two classes of nonlinear integral equations*, Univ. Federal de Pernambuco, Notas e Comun. Nr. 99, 1979.
- [23] I.A. Rus, *Metrical fixed point theorems*, Univ. of Cluj-Napoca, 1979.
- [24] I.A. Rus, *Principii și aplicații ale teoriei punctului fix*, Ed. Dacia, Cluj-Napoca, 1979.
- [25] I.A. Rus, *An iterative method for the solution of the equation $x = f(x, \dots, x)$* , L'Anal. Numérique et la Théorie de l'Approximation, 10(1981), Nr. 1, 95-100.
- [26] I.A. Rus, *Generalized contractions*, Babeș-Bolyai Univ., Preprint Nr. 3, 1983, 1-130.
- [27] I.A. Rus, *Basic problems of the metric fixed point theory revisited (I)*, Studia Univ. Babeș-Bolyai, 34(1989), Nr. 2, 61-68.
- [28] I.A. Rus, *Weakly Picard mappings*, Comment Math. Univ. Caroline, 34, 4(1993), 769-773.
- [29] I.A. Rus, *Some open problems in fixed point theory by means of fixed point structures*, Libertas Math., 14(1994), 65-84.

-
- [30] I.A. Rus, *Picard operators and applications*, Babeş-Bolyai Univ., Preprint Nr. 3, 1996.
- [31] I.A. Rus, *Ecuatii diferențiale, Ecuatii integrale și Sisteme dinamice*, Transilvania Press, Cluj-Napoca, 1996.
- [32] J. Sotomayor, *Smooth dependence of solution of differential equation on initial data: a simple proof*, Bol. Soc. Brasil. Mat., 4(1973), no. 1, 55-59.
- [33] C.A. Stuart, *Positive solution of a nonlinear integral equation*, Math. Ann., 192(1971), 119-124.
- [34] C.A. Stuart, *Existence theorems for a class of nonlinear integral equations*, Math. Z., 137(1974), 49-64.
- [35] M. Wertheim, *Analytic solution of the Percus-Yevick equation*, J. Math. Phys., 5(1964).

Approximation Methods and Existence Problems for Nonlinear Equations in Banach Spaces

Cezar Avramescu, Octavian Mustafa *

March 1997

Abstract

Let X be a Banach space, D a nonvoid subset of X and $M : D \rightarrow X$ an operator.

We consider the equation

$$(M) \quad x = Mx$$

If the properties of the operator M are not enough to ensure the existence of at least one solution for (M) , we intend to approximate M with some suitable operator M_n for which the equation

$$(M_n) \quad x = M_n x$$

could be solved easier and to use convergence techniques in order to prove the existence of solutions for (M) .

1 Approximable operators

Let X be a Banach space, D nonvoid subset of X and $M : D \rightarrow X$ an operator. We note by I the identity map on X .

*1]University of Craiova, Dept. of Mathematics

Let (X_n) and (Y_n) be two families of subsets of X (not necessarily closed); one denotes by D_n the intersection between D and X_n and supposes that

$$D_n \neq \emptyset, (\forall) n.$$

1.1 Definition

The operator M is considered to be *approximable* on D for the pair (X_n, Y_n) with the operators $M_n : D_n \rightarrow Y_n$ if and only if the *approximation equation* is valid, i.e.

$$(1.1) \quad \lim_{n \rightarrow \infty} \sup_{x \in D_n} \|M_n x - Mx\| = 0.$$

The definition 1.1 is easily satisfied in the most usual case of

$$M_n := M|_{D_n},$$

where X_n is an arbitrary subspace of X and

$$Y_n = \text{span } M(D_n).$$

A classical case is the one of X_n replaced with X for each n , D and $M : D \rightarrow X$ being a bounded subset of X and respectively a compact operator. Now, the existence of some satisfying (1.1) compact operator M_n on D to the space Y_n is assured; supplementary,

$$\dim Y_n < \infty,$$

for each n .

2 An existence principle

The aim of this section is to present a simple existence principle regarding the solutions of the equation

$$(M) \quad x = Mx$$

based on the fact that the *approximation equation*

$$(Mn) \quad x = M_n x$$

has some solutions, too.

2.1 Proposition

If the supposition that

- (i) M satisfies (1.1);
- (ii) $\mathcal{R}(I - M)$ is closed;
- (iii) the equation (Mn) has some solution for each n ,

is made then the equation (M) admits at least one solution.

Proof.

Let's consider

$$(2.1) \quad x_n = M_n x_n, \quad x_n \in D_n \subset D, \quad (\forall) n.$$

From (1.1) it follows that

$$x_n - Mx_n = M_n x_n - Mx_n \xrightarrow{n \rightarrow \infty} 0.$$

So,

$$(I - M)(x_n) \xrightarrow{n \rightarrow \infty} 0,$$

which implies

$$0 \in \overline{\mathcal{R}(I - M)}.$$

Due to the assumption (ii), the conclusion is evident.

■

2.2 Remark

For a closed bounded subset D of X and a demicompact continuous operator M , (ii) is accomplished; supplementary, each sequence (x_n) provided by (2.1) contains a subsequence which converges to a solution of the equation (M) . In particular, this always happens for a compact operator M .

■

2.3 Remark

One conclusion of the foregoing proof is that the relation (1.1) could be replaced with a less restrictive but even harder to control one, which is

$$(2.2) \quad \lim_{n \rightarrow \infty} \sup_{x \in \Phi_n} \|M_n x - Mx\| = 0.$$

where

$$(2.3) \quad \Phi_n := \mathcal{FLX} \{M_n, \Omega_n\}.$$

3 Main result

We start by enumerating the hypothesis we are going to use. So,

- Ω is a bounded subset of X ;
- $M : \overline{\Omega} \rightarrow X$ is an operator;
- X_n is a closed subspace of X ;
- $M_n : \overline{\Omega}_n \subset X_n \rightarrow X_n$ is a compact operator,

for each n .

Next, we denote by $\partial_n \Omega_n$ the boundary of Ω_n on X_n ; the closure operator on X_n is the same as the one on X , but

$$(!) \quad \partial_n \Omega_n \subset \partial \Omega_n,$$

where ∂ signifies the boundary on X .

We also consider that

$$\Phi := \mathcal{FLX} \{M, \overline{\Omega}\}, \Phi_n := \mathcal{FLX} \{M_n, \overline{\Omega}_n\},$$

for each positive integer n ;

$$A := \{n \mid 0 \in (I - M_n) \partial_n \Omega_n\};$$

$$B := \{n \mid n \notin A, \deg_{LS}(I - M_n, \Omega_n, 0) \neq 0\},$$

where \deg_{LS} is the Leray-Schauder topological degree.

3.1 Proposition

As a supplement to our previous hypothesis, let's suppose that

- (i) M is approximable on $\overline{\Omega}$ for the pair (X_n, Y_n) with the operators M_n ;
- (ii) $\mathcal{R}[(I - M)\overline{\Omega}]$ is closed;
- (iii) one of the sets A and B is infinite.

Then,

$$(3.1) \quad \Phi \neq \emptyset.$$

Proof.

It's sufficient to show that

$$(3.2) \quad \Phi_n \neq \emptyset$$

for an infinity of positive integers n .

If A is infinite then the relation

$$x_n = M_n x_n, x_n \in \partial_n \Omega_n \subset \partial \Omega_n \subset \overline{\Omega}$$

remains valid for an infinity of n . Using (1.1) for $D_n = \partial_n \Omega_n$ and the proposition 2.1., the conclusion follows instantly.

If B is infinite then

$$\deg_{LS}(I - M_n, \Omega_n, 0) \neq 0$$

also for an infinity of n , providing all these positive integers for

$$\Phi_n \neq \emptyset.$$

4 Construction

We'll indicate from now on some possibility to construct *approximation operators* M_n . Assuming that there is a countable family of *projectors*

$$\Pi_n : X \rightarrow X, n \in \mathbb{N}^*,$$

with the property of

$$(4.1) \quad \lim_{n \rightarrow \infty} \Pi_n x = x, x \in X,$$

it follows that for some $a > 0$ we have

$$(4.2) \quad \|\Pi_n\| \leq a, n \in \mathbb{N}^*.$$

Let's denote by X_n the *range* of X under Π_n . For a nonvoid subset Ω of X , we consider

$$\Omega_n := \Omega \cap X_n$$

and suppose that Ω_n is nonvoid for each positive integer n .

If

$$(4.3) \quad M : \bar{\Omega} \rightarrow X$$

is a given operator and we consider

$$(4.4) \quad M_n := \Pi_n Mx,$$

then from this **arrangement**,

$$(4.5) \quad \lim_{n \rightarrow \infty} M_n x = Mx, (\forall) x \in \bar{\Omega}.$$

If M has some supplementary properties then the convergence (4.5) is a uniform one on $\bar{\Omega}$ as, for example, in the next

4.1 Proposition

If $M : \overline{\Omega} \subset X \rightarrow X$ is compact then

$$(4.6) \quad \lim_{n \rightarrow \infty} \sup_{x \in \overline{\Omega}} \|M_n x - Mx\| = 0.$$

Proof.

If it weren't for (4.6) there would be an infinity of x_n in $\overline{\Omega}$ with

$$(4.7) \quad \|M_n x - Mx\| \geq \varepsilon_0 > 0$$

or

$$\|(I - \Pi_n) Mx_n\| \geq \varepsilon_0.$$

Due to the compactness of $M\overline{\Omega}_n$, (Mx_n) contains a convergent subsequence with limit point x .

But

$$\|(I - \Pi_n) Mx_n\| \leq \|(I - \Pi_n)(Mx_n - x)\| + \|(I - \Pi_n)x\| \leq (1 + a) \cdot$$

$$\cdot \|Mx_n - x\| + \|(I - \Pi_n)x\|,$$

allowing us to conclude the existence of a **going to 0** subsequence of $((I - \Pi_n) Mx_n)$,

a clear contradiction of (4.7).

4.2 Proposition

Supposing that

- (i) $M : \overline{\Omega} \subset X \rightarrow X$ is a compact operator;
- (ii) Ω_n is an opened subset of ;
- (iii) one of the sets A and B is infinite,

the equation (M) has some solution in $\overline{\Omega}$.

■

The simple fact of Ω_n being an opened subset of X_n does not provide the necessity for Ω to be opened in X . Then the classical degree $\deg_{LS}(I - M, \Omega, 0)$, if for each x in $\partial\Omega$ Mx is different from x , has no **meaning**.

Nevertheless, the converse is true. That is if Ω is opened in X , Ω_n is an opened subset of X_n . The compactness of M also implies the compactness of $M_n : \Omega \rightarrow X$ and of $M_n : \Omega_n \rightarrow X_n$.

If

$$(4.8) \quad x \neq Mx, x \in \partial\Omega,$$

then according to (4.6) it follows that

$$(4.9) \quad x \neq M_n x, x \in \partial\Omega,$$

for each n greater than some n_0 , providing the existence of the degree

$$(4.10) \quad \deg_{LS}(I - M_n, \Omega, 0), n \geq n_0.$$

The assumption (4.8) enable us to state this **well known** relation

$$(4.11) \quad \|x - Mx\| \geq c > 0, x \in \partial\Omega,$$

which, after a classical argumentation, ensure that

$$(4.12) \quad \lim_{n \rightarrow \infty} \deg_{LS}(I - M_n, \Omega, 0) = \deg_{LS}(I - M, \Omega, 0).$$

From the reduction property of the topological degree, it follows that

$$(4.13) \quad \deg_{LS}(I - M_n, \Omega, 0) = \deg_{LS}(I - M_n, \Omega_n, 0).$$

The right member of the preceeding relation is often easier to determine.

5 Examples

In here we'll outline two examples of constructing the *projector* Π_n .

5.1 Example

For $X = \left\{ x : \mathbf{R}^n \rightarrow \mathbf{R}^n \mid x \text{ continuous, } (\exists) \lim_{t \rightarrow \pm\infty} x(t) < \infty \right\}$, with the norm $\|x\| := \sup_{t \in \mathbf{R}} \|x(t)\|_{\mathbf{R}^n}$, Π_n can be defined as

$$(\Pi_n x)(t) = \begin{cases} x(t), & t \in [-n, n] \\ x(n), & t \geq n \\ x(-n), & t \leq -n \end{cases},$$

for each x .

Of course, $\Pi_n : X \rightarrow X$ is a continuous projector which satisfies (4.1).

5.2 Example

Let's consider $X = \{x : \mathbf{R}^n \rightarrow l^1 \mid x \text{ continuous, } x(t + \omega) = x(t), (\forall) t \in \mathbf{R}\}$ with the norm $\|x\| := \sup_{t \in \mathbf{R}} \|x(t)\|_{l^1}$. For every member x of X we denote by $(x_n(t))$, with $x_n : \mathbf{R} \rightarrow \mathbf{R}$, $n \geq 1$, the sequence $x(t)$, $t \in \mathbf{R}$. It's not at all difficult to see that

$$\sum_1^\infty x_n(t)$$

converges absolutely and uniformly on $[0, \omega]$ and so on \mathbf{R} , too. The projector

$\Pi_n : X \rightarrow X$ is introduced by

$$(\Pi_n x)(t) := (x_1(t), \dots, x_n(t), 0, \dots).$$

Then X_n is exactly the space

$$C_\omega^n = \{x : \mathbf{R} \rightarrow \mathbf{R}^n \mid x \text{ continuous, } x(t + \omega) = x(t), (\forall) t \in \mathbf{R}\}.$$

6 Discussions

We'll study the second example in order to show what are the real advantages of this theory.

6.1 Hypothesis

For $\omega > 0$ an arbitrary positive number and l^1 let's consider

$$\rho_n(x) := \sum_{i>n} |x_i|, x \in l^1$$

We remind that

$$C([0, \omega], l^1) := \{x : [0, \omega] \rightarrow l^1 \mid x \text{ continuous}\}.$$

The *continuity* of some $x : [0, \omega] \rightarrow l^1$ implies the uniform convergence of $\sum_{n \geq 1} |x_n(t)|$ allowing us to define the *norm* $\|x\| := \sup_{t \in [0, \omega]} \|x(t)\|_{l^1}$; in which case, $C([0, \omega], l^1)$ becomes a Banach space. We also remind that a subset A of $C([0, \omega], l^1)$ is *relatively compact* if and only if

- a) $\exists (r > 0) \forall (x \in A) \implies (\|x\| \leq r);$
- b) $\forall (\varepsilon > 0) \forall (n > n_0) \forall (x \in A) \implies (\rho_n(x(t)) < \varepsilon);$
- c) $\forall (\varepsilon > 0) \exists (\delta > 0) \forall (t_1, t_2 \in [0, \omega], |t_1 - t_2| < \delta)$

$$\forall (x \in A) \implies (\|x(t_1) - x(t_2)\|_{l^1} < \varepsilon).$$

Let X be a **special** subspace of $C([0, \omega], l^1)$, i.e.

$$X = \{x \in C([0, \omega], l^1) \mid x(0) = x(\omega)\}.$$

Which is, of course, a *one to one* range of the space of the continuous

ω -periodical maps on \mathbf{R} to l^1 . In $C([0, \omega], l^1)$ we define the *projector* Π_n

as

$$(\Pi_n x)(t) := (x_1(t), \dots, x_n(t), 0, \dots)$$

and we also consider the spaces

$$C_n := \Pi_n C([0, \omega], \mathbf{R}^n),$$

$$X_n := \Pi_n X.$$

We are asking ourselves if the differential equation

$$(6.1) \quad x' = f(t, x),$$

where $f : [0, \omega] \times l^1 \rightarrow l^1$ is a continuous function with a *property of periodicity*:

$$f(t + \omega, x) = f(t, x),$$

has or has not some solution in X (the periodical **generalized** solutions of (6.1)).

The problem itself is but the **construction** of a suitable operator T and the **view** of all the periodical solutions of (6.1) as solutions of

$$(6.1') \quad x = Tx.$$

The advanced theory of the topological degree studies such matters in either X or $C([0, \omega], l^1)$.

In fact, we are looking for compact operators T for which $\mathcal{D}(T)$ would be **precisely** the closure of an opened bounded set.

The set

$$\Omega = \left\{ x \in C([0, \omega], l^1) \mid x(t) := (x_i(t)), |x_i(t)| \leq c_i \right\},$$

where $c := (c_i) \in l^1$,

is not opened; nevertheless, its intersection with C_n or X_n is an opened set under the topology induced by the entire space.

Let's consider, on $C([0, \omega], l^1)$, the operator T :

$$(Tx)(t) = x(\omega) + \int_0^t f(s, x(s)) ds.$$

It's obvious the all the solutions of (6.1') are also solutions for (6.1) and conversely. For

$$T_n := \Pi_n T$$

and if, for example, $f := (f_i)$ satisfies a *bounding condition* as

$$|f_i(t, x(t))| \leq \alpha_i \cdot |x_i(t)|,$$

where $(\alpha_i) \in l^1$, then one can easily show that

$$\lim_{n \rightarrow \infty} \sup_{x \in \bar{\Omega}} \|T_n x - Tx\| = 0.$$

Because of the mission condition of *being opened*, Ω doesn't allow a **classical definition** for the topological degree of the operator T on it; however, if

$$x \neq T_n x, x \in \partial_n \left(\Omega \cap C([0, \omega], l^1) \right), (\forall) n \geq 1$$

we can define

$$\deg_{LS}(I - T_n, \Omega \cap C([0, \omega], \mathbf{R}^n), 0)$$

In this particular case ∂_n is the boundary operator on $\Pi_n C([0, \omega], l^1)$.

If the result is not 0, the equation (6.1) has some periodical solution.

We can also apply directly the topological degree theory on X ; the **advantage** is that the space X_n is endowed with an S^1 -action, i.e. a continuous mapping

$$S^1 \times X_n \rightarrow X_n \quad (\tau, x) \mapsto \tau * x$$

compatible with the *group law* (+) :

$$\tau_1 * (\tau_2 * x) = (\tau_1 + \tau_2) * x.$$

for all $\tau_i \in S^1$, $x \in X_n$, which is indeed a continuous representation of S^1

into the *group of isometries* of X_n , defined by

$$(\tau * x)(t) := x(t + \tau).$$

In fact, in the precise situation of an autonomous equation

$$(6.2) \quad x'(t) = g(x(t))$$

we can build an operator such as the solutions of (6.1') are exactly the periodical solutions of (6.2). We define on X the *projector* P as

$$Px := \frac{1}{\omega} \cdot \int_0^{\omega} x(t) dt.$$

Now, (6.2) becomes

$$(6.3) \quad x = Mx,$$

where

$$\begin{aligned} Mx &:= Px + [P + K \cdot (I - P)] Gx, \\ (Kv)(t) &:= \int_0^t v(s) ds - \frac{1}{\omega} \cdot \int_0^{\omega} \left\{ \int_0^t v(s) ds \right\} dt, \\ (Gx)(t) &:= g(x(t)). \end{aligned}$$

Then, let's have

$$\Omega_n := \Omega \cap X_n.$$

If we admit that

$$G_n x = x, \quad (\forall) x \in \partial_n \Omega_n,$$

where

$$G_n := \Pi_n G,$$

it's possible to define the degree

$$d_n := \deg_{LS}(I - G_n, \Omega_n, 0).$$

It one supposes that

$$(6.4) \quad |g_i(x)| \leq a_i |x_i|, \quad g(x) = (g_i(x)), \quad (a_i) \in l^1,$$

then

$$\lim_{n \rightarrow \infty} \sup_{x \in \Omega_n} \|M_n x - Mx\| = 0,$$

where

$$M_n := \Pi_n M.$$

It's easy to notice that $\bar{\Omega}_n$ is invariant and M_n is equivariant under S^1 -action, so

$$\deg_{LS}(I - M_n, \Omega_n, 0) = (-1)^n \cdot \deg_B(g|_{\mathbb{R}^n}, \Omega_n, 0),$$

\deg_B being the Brouwer topological degree (see [2] for details). Finally, for

$$\deg_B(g|_{\mathbb{R}^n}, \Omega_n, 0) \neq 0, n \geq 1$$

the equation (6.2) has some solution in X . Using various kinds of *continuation theorems* one can easily compose existence theorems for (6.1). ■

7 Bibliography

7.1 Zeidler, E

"*Nonlinear Functional Analysis*", 1st volume, Springer, N.Y., 1986.

7.2 Mawhin, J

"*Topological Degree and Boundary Value Problems for Nonlinear Differential Equations*", **Lecture Notes in Math.**, No. 1537, Springer, Berlin, 1993, 74-142.

Weak solutions for the nonlinear one dimensional wave equation in adiabatic case.

S. Birăuș, Șt. Balint, A.M. Balint
West University of Timișoara
Bd. V. Pârvan, Nr. 4, 1900 Timișoara, România

This paper presents a shock-capturing method using Greenberg's results [2]. We consider the nonlinear wave equation $\frac{\partial^2 \chi}{\partial t^2} = \frac{\partial}{\partial x} (p(\frac{\partial \chi}{\partial x}))$ and a related infinite system of differential equations ; we find some solutions for this system and construct weak solutions for the nonlinear wave equation.

References :

- [1] von Neuman, J. - Proposal and analysis of numerical method for the treatment of hydrodynamical shock problems pp. 361-379, Collected Works, vol VI, Pergamon Press, Oxford, 1963.
- [2] J. M. Greenberg - The Shock Generation Problem for a Discrete Gas with Short-Range Repulsive Forces, Comm. on Pure and Appl. Mathematics, vol. XLV, 1125-1139, (1992).

Weak Solutions and Hydrodynamical Shock Generation by Non Linear Oscillations in the case of One Dimensional Non Linear Wave Equation

V. Iordan, Șt. Balint, A.M. Balint
West University of Timișoara
Bd. V. Pârvan No. 4, 1900 Timișoara, România

Abstract

In this paper we generalize the Greenberg's results by [7]. We obtain a weak approximation of the solutions of the nonlinear wave equation, in order to give a numerical treatment of hydrodynamical shock problems. A weak approximation of the solutions of the nonlinear wave equation has been obtained using the nonstationary solutions of the infinite system of ordinary differential equations [9,10,11]. Moreover, we determinate the lines of shock

$x = \frac{2v_0}{\alpha - \lambda + v_0} t$, in the case $\alpha > \lambda + \max_N \{v_0 \cdot I\}$.

1. Introduction

The differential equations of hydrodynamics are a not too complicated type as long as the motion is continuous and isentropic. It is known, that almost all hydrodynamical setups cause a development of discontinuities, so-called shocks. These shocks almost never remain "straight" and as soon as they are "curved" or intersect each other, isentropy ceases.

J. von Neumann studied [1] the problem of hydrodynamical shocks and he considered the infinite system of differential equation

$$\dot{x}_1 = v_1, \quad \frac{1}{N} \dot{v}_1 = \sigma(N(x_2 - x_1)) - \sigma(2Nx_1) \quad (1.1)$$

$$\dot{x}_k = v_k, \quad \frac{1}{N} \dot{v}_k = \sigma(N(x_{k+1} - x_k)) - \sigma(N(x_k - x_{k-1})), \quad k = 2, 3, \dots \quad (1.2)$$

in order to give a weak approximation of the solutions of the nonlinear wave equation:

$$\frac{\partial^2 \chi}{\partial t^2} - \frac{\partial(\sigma(\frac{\partial \chi}{\partial x}))}{\partial x} = 0 \quad (1.3)$$

The infinite system (1.1), (1.2) were obtained by difference method.

J.M. Greenberg in the papers [5], [6], [7], [8] considered the system (1.1), (1.2), in the context of shocks generation for a discrete system of particles

which are in interaction and for the similar problems for the system of particles which shocks like the billiard balls.

In the discrete shocks generation problem we seek a solution to the infinite system of differential equations (1.1), (1.2). In this system $x_k(t)$ and $v_k(t)$ represent the position respective the velocity of the particle k of mass $1/N$, where N is a positive integer. The function $\sigma(N(x_{k+1}-x_k))$ represent the force acting between the particles $k, k+1$ which are supposed so that at the initial moment $t_0 = 0$ the space between particles is $1/N$.

In the paper [11] we constructed nonstationary solutions of the infinite system (1.1), (1.2) for make a weak approximation of the solutions of the nonlinear wave equation (1.3).

In our construction we used the periodic solutions of a system of two nonlinear ordinary differential equations of first order presented in [9]. In our papers [9], [10], [11] we supposed that the function σ satisfies the conditions:

a) $\sigma: (0, +\infty) \rightarrow (-\infty, 0]$ is of class C^1 ;

b) there exist $\lambda \in (0, 1)$ such that $\sigma(\xi) < 0$ for $\xi \in (0, \lambda)$,
 $\sigma(\xi) = 0$ for $\xi \geq \lambda$ and $\lim_{\xi \rightarrow 0^+} \sigma(\xi) = -\infty$;

c) σ is strictly increasing on $(0, \lambda)$;

d) the potential energy $U(\xi) = \int_{\lambda}^{\xi} \sigma(s) ds$ satisfies the condition $\lim_{\xi \rightarrow 0^+} U(\xi) = +\infty$.

Let be $(\xi(t), v(t))$ the solution of the system:

$$\begin{cases} \dot{\xi} = v, \\ \frac{1}{N} \dot{v} = -\sigma(2N\xi) + \sigma(2N(\beta - \xi)) \end{cases} \quad (1.4)$$

($N > 0$ integer, $\beta > 0$ real) which satisfies the initial conditions $\xi(0) = \xi_0$, $\xi_0 \in (0, \lambda/2N)$ and $v(0) = 0$.

Let be $T > 0$ the period of the solution $(\xi(t), v(t))$ and $t_1 > 0, v_0 > 0$ defined by:

$$t_1 = \inf\{t \mid t > 0, \xi(t) = \lambda/2N\}, v_0 = v(t).$$

In paper [11] we showed that a solution of the infinite system (1.1), (1.2) is the family of function $(x_k(t), v_k(t))$, $k=1, 2, \dots$ defined for $t \geq 0$ by the formulas:

$$x_1(t) = \xi(t), v_1(t) = v(t) \quad (1.5)$$

and for $k = 2, 3, \dots$

$$\begin{cases} x_k(t) = (k-1)\beta + \frac{\lambda}{2N} + v_0 \left(\frac{(k-1)T}{2} - t_1 \right) - v_0 t, & \text{for } 0 \leq t \leq \frac{(k-1)T}{2} - t_1 \\ v_k(t) = -v_0 \end{cases} \quad (1.6)$$

and

$$\begin{cases} x_k(t) = (k-1)\beta + \xi \left(t - \frac{(k-1)T}{2} \right) \\ v_k(t) = v \left(t - \frac{(k-1)T}{2} \right) \end{cases}, \quad \text{for } t \geq \frac{(k-1)T}{2} - t_1 \quad (1.7)$$

and satisfies the following initial conditions:

$$\begin{cases} x_1(0) = \xi_0 \in \left(0, \frac{\lambda}{2N}\right), & v_1(0) = 0 \\ x_k(0) = (k-1)\beta + \frac{\lambda}{2N} + v_0 \left(\frac{(k-1)T}{2} - t_1 \right), & v_k(0) = -v_0, \quad k = 2, 3, \dots \end{cases} \quad (1.8)$$

This solution is characterized by translates of a single periodic function. Moreover, we are able to evaluate the continuum limit of this solution; in particular, we obtain the limit motion $X^\infty(x, t)$ as the pointwise limit of the individual trajectories $x_k(t)$ as N tends to infinity along with $x = k/N$ fixed.

2. Weak solutions and hydrodynamical shocks study

For each integer N , we introduce the functions:

$$\chi^N(x, t) = \begin{cases} 2Nx_1(t)x, & 0 \leq x \leq \frac{1}{2N} \\ \text{and for } k = 1, 2, \dots \\ x_k(t) + N(x_{k+1}(t) - x_k(t)) \left(x - \frac{2k-1}{2N} \right), & \frac{2k-1}{2N} \leq x \leq \frac{2k+1}{2N} \end{cases} \quad (2.1)$$

$$\gamma^N(x, t) = \frac{\partial \chi^N}{\partial x}(x, t) = \chi_x^N(x, t) = \begin{cases} 2Nx_1(t), & 0 \leq x \leq \frac{1}{2N} \\ \text{and for } k = 1, 2, \dots \\ N(x_{k+1}(t) - x_k(t)), & \frac{2k-1}{2N} \leq x \leq \frac{2k+1}{2N} \end{cases} \quad (2.2)$$

$$v^N(x, t) = \frac{\partial \chi^N}{\partial t}(x, t) = \chi_t^N(x, t) = \begin{cases} 2Nv_1(t)x, & 0 \leq x \leq \frac{1}{2N} \\ \text{and for } k = 1, 2, \dots \\ v_k(t) + N(v_{k+1}(t) - v_k(t)) \left(x - \frac{2k-1}{2N} \right), & \frac{2k-1}{2N} \leq x \leq \frac{2k+1}{2N} \end{cases} \quad (2.3)$$

and

$$\sigma^N(x, t) = \sigma(\gamma^N(x, t)) = \begin{cases} \sigma(2Nx_1(t)), & 0 \leq x \leq \frac{1}{2N} \\ \text{and for } k = 1, 2, \dots \\ \sigma(N(x_{k+1}(t) - x_k(t))), & \frac{2k-1}{2N} \leq x \leq \frac{2k+1}{2N} \end{cases} \quad (2.4)$$

The numbers $x_k(t)$ and $v_k(t)$ are the particles trajectories and velocities defined in (1.5) - (1.7).

Remark: We first observe that χ_x^N and χ_t^N are weak solutions of

$$\frac{\partial \chi_x^N}{\partial t} - \frac{\partial \chi_t^N}{\partial x} = 0, \quad \text{for } x > 0, t > 0$$

that means

$$\int_a^b [\chi_x^N(x, t_2) - \chi_x^N(x, t_1)] dx = \int_{t_1}^{t_2} [\chi_t^N(b, t) - \chi_t^N(a, t)] dt, \quad (2.5)$$

for all $0 < a < b$ and $0 < t_1 < t_2$.

From (2.2) we have:

$$\begin{aligned} \int_a^b [\chi_x^N(x, t_2) - \chi_x^N(x, t_1)] dx &= \left(\frac{2k+1}{2N} - a \right) N(x_{k+1}(t_2) - x_k(t_2)) - \left(\frac{2k+1}{2N} - a \right) N(x_{k+1}(t_1) - x_k(t_1)) + \\ &+ \frac{1}{N} [x_{k+2}(t_2) - x_{k+1}(t_2) + x_{k+3}(t_2) - x_{k+2}(t_2) + \dots + x_m(t_2) - x_{m-1}(t_2) - x_{k+2}(t_1) + x_{k+3}(t_1) - \\ &- x_{k+2}(t_1) + x_{k+2}(t_1) - \dots - x_m(t_1) + x_{m-1}(t_1)] + \left(b - \frac{2m-1}{2N} \right) N(x_{m+1}(t_2) - x_m(t_2)) - \\ &- \left(b - \frac{2m-1}{2N} \right) N(x_{m+1}(t_1) - x_m(t_1)) = \left(\frac{2k+1}{2N} - a \right) N[x_{k+1}(t_1) - x_k(t_2) - x_{k+1}(t_1) + x_k(t_2)] + \\ &+ x_{k+1}(t_1) - x_{k+1}(t_2) + x_m(t_2) - x_m(t_1) + \left(b - \frac{2m-1}{2N} \right) N[x_{m+1}(t_2) - x_m(t_2) - x_{m+1}(t_1) + x_m(t_1)] \end{aligned}$$

and from (2.3) we have:

$$\begin{aligned} \int_{t_1}^{t_2} [\chi_t^N(b, t) - \chi_t^N(a, t)] dt &= \int_{t_1}^{t_2} \left[v_m(t) + N(v_{m+1}(t) - v_m(t)) \left(b - \frac{2m-1}{2N} \right) - v_k(t) - N(v_{k+1}(t) - v_k(t)) \cdot \right. \\ &\left. \left(a - \frac{2k-1}{2N} \right) \right] dt = x_m(t_2) - x_m(t_1) + N(x_{m+1}(t_2) - x_m(t_2)) \left(b - \frac{2m-1}{2N} \right) - M(x_{m+1}(t_1) - x_m(t_1)) \cdot \\ &\left(b - \frac{2m-1}{2N} \right) - x_k(t_2) + x_k(t_1) - N(x_{k+1}(t_2) - x_k(t_2)) \cdot \left(a - \frac{2k-1}{2N} \right) + N(x_{k+1}(t_1) - x_k(t_1)) \cdot \\ &\left(a - \frac{2k-1}{2N} \right) = x_m(t_2) - x_m(t_1) + N \left(b - \frac{2m-1}{2N} \right) [x_{m+1}(t_2) - x_m(t_2) - x_{m+1}(t_1) + x_m(t_1)] + \\ &+ N \left(\frac{2k+1}{2N} - a \right) [x_{k+1}(t_2) - x_{k+1}(t_1) - x_k(t_2) + x_k(t_1)] - N \cdot \frac{1}{N} [x_{k+1}(t_2) - x_{k+1}(t_1) - x_k(t_2) + x_k(t_1)] - \\ &- x_k(t_2) + x_k(t_1) = x_m(t_2) - x_m(t_1) + N \left(b - \frac{2m-1}{2N} \right) [x_{m+1}(t_2) - x_m(t_2) - x_{m+1}(t_1) + x_m(t_1)] + \\ &+ N \left(\frac{2k+1}{2N} - a \right) [x_{k+1}(t_2) - x_{k+1}(t_1) - x_k(t_2) + x_k(t_1)] \end{aligned}$$

It follows from here that χ_x^N and χ_t^N satisfy the relation (2.5).

Now we show that χ^N converges pointwise to function χ^∞ , for N tends to infinity.

Theorem 1. The sequence $\chi^N(x,t)$ defined for $N>0$ by the formula (2.1) converges pointwise to the function:

$$\chi^\infty(x,t) = \begin{cases} \alpha x - v_0 t, & 0 < t < \frac{\alpha - \lambda_1(v_0)}{2v_0} \cdot x \\ \frac{\alpha + \lambda_1(v_0)}{2} \cdot x, & t \geq \frac{\alpha - \lambda_1(v_0)}{2v_0} \cdot x \end{cases} \quad \text{for } N \rightarrow \infty \quad (2.6)$$

Proof: We will consider the next three situations determined by the solutions $x_k(t)$ of the infinite system (1.1), (1.2) :

$$a) 0 \leq t \leq \frac{(k-1)T}{2} - t_1$$

$$b) t \geq \frac{kT}{2} - t_1$$

$$c) t \in \left[\frac{(k-1)T}{2} - t_1, \frac{kT}{2} - t_1 \right]$$

a) For $0 \leq t \leq \frac{(k-1)T}{2} - t_1$ we have :

$$\begin{aligned} x_{k+1}(t) - x_k(t) &= k\beta + \frac{\lambda}{2N} + v_0 \left(\frac{kT}{2} - t_1 \right) - v_0 t - (k-1)\beta - \frac{\lambda}{2N} - v_0 \left(\frac{(k-1)T}{2} - t_1 \right) + \\ &+ v_0 t = \beta + v_0 \frac{T}{2} \end{aligned}$$

and:

$$\begin{aligned} \chi^N(x,t) &= (k-1)\beta + \frac{\lambda}{2N} + v_0 \left(\frac{(k-1)T}{2} - t_1 \right) - v_0 t + N \left(\beta + v_0 \frac{T}{2} \right) \left(x - \frac{2k-1}{2N} \right) = \\ &= (k-1)\beta + \frac{\lambda}{2N} + v_0 \frac{(k-1)T}{2} - v_0 t_1 - v_0 t + N \left(\beta + v_0 \frac{T}{2} \right) x - N \left(\beta + v_0 \frac{T}{2} \right) \cdot \frac{2k-1}{2N} = \\ &= \frac{\lambda}{2N} - v_0 t + N \left(\beta + v_0 \frac{T}{2} \right) x - \frac{1}{2} \left(\beta + v_0 \frac{T}{2} \right) - v_0 t_1 \end{aligned}$$

b) For $t \geq \frac{kT}{2} - t_1$ we have:

$$x_{k+1}(t) - x_k(t) = k\beta + \xi \left(t - \frac{kT}{2} \right) - (k-1)\beta - \xi \left(t - \frac{(k-1)T}{2} \right) = 2 \left[\beta - \xi \left(t - \frac{(k-1)T}{2} \right) \right]$$

(see [11]).

Therefore we deduce:

$$\begin{aligned}\chi^N(x, t) &= (k-1)\beta + \xi\left(t - \frac{(k-1)T}{2}\right) + 2N\left[\beta - \xi\left(t - \frac{(k-1)T}{2}\right)\right]\left(x - \frac{2k-1}{2N}\right) = (k-1)\beta + \\ &+ \xi\left(t - \frac{(k-1)T}{2}\right) + 2N\beta x - 2N\xi\left(t - \frac{(k-1)T}{2}\right)x - 2N\beta \cdot \frac{2k-1}{2N} + 2N\xi\left(t - \frac{(k-1)T}{2}\right) \cdot \frac{2k-1}{2N} = \\ &= \beta N\left(2x - \frac{k}{N}\right) + 2(k-Nx)\xi\left(t - \frac{(k-1)T}{2}\right)\end{aligned}$$

c) For $t \in \left[\frac{(k-1)T}{2} - t_1, \frac{kT}{2} - t_1\right]$ the solutions are:

$$x_k(t) = (k-1)\beta + \xi\left(t - \frac{(k-1)T}{2}\right) \quad \text{and}$$

$$x_{k+1}(t) = k\beta + \frac{\lambda}{2N} + v_0\left(\frac{kT}{2} - t_1\right) - v_0 t$$

In this way we obtain:

$$\begin{aligned}\chi^N(x, t) &= (k-1)\beta + \xi\left(t - \frac{(k-1)T}{2}\right) + N\left[\beta + \frac{\lambda}{N} + v_0\left(\frac{kT}{2} - t_1\right) - v_0 t - \xi\left(t - \frac{(k-1)T}{2}\right)\right]\left(x - \frac{2k-1}{2N}\right) \\ &= \beta\left(Nx - \frac{1}{2}\right) + v_0 \frac{kT}{2}\left(Nx - \frac{2k-1}{2}\right) + v_0 t\left(-Nx + \frac{2k-1}{2}\right) + \left(\frac{2k+1}{2} - Nx\right)\xi\left(t - \frac{(k-1)T}{2}\right) + \\ &+ \frac{\lambda}{2}\left(x - \frac{k}{N}\right) + v_0 t_1\left(-Nx + \frac{2k-1}{2}\right) + \frac{1}{2} \cdot \frac{\lambda}{2N}\end{aligned}$$

From a), b), c) we obtain:

$$\chi^N(x, t) = \begin{cases} \frac{\lambda}{2N} - v_0 t + N\left(\beta + v_0 \frac{T}{2}\right)x - \frac{1}{2}\left(\beta + v_0 \frac{T}{2}\right) - v_0 t_1, & \text{for } 0 \leq t \leq \frac{(k-1)T}{2} - t_1 \\ \beta\left(Nx - \frac{1}{2}\right) + v_0 t\left(-Nx + \frac{2k-1}{2}\right) + v_0 \frac{kT}{2}\left(Nx - \frac{2k-1}{2}\right) + \left(\frac{2k+1}{2} - Nx\right)\xi\left(t - \frac{(k-1)T}{2}\right) + \\ \quad + \frac{\lambda}{2}\left(x - \frac{k}{N}\right) + \frac{\lambda}{2M} \cdot \frac{1}{2}, & \text{for } \frac{(k-1)T}{2} - t_1 \leq t \leq \frac{kT}{2} - t_1 \\ \beta N\left(2x - \frac{k}{N}\right) + 2(k-Nx)\xi\left(t - \frac{(k-1)T}{2}\right), & \text{for } t \geq \frac{kT}{2} - t_1 \end{cases}$$

The period is :

$$T = \frac{2}{N} \int_{2N\xi_0}^{\lambda} \frac{dp}{\int_{2N\xi_0}^p -\sigma(s)ds} + \frac{2}{v_0}\left(\beta - \frac{\lambda}{N}\right) = \frac{2}{N}I + \frac{2}{v_0}\left(\beta - \frac{\lambda}{N}\right), \quad \text{where } I = \int_{2N\xi_0}^{\lambda} \frac{dp}{\int_{2N\xi_0}^p -\sigma(s)ds}.$$

(see [9]).

We remark that $v_0 I$ is bounded, indeed:

$$v_0 \cdot I = \sqrt{\int_{2N\xi_0}^{\lambda} -\sigma(u)du} \cdot \int_{2N\xi_0}^{\lambda} \frac{dp}{\sqrt{\int_{2N\xi_0}^p -\sigma(s)ds}} \leq \sqrt{-\sigma(2N\xi_0)(\lambda - 2N\xi_0)} \cdot 2M\sqrt{(\lambda - 2N\xi_0)} =$$

$$= 2M(\lambda - 2N\xi_0)\sqrt{-\sigma(2N\xi_0)}, \text{ because}$$

$$v_0^2 = \sqrt{\int_{2N\xi_0}^{\lambda} -\sigma(u)du} \leq \sqrt{\int_{2N\xi_0}^{\lambda} -\sigma(2N\xi_0)du} = \sqrt{-\sigma(2N\xi_0)(\lambda - 2N\xi_0)} \quad \text{and}$$

$$\begin{aligned} \int_{2N\xi_0}^{\lambda} \frac{dp}{\sqrt{\int_{2N\xi_0}^p -\sigma(s)ds}} &= \int_{2N\xi_0}^{\lambda} \frac{dp}{\sqrt{h(p)}} = \\ &= \int_{2N\xi_0}^{\lambda} \frac{dp}{\sqrt{h(2N\xi_0) + h'(2N\xi_0)(p - 2N\xi_0) + h''(2N\xi_0) \cdot (p - 2N\xi_0)^2/2!}} = \\ &= \int_{2N\xi_0}^{\lambda} \frac{1}{\sqrt{\rho - 2N\xi_0}} \cdot \frac{dp}{\sqrt{-\sigma(2N\xi_0) - \sigma'(2N\xi_0) \cdot (p - 2N\xi_0)/2}} \leq M \cdot \int_{2N\xi_0}^{\lambda} \frac{dp}{\sqrt{\rho - 2N\xi_0}} \leq \\ &\leq M\sqrt{\lambda - 2N\xi_0}. \end{aligned}$$

Let be $\alpha > \lambda + \max_N \{v_0 \cdot I\}$, choosing $\beta = \frac{\alpha + \lambda - v_0 \cdot I}{2N}$, we have:

$$\beta + v_0 \frac{T}{2} = \frac{\alpha}{N} \rightarrow 0 \text{ for } N \rightarrow \infty.$$

On the other hand we have $\frac{NT}{2} = \frac{\alpha}{2v_0} - \frac{\lambda - v_0 I}{2v_0}$ which implies:

$$\frac{(k-1)T}{2} - t_1 = \frac{k}{N} \cdot \frac{\alpha + v_0 I - \lambda}{2v_0} - \frac{1}{N} \cdot \frac{\alpha + v_0 I - \lambda}{2v_0} - t_1 \quad \text{and} \quad \frac{kT}{2} - t_1 = \frac{k}{N} \left(\frac{\alpha}{2v_0} + \frac{v_0 I - \lambda}{2v_0} \right) - t_1$$

Consequently for $N \rightarrow \infty$ along with $x = k/N$ fixed we obtain $\lim_{N \rightarrow \infty} \chi^N(x, t) = \chi^\infty(x, t)$,

where

$$\chi^\infty(x, t) = \begin{cases} \alpha x - v_0 t & , \text{ for } 0 < t < \frac{\alpha - \lambda_1(v_0)}{2v_0} x \\ \frac{\alpha + \lambda_1(v_0)}{2} x & , \text{ for } t \geq \frac{\alpha - \lambda_1(v_0)}{2v_0} x, \end{cases} \quad \text{where } \lambda_1(v_0) = \lambda - v_0 I$$

Theorem 2. The derivatives $\chi_t^N = \frac{\partial \chi^N}{\partial t}$ and $\chi_x^N = \frac{\partial \chi^N}{\partial x}$ converge weakly to the functions χ_t^∞ and χ_x^∞ defined in:

$$\chi_t^\infty(x, t) = \begin{cases} -v_0, & 0 < t < \frac{\alpha - \lambda_1(v_0)}{2v_0}x \\ 0, & t \geq \frac{\alpha - \lambda_1(v_0)}{2v_0}x \end{cases} \quad (2.7)$$

and

$$\chi_x^\infty(x, t) = \begin{cases} \alpha, & 0 < t < \frac{\alpha - \lambda_1(v_0)}{2v_0}x \\ \frac{\alpha + \lambda_1(v_0)}{2}, & t \geq \frac{\alpha - \lambda_1(v_0)}{2v_0}x \end{cases} \quad (2.8)$$

Proof: We prove that $\chi_t^N(x, t) \rightarrow \chi_t^\infty(x, t)$ for $N \rightarrow \infty$.

For $t \in \left(0, \frac{(k-1)T}{2} - t_1\right)$, we have $\chi_t^N(x, t) = -v_0 + N(v_0 - v_0)\left(x - \frac{2k-1}{2N}\right) = -v_0$

and for $t \geq \frac{kT}{2} - t_1$, $\chi_t^N(x, t) = v_k(t) + N(v_{k+1}(t) - v_k(t))\left(x - \frac{2k-1}{2N}\right)$. We observe that

for $1 \leq j \leq k$ and $t \geq kT/2 - t_1$,

$$v_{j+1}(t) = v\left(t - \frac{jT}{2}\right), \quad v_j(t) = v\left(t - \frac{(j-1)T}{2}\right) \text{ and } v(t) = -v\left(t - \frac{T}{2}\right) \quad (\text{from [10]}) \text{ and}$$

therefore:

$$v_{j+1}(t) + v_j(t) = v\left(t - \frac{jT}{2}\right) + v\left(t - \frac{(j-1)T}{2}\right) = v\left(t - \frac{jT}{2}\right) - v\left(t - \frac{(j-1)T}{2} - \frac{T}{2}\right) = v\left(t - \frac{jT}{2}\right) - v\left(t - \frac{jT}{2}\right) = 0$$

$$\text{Consequently, } \chi_t^N(x, t) = v_k(t) + N(-v_k(t) - v_k(t))\left(x - \frac{2k-1}{2N}\right) = (2k - 2Nx)v_k(t).$$

For $N \rightarrow \infty$, we have $\chi_t^N(x, t) \rightarrow 0$. In this way we obtain $\chi_t^N \rightarrow \chi_t^\infty$ for $N \rightarrow \infty$ and these prove that formula (2.7) is true.

Than, we prove that $\lim_{N \rightarrow \infty} \chi_x^N(x, t) = \chi_x^\infty(x, t)$.

To observe immediately that for $t \in \left[0, \frac{(k-1)T}{2} - t_1\right]$,

$$\begin{aligned} \chi_x^N(x, t) &= N(x_{k-1}(t) - x_k(t)) = N\left[k\beta + \frac{\lambda}{2N} + v_0\left(\frac{kT}{2} - t_1\right) - v_0t - (k-1)\beta - \frac{\lambda}{2N} - v_0\left(\frac{(k-1)T}{2} - t_1\right) + \right. \\ &\quad \left. + v_0t\right] = N\left[\beta + v_0\frac{T}{2}\right] = N\frac{\alpha}{N} = \alpha \end{aligned}$$

On the other hand, $t \geq kT/2 - t_1$, we have:

$$\begin{aligned}
\chi_x^N(x, t) &= N(x_{k+1}(t) - x_k(t)) = N \left[k\beta + \xi \left(t - \frac{kT}{2} \right) - (k-1)\beta - \xi \left(t - \frac{(k-1)T}{2} \right) \right] = \\
&= N \left[\beta + \xi \left(t - \frac{kT}{2} \right) - \xi \left(t - \frac{kT}{2} + \frac{T}{2} \right) \right] = N \left[\beta + \xi \left(t - \frac{kT}{2} \right) - \xi \left(t - \frac{kT}{2} \right) \right] = \\
&= N\beta = \frac{\alpha + \lambda - v_0 I}{2} = \frac{\alpha + \lambda_1(v_0)}{2}
\end{aligned}$$

These prove that the relation (2.8) is satisfied.

From relation (2.5) we deduce that χ_t^∞ and χ_x^∞ are weak solutions of

$$\frac{\partial \chi_x^\infty}{\partial t} = \frac{\partial \chi_t^\infty}{\partial x}; \text{ because}$$

$$\lim_{N \rightarrow \infty} \int_a^b \left(\frac{\partial \chi_x^N}{\partial t}(x, t_2) - \frac{\partial \chi_x^N}{\partial t}(x, t_1) \right) dx = \lim_{N \rightarrow \infty} \int_{t_1}^{t_2} \left(\frac{\partial \chi_t^N}{\partial x}(b, t) - \frac{\partial \chi_t^N}{\partial x}(a, t) \right) dt$$

and consequently:

$$\int_a^b \left(\frac{\partial \chi_x^\infty}{\partial t}(x, t_2) - \frac{\partial \chi_x^\infty}{\partial t}(x, t_1) \right) dx = \int_{t_1}^{t_2} \left(\frac{\partial \chi_t^\infty}{\partial x}(b, t) - \frac{\partial \chi_t^\infty}{\partial x}(a, t) \right) dt.$$

Moreover, they satisfy the Rankine-Hugoniot relation:

$$\frac{2v_0}{\alpha - \lambda_1(v_0)} (\chi_x^\infty - \chi_{x-}^\infty) + (\chi_t^\infty - \chi_{t-}^\infty) = 0 \text{ across the shock wave } x = \frac{2v_0}{\alpha - \lambda_1(v_0)} t.$$

Theorem 3. The sequence $\sigma^N(x, t)$ defined by $N > 0$ by the formula (2.4) has a weak limit.

Proof: Equations (1.6), (1.7) and the relation (2.4) imply that $\sigma^N \equiv 0$ in $x \geq \frac{2v_0}{\alpha - \lambda_1(v_0)} t + \frac{1}{N}$ and this guarantees that they converge pointwise to $\sigma^\infty \equiv 0$ in

$x \geq \frac{2v_0}{\alpha - \lambda_1(v_0)} t$. In the region $0 < x < \frac{2v_0}{\alpha - \lambda_1(v_0)} t + \frac{1}{N}$ we know that $\sigma(\xi_1(v_0)) \leq$

$\gamma^N \leq 0$ independently of N . Because $x_k(t)$ and $v_k(t)$ satisfy the infinite system (1.1), (1.2) and using (2.3) and (2.4) we have (for all $0 < a < b$ and $0 < t_1 < t_2$):

$$\int_a^b (\chi_t^N(x, t_2) - \chi_t^N(x, t_1)) dx = \frac{\chi_t^N(a, t_2) + v_{k+1}(t_2)}{2} \left(\frac{2k+1}{2N} - a \right) + \frac{1}{2N} (v_{k+1}(t_2) + v_{k+2}(t_2)) + \dots +$$

$$+ \frac{1}{2N} (v_{m-2}(t_2) + v_{m-1}(t_2)) + \frac{v_m(t_2) + \chi_t^N(t_2)}{2} \left(b - \frac{2m-1}{2N} \right) - \frac{\chi_t^N(a, t_1) + v_{k+1}(t_1)}{2} \left(\frac{2k+1}{2N} - a \right) -$$

$$- \frac{1}{2} (v_{k+1}(t_1) + v_{k+2}(t_1)) - \dots - \frac{1}{2N} (v_{m-2}(t_1) + v_{m-1}(t_1)) - \frac{v_m(t_1) + \chi_t^N(t_1)}{2} \left(b - \frac{2m-1}{2N} \right)$$

and

$$\int_{t_1}^{t_2} [\sigma(\chi_x^N(b, t)) - \sigma(\chi_x^N(b, t_1))] dt = \int_{t_1}^{t_2} [\sigma(N(x_{m+1}(t) - x_{m+1}(t))) - \sigma(N(x_{k+1}(t) - x_k(t)))] dt =$$

$$= \int_{t_1}^{t_2} [\sigma(N(x_{m+1}(t) - x_{m+1}(t))) - \sigma(N(x_m(t) - x_{m-1}(t))) + \sigma(N(x_m(t) - x_{m-1}(t))) -$$

$$+ \dots + \sigma(N(x_{k+2}(t) - x_{k+1}(t))) - \sigma(N(x_{k+1}(t) - x_k(t)))] dt = \int_{t_1}^{t_2} \left[\frac{1}{N} \dot{v}_{k+1}(t) + \frac{1}{N} \dot{v}_{k+2}(t) + \dots + \frac{1}{N} \dot{v}_m(t) \right] dt =$$

$$= \frac{1}{N} [v_{k+1}(t_2) - v_{k+1}(t_1) + v_{k+2}(t_2) - v_{k+1}(t_2) + \dots + v_m(t_2) - v_m(t_1)]$$

From these relations, we obtain:

$$\left| \int_a^b (\chi_x^N(x, t_2) - \chi_x^N(x, t_1)) dx - \int_{t_1}^{t_2} (\sigma^N(b, t_2) - \sigma^N(b, t_1)) dt \right| = \left| \frac{\chi_t^N(a, t_2) - \chi_t^N(a, t_1) + v_{k+1}(t_2) - v_{k+1}(t_1)}{2} \right.$$

$$\left. \left(\frac{2k+1}{2N} - a \right) + \frac{v_m(t_2) - v_m(t_1) + \chi_t^N(t_2) - \chi_t^N(t_1)}{2} \left(b - \frac{2m-1}{2N} \right) - \frac{1}{2N} v_{k+1}(t_2) + \frac{1}{2N} v_{k+1}(t_1) - \right.$$

$$\left. - \frac{1}{2N} v_m(t_1) + \frac{1}{2N} v_m(t_2) \right| \leq 6M \cdot \frac{1}{N}$$

where M is independent of N (because $v_k(t) = v(t - kT/2)$ is continue and periodic, so it is bounded).

If we now let $t_2 = \frac{\alpha - \lambda_1(v_0)}{2v_0} \cdot b$ and $t_1 = \frac{\alpha - \lambda_1(v_0)}{2v_0} \cdot a$ and exploit the limit

relations:

$$\lim_{N \rightarrow \infty} \int_a^b \chi_t^N \left(x, \frac{\alpha - \lambda_1(v_0)}{2v_0} \cdot a \right) dx = -(b-a)v_0,$$

$$\lim_{N \rightarrow \infty} \int_a^b \chi_t^N \left(x, \frac{\alpha - \lambda_1(v_0)}{2v_0} \cdot b \right) dx = 0, \quad \text{and}$$

$$\lim_{N \rightarrow \infty} \int_{\frac{\alpha - \lambda_1(v_0)}{2v_0} a}^{\frac{\alpha - \lambda_1(v_0)}{2v_0} b} \sigma^{(N)}(b, t) dt = 0$$

we find that (2.9) implies that for all $0 < a < b$

$$\lim_{N \rightarrow \infty} \int_{\frac{\alpha - \lambda_1(v_0)}{2v_0} a}^{\frac{\alpha - \lambda_1(v_0)}{2v_0} b} \sigma^N(a, t) dt = -(b - a)v_0.$$

The last relation guarantees that σ^N converge weakly to the constant function

$$\sigma^\infty = -\frac{2v_0^2}{\alpha - \lambda_1(v_0)} \text{ in } 0 < x < \frac{2v_0 t}{\alpha - \lambda_1(v_0)}$$

The above construction also implies that the pair

$$v^\infty(x, t) = \begin{cases} -v_0 & , 0 < t < \frac{\alpha - \lambda_1(v_0)}{2v_0} x \\ 0 & , t \geq \frac{\alpha - \lambda_1(v_0)}{2v_0} x \end{cases} \quad (2.10)$$

and

$$\sigma^\infty(x, t) = \begin{cases} -\frac{2v_0}{\alpha - \lambda_1(v_0)} & , 0 < x < \frac{\alpha - \lambda_1(v_0)}{2v_0} t \\ 0 & , x \geq \frac{\alpha - \lambda_1(v_0)}{2v_0} t \end{cases} \quad (2.11)$$

is a weak solution of

$$\frac{\partial \chi_x^\infty}{\partial t} - \frac{\partial \sigma^\infty}{\partial x} = 0 \quad \text{in } x > 0 \text{ and } t > 0 \text{ and satisfies the Rankine-Hugoniot equation}$$

$$\frac{2v_0}{(\alpha - \lambda_1(v_0))} (v_-^\infty - v_+^\infty) + (\sigma_-^\infty - \sigma_+^\infty) = 0 \quad \text{across the shock wave } x = \frac{2v_0}{\alpha - \lambda_1(v_0)} t.$$

It results that the continuum limit of solution (1.5) - (1.7) with the initial conditions (1.8) can be evaluate and the limit motion is the pointwise limit of the individual trajectories $x_k(t)$ for $N \rightarrow \infty$ along with $x = k/N$ fixed.

References

- [1] von Neumann I., Proposal and analysis of a numerical method for the treatment of hydrodynamical shock problems pp. 361-379 in *Collected Works*, vol. VI, Pergamonn, Oxford, 1963
- [2] Lax,P.D., On dispersive difference schemes, *Physica D*, 1986 pp. 250-254.
- [3] Lax,P.D., The zero dispersion limit, A deterministic analogue of turbulence, *Comm. Pure. Appl. Math.* 44,1991, pp.1047-1056.
- [4] Hou,T.Y., and Lax,P.D., Dispersive approximations in fluid dynamics. *Comm. Pure. Appl. Math.* 44,1991, pp.1-40.
- [5] Greenberg, I.M. and Hedstrom,G , A note on a model for the quasilinear wave equation, *Arch. Rat. Mech. Anal.* 40,1971, pp.160-165.
- [6] Greenberg, I.M., Continuum limits of discrete gases, *Arch. Rat. Mech. Anal.* 105,1989,pp.367-376.
- [7] Greenberg, I.M., The Shock Generation Problem for a Discrete Gas with Short-Range Repulsive Forces. *Comm. Pure. Appl. Math.* 45,1992, pp.1125-1139.
- [8] Greenberg, I.M., Continuum limits of discrete gases II, I.M. A Springer Monograph on Shock Induced Transitions and Phase Structure in General Media, Springer-Verlag
- [9] Balint,St.,Balint,A.M.,Baltean, D.G., Jadaneant,I., Iordan,V., Hydrodynamical shock problems and nonlinear oscillations (I)
- [10] Balint,St.,Balint,A.M.,Baltean, D.G , Iordan,V., Hydrodynamical shock problems and nonlinear oscillations (II)
- [11] Balint,St.,Balint,A.M.,Baltean, D.G , Iordan,V., Hydrodynamical shock problems and nonlinear oscillations (III)

The heat and mass transport by convection and diffusion during quartz crystal growth by hydrothermal system

Șt. Balint, A.M. Balint, D. Bălțean, A. Neculae
Univ. of the West Timișoara,
Blv. V. Pârvan no.4, 1900 Timișoara, Romania

Abstract

In this paper we give a short description of the physical model of the quartz crystal growth by the hydrothermal system. This is followed by a presentation of the mathematical model of the system, including equations governing the process. Because this model don't describe the solute (quartz) field, we continue by a solute field analysis proposal. In order to make this analysis, we make two kind of hypothesis concerning the neighbourhood of the growth interface, which is a thin region, but not a mathematical surface. The first hypothesis is that in this region there is already a "periodic" structure formed by microcells, like in crystal and the dispersion mechanism of the solute is due also to convection of solute by the microscopic velocity field in these microcells. The second hypothesis is that this region is like a bed of randomly distributed spheres and the dispersion mechanism of solute is due also to convection of the solute by the random velocity field generated at the microscale by the randomly distributed inclusions. In both situations we obtain a new effective convective-diffusive equation for this region. For realize this we used the method of homogenization, that is a multiple scale analysis in terms of a small ratio ε between the characteristic micro and macroscales.

1 The physical model of the quartz crystal growth by hydrothermal system

The schematic of the system is presented in fig. 1.

The system consists of two isothermal zones separated by a gradient region.

Typical values of temperatures for isothermal zones are: $T_h \approx 400^\circ\text{C}$, $T_c \approx 350^\circ\text{C}$.

In the gradient region the temperature decreases linearly.

The top of the autoclave is assumed to be adiabatic.

The solvent is water and the autoclave is filled 80 – 85%.

In steady state the pressure in the autoclave is $\bar{p} \approx 1500 \cdot 10^5 \text{ N/m}^2$ and in this way the solubility condition of the polycrystalline quartz in water is assured. The gravitational

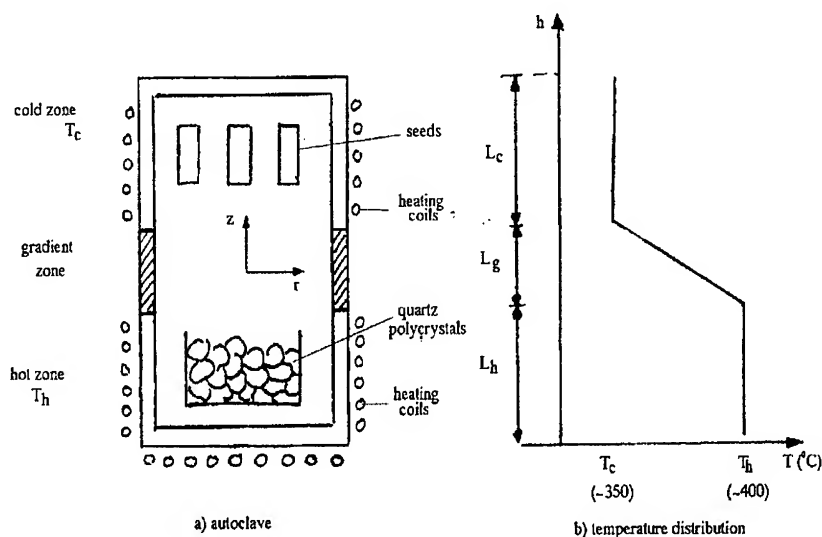


Figure 1: Schematic of crystal growth by hydrothermal system

acceleration is considered orthogonal to the growth direction (to the autoclave generator). The solution contains 2 – 5% of quartz and its (p,T) diagram is similar to the pure water (p,T) diagram which shows that in the above conditions only the liquid phase exists in the autoclave.

It is assumed that in the hot zone there is sufficiently polycrystalline quartz and the ratio between its surfaces and the seeds surfaces is sufficiently large for assuring the saturation value of the average concentration of the solute in the hot zone and cold zone.

The quartz is transported by convection and diffusion from the hot zone into the cold zone, where the solution becomes oversaturated and the quartz crystallizes on the surfaces of the seeds.

2 Mathematical model for quartz crystal growth by hydrothermal system. Equations governing the process.

The equations used for describing mass and heat transport in quartz crystal growth by the above presented hydrothermal system are the following:

$$(1) \quad \frac{\partial \bar{u}}{\partial t} + (\bar{u} \nabla) \bar{u} = -\nabla p + \nabla^2 \bar{u} - \frac{R_a}{P_r} \theta \bar{e}_z$$

the non-dimensional transient momentum equations in the solution

$$(2) \quad \frac{\partial \theta}{\partial t} + \bar{u} \nabla \theta = \frac{1}{Pr} \nabla^2 \theta$$

the non-dimensional energy equation in the solution

$$(3) \quad \nabla \bar{u} = 0$$

the non-dimensional mass continuity equation in the solution

The list of symbols used in these equations:

\bar{u} - non-dimensional velocity vector ($= \bar{v}r/\nu$)

\bar{v} - velocity vector

r - radius of the autoclave

\bar{R} - position vector

$\frac{\bar{R}}{r}$ - non-dimensional space variable

ν - kinematic viscosity

t - non-dimensional time ($= \tau\nu/r^2$)

τ - time

p - non-dimensional pressure ($= \bar{p}r^2/(\rho\nu^2)$)

\bar{p} - pressure

ρ - density of the solution

R_a - Rayleigh number ($= g\beta(T_h - T_c)r^3/\nu\alpha$)

g - gravitational acceleration

β - thermal expansion coefficient

T_h - hot temperature

T_c - cold zone temperature

α - thermal diffusivity

Pr - Prandtl number ($= \nu/\alpha$)

θ - non-dimensional temperature ($= (T - T_c)/(T_h - T_c)$)

\bar{e}_z - unit vector parallel to gravitational acceleration

Solutions of equations 1 to 3 requires simultaneous calculations of the velocity field \bar{u} and the temperature field θ in the solution.

For the steady state we can use the following methodology:

The value of the temperature θ on the walls of the autoclave will be used like boundary condition for finding the stationary solution $\theta^{(1)}$ of the non-dimensional energy equation 2 in which at this step we neglect \bar{u} .

Whith the above obtained temperature distribution in the solution $\theta^{(1)}$ we find a stationary solution $\bar{u}^{(1)}$ of the equation 1,3 corresponding to the boundary condition $\bar{u}^{(1)}|_{\partial} = 0$.

Using the velocity field $\bar{u}^{(1)}$ we find a stationary solution $\theta^{(2)}$ of equation 2 corresponding to the same boundary condition like $\theta^{(1)}$. With $\theta^{(2)}$ we find a stationary solution $\bar{u}^{(2)}$ of the equation 1,3 corresponding to the boundary conditions $\bar{u}^{(2)}|_{\partial} = 0$. With $\bar{u}^{(2)}$ we find $\theta^{(3)}$ and with $\theta^{(3)}$ we find $\bar{u}^{(3)}$. We stop this iterative process when $\bar{u}^{(i)}$, $\theta^{(i)}$ satisfies with sufficient accuracy equations 1,2 and 3.

Note that we solve the energy equation in the region A defined by the inner walls of the autoclave, the transient momentum equation and the mass continuity equation in the region A-S where S is the region occupied by the seeds and ∂ is the boundary of A-S.

The transport equation can be solved using Nekton solver. This solver is based on a spectral element technique which decomposes the flow domain in standard finite element fashion and expands the primitive variables using high-order Chebyshev polynomials. The convective and buoyancy terms are treated explicitly using a third-order Adams-Bashforth method and the diffusive terms are treated implicitly with a second order Crank-Nicolson scheme.

Solute field analysis in this model is not considered. This requires dynamic description of the growth process from the initial to final stage, including dynamic description of the quartz concentration.

3 A first step for the quartz field analysis proposal.

An analysis of the solute field in the context of quartz crystal growth by hydrothermal system is justified by the fact that the unequal repartitioning of the quartz influences the quality of the quartz crystal. The convection, the value of the diffusivity influence the repartitioning of the quartz. The unavoidable temperature gradients generate buoyancy driving forces (convection) which result in only nearly complete mixing [1].

A way to obtain uniform repartitioning could be to compute the evolution in time of the quartz concentration for given thermal conditions and to find from here how they influence the quality of the quartz crystal and in what way these conditions must be modified (generating control functions) in order to have the desired uniform distribution of the quartz at least in the neighbourhood of the crystallization surfaces. In this way we hope to assure the quality of the grown quartz crystal. This method requires dynamic description of the growth process from initial to final stages, inclusively dynamic description of the quartz concentration and solubilization. In order to make such a description in a first stage we complete the system of equations 1-3 with the convective-diffusive equation of the quartz concentration:

$$(4) \quad \frac{\partial c}{\partial \tau} + \bar{v} \cdot \nabla c = D(\nabla^2 c + \frac{k_T}{T} \nabla^2 T)$$

where c is the quartz concentration, \bar{v} is the velocity field given by eq.1, D is the diffusion coefficient of dopant, $k_T D$ is the thermodiffusion coefficient, T is the temperature given by eq.2. The constant k_T is called the thermodiffusion ratio and we can neglect it for small concentrations (see [2]).

At this stage we ignore the dynamic of the solubilization assuming that the average of the concentration in the hot zone respectively in the cold zone is equal to the saturation concentration corresponding to the hot respectively cold temperature.

The equation 4 describes with accuracy the evolution of the quartz concentration in the hot zone and in the cold zone, far from the crystallization surfaces. In the cold zone close to the crystallization surface this equation must be improved because the growth surface is not a mathematical surface. The growth surface is in fact a thin region which has one of the following characteristics:

1. There is already a "periodic" structure, formed by microcells, like in crystal and the dispersion mechanism of the quartz is due also to convection of quartz by the microscopic velocity field in these microcells.

2. This region is like a bed of randomly distributed fixed "spheres" and the dispersion mechanism of quartz is due also to convection of the quartz by the random velocity field generated at the microscale by the randomly distributed inclusions.

In both situations we must establish a new effective convective-diffusive equation for this region.

In order to deduce the new macroscopic convective-diffusive equation in the neighbourhood of the growth interface we use the method of homogenization, that is a multiple-scale perturbative analysis in terms of the small ratio ε between the characteristic micro and macro length scales. The method was first proposed in 1978 by Bensoussan, Lions and Papanicolau in [3]. Later it was extended in a series of books and articles ([4-12]).

In this method the dependent variables of the problem is assumed to be expressible as a regular expansion in terms of a small parameter ε equal to the ratio of the microscale to macroscale characteristic lengths. Finally the macroscopic equation, which is satisfied by the leading-order term of that expansion, is expected to arise naturally from the ensuring regular perturbation analysis.

4 The macroscopic (effective) convective-diffusive equation of quartz when we modeling the thin region in the neighbourhood of the growth interface by a spatial periodical structure.

For small concentrations, the microscopic convective-diffusive equation of the quartz is

$$(5) \quad \frac{\partial c}{\partial \tau} + \bar{v} \nabla c = D \nabla^2 c$$

with the boundary condition

$$(6) \quad \bar{n} \nabla c = 0 \quad \text{on} \quad \partial \omega$$

Here $\bar{v} = \bar{v}(\bar{y})$ is the fluid velocity in a cell Ω and is taken periodic in \bar{y} , D is the diffusion coefficient, ω denotes the "solid" part in the cell Ω , $\partial \omega$ denotes the boundary of the solid part and \bar{n} indicates a unit vector normal to $\partial \omega$, $\Omega' = \Omega - \omega$.

We consider the two length scales l and L corresponding to the cell size (i.e. the period of the structure) and the size of the region in question, respectively. Assume that $\varepsilon = l/L \ll 1$. Now we introduce the following hierarchy of time scales

$$(7) \quad \tau_1 = \frac{l}{V_0}, \quad \tau_2 = \frac{l^2}{D}, \quad \tau_3 = \frac{L}{V_0}, \quad \tau_4 = \frac{L^2}{D}$$

where V_0 is the characteristic value of the velocity field.

There are two related non-dimensional numbers which appear here - the local and global

Peclet numbers:

$$(8) \quad Pe_l = \frac{\tau_2}{\tau_1} = \frac{LV_0}{D}, \quad Pe_g = \frac{\tau_4}{\tau_3} = \frac{LV_0}{D} = \frac{1}{\varepsilon} Pe_l$$

representing the ratio between convection and diffusion locally and globally, respectively.

We assume that convection and diffusion balance each other at the microscale, that means $Pe_l = O(1)$. In this case, $Pe_g = O(\varepsilon^{-1})$, what means that convection dominates diffusion at the macroscale.

We note by \bar{R} the macroscopic position vector, with $|\bar{R}| = O(L)$. Scaling the space variables according to

$$(9) \quad \bar{x} = \frac{\bar{R}}{L}$$

we introduce the corresponding microscopic variables

$$(10) \quad \bar{y} = \frac{\bar{R}}{l} = \frac{\bar{x}}{\varepsilon}$$

Now we introduce the following three time scales:

$$(11) \quad t = \frac{\tau}{\tau_2}, \quad T_1 = \frac{\tau}{\tau_3}, \quad T_2 = \frac{\tau}{\tau_4}$$

Assume that the effective concentration c depends on $\varepsilon, \bar{x}, \bar{y}, t, T_1, T_2$ and can be expanded as follows:

$$(12) \quad c(\varepsilon, \bar{x}, \bar{y}, t, T_1, T_2) = \sum_{n=0}^{\infty} \varepsilon^n c_n(\bar{x}, \bar{y}, t, T_1, T_2)$$

The dependence on \bar{y} will be assumed periodic and we assume that $\int_{\Omega'} c_n d\bar{y} = 0$, for $n=1,2,\dots$

For the time derivatives formulas 11 give:

$$(13) \quad \frac{\partial}{\partial \tau} = \frac{D}{L^2} \left(\frac{\partial}{\partial T_2} + Pe_l \varepsilon^{-1} \frac{\partial}{\partial T_1} + \varepsilon^{-2} \frac{\partial}{\partial t} \right)$$

and for the space derivatives formulas 9 and 10 give:

$$(14) \quad \nabla_{\bar{R}} = \frac{1}{L} \left(\nabla_{\bar{x}} + \frac{1}{\varepsilon} \nabla_{\bar{y}} \right), \quad \nabla_{\bar{R}}^2 = \frac{1}{L^2} \left(\nabla_{\bar{x}}^2 + \frac{2}{\varepsilon} \nabla_{\bar{x}} \nabla_{\bar{y}} + \frac{1}{\varepsilon^2} \nabla_{\bar{y}}^2 \right)$$

Substituting 12 in 5, using 13, 14 and collecting equal powers of ε on gets:

$$(15) \quad \begin{cases} \Delta_{\bar{y}} c_0 - \bar{u} \nabla_{\bar{y}} c_0 - \frac{\partial c_0}{\partial t} = 0 \\ \bar{n} \nabla_{\bar{y}} c_0 = 0 \quad \text{on} \quad \partial \omega \end{cases} \quad \text{for} \quad O(\varepsilon^{-2})$$

$$(16) \quad \begin{cases} \Delta_{\bar{y}} c_1 - \bar{u} \nabla_{\bar{y}} c_1 - \frac{\partial c_1}{\partial t} = \bar{u} \nabla_{\bar{x}} c_0 - 2 \nabla_{\bar{x}} \nabla_{\bar{y}} c_0 + Pe_l \frac{\partial c_0}{\partial T_1} \\ \bar{n} \nabla_{\bar{y}} c_1 + \bar{n} \nabla_{\bar{x}} c_0 = 0 \quad \text{on} \quad \partial \omega \end{cases} \quad \text{for} \quad O(\varepsilon^{-1})$$

$$(17) \begin{cases} \Delta_{\bar{y}} c_2 - \bar{u} \nabla_{\bar{y}} c_2 - \frac{\partial c_2}{\partial t} = \bar{u} \nabla_{\bar{x}} c_1 - 2 \nabla_{\bar{x}} \nabla_{\bar{y}} c_1 + P e_l \frac{\partial c_1}{\partial T_1} - \nabla_{\bar{x}}^2 c_0 + \frac{\partial c_0}{\partial T_2} \\ \bar{n} \nabla_{\bar{y}} c_2 + \bar{n} \nabla_{\bar{x}} c_1 = 0 \quad \text{on } \partial \omega \end{cases} \quad \text{for } O(1)$$

where we have put

$$(18) \quad \bar{u} = P e_l \frac{\bar{v}}{V_0}$$

A function $c_0 = c_0(\bar{x}, T_1, T_2)$ satisfies 15. For such a solution of 15 equation 16 becomes

$$(19) \quad \begin{cases} \Delta_{\bar{y}} c_1 - \bar{u} \nabla_{\bar{y}} c_1 - \frac{\partial c_1}{\partial t} = \bar{u} \nabla_{\bar{x}} c_0 + P e_l \frac{\partial c_0}{\partial T_1} \\ \bar{n} \nabla_{\bar{y}} c_1 + \bar{n} \nabla_{\bar{x}} c_0 = 0 \quad \text{on } \partial \omega \end{cases}$$

The solvability condition for 19 gives

$$(20) \quad P e_l \frac{\partial c_0}{\partial T_1} = - \langle \bar{u} \rangle \nabla_{\bar{x}} c_0$$

where we have put

$$(21) \quad \langle \bar{u} \rangle = \frac{1}{|\Omega'|} \int_{\Omega'} \bar{u}(\bar{y}) d\bar{y}$$

For the equation 19 we look for a solution of the form

$$(22) \quad c_1(\bar{x}, \bar{y}, t, T_1, T_2) = \bar{\chi}(\bar{y}, t) \nabla_{\bar{x}} c_0(\bar{x}, T_1, T_2)$$

Substitutioning 22 in 19 we find:

$$(23) \quad \begin{cases} \frac{\partial \bar{\chi}}{\partial t} + (\bar{u} \nabla_{\bar{y}}) \bar{\chi} - \Delta_{\bar{y}} \bar{\chi} = \langle \bar{u} \rangle - \bar{u} \\ (\bar{n} \nabla_{\bar{y}}) \bar{\chi} = -\bar{n} \end{cases}$$

The problem 23 has an unique stationary solution $\bar{\chi} = \bar{\chi}(\bar{y})$ which is periodic and satisfies $\langle \bar{\chi} \rangle = \frac{1}{|\Omega'|} \int_{\Omega'} \bar{\chi}(\bar{y}) d\bar{y} = 0$. We consider this function $\bar{\chi} = \bar{\chi}(\bar{y})$ and $c_1 = \bar{\chi} \nabla_{\bar{x}} c_0$.

Substituting in 17 we find

$$(24) \quad \begin{cases} \Delta_{\bar{y}} c_2 - \bar{u} \nabla_{\bar{y}} c_2 - \frac{\partial c_2}{\partial t} = \bar{u} \nabla_{\bar{x}} (\bar{\chi} \nabla_{\bar{x}} c_0) - 2 \nabla_{\bar{x}} \nabla_{\bar{y}} (\bar{\chi} \nabla_{\bar{x}} c_0) + P e_l \frac{\partial c_1}{\partial T_1} - \Delta_{\bar{x}} c_0 + \frac{\partial c_0}{\partial T_2} \\ \bar{n} \nabla_{\bar{y}} c_2 = -\bar{n} \nabla_{\bar{x}} c_1 \end{cases}$$

The solvability condition of the equation 24 gives:

$$(25) \quad \frac{\partial c_0}{\partial T_2} = \sum_{i=1}^3 \sum_{j=1}^3 \left(\delta_{ij} - \frac{1}{|\Omega'|} \int_{\Omega'} \chi_j u_i d\bar{y} + \frac{2}{|\Omega'|} \int_{\Omega'} \frac{\partial \chi_j}{\partial y_i} d\bar{y} - \frac{1}{|\Omega'|} \int_{\partial \omega} n_i \chi_j d\sigma \right) \frac{\partial^2 c_0}{\partial x_i \partial x_j}$$

or

$$(26) \quad \frac{\partial c_0}{\partial T_2} = \left[I - \langle \bar{\chi} \bar{u} \rangle + 2 \langle \nabla \bar{\chi} \rangle - \frac{1}{|\Omega'|} \int_{\partial \omega} \bar{n} \bar{\chi} d\sigma \right] \nabla_{\bar{x}} \nabla_{\bar{x}} c_0$$

Substituting $c_0 = c_0(\bar{x}, T_1, T_2)$ in 13 and using 20, 26 we find that c_0 satisfies the equation

$$(27) \quad \frac{\partial c_0}{\partial \tau} + \langle \bar{v} \rangle \cdot \nabla_R c_0 = D \left[I - \langle \bar{\chi} \bar{u} \rangle + 2 \langle \nabla \bar{\chi} \rangle - \frac{1}{|\Omega'|} \int_{\partial \omega} \bar{n} \bar{\chi} d\sigma \right] \nabla_R \nabla_R c_0$$

This is the macroscopic convective-diffusive equation of the quartz in the neighbourhood of the crystallization front.

The quantity defined by

$$(28) \quad D^* = D \left[I - \langle \bar{\chi} \bar{u} \rangle + 2 \langle \nabla \bar{\chi} \rangle - \frac{1}{|\Omega'|} \int_{\partial \omega} \bar{n} \bar{\chi} d\sigma \right]$$

is the diffusivity tensor of the quartz in this region.

The expression of the effective diffusivity tensor for periodic porous media was subject of several papers, see for example [10], [12].

For the case of spatially periodic porous media a formula was first obtained by Brenner in [13]. Brenner considers that only the symmetric part of D^* enters in the macroscopic equation 27.

In order to find the symmetric part we consider D_{ij} from 25

$$(29) \quad D_{ij} = D \left[\delta_{ij} - \frac{1}{|\Omega'|} \int_{\Omega'} \chi_i u_j d\bar{y} + \frac{2}{|\Omega'|} \int_{\Omega'} \frac{\partial \chi_i}{\partial y_j} d\bar{y} - \frac{1}{|\Omega'|} \int_{\partial \omega} \chi_i n_j d\sigma \right]$$

and using Gauss formula we find

$$(30) \quad D_{ij} = D \left[\delta_{ij} - \frac{1}{|\Omega'|} \int_{\Omega'} \chi_i u_j d\bar{y} + \frac{1}{|\Omega'|} \int_{\Omega'} \frac{\partial \chi_i}{\partial y_j} d\bar{y} \right]$$

The symmetric part \tilde{D}_{ij} is given by

$$(31) \quad \tilde{D}_{ij} = D \left[\delta_{ij} - \frac{1}{|\Omega'|} \frac{1}{2} \int_{\Omega'} (\chi_i u_j + \chi_j u_i) d\bar{y} + \frac{1}{|\Omega'|} \frac{1}{2} \int_{\Omega'} \left(\frac{\partial \chi_i}{\partial y_j} + \frac{\partial \chi_j}{\partial y_i} \right) d\bar{y} \right]$$

The dispersion tensor given by 30 depends on the flow in the cell Ω . To calculate the dispersion tensor one must solve the Ω cell problem defined by 23. This linear Ω cell problem defined by 23 can, in principle, be solved numerically for $\bar{\chi}$ for any Ω cell geometry and velocity field \bar{v} in the Ω cell.

A choice for the velocity field \bar{v} in the cell Ω is the velocity field \bar{v} generated by the macroscopic convective velocity field. That is the Brinkmann velocity field given by the equation

$$(32) \quad \begin{cases} \nabla p + \frac{\mu}{\sigma} \bar{v} - \mu \nabla^2 \bar{v} = \bar{F} \\ \nabla \cdot \bar{v} = 0 \end{cases}$$

where σ denotes the permeability of the thin region which in the dilute limit equals to the ratio between the fluid velocity and the force per unit volume exerted on the fluid by the solid ω ; μ is the dynamic viscosity; $\bar{F} = -6\pi\mu a \bar{V}$; a is the radius of the solid part and \bar{V} is the average of the convective velocity field in the cold zone.

Another choice of the velocity field \bar{v} in the cell Ω can be the slow flow past a sphere given by the equation

$$(33) \quad \begin{cases} \nabla p - \mu \nabla^2 \bar{v} = 0 \\ \nabla \bar{v} = 0 \end{cases}$$

For an axisymmetric flow, using appropriate spherical polar coordinates ($x = r \sin \theta \cos \varphi$, $y = r \sin \theta \sin \varphi$, $z = r \cos \theta$) we have in the plane $\varphi = \pi/2$:

$$(34) \quad \bar{v} = (v_r(r, \theta), v_\theta(r, \theta), 0)$$

We may automatically satisfy the condition $\nabla \bar{v} = 0$ by introducing Stokes stream function $\psi(r, \theta)$ such that

$$(35) \quad v_r = \frac{1}{r^2 \sin \theta} \frac{\partial \psi}{\partial \theta} ; \quad v_\theta = -\frac{1}{r \sin \theta} \frac{\partial \psi}{\partial r}$$

In these conditions we have:

$$(36) \quad \psi = \frac{1}{4} |\bar{V}| \left(2r^2 + \frac{a^3}{r} - 3ar \right) \sin^2 \theta$$

where $|\bar{V}|$ is the average of the velocity field in the lower cell ($\bar{V} = |\bar{V}| \bar{e}_z$).

5 The effective convective-diffusive equation of the quartz in the case when we modelling the thin region in the neighbourhood of the growth interface by a fixed bed of randomly distributed spheres.

We started again from the convective-diffusive equation for small concentrations

$$(37) \quad \frac{\partial c}{\partial \tau} + \bar{v} \nabla c = D \nabla^2 c$$

In this equation c is the concentration of quartz, τ is the time, \bar{v} is the random incompressible velocity field generated at the microscale by the randomly-distributed spheres which is statistically homogenous and infinitely extended, D is the diffusion coefficient.

Following R. Mauri's considerations from [12] for a fixed bed of randomly distributed spheres we consider the two length scales l and L , indicating a typical correlation length of the random velocity field \bar{v} generated at the microscale by the randomly-distributed spheres and a characteristic linear dimension of the macroscale (size of the bed). We assume that $\varepsilon = l/L \ll 1$ and we introduce the time scales

$$(38) \quad \tau_1 = \frac{l}{V_o}, \quad \tau_2 = \frac{l^2}{D}, \quad \tau_3 = \frac{L}{V_o}, \quad \tau_4 = \frac{L^2}{D}$$

where V_0 is the characteristic value of the velocity field.

We consider the local and global Peclet numbers:

$$(39) \quad Pe_l = \frac{\tau_2}{\tau_1} = \frac{lV_0}{D}, \quad Pe_g = \frac{\tau_4}{\tau_3} = \frac{LV_0}{D} = \frac{1}{\varepsilon} Pe_l$$

and assume that convection and diffusion balance each other at the microscale, that means $Pe_l = O(1)$. In this case, $Pe_g = O(\varepsilon^{-1})$, what means that convection dominates diffusion at the macroscale.

We note by \bar{R} the macroscopic position vector and we scale the space variables according to

$$(40) \quad \bar{x} = \frac{\bar{R}}{L}$$

The corresponding microscopic variables \bar{y} are given by

$$(41) \quad \bar{y} = \frac{\bar{R} - \bar{x}}{l} = \frac{\bar{x}}{\varepsilon}$$

Introducing the following three time scales:

$$(42) \quad t = \frac{\tau}{\tau_2}, \quad T_1 = \frac{\tau}{\tau_3}, \quad T_2 = \frac{\tau}{\tau_4}$$

we assume that the effective concentration c depends on $\varepsilon, \bar{x}, \bar{y}, t, T_1, T_2$ and can be expanded as follows:

$$(43) \quad c(\varepsilon, \bar{x}, \bar{y}, t, T_1, T_2) = \sum_{n=0}^{\infty} \varepsilon^n c_n(\bar{x}, \bar{y}, t, T_1, T_2)$$

We note that the stationary random velocity field \bar{v} depends only on \bar{y} ; each term c_n in the expansion 43 is locally ergodic (expressible as a product of an ergodic \bar{y} dependent function by an \bar{x}, T_1, T_2 dependent part); the ensemble average of c_n denoted by $\langle c_n \rangle$ satisfies

$$(44) \quad \langle c_n \rangle = \bar{c} \delta_{n0}$$

and each c_n is locally random.

For the time derivatives we have:

$$(45) \quad \frac{\partial}{\partial \tau} = \frac{D}{L^2} \left(\frac{\partial}{\partial T_2} + Pe_l \varepsilon^{-1} \frac{\partial}{\partial T_1} + \varepsilon^{-2} \frac{\partial}{\partial t} \right)$$

and for the space derivatives:

$$(46) \quad \nabla_R = \frac{1}{L} \left(\nabla_{\bar{x}} + \frac{1}{\varepsilon} \nabla_{\bar{y}} \right), \quad \nabla_R^2 = \frac{1}{L^2} \left(\nabla_{\bar{x}}^2 + \frac{2}{\varepsilon} \nabla_{\bar{x}} \nabla_{\bar{y}} + \frac{1}{\varepsilon^2} \nabla_{\bar{y}}^2 \right)$$

Considering \bar{u} defined by

$$(47) \quad \bar{u} = Pe_l \frac{\bar{v}}{V_0}$$

substituting 43 in 37, using 45, 46 and collecting equal powers of ε on gets:

$$(48) \quad \Delta_{\bar{y}} c_0 - \bar{u} \nabla_{\bar{y}} c_0 - \frac{\partial c_0}{\partial t} = 0 \quad \text{for } O(\varepsilon^{-2}).$$

$$(49) \quad \Delta_{\bar{y}} c_1 - \bar{u} \nabla_{\bar{y}} c_1 - \frac{\partial c_1}{\partial t} = \bar{u} \nabla_{\bar{x}} c_0 - 2 \nabla_{\bar{x}} \nabla_{\bar{y}} c_0 + P e_l \frac{\partial c_0}{\partial T_1} \quad \text{for } O(\varepsilon^{-1})$$

$$(50) \quad \Delta_{\bar{y}} c_2 - \bar{u} \nabla_{\bar{y}} c_2 - \frac{\partial c_2}{\partial t} = \bar{u} \nabla_{\bar{x}} c_1 - 2 \nabla_{\bar{x}} \nabla_{\bar{y}} c_1 + P e_l \frac{\partial c_1}{\partial T_1} - \nabla_{\bar{x}}^2 c_0 + \frac{\partial c_0}{\partial T_2} \quad \text{for } O(1)$$

A function $c_0 = c_0(\bar{x}, T_1, T_2)$ satisfies 48. For such a function 49 becomes

$$(51) \quad \Delta_{\bar{y}} c_1 - \bar{u} \nabla_{\bar{y}} c_1 - \frac{\partial c_1}{\partial t} = \bar{u} \nabla_{\bar{x}} c_0 + P e_l \frac{\partial c_0}{\partial T_1}$$

Now we impose that equation 51 is solvable; that means that ensemble averages of its left hand side and right hand side are identically equal to each other. Using that c_1 is locally random we find:

$$(52) \quad P e_l \frac{\partial c_0}{\partial T_1} = - \langle \bar{u} \rangle \nabla_{\bar{x}} c_0$$

where $\langle \bar{u} \rangle$ is the ensemble average of \bar{u} and is the effective quartz velocity.

If we look for solution of equation 49 of the form

$$(53) \quad c_1(\bar{x}, \bar{y}, t, T_1, T_2) = \bar{\chi}(\bar{y}, t) \nabla_{\bar{x}} c_0(\bar{x}, T_1, T_2)$$

we find

$$(54) \quad \frac{\partial \bar{\chi}}{\partial t} + (\bar{u} \nabla_{\bar{y}}) \bar{\chi} - \Delta_{\bar{y}} \bar{\chi} = \langle \bar{u} \rangle - \bar{u}$$

Condition 44 for $n=1$ implies that $\bar{\chi}$ satisfies also

$$(55) \quad \langle \bar{\chi} \rangle = 0$$

If we consider $\bar{\chi}$ satisfying 54, 55 and $c_1 = \bar{\chi} \nabla_{\bar{x}} c_0$ equation 50 becomes

$$(56) \quad \Delta_{\bar{y}} c_2 - \bar{u} \nabla_{\bar{y}} c_2 - \frac{\partial c_2}{\partial t} = \bar{u} \nabla_{\bar{x}} (\bar{\chi} \nabla_{\bar{x}} c_0) - 2 \nabla_{\bar{x}} \nabla_{\bar{y}} (\bar{\chi} \nabla_{\bar{x}} c_0) + P e_l \frac{\partial c_1}{\partial T_1} - \Delta_{\bar{x}} c_0 + \frac{\partial c_0}{\partial T_2}$$

We apply the solvability condition to this equation and considering that c_2 is locally random we obtain

$$(57) \quad \frac{\partial c_0}{\partial T_2} = \sum_{i=1}^3 \sum_{j=1}^3 \left(\delta_{ij} - \langle \chi_j u_i \rangle + 2 \langle \frac{\partial \chi_j}{\partial y_i} \rangle \right) \frac{\partial^2 c_0}{\partial x_i \partial x_j}$$

or

$$(58) \quad \frac{\partial c_0}{\partial T_2} = [I - \langle \bar{\chi} \bar{u} \rangle + 2 \langle \nabla \bar{\chi} \rangle] \nabla_{\bar{x}} \nabla_{\bar{x}} c_0$$

Substituting c_0 in the equation 45 we find

$$(59) \quad \frac{\partial c_0}{\partial \tau} + \langle \bar{v} \rangle \nabla_{\bar{R}} c_0 = D [I - \langle \bar{\chi} \bar{u} \rangle + 2 \langle \nabla \bar{\chi} \rangle] \nabla_{\bar{R}} \nabla_{\bar{R}} c_0$$

This is the macroscopic convective-diffusive equation of the quartz in the neighbourhood of the crystallization front if we assume that this is a fixed bed of randomly distributed spheres. The quantity defined by

$$(60) \quad D^* = D [I - \langle \bar{\chi} \bar{u} \rangle + 2 \langle \nabla \bar{\chi} \rangle]$$

is the diffusivity tensor in this region.

The symmetric part of this tensor is

$$(61) \quad \tilde{D}_{ij} = D \left[\delta_{ij} - \frac{1}{2} (\langle \chi_i u_j + \chi_j u_i \rangle) + \left(\langle \frac{\partial \chi_i}{\partial y_j} + \frac{\partial \chi_j}{\partial y_i} \rangle \right) \right]$$

The dispersion tensor depends on the flow. To calculate it one must solve the problem 54,55. This linear problem can, in principle, be solved. In the papers [12],[14] this linear problem is solved for a Birkmann velocity field given by the equations

$$(62) \quad \begin{cases} \nabla p + \frac{\mu}{\sigma} \bar{v} - \mu \nabla^2 \bar{v} = \bar{F} \delta(r) + O(\phi) \\ \nabla \bar{v} = 0 \end{cases}$$

where σ denotes the permeability of the bed which, in the dilute limit, equals to the ratio between the fluid velocity and the force per unit volume exercised on the fluid by the bed particles; $\bar{F} = -6\pi\mu a \bar{V}$; a is the radius of the solid part and \bar{V} is the average of the convective velocity field in the neighbourhood of the crystallization front.

6 A conclusion

A solution c_0 of the effective convective-diffusive equation depends on the initial value, on the boundary condition and, via the velocity field \bar{v} , on the thermal conditions (T_h, T_c) .

Changing the thermal conditions at a moment τ_1 we will have other solution $c_0^{(1)}$ for which c_0 is an initial value and for which the boundary conditions are given by the values of c_0 on the boundary. In this way, changing the thermal conditions we hope to realize the uniform concentration distribution.

References

- [1] Wang, C.: Ph.D Thesis, Dept. of Materials Science and Engineering, M.I.T. Cambridge, Mass. 1984
- [2] Landau, L. and Lifchitz, E.; *Mecanique des fluides*, ed. Mir, 1971, pg.284
- [3] Bensoussan A., Lions J.L., Papanicolau G.; "Asymptotic Analysis for Periodic Structures", North-Holland, Amsterdam (1978)
- [4] E. Sanchez-Palencia, *Non-homogenous Media and Vibration Theory*, Springer-Verlag, Berlin (1980)

-
- [5] J.L. Ericksen, D. Kinderlehrer, R. Kohn and J.L. Lions, Homogenization and Effective Moduli of Materials and Media, Springer-Verlag, Berlin (1986)
 - [6] E. Sanchez-Palencia and A. Zaoui, Homogenization Techniques for Composite Media, Springer-Verlag, Berlin (1987)
 - [7] T. Levy and E. Sanchez-Palencia, Suspensions of solid particles in a Newtonian fluid, J. Non-Nerv. Fl. Mech. 13 (1983) 13
 - [8] C.L. Winter, C.M. Neuman and S.P. Neuman, A perturbation expression for diffusion in a random velocity field. SIAM J. Appl. Math. 44 (1984) 411
 - [9] T. Levy and R.K.T. Hsieh, Homogenization mechanics of a non dilute suspension of magnetic particles, Int. J. Engng. Sci. 26 (1988) 1087
 - [10] J. Rubinstein and R. Mauri, Dispersion and convection in periodic porous media, SIAM J. Appl. Math. 46 (1986) 1018
 - [11] R. Mauri, Dispersion, convection and reaction in porous media, Phys. Fluids A 3 (1991) 743
 - [12] R. Mauri, Heat and mass transport in random velocity fields with application to dispersion in porous media, Journal of Engineering Mathematics 29 (1995) 77-89
 - [13] Brenner; Phil. Trans. R. Soc. Lond. A297 (1980) 81
 - [14] D.L. Koch and J.F. Brady, J. Fluid Mech. vol154 (1985) 399-427

A theoretical and numerical approach of a distributed control model for a free boundary problem

Ruxandra Stavre

Institute of Mathematics of the Romanian Academy,

P. O. Box 1-764, RO-70700, Bucharest, Romania,

fax: (401)2229826, e-mail: RSTAVRE@IMAR.RO

Abstract. The flow of an incompressible fluid through a non-homogeneous dam is considered. A distributed control problem associated with this free boundary problem is studied. The aim of this paper is to minimize the total pressure of the fluid, the control being the permeability coefficient of the dam. The first order necessary conditions of optimality are derived for a family of regular control problems. A finite element approximation of the optimality system is introduced and the convergence of the proposed algorithms is studied. Some numerical results are discussed, for the case of the non-homogeneous rectangular dam.

Mathematics Subject Classification (1991): 35R35, 49J20, 65N30, 76S05

A theoretical and numerical approach of a control problem

1. Introduction

The flow of an incompressible fluid through a non-homogeneous dam with general geometry was studied, for instance, in: Alt (1979), Alt (1980), Friedman and Huang (1985), Stavre and Vernescu (1985), Stavre and Vernescu (1989). In Alt (1979), Friedman and Huang (1985), Stavre and Vernescu (1985) this free boundary problem

was studied from a theoretical point of view, while in Alt (1980), Stavre and Vernescu (1989) numerical methods were used for solving it.

We introduce and study an optimal control model associated with this free boundary problem. We want to minimize the "total pressure" of the fluid in the dam, given by the functional:

$$(1.1) \quad J(k) = \int_D p(x, y) dx dy,$$

where the control k is the permeability coefficient of the dam, $D \subset \mathbb{R}^2$ is the cross-section of the dam and p , the pressure of the fluid. The purpose of the paper is to obtain the optimality system (the necessary conditions of optimality) and to approximate it in order to compute an optimal control k^* , characterized as a minimum point for the functional J , defined by (1.1).

Other optimal control models associated with the homogeneous dam problem were studied in Barbu (1984), Friedman and Yaniro (1985), Friedman, Huang and Yong (1987). In Friedman and Yaniro (1985), Friedman, Huang and Yong (1987) the control variable is the rate allowed to withdraw water from the bottom of the dam and in Barbu (1984) the control is the highest level of the fluid in the reservoirs.

The plan of the paper is as follows. In Section 2 we define the distributed control problem and we prove an existence result. The necessary conditions of optimality are deduced in the next section, by approximating the control problem by a family of control problems which are regular. Section 4 deals with the finite element approximation of the optimality system associated with the family of regularized control problems; the convergence of the proposed algorithms is also discussed. In the last section, some numerical results are presented, for the case of a non-homogeneous, rectangular dam.

2. The control problem

First we describe the mathematical formulation of the physical problem, introduced in Brezis, Kinderlehrer and Stampacchia (1978), Carrillo-Menendez and Chipot (1982) for the homogeneous dam and in Stavre and Vernescu (1985) for the non-homogeneous case.

The cross-section of the dam is denoted by D , where $D \subset \mathbb{R}^2$ is open, bounded, connected, with the boundary ∂D , which is locally a Lipschitz graph. The boundary is formed by three disjoint parts: S_1 —the impervious part, S_2 —the part in contact with the air and $S_3 = S_{3,1} \cup S_{3,2}$ —the part in contact with the reservoirs ($S_{3,1}$, $S_{3,2}$ being the connected components of S_3).

We denote by h_i the level of the fluid in the reservoir with bottom $S_{3,i}$, $i = 1, 2$ and we define $f : S_2 \cup S_3 \mapsto \mathbb{R}$,

$$(2.1) \quad f = \begin{cases} 0 & \text{on } S_2, \\ h_i - y & \text{on } S_{3,i} \quad i = 1, 2. \end{cases}$$

The variational formulation of the physical problem is (see Stavre and Vernescu (1985)):

$$(VP)_k \begin{cases} \text{Find } p_k \in H^1(D), p_k \geq 0 \text{ a.e. in } D, p_k = f \text{ on } S_2 \cup S_3, \\ \int_D k(\nabla p_k \cdot \nabla \varphi + H(p_k) \frac{\partial \varphi}{\partial y}) dx dy \leq 0 \quad \forall \varphi \in H^1(D), \varphi = 0 \text{ on } S_3, \varphi \geq 0 \text{ on } S_2 \end{cases}$$

where k is the permeability coefficient of the dam, p_k the corresponding pressure of the fluid and H , the Heaviside function. It is obvious that the pressure of the fluid in the dam depends on the function k .

We suppose that k is a control variable belonging to the following bounded, closed, convex set:

$$(2.2) \quad K = \{v \in H^1(D) / \|v\|_{H^1(D)} \leq r, \alpha \leq v \leq \beta \text{ a.e. in } D, \frac{\partial v}{\partial y} \geq 0 \text{ a.e. in } D\},$$

where α , β , r are positive constants, with r large enough.

Since $(VP)_k$ has not, in general, a unique solution p_k (see Stavre and Vernescu (1985)), the correspondence $k \mapsto p_k$ is multi-valued.

We define:

$$(2.3) \quad P_k = \{p / p \text{ solution of } (VP)_k\},$$

and we introduce the following problem:

$$(2.4) \quad \begin{cases} \text{Find } (k^*, p^*) \in K \times P_{k^*}, \\ \int_D p^* dx dy \leq \int_D p dx dy \quad \forall (k, p) \in K \times P_k. \end{cases}$$

It is known from Stavre and Vernescu (1985) (Theorem 4.2) that there exists a unique solution \bar{p}_k of $(VP)_k$ so that the boundary of each connected component of $\{\bar{p}_k > 0\}$ is in contact with at least a reservoir (S_3 -connected solution). Hence, the correspondence $k \mapsto \bar{p}_k$ is uni-valued.

Lemma 2.1 *Let k_0 be an element of K and let \bar{p}_{k_0}, p_{k_0} be the S_3 -connected solution of $(VP)_{k_0}$ and another solution of $(VP)_{k_0}$, respectively. Then:*

$$(2.5) \quad \int_D \bar{p}_{k_0} dx dy < \int_D p_{k_0} dx dy.$$

Proof. There exists at least a connected set $C_1 \subset \{p_{k_0} > 0\}$ so that $\partial C_1 \cap S_3 = \emptyset$. We denote by C the union of all the connected components of $\{p_{k_0} > 0\}$ with the above property and we define:

$$(2.6) \quad p_{k_0}^* = \begin{cases} p_{k_0} & \text{in } D - \bar{C}, \\ 0 & \text{in } \bar{C}. \end{cases}$$

It can be proved, as in Stavre and Vernescu (1985) (Theorem 3.7), that $p_{k_0}^*$ is a solution for $(VP)_{k_0}$. Moreover, from (2.6) it follows that $p_{k_0}^*$ is S_3 -connected; hence $p_{k_0}^* = \bar{p}_{k_0}$. Since, from (2.6) we get $\bar{p}_{k_0} < p_{k_0}$ in C , the assertion of the lemma is obtained.

We introduce another minimum problem:

$$(2.7) \quad \begin{cases} \text{Find } k^* \in K, \\ \int_D \bar{p}_{k^*} dx dy \leq \int_D \bar{p}_k dx dy, \quad \forall k \in K, \end{cases}$$

and we prove, by using Lemma 2.1, the following:

Proposition 2.2 (2.4) has a solution iff (2.7) has a solution.

Proof. Let (k^*, p^*) be a solution of (2.4). Hence:

$$\int_D p^* dx dy \leq \int_D \bar{p}_{k^*} dx dy.$$

By using Lemma 2.1, it follows $p^* = \bar{p}_{k^*}$ and, from (2.4) for $p = \bar{p}_k$, $k \in K$, we obtain:

$$\int_D \bar{p}_{k^*} dx dy \leq \int_D \bar{p}_k dx dy \quad \forall k \in K.$$

Conversely, if k^* is a solution of (2.7), we define $p^* = \bar{p}_{k^*} \in P_{k^*}$ and, by using again Lemma 2.1, the proof is achieved.

We shall study in the sequel the problem (2.7).

We define the functional $J : K \mapsto \mathbb{R}_+$,

$$(2.8) \quad J(k) = \int_D \bar{p}_k dx dy.$$

(2.7) can be written as the following control problem:

$$(CP) \begin{cases} \text{Find } k^* \in K, \\ J(k^*) = \min\{J(k) / k \in K\}. \end{cases}$$

The last result of this section is an existence theorem.

Theorem 2.3 (CP) has at least a solution.

Proof. Let $\{k_n\}_{n \in \mathbb{N}} \subset K$ be a minimizing sequence. Since K is bounded in $H^1(D)$, closed and convex, it follows that $k_{n_s} \rightarrow k_0$ weakly in $H^1(D)$ when $s \rightarrow \infty$ and $k_0 \in K$.

Taking into account that $\{H(\bar{p}_{k_{n_s}})\}_{s \in \mathbb{N}}$ is bounded in $L^\infty(D)$ and, from $(VP)_{k_{n_s}}$, $\{\bar{p}_{k_{n_s}}\}_{s \in \mathbb{N}}$ is bounded in $H^1(D)$, we get, by passing to the limit on a subsequence in $(VP)_{k_{n_s}}$:

$$(2.9) \quad \int_D k_0 (\nabla p_0 \cdot \nabla \varphi + \bar{H} \frac{\partial \varphi}{\partial y}) dx dy \leq 0 \quad \forall \varphi \in H^1(D), \varphi = 0 \text{ on } S_3, \varphi \geq 0 \text{ on } S_2,$$

where p_0 is the weak limit in $H^1(D)$ of a subsequence of $\{\bar{p}_{k_n}\}_{n \in \mathbb{N}}$ and \bar{H} is the weak star limit in $L^\infty(D)$ of a subsequence of $\{H(\bar{p}_{k_n})\}_{n \in \mathbb{N}}$. With the same technique as in Stavre and Vernescu (1985), we get $\bar{H} = H(p_0)$ and, hence, p_0 verifies $(VP)_{k_0}$. Moreover, $\int_D p_0 dx dy = \min\{J(k) / k \in K\}$. This equality and Lemma 2.1 imply $p_0 = \bar{p}_{k_0}$ and therefore, the theorem has been proved.

For simplicity we shall assume in the sequel that D has a geometry which ensures the uniqueness of the solution of $(VP)_k$, $\forall k \in K$ (for instance, S_1 given by $y = 0$, $x \in (0, a)$). We shall denote the unique solution of $(VP)_k$ by p_k .

In the next section, (CP) will be approximated by a family of regularized problems, for which we shall deduce the necessary conditions of optimality.

3. The optimality system

We introduce in the sequel the following family of regularized control problems:

$$(CP)_\varepsilon \begin{cases} \text{For } \varepsilon > 0, \text{ find } k_\varepsilon^* \in K, \\ J_\varepsilon(k_\varepsilon^*) = \min\{J_\varepsilon(k) / k \in K\}, \end{cases}$$

where $J_\varepsilon(k) = \int_D p_k^\varepsilon dx dy$, p_k^ε being a solution of:

$$(VP)_k^\varepsilon \begin{cases} p_k^\varepsilon \in H^1(D), p_k^\varepsilon = f \text{ on } S_2 \cup S_3, \\ \int_D k(\nabla p_k^\varepsilon \cdot \nabla \varphi + H_\varepsilon(p_k^\varepsilon) \frac{\partial \varphi}{\partial y}) dx dy = 0 \quad \forall \varphi = 0 \text{ on } S_2 \cup S_3, \end{cases}$$

with $H_\varepsilon(x) = \frac{x^{+2}}{x^2 + \varepsilon^2}$, $x^+ = \max(x, 0)$.

Before studying the family of control problems $(CP)_\varepsilon$, we remark that $(VP)_k^\varepsilon$ is of the same type as $(VP)_\varepsilon$ considered in Stavre and Vernescu (1985), but with a more regular function H_ε . We shall use the regularity of H_ε in the next section, for obtaining the convergence of a sequence of solutions of the discrete optimality system to a solution of the optimality system, associated with $(CP)_\varepsilon$.

The proof of the next theorem is similar to those of Theorems 3.1, 3.2 from Stavre and Vernescu (1985), therefore we shall omit it.

Theorem 3.1 For any $\varepsilon > 0$, $k \in K$, there exists a unique solution p_k^ε of $(VP)_k^\varepsilon$ with the properties: $p_k^\varepsilon \in C(D \cup S_2 \cup S_3)$, $p_k^\varepsilon \geq 0$ in D .

The sense of the approximation of $(VP)_k$ by the family $(VP)_k^\varepsilon$, $\varepsilon > 0$ is given by:

Theorem 3.2 Let p_k^ε and p_k be the unique solution of $(VP)_k^\varepsilon$ and $(VP)_k$, respectively. Then $p_k^\varepsilon \rightarrow p_k$ weakly in $H^1(D)$, when $\varepsilon \rightarrow 0$.

Proof. By choosing in $(VP)_k^\varepsilon$ $\varphi = p_k^\varepsilon - v$, $v \in H^1(D)$, $v = f$ on $S_2 \cup S_3$ and by taking into account the properties of k and H_ε , we obtain the boundedness in $H^1(D)$ of the sequence $\{p_k^\varepsilon\}_{\varepsilon > 0}$. Moreover, $\{H_\varepsilon(p_k^\varepsilon)\}_{\varepsilon > 0}$ is bounded in $L^\infty(D)$. Hence, we obtain, on a subsequence: $p_k^\varepsilon \rightarrow p$ weakly in $H^1(D)$, $H_\varepsilon(p_k^\varepsilon) \rightarrow \bar{H}$ weakly star in $L^\infty(D)$, when $\varepsilon \rightarrow 0$. Moreover, $p = f$ on $S_2 \cup S_3$, $p \geq 0$ a.e. in D , $0 \leq \bar{H} \leq 1$ a.e. in D .

By applying the Stokes formula for $\varphi \in H^1(D)$, $\varphi = 0$ on S_3 , $\varphi \geq 0$ on S_2 it follows, as in Stavre and Vernescu (1985):

$$(3.1) \int_D k(\nabla p_k^\varepsilon \cdot \nabla \varphi + H_\varepsilon(p_k^\varepsilon) \frac{\partial \varphi}{\partial y}) dx dy \leq 0 \quad \forall \varphi \in H^1(D), \varphi = 0 \text{ on } S_3, \varphi \geq 0 \text{ on } S_2.$$

By passing to the limit, on a subsequence, in (3.1), we get:

$$(3.2) \int_D k(\nabla p \cdot \nabla \varphi + \bar{H} \frac{\partial \varphi}{\partial y}) dx dy \leq 0 \quad \forall \varphi \in H^1(D), \varphi = 0 \text{ on } S_3, \varphi \geq 0 \text{ on } S_2.$$

If we choose $\varphi \in \mathcal{D}(D)$ in (3.2) we obtain:

$$(3.3) \quad \operatorname{div}(k \nabla p) + \frac{\partial}{\partial y}(k \bar{H}) = 0 \text{ in } \mathcal{D}'(D)$$

and, since $k \bar{H} \in L^\infty(D)$, by using elliptic regularity (see Gilbarg and Trudinger (1977)), we deduce that $p \in C(D \cup S_2 \cup S_3)$.

In order to conclude that $\bar{H} = H(p)$, we have to prove:

$$(i) \quad \bar{H} = 1 \text{ a.e. in } \{p > 0\},$$

$$(ii) \quad \bar{H} = 0 \text{ a.e. in } D - \{p > 0\},$$

$$(iii) \quad \operatorname{mes}(D \cap \partial\{p > 0\}) = 0.$$

We begin with the proof of the assertion (i). We have:

$$(3.4) \quad \int_{\{p>0\}} \bar{H} dx dy = \liminf_{\varepsilon \rightarrow 0} \int_{\{p>0\}} H_\varepsilon(p_k^\varepsilon) dx dy.$$

Let δ be a fixed positive number. It can be easily proved that:

$$(3.5) \quad \int_{\{p>0\}} H_\varepsilon(p_k^\varepsilon) dx dy > \int_{\{p>\delta\} \cap \{p_k^\varepsilon > \delta\}} dx dy - \frac{\varepsilon^2}{\delta^2 + \varepsilon^2} \int_{\{p>\delta\} \cap \{p_k^\varepsilon > \delta\}} dx dy.$$

By passing to the inferior limit with $\varepsilon \rightarrow 0$ in (3.5) and combining this with (3.4), we get:

$$(3.6) \quad \int_{\{p>0\}} \bar{H} dx dy \geq \int_{\{p>\delta\}} dx dy \quad \forall \delta > 0.$$

By passing to the limit in (3.6) with $\delta \rightarrow 0$ and by taking into account that $\bar{H} \leq 1$ a.e. in D , we obtain the assertion (i).

For obtaining (ii) and (iii) we need only (3.2) and (i); hence, the proof of (ii) and (iii) is that of Lemma 3.1 of Stavre and Vernescu (1989).

Since $\bar{H} = H(p)$, it follows from (3.2) that p is the unique solution of $(VP)_k$. We remark that the uniqueness of the solution of $(VP)_k$ gives the uniqueness of the weak limit point in $H^1(D)$ of the sequence $\{p_k^\varepsilon\}_{\varepsilon>0}$, which completes the proof.

Theorem 3.3 For any $\varepsilon > 0$, $(CP)_\varepsilon$ has at least a solution.

Proof. Let $\{k_n^\varepsilon\}_{n \in \mathbb{N}} \subset K$ be a minimizing sequence for J_ε . It follows that on a subsequence, denoted also by k_n^ε , we have: $k_n^\varepsilon \rightarrow k_\varepsilon^*$ weakly in $H^1(D)$, $k_n^\varepsilon \rightarrow k_\varepsilon^*$ weakly star in $L^\infty(D)$, $k_n^\varepsilon \rightarrow k_\varepsilon^*$ a.e. in D , when $n \rightarrow \infty$ and $k_\varepsilon^* \in K$. Moreover, $\lim_{n \rightarrow \infty} J_\varepsilon(k_n^\varepsilon) = \min\{J_\varepsilon(k) / k \in K\}$.

By taking in $(VP)_{k_n^\varepsilon}^\varepsilon$ $\varphi = p_{k_n^\varepsilon}^\varepsilon - v$, with $v = f$ on $S_2 \cup S_3$ and by using the properties of k_n^ε and H_ε we obtain, on a subsequence: $p_{k_n^\varepsilon}^\varepsilon \rightarrow p^\varepsilon$ weakly in $H^1(D)$ and $H_\varepsilon(p_{k_n^\varepsilon}^\varepsilon) \rightarrow H_\varepsilon(p^\varepsilon)$ strongly in $L^2(D)$, when $n \rightarrow \infty$. By passing to the limit in $(VP)_{k_n^\varepsilon}^\varepsilon$ on a subsequence, when $n \rightarrow \infty$ it follows that p^ε satisfies $(VP)_{k_\varepsilon^*}^\varepsilon$ and hence, $p^\varepsilon = p_{k_\varepsilon^*}^\varepsilon$. This yields:

$$\min\{J_\varepsilon(k) / k \in K\} = \lim_{n \rightarrow \infty} \int_D p_{k_n^\varepsilon}^\varepsilon dx dy = \int_D p_{k_\varepsilon^*}^\varepsilon dx dy = J_\varepsilon(k_\varepsilon^*).$$

We establish next the relation between the regularized minimum problems $(CP)_\varepsilon$, $\varepsilon > 0$ and the initial control problem.

Theorem 3.4 *For any $\varepsilon > 0$, let $k_\varepsilon^* \in K$ be a minimum point of J_ε . Then, any weak limit point in $H^1(D)$, k^* , of $\{k_\varepsilon^*\}_{\varepsilon>0}$ is a solution for (CP) . Moreover:*

$$(3.7) \quad \lim_{\varepsilon \rightarrow 0} J_\varepsilon(k_\varepsilon^*) = \min\{J(k) / k \in K\}.$$

Proof. From the definition (2.2) and $\{k_\varepsilon^*\}_{\varepsilon>0} \subset K$ it follows that there exists at least an element $k^* \in K$ such that, we have, on a subsequence: $k_\varepsilon^* \rightarrow k^*$ weakly in $H^1(D)$, $k_\varepsilon^* \rightarrow k^*$ weakly star in $L^\infty(D)$, $k_\varepsilon^* \rightarrow k^*$ a.e. in D , when $\varepsilon \rightarrow 0$.

From $(VP)_{k_\varepsilon^*}^\varepsilon$ we obtain, as before, the boundedness in $H^1(D)$ of $\{p_{k_\varepsilon^*}^\varepsilon\}_{\varepsilon>0}$.

Moreover $\{H_\varepsilon(p_{k_\varepsilon^*}^\varepsilon)\}_{\varepsilon>0}$ is bounded in $L^\infty(D)$. We can now extract subsequences such that $p_{k_\varepsilon^*}^\varepsilon \rightarrow p$ weakly in $H^1(D)$, $H_\varepsilon(p_{k_\varepsilon^*}^\varepsilon) \rightarrow \bar{H}$ weakly star in $L^\infty(D)$, when $\varepsilon \rightarrow 0$, with $p = f$ on $S_2 \cup S_3$, $p \geq 0$ in D , $0 \leq \bar{H} \leq 1$ a.e. in D .

For any $\varphi \in H^1(D)$, $\varphi = 0$ on S_3 , $\varphi \geq 0$ on S_2 we obtain from $(VP)_{k_\varepsilon^*}^\varepsilon$, as in Theorem 3.2:

$$(3.8) \quad \int_D k_\varepsilon^* (\nabla p_{k_\varepsilon^*}^\varepsilon \cdot \nabla \varphi + H_\varepsilon(p_{k_\varepsilon^*}^\varepsilon) \frac{\partial \varphi}{\partial y}) dx dy \leq 0.$$

By passing to the limit in (3.8), on a subsequence, with $\varepsilon \rightarrow 0$, we get:

$$(3.9) \quad \int_D k^* (\nabla p \cdot \nabla \varphi + \bar{H} \frac{\partial \varphi}{\partial y}) dx dy \leq 0 \quad \forall \varphi \in H^1(D), \varphi = 0 \text{ on } S_3, \varphi \geq 0 \text{ on } S_2.$$

We conclude, with the same proof as in Theorem 3.2, that $\bar{H} = H(p)$ and, hence, $p = p_{k^*}$, the unique solution of $(VP)_{k^*}$.

On the other hand we have $J_\varepsilon(k_\varepsilon^*) \leq J_\varepsilon(k) \quad \forall k \in K, \forall \varepsilon > 0$, i.e.:

$$(3.10) \quad \int_D p_{k_\varepsilon^*}^\varepsilon dx dy \leq \int_D p_k^\varepsilon dx dy \quad \forall k \in K, \forall \varepsilon > 0.$$

Taking $\varepsilon \rightarrow 0$ in (3.10) and using Theorem 3.2 and the weak convergence in $H^1(D)$ of $\{p_{k_\varepsilon^*}^\varepsilon\}_{\varepsilon>0}$ to p_{k^*} we obtain $J(k^*) \leq J(k) \quad \forall k \in K$; hence, the first assertion of the theorem holds.

For proving (3.7), we first remark that the boundedness of $\{p_{k_\varepsilon}^\varepsilon\}_{\varepsilon>0}$ in $H^1(D)$ implies the boundedness of $\{J_\varepsilon(k_\varepsilon^*)\}_{\varepsilon>0}$ in \mathbb{R} .

If we suppose, by contradiction, that there exists two subsequences such that $J_{\varepsilon_s}(k_{\varepsilon_s}^*) \rightarrow l_1$, when $s \rightarrow \infty$ and $J_{\varepsilon_q}(k_{\varepsilon_q}^*) \rightarrow l_2$, when $q \rightarrow \infty$, with $l_1 \neq l_2$ we obtain, as before, that, on a subsequence, we have: $k_{\varepsilon_s}^* \rightharpoonup k_1$, $p_{k_{\varepsilon_s}^*}^{\varepsilon_s} \rightarrow p_{k_1}$ weakly in $H^1(D)$, when $s \rightarrow \infty$ and $k_{\varepsilon_q}^* \rightarrow k_2$, $p_{k_{\varepsilon_q}^*}^{\varepsilon_q} \rightarrow p_{k_2}$ weakly in $H^1(D)$, when $q \rightarrow \infty$.

From (3.10), for $\varepsilon = \varepsilon_s$, $k = k_2$ we get, as $s \rightarrow \infty$ $l_1 \leq l_2$ and, for $\varepsilon = \varepsilon_q$, $k = k_1$ we get, as $q \rightarrow \infty$ $l_1 \geq l_2$; hence, a contradiction with $l_1 \neq l_2$.

Thus, (3.7) holds.

In the sequel, we shall derive the necessary conditions of optimality associated with $(CP)_\varepsilon$.

We first establish the following:

Lemma 3.5 *For any $k, k_0 \in K$, $\varepsilon > 0$, we have:*

$$(3.11) \quad J'_\varepsilon(k_0) \cdot (k - k_0) = \int_D q^\varepsilon dx dy,$$

where $q^\varepsilon \in H^1(D)$ is the unique weak solution of the problem:

$$(3.12) \quad \begin{cases} \operatorname{div}(k_0 \nabla q^\varepsilon) + \frac{\partial}{\partial y}(k_0 H'_\varepsilon(p_{k_0}^\varepsilon) q^\varepsilon) \\ = \operatorname{div}((k_0 - k) \nabla p_{k_0}^\varepsilon) + \frac{\partial}{\partial y}((k_0 - k) H_\varepsilon(p_{k_0}^\varepsilon)) \text{ in } D, \\ q^\varepsilon = 0 \text{ on } S_2 \cup S_3, \\ k_0 \left(\frac{\partial q^\varepsilon}{\partial n} + H'_\varepsilon(p_{k_0}^\varepsilon) q^\varepsilon n_y \right) = (k_0 - k) \left(\frac{\partial p_{k_0}^\varepsilon}{\partial n} + H_\varepsilon(p_{k_0}^\varepsilon) n_y \right) \text{ on } S_1, \end{cases}$$

where $\vec{n} = (n_x, n_y)$ is the outward unit normal to ∂D .

Proof. We begin by proving that the solution of (3.12) is unique. Let us suppose that there exists two solutions of (3.12), q_1^ε , q_2^ε and let us define $Q^\varepsilon = q_1^\varepsilon - q_2^\varepsilon$. $Q^\varepsilon \in H^1(D)$ satisfies the following variational problem:

$$(3.13) \quad \begin{cases} \int_D k_0 (\nabla Q^\varepsilon \cdot \nabla \varphi + H'_\varepsilon(p_{k_0}^\varepsilon) Q^\varepsilon \frac{\partial \varphi}{\partial y}) dx dy = 0 \quad \forall \varphi \in H^1(D), \varphi = 0 \text{ on } S_2 \cup S_3, \\ Q^\varepsilon = 0 \text{ on } S_2 \cup S_3. \end{cases}$$

If $Q^\varepsilon \neq 0$ in D , we can suppose that $\text{mes}(\{Q^\varepsilon > 0\}) > 0$.

For $\delta > 0$ given, we take $\varphi = \frac{(Q^\varepsilon - \delta)^+}{Q^\varepsilon}$ in (3.13) and we obtain:

$\| \ln(1 + \frac{(Q^\varepsilon - \delta)^+}{\delta}) \|_{H^1(D)} \leq c$, the constant being independent of δ . When δ tends to 0 we obtain $Q^\varepsilon \leq 0$ a.e. in D . It follows that $Q^\varepsilon = 0$ in D and, hence, $q_1^\varepsilon = q_2^\varepsilon$ in D .

Let $t \in (0, 1)$. We denote $(p_{k_0+t(k-k_0)}^\varepsilon - p_{k_0}^\varepsilon)/t$ by q_t^ε ; hence,

$$\lim_{t \rightarrow 0} \frac{J_\varepsilon(k_0 + t(k - k_0)) - J_\varepsilon(k_0)}{t} = \lim_{t \rightarrow 0} \int_D q_t^\varepsilon dx dy.$$

We prove next that $\{q_t^\varepsilon\}_{t \in (0,1)}$ is bounded in $H^1(D)$.

By computing $\frac{(VP)_{k_0+t(k-k_0)}^\varepsilon - (VP)_{k_0}^\varepsilon}{t}$ for $\varphi = q_t^\varepsilon$, we get:

$$(3.14) \quad \|q_t^\varepsilon\|_{H^1(D)} \leq c_1 \|q_t^\varepsilon\|_{L^2(D)} + c_2,$$

the constants c_1, c_2 being independent of t .

If $\{q_t^\varepsilon\}_{t \in (0,1)}$ is bounded in $L^2(D)$, we obtain, from (3.14), the boundedness of the sequence in $H^1(D)$.

Let us suppose that $\{q_t^\varepsilon\}_{t \in (0,1)}$ is unbounded in $L^2(D)$. For a subsequence, denoted again by $\{q_t^\varepsilon\}_{t \in (0,1)}$ we have $\lim_{t \rightarrow 0} \|q_t^\varepsilon\|_{L^2(D)} = \infty$.

We define $Q_t^\varepsilon = \frac{q_t^\varepsilon}{\|q_t^\varepsilon\|_{L^2(D)}}$. It is obvious that $\|Q_t^\varepsilon\|_{L^2(D)} = 1$ and, from (3.14), that $\{Q_t^\varepsilon\}_{t \in (0,1)}$ is bounded in $H^1(D)$. Thus we can extract a subsequence such that $Q_t^\varepsilon \rightarrow Q^\varepsilon$ weakly in $H^1(D)$, when $t \rightarrow 0$.

Moreover, $\|Q^\varepsilon\|_{L^2(D)} = 1$.

By considering the problem satisfied by Q_t^ε and by passing to the limit with $t \rightarrow 0$, we obtain that Q^ε is the solution of (3.13), i.e. $Q^\varepsilon = 0$ in D , which contradicts $\|Q^\varepsilon\|_{L^2(D)} = 1$.

The sequence $\{q_t^\varepsilon\}_{t \in (0,1)}$ being bounded in $H^1(D)$, it follows that it has at least a weak limit point in $H^1(D)$, q^ε , which is the solution of (3.12).

From the uniqueness of the solution of (3.12), we obtain that the weak limit point of $\{q_t^\varepsilon\}_{t \in (0,1)}$ is unique, which completes the proof.

The main result of this section, the necessary conditions of optimality associated with $(CP)_\varepsilon$, is a consequence of the above lemma.

Theorem 3.6 For any $\varepsilon > 0$ let k_ε^* be a solution of $(CP)_\varepsilon$. Then, there exists the unique elements $p_{k_\varepsilon^*}^\varepsilon, Q_{k_\varepsilon^*}^\varepsilon \in H^1(D)$, which satisfy the optimality system:

$$(OS) \left\{ \begin{array}{l} \left\{ \begin{array}{l} \operatorname{div}(k_\varepsilon^* \nabla p_{k_\varepsilon^*}^\varepsilon) + \frac{\partial}{\partial y}(k_\varepsilon^* H_\varepsilon(p_{k_\varepsilon^*}^\varepsilon)) = 0 \text{ in } D, \\ p_{k_\varepsilon^*}^\varepsilon = f \text{ on } S_2 \cup S_3, \\ k_\varepsilon^* \left(\frac{\partial p_{k_\varepsilon^*}^\varepsilon}{\partial n} + H_\varepsilon(p_{k_\varepsilon^*}^\varepsilon) n_y \right) = 0 \text{ on } S_1, \end{array} \right. \\ \left\{ \begin{array}{l} \operatorname{div}(k_\varepsilon^* \nabla Q_{k_\varepsilon^*}^\varepsilon) - k_\varepsilon^* H'_\varepsilon(p_{k_\varepsilon^*}^\varepsilon) \frac{\partial Q_{k_\varepsilon^*}^\varepsilon}{\partial y} = 1 \text{ in } D, \\ Q_{k_\varepsilon^*}^\varepsilon = 0 \text{ on } S_2 \cup S_3, \\ k_\varepsilon^* \frac{\partial Q_{k_\varepsilon^*}^\varepsilon}{\partial n} = 0 \text{ on } S_1, \end{array} \right. \\ \int_D (\nabla p_{k_\varepsilon^*}^\varepsilon \cdot \nabla Q_{k_\varepsilon^*}^\varepsilon + H_\varepsilon(p_{k_\varepsilon^*}^\varepsilon) \frac{\partial Q_{k_\varepsilon^*}^\varepsilon}{\partial y}) (k - k_\varepsilon^*) dx dy \geq 0 \quad \forall k \in K. \end{array} \right.$$

Proof. It is obvious that $(OS)_I$ has a unique solution, $p_{k_\varepsilon^*}^\varepsilon$, since it represents $(VP)_{k_\varepsilon^*}^\varepsilon$.

The uniqueness of the solution $Q_{k_\varepsilon^*}^\varepsilon$ of $(OS)_{II}$ is given by the general results of Chicco (1970).

We denote by q^* the function given by Lemma 3.5, corresponding to $k_0 = k_\varepsilon^*$. It is obvious that:

$$(3.15) \quad \int_D q^* dx dy \geq 0.$$

By taking $\varphi = q^*$ in the variational formulation of $(OS)_{II}$, $\varphi = Q_{k_\varepsilon^*}^\varepsilon$ in the variational formulation of (3.12) for $k_0 = k_\varepsilon^*$ and by using (3.15), we obtain $(OS)_{III}$, which completes the proof.

The next section deals with the finite element approximation of (OS) .

4. The approximation of the control system

Let $\{\mathcal{T}_h\}_{h>0}$ be a regular family of triangulations of \bar{D} and let $K_h \times V_h \times H_h$ be an internal approximation of $K \times V \times H$ (see Glowinski, Lions and Tremolieres (1981)),

where:

$$(4.1) \quad \begin{cases} V = \{v \in H^1(D) / v = f \text{ on } S_2 \cup S_3\}, \\ H = \{v \in H^1(D) / v = 0 \text{ on } S_2 \cup S_3\}. \end{cases}$$

We consider the discrete optimality system:

$$(4.2) \quad \begin{cases} (k_h^*, p_h^*, Q_h^*) \in K_h \times V_h \times H_h, \\ \int_D k_h^* (\nabla p_h^* \cdot \nabla \varphi_h + H_\varepsilon(p_h^*) \frac{\partial \varphi_h}{\partial y}) dx dy = 0 \quad \forall \varphi_h \in H_h, \\ \int_D k_h^* (\nabla Q_h^* \cdot \nabla \varphi_h + H'_\varepsilon(p_h^*) \frac{\partial Q_h^*}{\partial y} \varphi_h) dx dy = - \int_D \varphi_h dx dy \quad \forall \varphi_h \in H_h, \\ \int_D (\nabla p_h^* \cdot \nabla Q_h^* + H_\varepsilon(p_h^*) \frac{\partial Q_h^*}{\partial y}) (k_h - k_h^*) dx dy \geq 0 \quad \forall k_h \in K_h. \end{cases}$$

(4.2) approximates the optimality system (OS) in the sense given by the next theorem:

Theorem 4.1 *There exists a subsequence $\{(k_{h_m}^*, p_{h_m}^*, Q_{h_m}^*)\}_{m \in \mathbb{N}}$ such that: $k_{h_m}^* \rightarrow k_\varepsilon^*$ weakly in $H^1(D)$, $k_{h_m}^* \rightarrow k_\varepsilon^*$ weakly star in $L^\infty(D)$, $k_{h_m}^* \rightarrow k_\varepsilon^*$ a.e. in D , $p_{h_m}^* \rightarrow p_\varepsilon^*$ strongly in $H^1(D)$, $Q_{h_m}^* \rightarrow Q_\varepsilon^*$ strongly in $H^1(D)$, when $m \rightarrow \infty$ and $(k_\varepsilon^*, p_\varepsilon^*, Q_\varepsilon^*)$ is solution for (OS).*

Proof. The assertions of the theorem concerning $\{k_{h_m}^*\}_{m \in \mathbb{N}}$ are a consequence of the fact that $\{k_h^*\}_{h>0} \subset K_h \subset K$.

For $\varphi_{h_m} = p_{h_m}^* - v_{h_m}$, with $\{v_{h_m}\}_{m \in \mathbb{N}} \subset V_{h_m}$ a strongly convergent sequence in $H^1(D)$, (4.2)₂ gives the boundedness in $H^1(D)$ of $\{p_{h_m}^*\}_{m \in \mathbb{N}}$ and, hence, the existence of a weak limit point in $H^1(D)$, denoted p_ε^* . We can now pass to the limit, on a subsequence, in (4.2)₂ and we obtain that p_ε^* satisfies (OS)_I; therefore $p_\varepsilon^* = p_{k_\varepsilon^*}^*$. From the uniqueness of the solution of (OS)_I we deduce that $\{p_{h_m}^*\}_{m \in \mathbb{N}}$ has a unique limit point. We also obtain from (OS)_I:

$$(4.3) \quad \int_D k_\varepsilon^* (\nabla p_{k_\varepsilon^*}^* \cdot \nabla \varphi_h + H_\varepsilon(p_{k_\varepsilon^*}^*) \frac{\partial \varphi_h}{\partial y}) dx dy = 0 \quad \forall \varphi_h \in H_h.$$

By computing (4.2)₂-(4.3) for $h = h_m$, with $\varphi_{h_m} = p_{h_m}^* - v_{h_m}$, $\{v_{h_m}\}_{m \in \mathbb{N}} \subset$

$V_{h_m}, v_{h_m} \rightarrow v$ strongly in $H^1(D)$ when $m \rightarrow \infty$, we get:

$$(4.4) \quad \begin{aligned} & \int_D k_{h_m}^* |\nabla(p_{h_m}^* - p_{k_\varepsilon}^\varepsilon)|^2 dx dy = - \int_D k_{h_m}^* \nabla(p_{h_m}^* - p_{k_\varepsilon}^\varepsilon) \cdot \nabla p_{k_\varepsilon}^\varepsilon dx dy \\ & + \int_D k_{h_m}^* \nabla(p_{h_m}^* - p_{k_\varepsilon}^\varepsilon) \cdot \nabla v_{h_m} dx dy - \int_D (k_{h_m}^* - k_\varepsilon^*) \nabla p_{k_\varepsilon}^\varepsilon \cdot \nabla(p_{h_m}^* - v_{h_m}) dx dy \\ & - \int_D (k_{h_m}^* - k_\varepsilon^*) H_\varepsilon(p_{h_m}^*) \frac{\partial}{\partial y} (p_{h_m}^* - v_{h_m}) dx dy \\ & - \int_D k_\varepsilon^* (H_\varepsilon(p_{h_m}^*) - H_\varepsilon(p_{k_\varepsilon}^\varepsilon)) \frac{\partial}{\partial y} (p_{h_m}^* - v_{h_m}) dx dy. \end{aligned}$$

By using the properties of $\{k_{h_m}^*\}_{m \in \mathbb{N}}$, $\{p_{h_m}^*\}_{m \in \mathbb{N}}$, $\{v_{h_m}\}_{m \in \mathbb{N}}$ and of the function H_ε it follows that for $m \rightarrow \infty$ the right member vanishes. Hence (4.4) gives $p_{h_m}^* \rightarrow p_{k_\varepsilon}^\varepsilon$ strongly in $H^1(D)$, when $m \rightarrow \infty$.

We prove next that $\{Q_{h_m}^*\}_{m \in \mathbb{N}}$ is bounded in $H^1(D)$. If $\{Q_{h_m}^*\}_{m \in \mathbb{N}}$ is bounded in $L^2(D)$, we obtain, from (4.2)₃, with $\varphi_{h_m} = Q_{h_m}^*$, the boundedness of $\{Q_{h_m}^*\}_{m \in \mathbb{N}}$ in $H^1(D)$. If $\{Q_{h_m}^*\}_{m \in \mathbb{N}}$ is not bounded in $L^2(D)$, we can extract a subsequence, denoted also by $\{Q_{h_m}^*\}_{m \in \mathbb{N}}$ with $\|Q_{h_m}^*\|_{L^2(D)} \rightarrow \infty$ when $m \rightarrow \infty$. We define $R_m = \frac{Q_{h_m}^*}{\|Q_{h_m}^*\|_{L^2(D)}}$. It is obvious that $\|R_m\|_{L^2(D)} = 1$ and $\{R_m\}_{m \in \mathbb{N}}$ is bounded in $H^1(D)$.

Multiplying (4.2)₃ for $h = h_m$ with $\frac{1}{\|Q_{h_m}^*\|_{L^2(D)}}$ we obtain:

$$(4.5) \quad \begin{aligned} & \int_D k_{h_m}^* (\nabla R_m \cdot \nabla \varphi_{h_m} + H'_\varepsilon(p_{h_m}^*) \frac{\partial R_m}{\partial y} \varphi_{h_m}) dx dy = \\ & - \frac{1}{\|Q_{h_m}^*\|_{L^2(D)}} \int_D \varphi_{h_m} dx dy \quad \forall \varphi_{h_m} \in H_{h_m}. \end{aligned}$$

For passing to the limit in (4.5), we use the properties: the embedding $H^1(D) \subset L^p(D) \forall 1 \leq p < \infty$ is compact, $k_{h_m}^* \rightarrow k_\varepsilon^*$ a.e. in D , $\varphi_{h_m} \rightarrow \varphi$ strongly in $H^1(D)$, on a subsequence $R_m \rightarrow R$ weakly in $H^1(D)$ and $H'_\varepsilon(p_{h_m}^*) \rightarrow H'_\varepsilon(p_\varepsilon^*)$ strongly in $L^4(D)$. The last assertion is a consequence of the regularity of the function H_ε . Passing to the limit with $m \rightarrow \infty$ in (4.5), we get:

$$(4.6) \quad \int_D k_\varepsilon^* (\nabla R \cdot \nabla \varphi + H'_\varepsilon(p_\varepsilon^*) \frac{\partial R}{\partial y} \varphi) dx dy = 0.$$

Combining (4.6) with $R = 0$ on $S_2 \cup S_3$, we obtain $R = 0$ in D i.e. a contradiction with $\|R\|_{L^2(D)} = 1$. Hence $\{Q_{h_m}^*\}_{m \in \mathbb{N}}$ is bounded in $H^1(D)$, which ensures the existence of a weak limit point in $H^1(D)$, Q_ε^* . Passing to the limit, as in (4.5),

on a subsequence, in (4.2)₃ for $h = h_m$ we obtain that Q_ε^* is the unique solution of (OS)_{II}, i.e. $Q_\varepsilon^* = Q_{k_\varepsilon^*}^*$. From the uniqueness of the solution of (OS)_{II} we obtain that $\{Q_{h_m}^*\}_{m \in \mathbb{N}}$ has a unique weak limit point. With a similar technique as in the first part of the proof, we obtain $Q_{h_m}^* \rightarrow Q_\varepsilon^*$ strongly in $H^1(D)$. Finally, by passing to the limit in (4.2) for $h = h_m$ it follows that $(k_\varepsilon^*, p_\varepsilon^*, Q_\varepsilon^*)$ satisfies (OS), which completes the proof.

In order to solve (4.2), we propose the following algorithm: for $k_{h0} \in K_h$ given, for any $m \in \mathbb{N}^*$ and for a suitable choice of a positive number ρ_m , we define $(k_{hm+1}^*, p_{hm}^*, Q_{hm}^*) \in K_h \times V_h \times H_h$ as a solution of the following problem:

$$(4.7) \begin{cases} \int_D k_{hm}^* (\nabla p_{hm}^* \cdot \nabla \varphi_h + H_\varepsilon(p_{hm}^*) \frac{\partial \varphi_h}{\partial y}) dx dy = 0 \quad \forall \varphi_h \in H_h, \\ \int_D k_{hm}^* (\nabla Q_{hm}^* \cdot \nabla \varphi_h + H'_\varepsilon(p_{hm}^*) \frac{\partial Q_{hm}^*}{\partial y} \varphi_h) dx dy = - \int_D \varphi_h dx dy \quad \forall \varphi_h \in H_h, \\ k_{hm+1}^* = \begin{cases} P_{K_h}(k_{hm}^* - \rho_m \frac{f_{hm}}{\|f_{hm}\|_{L^2(D)}}) & \text{if } \|f_{hm}\|_{L^2(D)} \neq 0, \\ k_{hm}^* & \text{if } \|f_{hm}\|_{L^2(D)} = 0, \end{cases} \end{cases}$$

where $f_{hm} = \nabla p_{hm}^* \cdot \nabla Q_{hm}^* + H_\varepsilon(p_{hm}^*) \frac{\partial Q_{hm}^*}{\partial y}$ and P_{K_h} is the projection map of the internal approximation of $L^2(D)$ on K_h . The projection map can be defined since K is a closed, convex subset of $L^2(D)$.

Proposition 4.2 *There exists sequences $\{\rho_m\}_{m \in \mathbb{N}}$, with $\rho_m \rightarrow 0$ when $n \rightarrow \infty$ such that $\{(k_{hm}^*, p_{hm}^*, Q_{hm}^*)\}_{m \in \mathbb{N}}$, defined by (4.7), is convergent to a solution of (4.2)₁–(4.2)₃.*

Proof. From (4.7)₃ and from the properties of the projection map it follows:

$$\|k_{hm+1}^* - k_{hm}^*\|_{L^2(D)} \leq \rho_m \quad \forall m \in \mathbb{N}.$$

We can find sequences $\{\rho_m\}_{m \in \mathbb{N}}$, $\rho_m \rightarrow 0$ when $n \rightarrow \infty$ such that the above inequality lead us to the fact that $\{k_{hm}^*\}_{m \in \mathbb{N}}$ is a Cauchy sequence in $L^2(D)$, hence strongly convergent to an element $k_h^* \in L^2(D)$. It can be proved as in Theorem 4.1 that $p_{hm}^* \rightarrow p_h^*$, $Q_{hm}^* \rightarrow Q_h^*$ strongly in $H^1(D)$ when $m \rightarrow \infty$, with (k_h^*, p_h^*, Q_h^*) satisfying (4.2)₁–(4.2)₃.

It is obvious that the interest is to obtain a sequence $\{k_{hm}^*\}_{m \in \mathbb{N}}$ which approximate a discrete optimal control k_h^* . The difficulty of the numerical computations will be to choose, for any $m \in \mathbb{N}^*$, $\rho_m > 0$ such that the above assertion on $\{k_{hm}^*\}_{m \in \mathbb{N}}$ hold and $J_\varepsilon(P_{K_h}(k_{hm}^* - \rho_m \frac{f_{hm}}{\|f_{hm}\|_{L^2(D)}})) \leq J_\varepsilon(k_{hm}^*)$, $k_{hm}^* - \rho_m \frac{f_{hm}}{\|f_{hm}\|_{L^2(D)}} \in K$.

We finish this section with the remark that the nonlinear problem (4.7)₁ was solved in Stavre and Vernescu (1989) for a less regular H_ε .

5. Numerical results

Our numerical tests have been performed for $D = (0, a) \times (0, h_1)$. We are interested in comparing the results for different values of $k_{h0} \in K_h$ and for different grids of the domain D . Let $\{\mathcal{T}_h\}_{h>0}$ be a regular family of triangulations of \bar{D} such that $\bar{D} = \bigcup_{T \in \mathcal{T}_h} T$, the finite elements T being triangles, as in Fig. 1. Let Σ_h be the set of mesh points in \bar{D} . V_h , H_h and K_h of Section 4 are given by:

$$\begin{cases} V_h = \{v_h \in C^0(\bar{D}) / v_h(n_i) = f(n_i) \forall n_i \in \Sigma_h \cap (S_2 \cup S_3), v_h|_T \in P_1 \forall T \in \mathcal{T}_h\}, \\ H_h = \{v_h \in C^0(\bar{D}) / v_h(n_i) = 0 \forall n_i \in \Sigma_h \cap (S_2 \cup S_3), v_h|_T \in P_1 \forall T \in \mathcal{T}_h\}, \\ K_h = K \cap \{v_h \in C^0(\bar{D}) / v_h|_T \in P_1 \forall T \in \mathcal{T}_h\}. \end{cases}$$

The aim of the first experiment is to compare the minimum values of the functional J_ε , the expressions of the pressure and the expressions of the permeability coefficient for different values of k_{h0} . The data common to all runs in the first experiment are: $a = 4$, $h_1 = 5$, $h_2 = 1.5$, $\alpha = 1$, $\beta = 50$, $r = 100$, $\varepsilon = 0.1$, for a mesh size $h = \Delta x = \Delta y = 0.25$. The following expressions of k_{h0} have been considered:

$$k_{h0}^1(x, y) = \begin{cases} 4, & \text{if } y \in [0, \frac{h_1}{2}), \\ 10, & \text{if } y \in [\frac{h_1}{2}, h_1], \end{cases} \quad k_{h0}^2(x, y) = \begin{cases} 4, & \text{if } y \in [0, \frac{h_1}{2}), \\ 4(y - \frac{h_1}{2} + 1), & \text{if } y \in [\frac{h_1}{2}, h_1], \end{cases}$$

$$k_{h0}^3(x, y) = \begin{cases} 2, & \text{if } x \in [0, \frac{a}{2}), \\ 2(x - \frac{a}{2} + 1), & \text{if } x \in [\frac{a}{2}, a], \end{cases} \quad k_{h0}^4(x, y) = 4.$$

In each case, the computed values of the functional J_ϵ decrease from one iteration to another. The CPU time for one iteration was 75 seconds and satisfactory convergence was obtained after 10-15 iterations. In all these cases, we obtained almost the same nodal values for the pressure; the minimum values of J_ϵ are contained in the interval $[14.76; 14.82]$. The expressions of the computed permeability coefficient which gives the minimum of J_ϵ , $k_{h_{min}}$, were different for different k_{h0} , but the ratio $k_{h_{min}}^l / k_{h0}^l$, $l = 1, \dots, 4$, was almost the same. We give below the nodal values of $k_{h_{min}}$

corresponding to k_{h0}^2 .

2.24	2.64	3.13	3.43	3.63	3.78	3.89	3.97	4.03	4.07	4.09	4.08	4.06	3.99	3.82	3.48	3.28
2.55	2.92	3.24	3.48	3.66	3.80	3.90	3.98	4.03	4.07	4.10	4.10	4.09	4.05	3.95	3.79	3.54
2.88	3.09	3.33	3.52	3.68	3.80	3.90	3.98	4.03	4.07	4.10	4.10	4.09	4.05	3.96	3.85	3.73
3.08	3.23	3.40	3.56	3.70	3.81	3.90	3.98	4.03	4.07	4.10	4.10	4.09	4.05	3.98	3.86	3.89
3.22	3.33	3.47	3.60	3.72	3.82	3.90	3.98	4.03	4.07	4.10	4.10	4.09	4.05	3.99	3.97	4.03
3.32	3.41	3.53	3.64	3.74	3.83	3.90	3.98	4.03	4.07	4.10	4.10	4.09	4.05	4.04	4.08	4.17
3.40	3.47	3.57	3.67	3.76	3.84	3.90	3.99	4.03	4.07	4.10	4.10	4.09	4.06	4.09	4.17	4.26
3.46	3.52	3.61	3.70	3.78	3.85	3.91	3.99	4.04	4.08	4.11	4.11	4.09	4.09	4.09	4.17	4.26
3.50	3.55	3.64	3.72	3.80	3.86	3.92	3.99	4.04	4.08	4.11	4.11	4.09	4.09	4.09	4.17	4.26
3.52	3.57	3.67	3.75	3.82	3.87	3.92	4.00	4.05	4.08	4.11	4.11	4.10	4.09	4.09	4.18	4.26
3.53	3.59	3.69	3.77	3.84	3.91	3.92	4.00	4.05	4.08	4.11	4.11	4.10	4.09	4.09	4.18	4.26
4.54	4.61	4.72	4.79	4.85	4.89	4.92	4.95	4.97	4.99	5.00	5.02	5.03	5.03	5.03	5.02	5.01
5.58	5.66	5.75	5.81	5.86	5.90	5.92	5.95	5.97	5.98	6.00	6.01	6.02	6.02	6.02	6.01	5.01
6.64	6.71	6.78	6.83	6.87	6.91	6.93	6.95	6.97	6.98	6.99	7.00	7.01	7.01	7.01	7.02	7.03
7.70	7.76	7.82	7.86	7.89	7.92	7.94	7.96	7.97	7.98	7.99	8.00	8.00	8.01	8.03	8.03	8.06
8.76	8.81	8.85	8.88	8.91	8.93	8.95	8.96	8.97	8.98	8.98	8.98	8.98	8.99	9.02	9.05	9.07
9.82	9.86	9.89	9.91	9.92	9.94	9.96	9.97	9.98	9.99	9.98	9.98	9.98	10.00	10.03	10.06	10.07
10.87	10.90	10.92	10.93	10.94	10.95	10.97	10.99	11.00	11.00	11.00	11.00	11.00	11.01	11.03	11.05	11.06
11.93	11.95	11.94	11.94	11.95	11.96	11.98	12.01	12.03	12.04	12.05	12.05	12.05	12.04	12.03	12.04	12.03
12.98	12.99	12.98	12.97	12.96	12.96	12.96	12.96	12.96	12.96	12.97	12.98	13.00	13.02	13.04	13.03	13.02
14.05	14.14	14.25	14.35	14.44	14.51	14.58	14.62	14.64	14.62	14.54	14.43	14.29	14.16	14.07	14.02	14.00

As it can be seen, the differences between $k_{h_{min}}$ and k_{h0} are greater near S_3 . There exists a good reason for this: the pressure of the fluid, which must be minimized, has the greatest values near the boundary in contact with the reservoirs.

The purpose of the second experiment is to compare the minimum values of J_ϵ for two different grids. We took: $a = 1.5$, $h_1 = 2.5$, $h_2 = 1.2$, $\alpha = 1$, $\beta = 50$, $r = 100$, $\epsilon = 0.1$ and $k_{h0} = k_{h0}^2$. The two different values of the mesh size h were 0.25 and

0.1. In the first case the minimum of J_ϵ was 2.21554 and in the second one, 2.22281.

For all the examples, the stopping test was:

$$|k_{hm+1}(n_i) - k_{hm}(n_i)| \leq 0.01 \quad \forall n_i \in \Sigma_h.$$

References

- Alt, H.W. (1979): Strömungen durch inhomogene poröse Medien mit freiem Rand. J. Reine Angew. Math. **305**, 89-115
- Alt, H.W. (1980): Numerical Solution of Steady-State Porous Flow Free Boundary Problems. Numer. Math. **36**, 73-98
- Barbu, V. (1984): Optimal Control of Variational Inequalities. Pitman, London
- Brezis, H., Kinderlehrer, D., Stampacchia, G. (1978): Sur une nouvelle formulation du problème de l'écoulement à travers une digue. C. R. Acad. Sci. Paris **287**, 711-714
- Carrillo-Menendez, J., Chipot, M. (1982): On the dam problem. J. Diff. Eqns. **45**, 234-271
- Chicco, M. (1970): Principio di massimo per soluzioni di problemi al contorno misti per equazioni ellittiche di tipo variazionale. Boll. U. M. I. **3**, 384-394
- Friedman, A., Huang, S. (1985): The Inhomogeneous Dam Problem with Discontinuous Permeability. Technical Report, Purdue University
- Friedman, A., Yaniro, D. (1985): Optimal control for the dam problem. Appl. Math. Optim. **13**, 59-78
- Friedman, A., Huang, S., Yong, J. (1987): Bang-Bang Optimal Control for the Dam Problem. Appl. Math. Optim. **15**, 65-85
- Gilbarg, D., Trudinger, N. (1977): Elliptic Partial Differential Equations of Second Order. Springer, Berlin Heidelberg New York
- Glowinski, R., Lions, J.L., Tremolières, R. (1981): Numerical Analysis of Varia-

tional Inequalities. North-Holland, Amsterdam

Stavre, R., Vernescu, B. (1985): Incompressible fluid flow through a non-homogeneous and anisotropic dam. Nonlin. Anal. TMA **9**, 799-810

Stavre, R., Vernescu, B. (1989): Free boundary properties in non-homogeneous porous media fluid flow. Int. J. Engng. Sci. **27**, 399-409

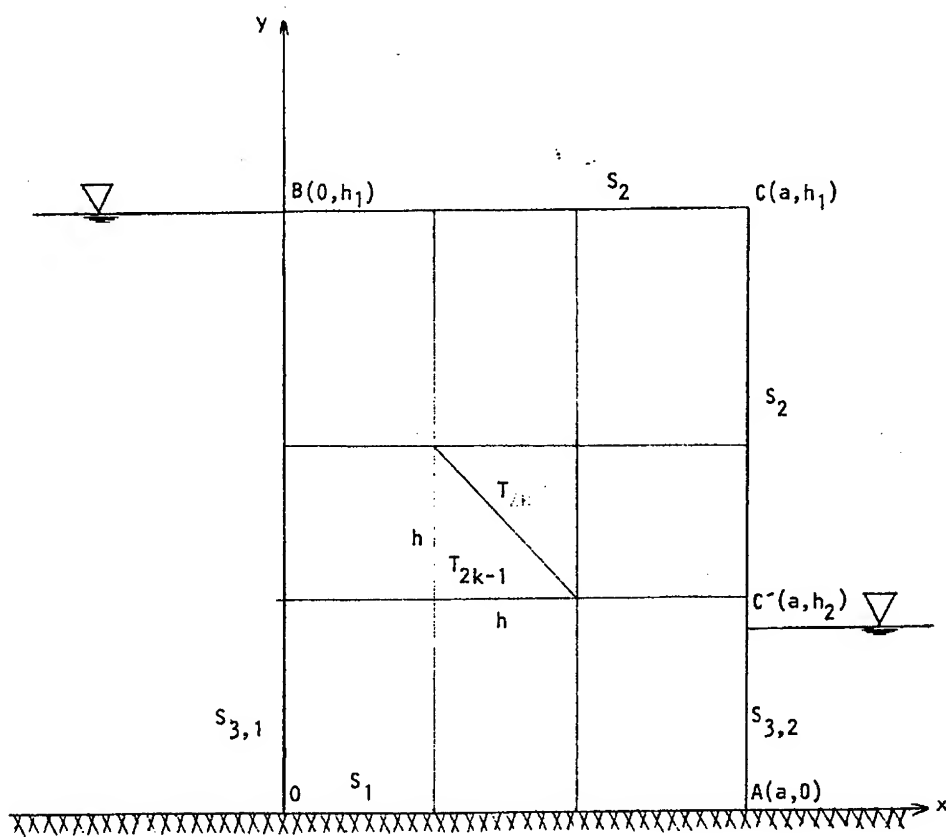


Fig. 1 The finite element mesh

THE EXACT SOLUTION IN THE CASE OF CERTAIN NON-LINEAR CAUCHY PROBLEM

By Vasile Marinca

"Politehnica" University Timișoara
Bd. Mihai Viteazul Nr.1

Abstract

The aim of this paper is to give a constructive existence frame for the analytic solutions by means of the linear equivalence method (LEM) for polynomial operators. Local representations of the solution are obtained by using Laplace transformation in combination with the matrix calculus. We obtain exactly solution in the form of series. The examples are given.

1. INTRODUCTION

The main idea of many of the papers dealing with nonlinear systems was to make an approach with linear cases. This was chiefly done by considering linear approximating operators, and therefore is the most part of cases only "small" nonlinearities could be controlled; convenient generalization could not be found. But common linearizations are in fact approximations that cut off the influence of the non-linear terms and thus do not provide exact informations on the behaviour of the solution. From the numerical point of view, collocation [2], shooting [1] and finite element method were used to get numerical approximations of the solution.

The problem of the differential polynomial operators appears in many concrete models of mathematical physics, elasticity and plasticity, mechanics of fluids etc. The large extension of polynomials models for various phenomena resulted in their study as a separate class of operators. A theoretic frame for polynomial operators was firstly set up in [3], the obtained results aiming especially generalization of Weierstrass's theorem and existence of solutions for abstract second degree polynomial equations.

In this paper it is given a constructive method for the analytic solutions of the certain polynomial problem, based on a linearization mapping, introduced and studied in [4, 5, 6]. It is proved that every polynomial differential system is equivalent to a linear system. The linear operator proposed here is not an approximation; it fully replaces the polynomial system. Is established a one-to-one correspondence between the solutions of initial polynomial problems and its linear equivalent system.

2. THE LINEAR EQUIVALENCE METHOD

The LEM was initially introduced for first order polynomial differential system [4], but it was extended without difficulties to canonic first order non-linear differential systems with right side analytic with respect to the unknown functions [6].

Let us consider the system

$$y' = P(x, y) \quad x \in [a, b] \subset \mathbb{R} \quad (1)$$

for $y = (y_j(x))_1^n \in (C^1([a, b]))^n$, where $P(x, y) = (P_j(x, y))_1^n$ are given by

$$P_j(x, y) = \sum_{|\nu| \leq p_j} a_{j\nu} y^\nu \quad (2)$$

In the relation (2), $p_j \in \mathbb{N}$ are fixed, ν are n -dimensional multiindices, $a_{j\nu}$ = constants, $a_{j0} = a_{j(0,0,\dots,0)} = 0$. Let us introduce also the initial conditions

$$y(x_0) = y_0, \quad x_0 \in [a, b] \quad (3)$$

Let be the exponential mapping:

$$v(x, z) = e^{(y, z)}, \quad (y, z) = \sum_{i=1}^n y_i z_i, \quad z \in \mathbb{R}^n \quad (4)$$

which, formally introduced in (1), leads to a linear P.D.E. of first order with respect to x :

$$\frac{\partial v}{\partial x} - (z, P(x, D)) v = 0 \quad (5)$$

where

$$(z, P(x, D)) = \sum_{j=1}^n z_j P_j(x, D)$$

$P_j(x, D)$ representing the corresponding to $P_j(x, y)$ differential polynomial:

$$P_j(x, D) = \sum_{|v| \leq p_j} a_{jv} \frac{\partial^{|v|}}{\partial z^v} ; \quad \frac{\partial^{|v|}}{\partial z^v} = \frac{\partial^{v_1+v_2+\dots+v_n}}{\partial z_1^{v_1} \partial z_2^{v_2} \dots \partial z_n^{v_n}} \quad (6)$$

Conditions (3) give

$$v(x_0, z) = e^{(y_0, z)} \quad (7)$$

The linear PDE (5) was called the linear equivalent of the polynomial system (1)

Proposition 1 [6]. The mapping $v(x, z)$, given by (4), establishes a one-to-one correspondence between the solutions of the initial polynomial problems (1), (3) and the analytic with respect to z solutions of its linear equivalent (5) under conditions (7).

More precisely, any solution of (1), (3) is such that the corresponding $v(x, z)$ satisfies the linear problem (5), (7) and conversely, any analytic with respect to z solution of (5), (7) is of the exponential form (4), with y solution of the polynomial initial problem (1), (3).

To use this proposition, let us expand $v(x, z)$ with respect to z under the form

$$v(x, z) = \sum_{|y| \geq 0} v_y(x) \frac{z^y}{y!} ; \quad v_0(x) = 1 ; \quad x \in [a, b] , \quad y \in \mathbb{N}^n \quad (8)$$

Introducing it in (5), gives the associated linear equivalent system of ordinary differential equations:

$$\frac{dv_y}{dx} = \sum_{j=1}^n \gamma_j \sum_{|v| \leq p_j} a_{jv} v_{y+v-s_j} ; \quad y = (y_1, y_2, \dots, y_j, \dots, y_n) \quad (9)$$

where

$$e_j = (\delta_j^k)_{1 \leq k \leq n} \quad (10)$$

δ_j^k being the Kronecker symbol.

The conditions (7) give

$$v_y(x_0) = y^y , \quad |y| \in \mathbb{N}^n \quad (11)$$

$$v_Y(x) = \sum_{i=0}^{\infty} v_Y^i (x - x_0)^i \quad (12)$$

Then, the equations (9) become:

$$(i+1)v_Y^i = \sum_{j=1}^n \gamma_j \sum_{|v| \leq p_j} a_{j,v} v_Y^{i-v}, \quad i \in \mathbb{N} \quad (13)$$

Proposition 2. The linear explicit algorithm (13) with conditions

$$v_0^0 = 1; \quad v_0^i = 0; \quad v_Y^0 = y_0^Y; \quad i \in \mathbb{N}^*; \quad \Theta = (0, 0, \dots, 0) \quad (14)$$

is convergent for

$$\begin{aligned} |x - x_0| &< \frac{1}{(p+1)CQ}; \quad p = \max_{1 \leq j \leq n} \{p_j\}; \quad C = \max\{a_{j,v}, 1 \leq j \leq n, |v| \leq p_j\}; \\ Q &= \sum_{|v| \leq p} |y_0^{Y-v}| \end{aligned} \quad (15)$$

Proof: For the first iteration we obtain:

$$|v_Y^1| = \left| \sum_{j=1}^n \gamma_j \sum_{|v| \leq p_j} a_{j,v} y_0^{Y-v} \right| \leq C \sum_{j=1}^n \gamma_j \sum_{|v| \leq p_j} |y_0^{Y-v}| \leq C |Y| Q |y_0^Y|$$

In general case, for the m^{th} iteration we obtain

$$|v_Y^m| \leq \frac{|Y|(|Y|+p)(|Y|+2p) \dots (|Y|+(m-1)p)}{m!} (CQ)^m |y_0^Y|$$

These results were used in (12) and therefore:

$$\begin{aligned} |v_Y(x)| &\leq \sum_{m=0}^{\infty} |v_Y^m| |x - x_0|^m \leq \sum_{m=0}^{\infty} \frac{|Y|(|Y|+p) \dots (|Y|+(m-1)p)}{m!} (CQ |x - x_0|)^m |y_0^Y| \leq \\ &\leq \sum_{m=0}^{\infty} |Y| \left(\frac{|Y|}{2} + \frac{p}{2} \right) \left(\frac{|Y|}{3} + \frac{2p}{3} \right) \dots \left(\frac{|Y|}{m} + \frac{(m-1)p}{m} \right) (CQ |x - x_0|)^m |y_0^Y| \leq \\ &\leq \sum_{m=0}^{\infty} ((|Y|+p) CQ |x - x_0|)^m |y_0^Y| \end{aligned}$$

For $|Y| = 1$ and x defined in (15), algorithm (13) is convergent.

Remark. For $|Y| = 1$ in [6] it is shown that algorithm (13) is convergent to the solution y of the problem (1), (3):

$$y(x) = \sum_{i=0}^{\infty} v_{e_j}^i (x-x_0)^i = v_{e_j}(x), \quad (16)$$

where

$$y = e_j \text{ if } |y| = 1$$

The solution y given by (16) is consistent.

3. THE SOLUTION OF THE SYSTEM (9)

The system (9) is linear and therefore using the Laplace transform:

$$\mathcal{L}v_y(x) = \bar{v}_y(s) = \int_0^{\infty} v_y(x) e^{-sx} dx \quad (17)$$

we can write the system (9) in the form:

$$s\bar{v}_y(s) - \sum_{j=1}^n \gamma_j \sum_{|v| \leq p_j} a_{jv} \bar{v}_{y+v-e_j}(s) = \bar{y}_0^y \quad (18)$$

With the notations:

$$V_1 = \{\bar{v}_y\}_{|y|=1}; \quad V = \{V_1\}_{1 \in \mathbb{N}^n}; \quad Y_{01} = \{\bar{y}_0^y\}_{|y|=1}; \quad Y_0 = \{Y_{01}\}_{1 \in \mathbb{N}^n} \quad (19)$$

the equations (18) can be write:

$$AV = Y_0 \quad (20)$$

where we notice that

$$A = \begin{bmatrix} A_{11} & A_{12} & A_{13} & \dots & A_{1p} & 0 & 0 & \dots \\ 0 & A_{22} & A_{23} & \dots & A_{2p} & A_{2,p+1} & 0 & \dots \\ 0 & 0 & A_{33} & \dots & A_{3,p+1} & 0 & \dots \\ \dots & \dots & \dots & A_{kk} & \dots & A_{k,k+p-1} & \dots \\ \dots & \dots & \dots & \dots & \dots & \dots & \dots \end{bmatrix} \quad (21)$$

and the cells A_{ij} are perfectly determined by the coefficients a_{ij} . The matrix A is row-and column-finite and it has a $(p+1)$ - cellular diagonal structure and may be easily generated, its form allowing the calculus by blockpartitioning ($p = \max \{p_i\}$) but the system (20) is infinite.

We introduce the matrix

$$B = \begin{bmatrix} B_{11} & B_{12} & B_{13} & \dots & B_{1,k} & \dots \\ 0 & B_{22} & B_{23} & \dots & B_{2,k} & \dots \\ 0 & 0 & B_{33} & \dots & B_{3,k} & \dots \\ \dots & \dots & \dots & \dots & \dots & \dots \end{bmatrix} \quad (22)$$

such that $BA = \text{diag} (E_1, E_2, \dots, E_l, \dots)$ where $E_i = \delta_i^k$ - the unit matrix of $(n-1+i)$ order. The equation (20) becomes:

$$V = BY_0 \quad (23)$$

and the cells B_{ik} can be determined by recurrence:

$$\begin{aligned} B_{11} &= A_{11}^{-1}; \quad B_{1,k} = -\left(\sum_{i=1}^{k-1} B_{1,i} A_{ik}\right) A_{kk}^{-1}, \quad 2 \leq k \leq p \\ B_{1,p+k} &= -\left(\sum_{i=1}^{p-1} B_{1,i} A_{i,p+k}\right) A_{p,p+k}^{-1}, \quad k \geq 1 \end{aligned} \quad (24)$$

Taking into account (16), in relation (23) is important only the first row:

$$V_1(s) = \sum_{i=1} B_{1,i}(s) Y_{0,i} \quad (25)$$

Using the inverse Laplace transform:

$$\mathcal{L}^{-1} \bar{V}_1(s) = v_1(x) \quad (26)$$

from the relation (25), we can determine the solution

$$y(x) = \mathcal{L}^{-1} \bar{V}_1(s), \quad |y| = 1 \quad (27)$$

4. EXAMPLES

a) Consider the initial problem for the equation

$$\begin{aligned} y'' + yy'^2 + y^3 &= 0 \\ y(0) &= 0, \quad y'(0) = 1 \end{aligned} \quad (28)$$

An exact solution of this problem is $y(x) = \sin x$. Let us obtain approximations by linearization. The linear system corresponding to (28) is

$$\frac{dv_{ij}}{dx} = i v_{i-1,j+1} - j(v_{i+1,j+1} + v_{i+3,j-1}), \quad i+j \geq 1 \quad (29)$$

The matrix A is:

$$A = \begin{bmatrix} A_{11} & A_{13} & 0 & 0 & \dots \\ 0 & A_{33} & A_{35} & 0 & \dots \\ 0 & 0 & A_{55} & A_{57} & \dots \\ \dots & \dots & \dots & \dots & \dots \end{bmatrix} \quad (30)$$

Where the cells A_{ij} are given by

$$A_{2j-1,2j-1} = \begin{bmatrix} s & 1-2j & 0 & 0 & 0 & \dots & 0 & 0 \\ 0 & s & 2-2j & 0 & 0 & \dots & 0 & 0 \\ 0 & 0 & s & 3-2j & 0 & \dots & 0 & 0 \\ 0 & 0 & 0 & s & 4-2j & \dots & 0 & 0 \\ \dots & \dots & \dots & \dots & \dots & \dots & \dots & \dots \\ 0 & 0 & 0 & 0 & 0 & \dots & s & -1 \\ 0 & 0 & 0 & 0 & 0 & \dots & 0 & s \end{bmatrix} \quad \text{of } (2j) \times (2j) \text{ order}$$

$$A_{2j-1,2j+1} = \begin{bmatrix} 0 & 0 & 0 & 0 & 0 & 0 & \dots & 0 & 0 & 0 & 0 \\ 1 & 0 & 1 & 0 & 0 & 0 & \dots & 0 & 0 & 0 & 0 \\ 0 & 2 & 0 & 2 & 0 & 0 & \dots & 0 & 0 & 0 & 0 \\ 0 & 0 & 3 & 0 & 3 & 0 & \dots & 0 & 0 & 0 & 0 \\ 0 & 0 & 0 & 4 & 0 & 4 & \dots & 0 & 0 & 0 & 0 \\ \dots & \dots & \dots & \dots & \dots & \dots & \dots & \dots & \dots & \dots & 0 \\ 0 & 0 & 0 & 0 & 0 & 0 & \dots & 2j-1 & 0 & 2j-1 & 0 \end{bmatrix} \quad \text{of } (2j) \times (2j+2) \text{ order}$$

The first row $B_{1,lj-1}$ of the matrix B given by (22) is:

$$B_{11} = A_{11}^{-1}; \quad B_{1,2j-1} = -B_{1,2j-3} A_{2j-3,2j-1} A_{2j-1,2j-1}^{-1}$$

and the column matrices V and Y are:

$$V = \{V_{2j-1}\}_{j \in \mathbb{N}^*}; \quad V_{2j-1} = \{\bar{V}_{ik}(s)\}_{1 \leq k \leq 2j-1}; \quad Y_0 = \{Y_{0,2j-1}\}; \quad Y_{0,2j-1} = \{\delta_{2j}^1\}_{1 \leq i \leq 2j}$$

The solution $V_1(s)$ given by (25) can be write by truncations:

$$V_1(s) = \sum_{j=1}^m B_{1,2j-1} Y_{0,2j-1}, \quad m \in \mathbb{N}^*$$

For different values of m , we obtain:

Table 1

m	$y(x)$
2	$x - \frac{x^3}{3!} - \frac{1}{20}x^5$
3	$x - \frac{x^3}{3!} + \frac{x^5}{5!} + \frac{1}{40}x^7 + \frac{1}{480}x^9$
4	$x - \frac{x^3}{3!} + \frac{x^5}{5!} - \frac{x^7}{7!} - \frac{13}{1080}x^9$
5	$x - \frac{x^3}{3!} + \frac{x^5}{5!} - \frac{x^7}{7!} + \frac{x^9}{9!} + \frac{7}{2160}x^{11}$

In this case $p = 3$, $c = 1$, $Q = 3$ therefore $x < 1/9$. From the above approximation it follows that if m increases, the coefficients of the approximation polynomial tends to the coefficients of Taylor's development of the exact solution and the m^{th} approximation is better than the corresponding development up to m .

b) Consider a straight bar of length L , reported to a left hand frame of reference Oxy . Assuming the Bernoulli-Euler hypothesis of plane sections, the axis $y = y(x)$ of the bar must verify the Bernoulli-Euler equation [7]:

$$y'' = \frac{M}{EI} \sqrt{1 + y'^2}^3 \quad (31)$$

where M is bending moment and EI the rigidity of bar (M, E, I - constants). Equation (31) must be completed with boundary conditions, whose nature depends of the nature of the physical problem. For instance, the cantilever bar requires Cauchy conditions:

$$y(0) = 0, \quad y'(0) = 0. \quad (32)$$

In order to make easier the application of the results in previous section, we shall firstly consider the transformation

$$w = \sqrt{1 + y'^2}; \quad u = y' \quad (33)$$

By thus, the Bernoulli Euler equation (31), becomes

$$\frac{dw}{dx} = kw^3; \quad \frac{du}{dx} = kw^3; \quad \left(k = \frac{M}{EI}\right); \quad y = (w, u) \quad (34)$$

Let us take $x \in [0, L]$. Conditions (30) become

$$w(0) = 1; \quad u(0) = 0 \quad (35)$$

The linear equivalence mapping will depend on two real parameters z_1 and z_2 , say

$$v(x, z_1, z_2) = e^{z_1 w + z_2 u} \quad (36)$$

The linear system corresponding to (34) is

$$v'_{ij} = k(i v_{i+1, j+1} + j v_{i+3, j-1})$$

The matrix A becomes:

$$A = \begin{bmatrix} A_{11} & A_{13} & 0 & 0 & \dots \\ 0 & A_{33} & A_{35} & 0 & \dots \\ 0 & 0 & A_{53} & A_{57} & \dots \\ \dots & \dots & \dots & \dots & \dots \end{bmatrix}$$

with

$$A_{2i-1, 2i-1} = \begin{bmatrix} s & 0 & 0 & \dots & 0 \\ 0 & s & 0 & \dots & 0 \\ 0 & 0 & s & \dots & 0 \\ \dots & \dots & \dots & \dots & \dots \\ 0 & 0 & 0 & \dots & s \end{bmatrix} \quad \text{of } (2i) \times (2i) \text{ order}$$

$$A_{2i-1, 2i+1} = k \begin{bmatrix} 0 & 1-2i & 0 & 0 & 0 & \dots & 0 & 0 & 0 & 0 \\ -1 & 0 & 2-2i & 0 & 0 & \dots & 0 & 0 & 0 & 0 \\ 0 & -2 & 2 & 3-2i & 0 & \dots & 0 & 0 & 0 & 0 \\ 0 & 0 & -3 & 0 & 4-2i & \dots & 0 & 0 & 0 & 0 \\ \dots & \dots & \dots & \dots & \dots & \dots & \dots & \dots & \dots & \dots \\ 0 & 0 & 0 & 0 & 0 & \dots & 0 & -1 & 0 & 0 \\ 0 & 0 & 0 & 0 & 0 & \dots & 1-2i & 0 & 0 & 0 \end{bmatrix}$$

of $(2i) \times (2i+2)$ order

Unlike example a), $Y_{0,ij-1} = \{\delta_i^1\}_{1 \leq i \leq j}$, but in the solution

$$V_1(s) = \sum_{j=1}^n B_{1,2j-1} Y_{0,2j-1}$$

we consider the second row and, for different values of n we obtain:

Table 2

n	$y'(x)$	$y(x)$
2	kx	$\frac{kx^2}{2}$
4	$kx + \frac{(kx)^3}{2}$	$\frac{kx^2}{2} + \frac{k^3 x^4}{8}$
6	$kx + \frac{(kx)^3}{2} + \frac{3}{8} (kx)^5$	$\frac{kx^2}{2} + \frac{k^3 x^4}{8} + \frac{3}{40} k^5 x^6$
8	$kx + \frac{(kx)^3}{2} + \frac{3}{8} (kx)^5 + \frac{5}{16} (kx)^7$	$\frac{kx^2}{2} + \frac{k^3 x^4}{8} + \frac{3}{40} k^5 x^6 + \frac{5}{112} k^7 x^8$

For a steel bar: $E = 21000 \text{ [kN/cm}^2\text{]}$, $M = 40 \text{ [kN/cm]}$, $I = 1/2 \text{ [cm}^4\text{]}$ we obtain $k = 3,8095 \cdot 10^{-3} \text{ [1/cm]}$. From the relation (31) we define

$$\epsilon = \max_{x \in [0, L]} |y'' - k \sqrt{1 + y'^2}|$$

such that result the following values for ϵ ($L = 100 \text{ [cm]}$):

Table 3

n	ϵ
2	$8,57 \cdot 10^{-4}$
4	$1,62 \cdot 10^{-4}$
6	$2,82 \cdot 10^{-5}$
8	$3,89 \cdot 10^{-6}$

5. CONCLUSIONS

The exposed method has many advantages, especially for the constructive existence of solutions for polynomial differential operators and offers a general tool that might to used for any physical phenomenon. Local representations of the solution are obtained by using a matrix that depends only on the operator and not on the initial conditions.

R E F E R E N C E S

- [1] LAMBERT, J.D. "A Modification of the Shooting Method for Two-point Boundary Value Problems" - Intern.Schrift. Numerische Math., Birkhäuser Verlag, Basel und Stuttgart 19 pp.133-143 (1974).
- [2] MEIROVITCH, L. "Analytical methods in vibrations" Mac Millan Comp. N.Y., London (1967).
- [3] RALL, L.B. "Solutions for Abstract Polynomial Equations by Iterative Method" MRC Report # 892 (1968).
- [4] TOMA, I. "On Polynomial Differential Equations", Bull.Math Soc.Sci.Math.de la RSR, 24(72), 4, pp.417-424 (1980).
- [5] TOMA, I. "Extension of Linearization Method for Polynomial Operators", Rev. Roum.des Math.Pures et Appl, 31(6), pp.531-538 (1983).
- [6] TOMA, I., "Metoda echivalenței lineare și aplicațiile ei", Ed.Flores (1995).
- [7] TEODORESCU, P.P., ILLE, V. "Teoria elasticității și introducere în mecanica solidelor deformabile" Ed.Dacia, Cluj-Napoca (1979).

ON THE MINIMALLY SUPPORTED FREQUENCY WAVELETS AND SCALING FUNCTIONS

P. GĂVRUȚĂ

Department of Mathematics, "Politehnica" University,
Piața Horațiu No. 1, 1900 - Timișoara, Romania

Abstract We give a new characterization of minimally supported frequency wavelets (unimodular wavelets).

We present also an elementary proof for the characterization of the scaling function of a multiresolution analysis and as an application we give an extension of a result of D. - X. Zhou concerning the Lemarié - Meyer scaling function.

A wavelet for $L^2(\mathbb{R})$ is a function $\psi \in L^2(\mathbb{R})$ so that

$\{\psi_{j,k}\}_{j,k \in \mathbb{Z}}$ is an orthonormal basis for $L^2(\mathbb{R})$, where

$$\psi_{j,k}(x) = 2^{j/2} \psi(2^j x - k), \quad x \in \mathbb{R}; j, k \in \mathbb{Z}.$$

They are useful in many areas of mathematics, image and signal processing, turbulence, optics, physics, medicine. See for example the books [3], [4], [5], [10], [15].

If ψ is an wavelet for $L^2(\mathbb{R})$, then ψ is an admissible function; more exactly we have the following result.

PROPOSITION 1. If ψ is a wavelet for $L^2(\mathbb{R})$, then

$$\int_0^\infty \frac{|\hat{\psi}(\omega)|^2}{\omega} d\omega < \infty.$$

P. Lemarié proves in [12] this result using the Poisson formula.

The orthonormality of the system $\{\psi_{j,k}\}_{j,k \in \mathbb{Z}}$ in $L^2(\mathbb{R})$ can be characterized in the following way.

LEMMA 1. Let be $\psi \in L^2(\mathbb{R})$. Then $\{\psi_{j,k}\}_{j,k \in \mathbb{Z}}$ is an orthonormal system in $L^2(\mathbb{R})$ if and only if

$$\sum_{k \in \mathbb{Z}} \hat{\psi}(2^j(\omega + 2k\pi)) \overline{\hat{\psi}(\omega + 2k\pi)} = \delta_{j,0} \quad (1)$$

for a.e. $\omega \in [-\pi, \pi]$, $j \geq 0$.

For a proof see [8] or [2]. ($\hat{\psi}$ denotes the Fourier transform of ψ).

The wavelets in $L^2(\mathbf{R})$ can be characterized also.

THEOREM I. Let $\psi \in L^2(\mathbf{R})$ with $\|\psi\|_2 = 1$. Then ψ is a wavelet for $L^2(\mathbf{R})$ if and only if

$$\sum_{j \in \mathbf{Z}} |\hat{\psi}(2^j \omega)|^2 = 1, \quad (2)$$

for a.e. $\omega \in \mathbf{R}$;

$$\sum_{j=0}^{\infty} \hat{\psi}(2^j \omega) \overline{\hat{\psi}(2^j(\omega + 2k\pi))} = 0, \quad (3)$$

for a.e. $\omega \in \mathbf{R}$, $k \in \mathbf{N}$ odd.

See [7], [8], [9].

In particular, if $\psi \in L^2(\mathbf{R})$ is a unimodular function, that is

$$|\hat{\psi}(\omega)| = 1 \quad \text{for } \omega \in \text{supp } \hat{\psi},$$

we have the following result.

THEOREM II. Let ψ be a unimodular function in $L^2(\mathbf{R})$. Then ψ is a wavelet for $L^2(\mathbf{R})$ if and only if the following hold:

$$\sum_{k \in \mathbf{Z}} |\hat{\psi}(\omega + 2k\pi)|^2 = 1 \quad \text{a.e. } \omega \in [-\pi, \pi]; \quad (4)$$

$$\sum_{k \in \mathbf{Z}} |\hat{\psi}(2^j \omega)|^2 = 1 \quad \text{a.e. } \omega \in \mathbf{R}; \quad (5)$$

See [8], [6].

We can prove the following theorem.

THEOREM III. Let ψ be a unimodular function in $L^2(\mathbf{R})$ so that $\|\psi\|_2 =$

1. Then ψ is a wavelet for $L^2(\mathbf{R})$ if and only if the following hold:

$$\sum_{k \in \mathbf{Z}} |\hat{\psi}(\omega + 2k\pi)|^2 = \sum_{j \in \mathbf{Z}} |\hat{\psi}(2^j \omega)|^2 \quad \text{a.e. } \omega \in \mathbf{R}; \quad (6)$$

Proof. We denote

$$\Psi_1(\omega) = \sum_{k \in \mathbf{Z}} |\hat{\psi}(\omega + 2k\pi)|^2$$

and

$$\Psi_2(\omega) = \sum_{k \in \mathbb{Z}} |\hat{\psi}(2^k \omega)|^2.$$

If $\{c_n\}_{n \in \mathbb{Z}}$ is the sequence of Fourier coefficients for Ψ_1 , we have

$$c_n = \frac{1}{2\pi} \int_{-\pi}^{\pi} \Psi_1(\omega) e^{-in\omega} d\omega = \frac{1}{2\pi} \int_0^{\pi} \Psi_1(\omega - \pi) e^{-in(\omega - \pi)} d\omega + \frac{1}{2\pi} \int_0^{2\pi} \Psi_1(\omega) e^{-in\omega} d\omega$$

From (6) it follows

$$\Psi_1(\omega - \pi) = \Psi_1(2\omega - 2\pi) = \Psi_1(2\omega) = \Psi_1(\omega)$$

hence

$$c_n = (1 + e^{in\pi}) \frac{1}{2\pi} \int_0^{\pi} \Psi_1(\omega) e^{-in\omega} d\omega.$$

It follows

$$c_{2m} = \frac{1}{\pi} \int_0^{\pi} \Psi_1(\omega) e^{-i2m\omega} d\omega = \frac{1}{\pi} \int_0^{\pi} \Psi_1(2\omega) e^{-i2m\omega} d\omega = \frac{1}{2\pi} \int_0^{2\pi} \Psi_1(\omega) e^{-im\omega} d\omega$$

hence $c_{2m} = c_m$, $m \in \mathbb{Z}$. From this relation it follows

$$c_{2^s m} = c_m \quad \text{for } s \in \mathbb{N}$$

If $m \neq 0$ we have

$$\lim_{s \rightarrow \infty} 2^s m = \begin{cases} \infty, & \text{if } m > 0 \\ -\infty, & \text{if } m < 0 \end{cases}$$

Then, from Riemann - Lebesgue Lemma it follows

$$\lim_{s \rightarrow \infty} c_{2^s m} = 0, \quad m \neq 0$$

hence $c_m = 0$, $m \neq 0$. It follows

$$\Psi_1(\omega) = c_0 = \frac{1}{2\pi} \int_0^{2\pi} \left(\sum_{k \in \mathbb{Z}} |\hat{\psi}(\omega + 2k\pi)|^2 \right) d\omega = \frac{1}{2\pi} \int_{-\infty}^{\infty} |\hat{\psi}(\omega)|^2 d\omega = 1$$

by Plancherel formula.

Multiresolution analysis provides a natural framework for the construction of wavelets. See [3], [4], [5], [10], [15].

A multiresolution analysis for $L^2(\mathbb{R})$ consists of a sequence $\{V_j\}_{j \in \mathbb{Z}}$ of closed subspaces of $L^2(\mathbb{R})$ such that

$$V_j \subset V_{j+1} \quad \text{for all } j \in \mathbb{Z}; \quad (7)$$

$$f \in V_j \Leftrightarrow f(2^j \cdot) \in V_{j+1} \quad \text{for all } j \in \mathbb{Z}; \quad (8)$$

$$\bigcap_{j \in \mathbb{Z}} V_j = \{0\}; \quad (9)$$

$$\overline{\bigcup_{j \in \mathbb{Z}} V_j} = L^2(\mathbb{R}); \quad (10)$$

there exists $\varphi \in V_0$ so that $\{\varphi(\cdot - k)\}_{k \in \mathbb{Z}}$ is an orthonormal basis for V_0 . (11)

The function φ is called a scaling function for the multiresolution analysis $\{V_j\}_{j \in \mathbb{Z}}$.

Recently, E. Hernández, X. Wang and G. Weiss [9] give the following characterization of a scaling function.

THEOREM IV. A function $\varphi \in L^2(\mathbb{R})$ is a scaling function of an multiresolution analysis of $L^2(\mathbb{R})$ if and only if

$$\sum_{k \in \mathbb{Z}} |\hat{\varphi}(\omega + 2k\pi)|^2 = 1 \quad \text{for a.e. } \omega \in [-\pi, \pi]; \quad (12)$$

$$\lim_{j \rightarrow \infty} |\hat{\varphi}(2^{-j}\omega)| = 1 \quad \text{for a.e. } \omega \in \mathbb{R} \quad (13)$$

$$\hat{\varphi}(2\omega) = m_0(\omega)\hat{\varphi}(\omega) \text{ a.e. on } \mathbb{R}, \quad (14)$$

for some 2π - periodic function m_0 .

The function m_0 is called the low-pass filter associated with φ .

The key in their proof is the following result.

PROPOSITION 2. We suppose that (7), (8) and (11) holds. Then (10) \Leftrightarrow (13).

It is well-known that the function defined by

$$\hat{\psi}(2\omega) = e^{-i\omega} v(2\omega) \overline{m_0(\omega + \pi)} \hat{\varphi}(\omega), \quad (15)$$

a.e. $\omega \in \mathbb{R}$, where v is 2π -periodic, measurable function such that

$$|v(\omega)| = 1 \quad \text{for a.e. } \omega \in [-\pi, \pi],$$

is a wavelet for $L^2(\mathbb{R})$. We say that ψ is associated with a multiresolution analysis.

It is possible to construct a wavelet ψ for $L^2(\mathbb{R})$ which is not associated with a multiresolution analysis. See [5].

G.Gripenberg [7] gives a characterization of the wavelets associated with a multiresolution analysis.

THEOREM V. A wavelet $\psi \in L^2(\mathbb{R})$ is associated with an multiresolution analysis if and only if

$$D_\psi(\omega) = 1 \quad \text{for a.e. } \omega \in [-\pi, \pi] \quad (16)$$

where

$$D_\psi(\omega) = \sum_{j=1}^{\infty} \sum_{k \in \mathbb{Z}} |\hat{\psi}(2^j(\omega + 2k\pi))|^2. \quad (17)$$

Using an idea of P.Auscher [1], E.Hernández, X.Wang and G.Weiss [9] give another proof for this theorem. The key of their proof is the following proposition.

PROPOSITION 3. Let be $\psi \in L^2(\mathbb{R})$ a wavelet. Denote

$$\tilde{\Psi}_j(\omega) = \{\hat{\psi}(2^j(\omega + 2k\pi)); k \in \mathbb{Z}\} \quad \text{a.e. } \omega \in [-\pi, \pi],$$

$j \geq 1$ and $F_\psi(\omega)$ the closed subspace of $l^2(\mathbb{Z})$ generated by the system $\{\tilde{\Psi}_j(\omega); j \geq 1\}$. Then

$$\dim F_\psi(\omega) = D_\psi(\omega).$$

In the following we give more simple and elementary proofs for the Propositions 1,2.

Moreover, as an application of Theorem IV, we give a more simple proof (in a more general form) of a result of D.-X.Zhou concerning the Lemarié-Meyer scaling function.

We use the following lemma.

LEMMA 2 Let be $\varphi \in L^2(\mathbb{R})$ so that the system $\{\varphi(\cdot - k)\}_{k \in \mathbb{Z}}$ is an orthonormal basis for the closed subspace V_0 of $L^2(\mathbb{R})$ and we denote

$$V_j = \{f(2^j \cdot) | f \in V_0\}, \quad j \in \mathbb{Z}.$$

We denote also by P_j the orthogonal projection of $L^2(\mathbb{R})$ on V_j . If $f \in L^2(\mathbb{R})$ is so that \hat{f} is bounded and the support of \hat{f} is in $[-R, R]$ for $R > 0$, then for $j \in \mathbb{Z}$, $j \geq \log_2 \frac{R}{\pi}$ we have

$$\|P_j f\|_2^2 = \frac{1}{2\pi} \int_{-\infty}^{\infty} |\hat{f}(\omega)|^2 |\hat{\psi}(2^{-j}\omega)|^2 d\omega. \quad (18)$$

Proof. We have as in [9]

$$\begin{aligned} \|P_j f\|_2^2 &= \sum_{k \in \mathbb{Z}} |\langle f, \varphi_{j,k} \rangle|^2 = \frac{1}{4\pi^2} \sum_{k \in \mathbb{Z}} |\langle \hat{f}, \hat{\varphi}_{j,k} \rangle|^2 = \\ &= \frac{1}{4\pi^2} \sum_{k \in \mathbb{Z}} \left| \int_{-\infty}^{\infty} 2^{-j/2} \hat{f}(\omega) \overline{\hat{\psi}(2^{-j}\omega)} e^{i2^{-j}k\omega} d\omega \right|^2. \end{aligned}$$

The support of function $\omega \rightarrow \hat{f}(\omega) \overline{\hat{\psi}(2^{-j}\omega)}$ is in $[-\pi 2^j, \pi 2^j]$ for $j \geq \log_2 \frac{R}{\pi}$.

An application of Parseval formula on $[-\pi 2^j, \pi 2^j]$ gives (18).

PROOF OF PROPOSITION 1. If ψ is a wavelet for $L^2(\mathbb{R})$, we have for $f \in L^2(\mathbb{R})$ so that \hat{f} is bounded and the support of \hat{f} is in $[-\pi, \pi]$

$$\|f\|_2^2 = \sum_{j,k \in \mathbb{Z}} |\langle f, \psi_{j,k} \rangle|^2 \geq \sum_{j=0}^{\infty} \frac{1}{2\pi} \int_{-\infty}^{\infty} |\hat{f}(\omega)|^2 |\hat{\psi}(2^{-j}\omega)|^2 d\omega.$$

We take f so that

$$\hat{f}(\omega) = \begin{cases} \frac{1}{\sqrt{\omega}} & \text{if } \omega \in [\frac{\pi}{2}, \pi] \\ 0 & \text{if } \omega \notin [\pi/2, \pi] \end{cases}.$$

It follows

$$\frac{1}{2\pi} \sum_{j=0}^{\infty} \int_{\frac{\pi}{2}}^{\pi} \frac{|\hat{\psi}(2^{-j}\omega)|^2}{\omega} d\omega = \frac{1}{2\pi} \sum_{j=0}^{\infty} \int_{\frac{\pi}{2^{j+1}}}^{\frac{\pi}{2^j}} \frac{|\hat{\psi}(\omega)|^2}{\omega} d\omega = \frac{1}{2\pi} \int_0^{\pi} \frac{|\hat{\psi}(\omega)|^2}{\omega} d\omega \leq \|f\|_2^2 < \infty.$$

PROOF OF PROPOSITION 2. If (10) holds, then

$$\|P_j f\|_2^2 \xrightarrow{(j \rightarrow \infty)} \|f\|_2^2$$

for every $f \in L^2(\mathbb{R})$. For f with $\hat{f} = \chi_{[-\pi, \pi]}$ it follows by (18)

$$\lim_{j \rightarrow \infty} \frac{1}{2\pi} \int_{-\pi}^{\pi} |\hat{\psi}(2^{-j}\omega)|^2 d\omega = 1$$

and since the sequence $\{|\hat{\psi}(2^{-j}\omega)|\}_{j \geq 1}$ is nondecreasing ([9]) it follows (13).

If (13) holds, from Lebesgue Theorem we have by (18)

$$\|P_j f\|_2^2 \xrightarrow{(j \rightarrow \infty)} \frac{1}{2\pi} \int_{-\infty}^{\infty} |\hat{f}(\omega)|^2 d\omega = \|f\|_2^2$$

for all $f \in L^2(\mathbb{R})$ with \hat{f} bounded and the support of \hat{f} compact. Since these functions are dense in $L^2(\mathbb{R})$ we have (10).

In [17], D.-X. Zhou give an example to show that the center of a skew-symmetric scaling function $\varphi \in L^2(\mathbb{R})$ may not be in $\mathbb{Z}/2$. His proof used a result of R.Q. Jia and C.A. Micchelli [11].

In the following we give an extension of Zhou's result as an application of Theorem IV.

THEOREM VI. Let be $0 < \varepsilon \leq \pi/3$ and $\varphi \in L^2(\mathbb{R})$ such that

$$\hat{\varphi} \text{ is continuous and even:} \quad (19)$$

$$\text{supp } \hat{\varphi} \subset [-\pi-\varepsilon, \pi+\varepsilon] \quad (20)$$

$$\hat{\varphi}(\omega)=1, \quad \omega \in [-\pi+\varepsilon, \pi-\varepsilon]; \quad (21)$$

$$|\hat{\varphi}(\omega)|^2 + |\hat{\varphi}(2\pi-\omega)|^2=1, \quad \omega \in [\pi-\varepsilon, \pi+\varepsilon]. \quad (22)$$

Let be $a \in \mathbb{R}$ and $\varphi_a := \varphi(\cdot - a)$. Then φ_a is a scaling function for a multiresolution analysis.

Proof. We take

$$m_0(\omega) = e^{ia\omega} \sum_{k \in \mathbb{Z}} e^{2\pi k a i} \hat{\varphi}(2\omega + 4k\pi) \quad (23)$$

and prove that

$$\hat{\varphi}_a(\omega) = m_0\left(\frac{\omega}{2}\right) \hat{\varphi}_a\left(\frac{\omega}{2}\right) \quad (24)$$

or equivalent

$$\hat{\varphi}(\omega) = m_0\left(\frac{\omega}{2}\right) e^{-ia\frac{\omega}{2}} \hat{\varphi}\left(\frac{\omega}{2}\right) \quad (25)$$

We have two cases

a) $\omega \notin \text{supp } \hat{\varphi}$. If $\hat{\varphi}(\omega/2) = 0$, then (25) holds.

If $\hat{\varphi}(\omega/2) \neq 0$ it follows $-\pi - \varepsilon \leq \omega/2 \leq \pi + \varepsilon$, hence $\omega + 4\pi \geq 2\pi - 2\varepsilon$ and $\omega - 4\pi \leq -2\pi + 2\varepsilon$ and from the condition $0 < \varepsilon \leq \pi/3$ it follows $\omega + 4\pi \geq \pi + \varepsilon$ and $\omega - 4\pi < -\pi - \varepsilon$, hence

$$\hat{\varphi}(\omega + 4k\pi) = 0 \quad \text{for } k \neq 0.$$

It follows

$$m_0\left(\frac{\omega}{2}\right) = e^{ia\omega} \hat{\varphi}(\omega) = 0.$$

b) $\omega \in \text{supp } \hat{\varphi}$. It follows $-\pi - \varepsilon \leq \omega \leq \pi + \varepsilon$ and from condition $0 < \varepsilon \leq \pi/3$ it follows $-\pi + \varepsilon \leq \omega/2 \leq \pi - \varepsilon$ hence $\hat{\varphi}(\omega/2) = 1$. On the other hand, from

(23) it follows $m_0\left(\frac{\omega}{2}\right) = e^{ia\frac{\omega}{2}} \hat{\varphi}(\omega)$. Hence, (25) holds.

The conclusion it follows from Theorem IV.

REMARK. We can prove a converse of the above result:

Let be $0 < \varepsilon$, $\varepsilon' < \pi$ and $\varphi \in L^2(\mathbb{R})$ so that

$$\hat{\varphi} \text{ is continuous and even} \quad (26)$$

$$\text{supp } \hat{\varphi} = [-\pi - \varepsilon', \pi + \varepsilon'] \quad (27)$$

$$\hat{\varphi}(\omega) = 1, \quad \omega \in [-\pi + \varepsilon, \pi - \varepsilon] \quad (28)$$

$$|\hat{\varphi}(\omega)| < 1, \quad \omega \notin [-\pi + \varepsilon, \pi - \varepsilon]. \quad (29)$$

If φ is a scaling function with a continuous low-pass filter, then $\varepsilon' = \varepsilon \leq \pi/3$ and the relation (22) holds.

For other properties of Lemarié-Meyer wavelets see [16], [18].

DISCUSSION. 1. Proposition 1 can be also proved using the relation (5). See [12] or the recently book

[HW] E. Hernández, G. Weiss, A. First Course on Wavelets, CRC Press, 1996

2. We can prove the Theorem III without to use the Riemann-Lebesgue lemma. Indeed, from

$$c_n = \left(1 + e^{in\pi}\right) \frac{1}{2\pi} \int_0^\pi \psi_1(\omega) e^{-in\omega} d\omega,$$

it follows that $c_n = 0$ for all $n \in 2\mathbb{Z} + 1$. If m is even and $m \neq 0$, we can write $m = 2^p n$ with $p \in \mathbb{N}$ and $n \in 2\mathbb{Z} + 1$. It follows

$$c_m = c_{n2^p} = c_n = 0$$

since n is odd.

3. The formula (18) was obtained, but using the Poisson formula in W.R.Madych, Some Elementary Properties of Multiresolution Analyses of $L^2(\mathbb{R}^n)$, in Wavelets - A Tutorial in Theory and Applications (C.K.Chui, ed.), Academic Press, 1992, 259-294 and, with essentially the same argument as in our paper, in [HW]. Also the proof of Proposition 2 is essentially the same argument given in [HW] (pages 382 and 384).

Our results were independently obtained in the preprint P.Găvruta, On a characterization of the scaling functions and some classes of wavelets, SLOHA, Univ. of Timișoara, No.5/1996,

ACKNOWLEDGEMENTS. I am pleased to express my gratitude to Professor E.Hernández for his comments on this paper.

REFERENCES

1. Auscher, P., Solution of two problems on wavelets, *Journal of Geometric Analysis*, vol.5, No.2, 1995
2. A.Bonami, F.Soria, G.Weiss, Band-limited wavelets, in *Fourier Analysis and Partial Differential Equations* (Ed.J.Garcia-Cuerva, E.Hernandez, F.Soria, J.L.Torrea), CRC Press, Boca Raton-London-Tokyo, 1995 (21-56)
3. C.K.Chui, *An Introduction to Wavelets*, Academic Press, New York, 1992
4. A.Cohen, *Ondelettes et traitement numérique du signal*, Masson, 1992
5. I.Daubechies, *Ten Lectures on Wavelets*, CBMS-NSF Regional Conference Series in Applied Mathematics 61, SIAM, 1992
6. X.Fang, X.Wang, Construction of Minimally-Supported-Frequencies Wavelets, preprint
7. G.Gripenberg, A necessary and sufficient condition for the existence of a father wavelet, *Studia Math.* 114(1995), no.3, pp.207-226
8. Y-H. Ha, H.Kang, J.Lee, J.Seo, Unimodular wavelets for L^2 and the Hardy space H^2 , *Michigan Math.J.*, 41, 1994, pp.345-361
9. E.Hernández, X.Wang, G.Weiss, Characterization of Wavelets, Scaling Functions and Wavelets Associated with Multiresolution Analysis, Preprint
10. G. Kaiser, *A Friendly Guide to Wavelets*, Birkhauser; Boston, Basel, Berlin, 1994
11. R.Q. Jia and C.A. Micchelli, Using the refinement equation for the construction of pre-wavelets. II. Power of two, in *Curves and Surfaces* (P.J.Laurent, A.Le Méhauté, and L.L.Schumaker, Eds.) Academic Press, 1991, pp.209-246
12. P.G.Lemarié, Sur l'existence des analyses multi-résolutions en théorie des ondelettes, *Revista Matemática Iberoamericana*, vol.8, No.3, 1992, pp.457-474
13. P.G. Lemarié, Y.Meyer, Ondelettes et Basis Hilbertiennes, *Revista Matemática Iberoamericana*, 2(1986), pp. 1-18

14. S.Mallat, Multiresolution approximations and wavelet orthonormal bases for $L^2(\mathbb{R})$, Trans Amer. Math.Soc., 315, 1989, pp.69-87
15. Y.Meyer, Ondelettes et Operateurs. I. Ondelettes; Herman, Paris, 1990
16. A.I.Zayed and G. G.Walter, Characterization of Analytic Functions in Terms of Their Wavelet Coefficients, J. of Complex Variable: Theory and Applications, to appear
17. D.-X. Zhou, Construction of Real-Valued Wavelets by Symmetry, Journal of Approximation Theory, 1995, pp.323-331
18. G.G.Walter, Translation and Dilation Invariance in Orthogonal Wavelets, Appl. Comp.Harmonic Analysis, 1 (1994), pp.344-349

SOME COMPLEXITY ISSUES CONCERNING A SPECIFIC NONLINEAR DYNAMIC SYSTEM

Ligia-Loretta Cristea, Nicolae Szirbik, Ștefan Holban
Technical University of Timișoara
România

Abstract

We study the numerical methods to compute the parameters for a specific N -dimensional nonlinear dynamic system in order to have a desired behavior. Desired behavior can be stated as a sequence of stable fixpoints. More complicated asymptotic behaviors include limit cycles and even chaos. Chaotic phenomena can occur during the gradient descent computation in both cases, continuous or discrete. This has a simple explanation, the gradient descent heuristic can be reduced to an asymptotic behavior of a new system described by equations of the same type as the basic system. This system is N^2 -dimensional and is far more complex and chaotic than the studied one. Some proposed methods to avoid this will be presented.

1. Introduction

There are a lot of engineering applications which need a "black-box" capable of receiving a time dependent function, say $I(t)$, or a set of functions, defining a vector function $I(t)$ with dimension n , and transforming this function into another time dependent vector function $O(t)$, with dimension m . The most obvious application is the system controller, which in the most cases have a mathematically deductible formal structure, by identification and modelling of the controlled system.

But in many cases, the system is too complicate or uncertain to have an appropriate model, or the application is defined by experimentally obtained data, so is impossible to build a formal system which describes the "black-box" in terms of a well determined transfer function. In this cases, it is possible to use an adaptive system, which has a specific but general, all-purpose form. Why specific? The system has a very strict formal description, and the behavior of such systems has been studied since 1987 [Crutchfield & McNamara 87], [Pineda 88], [Renals & Rowher 90]. Why general? Because the same form can be used in various applications, ranging from signal processing to control and robotics. The difference between two systems of this kind, applied to different problems is laying in the value of the parameters (name them **weights**). In order to implement an application using this type of adaptive system, we must have measured needed behaviors, that is, a set of pairs of samples for the functions $(I(t), O(t))$. This is experimental data, and the functions are delivered as number time series, with a constant or a variable sample rate. We will name this set of pairs, the **prescribed base B**.

To adjust the weights through a numerical method based on gradient descent we have to tackle with the great complexity of this kind of computation. The algorithms are not yet studied enough from this point of view, because obtaining a "desired behavior" is a vague goal and has yet to be formally described. There are some papers which consider that these algorithms are NPH and intractable in their implementation, especially for large-scale problems [Hornik 91], [Jordan 89]. Analytically, is simple to prove that the complexity is

around $O(N^5)$, where N is an average between the number of equations used, the length of the series describing B , the number of pairs (I,O) which are describing the desired behavior.

However, the main critical issue in computing the weights is "bifurcation" of the system's dynamics. In general, asymptotic behavior of a nonlinear dynamical system changes qualitatively at certain points in its parameter space [Guckenheimer & Holmes 83], [Wiggins 90]. For example, a stable fixed point can change into an unstable fixed point or even disappear with a continuous change of the system parameters. This problem is worsening the computation complexity, because the gradient descent must be restarted from scratch.

The model of these dynamic systems has been widely used by the community of connectionism. It describes a connectionist architecture named "fully recurrent network". It is noteworthy that the same behaviors can be obtained using more simplified architectures which permit weight adjustment through gradient-descent methods of complexity $O(n^3)$ or even $O(2n+n^2)$. Sometimes, simpler "feedforward network" architectures can be used, these yield a computational burden of $O(n^2)$. As a conclusion, we say that there is no reason to use the recurrent architecture when a simple architecture suffices; but on the other hand, there are a lot of methods to improve the performance of the $O(n^5)$ algorithm, and a lot of artifices to avoid chaotic behavior [Pearlmutter 95].

The paper is structured in the following way: section 2 presents the formal description of the studied system, section 3 presents two ways of implementation of the system on a digital computer, pro's and con's, and a simple example based explanation for the chaotic behavior, section 4 deals with the pseudo-continuous system weight adjustment process; section 5 introduces three enhancements of the system which had been studied by us; section 6 concludes about the feasibility of this type of system in practical, real-life applications. Also, the complete deduction of the used methods are presented in appendices A and B.

2. The system formal description

Consider a dynamic system, governed by a set of coupled first order differential equations, coupled by a matrix of parameters w_{ij} or weights ($i=1,n$; $j=u+n$).

$$\frac{dy_i(t)}{dt} = -y_i(t) + g(h_i(t) + x_i(t)) \quad (i=1, u ; u=N) \quad (1)$$

where $g(x)$ is a nonlinear function with saturation (e.g. the sigmoid) and:

$$h_i(t) = \sum_{j=u+n+1}^{u+n} w_{ij} y_j(t) \quad (i=1, u) \quad (2)$$

$$x_i(t) = \sum_{k=1}^n w_{ik} I_k(t) \quad (i=1, u) \quad (3)$$

These weights are subject to application dependent adaptation, and their values are the only adjustable entities in such a system. The form of the system will remain unchanged in all possible applications. This kind of system is also known as "the fully recurrent continuous connectionist network" [Werbos 88]. From a computational point of view, the system is an analog computer, which has as inputs the $I_j(t)$ functions ($j=1,m$), and as outputs we can select a small number of the states $y_i(t)$ $i=1,m$.

The state space of the system has the dimension u (name it $U \subset \mathbb{R}^u$), but we are using only

a small subspace with dimension m (name it $M \subset \mathbb{R}^m$). The output of the system can be a trajectory in the subspace M , which is a projection of a trajectory in the space U , and this u -dimensional trajectory represents the overall behavior of the system. The dimensions $u-m$ (the rest which are not directly used as outputs) are used as a "time-memories" through their attached weights in the subsequent equations ($m+1, \dots, u$). Setting randomly the weights in the matrix W , he will have a difference between the output $Y_p(t)$ and the desired output $O_p(t)$:

$$J_p(t) = O_p(t) - Y_p(t) \quad (p=1, P) \quad (4)$$

The vector function $J_p(t)$ can be expressed as a function of w_{ij} , and a gradient-descent method to minimize $J_p(t)$ in an interval $[t_0, t_f]$ can be applied, in order to adjust the weights, to obtain the desired behavior of our system.

3. Implementing the system on a digital computer

It is possible to use a discrete variant of the above presented system, because the "original" model is implementable only on analog computers. There are such computers, but they are extremely application dependent, and though accuracy and speed of such architectures are excellent, the applications reported in papers [Doya & Yoshizawa 89], [Pearlmutter 89], [Williams & Zipser 90] reason that its mean a large cost. Using an all-purpose, reconfigurable digital architecture is far more inexpensive. However some problems appear in the digital case. The functioning of the system can be based on two paradigms:

I. - The speed of the "internal" computation is the same with the speed of the sampling rate associated with the time number series $I_p[t]$ and $O_p[t]$ defining the driving function $I_p(t)$ and the desired output $O_p(t)$ ($p = 1, P$). P is the number of pairs which in the set $B = \{(I_p[t], O_p[t])\}$, the prescribed base. In this case, the system will be a pure discrete system, described by the equations:

$$y_i[t] = g\left(\sum_{j=u+1}^{u+n} w_{ij} \cdot y_j[t-1] + \sum_{j=1}^n w_{ij} \cdot I_j[t]\right) \quad (j=1, u) \quad (5)$$

The demonstration of w_{ij} update formula via gradient-descent is given in appendix A [Williams & Zipser 89]. It is simple to demonstrate that the complexity of computation of the weight adjustment is $O(n^4P)$ [Pearlmutter 89]. But the performance of such a system is extremely poor, due to the discretisation of the initial system (1).

II. - The second paradigm is to use a pseudo-continuous system, where the "internal" speed is much higher. That is fairly possible because the speed of recent digital processors is in the range of 20-30 Mflops (millions_of_floating_point_operations / second); also, signal processor usage is highly recommended [Haykin 94]. It is noteworthy that the speeds of modifications of the input $I(t)$ and the output $O(t)$ are "slow" compared with the internal speed.

When a continuous time system is simulated on a digital computer, it is usually converted into a set of simple first order equations, which is formally identical to the discrete time system, but in this case, the speed of $I_p[t]$ (i.e. the sampling rate) is far more lower than the difference between moments t and $t+1$ (the "time step") in the equations describing the discrete system expressed by (5).

There are some advantages running the discrete time system as a simulation of a continuous time system. First, more sophisticated and faster simulation techniques than simple first order equations can be used. Second, even if simple first order equations are used, the size of the

time step can be varied to suit changing circumstances; for instance if the system is being used for a signal processing application and afterwards faster sensors and computers becomes available, the size of the time step can be decreased without re-computing the coupling parameters from W [Lepedes & Farber 87]. Third advantage is somewhat more subtle. Even for tasks which themselves have no temporal content, such as constraint satisfaction, the best way for such a system to perform the required computation is for each output to represent nearly the same thing at nearby points in time. Using continuous time equations makes this the default behavior; in the absence of other forces, units will tend to retain their state through time. In contrast, in purely discrete time systems, there is no a-priori reason for the one equation's state at one point in time to have any special relationship to its state at the next point in time [Jordan 86].

Basically, from any point y from R^n , if the driving functions $I(t)$'s are considered constant, the system will evolve to a stable state, in a so-called fixed point (a process named "relaxation", [Pineda 88]). These points can be computed. If the output desired functions $O(t)$ are crossing these points, the trajectory in the state space will be formed by small relaxation trajectories from one fixed point to another. The problem is that we cannot know in advance the final form of the system, given by its computed weights through gradient descent. But it is desirable to have the output trajectories crossing the adjacent regions with the fixed points (the basins of attraction). This zones of R^n are named "working regions". Sometimes, crossing from one working region to another, a bifurcation can appear. In order to illustrate this, we consider a very trivial example of a bifurcation of such a system to see what kind of problems can arise [Doya 93]. Suppose a system consisting of a single equation, a single input "b" and single output "x". The used function for $g(x)$ is the sigmoid (a continuous squashing function):

$$\sigma \frac{dx(t)}{dt} = -x(t) + \frac{1}{1 + e^{-(wx(t) + b)}} \quad (6)$$

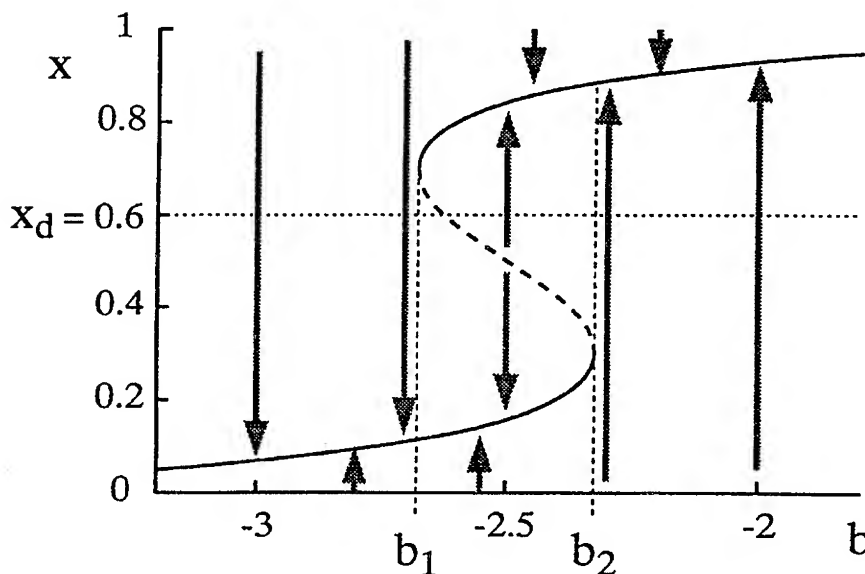


Figure 1: The bifurcation diagram

The output of this "system" converges to a fixed point solution that satisfies:

$$x = \frac{1}{1 + e^{-[wx+b]}} \quad (7)$$

Figure 1 shows the change of the fixed points with the change of b ($w=5$ - set initially). The solid and dashed curves represent the stable and unstable fixed points respectively. Suppose the desired output is constant and it is $x_d=0.6$ and the input is initially set as $b=0.0$. At first, the output trajectory converges to the upper branch of the stable fixed point and then b is decreasing. When b becomes smaller than a certain value b_1 , the stable fixed point on the upper branch vanishes and the state jumps to another stable point in the lower branch. This case is the one-dimensional situation of "saddle-node" bifurcation. If b is increasing, when it will reach b_2 , another saddle point bifurcation occurs. In large scale systems, Hopf bifurcations and homoclinic bifurcations can appear [Wiggins 90]. Using the pseudo-continuous implementation, all these problems remain. Even in the purely discrete case, using a small number of samples for $I(t)$'s and $O(t)$'s ($t=1, \text{stop}$, see appendix A), bifurcations inducing chaotic behavior can appear.

4. Adjusting the weights to obtain the desired behavior

For each pair in B , all weights must be updated once. This is a **step** or "epoch" for the coupling parameters' adaptive computation. It is hard to estimate the number of steps which are needed to approximate the current behavior as close as possible to the desired behavior. But experiments done to implement various applications, give for the needed step number a range between 1,000 and 100,000 [Rowher 90], [Szirbik 95].

You can see in appendix B the deduction of the formula adjusting the weights in the continuous variant [Pineda 88]. For one pair (I, O) the adjustment of one particular weight is given by (b-13) and subsequently:

$$\Delta w_{ij} = \eta \cdot \int_{t_0}^{t_f} g'(u_i^*) \cdot x_j^* \cdot \sum_{k=1}^N J_k \cdot (L^{-1})_{kj} \cdot dt \quad (8)$$

where x_j^* with infinitum superscript means a fixed point. The complexity of computation applying this formula, working numerically on a digital computer, is $O(PN^3)$, which is with one degree higher as the discrete case (P is the total number of pairs - if the number is low here and in a discrete case, the number is big, the complexities are in the same range - and this is a normal case, in the discrete variant more pairs are needed than in the continuous case [Szirbik 95]). What makes the things worse is that the computing process, viewed as a relaxation in the weight space, as presented by (b-18) can have bifurcations. Experimentally, this is the case, because the weight space is quadratic with respect to the initial state space (N^2), and the phenomena occurring here is far more complex. Chaotic behavior is more often encountered in the weight adjustment phase than in the functioning phase. That is extremely dangerous because after 90% of the overall computation time (for example), all the current results can be severely damaged, because the weight matrix, which is a moving point in the weight space, jumps from the current position somewhere very distant from the points which are giving approximate desired behaviors. Thus, all the computation effort made is lost, and the adjustment process must be restarted from another point in the weight space (randomly set).

An immediate method to avoid these undesired phenomena is to trace down the last part of the weight trajectory and turn back when the discontinuity (jump) appear, starting from a

previous position with a new value for η (the gradient descent step size) - usually a lower value [Tsung & al 90].

5. System enhancement

We studied methods to improve the performance of the weight computing not starting from the intrinsic of the computing process, but from the structure of the system. The former methods have been studied intensely and presented in papers (an excellent review can be found in [Pearlmutter 95]). The latter involves hybridizations of the system, that is, modifications of its form. Three methods have been experimented:

- i. - linear equations along the non-linear ones.
- ii. - discrete equations along the pseudo-continuous ones.
- iii. - desired behavior complementary adjustment.

Method i. In many cases, the mapping between the input and the output is linear. It is wasting of computing power to express these dependencies through weights attached to nonlinear equations. We have seen that the inclusion in the system (or even replacement) of a number of "hidden" equations which are purely linear, enhances dramatically the weights computation process. First, the computational complexity is more simple for these weights (equation (8) is reduced to a simple sum), but the number of epochs needed to obtain the desired behavior is decreasing only 10-15% with respect with the fully nonlinear system. This enhancement is application dependent, but all applications have some degree of linear mapping.

Method ii. Sometimes the temporal link between input and output is not very strong. We included in the system discrete equations (or replaced continuous equations) updating the weights using (a-22). The number of epochs is increasing in this case with 5-10%, but sometimes in very favorable cases, when the temporal link is not present at all, the number of epochs is decreasing with 10-20%. More important is that we reduced computational complexity for these weights from $O(N^2)$ to $O(N)$. Methods i and ii have to be studied in depth, because we believe that is a relation between the form of the trajectories from the prescribed base B and the percent of hybrid equation used. We used a very crude and rigid 25% linear-continuous, 25% discrete-nonlinear, and 50% nonlinear continuous equation percentage. Also, the order of updating the weights is important, because we used different strategies, and it appears that in the first case the linear weights are to be updated, afterwards the discrete ones, and only in the last the nonlinear continuous.

Method iii. After each epoch, the fixpoints of the current system can be computed. The weight computing process tries to put the fixpoints in the most appropriate places, to have the desired trajectories crossing them. But this is not always possible, and "overshooting" effects can be detected in the last phase of the process. This creates premises for chaotic behavior of the system, and yields an increase in the number of epochs (after "overshoot" the system is to be "fixed" again). We have modified the trajectories in the prescribed base B, allowing only small changes, but in order to place the trajectories as near as possible (without altering the prescribed base with more than 0.5-1%) with the current fixpoints. The method saved 50-80% of the needed number of epochs. It is a way to help gradient descent to find its minima, not by moving in the weight space, but by modifying the landscape of the J function, to "move" the minima near the current point. The fixpoint computation at every epoch is computationally expensive, but is useful to invoke this method only in the last part of the computing process, and seldom, for example, once at every ten epochs. It is very hard to study analytically why these effects appears in the computation process, due to the system modifications and hybridizations. At last, it is noteworthy to say that in the functional phase of the system, the linear and discrete "processing units" are more faster.

6. Conclusions

This kind of system can be used in many engineering applications, but the main problem is the dimensionality of inputs, outputs, internal state space, the number of pairs P , and the sampling rate of the number time series describing $I(t)$ and $O(t)$. Results of computation time for these systems are presented in [Szirbik 95]. The maximum number of equations are in the range of 700-800, the inputs and outputs are 30-40 dimensional; $P=40-50$, and the sampling rate varies from 25 to 60. Of course, the form of $I(t)$ and $O(t)$ is crucial. But for ordinary applications, the above numbers are feasible on today's computers.

Applying the hybridization methods to our system, using linear mapping between input and output, using simpler discrete equations for trajectories with slow dynamic the performance of learning was reduced not in terms of "epochs" but in terms of complexity. The number of epochs was reduced using an on-line "working region" detector. We want to emphasize that this research is only at its start and on-going, and this paper is not yet presenting certain and verified results. These are only observations along the weights computation process, and of course, in order to have scientifically proven results, to eliminate false or non-characteristic results, more tests have to be done in the near future. As a far target, it will be important to find the theoretical backgrounds for the presented effects.

Acknowledgements

We are indebted to Ștefan Balint, from The University of Sciences from Timișoara, Romania for the opportunity offered by him to present these ideas. Also, the discussions with Scott Fahlman from Carnegie-Mellon University, Pittsburgh, PA, were extremely useful. Siva Banda and Mark Mears from Wright Labs, Dayton, OH, offered excellent feed-back from the practical point of view.

Appendix A (the deduction of the gradient descent method for the discrete variant)

The discrete system is expressed by the equations:

$$V_i(t) = g(h_i(t)) = g\left(\sum_{j=0}^L w_{ij} \cdot z_j(t-1)\right) \quad (i=1, N) \quad (a-1)$$

The driving function of the input is expressed as x :

$$z_i(t) = \begin{cases} -1 & \text{if } j=0 \\ x_j(t) & \text{if } j=1, n \\ V_{j-n}(t) & \text{if } j=n+1, L \end{cases} \quad (j=0, L) \quad (a-2)$$

The used output:

$$O_i(t) = V_i(t) \quad (i=1, m) \quad (a-3)$$

Name h the internal input of one unit:

$$h_i(t) = \sum_{j=0}^L w_{ij} \cdot z_j(t-1) \quad (i=1, N) \quad (a-4)$$

The difference between the desired output defined as time number series $d_i^s(t)$ is a function $E_s(W)$, (s is the index for a single pair $(X^s(t), D^s(t))$):

$$E^s(W) = \frac{1}{2} \sum_{t=1}^{stop} \sum_{i=1}^m [d_i^s(t) - o_i^s(t)]^2 \quad (s=1, P) \quad (a-5)$$

The weights are updated like:

$$w_{ij}^{new} = w_{ij}^{old} + \Delta w_{ij}^s \quad (s=1, P) \quad (a-6)$$

The gradient component for w_{ij} is:

$$\frac{\partial E^s}{\partial w_{ij}} = \frac{1}{2} \sum_{t=1}^{stop} \sum_{k=1}^m \frac{\partial [d_k^s(t) - o_k^s(t)]^2}{\partial w_{ij}} = \quad (a-7)$$

except this particular w_{ij} , all the rest of the weights are considered constants:

$$= -\frac{1}{2} \sum_{t=1}^{stop} \sum_{k=1}^m 2 [d_k^s(t) - o_k^s(t)] \frac{\partial o_k^s(t)}{\partial w_{ij}} = \quad (a-8)$$

and obtain:

$$= -\sum_{t=1}^{stop} \sum_{k=1}^m \delta_k^s(t) \frac{\partial o_k^s(t)}{\partial w_{ij}} \quad (i=1, N; j=1, L) \quad (a-9)$$

δ is the difference between the desired output and the obtained one at moment t :

$$\delta_k^s = [d_k^s(t) - o_k^s(t)] \quad (k=1, m) \quad (a-10)$$

And the derivative will be:

$$r_{kij}^s(t) = \frac{\partial o_k^s(t)}{\partial w_{ij}} \quad (a-11)$$

Now, deducing this partial derivative means:

$$r_{kij}^s(t) = \frac{\partial}{\partial w_{ij}} g(h_k^s(t)) = \frac{\partial}{\partial w_{ij}} g\left(\sum_{l=0}^L w_{kl} \cdot z_l^s(t-1)\right) = \quad (a-12)$$

$g(x)$ must be differentiable (if it is the sigmoid $g'=g(1-g)$):

$$= g'(h_k^s(t)) \sum_{l=0}^L \frac{\partial}{\partial w_{ij}} (w_{kl} \cdot z_l^s(t-1)) = \quad (a-13)$$

using the Kronecker delta function:

$$= g'(h_k^s(t)) \left[\frac{\partial}{\partial w_{ij}} w_{kl} \cdot z_1^s(t-1) + \dots + \frac{\partial}{\partial w_{ij}} w_{kj} \cdot z_j^s(t-1) + \dots + \sum_{l=0}^L w_{kl} \frac{\partial z_l^s(t-1)}{\partial w_{ij}} \right] = \quad (a14)$$

yields:

$$= g'(h_k^s(t)) \left[K_{ik}^A \cdot z_j^s + \sum_{l=0}^L w_{kl} \frac{\partial z_l^s(t-1)}{\partial w_{ij}} \right] \quad (a-15)$$

The sum is split as:

$$\sum_{l=0}^L w_{kl} \frac{\partial z_l^s(t-1)}{\partial w_{ij}} = \sum_{l=0}^n w_{kl} \frac{\partial x_l^s(t-1)}{\partial w_{ij}} + \sum_{l=n+1}^L w_{kl} \frac{\partial z_l^s(t-1)}{\partial w_{ij}} \quad (a-16)$$

using a new index p:

$$\sum_{p=1}^N w_{k(p+n)} \frac{\partial z_p^s(t-1)}{\partial w_{ij}} = \sum_{p=1}^m w_{k(p+n)} \frac{\partial o_p^s(t-1)}{\partial w_{ij}} + \sum_{p=m+1}^N w_{k(p+n)} \frac{\partial v_p^s(t-1)}{\partial w_{ij}} \quad (a-17)$$

to separate between used outputs and the rest of the outputs:

$$y_p^s(t) = \begin{cases} o_p^s(t) & \text{if } p=1, m \\ v_p^s(t) & \text{if } p=m+1, N \end{cases} \quad (a-18)$$

considering the moment t-1:

$$\sum_{p=1}^N w_{k(p+n)} \frac{\partial y_p^s(t-1)}{\partial w_{ij}} \quad (a-19)$$

is simple to see that the term:

$$r_{pij}^s(t) = \frac{\partial y_p^s(t)}{\partial w_{ij}} \quad (p=1, N) \quad (a-20)$$

is recurrent:

$$r_{kij}^s(t) = g'(h_k^s(t)) \left[K_{ik}^A \cdot z_j^s(t-1) + \sum_{p=1}^N w_{k(p+n)} \cdot r_{pij}^s(t-1) \right] \quad (k=1, N) \quad (a-21)$$

So, the final formula for adjustment is:

$$\Delta w_{ij}^s = \eta \sum_{t=1}^{stop} \sum_{k=1}^m \delta_k^s(t) \cdot r_{kij}^s(t) \quad (a-22)$$

Appendix B (the deduction of the gradient descent method for the continuous variant)

For a single pair of desired functions, the error can be expressed as:

$$E = \frac{1}{2} \sum_{i=1}^N J(t)_i^2 \quad (b-1)$$

where the difference J is a time dependent function:

$$J_i(t) = [O_i(t) - x_i(t)] \quad (i=1, N) \quad (b-2)$$

Note that the system state variables are $x(t)$. A small step in the weight space:

$$\tau_w \frac{dw_{rs}}{dt} = - \frac{\partial E}{\partial w_{rs}} \quad (r, s=1, N) \quad (b-3)$$

which can be expressed as (we obtain somewhat similar to (a-9)):

$$\tau_w \frac{dw_{rs}}{dt} = - \frac{1}{2} \frac{\partial}{\partial w_{rs}} \sum_{k=1}^N J_k^2 = \sum_{k=1}^N J_k \frac{\partial x_k}{\partial w_{rs}} \quad (r, s=1, N) \quad (b-4)$$

computing the fixpoints:

$$x_i^* = g_i \left(\sum_{j=1}^N w_{ij} \cdot x_j^* + I_i \right) \quad (i=1, N) \quad (b-5)$$

these x_k with the infinite superscript are fixpoints of the free evolving system:

$$\frac{\partial x_i^*}{\partial w_{rs}} = g_i' \left(\sum_{j=1}^N w_{rj} \cdot x_j^* + I_r \right) \cdot \sum_{j=1}^N \left\{ \frac{\partial w_{ij}}{\partial w_{rs}} x_j^* + w_{ij} \frac{\partial x_j^*}{\partial w_{rs}} \right\} \quad (i=1, N) \quad (b-6)$$

Note (u is similar with h from the discrete variant):

$$u_r^* = \sum_{j=1}^N w_{rj} \cdot x_j^* + I_r \quad (r=1, N) \quad (b-7)$$

And, using again the Kronecker delta function:

$$K_{ij}^A = \begin{cases} 1 & \text{if } i=j \\ 0 & \text{if } i \neq j \end{cases} \quad (b-8)$$

we fix the indices i and j for this derivative, and the rest of the weights are held constant:

$$\frac{\partial w_{ij}}{\partial w_{rs}} = K_{ir}^A \cdot K_{js}^A \quad (b-9)$$

rewrite b-6 as:

$$\sum_{j=1}^N K_{ij}^A \frac{\partial x_j^*}{\partial w_{rs}} = g_i'(u_r^*) \left\{ K_{ir}^A \cdot x_s^* + \sum_{j=1}^N w_{ij} \frac{\partial x_j^*}{\partial w_{rs}} \right\} \quad (i=1, N) \quad (b-9-i)$$

taking all derivatives to the left side:

$$\sum_{j=1}^N [K_{ij}^A - g_i(u_i^*) \cdot w_{ij}] \frac{\partial x_j^*}{\partial w_{is}} = K_{ir}^A \cdot g_r(u_r^*) \cdot x_s^* \quad (i=1, N) \quad (b-9-ii)$$

note with:

$$L_{ij} = K_{ij}^A - g_i(u_i^*) \cdot w_{ij} \quad (b-9-iii)$$

and express (b-6) as a matriceal formula:

$$L \cdot \frac{\partial \bar{x}^*}{\partial w_{is}} = K_{ir}^A \cdot g_r(u_r^*) \cdot x_s^* \quad (b-10)$$

Multiply by the inverse matrix L^{-1} :

$$\frac{\partial \bar{x}^*}{\partial w_{is}} = (L^{-1}) \cdot K_{ir}^A \cdot g_r(u_r^*) \cdot x_s^* \quad (b-11)$$

and again, turning to individual equations form:

$$\frac{\partial x_k^*}{\partial w_{is}} = (L^{-1})_{kr} \cdot g_r(u_r^*) \cdot x_s^* \quad (k=1, N) \quad (b-12)$$

and finally, the adjustment formula:

$$\tau_w \frac{dw_{is}}{dt} = g_r(u_r^*) \cdot x_s^* \cdot \sum_{k=1}^N J_k \cdot (L^{-1})_{kr} \quad (r, s=1, N) \quad (b-13)$$

In order to compute the adjustments in the analog computer style, we note:

$$y_r^* = g_r(u_r^*) \cdot \sum_{k=1}^N J_k \cdot (L^{-1})_{kr} \quad (r=1, N) \quad (b-14)$$

which is:

$$\tau_w \frac{dw_{rs}}{dt} = y_r^* \cdot x_s^* \quad (r, s=1, N) \quad (b-15)$$

This are equations describing a new dynamic system, $N \times N$ dimensional.

$$\sum_{r=1}^N L_{rk} \frac{u_r^*}{g_r(u_r^*)} = J_k \quad (k=1, N) \quad (b-16)$$

Rewrite (b-14) using the expression of L:

$$0 = y_k^* + g_k(u_k^*) \left\{ \sum_{r=1}^N w_{rk} \cdot y_r^* + J_k \right\} \quad (k=1, N) \quad (b-17)$$

and this linear system has solutions fixpoints of the dynamic system:

$$\frac{dy_k}{dt} = -y_k + g'_k(u_k) \left\{ \sum_{i=1}^N w_{ik} y_i + J_k \right\} \quad (k=1, N) \quad (b-18)$$

This dynamic system describes the behavior of the weight adjustment computation, as a relaxation dissipative process.

REFERENCES

- Crutchfield, J.P., and McNamara, B.S., 1987, "Equations of motion from a data series", *Complex Systems*, 1/87, p417-452.
- Doya, K., and Yoshizawa, S., 1989, "Memorizing oscillatory patterns in the analog neural network", *Proceedings of IJCNN'89*, Washington D.C., I, p27-32.
- Doya, K., 1993, "Bifurcations in the learning of recurrent neural networks", *Proceedings of IEEE ICSCS*, p2770-2780.
- Guckenheimer, J., and Holmes, P., 1983, "Nonlinear oscillation, Dynamical systems, and Bifurcations of vector fields", Springer-Verlag, New-York, NY.
- Haykin, S., 1994, "Neural Networks", Macmillan, New-York, NY.
- Hornik, K., 1991, "Approximation capabilities of feedforward and recurrent neural networks", *Neural Networks*, 4/91, p251-257.
- Jordan, M.I., 1986, "Attractor dynamics and parallelism in a connectionist machine", *Proceedings of CSC'86*, p531-546.
- Jordan, M.I., 1989, "Serial order: A parallel distributed processing approach", in *Advances in Connectionist Theory* (eds. J.L. Elman & D.E. Rumelhart).
- Lapedes, A., and Farber, R., 1987, "Nonlinear signal processing using neural networks", TR, Theoretical Division, Los Alamos National Laboratory.
- Pearlmutter, B., 1989, "Learning state space trajectories in recurrent neural networks", *Neural Computation*, 1(2)/89, p263-262.
- Pearlmutter, B., 1995, "Gradient descent learning in dynamic recurrent neural networks", PhD thesis, Carnegie-Mellon University, Pittsburgh, PA.
- Pineda, F.J., 1988, "Dynamic and architecture for neural computation", *Journal of Complexity*, 4/88, p216-245.
- Renals, S., and Rowher, R., 1990, "A study of recurrent network dynamics", *Journal of Statistical Physics*, 58, p825-848.
- Rowher, R., 1990, "The MOVING TARGETS training algorithm", in *Advances in Neural Information processing Systems 2*, Morgan Kaufmann, San Mateo, CA.
- Szurbik, N.B., 1995, "Recurrent NNs learning on the ZOO multiprocessor; Speed-ups and other results", Research Progress Report, FWI, The Free University, Amsterdam.
- Tsung, F., Cottrell, G.W., and Selverston, A.I., 1990, "Some experiments on learning stable network oscillations", *Proceedings of the IJCNN'90*, San Diego, CA, 1, p169-174.
- Werbos, P.J., 1988, "Generalization of backpropagation with application to a recurrent gas market model", *Neural Networks*, 1/89, p339-356.
- Wiggins, S., 1990, "Introduction to applied nonlinear dynamical systems and chaos", Springer-Verlag, New-York, NY.
- Williams, R.J., and Zipser, D., 1989, "A learning algorithm for continually running fully recurrent neural networks", *Neural Computation*, 1/89, p270-280.
- Williams, R.J., and Zipser, D., 1990, "Gradient based learning algorithms for recurrent connectionist networks", TR-NU-CCS-90-9, Northeastern University, Chicago, IL.

INFLUENȚA rotațiilor elicopterului ÎN TANGAJ ȘI RULIU ASUPRA DISTRIBUȚIEI VITEZEI INDUSE PE ROTOR

Cpt. cdor. ing. VLĂSCLEANU NICULAE*

Cpt. cdor. ing. SAITOC MARIAN**

Când mișcarea elicopterului este curbilinie, apar pe pală noi forțe de inerție care influențează atât mișcarea sa de bătaie, cât și distribuția vitezei induse pe suprafața discului rotor.

Fie un rotor principal aflat la punct fix ($\mu = 0$) având o mișcare de rotație în tangaj cu viteza unghiulară $q > 0$. Considerând conceptul de arie efectivă ($B = 1$) și viteza de ruluu $p = 0$, incidența efectivă a unui element de pală va fi:

$$\alpha_e = \theta + \phi = \theta + \frac{1}{x} (\lambda - a_1 x \cdot \sin \psi + b_1 x \cdot \cos \psi + \bar{q} \cdot x \cdot \cos \psi) \quad (1)$$

și cum la punct fix $a_1 = -8\bar{q} / \gamma_L$, $b_1 = -\bar{q}$, incidența elementului de pală devine:

$$\alpha_e = \theta + \frac{\lambda}{x} - \frac{8\bar{q}}{\gamma_L} \sin \psi, \quad (2)$$

unde $\bar{q} = q / (R\Omega)$, $\gamma_L = ac\rho R^4 / J_0$ și $x = r / R$.

Deci incidențele la $\psi = 0$ și $\psi = \pi$, când $\lambda = \text{constant}$, nu se modifică, adică variația vitezei U_n datorată mișcării de bătaie corespunzătoare tangajului q este nulă. La orice alt azimut incidența devine variabilă prin termenul $-8\bar{q} / \gamma_L \cdot \sin \psi$, variație ce are ca efect implicit o variație a vitezei induse.

Pentru cazul general al zborului curbiliniu al elicopterului ($p = 0$ și $q = 0$) se presupune că viteza indusă, datorată rotațiilor p și q , are forma:

$$v = v_0 + v_1 \cdot x \cdot \sin \psi + v_2 \cdot x \cdot \cos \psi, \quad (3)$$

unde am considerat $v > 0$ dacă este orientată spre în jos.

Introducem notațiile:

$$\begin{cases} p_y = \frac{v_1}{v_0} = C \cdot |F_{cq}| \\ p_x = \frac{v_2}{v_0} = C \cdot |F_{cp}| \end{cases} \quad (4)$$

* Academia Tehnică Militară

** Statul Major al Aviației și Apărării Antiaeriene

unde C este un factor de multiplicare, iar F_{cq} și F_{cp} sunt forțele Coriolis datorate rotațiilor în tangaj, respectiv în ruliu:

$$\begin{cases} F_{cq} = \int_{m_p} 2q\Omega r \sin \psi \cdot dm = -2S_0 \cdot q \cdot \Omega \cdot \sin \psi \\ F_{cp} = \int_{m_p} 2p\Omega r \cos \psi \cdot dm = -2S_0 \cdot p \cdot \Omega \cdot \cos \psi \end{cases} \quad (5)$$

Presupunând că viteza indusă suplimentară este funcție liniară de r , din teorema impulsului aplicată fluxului prin rotor, determinăm factorul de multiplicare $C = 3/2$, astfel încât:

$$\begin{cases} p_y = \frac{3b \cdot S_0}{\frac{1}{2} \rho \cdot \pi R^2 \cdot R^2 \cdot C_T} \cdot \bar{q} \\ p_x = \frac{3b \cdot S_0}{\frac{1}{2} \rho \cdot \pi R^2 \cdot R^2 \cdot C_T} \cdot \bar{p} \end{cases} \quad (6)$$

iar distribuția de viteze induse va fi:

$$v_i = v_0 + p_y \cdot v_0 \cdot x \sin \psi + p_x \cdot v_0 \cdot x \cos \psi, \quad (7)$$

în care v_0 este viteza indusă medie determinată prin teoria ideală:

$$v_0 = \frac{C_T}{4\sqrt{\lambda^2 + \mu^2}} \cdot (R\Omega). \quad (8)$$

Dacă notăm $\lambda_0 = v_0 / (R\Omega)$, atunci componenta normală a vitezei efective pe elementul de pală devine:

$$\begin{aligned} U_n = \lambda \cdot R \cdot \Omega - p_y \cdot \lambda_0 \cdot r \cdot \Omega \sin \psi - p_x \cdot \lambda_0 \cdot r \cdot \Omega \cos \psi - r \frac{d\beta}{dt} - \\ - \mu \cdot R \cdot \Omega \cdot \beta \cdot \cos \psi + q \cdot r \cos \psi - p \cdot r \sin \psi = U'_n + \Delta U_n. \end{aligned} \quad (9)$$

Tracțiunea rotorului principal, în acest caz, devine:

$$T = \frac{b}{2\pi} \int_0^{2\pi} \int_0^{BR} \frac{1}{2} \rho ac (\theta U_t^2 + U_t \cdot U'_n + U_t \cdot \Delta U_n) dr \cdot d\psi, \quad (10)$$

unde:

$$\begin{aligned} U_t \cdot \Delta U_n = -p_y \cdot \lambda_0 (r^2 \Omega^2 \sin \psi + R \cdot r \cdot \Omega^2 \cdot \mu \sin^2 \psi) - \\ - p_x \cdot \lambda_0 (r^2 \Omega^2 \cos \psi + R \cdot r \cdot \Omega^2 \cdot \mu \sin \psi \cos \psi). \end{aligned} \quad (11)$$

Aportul acestei distribuții suplimentare a vitezei induse în crearea tracțiunii este:

$$\frac{\Delta C_T}{\sigma} = -\frac{B^2}{4} \cdot p_y \cdot \lambda_0 \cdot \mu. \quad (12)$$

Luând în considerare legea de variație a vitezei induse v determinată de tangajul q și ruliul p al elicopterului:

$$v = v_0 (1 + p_y \cdot x \sin \psi + p_x \cdot x \cos \psi), \quad (13)$$

se vor modifica atât coeficienții mișcării de bătaie, cât și coeficientul momentului rezistent la arbore. Astfel, vom avea o variație a momentului tracțiunii față de articulația orizontală:

$$\begin{aligned} \Delta M_T &= \frac{1}{2} \rho a c \cdot \int_0^{BR} U_T \cdot \Delta U_n r \cdot dr = \\ &= -\frac{1}{2} \rho a c (R\Omega)^2 \cdot R^2 \left(\frac{B^3}{6} p_y \cdot \lambda_0 \mu + \frac{B^4}{4} p_y \cdot \lambda_0 \sin \psi + \frac{B^4}{4} p_x \cdot \lambda_0 \cos \psi \right), \end{aligned} \quad (14)$$

ceea ce implică o modificare a coeficienților mișcării de bătaie:

$$\begin{cases} a_0 = \gamma_L \cdot \left[\frac{B^3}{3} \cdot \lambda + \frac{\theta}{4} B^2 (B^2 + \mu^2) - \frac{B^3}{6} \mu (\bar{p} + p_y \lambda_0) \right] - \frac{g S_0}{J_0 \Omega^2} \\ a_1 = \frac{2\mu \left(\lambda + \frac{4}{3} B\theta \right)}{B^2 + \frac{1}{2} \mu^2} - \frac{B^4 \cdot \bar{p} - \frac{8}{\gamma_L} \cdot \bar{q} + B^4 \cdot p_y \cdot \lambda_0}{B^2 \left(B^2 - \frac{1}{2} \mu^2 \right)} \\ b_1 = \frac{\frac{4}{3} B \mu a_0}{B^2 + \frac{1}{2} \mu^2} - \frac{B^4 \cdot \bar{q} - \frac{8}{\gamma_L} \bar{p} - B^4 \cdot p_x \cdot \lambda_0}{B^2 \left(B^2 + \frac{1}{2} \mu^2 \right)} \end{cases} \quad (15)$$

Cu ajutorul relațiilor (6) putem determina expresiile pentru $\lambda_0 \cdot p_x$ și $\lambda_0 \cdot p_y$, presupunând $\lambda_0 \ll \mu$, ($\mu > 0,15$):

$$\begin{cases} \lambda_0 \cdot p_x = \frac{3b \cdot S_0}{2\pi \cdot \rho \cdot R^4} \cdot \frac{\bar{p}}{\mu} \\ \lambda_0 \cdot p_y = \frac{3b \cdot S_0}{2\pi \cdot \rho \cdot R^4} \cdot \frac{\bar{q}}{\mu} \end{cases} \quad (16)$$

relații din care observăm că, cu cât viteza de înaintare pe traiectoria curbilinie este mai mică, (μ mai mic), cu atât este mai mare influența celor două rotații asupra distribuției vitezei induse pe suprafața discului rotor.

BIBLIOGRAFIE

1. BRAMWELL, A. R. – Helicopter dynamics, Ed. John Wiley, New York, 1976
2. MARINESCU, A.; ANGHEL, V. – Aerodinamica și dinamica elicopterului, Ed. Acad., București, 1992
3. PAYNE, P. R. – Helicopter dynamics and aerodynamics, Ed. Pitman, London, 1959
4. ȘTEFAN, S. – Ecuațiile mecanicii fluidelor, Ed. A. T. M., București, 1996

BĂTAIA LIBERĂ A PALEI ÎN ZBORUL CURBILINIU AL ELICOPTERULUI

Cpt. cdor. ing. VLĂSCLEANU NICULAE*

Cpt. cdor. ing. POPESCU VIRGIL**

Cpt. ing. SIMOTA DORIN**

Coeficienții primei armonici din dezvoltarea în serie Fourier a unghiului de bătaie:

$$\beta = a_0 - a_1 \cos \psi - b_1 \sin \psi, \quad (1)$$

se determină din condiția de echilibru a momentelor forțelor care acționează asupra palei, față de articulația orizontală. Dacă a_0 reprezintă unghiul de conicitate al rotorului, a_1 și b_1 reprezintă unghiurile de înclinare longitudinală (pozitiv spre spate, $\psi = 0$) respectiv laterală (pozitiv spre dreapta, $\psi = \pi/2$) a axei conului descris de pale față de axa de comandă (axa de bătaie pură).

Deplasările în bătaie ale palei, corespunzătoare armonicilor superioare, sunt de același ordin de mărime cu cele determinate de deformările aeroelastice. Steward W. a demonstrat [1] că amplificarea unei armonici superioare reprezintă circa (5...10)% din amplitudinea armonicii precedente.

Considerăm cazul zborului curbiliniu cu înaintare, cu viteza v constantă, elicopterului imprimându-i-se o rotație în tangaj q și o rotație în rulu p .

Condiția de echilibru a momentelor forțelor care acționează asupra palei în acest caz conduce la ecuația diferențială a mișcării de bătaie:

$$\frac{d^2\beta}{d\psi^2} + \beta = \frac{1}{J_0 \Omega^2} \int_0^R r \cdot dt - 2\bar{q} \sin \psi - 2\bar{p} \cos \psi - \frac{gS_0}{J_0 \Omega^2}, \quad (2)$$

în care:

$$M_T = \int_0^R r \cdot dT = \frac{acpR^4}{2} \int_0^1 \xi^2 \left(\theta + \frac{\eta}{\xi} \right) x \cdot dx \quad (3)$$

este momentul forțelor de tracțiune de pe pala aflată la azimutul ψ .

Prin urmare, unghiul de bătaie β pentru pala aflată la azimutul ψ trebuie să satisfacă ecuația diferențială (2), ecuație în care membrul drept constituie momentul excitator, funcție de variabila independentă - azimut.

* Academia Tehnică Militară

** Statul Major al Aviației și Apărării Antiaeriene

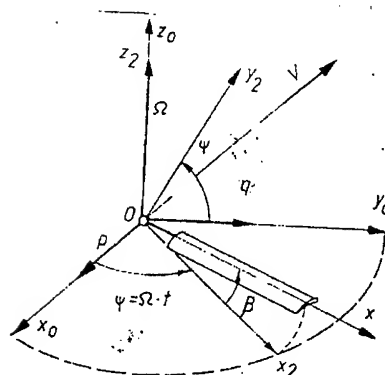


Fig. 1 Rotorul în zborul curbiliniu

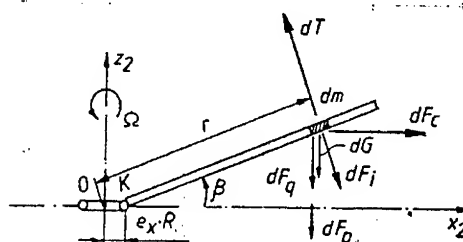


Fig. 2 Echilibrul momentelor de pală

În expresia (3) a momentului M_T s-au folosit relațiile vitezei și incidenței efective pentru un element de pală:

$$\begin{cases} U \equiv U_t = R\Omega \cdot \xi \\ \alpha_e = \theta + \frac{U_n}{U_t} = \theta + \frac{\eta}{\xi} \end{cases} \quad (4)$$

iar notațiile adimensionale ξ și η , pentru cazul considerat, devin:

$$\begin{cases} \xi = x + \mu \sin \psi \\ \eta = \lambda - \frac{x}{\Omega} \cdot \frac{d\beta}{dt} - \mu \cdot \beta \cos \psi + \bar{q} \cdot x \cdot \cos \psi - \bar{p} \cdot x \cdot \sin \psi \end{cases} \quad (5)$$

Căutând o soluție de forma (1) în ecuația diferențială (2), obținem expresiile coeficienților mișcării de bătaie:

$$\begin{cases} a_0 = \frac{\gamma_L}{2} \left[\frac{\lambda}{3} + \frac{\theta}{4} (1 + \mu^2) \right] - \frac{g \cdot S_0}{J_0 \cdot \Omega^2} - \frac{\gamma_L}{12} \bar{p} \cdot \mu = a'_0 - \Delta a_0 \\ a_1 = 2\mu \cdot \frac{\lambda + \frac{4}{3}\theta}{1 - \frac{1}{2}\mu^2} - \frac{\bar{p} + \frac{16}{3} \cdot \bar{q}}{1 - \frac{1}{2}\mu^2} = a'_1 - \Delta a_1 \\ b_1 = \frac{4a_0}{3} \cdot \frac{\mu}{1 + \frac{1}{2}\mu^2} - \frac{\bar{q} - \frac{16}{3} \cdot \bar{p}}{1 + \frac{1}{2}\mu^2} = b'_1 - \Delta b_1 \end{cases} \quad (6)$$

expresii în care am evidențiat efectul de întârziere produs de forțele Coriolis care apar în cazul rotațiilor elicopterului din zborul curbiliniu, în tangaj cu viteza unghiulară q și în ruliu cu viteza unghiulară p .

Dacă rotorului i se induce rotații în tangaj q și/sau în ruliu p , atunci axa conului descris de pale va urmări în rotație axa rotorului, care este solidară cu elicopterul, dar va fi permanent în urmă cu un anumit unghi. În relațiile (6) sunt evidențiate atât aceste unghiuri de întârziere (Δa_1 – longitudinal, Δb_1 – transversal), cât și unghiul de reducere a conicității (Δa_0).

Expresiile obținute pentru coeficienții mișcării de bătaie, confirmă presupunerea că noua mișcare provocată de p și q se stabilizează relativ repede. Sub influența acestor rotații, conul palelor se rotește împreună cu arborele, având înclinarea longitudinală mai mică cu Δa_1 , iar cea laterală mai mică cu Δb_1 . Astfel, planul acestei noi înclinări este deplasat în fază în raport cu planul de rotație cu $\Delta\psi$, unde:

$$\operatorname{tg} \Delta\psi = \frac{\Delta b_1}{\Delta a_1}. \quad (7)$$

De notat că aceste unghiuri de întârziere transformate în timpi de întârziere:

$$\tau_{q1} = \frac{\Delta a_1}{q}; \quad \tau_{q2} = \frac{\Delta b_1}{q}; \quad \tau_{p1} = \frac{\Delta a_1}{p}; \quad \tau_{p2} = \frac{\Delta b_1}{p}, \quad (8)$$

reprezintă întârzieri temporale ale rotorului, cu valori obișnuite de câteva sutimi de secundă, rezultând deci că rotorul elicopterului răspunde prompt la comenzi, este manevrabil.

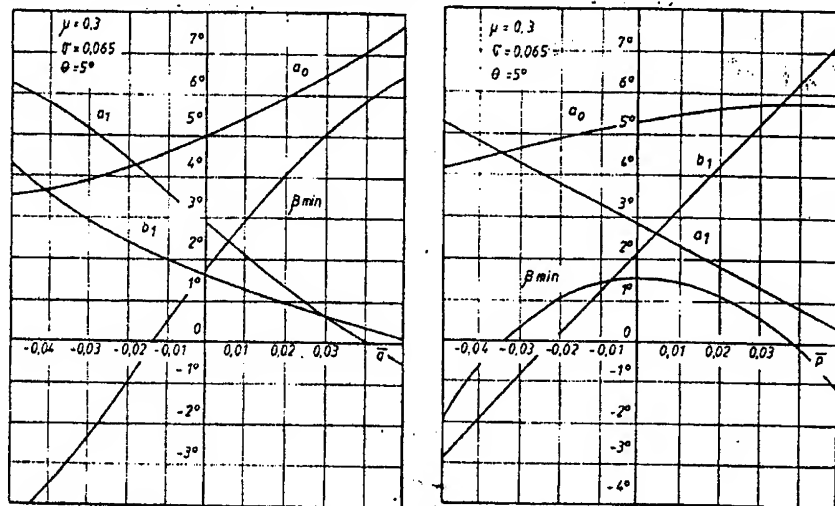


Fig. 3 Influența rotațiilor în ruliu și în tangaj asupra coeficienților mișcării de bătaie

Acum să considerăm cazul zborului la punct fix, elicopterul având o mișcare de tangaj cu viteza unghiulară q variabilă în timp, caz în care ecuația diferențială a mișcării de bătaie devine:

$$\frac{d^2\beta}{d\psi^2} + \frac{\gamma_L}{8} \cdot \frac{d\beta}{d\psi} + \beta = \frac{\gamma_L}{8} \bar{q} \cos \psi - 2\bar{q} \sin \psi + \frac{d\bar{q}}{d\psi} \cos \psi, \quad (9)$$

a cărei soluție de forma (1) conține coeficienți variabili, funcție de timp/azimut:

$$\beta = a_0(\psi) - a_1(\psi) \cdot \cos \psi - b_1(\psi) \cdot \sin \psi. \quad (10)$$

Cazul variației azimutale sinusoidale a vitezei unghiulare de tangaj, caz important în analiza stabilității palei și a rotorului, a fost analizat de Sissing și Zbrozek [1]. Considerând această variație de forma:

$$q = q_0 \cdot \sin(v\psi) \quad (11)$$

în ecuațiile (9) și (10), identificând coeficienții lui $\sin \psi$ și lui $\cos \psi$, se obține:

$$\begin{cases} \frac{\gamma_L}{8} a_1 + 2 \frac{da_1}{d\psi} - \frac{\gamma_L}{8} \cdot \frac{db_1}{d\psi} - \frac{d^2 b_1}{d\psi^2} = -2\bar{q}_0 \cdot \sin(v\psi) \\ \frac{\gamma_L}{8} \frac{da_1}{d\psi} + 2 \frac{d^2 a_1}{d\psi^2} - \frac{\gamma_L}{8} \cdot b_1 + 2 \frac{db_1}{d\psi} = \bar{q}_0 \cdot v \cdot \cos(v\psi) \end{cases} \quad (12)$$

Sissing a demonstrat că oscilațiile planului conului în raport cu planul de rotație nu coincid în fază cu oscilațiile în tangaj ale arborelui rotorului. Raportul k dintre frecvența tangajului și frecvența de rotație a arborelui rotor, în mișcarea perturbată tipică de bătaie, este inferior valorii de 0,1.

Pornind de la această constatare, Zbrozek a demonstrat că expresiile coeficienților $a_1(\psi)$ și $b_1(\psi)$ pot fi aduse la formele:

$$\begin{cases} a_1(\psi) = -\frac{16\bar{q}}{\gamma_L} + \left[\left(\frac{16}{\gamma_L} \right)^2 - 1 \right] \cdot \frac{d\bar{q}}{d\psi} \\ b_1(\psi) = -\bar{q} + \frac{24}{\gamma_L} \cdot \frac{d\bar{q}}{d\psi} \end{cases} \quad (13)$$

Pentru variația tangajului de forma (11), termenii doi din expresiile pentru a_1 și b_1 sunt foarte mici. Astfel, într-o mișcare de bătaie perturbată de un tangaj neuniform, coeficienții a_1 și b_1 sunt proporționali cu $\bar{q} = q/\Omega$, iar rotorul se comportă ca și când mișcarea perturbată ar fi staționară. Astfel, se justifică tratarea cvasistaționară a mișcării perturbate, ca o suscesiune de regimuri staționare, fapt ce simplifică considerabil analiza stabilității și manevrabilității elicopterului.

BIBLIOGRAFIE

1. BIELAWA, R. L. - Rotary wing structural dynamics aeroelasticity, Ed. AIAA, Washington, 1994
2. BRAMWELL, A. R. - Helicopter dynamics, Ed. John Wiley, New York, 1976

THE GENERAL PROPERTIES OF THE CONICAL MOTIONS

Richard Selescu*

National Institute for Aerospace Research "Elie Carafoli"
77538, Bucharest, 6, Romania

Abstract - This work is a presentation of the results obtained following some research performed in the first half year of 1994, having as object the study of the general properties specific to the conical fluid motions. These properties derive from the general properties of a certain flow, taking into account the definition of the conical flow. The cognition of these properties is useful not only for studying the proper conical flows, but also for solving the various problems advanced and treated in the framework of the conical motions theory, using the small disturbances approximate method. We mention that all the properties deduced in this work are not based on approximate assumptions, being valid with accuracy on the whole domain of the conical flows, both rotational and irrotational.

INTRODUCTION

The first chapter of the work is destined to define the conical motions and their classification from the viewpoint of the rotationality.

The second chapter is effectively dealing with the determination of the general properties of the above flows and with the study of these properties. For their deduction, it was started from the general equations established in the compressible fluid mechanics for a certain flow: the motion, energy, continuity and flow rate equations. Although we have also used the physical equation, we have considered unnecessary to mention it, since it did not constitute the object of some special mathematical transformations.

All the above equations have been written in the spherical coordinates system, having in view the advantage shown by this system if it is placed with the origin in the vertex of the conical flow. We mention that all the cinematics and dynamics of the tackled conical flows was treated by using the methods and notations adopted in the classical mechanics for the study of the material point motion (in this case, a very little fluid particle), therefore using the time as an independent variable.

Considering that the motion is steady, the trajectories of these fluid particles coincide with the flow streamlines.

This treating mode allows making evident some general properties specific to the conical flows, properties whose existence would have been more difficult to notice using the traditional methods of the fluid mechanics. We also mention, that in numerous situations are obtained some differential equations with partial derivatives, which can be sometimes reduced to ordinary differential equations, some of these being able to admit prime integrals. As a rule, as it was expected, the respective relations (deduced by artificial consideration of the time as an independent variable) do not contain any more the time variable, this being possible to be easily eliminated.

We shall introduce the following classical notations:

t - time

R, θ, ω - spherical coordinates of a certain mobile point in the conical flowfield, in the reference system with the axes origin placed in the flow vertex

$\dot{R}, \dot{\theta}, \dot{\omega}, \ddot{R}, \ddot{\theta}, \ddot{\omega}$ - first and respectively second order derivatives versus time of the adopted coordinates

$V_R = \dot{R}$ - radial velocity (along the radius vector)

$V_\theta = R\dot{\theta}$ - normal velocity (to the radius vector; is contained in the meridian plane)

$V_\omega = R\sin\theta\dot{\omega}$ - circumferential velocity (normal to the meridian plane)

$a_R = \ddot{R} - R\dot{\theta}^2 - R\sin^2\theta\dot{\omega}^2$ - radial acceleration

$a_\theta = R\ddot{\theta} + 2\dot{R}\dot{\theta} - R\sin\theta\cos\theta\dot{\omega}^2$ - normal acceleration

$a_\omega = R\sin\theta\ddot{\omega} + 2\sin\theta\dot{R}\dot{\omega} + 2R\cos\theta\dot{\theta}\dot{\omega}$ - circumferential acceleration

p - static pressure

ρ - gas density

γ - adiabatic exponent (the ratio of gas specific heats, that isobar to that isochor, $\gamma = C_p/C_v$)

K - isentropic constant ($K = p/\rho^\gamma$)

a - local speed of sound ($a^2 = dp/d\rho = \gamma K p^{1-\gamma}$)

W - maximum speed of sound (corresponding to the vacuum expansion)

Φ - potential of respective conical flow ($\Phi = R V_R = R \dot{R}$), (if existent)

* Senior Scientist, Department of Aerodynamics

1. CONICAL MOTIONS

We understand by conical motion (flow) the fluid motion (flow) in which the density, pressure, temperature, velocity, acceleration etc, so nearly all the physical quantities, are constant on a vector radius started from the origin of axes of a fixed reference system, origin which is placed in a particular point of the flow, called vertex, or focus. In the case of the vectorial quantities, like velocity and acceleration, but not the position vector, we understand the conservation of modulus, direction and sense of the respective vector along of such a radius vector.

There are some exceptions from this definition, like the radius vector length at the considered point and the second and superior order derivatives versus time of this length, as well as the derivatives versus time of the angular coordinates that define the position of the radius vector which is passing through the considered point (sometimes improper called angular velocities and accelerations).

We shall insist on the last aspect of the above definition. It is necessary that all the radius vectors on which takes place this invariance of the flow parameters to be concurrent in the same point (the conical flow vertex, or focus). Otherwise, even if the above invariance takes place along some straight lines, but which are not all concurrent in the same point, then that flow is not conical.

The conical flows represent an important motion class, especially supersonic. From the viewpoint of the motion rotationality, these flows are divided in two big categories: irrotational flows (isentropic in the whole considered fluid mass, to these belonging the one- and the two-dimensional flows, both plane and axisymmetric, as well as some particular three-dimensional flows, designated in [1] as helicoidal, or axisantisymmetric flows) and rotational flows (nonisentropic in the whole considered fluid mass, or isentropic along the stream- or vortexlines only, but having different values of the isentropic constant on the different stream- or vortexlines, to these belonging nearly all the three-dimensional conical flows).

2. THE GENERAL PROPERTIES SPECIFIC TO THE CONICAL FLOWS

2.1. THE FIRST EQUATION OF MOTION

From the motion equation for a certain three-dimensional flow written on radial direction, taking into consideration the conical flow definition, it results successively the following relations:

$$a_R = \ddot{R} - R\dot{\theta}^2 - R\sin^2\theta\dot{\omega}^2 = -\frac{1}{\rho}\frac{\partial p}{\partial R} = 0 ; \quad (1)$$

or

$$\ddot{R} \frac{d^2 R}{dt^2} = 0 ; \text{ or } \left| \ddot{R} \times \frac{d^2 R}{dt^2} \right| = \left| \ddot{R} \right| \left| \frac{d^2 R}{dt^2} \right| ; \quad (1')$$

(in a conical flow the acceleration is normal to the radius vector).

In the case of the plane conical flows, the equation (1) may be written successively in the forms

$$\ddot{R} - R\dot{\omega}^2 = 0 ; \quad \frac{d \ln R}{d\omega} \frac{d \ln |\ddot{R}|}{d\omega} = 1 , \quad (2)$$

or, in the initially adopted coordinates

$$\frac{d \ln R}{d\omega} \frac{d \ln |V_R|}{d\omega} = 1 , \quad (2')$$

since in the case of these flows, we have in the equation (1)

$$\theta = \frac{\pi}{2} ; \Rightarrow \sin\theta = 1 \text{ and } \dot{\theta} = \frac{d\theta}{dt} = 0 .$$

In the case of the axisymmetric flows, the fluid particle trajectory (the streamline) being contained in a meridian plane (the phenomenon being independent of ω), we have in the equation (1)

$$\omega = \omega_0 = \text{const.} ; \Rightarrow \dot{\omega} = \frac{d\omega}{dt} = 0 ,$$

in both cases resulting thus successively the same form of the first equation of motion

$$\ddot{R} - R\dot{\beta}^2 = 0 ; \quad \frac{d \ln R}{d\beta} \frac{d \ln |\ddot{R}|}{d\beta} = 1 , \quad (3)$$

where β represents the respective angular coordinate ($\beta = \omega$ - for the plane flows, or $\beta = \theta$ - for those axisymmetric), or

$$\frac{d \ln R}{d\beta} \frac{d \ln |V_R|}{d\beta} = 1 , \quad (4)$$

therefore

$$\arctan \frac{d \ln R}{d\beta} + \arctan \frac{d \ln |\dot{R}|}{d\beta} = \frac{\pi}{2} ; \text{ or } \arctan \frac{d \ln R}{d\beta} = \operatorname{arccot} \frac{d \ln |\dot{R}|}{d\beta} ; \quad (4')$$

(the curves $\ln R$ and $\ln |\dot{R}|$ are symmetrically inclined against the first axes bisectrix, for any value of ω , or of θ).

In this last case ($0 = \pi/2$, or $\omega = \omega_0$), the velocity is derived from the potential

$$\Phi = R V_R = R \dot{R} \quad \left(= \frac{dR}{d\beta} \frac{d\dot{R}}{d\beta} \right)$$

We logarithmise

$$\ln R |V_R| = \ln R + \ln |V_R| = \ln |\Phi| ;$$

we derive with respect to β and obtain

$$\frac{d \ln R}{d\beta} + \frac{d \ln |V_R|}{d\beta} = \frac{d \ln |\Phi|}{d\beta} . \quad (5)$$

If is known, or is given the conical flow potential $\Phi(\beta)$, then the classical system compound of the equations

(4) and (5) admits the solution:

$$\frac{d \ln R}{d\beta} = \frac{d \ln \sqrt{|\Phi|}}{d\beta} - \sqrt{\left(\frac{d \ln \sqrt{|\Phi|}}{d\beta} \right)^2 - 1} ; \quad \frac{d \ln |V_R|}{d\beta} = \frac{d \ln \sqrt{|\Phi|}}{d\beta} + \sqrt{\left(\frac{d \ln \sqrt{|\Phi|}}{d\beta} \right)^2 - 1} , \quad (6)$$

differential equations which can be easily integrated with respect to the variable β , being thus determined the quantities

$\ln R$ and $\ln |V_R|$; if we note

$$\frac{d \ln \sqrt{|\Phi|}}{d\beta} = \cosh w ; \quad \sqrt{\left(\frac{d \ln \sqrt{|\Phi|}}{d\beta} \right)^2 - 1} = \sinh w ; \quad \text{with } w = u + iv ,$$

(where w is a complex variable whose imaginary part coefficient, v , may have only two values: 0 and π , so that $\cosh w$ becomes a real quantity, $\pm \cosh u$, with the modulus $|\cosh w| \geq 1$), we find another form of solution

$$\begin{aligned} \frac{d \ln R}{d\beta} &= e^{-w} = e^{-\operatorname{arccosh} h \frac{d \ln \sqrt{|\Phi|}}{d\beta}} ; \quad \ln \frac{R}{R_0} = \int_{\beta_0}^{\beta} e^{-\operatorname{arccosh} h \frac{d \ln \sqrt{|\Phi|}}{d\beta}} d\beta ; \quad R = R_0 e^{\int_{\beta_0}^{\beta} e^{-\operatorname{arccosh} h \frac{d \ln \sqrt{|\Phi|}}{d\beta}} d\beta} ; \\ \frac{d \ln |V_R|}{d\beta} &= e^w = e^{\operatorname{arccosh} h \frac{d \ln \sqrt{|\Phi|}}{d\beta}} ; \quad \ln \frac{V_R}{V_{R0}} = \int_{\beta_0}^{\beta} e^{\operatorname{arccosh} h \frac{d \ln \sqrt{|\Phi|}}{d\beta}} d\beta ; \quad V_R = V_{R0} e^{\int_{\beta_0}^{\beta} e^{\operatorname{arccosh} h \frac{d \ln \sqrt{|\Phi|}}{d\beta}} d\beta} , \end{aligned} \quad (7)$$

where both V_R and V_{R0} have the same sign, the limits of the above integrals being respectively

β_0 - the initial value of the angular coordinate (ω or θ);

β - the current value of the angular coordinate, for which we must calculate the quantities R and V_R .

From the condition of existence for the roots in the solution (6) we have for $\beta > \beta_0$:

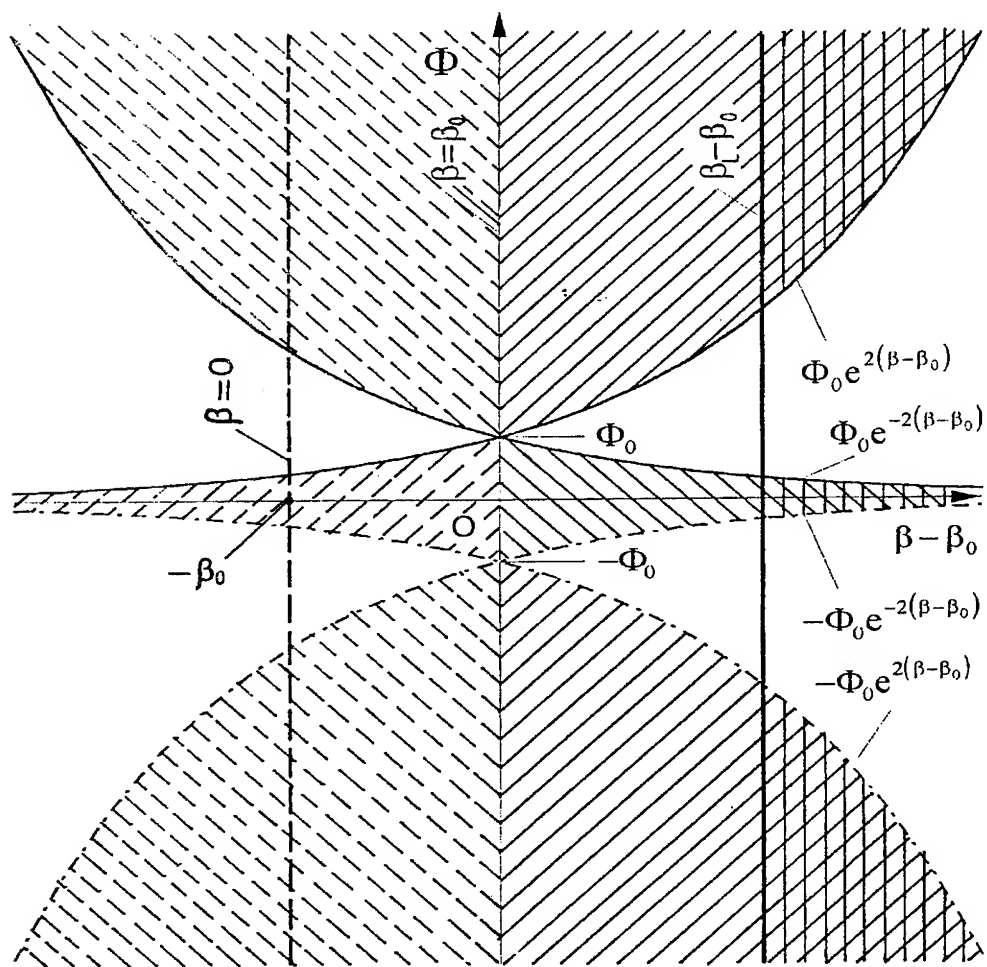
$$|\Phi| \geq \Phi_0 e^{2(\beta - \beta_0)} \quad \text{with} \quad \frac{d|\Phi|}{d\beta} \geq 2|\Phi| , \quad \text{or} \quad |\Phi| \leq \Phi_0 e^{-2(\beta - \beta_0)} \quad \text{with} \quad \frac{d|\Phi|}{d\beta} \leq -2|\Phi| , \quad (8)$$

and for $\beta < \beta_0$:

$$|\Phi| \leq \Phi_0 e^{2(\beta - \beta_0)} \quad \text{with} \quad \frac{d|\Phi|}{d\beta} \geq 2|\Phi| , \quad \text{or} \quad |\Phi| \geq \Phi_0 e^{-2(\beta - \beta_0)} \quad \text{with} \quad \frac{d|\Phi|}{d\beta} \leq -2|\Phi| , \quad (9)$$

(where $\Phi_0 = R_0 V_{R0} > 0$), relations which establish the existence domains for the potential $\Phi(\beta)$ (monotonic function of β) to obtain isentropic two-dimensional (plane and axisymmetric) conical flows, from the mathematical viewpoint only. It may be noticed that for both $\beta > \beta_0$ and $\beta < \beta_0$, isentropic two-dimensional conical flows can not exist in the domains comprised between the two above exponential curves and respectively, between their symmetric ones with respect to both β - and Φ -axis. In the (β, Φ) plane, any curve which is representing a variation of the two-dimensional conical flow potential Φ with the current β angle, along a certain streamline (i.e. for a given pair of the values β_0 and Φ_0) must pass through the point (β_0, Φ_0) , or through its symmetric one with respect to the β -axis.

This curve must also to be contained into the existence domain for Φ determined by the relations (8) and (9) and must satisfy the slope conditions given by these relations.



$$\Phi_0 = R_0 V_{R0} > 0$$

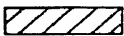
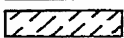
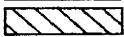

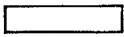
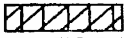
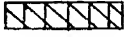
	- existence domain	$ \Phi \geq \Phi_0 e^{2(\beta - \beta_0)}$	} with $\frac{d \Phi }{d\beta} \geq 2 \Phi $
	- existence domain	$ \Phi \leq \Phi_0 e^{2(\beta - \beta_0)}$	
	- existence domain	$ \Phi \leq \Phi_0 e^{-2(\beta - \beta_0)}$	} with $\frac{d \Phi }{d\beta} \leq -2 \Phi $
	- existence domain	$ \Phi \geq \Phi_0 e^{-2(\beta - \beta_0)}$	
	- non-existence domain		
	} - physically incompatible solutions ($\beta > \beta_L$)		
			

Fig. 1. The existence domains for the potential $\Phi(\beta)$ of the two-dimensional (plane or axisymmetric) conical flow

The minimum possible value of the lower limit of the integrals which appear in the relations (7) is $\beta_0 = 0$, while the maximum possible value of the upper limit of these integrals, β_L , is given by the boundary condition

$$\int_{\beta_0}^{\beta_L} e^{\arccos h \frac{d \ln \sqrt{|\Phi|}}{d\beta}} d\beta = \ln \frac{V_{RL}}{V_{R0}}. \quad (10)$$

It can be noticed that in all the cases the unknown quantity β_L appears in both members of the equation (10), namely in the upper limit of the integral and in expression of V_{RL} .

Therefore we can write another condition for the existence domains of the potential $\Phi(\beta)$ to obtain isentropic two-dimensional (plane and axisymmetric) conical flows

$$\beta \leq \beta_L,$$

set this time from the physical viewpoint only (the compatibility of the solutions R and V_R - see the Figure 1).

The plane potential conical flows belong to a particular case of the class of helicoidal or axisymmetric conical flows, namely to that in which the streamlines are some conical helices, contained in the conical sheet of equation

$$\theta = \theta_0 = \text{const.}, \quad \text{with } \theta_0 \in [0, \pi],$$

therefore for which we have

$$\sin \theta = \sin \theta_0 = k; \quad \text{with } k \in [0, 1]; \quad \Rightarrow \dot{\theta} = \frac{d\theta}{dt} = 0,$$

resulting for the product of derivatives in the equation (3) the value k^2 .

The solution of the new system thus obtained is somewhat more general than the preceding one, in the roots of the relations (6) instead of 1 appearing now the term k^2 .

Analysing the equation (1) we remark that this last solution is also valid for a sub-class of three-dimensional potential conical flows, having the variables θ and ω bound by the differential equation

$$\sin \theta \frac{d\omega}{d\theta} = \pm \sqrt{k^2 - 1}, \quad \text{or } d\omega = \pm \sqrt{k^2 - 1} \frac{d\theta}{\sin \theta},$$

with the solution

$$\omega = \omega_0 \pm \sqrt{k^2 - 1} \ln \left| \tan \frac{\theta}{2} \right|, \quad \text{with } |k| \geq 1,$$

which represents two families (+ and -) of helicoid surfaces in which are comprised the flow streamlines, therefore another helicoidal flow.

The existence domains for $\beta > \beta_0$, similar to (8), of the potential $\Phi(\beta)$ for these two last flow sub-classes is adequately modified, becoming

$$|\Phi| \geq \Phi_0 e^{2k(\beta - \beta_0)} \quad \text{with } \frac{d|\Phi|}{d\beta} \geq 2k|\Phi|, \quad \text{or } |\Phi| \leq \Phi_0 e^{-2k(\beta - \beta_0)} \quad \text{with } \frac{d|\Phi|}{d\beta} \leq -2k|\Phi|,$$

where $0 < k < 1$ and respectively $|k| > 1$.

In the most general possible case are obtained helicoidal conical flows if we have in the equation (1)

$$\omega = f(\theta), \quad \text{or } \theta = f^{-1}(\omega) = g(\omega),$$

where by f^{-1} we have noted the inverse function of f .

The solution (6) remains valid, with the remark that instead of 1 is appearing now in the roots the square of a function $h(\beta)$

$$h(\theta) = 1 + \sin^2 \theta [f'(\theta)]^2 \quad \text{or } h(\omega) = \sin^2 \theta + [g'(\omega)]^2 = \sin^2 g(\omega) + [g'(\omega)]^2,$$

the existence domains for $\beta > \beta_0$, similar to (8), for the potential $\Phi(\beta)$ having now the form

$$|\Phi| \geq \Phi_0 e^{2 \int_{\beta_0}^{\beta} h(\beta) d\beta} \quad \text{with } \frac{d|\Phi|}{d\beta} \geq 2h(\beta)|\Phi|, \quad \text{or } |\Phi| \leq \Phi_0 e^{-2 \int_{\beta_0}^{\beta} h(\beta) d\beta} \quad \text{with } \frac{d|\Phi|}{d\beta} \leq -2h(\beta)|\Phi|,$$

in which, as till now, $\beta = 0$ or $\beta = \omega$.

The potential expression is

$$\Phi = R \dot{R} = R V_R.$$

In the case of the plane and axisymmetric conical flow, we obtain

$$\Phi' = \frac{d\Phi}{d\beta} = R' \dot{R} + R \ddot{R} = \frac{1}{\beta} (\dot{R}^2 + R \ddot{R}) = \frac{1}{\beta} (\dot{R}^2 + R^2 \dot{\beta}^2) = \frac{R}{R\beta} (\dot{R}^2 + R^2 \dot{\beta}^2) = \frac{R}{V_\beta} (V_R^2 + V_\beta^2) = \frac{R V^2}{V_\beta}.$$

It results

$$\frac{d \ln |\Phi|}{d\beta} = \frac{\Phi'}{\Phi} = \frac{RV^2}{V_\beta RV_R} = \frac{V^2}{V_R V_\beta} = \frac{V_R^2 + V_\beta^2}{V_R V_\beta} = \frac{V_R}{V_\beta} + \frac{V_\beta}{V_R}.$$

The significance of the logarithmic derivatives is :

$$\frac{d \ln R}{d\beta} = \frac{V_R}{V_\beta}; \quad \frac{d \ln |V_R|}{d\beta} = \frac{V_\beta}{V_R}, \quad \text{in which } V_\beta = V_\theta, \quad \text{or } V_\beta = V_\omega.$$

Let return to the first equation of motion introducing the notation

$$\dot{\phi}^2 = \dot{\theta}^2 + \sin^2 \theta \dot{\omega}^2 \quad (11)$$

the respective equation, written initially in the form (1), becomes

$$\ddot{R} - R\dot{\phi}^2 = 0, \quad (12)$$

where ϕ is defined by the following differential relation

$$d\phi = \sqrt{\dot{\theta}^2 + \sin^2 \theta \dot{\omega}^2} = \sin \theta \sqrt{\left(\frac{d\theta}{\sin \theta}\right)^2 + d\omega^2} = \sin \theta \sqrt{\left(d \ln \left| \tan \frac{\theta}{2} \right| \right)^2 + d\omega^2},$$

the general property (4) becoming thus valid for any three-dimensional conical flow (both potential and rotational), instead of the variable β appearing now the new variable ϕ .

2.2. THE OTHER TWO EQUATIONS OF MOTION

Let consider the system formed by the other two motion equations for a certain three-dimensional flow, written on the normal and respectively on the circumferential directions

$$a_\theta = R\ddot{\theta} + 2R\dot{\theta}\dot{\omega} - R\sin\theta\cos\theta\dot{\omega}^2 = -\frac{1}{\rho} \frac{\partial p}{R\partial\theta}; \quad a_\omega = R\sin\theta\ddot{\omega} + 2\sin\theta\dot{R}\dot{\omega} + 2R\cos\theta\dot{\theta}\dot{\omega} = -\frac{1}{\rho} \frac{\partial p}{R\sin\theta\partial\omega}.$$

Multiplying by $R\dot{\theta}$ and respectively by $R\sin\theta\dot{\omega}$ (both $\neq 0$), the two equations may be also written in the form

$$R^2\ddot{\theta}\dot{\theta} + 2R\dot{R}\dot{\theta}^2 - R^2\sin\theta\cos\theta\dot{\theta}\dot{\omega}^2 = -\frac{1}{\rho} \frac{\partial p}{\partial\theta}\dot{\theta}; \quad R^2\sin^2\theta\dot{\omega}\ddot{\omega} + 2R\sin^2\theta\dot{R}\dot{\omega} + 2R^2\sin\theta\cos\theta\dot{\theta}\dot{\omega}^2 = -\frac{1}{\rho} \frac{\partial p}{\partial\omega}\dot{\omega}.$$

By adding the equations of the last system, it results

$$R^2(\ddot{\theta}\dot{\theta} + \sin^2\theta\dot{\omega}\ddot{\omega} + \sin\theta\cos\theta\dot{\theta}\dot{\omega}^2) + 2R\dot{R}(\dot{\theta}^2 + \sin^2\theta\dot{\omega}^2) = -\frac{1}{\rho} \left(\frac{\partial p}{\partial\theta}\dot{\theta} + \frac{\partial p}{\partial\omega}\dot{\omega} \right).$$

Taking into account the conical flow definition

$$\frac{\partial p}{\partial R} = 0,$$

it results

$$\frac{\partial p}{\partial\theta}\dot{\theta} + \frac{\partial p}{\partial\omega}\dot{\omega} = \frac{dp}{dt} = \dot{p}.$$

The resulting motion equation may be still written

$$\frac{1}{2} R^2 \frac{d}{dt} (\dot{\theta}^2 + \sin^2\theta\dot{\omega}^2) + \frac{dR^2}{dt} (\dot{\theta}^2 + \sin^2\theta\dot{\omega}^2) = -\frac{1}{\rho} \frac{dp}{dt}.$$

Using the notation (11), introduced at the end of the preceding subchapter, the two motion equations are reduced in the case of a three-dimensional conical flow to the equation

$$R^2 \frac{1}{2} \frac{d(\dot{\phi}^2)}{dt} + \frac{dR^2}{dt} \dot{\phi}^2 = -\frac{\dot{p}}{\rho},$$

or in the compact form

$$R^2\dot{\phi}\ddot{\phi} + 2R\dot{R}\dot{\phi}^2 + \frac{\dot{p}}{\rho} = 0. \quad (13)$$

Then the system of the three motion equations may be reduced to an equivalent one (of only two equations)

$$\ddot{R} - R\dot{\phi}^2 = 0; \quad R^2\dot{\phi}\ddot{\phi} + 2R\dot{R}\dot{\phi}^2 + \frac{\dot{p}}{\rho} = 0, \quad (14)$$

where, according to the notation (11), we have

$$\dot{\phi}^2 = \dot{\theta}^2 + \sin^2\theta\dot{\omega}^2 = \frac{1}{R^2} (R^2\dot{\theta}^2 + R^2\sin^2\theta\dot{\omega}^2) = \frac{1}{R^2} (V_\theta^2 + V_\omega^2) = \frac{V_n^2}{R^2} = \frac{|\vec{R} \times \vec{V}|^2}{R^4},$$

and therefore

$$\dot{\varphi} = \sqrt{\dot{\theta}^2 + \sin^2 \theta \dot{\omega}^2} = \frac{|\vec{R} \times \vec{V}|}{R^2} = \frac{V_n}{R}, \quad (15)$$

where V_n is the velocity component normal to the radius vector

$$V_n = \sqrt{V_\theta^2 + V_\omega^2}.$$

It is interesting to signal out that in the case of a plane or an axisymmetric two-dimensional conical flow, the system (14) has absolutely the same form, in which we have $\dot{\varphi} = \dot{\beta}$ and respectively $\ddot{\varphi} = \ddot{\beta}$, with $\beta = \omega$, or respectively $\beta = \theta$, the quantity \dot{p} being replaceable by the expression $\gamma K \rho^{\gamma-1} \dot{\rho}$, obtained from the physical equation, written for an isentropic transformation ($p = K \rho^\gamma$).

2.3. THE ENERGY EQUATION

The energy equation for a certain three-dimensional flow (indifferently of rotationality) is written in the form

$$\frac{1}{2} (\dot{R}^2 + R^2 \dot{\theta}^2 + R^2 \sin^2 \theta \dot{\omega}^2) + \frac{a^2}{\gamma - 1} = \frac{W^2}{2}.$$

In the case of a conical flow, taking into account the first equation of motion (1), equation that we multiply by R ($\neq 0$), we have

$$R \ddot{R} - R^2 \dot{\theta}^2 - R^2 \sin^2 \theta \dot{\omega}^2 = 0,$$

whence results the expression

$$R^2 \dot{\theta}^2 + R^2 \sin^2 \theta \dot{\omega}^2 = R \ddot{R},$$

which replacing in the energy equation, we obtain

$$\frac{1}{2} (\dot{R}^2 + R \ddot{R}) + \frac{a^2}{\gamma - 1} = \frac{W^2}{2},$$

or also

$$\frac{1}{2} \frac{d(R \dot{R})}{dt} + \frac{a^2}{\gamma - 1} = \frac{W^2}{2}.$$

Introducing for the local speed of sound the notation

$$a = -\frac{dR_p}{dt} = \dot{R}_p,$$

where R_p has the significance of radius of the sphere of disturbance propagation, we obtain

$$\frac{1}{4} \frac{d^2(R^2)}{dt^2} + \frac{1}{\gamma - 1} \left(\frac{dR_p}{dt} \right)^2 = \frac{W^2}{2} = \frac{1}{4} \frac{d^2}{dt^2} (W^2 t^2 + 2At + B),$$

where A and B are some constants.

We are introducing now the notation

$$F = \frac{\gamma - 1}{4} (W^2 t^2 + 2At + B - R^2);$$

it results

$$\frac{d^2 F}{dt^2} - \left(\frac{dR_p}{dt} \right)^2 = 0,$$

or, using the notations

$$\ddot{F} = \frac{d^2 F}{dt^2} \quad \text{and} \quad \dot{R}_p = \frac{dR_p}{dt},$$

we have the form

$$\ddot{F} - \dot{R}_p^2 = 0,$$

and, after a series of transformations, the energy equation can be expressed in the case of a certain conical flow in the form

$$\frac{dF}{dR_p} \frac{d \ln |\ddot{F}|}{dR_p} = 1, \quad (16)$$

where

$$\dot{F} = \frac{dF}{dt} = \frac{\gamma-1}{4} \cdot 2(W^2 t + A - R\dot{R}) = \frac{\gamma-1}{2} (W^2 t + A - R V_R),$$

therefore

$$\arctan \frac{dF}{dR_p} + \arctan \frac{d \ln |F|}{dR_p} = \frac{\pi}{2}; \quad \text{or} \quad \arctan \frac{dF}{dR_p} = \operatorname{arccot} \frac{d \ln |F|}{dR_p}; \quad (16')$$

(the curves F and $\ln |F|$ are symmetrically inclined against the first axes bisectrix for any value of R_p).

Replacing the expressions of F and \dot{F} , the relation (16) may be written in the form

$$\frac{\gamma-1}{4} \frac{d}{dR_p} (W^2 t^2 + 2At + B - R^2) \frac{d}{dR_p} \ln |W^2 t + A - R V_R| = 1.$$

In the case of the plane and axisymmetric flows, the velocity admitting a potential Φ , it will be replaced the product $R V_R$ under the logarithm sign with this potential.

Returning to the system (14), it is shown that this system admits a prime integral, indifferently of the rotationality (nonisentropicity) of the considered conical flow.

We shall write the second equation of the system in the form

$$(R^2 \ddot{\varphi} + R \dot{R} \dot{\varphi}^2) + R \dot{R} \dot{\varphi}^2 + \frac{\dot{p}}{\rho} = 0,$$

or

$$\frac{1}{2} \frac{d}{dt} (R^2 \dot{\varphi}^2) + R \dot{R} \dot{\varphi}^2 + \frac{\dot{p}}{\rho} = 0.$$

It results from the first equation of the system (14)

$$\dot{\varphi}^2 = \frac{\ddot{R}}{R},$$

expression which we shall introduce in the preceding equation, thus obtaining

$$\frac{1}{2} \frac{d}{dt} (R^2 \dot{\varphi}^2) + R \dot{R} \dot{\varphi}^2 + \frac{\dot{p}}{\rho} = 0, \quad \text{or} \quad \frac{1}{2} \frac{d}{dt} (R^2 \dot{\varphi}^2 + \dot{R}^2) + \frac{\dot{p}}{\rho} = 0.$$

Since we are situated on a stream- or on a vortexline, even in the case in which the general flow is rotational (and therefore nonhomentropic, as that downstream of a curved or a conical nonaxisymmetric shock wave), the physical equation specific to the isentropic transformation remains valid on each flow stream- or vortexline (downstream of the respective shock wave), that is

$$p = K \rho^\gamma,$$

where K (the isentropic constant) differs from a streamline (vortexline) to another; in this case we may write

$$\dot{p} = \frac{dp}{d\rho} \frac{d\rho}{dt} = a^2 \dot{\rho} = \gamma K \rho^{\gamma-1} \dot{\rho},$$

where a is the local speed of sound; it results

$$\frac{1}{2} \frac{d}{dt} (\dot{R}^2 + R^2 \dot{\varphi}^2) + \gamma K \rho^{\gamma-2} \dot{\rho} = 0, \quad \text{or} \quad \frac{1}{2} \frac{d}{dt} (\dot{R}^2 + R^2 \dot{\varphi}^2) + \frac{\gamma K}{\gamma-1} \frac{d}{dt} (\rho^{\gamma-1}) = 0,$$

which admits the prime integral (the energy equation)

$$\frac{1}{2} (\dot{R}^2 + R^2 \dot{\varphi}^2) + \frac{\gamma K}{\gamma-1} \rho^{\gamma-1} = H = \frac{W^2}{2}, \quad (17)$$

or using the relation (12)

$$\frac{1}{2} (V_R^2 + V_n^2) + \frac{a^2}{\gamma-1} = H = \frac{W^2}{2},$$

where the constants H (the total or stagnation enthalpy) and respectively W (the maximum speed of gas) do not differ with the stream- (vortex-)line, these two constants being invariants for the whole flow, e.g. in the conical flow behind an attached non-axisymmetric conical shock wave, like that produced by a non-axisymmetric (say elliptic) cone without angle of incidence, or by a circular cone at angle of incidence.

We signal out that in the case of an axisymmetric conical flow, the equation (17) has absolutely the same form, in which instead of $\dot{\varphi}$ appears $\dot{\theta}$. The essential difference is that the quantity K , which occurs in the left side of the equation, is now constant in the whole fluid mass, e.g. the conical flow downstream of the attached conical shock wave produced by a circular cone without angle of incidence (homentropic flow).

2.4. THE CONTINUITY EQUATION

We shall start from the continuity equation for a certain three-dimensional steady motion, written in the spherical coordinates

$$\frac{1}{R^2} \frac{\partial(\rho R^2 V_R)}{\partial R} + \frac{1}{R \sin \theta} \frac{\partial(\rho V_\theta \sin \theta)}{\partial \theta} + \frac{1}{R \sin \theta} \frac{\partial(\rho V_\omega)}{\partial \omega} = 0,$$

equation which we shall multiply by R ($\neq 0$) and in which we shall replace the velocity components on the system axes, obtaining

$$\frac{1}{R} \frac{\partial(\rho R^2 \dot{R})}{\partial R} + \frac{1}{\sin \theta} \left[\frac{\partial(\rho R \sin \theta \dot{\theta})}{\partial \theta} + \frac{\partial(\rho R \sin \theta \dot{\omega})}{\partial \omega} \right] = 0.$$

Taking into account the fact that we are studying a conical flow and that R , θ and ω are independent variables, we have

$$\frac{\partial \rho}{\partial R} = \frac{\partial \dot{R}}{\partial R} = 0; \quad \frac{\partial R}{\partial \theta} = \frac{\partial R}{\partial \omega} = \frac{\partial(\sin \theta)}{\partial \omega} = 0 \quad \text{and} \quad \frac{\partial(\sin \theta)}{\partial \theta} = \frac{d(\sin \theta)}{d\theta} = \frac{d(\sin \theta)}{dt} \frac{dt}{d\theta} = \frac{1}{\theta} \frac{d(\sin \theta)}{dt}.$$

Grouping conveniently the terms and dividing by ρR ($\neq 0$), we obtain finally the following general form of the continuity equation, specific to the conical flows

$$\frac{\dot{\rho}}{\rho} + 2 \frac{\dot{R}}{R} + \frac{(\sin \theta)}{\sin \theta} \frac{\partial \dot{\theta}}{\partial \theta} + \frac{\partial \dot{\omega}}{\partial \omega} = 0. \quad (18)$$

where

$$(\sin \theta) = \frac{d(\sin \theta)}{dt} = \cos \theta \dot{\theta}.$$

In the following, we shall try to express in other form the two partial derivatives in equation (18). Thus we have

$$\dot{\theta} = \frac{d\theta}{dt} = \frac{\partial \dot{R}}{\partial R} \dot{R} + \frac{\partial \dot{\theta}}{\partial \theta} \dot{\theta} + \frac{\partial \dot{\omega}}{\partial \omega} \dot{\omega} \quad \text{and respectively} \quad \dot{\omega} = \frac{d\omega}{dt} = \frac{\partial \dot{R}}{\partial R} \dot{R} + \frac{\partial \dot{\theta}}{\partial \theta} \dot{\theta} + \frac{\partial \dot{\omega}}{\partial \omega} \dot{\omega}.$$

whence it results

$$\frac{\partial \dot{\theta}}{\partial \theta} = \frac{\dot{\theta}}{\dot{\theta}} - \frac{\partial \dot{R}}{\partial R} \frac{\dot{R}}{\dot{\theta}} - \frac{\partial \dot{\omega}}{\partial \omega} \frac{\dot{\omega}}{\dot{\theta}} \quad \text{and} \quad \frac{\partial \dot{\omega}}{\partial \omega} = \frac{\dot{\omega}}{\dot{\omega}} - \frac{\partial \dot{R}}{\partial R} \frac{\dot{R}}{\dot{\omega}} - \frac{\partial \dot{\theta}}{\partial \theta} \frac{\dot{\theta}}{\dot{\omega}}.$$

Taking into consideration the fact that we have a conical flow, there are the relations

$$\frac{\partial V_\theta}{\partial R} = \frac{\partial(R\dot{\theta})}{\partial R} = 0 \quad \text{and respectively} \quad \frac{\partial V_\omega}{\partial R} = \frac{\partial(R \sin \theta \dot{\omega})}{\partial R} = 0.$$

Developing, we obtain

$$\dot{\theta} + R \frac{\partial \dot{\theta}}{\partial R} = 0 \quad \text{and respectively} \quad \sin \theta \dot{\omega} + R \dot{\omega} \frac{\partial(\sin \theta)}{\partial R} + R \sin \theta \frac{\partial \dot{\omega}}{\partial R} = 0,$$

or, since θ and R are independent variables, we have $\frac{\partial(\sin \theta)}{\partial R} = 0$, and the last relation becomes

$$\dot{\omega} + R \frac{\partial \dot{\omega}}{\partial R} = 0.$$

Then, in the case of a certain conical flow, we have

$$\frac{\partial \dot{\theta}}{\partial R} = -\frac{\dot{\theta}}{R}; \quad \frac{\partial \dot{\omega}}{\partial R} = -\frac{\dot{\omega}}{R}.$$

Replacing in the expressions of the partial derivatives $\frac{\partial \dot{\theta}}{\partial \theta}$ and $\frac{\partial \dot{\omega}}{\partial \omega}$, we shall obtain

$$\frac{\partial \dot{\theta}}{\partial \theta} = \frac{\dot{\theta}}{\dot{\theta}} + \frac{\dot{\theta}}{R} \frac{\dot{R}}{\dot{\theta}} - \frac{\partial \dot{\omega}}{\partial \omega} \frac{\dot{\omega}}{\dot{\theta}} = \frac{\dot{R}}{R} + \frac{\dot{\theta}}{\dot{\theta}} - \frac{\partial \dot{\omega}}{\partial \omega} \frac{\dot{\omega}}{\dot{\theta}}; \quad \text{and} \quad \frac{\partial \dot{\omega}}{\partial \omega} = \frac{\dot{\omega}}{\dot{\omega}} + \frac{\dot{\omega}}{R} \frac{\dot{R}}{\dot{\omega}} - \frac{\partial \dot{\theta}}{\partial \theta} \frac{\dot{\theta}}{\dot{\omega}} = \frac{\dot{R}}{R} + \frac{\dot{\omega}}{\dot{\omega}} - \frac{\partial \dot{\theta}}{\partial \theta} \frac{\dot{\theta}}{\dot{\omega}}.$$

For example, in the case of the two-dimensional axisymmetric conical flow, we have $\dot{\theta} \neq 0$ and $\dot{\omega} = 0$, resulting thus

$$\frac{\partial \dot{\theta}}{\partial \theta} = \frac{\dot{R}}{R} + \frac{\dot{\theta}}{\dot{\theta}}; \quad \text{and respectively} \quad \frac{\partial \dot{\omega}}{\partial \omega} = 0,$$

being obtained for the equation (18) the following simple form

$$\frac{\dot{\rho}}{\rho} + 3 \frac{\dot{R}}{R} + \frac{(\sin \theta)}{\sin \theta} \frac{\dot{\theta}}{\dot{\theta}} = 0.$$

The equation (18) is valid for any conical flow, indifferently if this is or is not potential, representing the new general form of the continuity equation of these flows.

In the case of the homentropic certain (nonconical) flow, the velocity \vec{V} admits (is derived from) a potential Φ ; the cancellation of the velocity rotational curl is expressed in the spherical coordinates under the symbolic form

$$\text{rot } \vec{V} = \nabla \times \vec{V} = \frac{1}{R^2 \sin \theta} \begin{vmatrix} \vec{u}_R & R \vec{u}_\theta & R \sin \theta \vec{u}_\omega \\ \frac{\partial}{\partial R} & \frac{\partial}{\partial \theta} & \frac{\partial}{\partial \omega} \\ V_R & R V_\theta & R \sin \theta V_\omega \end{vmatrix} = 0,$$

from which are resulting the irrotationality relations

$$\frac{\partial(R V_\theta)}{\partial R} = \frac{\partial V_R}{\partial \theta}; \quad \frac{\partial(R \sin \theta V_\theta)}{\partial R} = \frac{\partial V_R}{\partial \omega} \quad \text{and} \quad \frac{\partial(R \sin \theta V_\omega)}{\partial \theta} = \frac{\partial V_R}{\partial \omega}.$$

From the first two conditions it results

$$V_\theta + R \frac{\partial V_\theta}{\partial R} = \frac{\partial V_R}{\partial \theta}; \quad \sin \theta V_\omega + R \sin \theta \frac{\partial V_\omega}{\partial R} = \frac{\partial V_R}{\partial \omega},$$

and since in the case of a conical flow we have

$$\frac{\partial V_\theta}{\partial R} = \frac{\partial V_\omega}{\partial R} = 0,$$

it results

$$V_\theta = \frac{\partial V_R}{\partial \theta} \quad \text{and respectively} \quad V_\omega = \frac{1}{\sin \theta} \frac{\partial V_R}{\partial \omega}.$$

Using the adopted notations, we obtain two relations which allow us to express the derivatives $\dot{\theta}$ and $\dot{\omega}$ for the potential conical flows in the form

$$\dot{\theta} = \frac{1}{R} \frac{\partial \dot{R}}{\partial \theta} \quad \text{and adequately} \quad \dot{\omega} = \frac{1}{R \sin^2 \theta} \frac{\partial \dot{R}}{\partial \omega}.$$

In some particular cases, the equation (18), written for potential flow, are admitting prime integrals (the flow rate equation), the constants C_i which appear in these integrals being kept along the streamlines or on the stream- (field-) surfaces.

It results that, in the case of these usual potential conical flows, the equation (18) is transformed from an equation with partial derivatives to an ordinary differential equation, whose prime integral (the flow rate equation) may be written in the general form

$$\rho R^n \sin^{n-2} \beta \dot{\beta} = C_n; \quad (19)$$

(with $\beta = \theta$, or $\beta = \omega$, as in the case of the first equation of motion), where the exponent n has the following values

$n = 1$ - for the one-dimensional (parallel and uniform) flows;

$n = 2$ - for the plane two-dimensional flows;

$n = 3$ - for the axisymmetric two-dimensional flows,

the flow rate equation having respectively the forms

$$\begin{aligned} n = 1; \quad \beta = \theta; \quad \rho \frac{R \dot{\theta}}{\sin \theta} &= \rho \frac{V_\theta}{\sin \theta} = \rho V = C_1 = \frac{m}{A}; \\ n = 2; \quad \beta = \omega; \quad \rho R^2 \dot{\omega} &= \rho R V_\omega = C_2 = \frac{m}{l}; \\ n = 3; \quad \beta = \theta; \quad \rho R^3 \sin \theta \dot{\theta} &= \rho R^2 \sin \theta V_\theta = C_3 = \frac{m}{\pi}. \end{aligned} \quad (20)$$

It can be noted that in the equation (19) corresponding to $n = 3$, the quantity $\pi R^2 \sin \theta$ represents just the side area of the current circular cone of vertex half angle θ ; in the expressions of the constants C_n intervene the following quantities

m - the mass flow rate;

A - the area of the section normal to the flow velocity;

l - the width (depth) of this section.

An other case of prime integrability of the equation (18) is given by the three-dimensional conical flows having the variables θ and ω bound by certain differential relation (the so called helicoidal or axisantisymmetric flows -see [1] and also the subchapter 2.1).

REFERENCES

1. Selescu, R. - Studiul proprietatilor generale specifice ale curgerilor conice, IMFDZ report, code P 1446, Bucharest, june 1994.

DETERMINING THE LIQUID (WATER) DEPTH FOR SATISFYING THE GAS - HYDRODYNAMIC ANALOGY

Richard Selescu *

National Institute for Aerospace Research "Elie Carafoli", INCAS
77538, Bucharest, 6, Romania

Abstract The liquid (water) depth necessary for satisfying the gas - hydrodynamic analogy, from the viewpoint of the disturbance propagation velocity, is deduced in this work, considering the real physical phenomenon, which consists in the superposition of the gravity waves with the capillary ones. Both the direct problem (having as unknown quantity the liquid depth and as parameter the ratio between this depth and the wave wavelength) and the inverse problem (in which the roles of the unknown quantity and respectively that of the parameter are inverted) are solved. Some possible applications of the analogy to the hydrodynamics of the supercritical plane two-dimensional flows in liquids of limited depth are presented.

1. INTRODUCTION

As it is well-known from the waves theory, the expression of the velocity c of surface waves propagation in a liquid is given by the relation (see [1], [5], [6])

$$c^2 = \frac{\lambda^2}{\tau^2} = \frac{\omega^2}{k^2} = \left(\frac{g\lambda}{2\pi} + \frac{2\pi\sigma}{\rho\lambda} \right) \tanh \frac{2\pi h}{\lambda} ,$$

obtained by considering a simple solution in the form

$$f(z, t) = A \cos(kz - \omega t) = A \cos k(z - ct) = A [\cos k(x - ct) \cosh ky - i \sin k(x - ct) \sinh ky] ,$$

(which admits $\psi = 0$ for the ground level $y = 0$, that is on the real axis) for the differential equation with partial derivatives due to U. Cisotti, which may be written in the compact symbolic form below :

$$\left(\frac{\partial^2}{\partial t^2} + ig \frac{\partial}{\partial z} - i \frac{\sigma}{\rho} \frac{\partial^3}{\partial z^3} \right) [f(z + ih, t) - f(z - ih, t)] = 0 ,$$

by replacing in this equation the above given simple solution and by cancelling its imaginary part, thus resulting the condition

$$-\omega^2 \cosh kh + kg \sinh kh + \frac{k^3 \sigma}{\rho} \sinh kh = 0 .$$

The following quantities are intervening here:

$z = x + iy$ - the complex variable in the vertical plane of the motion;

t - the time

$f(z, t) = \varphi(x, y, t) + i \psi(x, y, t)$ - the complex potential of the plane motion (real on the real axis

$y = 0$ of the z - plane)

A - the wave amplitude

λ - the wave wavelength;

τ - the period of motion

$k = \frac{2\pi}{\lambda}$ - the wave number;

$\omega = \frac{2\pi}{\tau}$ - the cyclic (angular) frequency

g - the acceleration of gravity

σ - the surface tension (the capillary constant) of the liquid

ρ - the density of the liquid

h - the depth of the liquid.

*) Senior Scientist, Department of Aerodynamics

It can be noticed that the above expression of the velocity of surface waves represents the sum (superposition) of two contributions, namely: the first term of the sum is due to the gravity wave, while the second term is due to the capillary wave.

We mention that, till now it was considered that, due to the great value of the wavelength λ , the second term (the capillary wave effect) may be neglected with respect to the first one (the gravity wave effect).

In this work, that reproduces the chapter 3 of [2], we propose to consider the real physical phenomenon, i.e. that consisting in the superposition of the two above mentioned effects.

2. SOLVING THE DIRECT PROBLEM

We shall deduce the depth h of the incident (undisturbed) liquid flow, needed for satisfying the gas - hydrodynamic analogy (existent between the plane two-dimensional supersonic flow of a fictitious monoatomic perfect gas and the quasi-two-dimensional supercritical flow in the thin layer at the free surface of a little depth liquid), from the viewpoint of the disturbance propagation velocity.

With the view to doing this, we shall introduce the notation

$$\chi = \frac{2\pi h}{\lambda} = kh,$$

by the use of which, the initial relation becomes

$$c^2 = \left(\frac{gh}{\chi} + \frac{\sigma}{\rho h} \chi \right) \tanh \chi.$$

We shall impose now the condition of equality between the exact expression of the propagation velocity of the mixed wave, given by this relation, and the approximate expression of the propagation velocity of the gravity wave in a little depth liquid, (which is used in defining the liquid flow Froude number, the last one being the analogous quantity with the gas flow Mach number)

$$c^2 = gh,$$

for having satisfied the gas - hydrodynamic analogy, since the expression of the propagation velocity of the disturbance (the speed of sound) in gases, and in the case of the fictitious monoatomic gas, is given by the relation

$$a^2 = \gamma \frac{R}{\mu} T = 2 \frac{R}{\mu} T,$$

where we have

$$\gamma = \frac{N+2}{N} \quad (\text{with } N=2) - \text{the adiabatic exponent of the fictitious monoatomic gas}$$

N - the number of the degrees of freedom for the respective gas molecules($N=2$ translations only). It is the case of the molecules of a gas closed in a container having one of its three dimensions negligible, so that these molecules are moving practically in a plane. In order to estimate the magnitude of the extremely little distance (gap) needed between the two parallel plane walls of the container, we give in the Table no.1, reproduced from [3], the diameters d of molecules of some monoatomic gases, expressed in ångströms ($1 \text{ Å} = 10^{-8} \text{ cm}$). These diameters have been computed from the results of measurements of the respective gases viscosity.

Table no.1

Monoatomic gas	Helium (He)	Argon (Ar)	Krypton (Kr)	Xenon (Xe)
Diameter of molecules, d (Å)	1.9	2.9	3.14	4.0

R - the universal constant of the perfect gases

μ - the mole (the molecular weight) of the respective monoatomic perfect gas

T - the absolute static temperature of the fictitious gas with $\gamma = 2$, this temperature representing the analogous physical quantity with the little depth h of the considered liquid (water).

It results the following algebraic equation

$$\left(\frac{gh}{\chi} + \frac{\sigma}{\rho h} \chi \right) \tanh \chi = gh ,$$

or

$$\frac{gh}{\chi} + \frac{\sigma}{\rho h} \chi = gh \coth \chi ,$$

or more

$$\frac{1}{\chi} + \frac{\sigma}{\rho gh^2} \chi = \coth \chi ,$$

with the unknown quantity h , where χ is a positive real non-dimensional parameter, proportional to the ratio h/λ .

It results successively

$$\frac{\sigma}{\rho gh^2} = \frac{1}{\chi} \left(\coth \chi - \frac{1}{\chi} \right)$$

and

$$h^2 = \frac{\sigma}{\rho g} \frac{\chi}{\coth \chi - \frac{1}{\chi}} = \frac{\sigma}{\rho g} \frac{1}{\frac{1}{\chi} \left(\frac{1}{\tanh \chi} - \frac{1}{\chi} \right)} .$$

It must be noticed the fact that the framed formula allows the determining the depth h of the incident (undisturbed) liquid (water) layer necessary for gas - hydrodynamic quantitative analogy (without neglecting the capillary wave contribution in the expression of the propagation velocity c , in this formula appearing both σ and ρ). This formula also shows us that, for any value of the ratio h/λ , there is a corresponding value h (not always, but usually little) for which the disturbance propagation velocity c has the critical value, $c = \sqrt{gh}$.

One can also notice that in the case when χ tends to zero ($h \ll \lambda$), therefore the case of the large wavelength waves (practically infinite), the quantity h^2 necessary for satisfying the gas-hydrodynamic analogy tends to the value $\frac{3\sigma}{\rho g}$ (which is the absolute minimum value of h^2 , that is on its whole existence

domain), since, by expanding the function $\coth \chi$ in a power series around the origin, therefore inside the convergence interval $\left(|\chi| < \pi, \text{ i.e. } \frac{h}{\lambda} < \frac{1}{2} \right)$, we have

$$\coth \chi = \frac{1}{\chi} + \frac{\chi}{3} - \frac{\chi^3}{45} + \frac{2\chi^5}{945} - \frac{\chi^7}{4725} + \dots = \sum_{k=0}^{\infty} \frac{2^{2k} B_{2k}}{(2k)!} \chi^{2k-1} = \frac{1}{\chi} + \sum_{k=1}^{\infty} \frac{2^{2k} B_{2k}}{(2k)!} \chi^{2k-1} ,$$

while the difference from the denominator of h^2 becomes

$$\coth \chi - \frac{1}{\chi} = \frac{\chi}{3} \left(1 - \frac{\chi^2}{15} + \frac{2\chi^4}{315} - \frac{\chi^6}{1575} + \dots \right) = \sum_{k=1}^{\infty} \frac{2^{2k} B_{2k}}{(2k)!} \chi^{2k-1} ,$$

wherefrom results the value of the product in this denominator

$$\frac{1}{\chi} \left(\coth \chi - \frac{1}{\chi} \right) = \frac{1}{3} \left(1 - \frac{\chi^2}{15} + \frac{2\chi^4}{315} - \frac{\chi^6}{1575} + \dots \right) = \sum_{k=1}^{\infty} \frac{2^{2k} B_{2k}}{(2k)!} \chi^{2(k-1)} ,$$

which, for χ tending to 0, tends to the value $\frac{1}{3}$. In all these three expressions we have denoted by the symbol B_{2k} the Bernoulli numbers.

Therefore, we shall have the following conditions for the depth of the incident supercritical liquid flow and for the critical velocity in the case of the infinite wavelength waves ($\lambda \rightarrow \infty$)

$$h_{\infty} = h_{\min} = \sqrt{\frac{3\sigma}{\rho g}} \quad \text{and respectively} \quad c_{\infty} = c_{\min} = \sqrt{gh_{\infty}} = \sqrt{3g \frac{\sigma}{\rho}} ,$$

which, for water at a temperature of about 20°C , lead to the values

$$h_{\infty} = 4.715 \text{ mm} \quad \text{and} \quad c_{\infty} = 0.215 \text{ m/s} .$$

But, as it is well-known, both the surface tension σ , and the density ρ of the liquids, and particularly of water, vary with the environmental temperature t , following some physical laws. In the first three columns of the Table no.2 we have reproduced from [4] the values of the coefficient σ of the surface tension of water with respect to the dry air and those of the water density ρ , for some common values of the environmental temperature t , inside the interval contained between 0 and 34°C.

In the last three columns of this table, we have written down the calculated values of the ratio $\frac{\sigma}{\rho g}$, expressed in mm^2 , those of the depth h_{∞} necessary for satisfying the gas - hydrodynamic analogy, expressed in mm and calculated by applying the previously established framed formula, as well as those of the critical velocity of surface wave propagation, $c_{\infty} = \sqrt{gh_{\infty}}$, expressed in m/s , therefore for the case of infinite wavelength waves. For the acceleration g of gravity, we have considered the value $9.80665 \text{ m/s}^2 = 9.80665 \text{ N/kg}$, corresponding to a 45 degrees latitude.

Table no.2

$t (^{\circ}\text{C})$	$\sigma \text{ (dyn/cm)}$	$\rho \text{ (g/cm}^3\text{)}$	$\frac{\sigma}{\rho g} \cdot 10^6 \text{ (mm}^2\text{)}$	$h_{\infty} \text{ (mm)}$	$c_{\infty} \text{ (m/s)}$
0	75.49	0.99987	7.6988	4.806	0.2171
5	74.75	0.99999	7.6225	4.782	0.21655
10	74.01	0.99973	7.5490	4.759	0.2160
12	73.70	0.99952	7.5189	4.749	0.2158
14	73.41	0.99927	7.4912	4.741	0.2156
15	73.26	0.99913	7.4769	4.736	0.2155
16	73.11	0.998970	7.4628	4.732	0.2154
18	72.82	0.998623	7.4358	4.723	0.2152
20	72.53	0.998232	7.4091	4.715	0.2150
21	72.37	0.998021	7.3943	4.710	0.2149
22	72.22	0.997799	7.3806	4.706	0.2148
23	72.08	0.997567	7.3680	4.702	0.2147
24	71.93	0.99732	7.3545	4.697	0.2146
25	71.78	0.99707	7.3410	4.693	0.2145
26	71.63	0.99681	7.3276	4.689	0.2144
28	71.33	0.99626	7.3009	4.680	0.2142
30	71.03	0.99567	7.2745	4.672	0.2140
32	70.74	0.99505	7.2494	4.663	0.21385
34	70.44	0.99440	7.2233	4.655	0.2137

One can notice that the variation with the temperature of the depth h_{∞} of the water incident supercritical flow, necessary for satisfying the gas - hydrodynamic analogy, is negligible (between 4.806 mm and 4.655 mm , therefore of only 3.24 %), while the corresponding one of the critical velocity c_{∞} of surface wave propagation is totally insignificant (between 0.2171 m/s and 0.2137 m/s , therefore of only 1.61 %).

In the case $\chi = \pi$ (the upper limit of the convergence interval for the series expansion of the function $\coth \chi$), therefore $\frac{h^*}{\lambda^*} = \frac{1}{2}$, we immediately obtain the following formula:

$$h^{*2} = \frac{\pi}{\coth \pi - \frac{1}{\pi}} \frac{\sigma}{\rho g} = \frac{\pi^2}{\pi \coth \pi - 1} \frac{\sigma}{\rho g} \approx 4.583376 \frac{\sigma}{\rho g} \approx 1.527792 h_{\infty}^2 ,$$

wherefrom it results

$$h^* = \frac{\pi}{\sqrt{\pi \coth \pi - 1}} \sqrt{\frac{\sigma}{\rho g}} \approx 2.140882 \sqrt{\frac{\sigma}{\rho g}} \approx 1.236039 h_\infty ; \quad \lambda^* = 2h^* \approx 4.281764 \sqrt{\frac{\sigma}{\rho g}} \approx 2.472078 h_\infty$$

and correspondingly, the value of the critical velocity of surface wave propagation

$$c^* = \sqrt{gh^*} \approx \sqrt{1.236039 gh_\infty} \approx 1.111773 \sqrt{gh_\infty} = 1.111773 c_\infty .$$

3. SOLVING THE INVERSE PROBLEM

Of course, one may also set the inverse problem, this consisting in calculating the value of the ratio χ previously defined, for a given value h of the liquid depth of an incident supercritical flow.

In this case the roles of the unknown quantity and respectively that of the independent non-dimensional positive parameter are inverted, the algebraic equation with the unknown h becoming a transcendental equation with the unknown χ .

This equation may be solved approximately by appreciating as satisfactory (from the viewpoint of the accuracy in the calculus of the solutions χ) the expansion in a power series of the function $\coth \chi$ and the keeping of only first five terms of this expansion, thus being obtained a bicubic algebraic equation

$$\frac{\sigma}{\rho gh^2} = \frac{1}{3} - \frac{\chi^2}{45} + \frac{2\chi^4}{945} - \frac{\chi^6}{4725} ,$$

which, by effecting the substitution

$$\chi^2 = Y > 0$$

is transformed in the following cubic algebraic equation, with the unknown quantity Y

$$\frac{Y^3}{4725} - \frac{2Y^2}{945} + \frac{Y}{45} - \frac{1}{3} + \frac{\sigma}{\rho gh^2} = 0 ,$$

or more, using the notation h_∞ (previously introduced and framed)

$$Y^3 - 10Y^2 + 105Y - 1575 \left(1 - \frac{h_\infty^2}{h^2}\right) = 0 ,$$

solvable by applying the Cardan's formulas, keeping only the positive solution of this approximate equation. One may notice that in the case $h = h_\infty$, it is obtained the trivial solution $Y = 0$, and respectively $\chi = 0$, previously mentioned (the case $\lambda \rightarrow \infty$). This means that our approximate equation accurately satisfies for $\chi = 0$ the same boundary condition as the original transcendental one.

In the case when the values of the non-dimensional positive unknown quantity χ are expected to be (very) close to the value π , this meaning $\frac{h}{\lambda}$ (very) close to $\frac{1}{2}$, it is recommended to expand the function

$\coth \chi$ in a power series around the point $\chi = \pi$ (the upper limit of the previous convergence interval), therefore in a Taylor series, and to keep a number of only four terms

$$\coth \chi = \coth \pi - \frac{\chi - \pi}{\sinh^2 \pi} \left[1 - \coth \pi \cdot (\chi - \pi) - \left(\frac{1}{3} - \coth^2 \pi \right) (\chi - \pi)^2 \right] ,$$

obtaining thus the following quartic algebraic equation

$$\frac{\sigma}{\rho gh^2} = \frac{1}{\chi} \left\{ \coth \pi - \frac{\chi - \pi}{\sinh^2 \pi} \left[1 - \coth \pi \cdot (\chi - \pi) - \left(\frac{1}{3} - \coth^2 \pi \right) (\chi - \pi)^2 \right] - \frac{1}{\chi} \right\} ,$$

which may be solved by applying the Hudde's formulas, keeping only the positive solution of the above approximate equation. We can easily see that for the value $\chi = \pi$, the above equation satisfies the same boundary condition as the original transcendental one:

$$\frac{\sigma}{\rho gh^2} = \frac{1}{\pi} \left(\coth \pi - \frac{1}{\pi} \right) ,$$

where by h^* , as previously, we have denoted the liquid depth in the case $\frac{h}{\lambda} = \frac{1}{2}$.

4. SOME POSSIBLE APPLICATIONS

All the results obtained in the Chapters 2 and 3 of this work have a special significance, the gas - hydrodynamic analogy being applied in the experimental aero - gasdynamics of the plane two-dimensional supersonic flows. Their applications consist in the qualitative determining (visualization) of the shock waves and expansion fans pattern, as well as the determining of the characteristic physical quantities of the jumps performed through normal or oblique shock waves, corresponding to that of the respective hydraulic jumps obtained in the analogue plane quasi-two-dimensional supercritical liquid flows of little depth. The experiment must be achieved in a horizontal channel with a free surface, using in the upstream a sluice-type nozzle, which produces a test section flow with a very smooth surface and also permits to adjust the water height upstream the sluice gate. This adjustment is needed to give the possibility of varying the velocity of the incident supercritical liquid flow in the channel, and therefore the Froude number F_∞ of this undisturbed flow, always keeping the same depth h_∞ at the upstream end of the channel (downstream the sluice gate), and therefore the same critical velocity c_∞ of the incident flow.

In order to avoid the horizontal flow non-uniformity due to the boundary layer which appears and develops itself on the floor and the side walls of the channel, it is suggested for this floor the use of a moving belt, having in its cross section the profile of the letter C and the same sense of displacement as the liquid flow. The linear velocity of this belt must equalize the free surface potential velocity of the undisturbed supercritical liquid flow (of magnitude $V_\infty = F_\infty c_\infty$) in the channel, having the little depth h_∞ , so that the vertical gradient of the horizontal flow velocity would be as small as possible.

5. COMPARISON WITH OTHER RESULTS

Some authors ([5], [6]) have tried to solve the direct problem by using an experimental way. Thus, A.H.Shapiro concludes that "the analogy method is reliable only with water depths of the order of 0.25 inch" (= 6.35 mm). His "experiments show that with this depth the measured Froude number is consistent with the Froude number obtained by other methods, but with larger depths the wave angles give incorrect results". Citing a paper by Th. von Kármán, the author asserts that "for this height the capillary waves behave most nearly like gravity waves; second, depths of a foot or more may be used (requiring proportionately larger channels and models), with the aim of making the gravity waves so large that capillary effects are secondary". A.O.Ditman & coll. "recommend to use a depth of undisturbed liquid layer $h \cong 6$ mm ; for this depth the velocity c practically does not depend on λ and is given by $c^2 = gh$ ". In the opinion of the author of this work, both values are overrated, they ignoring the floor boundary layer thickness, their experiments being performed without any kind of moving belt in order to avoid this layer.

REFERENCES

1. Carafoli, E., Oroveanu, T. - Mecanica fluidelor, vol.II, Bucharest, Editura Academiei R.P.R., 1955, pp. 390 - 391 ;
2. Selescu, R. - Analiza cantitativa a analogiei gazo - hidrodinamice in cazul curgerilor bidimensionale plane cu unde de soc si respectiv cu salturi hidraulice, Bucharest, I.M.F.D.Z. report, code P 1585, april 1995, pp. 37 - 42 ;
3. Koshkin, N., Shirkevich, M. - Handbook of Elementary Physics (translated from the Russian), Moscow, Mir Publishers, 1968, p. 75 ;
4. * * * - Indrumar matematic si tehnic (translated from the Russian, adapted), Bucharest, Editura Tehnica, 1964, pp. 525 - 526 and 554 ;
5. Shapiro, A.H. - Free Surface Water Table, article H,1 in "Physical Measurements in Gas Dynamics and Combustion", vol.IX - High Speed Aerodynamics and Jet Propulsion, editors: Part 1. R.W. Ladenburg; Part 2. B.Lewis, R.N.Pease, H.S.Taylor, London, Geoffrey Cumberlege, Oxford University Press, 1955, pp. 313 - 314 and 318 - 319 ;
6. Ditman, A.O., Savtchuk, V.D., Yakubov, J.R. - Metody analogui v aerodinamike letatel'nykh apparatov, Moscow, Mashinostroyeniye, 1987, pp. 116 - 117 and 121 .

Flow of a Ferromagnetic Fluid in an axial magnetic field

E.Tulcan*, S. Balint**

* Faculty of Physics, West University Timisoara

** Faculty of Mathematics, West University Timisoara

Abstract

We investigate theoretically the flow of a magnetic fluid in a horizontal circular pipe in the presence of a longitudinal magnetic field using the equations of quasi-steady ferrohydrodynamics derived by Neuringer and Rosensweig. The solution is compared with the results presented by S.Kamiyama.

1. Introduction

Ferromagnetic fluids are a suspension of many particles of a solid ferromagnetic material (diameter ≈ 10 nm and number density $\approx 10^{23}$ particles/m³) coated with a molecular layer of a dispersant and suspended in a liquid carrier.

Pipe flow problems of magnetic fluids in an applied magnetic field are important as the basic studies of hydrodynamics of magnetic fluid and as the

problems related closely to the development of applied devices such as new energy conversion system.

2. Theoretical analysis

When the magnetic fluid is placed in a field \vec{H} , the particle is acted upon by the torque $\mu_0(\vec{m} \times \vec{H})$ which causes a magnetic moment \vec{m} in the direction of magnetic field \vec{H} .

If we assume that the magnetization \vec{M} of the magnetic fluid is collinear with the magnetic field \vec{H} the system of equations for magnetic fluids established by Rosensweig [1] is :

- the continuity equation

$$\nabla \cdot \vec{u} = 0 \quad (1)$$

- the equation of motion

$$\rho \frac{D\vec{u}}{Dt} = -\nabla p + \eta \nabla^2 \vec{u} + \mu_0 (\vec{M} \cdot \nabla) \vec{H} \quad (2)$$

- the Maxwell equation

$$\nabla \times \vec{H} = 0 \quad \nabla \cdot \vec{B} = 0 \quad (3)$$

First we consider the steady laminar pipe flow in an axial magnetic field $H_z(z)$ as shown in Fig. 1

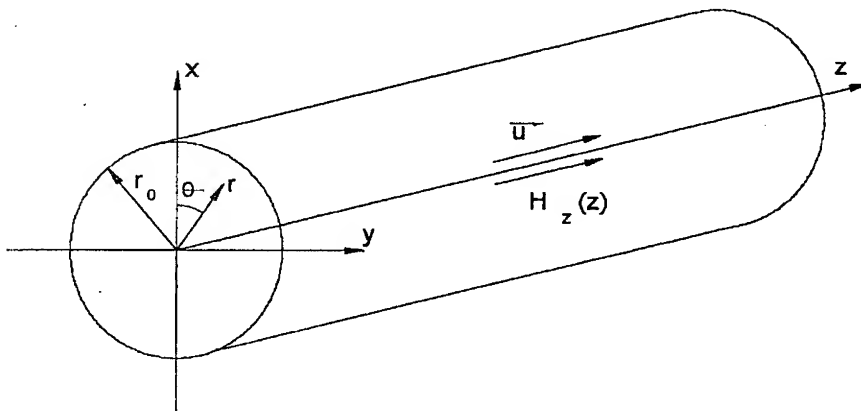


Fig. 1. Cylindrical coordinate system.

The basic equations (1) - (3) are applied to this problem.

With the continuity equation (1), the equation of motion (2) reduces to:

$$\frac{dp}{dz} = \eta \frac{1}{r} \frac{d}{dr} \left(r \frac{du_z}{dr} \right) + \mu_0 M_z \frac{dH_z}{dz} \quad (4)$$

Let us introduce the following dimensionless quantities:

$$r^* = \frac{r}{r_0}, \quad z^* = \frac{z}{z_0}, \quad u_z^* = \frac{u_z}{u_0}, \quad h^* = \frac{H_z}{M_{0\max}}, \quad p^* = \frac{pr_0}{\eta u_0} \quad (5)$$

Here r_0 is pipe radius, u_0 is mean flow velocity and M_0 is the equilibrium magnetization expressed by the Langevin function L :

$$M_0 = NmL(\xi) \quad (6)$$

where $L(\xi) = \coth \xi - \xi^{-1}$, $\xi = \mu_0 mH/kT$

Then, equation (4) is expressed as

$$\frac{dp^*}{dz^*} - \frac{\mu_0 r_0}{\eta u_0} M_{0\max} H_{\max} M_z^* \frac{dh^*}{dz^*} = \frac{1}{r^*} \frac{d}{dr^*} \left(r^* \frac{du_z^*}{dr^*} \right) \quad (7)$$

Applying the boundary condition of $u_z^* = 0$ at $r^* = 1$ to equation (7) we obtain the solution as

$$u_z^* = \frac{k}{4} (r^{*2} - 1) \quad (8)$$

where

$$k = \frac{dp}{dz^*} - \frac{\mu_0 r_0}{\eta u_0} M_{0\max} H_{\max} M_z^* \frac{dh^*}{dz^*} \quad (9)$$

Applying the continuity equation, the velocity profile is represented by

$$u_z^* = 2(1 - r^{*2}) \quad (10)$$

If we give up at the dimensionless quantities, we have the solution as

$$u_z(r) = 2u_0 \left(1 - \frac{r^2}{r_0^2} \right) \quad (11)$$

where the mean flow velocity is

$$u_0 = \frac{\mu_0 M_z \frac{dH_z}{dz} - \frac{dp}{dz}}{8\eta} r_0^2 \quad (12)$$

The same problem was presented by Kamiyama [2], [3]. On these papers the description of motion of a magnetic fluid is made with basic equations proposed by Shliomis.

That is, equation of motion which have an additional rotational friction term

$$\rho \frac{D\bar{u}}{Dt} = -\nabla p + \eta \nabla^2 \bar{u} + \mu_0 (\bar{M} \cdot \nabla) \bar{H} + \frac{1}{2\tau_s} \nabla \times (\bar{S} - I\bar{\Omega}) \quad (13)$$

equation of internal angular momentum:

$$\frac{D\bar{S}}{Dt} = \mu_0 (\bar{M} \times \bar{H}) - \frac{1}{\tau_s} (\bar{S} - I\bar{\Omega}) + \gamma \nabla^2 \bar{S} \quad (14)$$

and the following equation for $d\bar{M}/dt$

$$\frac{D\bar{M}}{Dt} = \frac{1}{I} (\bar{S} \times \bar{M}) - \frac{1}{\tau_B} \left(\bar{M} - M_0 \frac{\bar{H}}{H} \right) \quad (15)$$

where

\bar{S} - internal angular momentum

$\bar{\Omega}$ - local angular velocity of fluid

I - sum of moment of inertia of particles per unit volume

τ_s - relaxation time of particle rotation due to frictional resistance of fluid

τ_B - Brownian time of rotational diffusion

$$\gamma = \frac{1}{2} \tau_B$$

The solution have the same form (11), but the mean flow velocity is

$$u_0 = \frac{\mu_0 M_z \frac{dH_z}{dz} - \frac{dp}{dz}}{8(\eta + \Delta\eta)} r_0^2 \quad (16)$$

This solution show that the viscosity increases according to Kamiyama [4], with

$$\Delta\eta = \frac{3}{2} \varphi \eta_0 \frac{Ah^* L^*}{1 + Ah^* L^*} \quad (17)$$

where $\varphi = \frac{4}{3} \pi a^3 N$ is the volumetric concentration of particles and

$$A = \mu_0 \tau_s \tau_B H_{\max} M_{0\max} / I.$$

This rotational viscosity (17) have the order of η_0 (the viscosity of the carrier liquid). The difference between η and $\Delta\eta$ for a few sets of magnetic fluids according to Vékás [5] is of order two.

The solution (11), (12) is an exact solution of this problem which is very important from the mathematical point of view.

On the other hand, when we resolve the system of equation (13) ÷ (15) a few approximations is must be done.

3. Conclusions

If we put $\Delta\eta$ as a correction to η , from the beginning in equation of motion (2), we will obtain (11), (16) as an exact solution for the first set of equations. This step can be a good simplification for problems with not so simple geometry.

4. References

- [1] R. E. Rosensweig - *Ferrohydrodynamics* - Cambridge monographs on mechanics and applied mathematics (1985).
- [2] S. Kamiyama, K. Koike and N. Iizuka - *On the Flow of a Ferromagnetic Fluid in a Circular Pipe* - Bulletin of the JSME Vol 22 No 171 (1979).
- [3] S. Kamiyama and K. Mokuya - Trans. Jpn. Soc. Mech. Eng. , 47-424, B (1981) or Magn. Hidro. No1 (1982).
- [4] S. Kamiyama, K Koike - *Hydrodynamics of Magnetic Fluids* (1992).
- [5] L. Vékás, D. Bica, I. Potencz, E. Tulcan, D. Rolea, V. Sofonea - *Composition and Concentration Effects on the Rheological Behaviour of Magnetic Fluids* - Acta Physica Slovaca (1995).

**MATHEMATICAL PECULIARITIES IN MODEL ISSUES
OF AGGREGATION PROCESS OF TRIVALENT
IMPURITIES IN CUBIC SYMMETRY MONOCRYSTALS
NaCl-TYPE**

by
Gheorghe Dorin Stoicescu
Faculty of Science, Lucian Blaga University of Sibiu

In the ionic crystals doped with aliovalent impurities are induced vacancies in order to compensate the electric charges. These vacancies place themselves in the nearest neighbourhood of the first sphere of coordination (*positions nn*) or in the second sphere of coordination (*nnn -next nearest neighbour*). In this way dipols impurity vacancy (**I-V**) are formed, with electric moment different from zero. In determined conditions of temperature the dipols diffuse in the crystal and agglomerate to form dipolar complexes of variable proportions .

The agglomeration of dipols is accompanied by the modification of the optic, electric and mechanical properties of the material. The dipols' diffusion in the crystal is produced through the jump of vacancies, which change their place either with the own atoms of the basic net or the impurity atoms. The more the dipols agglomerate, the more the dielectric absorption decreases, because in an electric field the isolated dipols absorbate energy in the process of reorientation jumping, while in the case of coupled dipols the reorientation jumps are more difficult. They suffer some supplementary reciprocal interactions, which are proportional with the complexes extension, to whom they belong.

The theoretical description of the experimental observations made in the case of doping with bivalent impurities (structures of type I-V) is excellent realised by the model proposed by Stasiw and Teltow [1].

In the case of doping with trivalent impurities (structures I-2V), the presence of two charge compensatory vacancies in the neighbourhood makes the mentioned model becomes inoperant.

In our studies only the vacancies placed in the nn positions were considered. In this approximation are formed four distinct structures, called $\alpha, \beta, \gamma, \delta$ in the order of decreasing energy of coulombian interaction.

According to the Boltzmann distribution of vacancies on structures it can be noticed that only three structures present significant populations. The share of the α structure is, compared with the γ one, of an 10^{-6} order at the 300 K temperature.

To determinate the expresion of polarisation, in both constant field and in variable field, it has been considered as follows:

- all the vacancies induced are coupled with the impurity ions;
- the I-2V structures are isolated;
- the transition probabilities between the different kinds of structures (without field) depends only on the structure;
- there are considered only the transitions produced by the jump of only one vacancy and, furthermore, only on a distance of $a\sqrt{7}$ (a is the semiconstant of the cristaline network);
- a vacancy changes place with the impurity ion through several jumps and this leads to structures in which the vacancy places itself in a nnn position (a jump on a distance superior to $a\sqrt{2}$) and therefore they are omitted;
- the jumps of one vacancy are realised with a transition frequency ν_{ij} (between the i and the j structures). In the case of the jumps only on the distance $a\sqrt{2}$ only the transitions $\nu_{\gamma\gamma}, \nu_{\beta\gamma}, \nu_{\gamma\beta}, \nu_{\gamma\delta}$ and $\nu_{\delta\gamma}$ remain different from zero;
- the jump frequencies can be described like the processes of thermic activation by relations of Arrhenius;
- because the quotient w_{ij}/w_{ji} depends only on the interaction E_i and E_j , it will result that:

$$\nu_{ij}/\nu_{ji} = \exp[(E_i - E_j)/KT]$$

- in the presence of the external field, the dipol's energy depends both on the structure and on the configuration inside the structure :

$$E_{ij}^{(E=0)} \equiv E_i \rightarrow E_i - \vec{E} \cdot \vec{p}_{it} \equiv E_{it}$$

- the presence of the external field determines an asymmetrisation of the potential barrier;

- it is considered the weak field approximation, so the transition probability between the t_1 type in the i_1 structure and the t_2 type of the i_2 structure is influenced in the following way:

$$w_{i_1 t_1 \rightarrow i_2 t_2} \rightarrow w_{i_1 t_1 \rightarrow i_2 t_2} (1 - \vec{p}_{i_1 t_1} \cdot \vec{E} / KT)$$

This permits that the variation equations of the populations in the presence of the field can be obtained from those written in the absence of the field, by introducing the modification:

$$\nu_{ij} N_{it} \rightarrow \nu_{ij} \left(1 - \frac{\vec{p}_{it} \cdot \vec{E}}{KT}\right) \cdot N_{it}$$

With all these considerations there have been obtained equations of variation of the populations for the different structures and active types, in the presence of the field. From these equations there has been afterwards deduced the functions **sum S** and **difference D** for the populations on the same structure.

In the weak fields approximation the presence of the perturbator parameter $x = qaE/\hbar t \gg 1$ permits the development of the solutions in a series of powers of x and t . Therefore in the linear approximation in x the differences are proportions with the external field E .

This is a very important conclusion for the case of variable fields.

By using these considerations there have been written the temporal evolution equations, and it has been noticed that the populations $N_{\beta 00}, N_{\beta + -}, N_{\delta 00}, N_{\gamma + -}, N_{\delta + -}$ (the notation also indicates the orientation of the dipolar momentum in the field) do not variate and remain to their equilibrium values.

From the fact that the projection for the dipolar electric moment is zero in the types $\beta 00, \beta + -, \gamma + -, \delta 00, \delta + -$ it results that the polarisation can be described by the relation:

$$P(E, t) = 4ga [D_{\beta}(t) + 2D_{\delta}(t)]$$

where the D functions represent the difference in the populations for the studied structures.

The solving for the evolution equations for the differences of populations results in two different solutions:

$$\gamma_{12} = \frac{1}{2} (\gamma + 4\gamma_{\beta\delta}) [1 \mp \sqrt{1-\rho}]$$

with

$$\gamma \equiv 2\gamma_{\beta\delta} + \gamma_{\delta\delta} + 2\gamma_{\gamma\delta};$$

$$\rho \equiv \frac{16\gamma_{\beta\delta}(\gamma - \gamma_{\delta\beta})}{(\gamma + 4\gamma_{\beta\delta})^2}$$

which indicates the presence of two modes of relaxation in the considered model. Therefore the time evolution for the D_i differences can be described through relations of the following type:

$$D_i(t) = d_{ci} + d_{1i} e^{-\gamma_1 t} + d_{2i} e^{-\gamma_2 t}$$

The polarisation in constant field can be obtained as an expression of the kind:

$$P(t, E = \text{const}) = \frac{4cg^2 a^2 E}{KT} \left[(C_{1\beta} + 2C_{1\delta}) e^{-\gamma_1 t} + (C_{2\beta} + 2C_{2\delta}) e^{-\gamma_2 t} \right]$$

where C_{ij} are expressions which contain exclusively the transition probabilities between the active structures.

In the case of variable fields, by using the analyticity of the solutions as functions of the field and time it can be obtained the variation in weakfield and slowly variable, as well as the complete dependence of ω and the relaxation times:

$$P(t) = \frac{4g^2 a^2 c E}{KT} \left[\frac{\tilde{F}_1}{1 + \omega^2 \tau_1^2} + \frac{\tilde{F}_2}{1 + \omega^2 \tau_2^2} - \right. \\ \left. - j\omega \left(\frac{\tau_1 \tilde{F}_1}{1 + \omega^2 \tau_1^2} + \frac{\tau_2 \tilde{F}_2}{1 + \omega^2 \tau_2^2} \right) \right]$$

where F represent factors which are dependent exclusively on the frequencies of jump.

Brun and Dansas [2] treated the same problem , but they considered in the beginning the equilibrium status in constant field and followed (studied) the relaxation produced by the elimination of the field. In this way there has been avoided the hypotheses regarding the modification of the probabilities induced by the modification of the field. By considering also the structures formed with the vacancies placed in *nnn* positions they have obtained an equation system whose dimensions made impossible the deduction of the population implicated in the different relaxation modes.

By working in the other alternative (using the equilibrium status in the absence of the field and following the evolution of the system, if the field is introduced) it can be obtained the result wich is in accordance with those obtained by Brun and Dansas, which can constitute a verification of the hereby proposed model.

But in adition it is directly exploited the extension of the deduced equations for the case of variable fields [3]

Bibliography

- [1] O Stasiw, J Teltow Ann der Physik 1 261 (1947)
- [2].A.Brun, P.Dansas, Phys.Stat.Sol., **b66**, 201, (1974)
- [3].G.D.Stoicescu, Thesis, Babes-Bolyai University, Cluj-Napoca, 1990

UNIFORM ROTATIONS OF A LIQUID-FILLED SPACECRAFT IN A CONSTANT FORCE FIELD

Madeleine Pascal* and Dan Comănescu**

* - Universite Pierre et Marie Curie, 4 place Jussieu 75252 Paris, France

** - West University of Timișoara , bd. Parvan no.4 Timișoara , Romania

Abstract

We are concerned by the uniform rotations of a rigid body or a liquid filled spacecraft with a fixed point when the spacecraft is completely or partially filled with an incompressible , inviscid or viscous fluid.

0. Introduction

The problem of the rotation of a liquid filled spacecraft is a classical problem . This problem was subject of theoretical and experimental investigations beginning with the end of XIXth century . The investigations were stimulated by the developement of the spatial industry . Important contributions are in the papers of: Greenhill, Hough, Poincare, Cetaev, Moiseyev, Rumiantsev, Sobolev, Greenspan , etc. The most of this studies concern the problem of the stability of an assumed possible uniform rotation .

The purpose of this paper is to find the uniform rotations of a rigid body or a liquid-filled spacecraft with a fixed point in a constant force field . We consider the cases when the spacecraft is completely or partially filled with an incompressible, inviscid or viscous fluid.

I. Uniform rotations of a rigid body about a fixed point in a constant force field

1.0 Introduction

Let O be the fixed point, \vec{f} the body force per unit mass, I the inertia tensor of the rigid body with respect to O , D the rigid body domain, G the mass center of the rigid body and M the mass of the rigid body.

We introduce two coordinate systems, the first $\mathcal{R}(O, \vec{e}_1, \vec{e}_2, \vec{e}_3)$ in which we have :

$$(I.1) \quad \vec{e}_3 = \frac{\vec{f}}{\|\vec{f}\|} ,$$

and the body-coordinate system $\mathcal{R}'(O, \vec{e}_1', \vec{e}_2', \vec{e}_3')$.

We also denote $\vec{\omega}$ the angular velocity.

Definition A motion is called a *uniform rotation* if

$$(I.2) \quad \vec{\omega} = \vec{\omega}_0$$

$\vec{\omega}_0$ constant in \mathcal{R} and $\vec{\omega}_0 \neq \vec{0}$.

Remark I.1 If we have a uniform rotation then there is a body-fixed coordinate system $\mathcal{R}''(O, \vec{e}_1'', \vec{e}_2'', \vec{e}_3'')$ with

$$(I.3) \quad \vec{e}_3'' = \frac{\vec{\omega}_0}{\|\vec{\omega}_0\|}$$

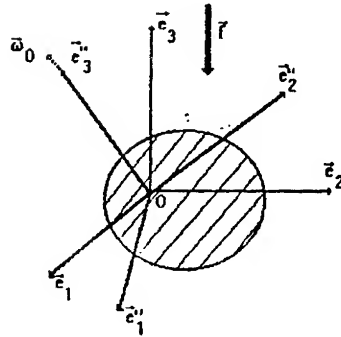
I. 1 Uniform rotations

The equation of rotation of the rigid body is

$$(I.4) \quad I\dot{\vec{\omega}} + \vec{\omega} \times I\vec{\omega} = M\vec{OG} \times \vec{f}$$

Then for uniform rotations we have :

$$(I.5) \quad \vec{\omega}_0 \times I\vec{\omega}_0 = M\vec{OG}_0 \times \vec{f}$$



with G_0 position of the mass center for uniform rotations.

Let us denote x_{1G}, x_{2G}, x_{3G} the components of \vec{OG}_0 in \mathcal{R}'' and ξ_1, ξ_2, ξ_3 the components of \vec{e}_3 in \mathcal{R}'' .

Remark I.2 The components of $\vec{\omega}_0$ in \mathcal{R}'' are $0, 0, \omega_0$.

The projections of the relation (I.5) on the axis of \mathcal{R}'' are:

$$-I_{23}\omega^2_0 = Mf(x_{2G}\xi_3 - x_{3G}\xi_2)$$

$$(I.6) \quad I_{13}\omega^2_0 = Mf(x_{3G}\xi_1 - x_{1G}\xi_3)$$

$$0 = x_{1G}\xi_2 - x_{2G}\xi_1$$

with $I = \sum_{i,j=1}^3 I_{ij} \vec{e}_i'' \otimes \vec{e}_j''$.

Let us denote (φ, ψ, θ) the Euler's angles of \mathcal{R}'' with respect to \mathcal{R} . We obtain:

$$\xi_1 = \sin\theta \sin\varphi$$

$$(I.7) \quad \xi_2 = \sin\theta \cos\varphi$$

$$\xi_3 = \cos\theta$$

For a uniform rotation , if we use the kinematic Euler's formula , we obtain

$$(I.8) \quad \varphi(t) = \varpi_0 t + \varphi_0$$

with φ_0 as a constant.

Using the Euler's angles we obtain for the uniform rotations the following:

$$-I_{23}\varpi_0^2 = Mf(x_{2G}\cos\theta - x_{3G}\sin\theta\cos(\varpi_0 t + \varphi_0))$$

$$(I.9) \quad I_{13}\varpi_0^2 = Mf(x_{3G}\sin\theta\sin(\varpi_0 t + \varphi_0) - x_{1G}\cos\theta))$$

$$0 = \sin\theta(x_{1G}\cos(\varpi_0 t + \varphi_0) - x_{2G}\sin(\varpi_0 t + \varphi_0))$$

Theorem I.1 If we have a uniform rotation with $\vec{\varpi}_0$ as the angular velocity and $O \neq G$ then $\vec{\varpi}_0 \parallel \vec{f}$.

Proof 1

If $x_{1G} \neq 0$ or $x_{2G} \neq 0$ then the relation $(I.9)_3$ implies:

$$(I.10) \quad \sin\theta(t) = 0 \quad \forall t$$

then

$$(I.11) \quad \theta(t) \in \{0, \pi\}$$

If $x_{1G} = x_{2G} = 0$ we obtain:

$$(I.12) \quad x_{3G} \neq 0$$

and

$$(I.13) \quad \frac{I_{23}\varpi_0^2}{Mf x_{3G}} = \sin\theta(t)\cos(\varpi_0 t + \varphi_0)$$

$$(I.14) \quad \frac{I_{13}\varpi_0^2}{Mf x_{3G}} = \sin\theta(t)\sin(\varpi_0 t + \varphi_0)$$

and

$$(I.15), \quad \sin^2\theta(t) = \frac{\varpi_0^4(I_{13}^2 + I_{23}^2)}{M^2 f^2 x_{3G}^2}$$

hence θ is a constant and by the formula (I.14) ($I_{13}, I_{23}, M, f, x_{3G}, \varpi_0$ are constants) we obtain $\sin\theta(t) = 0$ and:

$$\theta \in \{0, \pi\}$$

Proof 2 If we have $x_{1G} \neq 0$ then :

$$(I.17) \quad \xi_2 = \frac{x_{2G}\xi_1}{x_{1G}}$$

$$(I.18) \quad \xi_3 = \frac{x_{3G}\xi_1}{x_{1G}} - \frac{I_{13}\varpi_0^2}{Mf x_{1G}}$$

but

$$(I.19) \quad \xi_1^2 + \xi_2^2 + \xi_3^2 = 1$$

then

$$(I.20) \quad \frac{x_{1G}^2 + x_{2G}^2 + x_{3G}^2}{x_{1G}^2} \xi_1^2 - \frac{2I_{13}\varpi_0^2}{Mf x_{1G}} \xi_1 + \frac{I_{13}^2\varpi_0^4 - M^2 f^2 x_{1G}^2}{M^2 f^2 x_{1G}^2} = 0$$

ξ_1 is a continuous function which satisfies (I.20) for all t , then ξ_1 is a constant in \mathcal{R}'' , hence \vec{e}_3 is constant in \mathcal{R}''

We also have:

$$(I.21) \quad \left(\frac{d\vec{e}_3}{dt}\right)_{\mathcal{R}} = \left(\frac{d\vec{e}_3}{dt}\right)_{\mathcal{R}''} = \vec{0},$$

$$(I.22) \quad \left(\frac{d\vec{e}_3}{dt}\right)_{\mathcal{R}''} = \vec{\varpi}_0 \times \vec{e}_3$$

hence

$$(I.23) \quad \vec{\omega}_0 \parallel \vec{f}$$

The same argument is also possible for the case $x_{2G} \neq 0$

If we have $x_{1G} = x_{2G} = 0$ then:

$$(I.24) \quad \xi_1 = \frac{I_{13}\omega_0^2}{Mf x_{3G}}$$

$$(I.25) \quad \xi_2 = \frac{I_{23}\omega_0^2}{Mf x_{3G}}$$

The above proof is based on the formulas (I.19), (I.21) and (I.22).

Theorem I.2 It is possible a uniform rotation about an axis parallel to \vec{f} which contains O if and only if the point G is on the axis which is parallel to \vec{f} and contains the point A ($\vec{OA} = -\frac{\omega_0^2}{Mf^2} I \vec{f}$).

Proof

We have :

$$(I.26) \quad \xi_1 = \xi_2 = 0 \text{ and } \xi_3 = 1$$

The relation (I.6) becomes:

$$(I.27) \quad x_{1G} = -\frac{I_{13}\omega_0^2}{Mf}$$

$$x_{2G} = -\frac{I_{23}\omega_0^2}{Mf}$$

The result is an immediate consequence.

Theorem I.3 If $O = G$ it is possible a uniform rotation with $\vec{\omega}_0$ as the angular velocity if and only if $\vec{\omega}_0$ is a main direction for I .

Proof

In this case the equation for the uniform rotation is:

$$(I.28) \quad \vec{\omega}_0 \times I \vec{\omega}_0 = \vec{0}$$

II. Uniform rotations of a completely liquid-filled spacecraft about a fixed point in a constant force field

Let us consider a rigid spacecraft and an incompressible fluid .

We consider firstly the model of inviscid fluid and secondly the model of viscous fluid.

We denote O the fixed point , \vec{f} the body force per unit mass , I the inertia tensor of the spacecraft with respect to O , τ the fluid domain , ρ the fluid density, G the mass center of the total system , M the mass of the total system , \vec{K}_0 the angular momentum of the total system with respect to point O , \vec{M}_0 the moment of the forces with respect to point O , \vec{v} the absolute velocity of the fluid , \vec{n} the outer normal direction of the surface $\partial\tau$.

We note $\mathcal{R}(O, \vec{e}_1, \vec{e}_2, \vec{e}_3)$ the space-fixed coordinate system with :

$$(II.1) \quad \vec{e}_3 = \frac{\vec{f}}{\|\vec{f}\|}$$

, $\mathcal{R}(O, \vec{e}_1', \vec{e}_2', \vec{e}_3')$ a spacecraft-fixed coordinate system and $\vec{\omega}$ the angular velocity.

A motion is called a uniform rotation if:

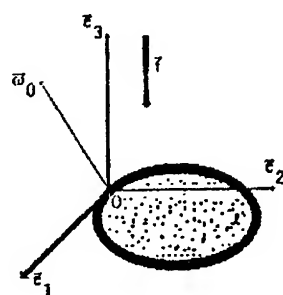
$$(II.2) \quad \vec{\omega} = \vec{\omega}_0 \text{ constant}$$

and

$$(II.3) \quad \vec{v} = \vec{\omega}_0 \times \vec{OP} \text{ in } \tau$$

Remark II.1 If we have a uniform rotation then the system has a rigid body motion.

II.1. Uniform rotations



The equations of the problem for a *inviscid* fluid are:

$$(II.4) \quad \frac{d\vec{K}_0}{dt} = \vec{M}_0$$

$$(II.5) \quad \frac{d\vec{v}}{dt} = -\frac{1}{\rho} \vec{\nabla} p + \vec{f} \text{ in } \tau$$

$$(II.6) \quad \text{div} \vec{v} = 0 \text{ in } \tau$$

$$(II.7) \quad \vec{v}\vec{n} = (\vec{\omega} \times \vec{OP})\vec{n} \text{ on } \partial\tau$$

and for a viscous fluid we have :

$$(II.8) \quad \frac{d\vec{K}_0}{dt} = \vec{M}_0$$

$$(II.9) \quad \frac{d\vec{v}}{dt} = -\frac{1}{\rho} \vec{\nabla} p + \nu \Delta \vec{v} + \vec{f} \text{ in } \tau$$

$$(II.10) \quad \operatorname{div} \vec{v} = 0 \text{ in } \tau$$

$$(II.11) \quad \vec{v} = (\vec{\omega} \times \vec{OP}) \text{ on } \partial\tau$$

with ν the kinematic viscosity.

Remark II.2 We have:

$$(II.12) \quad \vec{M}_0 = M \vec{OG} \times \vec{f}$$

$$(II.13) \quad \vec{K}_0 = I \vec{\omega} + \int_{\tau} \rho \vec{OP} \times \vec{v} d\tau$$

Remark II.3 For a uniform rotation we have:

$$(II.14) \quad \vec{K}_0 = (I + J) \vec{\omega}$$

$$(II.15) \quad J \vec{\omega} = \int_{\tau} \rho \vec{OP} \times (\vec{\omega} \times \vec{OP}) d\tau$$

The uniform rotations for a inviscid fluid or a viscous fluid are defined by:

$$(II.16) \quad \vec{\omega}_0 \times (I + J) \vec{\omega}_0 = M \vec{OG}_0 \times \vec{f}$$

and

$$(II.17) \quad \vec{\omega}_0 \times (\vec{\omega}_0 \times \vec{OP}) = -\frac{1}{\rho} \vec{\nabla} p + \vec{f} \text{ in } \tau$$

Remark II.4 We have:

$$(II.18) \quad \vec{\omega}_0 \times (\vec{\omega}_0 \times \vec{OP}) = -\frac{1}{2} \vec{\nabla} (\vec{\omega}_0 \times \vec{OP})^2$$

$$(II.19) \quad \vec{f} = \vec{\nabla} (\vec{f} \vec{OP})$$

then for a uniform rotation we have the equation:

$$\vec{\omega}_0 \times (I + J)\vec{\omega}_0 = M\vec{OG} \times \vec{f}$$

and the fluid pressure is:

$$(II.20) \quad p = \frac{\rho}{2}(\vec{\omega}_0 \times \vec{OP})^2 + \rho\vec{f}\vec{OP} + p_0^* \text{ in } \tau$$

with p_0^* a constant. Using the theorems of the first chapter we have immediately:

Theorem II.1 If we have a uniform rotation with $\vec{\omega}_0$ as the angular velocity and $O \neq G$ then $\vec{\omega}_0 \parallel \vec{f}$.

Theorem II.2 An uniform rotation about an axis parallel to \vec{f} which contains O is possible if and only if the point G is on the axis which is parallel to \vec{f} and contains the point A ($\vec{OA} = -\frac{\vec{\omega}_0^2}{Mf^2}(I + J)\vec{f}$).

Theorem II.3 If $O = G$ an uniform rotation is possible if and only if $\vec{\omega}_0$ is a main direction for $(I + J)$.

Remark II.5 For a uniform rotation we denote $\mathcal{R}''(O, \vec{e}_1'', \vec{e}_2'', \vec{e}_3'')$ the body fixed coordinate system with:

$$(II.21) \quad \vec{e}_3'' = \frac{\vec{\omega}_0}{\|\vec{\omega}_0\|}$$

We have:

$$(II.22) \quad \left(\frac{d\vec{e}_3}{dt}\right)_{\mathcal{R}''} = \vec{e}_3 \times \vec{\omega}_0$$

The projections on the axis of \mathcal{R}'' are:

$$(II.23) \quad \begin{aligned} \dot{\xi}_1 &= \omega_0 \xi_2 \\ \dot{\xi}_2 &= -\omega_0 \xi_1 \\ \dot{\xi}_3 &= 0 \end{aligned}$$

then we have the constants A_1, A_2, A_3, A_4, A_5 so:

$$\begin{aligned} \xi_1(t) &= A_1 \cos \omega_0 t + A_2 \sin \omega_0 t \\ (2.24) \quad \xi_2(t) &= A_3 \cos \omega_0 t + A_4 \sin \omega_0 t \\ \xi_3(t) &= A_5 \end{aligned}$$

We note x_1, x_2, x_3 the components of a fluid particle in \mathcal{R}'' . We obtain:

$$(II.25) \quad p = \frac{\rho \omega^2}{2} (x_1^2 + x_2^2) + \rho f (A_1 \cos \omega_0 t + A_2 \sin \omega_0 t) x_1 + \rho f (A_3 \cos \omega_0 t + A_4 \sin \omega_0 t) x_2 + \rho f A_5 x_3 + p_0^*$$

therefore:

If $O \neq G_0$ (i.e. $\vec{\omega}_0 \parallel \vec{f}$) the fluid pressure is constant.

If $O = G$, the fluid pressure is time variant.

III. Uniform rotation of a partially filled spacecraft about a fixed point in a constant force field

We use here the notation of the previous chapter and introduce: $(\partial \tau)_W$ the fluid boundary on cavity wall; $(\partial \tau)_F$ the free surface and

$$(III.1) \quad F(P, t) = 0$$

as the equation of the free surface.

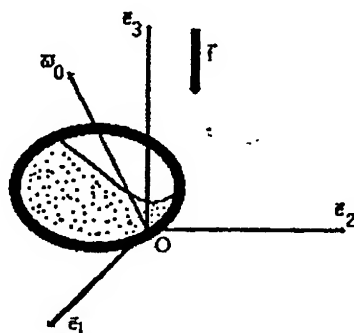
III.1 Uniform rotations

The equations of the problem for an *inviscid* fluid are:

$$(III.2) \quad \frac{d\vec{K}_0}{dt} = \vec{M}_0$$

$$(III.3) \quad \frac{d\vec{v}}{dt} = -\frac{1}{\rho} \vec{\nabla} p + \vec{f} \text{ in } \tau$$

$$(III.4) \quad \text{div} \vec{v} = 0 \text{ in } \tau$$



$$(III.5) \quad \vec{v}\vec{n} = (\vec{\omega} \times \vec{OP})\vec{n} \text{ on } (\partial\tau)_W$$

$$(III.6) \quad p = p_0 \text{ on } (\partial\tau)_F$$

$$(III.7) \quad \vec{v}\vec{n} + \frac{\partial F / \partial t}{\|\vec{\nabla} F\|} = (\vec{\omega} \times \vec{OP})\vec{n} \text{ on } (\partial\tau)_F$$

Remark III.1 F is defined in the body-fixed coordinate system.

For a viscous fluid we have:

$$(III.8) \quad \frac{d\vec{K}_0}{dt} = \vec{M}_0$$

$$(III.9) \quad \frac{d\vec{v}}{dt} = -\frac{1}{\rho}\vec{\nabla}p + \vec{f} + \nu \Delta \vec{v} \text{ in } \tau$$

$$(III.10) \quad \text{div} \vec{v} = 0 \text{ in } \tau$$

$$(III.11) \quad \vec{v} = (\vec{\omega} \times \vec{OP}) \text{ on } (\partial\tau)_W$$

$$(III.12) \quad \mathcal{T}\vec{n} = -p_0\vec{n} \text{ on } (\partial\tau)_F$$

$$(III.13) \quad \vec{v}\vec{n} + \frac{\partial F/\partial t}{\|\vec{\nabla}F\|} = (\varpi \times \vec{OP})\vec{n} \text{ on } (\partial\tau)_F$$

with $\mathcal{T} = -p\mathcal{E} + \mu(\nabla\vec{v} + (\nabla\vec{v})^t)$ with μ the coefficient of viscosity.

Definition A motion is called an uniform rotation if:

$$(III.14) \quad \vec{\omega} = \vec{\omega}_0 \text{ constant}$$

and

$$(III.15) \quad \vec{v} = \vec{\omega}_0 \times \vec{OP} \text{ in } \tau$$

Remark III.2 If we have a uniform rotation then the system has a rigid body motion. In this case we have $\nabla\vec{v} + (\nabla\vec{v})^t = 0$. The uniform rotations for a inviscid fluid or a viscous fluid are:

$$(III.16) \quad \vec{\omega}_0 \times (I + J)\vec{\omega}_0 = M\vec{OG}_0 \times \vec{f}$$

and

$$(III.17) \quad \vec{\omega}_0 \times (\vec{\omega}_0 \times \vec{OP}) = -\frac{1}{\rho}\vec{\nabla}p + \vec{f} \text{ in } \tau$$

$$(III.18) \quad p = p_0 \text{ on } (\partial\tau)_F$$

$$(III.19) \quad \frac{\partial F}{\partial t} = 0 \text{ on } (\partial\tau)_F$$

Remark III.3 For a uniform rotation we have the fluid pressure:

$$(III.20) \quad p = \frac{\rho}{2}(\vec{\omega}_0 \times \vec{OP})^2 + \rho\vec{f}\vec{OP} + p_0^* \text{ in } \tau$$

then the equations are (III.16), (III.18), (III.19) and (III.20).

Theorem III.1 If we have a uniform rotation with $\vec{\omega}_0$ as its angular velocity then $\vec{\omega}_0 \parallel \vec{f}$.

Proof On the free surface we have:

$$p_0 = \frac{\rho\omega^2}{2}(x_1^2 + x_2^2) + \rho f(A_1 \cos \omega_0 t + A_2 \sin \omega_0 t)x_1 + \rho f(A_3 \cos \omega_0 t + A_4 \sin \omega_0 t)x_2 +$$

$$(III.21) \quad + \rho f A_5 x_3 + p_0^*$$

we obtain:

$$F(t, x_1, x_2, x_3) = \frac{\rho\omega^2}{2}(x_1^2 + x_2^2) + \rho f(A_1 \cos \omega_0 t + A_2 \sin \omega_0 t)x_1 + \rho f(A_3 \cos \omega_0 t +$$

$$(III.22) \quad + A_4 \sin \omega_0 t)x_2 + \rho f A_5 x_3 + p_0^* - p_0$$

and

$$(III.23)$$

$$\frac{\partial F}{\partial t}(t, x_1, x_2, x_3) = -\rho f \omega_0 (A_1 x_1 + A_3 x_2) \sin \omega_0 t + \rho f \omega_0 (A_2 x_1 + A_4 x_2) \cos \omega_0 t$$

Actually we have on free surface:

$$A_1 x_1 + A_3 x_2 = 0$$

$$A_2 x_1 + A_4 x_2 = 0$$

This relation implies:

$$(III.25) \quad A_1 = A_2 = A_3 = A_4 = 0$$

If we connect it with the relation (II.24) we reach to:

$$(III.26) \quad \xi_1 = \xi_2 = 0$$

Theorem III.2 An uniform rotation about an axis parallel to \vec{f} which contains O is possible if and only if the point G is on the axis which is parallel to \vec{f} and contains the point A ($\vec{OA} = -\frac{\omega_0^2}{Mf^2}(I + J)\vec{f}$).

If we have a uniform rotation then the equation of the free surface is:

$$(III.27) \quad F(t, x_1, x_2, x_3) = \frac{\rho\omega^2}{2}(x_1^2 + x_2^2) + \rho f x_3 + p_0^*$$

Proof Using the theorem I.2 we obtain the necessary conditions for a uniform rotation.

If the condition are fulfilled then the relation (III.16) is fulfilled. The relation (III.20) and (III.18) imply (III.28) and in this case (III.19) is fulfilled.

References

- [1] GREENSPAN H.P. The theory of rotating fluids. Cambridge University Press, 1969.
- [2] MOISEYEV N.N., RUMYANTSEV V.V. , Dynamic stability of bodies containing fluid , Springer-Verlag, 1968.
- [3] DUFFAUT Y., These, Universite Pierre et Marie Curie, 1994.
- [4] DRAGOS L., Principiile mecanicii analitice , Editura Tehnica, Bucuresti, 1976.
- [5] IACOB C., Mecanica teoretica, Ed. Didactica si Pedagogica, Bucuresti, 1980.

ON NUMERICAL MODELLING OF WALL BOUNDARY
CONDITIONS IN SOLVING WIND TUNNEL WALL
INTERFACE PROBLEM

BOSKO RASUO

UNIVERSITY OF BELGRADE

It is well known that even the best wind tunnels do not provide the flow over a model that would exactly simulate the free air stream condition i.e. to be the same as the flow in free air. Hence, the problem of wind tunnel wall interference accompanies experimental and theoretical investigations when designing a wind tunnel as well as during its operation.

An survey physical and mathematical properties of various types of wind tunnel walls is given in this paper. The paper discusses some newer developments, but concentrates mainly on the specification of wall boundary conditions that are of importance for the calculation of wall interference.

In this paper a single expression approximately representing the boundary conditions of solid, porous and slotted walls and an open jet have been developed. Also, discussed are wall boundary conditions experimentally determined by measuring static pressure distribution at the vicinity of work section walls.

Linearized compressible-flow analysis is applied to the study of wind tunnel wall interference for subsonic and transonic flow in two-dimensional test section having closed or ventilated (slotted or porous) walls.

APPLICATION OF CENTRAL LIMIT THEOREMS TO MACROTRANSPORT PROCESSES

BY C. TIMOFTE

Department of Mathematics, Faculty of Physics, University of Bucharest,
Bucharest-Magurele, Romania

Abstract. Using a central limit theorem we shall describe a large class of material and non-material dispersive phenomena occurring in macrohomogeneous systems. More precisely, we focus on the diffusions X_t generated by an operator $L = 1/2 \sum_{i,j=1}^k a_{ij}(x) \partial^2 / \partial x_i \partial x_j + \sum_{i=1}^k U_0 b_i(x) \partial / \partial x_i$ having periodic coefficients. A central limit theorem asserts that $\lambda^{-1/2}(X_{\lambda t} - \lambda U_0 \bar{b} t)$, $t \geq 0$, converges in distribution to a Brownian motion as $\lambda \rightarrow \infty$. Here \bar{b} is the mean of $b(x) = (b_1(x), \dots, b_k(x))$. This article analyzes the functional dependence of the dispersion matrix \bar{D} of this limiting Brownian motion on the velocity parameter U_0 and the period "a". We shall give precise analytical conditions on the geometry of b_i 's which determine the asymptotic behavior of \bar{D}_{ij} 's as functions of a and U_0 . The results are shown to apply both for material and non-material dispersion phenomena. Dispersion coefficients are computed in several examples which provide closed-form solutions of \bar{D}_{ij} and exhibit their expected growth as functions of a and U_0 .

1. Introduction. Based upon a rigorous, physicomathematical description of microtransport processes occurring in heterogeneous systems, macrotransport processes describe a large class of material and non-material dispersive phenomena occurring in macrohomogeneous systems.

Applications of macrotransport theory are presently recognized in numerous fields of scientific and engineering research. In the last years, the application of microcontinuum theory to increasingly complex macrocontinuum systems has underlined the need for a wider theoretical context than previously provided by classical microtransport theory.

Various methods have been developed for obtaining the macroscale behavior and properties of some heterogeneous complex systems. These include the method of moments, the homogenization method, the statistical and volume-averaging methods and the probabilistic methods based on central limit theorems ([1], [2], [4], [6]).

We shall present now a probabilistic method based on a central limit theorem for Markov processes ([2], [9]).

More precisely, we focus on the diffusions X_t generated by a differential operator :

$$L = \frac{1}{2} \sum_{i,j=1}^k a_{ij}(x) \frac{\partial^2}{\partial x_i \partial x_j} + \sum_{i=1}^k U_0 b_i(x) \frac{\partial}{\partial x_i} \quad (1.1)$$

whose coefficients satisfy the following assumptions :

- (1) The matrix $((a_{ij}(x)))$ is symmetric and positive definite.
- (2) The functions $a_{ij}(x)$ and $b_i(x)$ are real valued and periodic, i.e. $a_{ij}(x + \nu) = a_{ij}(x)$, $b_i(x + \nu) = b_i(x)$ for any x and any vector ν with integer coordinates.
- (3) The functions $a_{ij}(x)$ have bounded second order derivatives and $b_i(x)$ have continuous first order derivatives.
- (4) U_0 is a real parameter.

Let $(\Omega, \mathcal{A}, P^x)$ be a probability space on which are defined :

- (i) - a random vector X_0 with values in \mathbb{R}^k and distribution π^i .
- (ii) a standard k -dimensional Brownian motion $B(t) = (B_1(t), \dots, B_k(t))$ which is independent of X_0 .

Let $\{X(t), t \geq 0\}$ be the solution (continuous and nonanticipative) of Itô's stochastic integral equation :

$$X_t = X_0 + \int_0^t U_0 b(X(s)) ds + \int_0^t \sigma(X(s)) dB(s) \quad (1.2)$$

where $\sigma(x)$ is the positive square root of $((a_{ij}(x)))$.

The periodicity of the coefficients allows us to work on the state space $T^k = [0, 1]^k$ with the process $\tilde{X}(t) = X(t) \pmod{1}$ having a transition probability density function $\dot{p}(t; x, y)$ and an invariant probability density $\pi(x)$ on $[0, 1]^k$ such that :

$$\int_{[0,1]^k} \dot{p}(t; x, y) \pi(x) dx = \pi(y) \quad \text{a.e. on } [0, 1]^k \quad (1.3)$$

Let us consider the real Hilbert space $L^2([0, 1]^k, \pi)$ with the inner product :

$$\langle f, g \rangle = \int_{[0,1]^k} f(y)g(y)\pi(y)dy \quad (1.4)$$

and let $\{\tilde{T}_t, t \geq 0\}$ be the strongly continuous semigroup of contractions on this space, defined by :

$$(\tilde{T}_t f)(x) = \int_{[0,1]^k} \dot{p}(t; x, y) f(y) dy, \text{ for } x \in [0, 1]^k \quad (1.5)$$

A central limit theorem asserts ([2]) that under the assumptions (1)-(4), no matter what the initial distribution π' is, the stochastic process:

$$\{Z_{t,\lambda} = \lambda^{-1/2}(X_{\lambda t} - \lambda U_0 t \bar{b}) \quad , \quad t \geq 0\} \quad (1.6)$$

converges weakly, as $\lambda \rightarrow \infty$, to a Brownian motion with zero drift and dispersion matrix $\bar{D} = ((\bar{D}_{ij}))$ given by :

$$\begin{aligned} \bar{D}_{ij} = & -U_0^2 \langle b_i, g_j \rangle - U_0^2 \langle b_j, g_i \rangle + \bar{a}_{ij} + \\ & + \int_{[0,1]^k} U_0 \left\{ g_i(y) \sum_{r=1}^k \frac{\partial}{\partial y_r} (a_{rj}(y) \pi(y)) + g_j(y) \sum_{r=1}^k \frac{\partial}{\partial y_r} (a_{ri}(y) \pi(y)) \right\} dy \end{aligned} \quad (1.7)$$

where :

$$\begin{cases} \bar{b}_i = \langle b_i, 1 \rangle & , \quad 1 \leq i \leq k \\ \bar{a}_{ij} = \langle a_{ij}, 1 \rangle & , \quad 1 \leq i, j \leq k \end{cases} \quad (1.8)$$

In (1.7) g_i is the unique solution in $\mathcal{D}_A \cap 1^\perp$ of the equation :

$$\hat{A} g_i = b_i - \bar{b}_i \quad (1.10)$$

and \hat{A} is the infinitesimal generator of the strongly continuous semigroup $\{\tilde{T}_t, t \geq 0\}$ on the domain \mathcal{D}_A .

In the particular case when $\text{div} b(x) = 0$ and the diffusion matrix is $a = \alpha I$, with α a strictly positive constant and I the $k \times k$ identity matrix, the dispersion coefficients are given by :

$$\bar{D}_{ij} = -U_0^2 \langle b_i, g_j \rangle - U_0^2 \langle b_j, g_i \rangle + \alpha \quad (1.11)$$

If, apart from the velocity parameter U_0 , we shall introduce a spatial scale parameter a , we shall be especially interested in the functional dependence of the asymptotic dispersion coefficients \bar{D}_{ij} on these two parameters.

As we shall see in §2, \bar{D}_{ij} depends only on the product aU_0 , the result being in accordance with all the experimental studies that have been done.

We shall give precise analytical conditions on the geometry of b_i 's which determine the asymptotic behavior of \bar{D}_{ij} 's for large aU_0 .

The results are shown to apply both for material and non-material macrotransport processes.

The objective in §3 is to show how central limit theorems such as described above can be used successfully in the study of solute macrodispersion in periodic media. Specific examples are given to illustrate the computation of the macrodispersion coefficients \bar{D}_{ij} as function of aU_0 .

The last section deals with the application of central limit theorems to thermal dispersion problems in periodic media.

The possibility of generalizing the macrotransport theory to such non-material processes has been demonstrated by introducing the notion of a generic conserved tracer entity, termed a "thermion" in the case of internal energy transport ([4],[9]).

By explicitly acknowledging the fictional or real existence of such a generic conserved tracer entity, we are able to extend the traditional methods underlying material macrotransport processes and, thereby, we get, by analogy, a macrotransport paradigm for thermal transport phenomena.

Dispersion coefficients are computed in two examples. The first one provides a closed-form solution of \bar{D}_{ij} , while in the second example the dispersion coefficients \bar{D}_{ij} are shown to exhibit their expected growth as functions of aU_0 .

2. The functional dependence of the asymptotic dispersion coefficients on the velocity and spatial scale parameters. The dependence of the asymptotic dispersion coefficients \bar{D}_{ij} on the velocity and scale parameters U_0 and a has been studied experimentally in laboratory columns and in many field situations for various models of heterogeneous porous media.

In 1989, R.N. Bhattacharya, V.K. Gupta and H.F. Walker ([3]) show that for the case of solute dispersion in periodic porous media, the macroscale dispersion matrix \bar{D} depends only on the product aU_0 . An extension to a more general class of diffusion processes is given in ([9]).

Let the large scale dispersion matrix \bar{D} be denoted by $\bar{D} = \bar{D}(a, U_0)$ to indicate its dependence on the spatial scale and velocity parameters. It is proved in ([9]) that if a central limit theorem holds for the solution $X(t)$ of Itô's stochastic equation :

$$\begin{cases} dX(t) = U_0 b(X(t)/a) dt + \sigma(X(t)/a) dB(t) \\ X(0) = X_0 \end{cases} \quad (2.1)$$

$$\begin{cases} dX(t) = U_0 b(X(t)/a) dt + \sigma(X(t)/a) dB(t) \\ X(0) = X_0 \end{cases} \quad (2.2)$$

then \bar{D} depends on a and U_0 only through their product aU_0 .

In particular :

$$\bar{D}(a, U_0) = \bar{D}(U_0, a) = \bar{D}(aU_0, 1) \quad (2.3)$$

This interchangeability of velocity and spatial scale parameters in the large-scale dispersion matrix enables us to consider that the spatial scale parameter a is held fixed at $a = 1$, while the velocity parameter U_0 is allowed to vary.

A more precisely analysis of the functional dependence of \bar{D}_{ij} on these two parameters can be done in the special case when a_{ij} 's are constants and b_i 's are continuously differentiable periodic functions satisfying the condition :

$$\text{div} b = 0 \quad (2.4)$$

Taking the period of b_i to be one in each coordinate, we can work on the state space $T = [0, 1]^k$ with the invariant distribution $\pi(x) \equiv 1$.

Let \mathcal{D} denote the following operator :

$$\mathcal{D} = \frac{1}{2} \sum_{i,j=1}^k a_{ij} \frac{\partial^2}{\partial x_i \partial x_j} \quad (2.5)$$

In this case, the macrodispersion coefficients are given by :

$$\bar{D}_{ij} = a_{ij} - U_0^2 \int_T g_i(x) (b_j(x) - \bar{b}_j) dx - U_0^2 \int_T g_j(x) (b_i(x) - \bar{b}_i) dx \quad (2.6)$$

We shall work with the following spaces of complex-valued functions on T ([3]):

$$H^0 = \left\{ h \left/ \int_T |h(x)|^2 dx < \infty, \int_T h(x) dx = 0 \right. \right. \\ \left. \left. \text{and } h \text{ satisfies periodic boundary conditions} \right\} \quad (2.7)$$

and :

$$E_{ij}(U_0) = U_0^2 \left\{ \| (\mathcal{D}^{-1} f_i)_N \|_1^2 + \sum_{n=1}^{\infty} \frac{|\beta_{in}|^2}{1 + U_0^2 \lambda_n^2} \right\} \quad (2.19)$$

Such expressions are given in ([3]) for the special case of solute dispersion in periodic porous media and in ([9]) for a more general class of diffusions generated by a differential operator of the form (1.1), whose coefficients satisfy the conditions :

(1) a_{ij} are constants and the matrix $((a_{ij}))$ is symmetric and positive definite.

(2) b_i are continuously differentiable periodic functions satisfying the condition $\text{div} \mathbf{b} = 0$.

It is obvious that $E_{ij}(U_0) = \mathcal{O}(U_0^2)$ if $\langle (\mathcal{D}^{-1} f_i)_N, (\mathcal{D}^{-1} f_j)_N \rangle_1 \neq 0$ and $E_{ij}(U_0) = o(U_0^2)$ otherwise.

We also note that \mathbf{N} is just the null space of $\mathbf{b} \cdot \nabla$ in \mathbf{H}^1 .

Proposition 2.1. If $f_i \in \mathbf{H}^1 \cap \mathbf{N}$, then either $f_i = 0$, in which case $E_{ij}(U_0) = 0$ for each j , or $E_{ii}(U_0) = \mathcal{O}(U_0^2)$.

Proof. Since $f_i \in \mathbf{H}^1 \cap \mathbf{N}$, it follows that :

$$\langle f_i, \mathcal{D}^{-1} f_i \rangle_1 = - \int_T f_i(\mathbf{x})^2 d\mathbf{x} \quad (2.20)$$

If $f_i = 0$, obviously $E_{ij}(U_0) = 0$, for each j .

If $f_i \neq 0$, then $(\mathcal{D}^{-1} f_i)_N \neq 0$ and finally, $E_{ii}(U_0) = \mathcal{O}(U_0^2)$.

The converse proposition is also true.

As an operator on \mathbf{H}^1 , $\mathbf{b} \cdot \nabla$ has the range \mathcal{R} in \mathbf{H}^0 :

$$\mathcal{R} = \{ f \in \mathbf{H}^0 / f = \mathbf{b} \cdot \nabla h, \text{ for some } h \in \mathbf{H}^1 \} \quad (2.21)$$

Theorem 2.2. If $f_i \in \mathcal{R}$, then :

$$\lim_{U_0 \rightarrow \infty} E_{ii}(U_0) = \| h_i \|_1^2 \quad (2.22)$$

where h_i is the unique element of $\mathbf{H}^1 \cap \mathbf{N}^\perp$ such that $f_i = \mathbf{b} \cdot \nabla h_i$.

Also, for $i \neq j$:

$$\begin{cases} E_{ij}(U_0) = \mathcal{O}(U_0) \simeq U_0 \langle h_i, \mathcal{D}^{-1} f_j \rangle_1 \end{cases} \quad (2.23)$$

$$\begin{cases} E_{ji}(U_0) = \mathcal{O}(U_0) \simeq -U_0 \langle \mathcal{D}^{-1} f_j, h_i \rangle_1 \end{cases} \quad (2.24)$$

for large U_0 .

In particular, if the inner products in (2.23) and (2.24) are zero, then $E_{ij}(U_0)$ and $E_{ji}(U_0)$ are $o(U_0)$.

Proof. Since $f_i \in \mathcal{R}$, it follows that :

$$h_i = \sum_{n=1}^{\infty} \gamma_{in} \Phi_n \quad (2.25)$$

and :

$$\mathcal{D}^{-1} f_i = H h_i = \sum_{n=1}^{\infty} i \lambda_n \gamma_{in} \Phi_n \quad (2.26)$$

Then :

$$\lim_{U_0 \rightarrow \infty} E_{ii}(U_0) = \lim_{U_0 \rightarrow \infty} U_0^2 \sum_{n=1}^{\infty} \frac{\lambda_n^2 |\gamma_{in}|^2}{1 + U_0^2 \lambda_n^2} = \sum_{n=1}^{\infty} |\gamma_{in}|^2 = \| h_i \|_1^2 \quad (2.27)$$

For $j \neq i$, we get :

$$E_{ij}(U_0) = U_0 \sum_{n=1}^{\infty} \frac{i U_0 \lambda_n \gamma_{in} \bar{\gamma}_{jn}}{1 + i U_0 \lambda_n} = \mathcal{O}(U_0) \simeq U_0 \sum_{n=1}^{\infty} \gamma_{in} \bar{\gamma}_{jn} = U_0 \langle h_i, \mathcal{D}^{-1} f_j \rangle_1 \quad (2.28)$$

and :

$$E_{ij}(U_0) = U_0^2 \left\{ \| (\mathcal{D}^{-1} f_i)_N \|_1^2 + \sum_{n=1}^{\infty} \frac{|\beta_{in}|^2}{1 + U_0^2 \lambda_n^2} \right\} \quad (2.19)$$

Such expressions are given in ([3]) for the special case of solute dispersion in periodic porous media and in ([9]) for a more general class of diffusions generated by a differential operator of the form (1.1), whose coefficients satisfy the conditions :

- (1) a_{ij} are constants and the matrix $((a_{ij}))$ is symmetric and positive definite.
 - (2) b_i are continuously differentiable periodic functions satisfying the condition $\text{div} \mathbf{b} = 0$.
- It is obvious that $E_{ij}(U_0) = \mathcal{O}(U_0^2)$ if $\langle (\mathcal{D}^{-1} f_i)_N, (\mathcal{D}^{-1} f_j)_N \rangle_1 \neq 0$ and $E_{ij}(U_0) = o(U_0^2)$ otherwise.

We also note that N is just the null space of $\mathbf{b} \cdot \nabla$ in H^1 .

Proposition 2.1. If $f_i \in H^1 \cap N$, then either $f_i = 0$, in which case $E_{ij}(U_0) = 0$ for each j , or $E_{ii}(U_0) = \mathcal{O}(U_0^2)$.

Proof. Since $f_i \in H^1 \cap N$, it follows that :

$$\langle f_i, \mathcal{D}^{-1} f_i \rangle_1 = - \int_T f_i(\mathbf{x})^2 d\mathbf{x} \quad (2.20)$$

If $f_i = 0$, obviously $E_{ij}(U_0) = 0$, for each j .

If $f_i \neq 0$, then $(\mathcal{D}^{-1} f_i)_N \neq 0$ and finally, $E_{ii}(U_0) = \mathcal{O}(U_0^2)$.

The converse proposition is also true.

As an operator on H^1 , $\mathbf{b} \cdot \nabla$ has the range \mathcal{R} in H^0 :

$$\mathcal{R} = \{f \in H^0 / f = \mathbf{b} \cdot \nabla h, \text{ for some } h \in H^1\} \quad (2.21)$$

Theorem 2.2. If $f_i \in \mathcal{R}$, then :

$$\lim_{U_0 \rightarrow \infty} E_{ii}(U_0) = \|h_i\|_1^2 \quad (2.22)$$

where h_i is the unique element of $H^1 \cap N^\perp$ such that $f_i = \mathbf{b} \cdot \nabla h_i$.

Also, for $i \neq j$:

$$\begin{cases} E_{ij}(U_0) = \mathcal{O}(U_0) \simeq U_0 \langle h_i, \mathcal{D}^{-1} f_j \rangle_1 \\ E_{ji}(U_0) = \mathcal{O}(U_0) \simeq -U_0 \langle \mathcal{D}^{-1} f_j, h_i \rangle_1 \end{cases} \quad (2.23)$$

$$(2.24)$$

for large U_0 .

In particular, if the inner products in (2.23) and (2.24) are zero, then $E_{ij}(U_0)$ and $E_{ji}(U_0)$ are $o(U_0)$.

Proof. Since $f_i \in \mathcal{R}$, it follows that :

$$h_i = \sum_{n=1}^{\infty} \gamma_{in} \Phi_n \quad (2.25)$$

and :

$$\mathcal{D}^{-1} f_i = H h_i = \sum_{n=1}^{\infty} i \lambda_n \gamma_{in} \Phi_n \quad (2.26)$$

Then :

$$\lim_{U_0 \rightarrow \infty} E_{ii}(U_0) = \lim_{U_0 \rightarrow \infty} U_0^2 \sum_{n=1}^{\infty} \frac{\lambda_n^2 |\gamma_{in}|^2}{1 + U_0^2 \lambda_n^2} = \sum_{n=1}^{\infty} |\gamma_{in}|^2 = \|h_i\|_1^2 \quad (2.27)$$

For $j \neq i$, we get :

$$E_{ij}(U_0) = U_0 \sum_{n=1}^{\infty} \frac{i U_0 \lambda_n \gamma_{in} \bar{\gamma}_{jn}}{1 + i U_0 \lambda_n} = \mathcal{O}(U_0) \simeq U_0 \sum_{n=1}^{\infty} \gamma_{in} \bar{\gamma}_{jn} = U_0 \langle h_i, \mathcal{D}^{-1} f_j \rangle_1 \quad (2.28)$$

and:

$$E_{ji}(U_0) = -U_0 \sum_{n=1}^{\infty} \frac{iU_0 \lambda_n \beta_{jn} \bar{\gamma}_{in}}{1 + iU_0 \lambda_n} = \mathcal{O}(U_0) \simeq -U_0 \sum_{n=1}^{\infty} \beta_{jn} \bar{\gamma}_{in} = -U_0 \langle \mathcal{D}^{-1} f_j, h_i \rangle_1 \quad (2.29)$$

for large U_0 ([9]).

These results are extensions of those given in ([3]) for the case of solute dispersion in periodic media.

A more precisely analysis of the asymptotic behavior of the dispersion coefficients \bar{D}_{ij} as functions of aU_0 can be done if we make more restrictive assumptions about b ([3],[9]).

3. Asymptotics of solute dispersion in periodic media Let us consider a non-reactive dilute solute injected into a porous medium saturated with a viscous incompressible fluid under laminar flow conditions.

Assume that the evolution of the solute concentration $C(t, \mathbf{x})$ is governed by the following parabolic differential equation :

$$\frac{\partial C}{\partial t} = \sum_{i,j=1}^3 D_{ij} \frac{\partial^2 C}{\partial x_i \partial x_j} - \sum_{i=1}^3 U_0 b_i \left(\frac{\mathbf{x}}{a} \right) \frac{\partial C}{\partial x_i} \quad (3.1)$$

subject to some initial condition:

$$C(0, \mathbf{x}) = C_0(\mathbf{x}) \quad (3.2)$$

In (3.1), $((D_{ij}))$ is a positive definite symmetric matrix, U_0 and a are strictly positive parameters and b_i are continuously differentiable periodic functions satisfying the condition $\text{div } \mathbf{b} = 0$.

As we said before, we can take the period of b_i to be one in each coordinate. So, the scale parameter a is held fixed at $a = 1$, while the velocity parameter U_0 is allowed to vary.

Analyzing the asymptotic behavior of $C(t, \mathbf{x})$ for large t is equivalent to analyzing the asymptotic behavior of the Markov process $\mathbf{X}(t)$ defined by the associate Itô's stochastic equation, for large t .

So, using a central limit theorem we get another partial differential equation with constant coefficients which governs the solute concentration for large t . This equation is called *the Fickian approximation* or *the macrotransport equation* and can be expressed as :

$$\frac{\partial \bar{C}}{\partial t} = \sum_{i,j=1}^3 \bar{D}_{ij} \frac{\partial^2 \bar{C}}{\partial x_i \partial x_j} - \sum_{i=1}^3 U_0 \bar{b}_i \frac{\partial \bar{C}}{\partial x_i} \quad (3.3)$$

Here, $\bar{\mathbf{U}} = U_0 \bar{\mathbf{b}}$ is the large-scale velocity and \bar{D}_{ij} are the large-scale dispersion coefficients, given by the above central limit theorem in terms of the coefficients D_{ij} and $U_0 b_i$ (see eq. (2.6)).

A similar result can be done in the case when the coefficients D_{ij} are periodic functions satisfying the assumptions (1)-(4). In this case, the macrodispersion coefficients \bar{D}_{ij} are given by (1.7).

We can also include in this analysis the case when we have an external force contribution \mathbf{F} by introducing the effective velocity :

$$\bar{\mathbf{U}} = \mathbf{U} + \mathbf{M} \cdot \mathbf{F} \quad (3.4)$$

The hydrodynamic mobility dyadic \mathbf{M} is given by the Nernst-Einstein-Planck relation :

$$\mathbf{M} = \frac{\mathbf{D}}{k_B T_0} \quad (3.5)$$

with k_B the Boltzmann constant and T_0 the absolute temperature.

More, the external force \mathbf{F} is assumed to be chosen such that to assure the spatial periodicity of $\bar{\mathbf{U}}$ ([9]).

As a concrete example, let us consider the case of the pure molecular diffusion of a non-reactive solute in a spatially periodic porous medium.

We shall take the molecular diffusivity dyadic \mathbf{D} to be isotropic, $\mathbf{D} = D(z)\mathbf{I}$, with $D(z)$ an integrable nonnegative definite function which is periodic with the period l_z .

Using the formulas given by the previous macrotransport paradigm we get :

$$\left\{ \begin{array}{l} \overline{D}_{11} = \overline{D}_{22} = \frac{1}{l_z} \int_0^{l_z} D(u) du \end{array} \right. \quad (3.6)$$

$$\left\{ \begin{array}{l} \overline{D}_{33} = \frac{l_z}{\int_0^{l_z} \frac{du}{D(u)}} \end{array} \right. \quad (3.7)$$

$$\left\{ \begin{array}{l} \overline{D}_{ij} = 0, \quad \text{for any } i \neq j, \quad i, j = \overline{1, 3} \end{array} \right. \quad (3.8)$$

As a second example, we shall consider the problem of the dispersion of a spherical particle of radius a , settling under the influence of gravity in an unbounded fluid, the latter undergoing a spatially periodic circulatory convective motion.

In the absence of the particle, the undisturbed incompressible spatially periodic fluid velocity vector field $u(r)$ satisfy the condition :

$$\int_{\tau_0} u(r) dr = 0 \quad (3.9)$$

over the volume τ_0 of a periodicity unit cell, r being the local position vector of a point within this cell relative to its centroid.

More, u is supposed to satisfy the quasistatic Stokes equation.

We shall take the molecular diffusivity dyadic of the form $D = DI$, with $D = \frac{k_B T_0}{6\pi\mu a}$.

For the low-Reynolds number flow, the instantaneous sedimentation velocity $U(r)$ of the sphere whose center is instantaneously situated at the position r may be determined via Faxén's law as:

$$U = U_\infty + \frac{F}{6\pi\mu a} \quad (3.10)$$

with:

$$U_\infty(r) = \left(1 + \frac{a^2}{6} \nabla^2\right) u(r) \quad (3.11)$$

and :

$$F = (\rho_p - \rho_f) V g \quad (3.12)$$

the net gravitational force on the sphere of density ρ_p and volume $V = 4\pi a^3/3$, in a fluid of density ρ_f .

It can be proved that U is periodic and satisfy the conditions :

$$\left\{ \begin{array}{l} \nabla \cdot U = 0 \end{array} \right. \quad (3.13)$$

$$\left\{ \begin{array}{l} \frac{1}{\tau_0} \int_{\tau_0} U(r) dr = \frac{F}{6\pi\mu a} \end{array} \right. \quad (3.14)$$

where τ_0 is the volume of the unit cell.

Using the general theory previously given, we get :

$$\overline{U} = \frac{F}{6\pi\mu a} \quad (3.15)$$

So, the sphere will, on average, sediment through the fluid at a settling velocity appropriate to a quiescent fluid, despite the presence of a local convection and a molecular diffusion. Thus, circulatory vortices in a macroscopically quiescent fluid cannot influence the mean settling velocity of the sphere.

For low Peclet numbers, using again a central limit theorem and an expansion in Bloch functions, we get ([9]) :

$$\frac{\bar{D}}{D} = 1 + \frac{1}{4\pi^2 D^2} \sum_{\mathbf{n}} \frac{\mathbf{U}_{\mathbf{n}} \mathbf{U}_{\mathbf{n}}}{K_{\mathbf{n}}^2} + \mathcal{O}(D^{-3}) \quad (3.16)$$

where the symbol \sum indicates the sum over all the integer vectors $\mathbf{n} \neq 0$.

The vectors $\mathbf{K}_{\mathbf{n}}$ are given by :

$$\mathbf{K}_{\mathbf{n}} = (n_1 s_1 + n_2 s_2 + n_3 s_3) \tau_0^{-1} \quad (3.17)$$

with s_j ($j = 1, 2, 3$) the reciprocal lattice vectors defined such that :

$$s_j \cdot l_k = \delta_{jk} \tau_0 \quad (3.18)$$

In (3.16) $\mathbf{U}_{\mathbf{n}}$ are the Bloch coefficients of the spatially periodic velocity field \mathbf{U}_{∞} , determined from the known function \mathbf{U}_{∞} via the quadrature :

$$\mathbf{U}_{\mathbf{n}} = \frac{1}{\tau_0} \int_{\tau_0} \mathbf{U}_{\infty}(\mathbf{r}) \exp(2\pi i \mathbf{K}_{\mathbf{n}} \cdot \mathbf{r}) d\mathbf{r} \quad (3.19)$$

To the order indicated, this agrees with the result obtained in ([5]) using the method of moments.

4. Thermal dispersion in periodic media. We shall extend now the macrotransport theory based on a central limit theorem to internal energy transport processes.

The possibility of such a generalization to non-material processes rests upon the analogous nature of the microscale phenomenological description underlying their transport.

It proves useful to contemplate the concept of a "tracer" for all forms of continuous transport, material or otherwise and, thereby, to establish a Lagrangian view both for material and non-material processes.

The viability of pursuing such a novel Lagrangian perspective in thermal dispersion problems has been demonstrated by introducing the notion of a generic conserved tracer entity, termed a "thermion" in the case of internal energy transport ([4]).

By explicitly acknowledging the existence of such a tracer, we are able to extend the previous results to internal energy transport processes and to establish a macrotransport paradigm for thermal transport phenomena.

In this case, the microtransport equation governing the evolution of the temperature $T(t, \mathbf{x})$ may be represented as:

$$\rho c_p \frac{\partial T}{\partial t} + \nabla \cdot \mathbf{J} = 0 \quad (4.1)$$

with:

$$\mathbf{J} = \rho c_p \mathbf{U} T - \mathbf{K}_T \cdot \nabla T \quad (4.2)$$

subject to appropriate initial and boundary conditions.

Introducing the Green's function $p(t; \mathbf{x}, \mathbf{y})$ by which the actual temperature field may be obtained:

$$T(t, \mathbf{x}) = \int_T (\rho c_p)(\mathbf{y}) p(t; \mathbf{y}, \mathbf{x}) T(0, \mathbf{y}) d\mathbf{y} \quad (4.3)$$

and considering the associate Itô's stochastic differential equation, we see that $\rho c_p p$ may be interpreted as the conditional probability density of the thermal tracer.

This connection between the temperature T and the probability density $\rho c_p p$ allows us to use the previous central limit theorem to get the desired Fickian approximation of the equation (4.1), the macrotransport coefficients $\overline{\rho c_p}$, $\overline{\mathbf{U}}$ and $\overline{\mathbf{K}_T}$ being expressed in terms of appropriate quadratures of the microscale data ([9]).

As a first particular example, we shall consider the problem of pure conduction in a layered medium ([9]).

The medium is assumed to possess thermophysical properties which vary only in the z direction, i.e.:

$$\begin{cases} \rho = \rho(z) \end{cases} \quad (4.4)$$

$$\begin{cases} c_p = c_p(z) \end{cases} \quad (4.5)$$

$$\begin{cases} K_T = K_T(z)I \end{cases} \quad (4.6)$$

and the phenomenological coefficients ρ , c_p and K_T are supposed to be integrable nonnegative definite periodic functions, having the period l_z .

With $\alpha = \frac{K_T}{\rho c_p}$, the evolution of the temperature $T(t, \mathbf{x})$ will be governed by the following equation:

$$\frac{\partial T}{\partial t} = \alpha \left(\frac{\partial^2 T}{\partial x^2} + \frac{\partial^2 T}{\partial y^2} + \frac{\partial^2 T}{\partial z^2} \right) + \frac{1}{\rho c_p} \frac{dK_T}{dz} \frac{\partial T}{\partial z} \quad (4.7)$$

subject to the initial condition $T(0, \mathbf{x}) = T_0(\mathbf{x})$.

Using the general formulas given by the above central limit theorem we are led to the following expressions for the effective volumetric specific heat $\overline{\rho c_p}$ and the effective thermal diffusivity dyadic $\overline{\alpha}$:

$$\overline{\rho c_p} = \frac{1}{l_z} \int_0^{l_z} \rho(u) c_p(u) du \quad (4.8)$$

and:

$$\begin{cases} \overline{\alpha}_{11} = \overline{\alpha}_{22} = \frac{1}{\int_0^{l_z} \rho(u) c_p(u) du} \cdot \int_0^{l_z} K_T(u) du \end{cases} \quad (4.9)$$

$$\begin{cases} \overline{\alpha}_{33} = \frac{1}{\int_0^{l_z} \rho(u) c_p(u) du} \cdot \frac{1}{\int_0^{l_z} \frac{1}{K_T(u)} du} \end{cases} \quad (4.10)$$

$$\begin{cases} \overline{\alpha}_{ij} = 0, \text{ for any } i \neq j, \quad i, j = 1, 3 \end{cases} \quad (4.11)$$

As a second example we shall consider the problem of internal energy dispersion in a two-dimensional periodic porous medium saturated with an incompressible viscous fluid having the velocity field $\mathbf{U}(\mathbf{x}) = U_0 \mathbf{b}(\mathbf{x})$ given by ([9]):

$$\begin{cases} b_1(x, y) = 2 - \cos(2\pi(\sin(2\pi x) - y)) \end{cases} \quad (4.12)$$

$$\begin{cases} b_2(x, y) = 2\pi \cos(2\pi x) \cdot b_1(x, y) \end{cases} \quad (4.13)$$

We assume that the spatial scale parameter a is held fixed at $a = 1$ and the phenomenological coefficients ρ , c_p and K_T are strictly positive constants.

Obviously, $\bar{b}_1 = 2$ and $\bar{b}_2 = 0$.

For this example, closed-form solutions of the macrotransport coefficients $\overline{\alpha}_{ij}$ cannot be obtained.

However, the analytical theory developed in §2 shows that, as $U_0 \rightarrow \infty$, $\overline{\alpha}_{11} = \alpha + \mathcal{O}(U_0^2)$, $\overline{\alpha}_{22} = \alpha + \mathcal{O}(1)$ and $\overline{\alpha}_{12} = \overline{\alpha}_{21} = \mathcal{O}(U_0)$.

This example reflects the influence of the geometry of the flow curves on the asymptotic behavior of the macrotransport coefficients.

REFERENCES

- [1] Bensoussan, A., Lions, J.L., Papanicolaou, G., *Asymptotic Analysis for Periodic Structures*, Amsterdam, North-Holland, 1978.
- [2] Bhattacharya, R.N., *A central limit theorem for diffusions with periodic coefficients*, Ann.Prob.13 (1985), 385-396.
- [3] Bhattacharya, R.N., Gupta, V.K., Walker, H., *Asymptotics of solute dispersion in periodic porous media*, SIAM J.Appl.Math.49 (1989), 86-98.
- [4] Brenner, H., Edwards, D.A., *Macrotransport Processes*, Butterworth-Heinemann, Boston, 1993.
- [5] Dungan, R.S., Brenner, H., *Sedimentation and dispersion of non-neutrally buoyant Brownian particles in cellular circulatory flows simulating local fluid agitation*, Phys.Rev. A38 (1988), 3601-3608.
- [6] Ene, H.I., Paşa, G.I., *Homogenization Method. Applications to the Theory of Composite Materials*, Ed. Acad. R.S.R., Bucharest, 1987.
- [7] Taylor, G.I., *Dispersion of soluble matter in a solvent flowing slowly through a tube*, Proc.Roy.Soc.SerA219 (1953), 186-203.
- [8] Timofte, C., *On the dispersion of a solute in some unbounded media*, Ann.Univ.Bucharest, Physica, XLIII (1994), 3-8.
- [9] Timofte, C., *Ph.D. Thesis*, Institute of Mathematics of the Romanian Academy, Bucharest, 1996 (in Romanian).
- [10] Timofte, C., *Heat transport in a random cylindrical tube*, Ann.Univ.Bucharest (1996) (to appear).

NONLINEAR APPROACH TO THE BEHAVIOUR OF THIN WALLED TURBINE BLADE SHAPED ELEMENTS

DOBROSLAV RUŽIĆ *, NINA ANDJELIĆ **

Faculty of Mechanical Engineering, University of Belgrade
27 marta 80, 11000 Belgrade, Serbia, Yugoslavia

* Professor, ** Assistant

ABSTRACT

Using the expressions for the works of external and internal forces and after the integration over the cross section six equilibrium equations and a seventh one relating the constrained torsion are derived for a thin walled beam with an arbitrary cross section taking into account the general sectorial coordinates. After the introduction of virtual displacements, the expressions for longitudinal displacements and corresponding strains are obtained. The attempt is made to investigate the influence of the second order terms and the dependence of these effects on the shape of the cross section. The obtained relations are applied to the cross section looking like a modified turbine blade section and it is shown that it is not recommended to neglect the influence of the secondary effects. Additional terms if taken into account have nonnegligible effects on the level of stress components especially in some particular cases of cross sectional shapes like those considered in the chosen example.

1. INTRODUCTION

Classical approach [1] to the theory of thin walled open section beams is extended in [2] by including the secondary sectorial coordinates. That procedure is still linear and it is extended in [3] to the second order theory for a thin-walled member with an open cross section having an arbitrary polygonal middle line. The similar approach is applied in [4] to the cross section with an arbitrary curvilinear middle line and with linearly varying thickness.

Here the attempt is made to investigate the influence of the second order terms and the dependence of these effects on the shape of the cross section with more complex variation of the thickness.

2. BASIC ASSUMPTIONS

According to the classical linear theory of thin-walled open section beams [1] normal stresses in cross sections are constant across the wall thickness and are proportional to the sectorial coordinate. More complex stress distribution [2] is obtained if the secondary sectorial coordinate is introduced assuming its linear distribution across the wall thickness.

Initial assumptions of the theory of thin walled beams are supposed to be valid:

{1} Cross sections do not change their shapes, or in another way, their projections to their initial planes behave like rigid plates. {2} Shear in the middle surface can be neglected. {3} Elements initially orthogonal to the middle surface stay orthogonal and straight during the deformation of the middle surface.

3. DISPLACEMENTS AND DEFORMATIONS

3.1 Displacements during the deformation

If i_i (index $i = 1, 2, 3$) are unit vectors of two centroidal principal axes of the cross section and of the longitudinal axis of the beam respectively, x_i are material coordinates of an arbitrary point which is not in the middle surface, u^* is the displacement vector, than position vectors r^* , before the deformation, and R^* , after the deformation, are defined by

$$r^* = x_i^* \cdot i_i, \quad (\text{index } i = 1, 2, 3) \quad (3.1)$$

$$R^* = r^* + u^* \quad (3.2)$$

If ξ_{iP} ($i = 1, 2$) are displacement components of an arbitrary pole P in directions of the axes x_i ($i = 1, 2$) in the plane of the cross section, φ_P is the rotation of the cross section around the pole P, and ω_P^* is the generalized sectorial coordinate [2], the position of the same arbitrary point after the deformation (3.2) can be written as

$$R^* = (x_i^* + u_i^*) i_i, \quad (3.3)$$

$$u_i^* = \xi_{iP} - / + (x_j^* - x_{jP}) \varphi_P, \quad (i = 1, 2; j \neq i). \quad (3.4)$$

$$u_3^* = - \xi_{1P} x_1^* - \varphi_P \omega_P^* + w_0, \quad w_0 = w_0(x_3). \quad (3.5)$$

3.2. Virtual displacements and deformations

When virtual displacements

$$\bar{u}^* = \bar{u}_i^* i_i \quad (3.6)$$

are applied to the points of the deformed beam the quantity R^* (3.3) becomes

$$R^* = (x_i^* + u_i^* + \bar{u}_i^*) i_i, \quad (3.7)$$

$$u_i^* = \xi_{iP} - / + (x_j^* - x_{jP}) \varphi_P. \quad (3.8)$$

Shear ϵ_{23} in the middle surface and ϵ_{23} in the longitudinal plane orthogonal to the middle surface introduced into the assumption {2} give

$$\epsilon_{23} = \bar{R}_{,2} \bar{R}_{,3} = \bar{u}_{1,2} (x_1 + u_1)_{,3} + \bar{u}_{1,3} (x_1 + u_1)_{,2} = 0 \quad (3.9)$$

or, if developed,

$$- \bar{u}_{3,2} (1 + u_{3,3}) = \bar{\varphi}_P' [x_1 x_{2,2} - x_2 x_{1,2} + x_{2P} x_{1,2} - x_{1P} x_{2,2} + u_1 x_{2,2} + x_1 u_{2,2} + u_1 u_{2,2} + x_{2P} u_{1,2} - u_2 x_{1,2} - x_2 u_{1,2} + u_2 u_{1,2} - x_{1P} u_{2,2}] + \bar{\varphi}_P [x_{2P,2} x_{1,3} + x_{2P,2} u_{1,3} + x_{2P,3} x_{1,2} + x_{2P,3} u_{1,2} - x_{1P,2} x_{2,3} - x_{1P,2} u_{2,3} - x_{1P,3} x_{2,2} - x_{1P,3} u_{2,2}] + \bar{\xi}_{1P}' (x_1 + u_1)_{,2} + \bar{\xi}_{2P}' (x_2 + u_2)_{,2}, \quad (3.10)$$

and into the assumption {3}

$$\bar{\epsilon}_{23} = \bar{R}_{,2} \bar{R}_{,3} = \bar{u}_{1,2} (x_1^* + u_1^*)_{,3} + \bar{u}_{1,3} (x_1^* + u_1^*)_{,2} = 0 \quad (3.11)$$

or

$$\begin{aligned}
- \bar{u}_{3,e}^* (1 + u_{3,3}^*) = & \bar{\varphi}_P^* [x_1^* x_{2,e}^* - x_2^* x_{1,e}^* + x_{2P} x_{1,e}^* - x_{1P} x_{2,e}^* + \frac{u_1^* x_{2,e}^* + x_1^* u_{2,e}^*}{2} + \\
& u_{2,e}^* + u_1^* u_{2,e}^* + x_{2P} u_{1,e}^* - u_2^* x_{1,e}^* - x_2^* u_{1,e}^* u_2^* u_{1,e}^* - x_{1P} u_{2,e}^*] + \bar{\varphi}_P [x_{2P,e} x_{1,3}^* + \\
& x_{2P,e} u_{1,3}^* + x_{2P,3} x_{1,e}^* + x_{2P,3} u_{1,e}^* - x_{1P,e} x_{2,3}^* - x_{1P,e} u_{2,3}^* - x_{1P,3} x_{2,e}^* - x_{1P,3} u_{2,e}^*] + \bar{\xi}_{1P}^* \\
& (x_1^* + u_1^*)_{,e} + \bar{\xi}_{2P}^* (x_2^* + u_2^*)_{,e}.
\end{aligned} \quad (3.12)$$

$$(\dots)' = d/dx_3; (\dots)_{,i} = \partial/\partial x_i; (i = 1, 2, 3); (\dots)_{,e} = \partial/\partial e; (\dots)_{,s} = \partial/\partial s$$

4. EQUILIBRIUM CONDITIONS

If A is the cross sectional area, σ_{3i} ($i = 1, 2, 3$) stress components in the cross section, and p load acting over the middle surface, virtual work \bar{W} of external forces and \bar{U} of internal forces for the given virtual displacements u^* are

$$\bar{W} = \int_A (\sigma_{3,3} \bar{u}^* + \sigma_3 \bar{u}_{3,3}) dA + \int_s \bar{p} \bar{u} ds \quad (4.1)$$

$$\bar{U} = - \int_A (\sigma_{33} \bar{\varepsilon}_{33}^* + \sigma_{33} \bar{\varepsilon}_{3,3}^*) dA. \quad (4.2)$$

After the introduction of real and virtual displacements and deformations into $\bar{W} + \bar{U} = 0$ (4.3)

an equation of the following form will be obtained

$$H_1 w_0 + H_2 \xi_P + H_3 \eta_P + H_4 \varphi_P + H_5 \xi_P' + H_6 \eta_P + H_7 \varphi_P' = 0 \quad (4.4)$$

The functions H_i ($i = 1, 2, \dots, 7$) defined by long expressions after some neglects become

$$H_1 = \int_A \{ \sigma_{33}' - [\sigma_{31} \xi_{1P}' + \sigma_{23} \xi_{2P}' - (\sigma_{31} x_2 - x_{2P}) - \sigma_{23} (x_1 - x_{1P})] \varphi_P' \} dA + \int_s p_3 ds, \quad (4.5)$$

$$H_2 = \int_A \{ \sigma_{31}' - [\sigma_{23} \varphi_P - (\xi_P' - \varphi_P' (x_2^* - x_{2P})) \sigma_{33}] \} dA + \int_s p_1 ds, \quad (4.6)$$

$$H_3 = \int_A \{ \sigma_{23}' - [\sigma_{31} \varphi_P - (\xi_{2P}' + \varphi_P' (x_1 - x_{1P})) \sigma_{33}] \} dA + \int_s p_2 ds, \quad (4.7)$$

$$\begin{aligned}
H_4 = & \int_A \{ \sigma_{23} (x_1 - x_{1P}) - \sigma_{31} (x_2 - x_{2P}) + [\xi_{1P} \sigma_{23} - \xi_{2P} \sigma_{31} - \sigma_{33} (\xi_{1P}' (x_2 - x_{2P}) - \\
& - \xi_{2P}' (x_1 - x_{1P})) + \varphi_P' \sigma_{33} ((x_1 - x_{1P})^2 + (x_2 - x_{2P})^2)] \} dA + \int_s [p_2 (x_1 - x_{1P}) - \\
& - p_1 (x_2 - x_{2P}) + \xi_{1P} p_2 - \xi_{2P} p_1 - \varphi_P (p_1 (x_1 - x_{1P}) + (x_2 - x_{2P}))] ds,
\end{aligned} \quad (4.8)$$

$$\begin{aligned}
H_5 = & \int_A \{ \sigma_{33}' x_1^* - \sigma_{31} - \varphi_P [\sigma_{33}' (x_2^* - x_{2P}) - \sigma_{23}] + \sigma_{33}' (\xi_{1P} + x_{2P} \varphi_P) + \\
& + g x_1^* \} dA + \int_s p_3 [x_1 - \varphi_P (x_2 - x_{2P}) + \xi_{1P}] ds,
\end{aligned} \quad (4.9)$$

$$\begin{aligned}
H_6 = & \int_A \{ \sigma_{33}' x_2^* - \sigma_{23} + \varphi_P (\sigma_{33}' x_1^* - \sigma_{31}) + \sigma_{33}' (\xi_{2P} - x_{1P} \varphi_P) + g' x_2^* \} dA + \\
& + \int_s p_3 [x_2 + \varphi_P (x_2 + \varphi_P (x_1 - x_{1P}) + \xi_{2P})] ds,
\end{aligned} \quad (4.10)$$

$$\begin{aligned}
H_7 = & \int_A \{ \sigma_{33} \omega_P^* - \sigma_{31} (x_2^* - x_{2P}) - \sigma_{23} (x_1 - x_{1P}) + 2 \sigma_{33} \varphi_P' e + \\
& + \xi_{1P} (\sigma_{33}' x_2^* - \sigma_{23}) - \xi_{2P} (\sigma_{33}' x_1^* - \sigma_{31}) - \sigma_{33}' (\xi_{1P} x_{2P} - \xi_{2P} x_{1P}) + g' \omega_P^* \} dA + \\
& + \int_s p_3 [\omega_P + \xi_{1P} (x_2 - x_{2P}) - \xi_{2P} (x_1 - x_{1P})] ds,
\end{aligned} \quad (4.11)$$

$$\text{with } g = \sigma_{31} [\xi_{1P}' - \varphi_P (x_2^* - x_{2P})] + \sigma_{23} [\xi_{2P}' + \varphi_P' (x_1 - x_{1P})]. \quad (4.12)$$

From (4.4) and (4.5) - (4.11) the following equations are obtained:

$$F_3' - (F_1 \xi_{1P}' + F_2 \xi_{2P}' + M_3 \varphi_P')' + p_3 = 0, \quad (4.13)$$

$$F_1' + [F_3 (\xi_{1P}' + x_{2P} \varphi_P') - M_2 \varphi_P' - F_2 \varphi_P']' + p_1 = 0, \quad (4.14)$$

$$F_2' + [F_3 (\xi_{2P}' - x_{1P} \varphi_P') + M_1 \varphi_P' + F_1 \varphi_P']' + p_2 = 0, \quad (4.15)$$

$$\begin{aligned}
M_3' + [F_2 \xi_{1P} - F_1 \xi_{2P} - \xi_{1P}' (M_2 - F_3 x_{2P}) + \xi_{2P}' (M_1 - F_3 x_{1P}) + \varphi_P' (F_3 x_1^2 + \\
+ 2 M_1 \beta_1 + 2 M_2 \beta_2 + B \beta \omega)]' + m_3 + p_2 \xi_{1P} - p_1 \xi_{2P} - \varphi_P m_3 = 0,
\end{aligned} \quad (4.16)$$

$$M_1' - F_1 + m_1 - \varphi_P (M_2' - F_2 + m_2) + (F_3' + p_3) (\xi_{1P} - x_{2P} \varphi_P) + D_1 = 0, \quad (4.17)$$

$$M_2' - F_2 + m_2 + \varphi_P (M_1' - F_1 + m_1) + (F_3' + p_3) (\xi_{2P} - x_{1P} \varphi_P) + D_2 = 0, \quad (4.18)$$

$$\begin{aligned}
B' - M \omega + b \omega + \xi_{1P} (M_2' - F_2 + m_2) - \xi_{2P} (M_1' - F_1 + m_1) - \\
- (F_3' + p_3) (\xi_{1P} x_{2P} - \xi_{2P} x_{1P}) + D_3 = 0,
\end{aligned} \quad (4.19)$$

F_i ($i = 1, 2, 3$) are two transversal and one axial force, M_i ($i = 1, 2, 3$) two bending and one torsional moment, B the bimoment, m_i ($i = 1, 2, 3$) distributed bending and torsional moments around the axes x_i , M_ω warping moment, m_ω distributed warping moment, expressions D_i , $i p^2$, β_i and β_ω are defined by

$$D_i = \int_A g' x_i dA, \quad (i = 1, 2); \quad D_3 = \int_A g' \omega_P^2 dA, \quad (4.20)$$

$$\begin{aligned} \beta_1 &= (\int_A x_1^2 (x_1^2 + x_2^2) dA) / 2 J_2 - x_{1P}, \\ \beta_2 &= \int_A x_2^2 (x_1^2 + x_2^2) dA / 2 J_1 - x_{2P}, \\ \beta_\omega &= \int_A \omega_P^2 (x_1^2 + x_2^2) dA / J_\omega, \quad J_\omega = \int_A \omega_P^2 dA. \end{aligned} \quad (4.21)$$

J_i are principal moments of inertia and J_ω sectorial moment of inertia [2] for the secondary coordinates x_i ($i = 1, 2$) and ω_P .

Six differential equations (4.13) - (4.18) are equilibrium conditions and the seventh one (4.19) is the particular equation for the constrained torsion of the thinwalled beam.

Linearizing some expressions, neglecting the influence of bending and warping shear stresses on the deformation, using relations [1], [2], [6] between M_i ($i = 1, 2$), B , ξ_{iP} ($i = 1, 2$), φ_P' and φ_P'' , and taking the shear center for the pole P the equations (4.13) - (4.19) reduce to

$$E J_2 \xi_1^{IV} - [N (\xi_{1P}' + x_{2P} \varphi')] + (\varphi M_2)'' + (\varphi m_2)' = p_1 + m_1', \quad (4.22)$$

$$E J_1 \xi_2^{IV} - [N (\xi_{2P}' - x_{1P} \varphi')] + (\varphi M_1)'' + (\varphi m_1)' = p_2 + m_2', \quad (4.23)$$

$$\begin{aligned} E J_\omega \varphi^{IV} - G I_t \varphi'' - [\varphi' (N i^2 + 2 \beta_1 M_1 + 2 \beta_2 M_2 + \beta_\omega M_\omega)]' - x_{2P} (N \xi_{1P}')' + \\ + x_{1P} (N \xi_{2P}')' + \xi_{1P}'' M_2 - \xi_{2P}'' M_1 - \xi_{1P}' m_1 + \xi_{2P}' m_2 + \varphi m_3 = m_3 + m_\omega \end{aligned} \quad (4.24)$$

$$\begin{aligned} m_3 &= \int_s [p_2 (x_1 - x_{1P}) - p_1 (x_2 - x_{2P})] ds; \\ m_3 &= \int_s [p_1 (x_1 - x_{1P}) - p_2 (x_2 - x_{2P})] ds; \quad m_\omega = \int_s p_3 \omega_P ds \end{aligned} \quad (4.25)$$

and are differential equations of the linearized second order theory for the considered thin walled beam.

5. NUMERICAL EXAMPLE

The above mentioned and derived expressions are applied to the thin walled beam with a cross section based on the shape of a turbine blade [6] section (Fig.1).

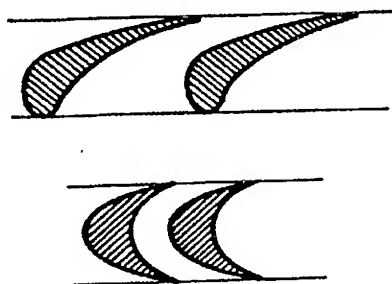


Fig.1

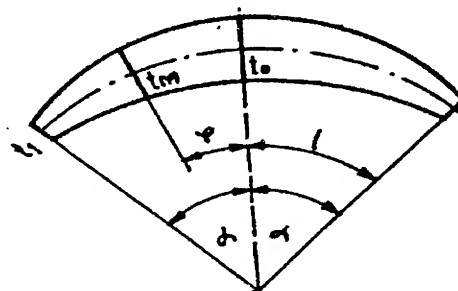


Fig.2

The section (Fig.2) considered in the numerical example has a curvilinear middle line and variable thickness which is supposed to be defined by

$$t(s) = t(\varphi) = t_0 \{1 - (1 - t_1/t_0) [1 - (1 - \varphi/\alpha)^n]\} \quad (5.1)$$

Geometrical characteristics area A , torsional constant I_t and sectorial moment of inertia J_ω defined by appropriate expressions [1], [6] are for the considered cross section from Fig.2

$$A = \int_0^\alpha t(\varphi) R d\varphi = 2 R \alpha t_0 [(1 - (1 - t_1/t_0) n / (n+1))], \quad (5.2)$$

$$I_t = (1/3) \int_0^\alpha t^3(\varphi) R d\varphi, \quad (5.3)$$

$$I_t / [(2/3) R \alpha t_0^3] = 1 - 3 n (1 - t_1/t_0) / (n+1) + \\ + 6 n^2 (1 - t_1/t_0)^2 / (n+1) (2n+1) - \\ - 6 n^3 (1 - t_1/t_0)^3 / (n+1) (2n+1) (3n+1), \quad (5.4)$$

$$J_\omega / (R^5 t_0 / 12) = 8 (t_1/t_0) \alpha^3 + 3 (1 - t_1/t_0) I_0 + \\ + 2 (e/R) (t_1/t_0) [12 - (t_1/t_0)^2 (t_0/R)^2] (\alpha \cos \alpha - \sin \alpha) - \\ - 6 (e/R) (1 - t_1/t_0) [4 - (t_1/t_0)^2 (t_0/R)^2] (2 I_3 - I_4 e/R) + \\ + 6 (e/R) (t_1/t_0) (1 - t_1/t_0)^2 (t_0/R)^2 (2 I_7 - I_5 e/R) + \\ + 2 (e/R) (1 - t_1/t_0)^3 (t_0/R)^2 (2 I_9 - I_6 e/R), \quad (5.5)$$

where

$$I_0 = \int_0^\alpha R^5 (1 - \varphi/\alpha)^n \varphi^2 d\varphi = 2 (R \alpha)^{n+3} / (n+1) (n+2) (n+3), \\ I_3 = \int_0^\alpha (1 - \varphi/\alpha)^n \varphi \sin \varphi d\varphi, \quad I_4 = \int_0^\alpha (1 - \varphi/\alpha)^n \sin^2 \varphi d\varphi, \\ I_5 = \int_0^\alpha (1 - \varphi/\alpha)^{2n} \sin^2 \varphi d\varphi, \quad I_6 = \int_0^\alpha (1 - \varphi/\alpha)^{3n} \sin^2 \varphi d\varphi, \\ I_7 = \int_0^\alpha (1 - \varphi/\alpha)^{2n} \varphi \sin \varphi d\varphi, \quad I_9 = \int_0^\alpha (1 - \varphi/\alpha)^{3n} \varphi \sin \varphi d\varphi. \quad (5.6)$$

All calculations are done for $R = 300$ mm, $t_0 = 26$ mm and $\alpha = 30^\circ$, beam length $L = 900$ mm. One end of the beam is supposed to be clamped and external torsional moment equal to one is applied to the other free end of the beam.

Normal stresses caused by bimoment and shear stresses caused by torsion are calculated according to the appropriate formulae [1], [2], [6]. After that the equivalent stresses are calculated according to the Tresca criterion.

The distributions of maximal values along the beam are shown in Fig.3 for normal stresses, in Fig.4 for shear stresses and for equivalent stresses in Fig.5.

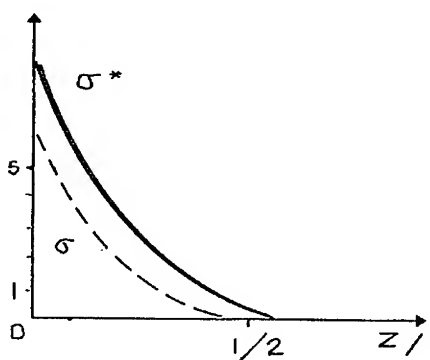


Fig. 3

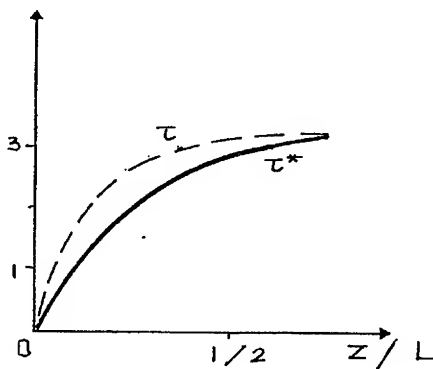


Fig. 4

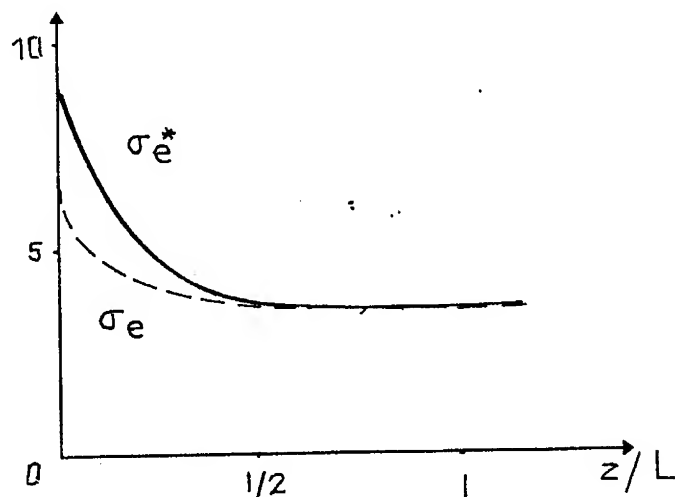


Fig. 5

6. CONCLUSION

As it can be seen from the shown diagrams it may be concluded that it is not recommendable to neglect the influence of the secondary effects for the considered sections because the nonnegligible differences in the stresses exist especially in the vicinity of the clamped ends.

References

- [1]. Vlassov B.Z., Tonkostennye uprugie sterzhni, Gosizd fiz-mat lit, Moskva, 1959.
- [2]. Kollbruner, C. F., Hajdin, N., Dunnwandige Stabe, Bd.1, Springer-Verlag, Berlin-Heidelberg-New York, 1972.
- [3]. Hajdin, N., A contribution to the non-linear theory of thin-walled member with open cross section (in Serbian), Symposium on Contemporary problems of nonlinear continuum mechanics. Tara, Serbia, 1980.
- [4]. Ruzic, D., Andjelic, N., One Approach to the Nonlinear Behaviour of Thin Walled Beams with Symmetrical Open Sections, Second Serbian-Greek Symposium on Solid Mechanics, Serbian Academy of Sciences and Arts, 14 - 15 November 1996, Belgrade, Yugoslavia.
- [5]. Vasiljevic, N., Steam turbines (in Serbian), Masinski fakultet, Beograd, 1990.
- [6]. Ruzic, D., Strength of Structures (in Serbian), Masinski fakultet, Beograd, 1995.
- [7]. Rnjak, N., A contribution to the analysis of behaviour of thin-walled structural elements of turbine blade shape (in Serbian), Magistrarska disertacija, Masinski fakultet, Beograd, 1993.

3D Numerical Simulation of Melt Flow in the Presence of Rotating Magnetic Fields

Daniel Vizman¹, Irina Nicoara¹ and Jochen Friedrich²

1. Department of Physics, West University of Timisoara, Romania

2. Institute of Material Science, Erlangen, Germany

Abstract

This paper gives the results of the numerical simulation of the isothermal convection due to a rotating magnetic field in a cylindrical Ga-melt volume. The governing equations to be solved are the Navier-Stokes equations coupled with the potential equation of the MHD2-approximation. In order to valid the numerical method, the Lorenz force distribution was analytically computed and later on compared with the numerical results. The temperature and velocity distribution are also presented.

1 Introduction

It is well known that the external magnetic fields are used in several industrial applications such as the continuous casting of the steel and aluminium and growth of single semiconductor crystals, where a contactless control is needed in order to damp melt flow fluctuations. The effect of rotating magnetic fields on the melt flow of electrically conducting materials was studied in many papers ([1]-[5]). Some of them considered the flow in an infinitely long liquid cylinder ([1],[2]) and the others

([3]-[5]) considered the flow in a cylinder of finite length. All of this papers are dealing with a 2D-axisymmetric modell. In this paper we present the results of the 3D-numerical simulation of the melt convection due to a rotating magnetic field in a cylindrical volume, the comparison between numerical calculations of Lorenz force and the exact solution in the case with no flow and the discussion of our results consequences for real processes.

2 Model description

2.1 Governing equation

The governing partial differential equations (in cartezian coordinates) can be written:

Conservation of mass:

$$\frac{\partial}{\partial y_i}(\rho u_i) = 0 \quad (1)$$

Conservation of momentum:

$$\frac{\partial}{\partial t}(\rho u_i) + \frac{\partial}{\partial y_j}(\rho u_i u_j + \tau_{ij}) = -\frac{\partial p}{\partial y_i} + s_i^u \quad (2)$$

Conservation of temperature:

$$\frac{\partial}{\partial t}(\rho T) + \frac{\partial}{\partial y_j}(\rho u_j T - \Gamma_T \frac{\partial T}{\partial y_j}) = s^T \quad (3)$$

In the above equation ρ is density, u_i i-th Cartesian component of velocity, p pressure, Γ_T the diffusion coefficient for temperature, s^T source term for temperature T , s_u source term for velocity, and τ_{ij} stress tensor

For a Newtonian fluid with dynamic viscosity μ , the stress tensor is defined:

$$\tau_{ij} = -\mu \left(\frac{\partial u_i}{\partial y_j} + \frac{\partial u_j}{\partial y_i} \right) \quad (4)$$

2.2 Source Terms for Momentum Equation

If we take in account the gravitational effect with the Boussinesq approximation, source term for velocity will be:

$$s_u^i = \rho(T_{ref})g^i\beta(T - T_{ref}) \quad (5)$$

where T_{ref} is the reference temperature, g^i i-th component of gravitational force, β thermal expansion coefficient.

When the flow is induced by a magnetic field we have to include the Lorentz force as source term in Navier-Stokes equations:

$$s_u^i = (\vec{j} \times \vec{B})_i \quad (6)$$

where \vec{B} is the intensity of magnetic field and \vec{j} current density.

The current density \vec{j} is determined by $\vec{j} = \sigma(\vec{E} + \vec{u} \times \vec{B})$ (σ is electrical conductivity). The electric field \vec{E} is described by the introduction of a scalar potential Φ (see [5]) and an additional term $\partial_t \vec{A}$:

$$\vec{E} = -\nabla\Phi - \frac{\partial \vec{A}}{\partial t} \quad (7)$$

\vec{A} is the vector potential and $\vec{B} = \nabla \times \vec{A}$. The condition $\nabla \cdot \vec{j} = 0$ yields the governing equation for scalar potential Φ . At the boundary $\vec{j} \cdot \vec{n} = 0$.

2.3 Rotating magnetic field

For a cylindrical cavity of radius R , the rotating magnetic field applied externally to the melt can be described by:

$$\vec{B} = [-\frac{B_0}{R}(x \sin \omega t - y \cos \omega t); \frac{B_0}{R}(x \cos \omega t + y \sin \omega t); 0] \quad (8)$$

The vector potential can be easily obtained:

$$\vec{A} = [0; 0; -\frac{B_0}{2R}((x^2 - y^2) \cos \omega t + 2xy \sin \omega t)] \quad (9)$$

where B_0 is the magnetic field amplitude, ω its frequency and (x, y, z) are the cartesian coordinates. While \vec{B} is rotating with frequency ω the quantities \vec{E} , \vec{j} , Φ will rotate with the same frequency. Consequently, the Lorentz force consists of a mean time-independent part and an oscillating part. So, the fluid flow has also a mean part and an oscillating one. In present work we assume that due to its high inertia the fluid is unable to follow this oscillating force component, therefore, our numerical analysis is limited to the time-independent mean force.

The follow integration:

$$\langle \vec{F}_L \rangle = \left(\frac{2\pi}{\omega}\right)^{-1} \int_0^{2\pi} \vec{j} \times \vec{B} dt \quad (10)$$

leads the mean Lorentz force components.

If we do not take in account fluid flow ($\vec{u} = 0$), the equation for scalar potential can be easy solved analytically for a finite cylinder of radius R . In this case, the analytical solution for Lorentz force is :

$$F_{lx} = F_\varphi \sin \varphi; \quad F_{ly} = F_\varphi \cos \varphi; \quad F_{lz} = 0 \quad (11)$$

where

$$F_\varphi = \sigma B_0^2 r \omega \left[\frac{1}{4} \left(\frac{r}{R}\right)^2 - \frac{1}{2} \sum_n \frac{J(2, \lambda_n \frac{r}{R}) J(3, \lambda_n)}{(J^2(2, \lambda_n) - J(1, \lambda_n) J(3, \lambda_n)) \lambda_n} \right. \\ \left. \left(\cosh \left(\lambda_n \frac{z}{R} \right) + \left(1 - \cosh \left(\lambda_n \frac{z_{max}}{R} \right) \right) \frac{\sinh \left(\lambda_n \frac{z}{R} \right)}{\sinh \left(\lambda_n \frac{z_{max}}{R} \right)} \right) \right]$$

$$r = (x^2 + y^2)^{\frac{1}{2}}; \quad J \text{ are the Bessel functions}$$

and λ_n are solutions of the equation

$$2 \frac{J(2, x)}{x} - J(3, x) = 0$$

2.4 Numerical discretization method

The present simulations were done with a three-dimensional, block structure finite volume code. The discretization procedure of the finite volume method is well known from its application to fluid flows [6]. In our case, the method was extended for modelling the scalar potential equation. The computational domain, e.g. a cylindrical cavity, is subdivided in 5 blocks. We use a three-dimensional, structured, non-orthogonal grid. Total number of control volumes is 45 000.

We have chosen a typical Rayleigh-Benard configuration as test case. Our geometry is a cylinder with high $h = 4\text{cm}$ and diameter $d = 4\text{cm}$. At the boundary is imposed a linear temperature profile with $T_u = 10^\circ\text{C}$ and $T_d = 30^\circ\text{C}$ (see Fig.1). Simulations were done for a galium melt.

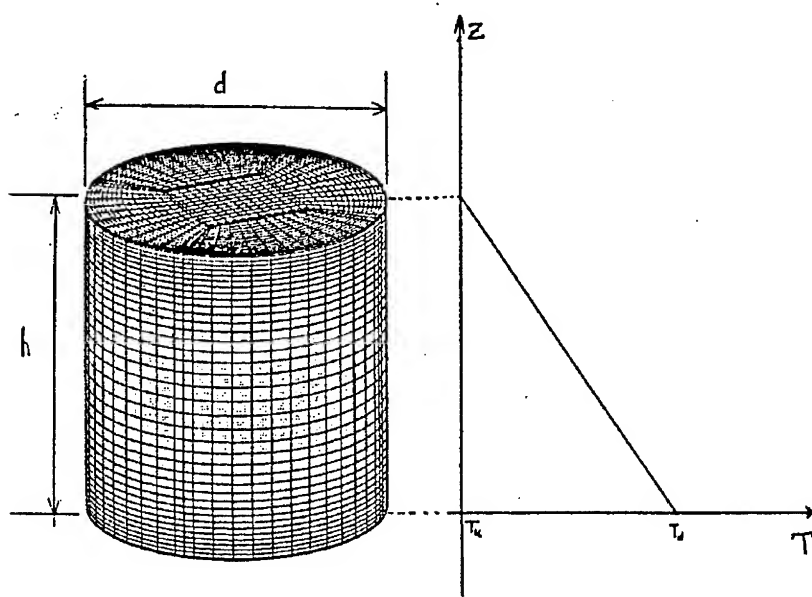


Figure 1: The geometry of test case is shown

3 Results and discussions

3.1 Numerical calculations and analytical solutions

In order to valid our numerical method we have done the numerical calculation of Lorentz force without taken into account the fluid flow ($\vec{u} = 0$). The analytical solution was found using eq. 11. A comparison of numerical and analytical solution of azimuthal Lorentz force is given in Fig. 2 and 3. Fig. 2 show the azimuthal Lorentz force along z-axis and fig. 3 along radius. It can be pointed up that the numerical and analytical calculation are in a good agreement.

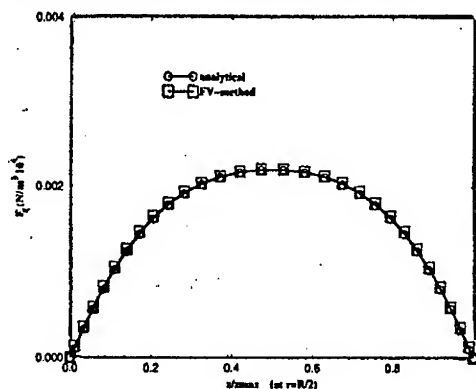


Figure 2: Comparison of analytical and numerical values of the azimuthal Lorentz force along z-axis

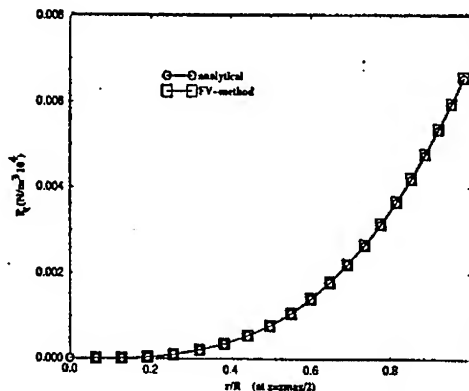


Figure 3: Comparison of analytical and numerical values of the azimuthal Lorentz force along radius

3.2 Influence of rotating magnetic field on the flow

This paragraph is devoted to the results of the numerical investigation of the rotating magnetic field on the melt flow. The results given below are done for the laminar time-independent state of the flow. The velocity field in the case with no magnetic field is shown in fig. 4. There are two section in the cylinder: one horizontal and one vertical. It can be observed from the horizontal section that the flow is a three-dimensional one. Due to the gravitation, the main motion can be found in the vertical section. The maximum of velocity is 1.6cm/s .

When a rotating magnetic field with amplitude 3.3mT is present, the flow configuration is completely different (see fig. 5). The main motion is now in the horizontal section and the maximum of velocity is 3.2cm/s . The secondary motion along z-axis is one order of magnitude smaller than the azimuthal rotation. Flow configuration is now an axisymmetric one.

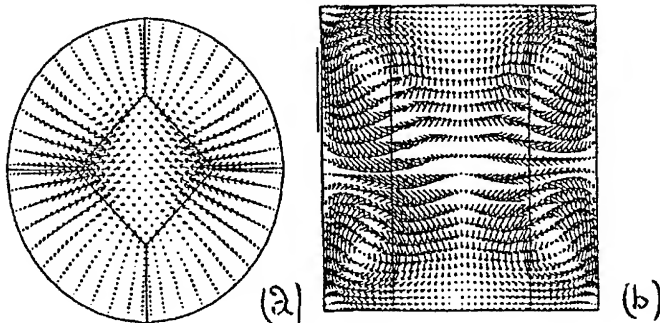


Figure 4: Velocity profile in a (a) horizontal and (b) vertical section with no magnetic field ($B_0 = 0\text{mT}$)

Fig.6 show the temperature distribution along centerline of cylinder with and without magnetic field. It can be observed that in the presence of a rotating magnetic field the temperature gradient along centerline is almost constant.

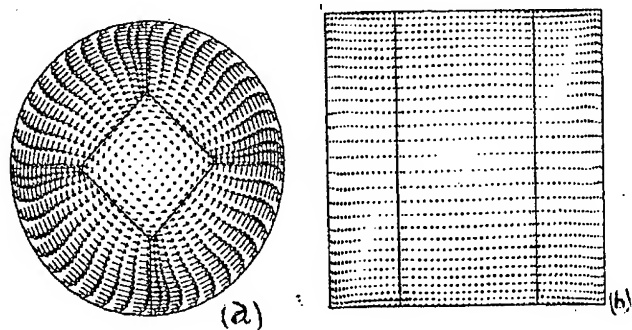


Figure 5: Velocity profile in a (a) horizontal and (b) vertical section with magnetic field ($B_0 = 3.3mT$)

The temperature isotherms in a vertical section are nearly flat in the presence of a rotating magnetic field (see fig. 7).

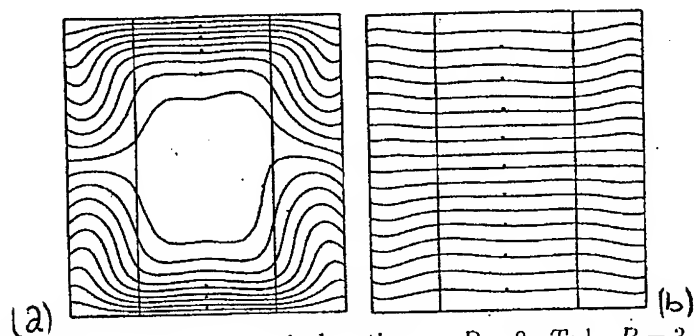


Figure 6: Isotherms in a vertical section: a. $B = 0mT$; b. $B = 3.3mT$

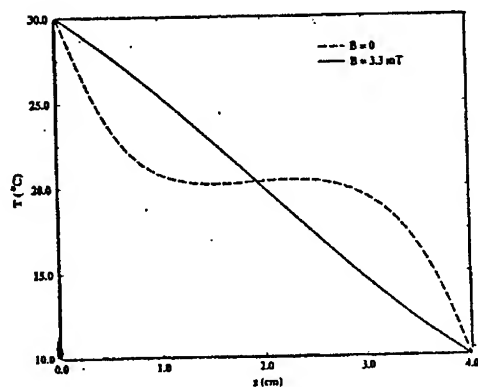


Figure 7: Temperature along z -axis in the middle of the fluid

4 Conclusions

A 3D Finite Volume method was implemented to study the influence of rotating magnetic fields on the fluid flow and its accuracy was tested by comparison with analytical solutions. A typical Rayleigh-Benard flow configuration was studied in the presence of a rotating magnetic field. An important conclusion is appropriate here, namely: a small magnetic field can have a great effect on the flow configuration. We conclude that the rotating magnetic fields can easily control the melt flow fluctuations.

References

- [1] A.B.Kapusta, *Magnitnaya Gidrodinamica* 2,1968, 71-76
- [2] E.Dahlberg, AB Atomenergi Rep. 1972 AE-447, Sweden
- [3] Yu.M.Gelfgat, J.Priede, M.Z.Sorkin, Energy transfer in MHD flows. Proc. of the International Conference,1991, Cadarache, France,181-186
- [4] J.Priede, Thesis (Salaspils 1993)
- [5] R.U.Bartz, G.Geberth, U.Wunderwald, E.Buhrig, Yu.M.Gelfgat, 2nd International Workshop on Modelling in Crystal Growth 1996(submitted to J.Crystal Growth)
- [6] M. Peric, Ph.D. Thesis, Imperial College of Science and Technology, University of London, 1985

Statistical solution for bioconvective flows

Dumitru HĂRĂGUŞ

Department of Mathematics, The West University of Timişoara,
Bd. V. Pârvan, 4, 1900 Timişoara, Romania
e-mail: haragus@tim1.uvt.ro

Abstract

For a system describing the bioconvective flows, the existence of statistical solutions is proved. Such solutions were introduced by Foiaş for the Navier-Stokes system.

1 Introduction

Statistical solutions for the initial boundary value problem for the Navier-Stokes system have been introduced by C.Foiaş [1]. In some functional frame the problem had the following form

$$u' + Au + B(u, u) = f, \quad u(0) = u_0, \quad (1.1)$$

with A linear operator and B bilinear map. In this paper a system describing bioconvective flows considered by Kan-On *et al.* [3] is treated. This problem can be written in the abstract form

$$u' + Au + B(u, u) + B_1u + B_2u = f, \quad u(0) = u_0, \quad (1.2)$$

where A, B_1, B_2 are linear operator and B bilinear map. Here A, B are different from A, B in (1.1) but they have similar properties. These together with some properties of the perturbations B_1 and B_2 permit us to define statistical solutions for (1.2) and to prove their existence.

The paper is organized as follows. In section 2 the system in [3] is written in the form (1.2). Statistical solutions for (1.2) are defined in Section 3 and their existence is proved in Section 4.

2 The system

Let Ω be a bounded domain in \mathbb{R}^3 with boundary $\partial\Omega \in \mathcal{C}^2$. Bioconvective flows in Ω are described by the following system, (cf. Kan-On *et al.* [3]):

$$\frac{\partial u}{\partial t} - \nu \Delta u + (u, \nabla)u + \nabla q = -km\chi + f \quad \text{in } \Omega \times (0, \infty), \quad (2.3)$$

$$\operatorname{div} u = 0 \quad \text{in } \Omega \times (0, \infty), \quad (2.4)$$

$$\frac{\partial m}{\partial t} - \theta \Delta m + (u, \nabla)m + U \frac{\partial m}{\partial x_3} = 0, \quad \text{in } \Omega \times (0, \infty), \quad (2.5)$$

where $u = (u_1, u_2, u_3) : \bar{\Omega} \times (0, \infty) \rightarrow \mathbb{R}^3$ denotes the velocity, $m : \bar{\Omega} \times (0, \infty) \rightarrow \mathbb{R}$ the concentration of microorganisms (more accurate $m(x, t)$ is the concentration in $(x_1, x_2, x_3) \in \Omega$ at time $t \geq 0$) and $q : \bar{\Omega} \times (0, \infty) \rightarrow \mathbb{R}$ the pressure of the culture fluid; ν, θ, κ, U are positive real parameters; $\chi = (0, 0, 1)$ and f is the external force. To this system we add the initial and the boundary conditions

$$u(x, 0) = u_0(x), \quad m(x, 0) = m_0(x), \quad x \in \Omega, \quad (2.6)$$

$$u(x, t) = 0, \quad \text{if } x \in \partial\Omega \quad \text{and } t > 0, \quad (2.7)$$

$$\theta \frac{\partial m}{\partial n} - Un_3(x)m = 0, \quad \text{if } x \in \partial\Omega \quad \text{and } t > 0, \quad (2.8)$$

where $n = (n_1, n_2, n_3)$ is the external normal to $\partial\Omega$.

Under suitable assumptions for U and θ in [3] is proved that the steady problem for (2.3)-(2.8), i.e.

$$\int_{\Omega} m \, dx = \alpha, \quad (2.9)$$

$$-\nu \Delta u + (u, \nabla)u + \nabla q = -km\chi + f, \quad \text{in } \Omega, \quad (2.10)$$

$$\operatorname{div} u = 0, \quad \text{in } \Omega, \quad (2.11)$$

$$-\theta \Delta m + (u, \nabla)m + U \frac{\partial m}{\partial x_3} = 0, \quad \text{in } \Omega, \quad (2.12)$$

$$u = 0, \quad \text{on } \partial\Omega, \quad (2.13)$$

$$\theta \frac{\partial m}{\partial n} - Un_3 m = 0, \quad \text{on } \partial\Omega, \quad (2.14)$$

has a solution $(u^\alpha, m^\alpha, p^\alpha)$, $\alpha \geq 0$. For the initial boundary value problem (2.3)-(2.8) consider solutions of the form $u = v + u^\alpha$, $m = \mu + m^\alpha$. Then it

yields the following system for v and μ :

$$\frac{\partial v}{\partial t} - \nu \Delta v + (u^\alpha, \nabla)v + (v, \nabla)u^\alpha + (v, \nabla)v + \nabla(q - p^\alpha) = -k\mu\chi, \quad \text{in } \Omega \times (0, T), \quad (2.15)$$

$$\operatorname{div} v = 0, \quad \text{in } \Omega \times (0, T), \quad (2.16)$$

$$\frac{\partial \mu}{\partial t} - \theta \Delta \mu + (u^\alpha, \nabla)\mu + (v, \nabla)m^\alpha + (v, \nabla)\mu + U \frac{\partial \mu}{\partial x_3} = 0, \quad \text{in } \Omega \times (0, T), \quad (2.17)$$

$$v = 0, \quad \text{on } \partial\Omega \times (0, T), \quad (2.18)$$

$$\theta \frac{\partial \mu}{\partial n} - Un_3\mu = 0, \quad \text{on } \partial\Omega \times (0, T), \quad (2.19)$$

$$v(x, 0) = a(x), \quad \mu(x, 0) = b(x), \quad x \in \Omega. \quad (2.20)$$

This problem can be written as an abstract initial value problem

$$u' + Au + B(u, u) + B_1u + B_2u = f, \quad u(0) = u_0, \quad (2.21)$$

in some Hilbert space.

Consider the Hilbert spaces $L^2(\Omega) := (L^2(\Omega))^3$, $H^1(\Omega) := (H^1(\Omega))^3$ where $L^2(\Omega)$ and $H^1(\Omega)$ are the usual Sobolev spaces, and define

$$\begin{aligned} \mathcal{V} &:= \{u \in (\mathcal{D}(\Omega))^3 \mid \operatorname{div} u = 0\}, \quad X_\sigma := \bar{\mathcal{V}}^{L^2(\Omega)}, \quad V_\sigma = \bar{\mathcal{V}}^{H^1(\Omega)}, \\ X_\mu &:= \{\mu \in L^2(\Omega) \mid \int_\Omega \mu dx = 0\}, \quad V_\mu := H^1(\Omega) \cap X, \quad H := X_\sigma \oplus X_\mu. \end{aligned}$$

The scalar product in H is denoted by (\cdot, \cdot) , i.e.

$$(u, v) = \sum_{i=1}^4 \int_\Omega u_i(x) v_i(x) dx, \quad u, v \in H,$$

and the corresponding norm by $|\cdot|$. For $u = (u_1, u_2, u_3, u_4) \in H$ denote $u_\sigma = (u_1, u_2, u_3) \in X_\sigma$.

In H consider the linear operator A_0 with domain

$$D(A_0) = \{u = (u_1, u_2, u_3, u_4) \mid u_\sigma \in \mathcal{V}, u_4 \in C^2(\bar{\Omega}) \cap X, \theta \frac{\partial u_4}{\partial n} - Un_3u_4 = 0\},$$

and defined by

$$A_0u = (-\nu \Delta u_\sigma, -\theta \Delta u_4).$$

This operator possesses a Friedrichs extension A , which is selfadjoint and has a compact inverse A^{-1} . Then $A^{\frac{s}{2}}$ exists, for $s \in [0, \infty)$, and is a closed linear operator with domain H^s . With the scalar product $(u, v)_s := (A^{\frac{s}{2}}u, A^{\frac{s}{2}}v)$, H^s is a Hilbert space; the corresponding norm is denoted by $|\cdot|_s$. For $s < 0$, H^s is the dual of H^{-s} . Remark that A is a sum: $A = A_\sigma \oplus A_\mu$, where A_σ is the Stokes operator and A_μ is the Laplace operator on the space of functions satisfying

$$\theta \frac{\partial \mu}{\partial n} - Un_3 \mu = 0, \text{ on } \partial\Omega.$$

Let b be the trilinear form

$$b(u, v, w) = \sum_{j=1}^4 \sum_{i=1}^3 \int_{\Omega} u_i(x) \frac{\partial v_j}{\partial x_i}(x) w_j(x) dx. \quad (2.22)$$

Consider the operators $B : H^1 \times H^1 \times H^1 \rightarrow H^{-1}$, $B_1, B_2 : H^1 \rightarrow H^{-1}$ defined by

$$(B(u, v), w) = b(u, v, w), \quad u, v, w \in H^1, \quad (2.23)$$

$$(B_1 u, v) = b(u^\alpha, u, v), \quad u, v \in H^1, \quad (2.24)$$

$$(B_2 u, v) = ((u_\sigma, \nabla) u^\alpha, v_\sigma) + ((u_\sigma, \nabla) m^\alpha, v_4) + \quad (2.25)$$

$$k(u_4 \chi, v_\sigma) - U(u_4, \frac{\partial v_4}{\partial x_3}), \quad u, v \in H^1,$$

(recall that (u^α, m^α) is a steady solution of (2.3)-(2.5) hence more accurate notation for $b(u^\alpha, u, v)$ is $b((u^\alpha, m^\alpha), u, v)$). In [2] have been proved that B is continuous,

$$(B(u, v), v) = 0, \quad u, v \in H^1, \quad (2.26)$$

and has continuous extensions $B : H \times H^1 \rightarrow H^{-2}$, $B : H^1 \times H \rightarrow H^{-2}$. Also B_1, B_2 are continuous, admit continuous extensions $B_1, B_2 : H \rightarrow H^{-2}$ and

$$(B_1 u, u) = 0. \quad (2.27)$$

With these notations the problem (2.3)-(2.8) is of the form (2.21).

A function $u \in L^2(0, T; H^1) \cap L^\infty(0, T; H)$, is called **weak or turbulent solution** of (2.21), for $u_0 \in H$ and $f \in L^2(0, T; H^{-1})$ if for all $v \in C^1([0, T]; H) \cap C([0, T]; H^1)$, with compact support in $[0, T]$ it satisfies

$$-\int_0^T (u(t), v'(t)) dt + \int_0^T ((u(t), v(t))) dt + \int_0^T (B(u(t), u(t)), v(t)) dt +$$

$$\begin{aligned} & \int_0^T (B_1 u(t), v(t)) dt + \int_0^T (B_2 u(t), v(t)) dt \\ &= (u_0, v(0)) + \int_0^T (f(t), v(t)) dt. \end{aligned} \quad (2.28)$$

Under suitable assumptions for (u^α, m^α) , the existence of such a solution is proved in [3].

3 The Definition of statistical solutions

Consider the class \mathcal{T} of all real functions $\Phi : [0, T] \times H^1 \rightarrow \mathbb{R}$ with the following properties (cf. [1]):

i) Φ is Fréchet differentiable with continuous differential from $[0, T] \times H^1$ into $\mathcal{L}(\mathbb{R} \times H^1; \mathbb{R})$ and $|\Phi_t(t, u)| \leq c_1 + c_2|u|$, for some positive constants c_1, c_2 which are independent of t and u .

ii) For $t \in [0, T]$, $\Phi(t, \cdot)$ is differentiable in the following sense: there exists $\Phi_u(t, u) \in H^1$ such that

$$\frac{1}{|v|} |\Phi(t, u+v) - \Phi(t, u) - (v, \Phi_u(t, u))| \rightarrow 0, \text{ as } v \rightarrow 0 \text{ in } H^1.$$

iii) $\Phi_u(\cdot, \cdot) : [0, T] \times H^1 \rightarrow H^1$ is continuous and $\|\Phi_u(\cdot, \cdot)\|$ is bounded on $[0, T] \times H^1$.

Definition 3.1. Let μ be a positive Borel measure on the Hilbert space H . Assume that

$$\mu(H) = 1 \text{ and } \int_H |u|^2 d\mu < \infty. \quad (3.29)$$

A family $\{\mu_t\}_{t \in [0, T]}$ of positive Borel measures on H is called **statistical solution** for (2.15) with the initial data μ if the following conditions are satisfied:

$$\sup \left\{ \int_H |u|^2 d\mu_t(u), \quad t \in [0, T] \right\} < \infty, \quad (3.30)$$

$$\int_0^T \int_H \|u\|^2 d\mu_t(u) dt < \infty, \quad (3.31)$$

$$\begin{aligned} & - \int_0^T \left[\int_H \Phi_t(t, u) d\mu_t(u) \right] dt + \int_0^T \left\{ \int_H [(u, \Phi_u(t, u))] + \right. \\ & \left. (B(u, u) + B_1 u + B_2 u, \Phi_u(t, u)) d\mu_t(u) \right\} dt = \end{aligned} \quad (3.32)$$

$$\int_H \Phi(0, u) d\mu(u) + \int_0^T \left[\int_H (f(t), \Phi_u(t, u)) d\mu_t(u) \right] dt, \text{ for any } \Phi \in \mathcal{T}.$$

4 Existence of statistical Solutions

The proof of the existence of statistical solutions for (2.15) is similar to the proof given by C. Foiaş in [1], p.254-272, for the Navier-Stokes system. For this reason we present here only a sketch of the proof.

Theorem 4.1. *Let α be a positive constant such that $2\alpha > 1 - \|B_2\|$, so there $C = 2(1 - \|B_2\| - \frac{1}{2\alpha}) > 0$. Then for any initial data μ there exists a statistical solution $\{\mu_t\}_{t \in [0, T]}$ of (2.15) which satisfies the inequality of energy*

$$\begin{aligned} \int_H \varphi(|u|^2) d\mu_t(u) + C \int_0^t \left[\int_H \varphi'(|u|^2) \|u\|^2 d\mu_\tau(u) \right] d\tau &\leq \\ &\leq \int_H \varphi(|u|^2) d\mu(u) + \alpha \int_0^t \left[\int_H \varphi'(|u|^2) |f(\tau)|_{-1}^2 d\mu_\tau(u) \right] d\tau, \end{aligned} \quad (4.33)$$

for any $\varphi \in C^1((0, \infty))$, $\varphi \geq 0$ and $0 \leq \varphi'(x) \leq c_p < \infty$, $x \in (0, \infty)$.

Proof. The operator A is selfadjoint and has a compact inverse so there exists an orthonormal system $\{w_k\}_{k \in \mathbb{N}^*} \subset H$ such that

$$Aw_k = \lambda_k w_k,$$

and

$$0 < \lambda_1 \leq \lambda_2 \leq \dots \leq \lambda_n \leq \dots \rightarrow \infty.$$

Let P_n be the projection associated to $Sp\{w_1, \dots, w_n\}$. For $u_0 \in H$ and $f \in L^2(0, T; H^{-1})$ we consider the initial boundary problem

$$u'_n + AP_n u_n + P_n B(u_n, u_n) + P_n B_1 u_n + P_n B_2 u_n = P_n f, \quad (4.34)$$

$$u_n(0) = P_n u_0. \quad (4.35)$$

From (4.34), (2.26) and (2.27) it follows

$$\frac{1}{2} \frac{d}{dt} |u_n(t)|^2 + \|u_n(t)\|^2 + (B_2 u_n(t), u_n(t)) = (f(t), u_n(t)). \quad (4.36)$$

For $\alpha > 1/[2(1 - \|B_2\|)]$, we have

$$(B_2 u_n(t), u_n(t)) + (f(t), u_n(t)) \leq \|B_2\| \|u_n(t)\|^2 + \frac{\alpha}{2} |f(t)|_{-1}^2 + \frac{1}{2\alpha} \|u_n(t)\|^2,$$

so from (4.36) we deduce

$$\frac{d}{dt}|u_n(t)|^2 + C\|u_n(t)\|^2 \leq \alpha|f(t)|_{-1}^2. \quad (4.37)$$

Integration of (4.37) from 0 to t yields

$$|u_n(t)|^2 + C \int_0^t \|u_n(\tau)\|^2 d\tau \leq |u_0|^2 + \alpha \int_0^t |f(\tau)|_{-1}^2 d\tau. \quad (4.38)$$

The problem (4.34)-(4.35) has a unique local solution u_n on some interval $[0, h_m]$ which due to (4.38) has a maximal solution on $[0, T]$. Define $S^{(n)}(t)$ by $u_n(t) = S^{(n)}(t)u_{0n}$ and the map $(t, u_0) \rightarrow S^{(n)}(t)u_0$ is continuous on $[0, T] \times P_n H$.

For $n \in \mathbb{N}^*$, $t > 0$, consider the Borel measures $\mu^{(n)}$ and $\mu_t^{(n)}$ defined by

$$\mu^{(n)}(\omega) = \mu(P_n^{-1}(\omega \cap P_n H))$$

$$\mu_t^{(n)}(\omega) = \mu(S_n^{-1}(t)(\omega \cap P_n H))$$

where ω is a Borel set from H .

Let \mathcal{C}_α , $\alpha \geq 0$, be the space of all real continuous functionals $\Phi(\cdot)$ on H such that

$$\|\Phi(\cdot)\|_{\mathcal{C}_\alpha} = \sup_{u \in H} \frac{\Phi(u)}{1 + |u|^\alpha} < \infty.$$

By $\mathcal{C}_{1,1}$ we denote the space of all $\Phi(\cdot) : H^1 \rightarrow \mathbb{R}$ such that

$$\|\Phi(\cdot)\|_{\mathcal{C}_{1,1}} = \sup_{u \in H^1} \frac{\Phi(u)}{1 + |u| \|u\|} < \infty.$$

Remark that for any $\Phi \in \mathcal{C}_2$,

$$\int_H \Phi(u) d\mu_t^{(n)} = \int_H \Phi(S^{(n)}(t)P_n u) d\mu(u). \quad (4.39)$$

Then from (4.38)-(4.39) follows

$$\int_H |u|^2 d\mu_t^{(n)} + C \int_0^t \left[\int_H \|u\|^2 d\mu_t^{(n)} \right] dt \leq \int_H |u|^2 d\mu(u) + c_1 = c_2,$$

where the constants c_1, c_2 , are independent of $t \in [0, T]$ and $n \in \mathbb{N}^*$. From this follows that the family $\{\mu_t^{(n)} \mid t \in [0, T]\}$, $n \in \mathbb{N}^*$, has the properties

$$\sup_n \left\| \int_H (1 + |u|^2) d\mu_t^{(n)}(u) \right\|_{L^\infty(0, T)} < \infty, \quad (4.40)$$

$$\sup_n \left\| \int_H (\|u\|^2) d\mu_t^{(n)}(u) \right\|_{L^1(0, T)} < \infty, \quad (4.41)$$

$$\int_H (\Phi(u) d\mu_t^{(n)}(u)) \text{ is measurable,} \quad (4.42)$$

for any $\Phi : H \rightarrow \mathbb{R}$ non-negative and weakly continuous. Lemma 1 in [1], p.246, implies the existence of the functionals $F^{(n)}$ continuous on $L^2(0, T; \mathcal{C}_{1,1})$, with continuous restriction to $L^2(0, T; \mathcal{C}_{1,1}) \cap L^1(0, T; \mathcal{C}_2)$ in the $L^1(0, T; \mathcal{C}_2)$ -topology and such that

$$F^{(n)}(\Phi) = \int_0^T \left[\int_H \Phi(t, u) d\mu_t^{(n)}(u) \right] dt, \quad (4.43)$$

for any $\Phi \in L^2(0, T; \mathcal{C}_{1,1}) \cap L^1(0, T; \mathcal{C}_2)$.

By applying Lemmas 3 and 4 in [1], p.254-265, we obtain in $L^1(0, T; \mathcal{C}_2)$ a cluster point F of the sequence $\{F^{(n)} \mid n \in \mathbb{N}^*\}$ and there exists a family $\{\mu_t\}_{0 \leq t < \infty}$ of (Borel) measures on H such that

$$F(\phi) = \int_0^T \left[\int_H \Phi(t, u) d\mu_t(u) \right] dt. \quad (4.44)$$

The family $\{\mu_t\}_{0 \leq t < \infty}$ is a statistical solution.

It remains to prove that $\{\mu_t\}_{0 \leq t < \infty}$ satisfies the inequality of energy. For this, let $\varphi \in \mathcal{C}^1((0, \infty))$, $\varphi \geq 0$ and $0 \leq \varphi'(x) \leq c_p < \infty$, $x \in (0, \infty)$. From (4.34) follows

$$\begin{aligned} & \frac{1}{2} \frac{d}{dt} \varphi(|u_n(t)|^2) + \varphi'(|u_n(t)|^2) [\|u_n(t)\|^2 + \\ & (B_2 u_n(t), u_n(t))] = \varphi'(|u_n(t)|^2) (f(t), u_n(t)), \end{aligned}$$

hence for all $t \in [0, T]$ we have

$$\frac{1}{2} \int_H \varphi(|u|^2) d\mu_t^{(n)}(u) + \int_0^t \int_H \varphi'(|u|^2) [\|u\|^2 + (B_2 u, u)] d\mu_\tau^{(n)}(u) d\tau = \quad (4.45)$$

$$\frac{1}{2} \int_H \varphi(|u|^2) d\mu^{(n)}(u) + \int_0^t \int_H \varphi'(|u|^2)(f(\tau), u) d\mu_\tau^{(n)}(u) d\tau.$$

Let $\rho \in L^1(0, T)$, $\rho \geq 0$. Multiplication of (4.45) by $\rho(t)$ and integration over $[0, T]$ yields

$$\begin{aligned} & \frac{1}{2} \int_0^T \int_H \rho(t) \varphi(|u|^2) d\mu_t^{(n)}(u) dt + \int_0^T \int_H \left(\int_\tau^T \rho(t) dt \right) \varphi'(|u|^2) [\|u\|^2 + \\ & (B_2 u, u)] d\mu_\tau^{(n)}(u) d\tau = \frac{1}{2} \int_0^T \int_H \rho(t) \varphi(|u|^2) d\mu_t^{(n)}(u) dt + \\ & \int_0^T \int_H \left(\int_\tau^T \rho(t) dt \right) \varphi'(|u|^2)(f(\tau), u) d\mu_\tau^{(n)}(u) d\tau. \end{aligned}$$

In the same manner as for (4.38) we obtain

$$\begin{aligned} & \int_0^T \int_H \rho(t) \varphi(|u|^2) d\mu_t^{(n)}(u) dt + C \int_0^T \int_H \left(\int_\tau^T \rho(t) dt \right) \varphi'(|u|^2) \|u\|^2 d\mu_\tau^{(n)}(u) d\tau \leq \\ & \int_0^T \int_H \rho(t) \varphi(|u|^2) d\mu_t^{(n)}(u) dt + \alpha \int_0^T \int_H \left(\int_\tau^T \rho(t) dt \right) \varphi'(|u|^2) |f(\tau)|_{-1}^2 d\mu_\tau^{(n)}(u) d\tau, \\ & \text{hence, because } \|P_k u\|^2 \leq \|u\|^2 \text{ for any } k \in \mathbb{N}^*, \\ & \int_0^T \int_H \rho(t) \varphi(|u|^2) d\mu_t^{(n)}(u) dt + C \int_0^T \int_H \left(\int_\tau^T \rho(t) dt \right) \varphi'(|u|^2) \|P_k u\|^2 d\mu_\tau^{(n)}(u) d\tau \leq \\ & \int_0^T \int_H \rho(t) \varphi(|u|^2) d\mu_t^{(n)}(u) dt + \alpha \int_0^T \int_H \left(\int_\tau^T \rho(t) dt \right) \varphi'(|u|^2) |f(\tau)|_{-1}^2 d\mu_\tau^{(n)}(u) d\tau, \end{aligned} \quad (4.46)$$

Since $\|P_k u\|^2 \in C(2)$ in (4.46) we can make $n \rightarrow \infty$, so

$$\int_0^T \int_H \rho(t) \varphi(|u|^2) d\mu_t(u) dt + C \int_0^T \int_H \left(\int_\tau^T \rho(t) dt \right) \varphi'(|u|^2) \|P_k u\|^2 d\mu_\tau(u) d\tau \leq$$

$$\int_0^T \int_H \rho(t) \varphi(|u|^2) d\mu(u) dt + \alpha \int_0^T \int_H \left(\int_\tau^T \rho(t) dt \right) \varphi'(|u|^2) |f(\tau)|_{-1}^2 d\mu_\tau(u) d\tau,$$

From this follows the inequality of energy (4.33).

References

- [1] Foiaş, C., *Statistical study of the Navier-Stokes equations, I*. Rend. Sem. Mat. Univ. Padova **49** (1973) 219-347.
- [2] Hărăguş, D., *On the bioconvective flow*. Universitatea din Timişoara, Preprint SEF nr. 97 (1994).
- [3] Kan-on, Y., Narukawa, K., Teramoto, Y., *On the equations of bioconvective flow*. J. Math. Kyoto Univ. **32**, 1 (1992) 135-153.
- [4] Temam, R., *Navier-Stokes equations, theory and numerical analysis*. North-Holland Publ. Comp. Amsterdam, 1979.

Dispersion of a solute in periodic porous media

Diana BALTEAN⁽¹⁾ Thérèse LÉVY⁽²⁾ Stefan BALINT⁽³⁾

⁽¹⁾ Universitatea de Vest din Timisoara and LMM, Université Paris 6

⁽²⁾ LMM, Université Pierre et Marie Curie Paris 6

⁽³⁾ Universitatea de Vest din Timisoara

Abstract

The aim of this paper is to study the problem of the transport of a passive solute in a porous medium by convection and dispersion. It is assumed that the media is a periodic system of cells, consisting of a solid part and a fluid part. The fluid is assumed to be incompressible and the flow can be described by Darcy's law. The effective equations are obtained using the homogenization method.

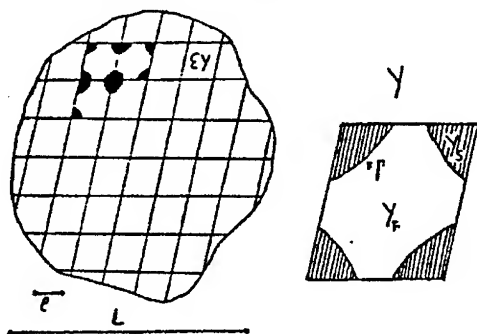
1 Introduction

The problem of a solute transport in a porous medium by convection and dispersion was studied in many papers [1],[2],[3]. In general, it is not possible to solve the full microscopic equations, so we would like to evaluate the effective (macroscopic) values of the dispersion coefficients and the convective velocity. Here the discussion was restricted to a strictly periodic structure applying the homogenization technique, that is a multiple scale perturbative analysis in terms of a small parameter ε . The homogenization method can be summarized as a three stage "recipe". In the first stage, each physical quantity is assumed to be representable by a function which depend separately on the macroscopic variable x and the microscopic one $y = \frac{x}{\varepsilon}$ such that the dependence on y is periodic. The non-dimensional equations are obtained and

the second section deals with that. In the second stage, all quantities, as well as their space derivatives, are expanded as regular perturbations of the small parameter ϵ . In the next section we perform two homogenization methods, the first one with a single time scale and the second one with two timescales. In our work, space and time are spanned through the macroscopic lengthscale and macroscopic timescales of convection and diffusion. An effective equation is obtained in the hypothesis that convection and diffusion are locally balanced. Under the assumption that the convection characteristic time is of order $O(\epsilon^{-2})$ we prove that the first method is simpler than the second one and we also find that the $O(1)$ term from the expansion of the concentration does not depend on the macroscopic diffusion characteristic time.

2 Formulation of the problem

Let us consider a spatially periodic porous material and two lengthscales l and L corresponding to the cell size and the size of the medium, respectively. The period will be a parallelepiped cell homothetic with the small ratio $\epsilon = l/L \ll 1$ of the region, denoted by Y , in which the fluid domain Y_F and the solid one Y_S have a smooth boundary Γ . The configuration of the medium is such that the ϵY_F parts are connected and the solid parts are fixed.



The fluid is considered to be viscous and incompressible. The fluid velocity verifies the Stokes equations and the non-slip condition on the solid boundary.

$$0 = -\nabla P + \mu \Delta \vec{V} \quad \text{in the fluid} \quad (1)$$

$$\nabla \cdot \vec{V} = 0 \quad \text{in the fluid} \quad (2)$$

$$\vec{V} = 0 \quad \text{on the solid boundaries} \quad (3)$$

Here $P = P(x, y)$ is the pressure in the fluid and μ the viscosity coefficient.

The convective-diffusive equation for the solute concentration $C(x, y, t)$ is:

$$\frac{\partial C}{\partial t} + \nabla \cdot (\vec{V}C) = D\Delta C \text{ in } Y_F \quad (4)$$

where D is the diffusion coefficient.

The initial condition:

$$C(x, y, 0) = f(x) \quad (5)$$

where f is a smooth function with a compact support in Ω (the domain occupied by the medium), and the boundary condition:

$$\bar{n}\nabla C = 0 \text{ on the solid boundaries} \quad (6)$$

where \bar{n} indicates a unit vector normal to the surface.

We want to perform an asymptotic analysis to pass from a microscopic description to the effective macroscopic equation.

To analyse this problem the following timescales are defined in [1]:

$$\tau_c = l/V_0, \quad \tau_d = l^2/D, \quad \tau_C = L/V_0, \quad \tau_D = L^2/D \quad (7)$$

where V_0 is the characteristic value of the velocity field. With those timescales one can define two related non-dimensional numbers (the local and global Peclet numbers):

$$Pe = \frac{\tau_d}{\tau_c} = \frac{lV_0}{D}, \quad Pe_L = \frac{\tau_D}{\tau_C} = \frac{LV_0}{D} \quad (8)$$

representing the ratio between convection and diffusion locally and globally.

In the following it will be analysed the case when diffusion and convection are balanced locally, i.e. $Pe=O(1)$ and $Pe_L=O(\frac{1}{\epsilon})$

3 The method of homogenization

3.1 Homogenization with one timescale

In this homogenization procedure time and space variables are scaled according to:

$$x' = \frac{x}{L}, \quad y' = \frac{y}{L} = \frac{x}{l} \quad (9)$$

$$\bar{t} = \frac{t}{\tau_C} \quad (10)$$

The gradient becomes:

$$\nabla = \frac{1}{L}(\nabla_{x'} + \frac{1}{\varepsilon}\nabla_{y'}) \quad (11)$$

We have:

$$C = C(\varepsilon, x', y', \bar{t}), \quad \vec{V} = \vec{V}(\varepsilon, x', y', \bar{t}), \quad f = f(x', y')$$

The non-dimensional convection-diffusion equation will be:

$$\text{Pe} \frac{\partial C}{\partial \bar{t}} + \text{Pe} \frac{\vec{V}}{V_0} (\nabla_{x'} + \frac{1}{\varepsilon} \nabla_{y'}) C = \varepsilon (\nabla_{x'} + \frac{1}{\varepsilon} \nabla_{y'})^2 C \quad (12)$$

Defining $u = \text{Pe} \frac{\vec{V}}{V_0}$ the adimensionalized velocity, (12) becomes:

$$\text{Pe} \frac{\partial C}{\partial \bar{t}} + u (\nabla_{x'} + \frac{1}{\varepsilon} \nabla_{y'}) C = \varepsilon (\nabla_{x'} + \frac{1}{\varepsilon} \nabla_{y'})^2 C \quad (13)$$

In the following we will drop the ' for simplicity.

Expand:

$$\begin{aligned} C &= C^{(0)} + \varepsilon C^{(1)} + \varepsilon^2 C^{(2)} + \dots \\ u &= u^{(0)} + \varepsilon u^{(1)} + \varepsilon^2 u^{(2)} + \dots \end{aligned} \quad (14)$$

We remind that the terms from the asymptotic expansion of the fluid velocity u are obtained by a homogenization method applied to the problem (1)-(3) and it was studied in [4],[5]. So, $u^0 = \vec{V}^0$ with:

$$\vec{V}^0 = -\frac{\partial P^0}{\partial x_i} \vec{v}^i \quad (15)$$

and \vec{v}^i the unique solution, in the weak sense, of the local problem:

$$\begin{cases} \nabla_y \cdot \vec{v}^i = 0 & \text{in } Y_F \\ 0 = -\nabla_y q^i + \mu \Delta_y \vec{v}^i + \vec{e}_i & \text{in } Y_F \\ \vec{v}^i = 0 & \text{on } \Gamma \end{cases}$$

\vec{v}_i and q_i being Y periodic, where \vec{e}_i is the unit vector in the direction of y_i axis.

The Darcy's law, obtained by averaging (15) is:

$$\langle \vec{V}^0 \rangle = -K \nabla_x P^0 \quad (16)$$

where $\langle g \rangle = \frac{1}{|Y|} \int_{Y_F} g dy$ is the cell average of function g and $K_{ij} = \langle v_i^j \rangle$.

$K = (K_{ij})$ is a tensor which depends only on the viscosity coefficient and the geometry of the period Y .

Following the homogenization technique we substitute the expansion (14) in the governing equation (13) and the boundary condition (6). We collect the equal powers of ε . At the leading order $O(\varepsilon^{-1})$ we obtain:

$$\begin{cases} u^0 \nabla_y C^{(0)} - \Delta_y C^{(0)} = 0 & \text{in } Y_F \\ n \nabla_y C^{(0)} = 0 & \text{on } \Gamma \end{cases} \quad (17)$$

(17) has a trivial solution $C^{(0)} = C^{(0)}(x, t)$. This solution is unique. To prove it we multiply the equation (17)₁ with a solution $C^{(0)}$ and integrate on Y_F :

$$\int_{Y_F} u^0 \nabla_y C^{(0)} C^{(0)} dy = \int_{Y_F} \Delta_y C^{(0)} C^{(0)} dy \quad (18)$$

Calculating the left side of the previous equality we obtain by using the Gauss's theorem:

$$\int_{Y_F} u^0 \nabla_y C^{(0)} C^{(0)} dy = - \int_{Y_F} u^0 \nabla_y C^{(0)} C^{(0)} dy$$

Thus,

$$\int_{Y_F} u^0 \nabla_y C^{(0)} C^{(0)} dy = 0$$

Calculating the right side of (18) we have:

$$\int_{Y_F} \Delta_y C^{(0)} C^{(0)} dy = - \int_{Y_F} [\nabla_y C^{(0)}]^2 dy$$

Thus,

$$\int_{Y_F} [\nabla_y C^{(0)}]^2 dy = 0$$

and consequently

$$\nabla_y C^{(0)} = 0 \quad (19)$$

which means that $C^{(0)}$ is constant in y .

At the next order $O(1)$ of equation (13) we have:

$$\begin{cases} \text{Pe} \frac{\partial C^{(0)}}{\partial t} + u^0 \nabla_x C^{(0)} + u^0 \nabla_y C^{(1)} + u^1 \nabla_y C^{(0)} = \\ \quad = 2 \nabla_x \nabla_y C^{(0)} + \Delta_y C^{(1)} & \text{in } Y_F \\ n \nabla_x C^{(0)} + n \nabla_y C^{(1)} = 0 & \text{on } \Gamma \end{cases} \quad (20)$$

and using (19) the problem becomes:

$$\begin{cases} u^0 \nabla_y C^{(1)} - \Delta_y C^{(1)} = -\text{Pe} \frac{\partial C^{(0)}}{\partial t} - u^0 \nabla_x C^{(0)} & \text{in } Y_F \\ n \nabla_y C^{(1)} = -n \nabla_x C^{(0)} & \text{on } \Gamma \end{cases} \quad (21)$$

First of all, we note that the solutions of (21) are defined up to an additive constant function with respect to y and the right side of equation (21)₁ must verify a compatibility condition. To obtain the compatibility condition we integrate on Y_F :

$$\int_{Y_F} (u^0 \nabla_y C^{(1)} - \Delta_y C^{(1)}) dy = \int_{Y_F} \left(-\text{Pe} \frac{\partial C^{(0)}}{\partial t} - u^0 \nabla_x C^{(0)} \right) dy \quad (22)$$

Using the Y periodicity of all functions and the boundary condition (21)₁ we obtain by computing the left side of (22):

$$\int_{Y_F} (u^0 \nabla_y C^{(1)} - \Delta_y C^{(1)}) dy = \int_{\Gamma} n \nabla_x C^{(0)} ds = \left(\int_{\Gamma} n ds \right) \nabla_x C^{(0)}_x = 0$$

Thus,

$$-\text{Pe} \frac{\partial C^{(0)}}{\partial t} = \frac{1}{n} \langle u^0 \rangle \nabla_x C^{(0)} \quad (23)$$

where $n = \frac{|Y_F|}{|Y|}$ is the porosity of the medium.

The condition (23) is also a necessary and sufficient condition for the existence and uniqueness of the solution for (21). To prove this we will give the equivalent variational formulation of this problem and apply the Lax-Milgram lemma.

Let us introduce the space of Y periodic functions:

$$V_y = \{w \in H^1(Y_F), w \text{ is } Y \text{ periodic and } \int_{Y_F} w dy = 0\} \quad (24)$$

which is a Hilbert space with the scalar product of $H^1(Y_F)$. We multiply the equation (21)₁ by a test function $w \in V_y$ and integrate on Y_F . Taking into account the Y periodicity of the functions, the properties $\nabla_y \cdot u^0 = 0$, $u^0 = 0$ on Γ and the condition (23) we obtain:

$$\begin{aligned} \int_{Y_F} u^0 \nabla_y C^{(1)} w dy - \int_{Y_F} \Delta_y C^{(1)} w dy &= \int_{Y_F} \frac{1}{n} \langle u^0 \rangle \nabla_x C^{(0)} w dy - \int_{Y_F} u^0 \nabla_x C^{(0)} w dy \\ \int_{Y_F} \nabla_y w (\nabla_y C^{(1)} - u^0 C^{(1)}) dy &= - \int_{\Gamma} n \nabla_x C^{(0)} w ds + \int_{Y_F} \left(\frac{1}{n} \langle u^0 \rangle - u^0 \right) \nabla_x C^{(0)} w dy \end{aligned}$$

The variational formulation is:

$$\left\{ \begin{array}{l} \text{Find } C^{(1)} \in V_y \text{ such that:} \\ \int_{Y_F} \nabla_y w (\nabla_y C^{(1)} - u^0 C^{(1)}) dy = - \int_{\Gamma} n \nabla_x C^{(0)} w ds + \\ + \int_{Y_F} \left(\frac{1}{n} \langle u^0 \rangle - u^0 \right) \nabla_x C^{(0)} w dy \quad \forall w \in V_y \end{array} \right. \quad (25)$$

To prove the existence and uniqueness of the solution for the problem (25) we will apply the Lax-Milgram lemma. We define the following functionals:

$$a : V_y \times V_y \rightarrow \mathbb{R} \quad (26)$$

$$a(v, w) = \int_{Y_F} \nabla_y v \nabla_y w dy - \int_{Y_F} v u^0 \nabla_y w dy$$

and

$$l : V_y \rightarrow \mathbb{R} \quad (L \in V_y') \quad (27)$$

$$\langle L, w \rangle = - \int_{\Gamma} n \nabla_x C^{(0)} w ds + \int_{Y_F} \left(\frac{1}{n} \langle u^0 \rangle - u^0 \right) \nabla_x C^{(0)} w dy$$

and we must verify that a is a bounded bilinear and coercive functional and L is a bounded linear functional on V_y . By Schwarz's inequality we have the following estimations:

$$\begin{aligned} |a(v, w)| &\leq \int_{Y_F} |\nabla_y v| |\nabla_y w| dy - \int_{Y_F} |v u^0 \nabla_y w| dy \leq \\ &\leq \|\nabla v\|_{L^2(Y_F)} \|\nabla w\|_{L^2(Y_F)} + \|v\|_{L^4(Y_F)} \|\nabla w\|_{L^2(Y_F)} \|u^0\|_{(L^4(Y_F))^3} \end{aligned}$$

Using the immersion Sobolev's inequality:

$$\|u^0\|_{(L^4(Y_F))^3} \leq \|u^0\|_{(H^1(Y_F))^3}$$

and the fact that u^0 is the unique solution (belonging to $(H^1(Y_F))^3$), obtained after resolving the problem (1)-(3) using the homogenization method, we obtain that it exists a constant $B_1 > 0$ such that:

$$|a(v, w)| \leq B_1 \|v\|_{H^1(Y_F)} \|w\|_{H^1(Y_F)} \quad (28)$$

Hence a is bounded. The bilinearity is obvious. For the coercivity we will use the Poincaré's inequality:

$$\int_{Y_F} v^2 dy \leq B_2 \int_{Y_F} |\nabla_y v|^2 dy$$

for all $v \in H^1(Y_F)$ and B_2 a positive number. Thus,

$$\|v\|_{H^1(Y_F)} = \|v\|_{L^2(Y_F)} + \|\nabla v\|_{L^2(Y_F)} \leq (B_2 + 1) \|\nabla v\|_{L^2(Y_F)} \quad (29)$$

If we compute $a(w, w)$ we obtain:

$$a(w, w) = \int_{Y_F} (\nabla_y w)^2 dy - \int_{Y_F} (u^0 \nabla_y w) w dy = \int_{Y_F} |\nabla_y w|^2 dy \quad (30)$$

We used the fact that:

$$\int_{Y_F} (u^0 \nabla_y v) w dy = - \int_{Y_F} (u^0 \nabla_y w) v dy$$

so

$$\int_{Y_F} (u^0 \nabla_y w) w dy = 0$$

Using the inequality (29) and the expression for a from (30) we obtain the coercivity:

$$a(w, w) = \|\nabla v\|_{L^2(Y_F)} \geq \frac{1}{B_2 + 1} \|v\|_{H^1(Y_F)}$$

The linearity of L is trivial. For the boundedness, using the Schwarz's inequality we have the following estimations:

$$\begin{aligned} | \langle L, w \rangle | &= \left| \frac{\partial C^{(0)}}{\partial x_i} \left[- \int_{\Gamma} n_i w ds + \int_{Y_F} \left(\frac{1}{n} \langle u_i^0 \rangle - u_i^0 \right) w dy \right] \right| \leq \\ &\leq (|\nabla_x C^{(0)}|^2)^{1/2} (|Y_F|^{1/2} \|\nabla w\|_{L^2(Y_F)} + \frac{|Y_F|^{1/2}}{n} (|Y_F| \|u_i^0\|_{L^2(Y_F)}^2)^{1/2}) \\ &\quad \cdot \|w\|_{L^2(Y_F)} \|w\|_{L^2(Y_F)} \|u^0\|_{(L^2(Y_F))^3} \end{aligned}$$

For a $C^{(0)}$ such that $|\nabla_x C^{(0)}|^2$ remain bounded it exists a constant $K > 0$ such that:

$$| \langle L, w \rangle | \leq K \|w\|_{H^1(Y_F)} = K \|w\|_{V_y}$$

The hypothesis of Lax-Milgram lemma are satisfied so the problem (25) has a unique solution.

In order to solve the problem (21) we search a solution of the following form:

$$C^{(1)} = \chi(y) \nabla_x C^{(0)}(x, t) + \bar{C}^1(x, t) \quad (31)$$

with $\chi(y)$ the solution of the following cell problem:

$$\begin{cases} (u^0 \nabla_y) \chi - \Delta_y \chi = \frac{1}{n} \langle u^0 \rangle - u^0 & \text{in } Y_F \\ (n \nabla_y) \chi = -n & \text{on } \Gamma \\ \chi & Y \text{ periodic} \end{cases} \quad (32)$$

If χ is a solution of the cell problem than $C^{(1)}$ defined by (31) will be a solution of (21). The solution of the problem (32) is determined only within an arbitrary additive constant vector. In consequence, we may assume the normalization condition:

$$\langle \chi \rangle = 0 \quad (33)$$

At the order $O(\varepsilon)$ we have:

$$\begin{cases} u^0 \nabla_y C^{(2)} - \Delta_y C^{(2)} = -Pe \frac{\partial C^{(1)}}{\partial t} - u^0 \nabla_x C^{(1)} - u^1 \nabla_x C^{(0)} \\ \quad - u^1 \nabla_x C^{(1)} + \Delta_x C^{(0)} + 2 \nabla_x \nabla_y C^{(1)} & \text{in } Y_F \\ n \nabla_y C^{(2)} = -n \nabla_x C^{(1)} & \text{on } \Gamma \end{cases} \quad (34)$$

The necessary and sufficient condition for the existence and unicity of the solution of problem (34) will be:

$$\int_{Y_F} (u^0 \nabla_y C^{(2)} - \Delta_y C^{(2)}) dy = \int_{Y_F} (-Pe \frac{\partial C^{(1)}}{\partial \bar{t}} - u^0 \nabla_x C^{(1)} - u^1 \nabla_x C^{(0)} - u^1 \nabla_x C^{(1)} + \Delta_x C^{(0)} + 2 \nabla_x \nabla_y C^{(1)}) dy$$

which becomes:

$$Pe < \frac{\partial \bar{C}^1}{\partial \bar{t}} > = D_{ij} \frac{\partial^2 C^{(0)}}{\partial x_i \partial x_j} - < u^1 > \nabla_x C^{(0)} - < u^0 > \nabla_x \bar{C}^1 \quad (35)$$

where

$$D_{ij} = n \delta_{ij} + \frac{2}{|Y|} \int_{Y_F} \frac{\partial \chi_j}{\partial y_i} dy - \frac{1}{|Y|} \int_{Y_F} u_i^0 \chi_j dy - \frac{1}{|Y|} \int_{\Gamma} n_i \chi_j ds$$

If we compute $\frac{\partial < C >}{\partial \bar{t}}$ up to $O(\varepsilon)$ we will obtain:

$$\frac{\partial < C >}{\partial \bar{t}} = \frac{V_0}{L} \frac{\partial < C >}{\partial \bar{t}} = \frac{V_0}{L} \left(\frac{\partial < C^{(0)} >}{\partial \bar{t}} + \varepsilon \frac{\partial < \bar{C}^1 >}{\partial \bar{t}} \right)$$

Using (35) and (23) in the above equality we obtain:

$$\frac{\partial < C >}{\partial \bar{t}} + \frac{1}{nPe} < u > \nabla_x < C > = \frac{\varepsilon}{nPe} D_{ij} \frac{\partial^2 < C >}{\partial x_i \partial x_j} \quad (36)$$

where the variable x is in fact the non-dimensional variable x' . If we come back to the dimensional variables we obtain the macroscopic convection-diffusion equation in dimensional form:

$$n \frac{\partial < C >}{\partial t} + < V > \nabla_x < C > = D_{ij}^* \frac{\partial^2 < C >}{\partial x_i \partial x_j} \quad (37)$$

where $D_{ij}^* = D D_{ij}$. The symmetric part of D_{ij}^* can be expressed in the following form:

$$\begin{aligned} \bar{D}_{ij}^* &= \frac{D}{2} (D_{ij} + D_{ji}) = D \left[n \delta_{ij} + \frac{1}{|Y|} \int_{Y_F} \left(\frac{\partial \chi_j}{\partial y_i} + \frac{\partial \chi_i}{\partial y_j} \right) dy - \right. \\ &\quad \left. - \frac{1}{2|Y|} \int_{Y_F} (u_i^0 \chi_j + u_j^0 \chi_i) dy - \frac{1}{2|Y|} \int_{\Gamma} (n_i \chi_j + n_j \chi_i) ds \right] \end{aligned}$$

Multiplying the equation for χ_j by χ_i and integrating on Y_F we obtain:

$$\int_{Y_F} u^0 \nabla_y \chi_j \chi_i dy - \int_{Y_F} \Delta_y \chi_j \chi_i dy = \int_{Y_F} \frac{1}{n} \langle u_j^0 \rangle \chi_i dy - \int_{Y_F} u_j^0 \chi_i dy \quad (38)$$

Using the Y periodicity and the boundary conditions, (38) becomes:

$$\int_{Y_F} u_j^0 \chi_i dy = - \int_{Y_F} u^0 \nabla_y \chi_i \chi_j dy - \int_{\Gamma} n_j \chi_i ds - \int_{Y_F} \nabla_y \chi_j \nabla_y \chi_i dy$$

which, introduced in the expression of \bar{D}_{ij}^* , gives:

$$\bar{D}_{ij}^* = D \left[n \delta_{ij} + \frac{1}{|Y|} \int_{Y_F} \left(\frac{\partial \chi_j}{\partial y_i} + \frac{\partial \chi_i}{\partial y_j} \right) dy + \frac{1}{|Y|} \int_{Y_F} \nabla_y \chi_j \nabla_y \chi_i dy \right] \quad (39)$$

If we define:

$$B_j = -y_j - \chi_j \quad (40)$$

than \bar{D}_{ij}^* can be expressed:

$$\bar{D}_{ij}^* = D \langle \nabla B_i \nabla B_j \rangle$$

with B_i the solution of the following cell problem:

$$\begin{cases} \Delta_y B_i - u^0 \nabla_y B_i = \frac{1}{n} \langle u_i^0 \rangle & \text{in } Y_F \\ n \nabla_y B_i = 0 & \text{on } \Gamma \\ B & Y\text{-periodic} \end{cases} \quad (41)$$

Because $\langle \chi \rangle = 0$ we will have $\langle B \rangle = - \langle y \rangle$ and so, the problem for B will be:

$$\begin{cases} \Delta_y B - (u^0 \nabla_y) B = \frac{1}{n} \langle u^0 \rangle & \text{in } Y_F \\ (n \nabla_y) B = 0 & \text{on } \Gamma \\ \langle B \rangle = - \langle y \rangle \\ B & Y\text{-periodic} \end{cases} \quad (42)$$

3.2 Homogenization with double timescale

In this section we will obtain the macroscopic convection-diffusion equation following the idea of Auriault, Mei and Chin [3]. Namely, we will make the same study as in section 3.1, but using two timescales :

$$T_1 = \frac{t}{\tau_C} = t \frac{V_0}{L}, \quad T_2 = \frac{t}{\tau_D} = t \frac{D}{L^2} \quad (43)$$

considered as independent. We obtain the following boundary value problem:

$$\begin{cases} \left(\frac{\partial}{\partial T_2} + \frac{Pe}{\varepsilon} \frac{\partial}{\partial T_1} \right) C + \frac{1}{\varepsilon} u (\nabla_x + \frac{1}{\varepsilon} \nabla_y) C = (\nabla_x + \frac{1}{\varepsilon} \nabla_y)^2 C & \text{in } Y_F \\ n(\nabla_x + \frac{1}{\varepsilon} \nabla_y) C = 0 & \text{on } \Gamma \end{cases} \quad (44)$$

After expanding u and C with (14) and equating the coefficients of like powers of ε we have the boundary value problems:

$$\begin{cases} u^0 \nabla_y C^{(0)} - \Delta_y C^{(0)} = 0 & \text{in } Y_F \\ n \nabla_y C^{(0)} = 0 & \text{on } \Gamma \end{cases} \quad (45)$$

at the order $O(\varepsilon^{-2})$,

$$\begin{cases} u^0 \nabla_y C^{(1)} - \Delta_y C^{(1)} = -Pe \frac{\partial C^{(0)}}{\partial T_1} - u^0 \nabla_x C^{(0)} - u^1 \nabla_y C^{(0)} + \\ \quad 2 \nabla_x \nabla_y C^{(0)} & \text{in } Y_F \\ n \nabla_y C^{(1)} = -n \nabla_x C^{(0)} & \text{on } \Gamma \end{cases} \quad (46)$$

at $O(\varepsilon^{-1})$ and at $O(1)$:

$$\begin{cases} u^0 \nabla_y C^{(2)} - \Delta_y C^{(2)} = -\frac{\partial C^{(0)}}{\partial T_2} - Pe \frac{\partial C^{(1)}}{\partial T_1} - u^0 \nabla_x C^{(1)} - u^1 \nabla_x C^{(0)} - \\ \quad -u^1 \nabla_y C^{(1)} - u^2 \nabla_y C^{(1)} + \Delta_x C^{(0)} + 2 \nabla_x \nabla_y C^{(1)} & \text{in } Y_F \\ n \nabla_y C^{(2)} = -n \nabla_x C^{(1)} & \text{on } \Gamma \end{cases} \quad (47)$$

The problem for $C^{(0)}$ is the same that in the above section, hence its solution will be $C^{(0)} = C^{(0)}(x, T_1, T_2)$.

Using the fact that $C^{(0)}$ does not depend on y , the problem (46) becomes:

$$\begin{cases} u^0 \nabla_y C^{(1)} - \Delta_y C^{(1)} = -Pe \frac{\partial C^{(0)}}{\partial T_1} - u^0 \nabla_x C^{(0)} & \text{in } Y_F \\ n \nabla_y C^{(1)} = -n \nabla_x C^{(0)} & \text{on } \Gamma \end{cases} \quad (48)$$

The solvability condition for (48) will be:

$$-Pe \frac{\partial C^{(0)}}{\partial T_1} = \frac{1}{n} \langle u^0 \rangle \nabla_x C^{(0)} \quad (49)$$

We look for solution of problem (48) of the form:

$$C^{(1)} = \chi(y) \nabla_x C^{(0)}(x, T_1, T_2) + \bar{C}^1(x, T_1, T_2) \quad (50)$$

where the vector function $\chi(y)$ is the unique solution of the problem (32), satisfying the normalization condition $\langle \chi \rangle = 0$.

We study now the problem at the next order $O(1)$, which now has the following formulation :

$$\begin{cases} u^0 \nabla_y C^{(2)} - \Delta_y C^{(2)} = -\frac{\partial C^{(0)}}{\partial T_2} - Pe \frac{\partial C^{(1)}}{\partial T_1} - u^0 \nabla_x C^{(1)} - u^1 \nabla_x C^{(0)} - \\ \quad - u^1 \nabla_x C^{(1)} + \Delta_x C^{(0)} + 2 \nabla_x \nabla_y C^{(1)} \quad \text{in } Y_F \\ n \nabla_y C^{(2)} = -n \nabla_x C^{(1)} \quad \text{on } \Gamma \end{cases} \quad (51)$$

The solvability condition for the equations (51) will be:

$$\int_{Y_F} (u^0 \nabla_y C^{(2)} - \Delta_y C^{(2)}) dy = \int_{Y_F} \left(-\frac{\partial C^{(0)}}{\partial T_2} - Pe \frac{\partial C^{(1)}}{\partial T_1} - u^0 \nabla_x C^{(1)} - \right. \quad (52) \\ \left. - u^1 \nabla_x C^{(0)} - u^1 \nabla_x C^{(1)} + \Delta_x C^{(0)} + 2 \nabla_x \nabla_y C^{(1)} \right) dy$$

If we compute the left hand side we find:

$$\int_{Y_F} (u^0 \nabla_y C^{(2)} - \Delta_y C^{(2)}) dy = \left(\int_{\Gamma} n_i \chi_j ds \right) \frac{\partial^2 C^{(0)}}{\partial x_i \partial x_j}$$

We have used the Y periodicity, the boundary condition $u = 0$ on Γ , the incompressibility of fluid flow, the condition (51)₂ and the fact that $\int_{\Gamma} n ds = 0$.

The right hand side becomes:

$$\begin{aligned} \int_{Y_F} \left[-\frac{\partial C^{(0)}}{\partial T_2} - Pe \frac{\partial C^{(1)}}{\partial T_1} - u^0 \nabla_x C^{(1)} - u^1 \nabla_x C^{(0)} - u^1 \nabla_x C^{(1)} + \Delta_x C^{(0)} + 2 \nabla_x \nabla_y C^{(1)} \right] dy = \\ = -|Y_F| \frac{\partial C^{(0)}}{\partial T_2} - |Y_F| Pe \frac{\partial C^{(1)}}{\partial T_1} - \left(\int_{Y_F} u_i^0 \chi_j dy \right) \frac{\partial^2 C^{(0)}}{\partial x_i \partial x_j} - |Y| \langle u^0 \rangle \nabla_x C^{(1)} - \end{aligned}$$

$$-|Y| \langle \mathbf{u}^1 \rangle \cdot \nabla_x C^{(0)} + |Y_F| \Delta_x C^{(0)} + 2 \left(\int_{Y_F} \frac{\partial \chi_j}{\partial y_i} dy \right) \frac{\partial^2 C^{(0)}}{\partial x_i \partial x_j}$$

Thus, (52) becomes:

$$n \frac{\partial C^{(0)}}{\partial T_2} = D_{ij} \frac{\partial^2 C^{(0)}}{\partial x_i \partial x_j} - \langle \mathbf{u}^1 \rangle \cdot \nabla_x C^{(0)} - \langle \mathbf{u}^0 \rangle \cdot \nabla_x \bar{C}^1 - n \text{Pe} \frac{\partial \bar{C}^1}{\partial T_1} \quad (53)$$

$$\frac{\partial \langle C \rangle}{\partial t} = \frac{\partial \langle C^{(0)} \rangle}{\partial t} + \varepsilon \frac{\partial \langle C^{(1)} \rangle}{\partial t} = \frac{D}{L^2} \left[\frac{1}{\varepsilon} \text{Pe} \frac{\partial C^{(0)}}{\partial T_1} + n \frac{\partial C^{(0)}}{\partial T_2} + n \text{Pe} \frac{\partial \bar{C}^1}{\partial T_1} \right]$$

at the order $O(1)$. Using (49) and (53) we get:

$$\frac{\partial \langle C \rangle}{\partial t} = \frac{D}{L^2} \left[D_{ij} \frac{\partial^2 C^{(0)}}{\partial x_i \partial x_j} - \langle \mathbf{u}^1 \rangle \cdot \nabla_x C^{(0)} - \langle \mathbf{u}^0 \rangle \cdot \nabla_x \bar{C}^1 - \frac{1}{\varepsilon} \langle \mathbf{u}^0 \rangle \cdot \nabla_x C^{(0)} \right]$$

But

$$\frac{1}{\varepsilon} \langle \mathbf{u}^0 \rangle \cdot \nabla_x \langle C \rangle = n \frac{1}{\varepsilon} \left[\langle \mathbf{u}^0 \rangle \cdot \nabla_x C^{(0)} + \varepsilon \langle \mathbf{u}^1 \rangle \cdot \nabla_x C^{(0)} + \varepsilon \langle \mathbf{u}^0 \rangle \cdot \nabla_x \bar{C}^1 \right]$$

at the order $O(1)$. Hence:

$$\frac{\partial \langle C \rangle}{\partial t} = \frac{D}{L^2} \left[D_{ij} \frac{\partial^2 C^{(0)}}{\partial x_i \partial x_j} - \frac{1}{n\varepsilon} \langle \mathbf{u} \rangle \cdot \nabla_x \langle C \rangle \right]$$

The effective equation in dimensional form will be:

$$n \frac{\partial \langle C \rangle}{\partial t} + \langle \tilde{\mathbf{V}} \rangle \cdot \nabla_x \langle C \rangle = D_{ij}^* \frac{\partial^2 \langle C \rangle}{\partial x_i \partial x_j} \quad (54)$$

that is the same effective equation obtained by homogenization with a single timescale.

We notice that we have computed $n \frac{\partial \langle C \rangle}{\partial t}$ up to $O(\varepsilon)$ in the following way: in the first case

$$\begin{aligned} \frac{\partial \langle C \rangle}{\partial t} &= \frac{V_0}{L} \left(\frac{\partial \langle C^{(0)} \rangle}{\partial \bar{t}} + \varepsilon \frac{\partial \langle \bar{C}^1 \rangle}{\partial \bar{t}} \right) = \\ &= \frac{D}{L^2} \left(\text{Pe} \frac{\partial \langle C^{(0)} \rangle}{\partial \bar{t}} + \varepsilon \text{Pe} \frac{\partial \langle \bar{C}^1 \rangle}{\partial \bar{t}} \right) \end{aligned} \quad (55)$$

with

$$\begin{cases} \text{Pe} \frac{\partial \langle C^{(0)} \rangle}{\partial t} = - \langle \mathbf{u}^0 \rangle \cdot \nabla_x C^{(0)} \\ \text{Pe} \frac{\partial \langle \tilde{C}^1 \rangle}{\partial t} = D_{ij} \frac{\partial^2 C^{(0)}}{\partial x_i \partial x_j} - (\langle \mathbf{u}^1 \rangle \cdot \nabla_x C^{(0)} + \langle \mathbf{u}^0 \rangle \cdot \nabla_x \tilde{C}^1) \end{cases} \quad (56)$$

while in the second method

$$\frac{\partial \langle C \rangle}{\partial t} = \frac{D}{L^2} \left[\frac{1}{\varepsilon} \text{Pe} \frac{\partial \langle C^{(0)} \rangle}{\partial T_1} + \frac{\partial \langle C^{(0)} \rangle}{\partial T_2} + \text{Pe} \frac{\partial \langle \tilde{C}^1 \rangle}{\partial T_1} \right] \quad (57)$$

with

$$\begin{cases} \text{Pe} \frac{\partial \langle C^{(0)} \rangle}{\partial T_1} = - \langle \mathbf{u}^0 \rangle \cdot \nabla_x C^{(0)} \\ \frac{\partial \langle C^{(0)} \rangle}{\partial T_2} + \text{Pe} \frac{\partial \langle \tilde{C}^1 \rangle}{\partial T_1} = D_{ij} \frac{\partial^2 C^{(0)}}{\partial x_i \partial x_j} - (\langle \mathbf{u}^1 \rangle \cdot \nabla_x C^{(0)} + \langle \mathbf{u}^0 \rangle \cdot \nabla_x \tilde{C}^1) \end{cases} \quad (58)$$

The conclusion is that, under the assumption that the characteristic velocity $V_0 = O(\varepsilon^2)$ (V_0 being the norm of \vec{V}_0 given by Darcy's law) which means that the macroscopic characteristic time $\tau_C = O(\varepsilon^{-2})$, there is no need to use the time scale $T_2 = O(\varepsilon^3)$ in the homogenization method in order to obtain the macroscopic convection-diffusion equation.

As it can be seen from (56) and (58) we can conclude that $C^{(0)}$ does not depend on T_2 , which is the time scale through the macroscopic diffusion characteristic time $\tau_D = O(\varepsilon^{-3})$. We also observe that if at the microscopic level the convection and diffusion are balanced, at the macroscopic level the convection will domine the diffusion.

References

- [1] J. Rubinstein and R. Mauri, Siam.J.Appl.Math., vol 46, no. 6, December 1986, pag 1018-1023
- [2] R. Mauri, Journal of Engineering Mathematics 29, 1995, pag 77-78
- [3] Chiang C. Mei, J.L. Auriault, Chin On Ng, Advances in applied mechanics, vol 32, 1996, pag 278-345
- [4] E. Sanchez-Palencia. Non Homogenous Media and Vibration Theory, Lecture Notes in Physics, no 127, Springer-Verlag, 1980
- [5] T. Lévy and E. Sanchez-Palencia, Int.J.Eng.Sci, vol 13,1975, pag 923-940

COMPUTER ANALYSIS AND SIMULATION OF TRANSIENT STATE AND PRESSURE RECOVERING IN FAST CYCLIC HYDRAULIC ACTUATORS

J.M. Janković

Aerospace Department, Faculty of Mechanical Engineering, University of Belgrade, F.R. Yugoslavia

ABSTRACT

In the paper is presented computer analysis of fast cyclic hydraulic servo-actuator transient state between its engage and full pressure recovering. In different mathematical forms hydraulic actuator dynamic model is assumed without any geometrical and physical discontinuities and ambiguity of initial pressure conditions. Fast cyclic hydraulic actuator can be assumed with two serial connected compressible fluid flows controlled by supply and return variable fluid flow restrictors enclosed in control servo-valve and separated by actuator piston, expressed by equivalent mass, viscous damping and arbitrary external force. Presented mathematical model includes transient state of fast cyclic hydraulic actuator, which can be described and determined by ambiguity of the initial pressure conditions in actuator chambers as result of the final state of its previous operations and existing fluid leakage which can produce arbitrary value of initial pressure. Initial condition of pressure is primarily caused by external force, which is arbitrary value during actuator operations. Relatively small pressure surge in the moment of change direction of piston motion as result of geometric and flow asymmetry of actuator and its control servo-valve is included in the model also.

INTRODUCTION

Hydraulic actuator is usually assumed with compressible fluid flow including the effects of its viscosity. Fluid compressibility is assumed as quasi-static change of its density depending of static pressure. Each of the mentioned effects produces local pressure drop and surge and corresponding actuator operational time delay, which is the limiting factor of its cyclic velocity. Dominant influence on actuators time delay (less than 3% of unit step discrete control piston stroke time) is caused by fluid volumetric compressibility.

In the paper following problems are treated:

- pressure discontinue changes in reverse of piston motion direction;
- nonlinear effects of actuator behavior and linearisation of its dynamic model.

EFFECTS OF SYSTEM DISCONTINUITIES

Any direction change of actuator motion produces pressure discontinuity in its source and return pipelines. This is caused by inversion of fluid flow which produce connection change between supply pipeline and actuator chambers. In the moment of fluid flow direction change each of actuator chambers inter-change connections with system pump and return pipeline and produce corresponding discrete change of pressure in actuator chambers. Possible pressure drop or surge is also caused by geometric asymmetry of servo valve. These effects are explained on the following figures.

On figure 1 is shown actuator motion asymmetry between direct and reverse modes. This asymmetry is result of pressure distribution along supply and return streamlines, shown on diagrams a) and c) on figure 3. Diagram a) corresponds to direct mode of actuator function represented by symmetrical pressure drops at supply and return branches of its servo-valve. The third step of pressure drop corresponds to the applied external force. On diagram c) is shown pressure distribution for reverse actuator mode. Main difference between these modes is in opposite directions of external force related to the streamline of fluid flow. For reverse mode external force support system pump as additional serial connected system source. This fact appears on figure 1 as different curve gradient for direct and reverse modes. However, absolute value of gradient is greater for reverse mode. More data about gradient value will be shown corresponding to the figure 6.

On figure 2 is presented actuator output on servo-valve control input assumed as transient step unit function. This approximation is very close to the real situation for digitally controlled actuators.

On diagrams b) and d) of figure 3 are shown, respectively, equivalent pressure drops for direct and reverse actuator modes corresponding to the conventional mathematical modeling of hydraulic actuator with total pressure drop on servo-valve by neglecting effects at its supply and return parts as two separated fluid flows. This usual approximation cannot be accepted if system model includes effects of hydraulic pressure drop and surge caused by fluid compressibility.

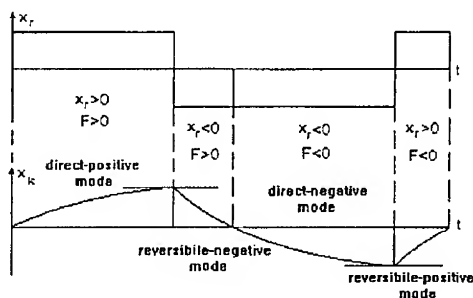


Fig. 1

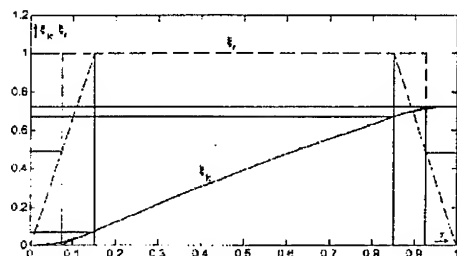


Fig. 2

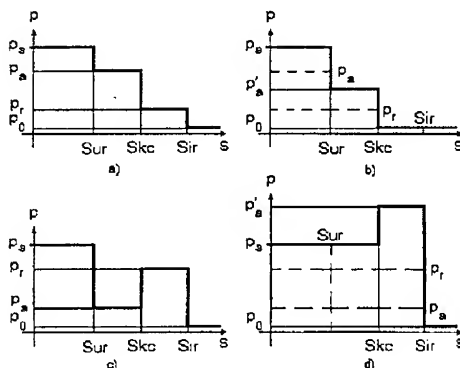


Fig. 3

CONVENTIONAL SYSTEM MODELING

Real state is described by pressure drop at supply and return parts of control servovalve and

corresponding pressure difference caused by external force:

$$\Delta p_{ul} = p_s - p_a \quad (1)$$

$$\Delta p_{iz} = p_r - p_0$$

$$p_a - p_r = \frac{|F|}{A_k} \operatorname{sgn}(F x_r) \quad (2)$$

where are: p_s supply static pressure, p_a static pressure in active chamber, p_r static pressure in return chamber of actuator cylinder, p_0 static pressure of return pipeline, F external force, x_r control of hydraulic relay and A_k equivalent area of the actuator piston. Function sgn denotes both directions of external load action, represented as direct and reverse modes of actuator function. Equations (1) and (2) defines basic formulation of system dynamic model. Closed formulation of mentioned pressure drops cannot be determined without additional approximations. If we assume that fluid flow through servo-valve is a turbulent, approximate expressions of corresponding equivalent pressure differences in accordance to the figures b) and d) are defined for incompressible fluid flow by following relations:

$$Q_s = Q_0 = \pm A_k \dot{x}_k = \pm \mu^* b_r^* x_r \sqrt{\frac{2}{\rho} (p_s - p_a')} \quad (3)$$

$$Q_s = Q_0 = \pm A_k \dot{x}_k = \mu^* b_r^* x_r \sqrt{\frac{2}{\rho} (p_r' - p_0)}$$

where are: Q_s supply fluid flow, Q_0 return fluid flow, x_k position of actuator piston, ρ fluid density, μ flow coefficient of actuator input and output relay and b_r equivalent wide of relay. Equivalent pressure values for direct and reverse modes are defined in the form:

$$p_r' = p_F + p_s$$

$$p_a' = p_F + p_0$$

SEPARATE FLOW MODELING

Previous relations (1) and (2) can be expanded for approximately symmetric supply and return flow characteristics of servo-valve in the following form (with assumed value of $p_0=0$) for direct and reverse modes:

$$p_a = p_s - \Delta p = \frac{1}{2} \left(p_s \pm \frac{F}{A_k} \right) \quad (4)$$

$$p_r = p_0 + \Delta p = \frac{1}{2} \left(p_s \mp \frac{F}{A_k} \right)$$

Corollary of expressions (4) is that nominal system pressure for zero external load is defined as

$$p_{sr} = \frac{p_s + p_0}{2} \quad (5)$$

It means that hydraulic system pressure for zero load must be equal to the p_{sr} . In the cases of continuous actuator function previous relation holds. In addition, this expression are satisfied for all regimes in which effects of pressure surge can be neglected. In opposite cases, presented mathematical system formulation does not hold. Then subjected mathematical model is not compatible. Corresponding to the relations (4) pressure drop can be determined in the form:

$$Q_s = Q_0 = A_k \dot{x}_k = \mu^+ b_r^+ x_r \sqrt{\frac{2}{\rho} (p_s - p_0 - p_F)} \quad (6)$$

$$Q_s = Q_0 = -A_k \dot{x}_k = -\mu^- b_r^- x_r \sqrt{\frac{2}{\rho} (p_s - p_0 + p_F)}$$

where p_F represent pressure drop caused by external load:

$$p_F = \pm \frac{F}{A_k} \quad (7)$$

Finally, static pressure in supply and return branches of actuator streamline can be expressed in expanded form:

$$p_s = \frac{1}{2} \left(p_s + p_0 + \frac{F}{A_k} \operatorname{sgn} x_r \right) \quad (8)$$

$$p_r = \frac{1}{2} \left(p_s + p_0 - \frac{F}{A_k} \operatorname{sgn} x_r \right)$$

Relations (8) are similar to the relations (4). In previous discussion hydraulic system pump is assumed as strong one. It means that the system pump is able to takes up system supply pressure to the maximal nominal value. This assumption is valid except for existence of system model incompatibilities. This problem can be solved by assuming system pump as a weak one at the initial moment of actuator engage. It follows that any regime of small external load must be assumed as of weak pump. This statement arise from the fact that static pressure in hydraulic system at any moment of its function is caused by external load and pressure loses. As consequence of previous statements, corresponding boundary conditions at actuator pipeline inlet must be determined at initial moment as maximal pump flow. Caused value of system static

pressure exists till the moment of pressure upgrading to its nominal system value. In that moment boundary conditions changes to the determined inlet pressure (equal maximal nominal value) and caused value of fluid flow (second part of flow cross the relive valve), which corresponds to the strong system pump.

If reducing valve is built in hydraulic system at actuator supply branch mentioned effects decreases. But in initial moment of actuator engage they cannot vanish completely. It means that each pump can't be strong one for the whole possible regimes, spatially at its initial moment.

BOUNDARY CONDITIONS

Corresponding actuator block diagrams for the cases of weak and strong system pump are presented on following figure 4.

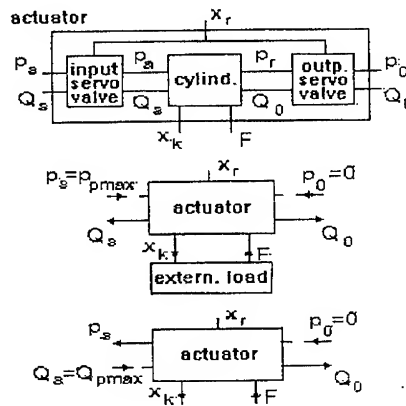


Fig.4

For geometric and flow symmetry of control servo-valve previous relations can be expressed in the form

$$A_k \dot{x}_k = \mu^+ b_r^+ x_r \sqrt{\frac{2}{\rho} (p_{pmax} - p)} \quad (9)$$

$$A_k \dot{x}_k = \mu^- b_r^- x_r \sqrt{\frac{2}{\rho} (p_{pmax} + p)}$$

or in expanded form:

$$A_k \dot{x}_k = \mu^s b_r^s x_r \sqrt{\frac{2}{\rho} \left(p_{pmax} - \frac{F}{A_k} \operatorname{sgn} x_r \right)} \quad (10)$$

where index s denotes parameters of symmetric servo-valve. Relation (10) is final mathematical model form of control servo-valve pressure drop for

the case of actuator symmetry. This formulation is well known. It must be noted that p_{pmax} is correct term only for strong system pump. For the cases of weak pump p_{pmax} becomes equal p_s , with corresponding changes of boundary conditions formulation, which gives following system model:

$$Q_{pmax} = A_k \dot{x}_k$$

$$Q_{pmax} = \mu^s b'_s x_l \sqrt{\frac{2}{\rho} (p_{pmax} - \frac{F}{A_k} \text{sgn } x_l)} \quad (11)$$

ACTUATOR MODELING WITH ASSUMED QUASI-STATIC FLUID COMPRESSIBILITY

Pressure drop in hydraulic systems can be caused by small external load or local increasing of fluid flow to be greater than maximal possible pump source flow. To prevent this it is suggested to separate corresponding branch of actuator supply by corresponding reducing valve. In these cases possible pressure surge are not of high influence and is determined by equivalent actuator stiffness together with potential external load. Pressure increases proportionally with piston displacement corresponding to its velocity. This pressure increasing is too slower than for the cases of pressure surge caused by fluid compressibility.

If actuator is assumed with quasistatic compressible fluid flow, system model can be presented for symmetric supply and return branch of fluid flow in the following form:

$$\mu b' x_l \sqrt{\frac{2}{\rho} (p_s - p_a)} =$$

$$= A_k \dot{x}_k \pm \beta A_k (H_{cl} \theta + x_k) \dot{p}_a + c(p_a - p_r)$$

$$\mu b' x_l \sqrt{\frac{2}{\rho} (p_r - p_0)} =$$

$$= A_k \dot{x}_k \mp \beta A_k (H_{cl} \theta - x_k) \dot{p}_a + c(p_a - p_r)$$

$$F = A_k (p_a - p_r) \quad (12)$$

where are: μ flow coefficient, b' equivalent geometric wide, x_l position of control valve throttle, p_s supply pressure of hydraulic system pump, p_a static pressure in supply chamber of actuator cylinder, p_r static pressure in return chamber of actuator cylinder, p_0 static pressure in return pipeline, A_k area of actuator piston, β coefficient of fluid compressibility, c coefficient of fluid leakage, H_{cl} piston stroke, θ coefficient of parasite volume of connected pipeline to actuator cylinder, x_k position of

piston and F applied external force (including inertia forces) to the actuator piston. Both signs in equations corresponds to the direct and reverse modes of actuator function.

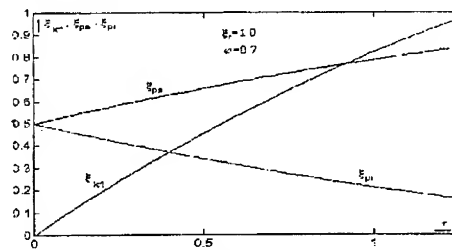


Fig.5

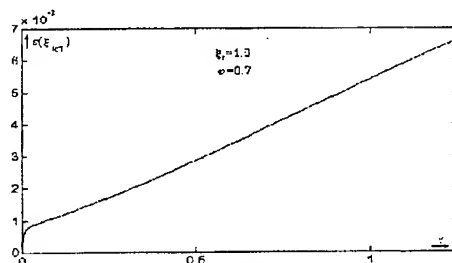


Fig.6

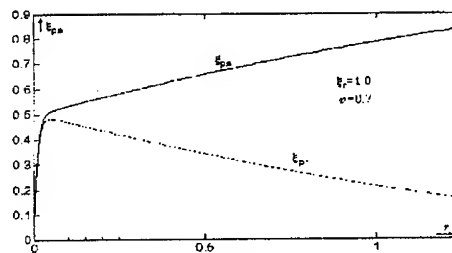


Fig.7

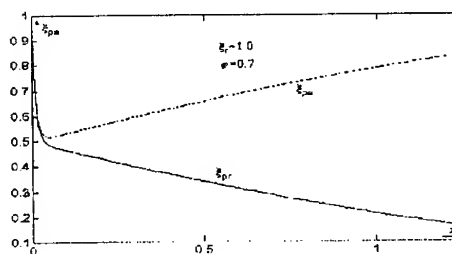


Fig.8

On figure 5 are presented simulation of actuator piston relative stroke and static pressure ratio in supply and return actuator chambers for usual mathematical form of actuator dynamic model. Initial pressure ratio values (equal 0.5) can exists in ideal

model only. In real cases, initial values of relative pressure in actuator chambers is the result of actuator history and fluid leakage, which produces it's ambiguity. Extreme case corresponds to the zero and unit values of initial pressure ratio. Corresponding simulation of supply and return pressure ratio are presented on figures 7 and 8.

All of the exposed diagrams are related to nondimensional ratio system coordinates, where are: x_{k1} piston position, x_{ps} static pressure in actuator supply chamber, x_{pr} static pressure in actuator return chamber, x_c control servovalve throttle position, q ratio of power reserve corresponding to applied external load. Presented system model enables its compatibility corresponding to the various initial conditions. On figure 5 are shown system simulation for incompressible fluid flow and corresponding model noncompatibility of initial conditions. Possible pressure difference between supply and return actuator chambers which is not compensated by external force produces piston "shock" motion, which can not be described by incompressible flow system modeling. Pressure difference can be caused by various effects which produces fast changes of fluid static pressure. Actuator locked position for longer time period is the reason for described effects also. Pressure drop or surge caused by fluid compressibility and initial condition discontinuity as result of closed control servo-valve throttle position are shown on the diagrams on figures 7 and 8. Piston position difference in relation with its incompressible model motion is defined on figure 6. Initial piston acceleration produces in practice piston shock motion, expressed in the later as increasing static error of its position (less than 1% for usual types of fluids). Mentioned effects are of high interest for digitally driven actuators. Supply and return pressure surge is presented on figure 7. Supply and return pressure drop are presented on figure 8. Because presented system model does not include previously explained real wave effects it is important to establish model in which corresponding effects are compatibly involved [3].

CONCLUSION

In difference with the facts presented in the paper [3], shown mathematical model of hydraulic actuator behavior is based on classical concept including quasistatic fluid compressibility, but involving the real actuator structure asymmetry and corresponding pressure and flow discontinuities as result of real actuator geometry. By neglecting these effects, it is possible to obtain the well known usual form of hydraulic actuator dynamic model.

REFERENCES

1. W. L Green, "Aircraft Hydraulic Systems", John Wiley and sons, UK, 1985;
2. G. Rudinger, "Wave Diagrams for Nonsteady Flow in Ducts", D. Van Nostrand company, Inc, Canada, 1955.
3. J. Jankovic, "Active Control of Static Pressure Drop and Expansion Wave Propagation in Hydraulic Pipelines Caused By Servo-actuator Engage", Bull. of Appl. Math., Budapest, Hungary, 1996.

Numerical Simulation of Euler Flows with Mach Effect

O. MANOLE and D. PANTAZOPOL

National Institute for Aerospace Research, Bd. Păcii 220, 77538 Bucharest, Romania

The paper presents an application of an unsteady Euler solver to simulate complex supersonic flow in which Mach effect is produced. The computational domain is discretized using an unstructured triangle based grid. The numerical method used to solve the Euler equation is a finite volume method based on the Steger-Warming flux splitting technique. Two geometries are investigated: channel with solid walls and a channel having a new modified boundary condition prescribed over a portion of the inferior wall. The numerical computed flow fields agree well with the experimental Schlieren photos. It is shown that the second geometry allows a simple modification of the flow configuration and can serve as a design tool for practical purposes.

Introduction

Supersonic flows in which Mach effect is produced have received greater attention in the last years. This interest is due to the research efforts made for obtaining a stable combustion in supersonic flows with minimum losses. A first step in this direction is to obtain a flexible method to simulate this type of flows.

Under certain flow conditions, the reflection of a shock wave at a wall leads to the situation sketched in Fig. 1. A supersonic, $M > 1$, flow in a channel forms an irregular reflection, called Mach effect, if the pressure ratio p_1/p_2 satisfies a certain correlation with the inflow Mach number. In Fig. 1 OP is the incident oblique shock wave corresponding to M and θ , OR is the reflected shock wave, OS is a shock wave which is very close to the normal at the wall from O and OV is a vortex sheet which evolves from point O.

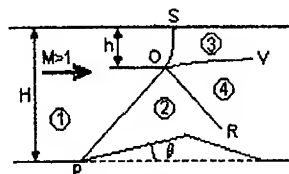


Fig. 1. Mach reflection - sketch

The flow around point O is highly complex but can be computed in a direct manner if at least an Euler (inviscid and nonconductive) flow it is assumed. From a practical point of view, one important parameter, which is a result of the computation, is the ratio h/H of the length of the almost normal shock wave OS to the width of the channel.

The correlation between the pressure ratio and the inflow Mach number, for stable flow configurations around point O, can be determined using the generalised Hugoniot-Rankine relations for stationary flows. More difficult it is to take into account the global continuity condition which has an essential influence on the stability of the complete configuration from Fig. 1.

The paper presents the results obtained using two geometries: (1) channel with solid walls, Fig. 2 having a shape similar to that shown in Fig. 1 and (2) channel with straight walls, with a new modified boundary condition imposed over a portion BC, see Fig. 3, of the inferior wall.

The second configuration was conceived to allow a simple and direct modification of the flow configuration and can serve as a first step in the inverse design of the channels designated to produce stable flow configurations with Mach effect.

Physical Model

We consider the two dimensional plane flow of a nonviscous and nonconductive fluid through a channel having the shape shown in Fig.2 or Fig.3

The flow is governed by the Euler equations

$$\frac{\partial U}{\partial t} + \frac{\partial f}{\partial x} + \frac{\partial g}{\partial y} = 0 \quad (1)$$

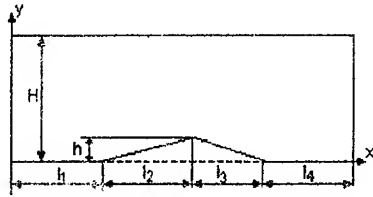


Fig.2. Geometry of the solid wall channel

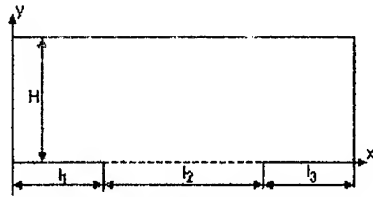


Fig.3. Geometry of the modified channel

where ρ - density, u, v - velocity components, ρe^* - total energy, p - pressure, $\gamma = c_p / c_v$ - specific heats ratio, $c = \sqrt{\gamma p / \rho}$ - the local speed of sound, H - total enthalpy.

In (1)...(5) the amounts are considered to be nondimensional being scaled with the following reference scales: l_0 - length, T_0 - temperature, $v_0 = \sqrt{2\gamma RT_0 / (\gamma + 1)}$ - velocity, p_0 - pressure, $\rho_0 = p_0 / v_0^2$ - density, $t_0 = l_0 / v_0$ - time. In nondimensional terms the gas constant is

$$\bar{R} = \frac{\gamma + 1}{2\gamma} \quad (6)$$

and the Mach number has the same value as in the case of dimensional quantities.

The boundary conditions which are specific to the above problem are: (a) the inflow is supersonic so all the flow parameters are imposed; (b) the outflow parameters are extrapolated from the nearest interior cells; (c) at the solid wall the normal velocity component is set to zero; (d) on the BC

$$U = \{\rho, \rho u, \rho v, \rho e^*\}^T \quad (2)$$

$$f = \{\rho u, \rho u^2 + p, \rho uv, \rho Hu\}^T \quad (3)$$

$$g = \{\rho v, \rho uv, \rho v^2 + p, \rho Hv\}^T \quad (4)$$

and the state equation

$$\rho H = \rho e^* + p = \frac{\gamma}{\gamma - 1} p + \rho \frac{u^2 + v^2}{2} \quad (5)$$

segment, Fig. 3, the value of the static pressure in the steady solution is imposed using a new modified boundary condition:

$$\frac{\partial u_n}{\partial n} = -\sigma \cdot \frac{\partial p}{\partial n} \quad (7)$$

which relates the normal components of the gradients of pressure and normal velocity component.

Numerical Method

The system of equations (1)...(5) is numerically integrated using an upwind scheme based on the Steger-Warming flux decomposition. The computational domain is discretized using an unstructured triangle based grid Fig.4.

The numerical flux decomposition is [2]

$$F = F^+ + F^- \quad (8)$$

$$F^\pm = \frac{\rho}{2\gamma} \begin{cases} \alpha \\ \alpha u + c(\lambda_3^\pm - \lambda_4^\pm)n_x \\ \alpha v + c(\lambda_3^\pm - \lambda_4^\pm)n_y \\ \alpha \frac{u^2 + v^2}{2} + cu_n(\lambda_3^\pm - \lambda_4^\pm) + c^2 \frac{\lambda_3^\pm + \lambda_4^\pm}{\gamma - 1} \end{cases} \quad (9)$$

where $\lambda_1 = u_n, \lambda_2 = u_n + c, \lambda_3 = u_n - c$ are the eigenvalues of the jacobian of the normal flux $F = n_x f + n_y g$ and

$$\alpha = 2(\gamma - 1)\lambda_1^\pm + \lambda_3^\pm + \lambda_4^\pm \quad (10)$$

$$\lambda^\pm = \frac{1}{2}(\lambda \pm |\lambda|) \quad (11)$$

$\vec{n} = n_x \vec{i} + n_y \vec{j}$ - the versor normal to BC.

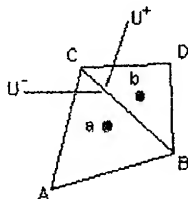


Fig. 4. Notations used in the definition of the numerical scheme

The numerical scheme is raised to the second order of accuracy using the MUSCL extrapolation in the form presented in [3]. The unknown values on the two sides of BC are computed using the relations (12) where $s_{a,b}$ are the flux limiters. An weighted interpolation based on the area of the surrounding cells was used to compute the nodal values of the flow parameters. The parameter k in (12) controls the upwind character of the extrapolation/interpolation method. In the numerical computations the value $k=1/3$, which ensures second order of accuracy for the one dimensional case, was used.

$$U^+ = U_b - \frac{s_b}{4} \left[(1 + ks) \Delta_b^- + (1 - ks) \Delta_b^+ \right]$$

$$U^- = U_a + \frac{s_a}{4} \left[(1 - ks) \Delta_a^- + (1 + ks) \Delta_a^+ \right]$$

$$\Delta_a^- = U_a - U_A \quad \Delta_a^+ = U_b - U_a$$

$$\Delta_b^- = U_b - U_a \quad \Delta_b^+ = U_D - U_b$$

$$s_{a,b} = \frac{2\Delta_{a,b}^+ \Delta_{a,b}^- + \varepsilon}{(\Delta_{a,b}^-)^2 + (\Delta_{a,b}^+)^2 + \varepsilon}$$

$$\varepsilon = 10^{-6} - \text{const}$$

(12)

The time integration method used was the modified Euler method [3] having second order of accuracy:

$$\begin{cases} U_a^{n+1/2} = U_a^n - \frac{\delta t}{2V_a} \sum_{(BC)} F^*(U^n) \Delta s_{BC} \\ U_a^n = U_a^n - \frac{\delta t}{V_a} \sum_{(BC)} F^*(U^{n+1/2}) \Delta s_{BC} \end{cases} \quad (13)$$

Because the numerical scheme is explicit the time integration step is limited by a Courant-Friedrichs-Levi condition considered in the form

$$\delta t = \alpha \frac{h}{\max_i \left\{ \left(\sqrt{u^2 + v^2} + \sqrt{\gamma p / \rho} \right)_i \right\}} \quad (14)$$

where α is a subunitary parameter due to the approximate character of the criterion (14) and h is a characteristic dimension of the mesh.

Adaptive mesh

In order to reduce the truncation error and to obtain sharp discontinuities we used an adaptive mesh algorithm based on the method presented in [4]. Due to the presence of the vortex sheet OV (Fig.1) across which Mach number distribution in the computed solution has a gradient with the order of magnitude equal to that occurring across a shock wave, the adaptation parameter (ϕ -notation) used in the numerical computation was the variation of the Mach number over each finite volume of the mesh.

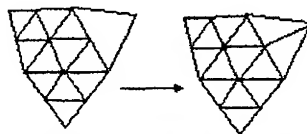


Fig. 5. Internal mesh compatibility

The adaptive mesh algorithm uses the following strategy: (1) a cell is divided into four "children" if $\phi > \phi_0$; the divided cell is marked "inactive" and kept in background for a later use; (2) when interface nodes appear in the mesh the neighbouring cell is divided in two as shown in Fig.5; (3) if $\phi < \phi_1$ for an "inactive" cell and all its "children" cells satisfy the same criterion, the cell is recovered and its "children" cells are removed from the mesh. Here ϕ_0 and ϕ_1 are constants with values computed through a simple statistical analysis of the distribution of ϕ over the mesh.

Tab.1. Parameter values for the computational cases

Computational Case	H	h	l1	l2	l3	l4	M
EFM 1	0.60	0.1635	0.30	0.5031	0.5031	0.50	1.80
EFM 5	0.65	0.1635	0.30	0.5031	0.5031	0.50	2.6015

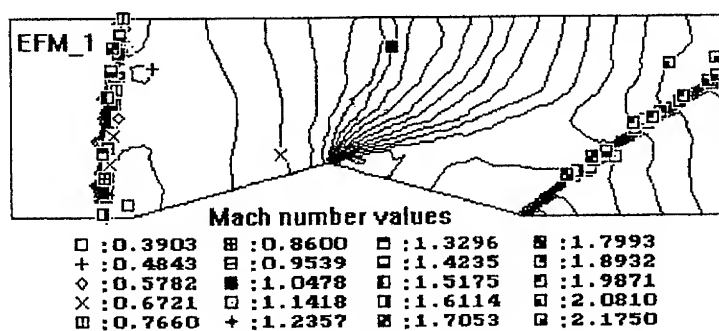


Fig.6

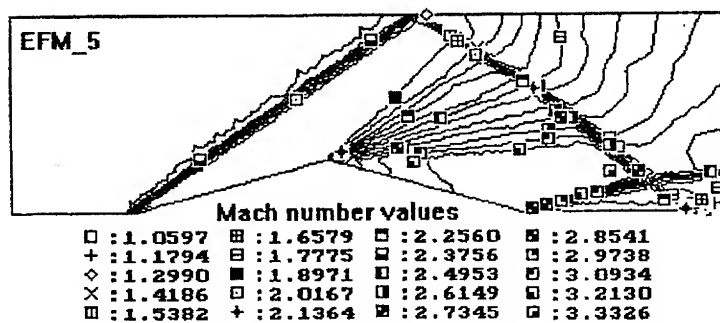


Fig.7

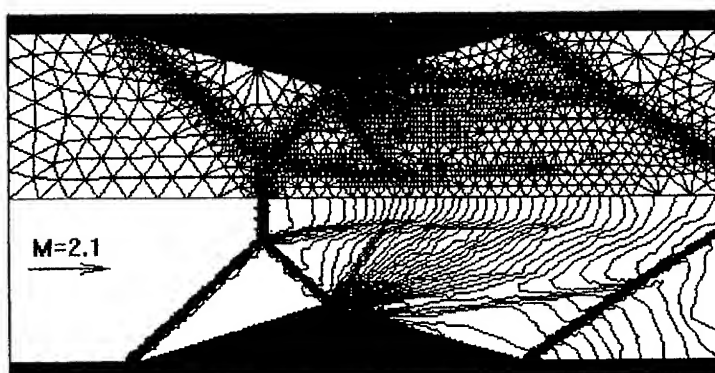


Fig.8. Izomach lines for M=2.1, H=0.5

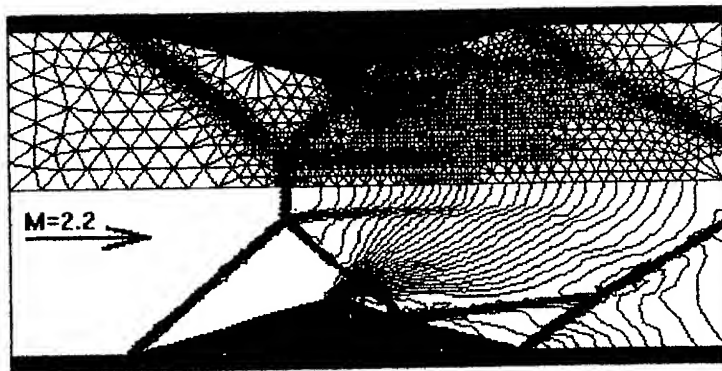


Fig.9. Izomach lines for $M=2.2$, $H=0.5$

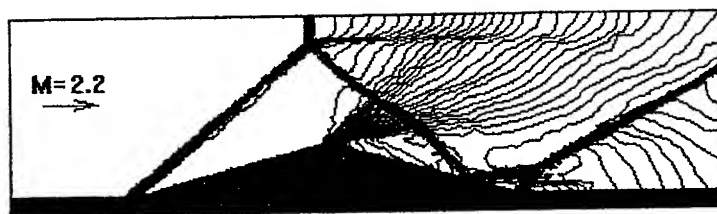
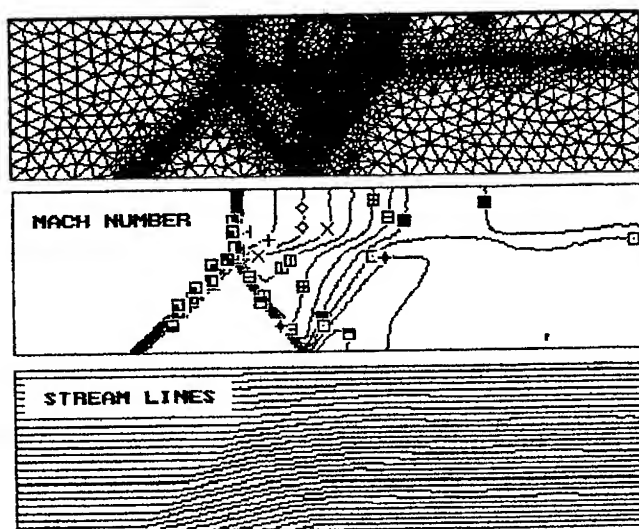


Fig.10. Izomach lines for $M=2.2$, $H=0.55$



A2:

H=0.5
L1=0.3
L2=0.5
L3=0.8

□ :	0.6333	□ :	1.2475
+	0.6948	□ :	1.3089
◇ :	0.7562	□ :	1.3703
×	0.8176	□ :	1.4317
□ :	0.8790	□ :	1.4931
□ :	0.9404	□ :	1.5545
□ :	1.0018	□ :	1.6160
□ :	1.0632	□ :	1.6774
□ :	1.1246	□ :	1.7388
+	1.1861	□ :	1.8002

$$\frac{P_{\text{externa}}}{P_{\text{current}}} = 2.0$$

Fig.11. Channel with modified boundary condition

Results and discussion

For the configuration shown in Fig.2 (channel with solid walls) several tests were performed. The values of the parameters are presented in Tab.1.

For a fixed geometry, the irregular reflection is obtained in a certain Mach number range. The inferior limit corresponds to the propagation of a normal shock towards the inflow, Fig.6. Downstream this normal shock the flow is subsonic and the convergent portion of the channel is set out. The superior limit corresponds to a regular reflection as shown in Fig.7 for inflow Mach number $M=2.6015$.

For an inflow $M=2.1$ and $M=2.2$ with $H=0.5$ the results presented in Fig. 8,9 show a good agreement with the Schlieren photos presented in [6].

The Mach tail has a greater length when Mach number decreases. From Fig. 10 for $M_{inflow}=2.2$ and $H=0.55$ it results a small decrease of the Mach tail which is due to a greater reserve given the situation of setting out the supersonic flow.

In order to obtain the longest Mach tail, the reflected shock wave OR (Fig.1) must intersect the inferior wall in the vicinity of the minimum section. This situation is very close to the inferior limit for a stable Mach effect and is difficult to be obtained for a channel having solid walls.

Using the modified boundary condition the flow configuration can be easily changed. The results presented in Fig. 11 correspond to the geometry described in Fig.3. There is a streamline which is equivalent in its first portion with a solid wall and can be used to design the wall for a given Mach number value and nearly greatest value of the corresponding Mach tail length.

Conclusions

The article presents a method to solve the unsteady bidimensional Euler equations.

A home made code based on the presented method was used to study the conditions under which Mach effect is produced.

Two geometries are presented in the paper: the solid wall channel which leads to difficulties in varying the parameters and a channel with a new modified boundary condition prescribed over a portion of the inferior wall. The flow parameter can be modified in a easier way using the second configuration. Also it can be used for design purposes.

Future work should consider the modelling of combustion phenomena associated with the presented type of flow.

References

- ¹ Steger J.L. and Warming R.F. - Flux Vector Splitting of the Inviscid Gasdynamic Equations with Application to Finite Difference Methods, *Journal of Computational Physics*, vol.40, No.2, April 1981, pp. 263-293.
- ² Anderson W.K., Thomas J.L. and van Leer B. - Comparison of Finite Volume Flux Vector Splittings for the Euler Equations, *AIAA Journal*, vol.24, No.9, Sept. 1986, pp. 1453-1460.
- ³ Batina J.T. - Unsteady Euler Airfoil Solutions Using Unstructured Dynamic Meshes, *AIAA Journal*, vol.28, No.8, August 1990, pp.1381-1388.
- ⁴ Rausch R.D., Batina J.T. and Yang H.T.Y. - Spatial Adaptation of Unstructured Meshes for Unsteady Aerodynamic Flow Computations, *AIAA Journal*, vol.30, No.5, May 1992, pp.1243-1251.
- ⁵ Manole O. and Pantazopol D. - Reflection and refraction of shock and combustion waves in gaseous flows - Boundary conditions, computational algorithms, flow configurations, *INCAS Report*, C-697/1996.
- ⁶ Gastebois, Phil., Bellet, J.C. and Soustre, J. - Etude experimentale de la similitude des configuration d'onde de choc se reflechissant avec effet de Mach, *Lab. D'Energetique, E.N.S.M.A. et C.E.A.T.*, Poitiers, 1970.

LATTICE BOLTZMANN MODELS FOR COMPLEX FLUIDS SUBJECTED TO TERRESTRIAL OR SPACE CONDITIONS

Victor SOFONEA

*Research Center for Hydrodynamics,
Cavitation and Magnetic Fluids
"Politehnica" University of Timișoara
Bd. Mihai Viteazul 1, R - 1900 Timișoara, Romania
e-mail: sofonea@linux1.mec.utt.ro*

Lattice gas and Lattice Boltzmann cellular automata techniques have been proved to be extremely useful tools for investigating fluid dynamics problems. Their parallel nature, the easy handling of irregular geometries and the possibility to incorporate the physics at a microscopic level, are major advantages of these techniques, when compared with other classical numerical methods for simulating complex fluid flow. After a brief outline of lattice Boltzmann techniques, the paper deals with their application to the following problems: (i) viscous flow between parallel plates; (ii) behavior of a liquid - vapor system placed in a tank subjected to terrestrial or space conditions, when the tank walls are wetted or not by the fluid; (iii) spinodal decomposition; (iv) structure formation and sound propagation in magnetic fluids.

General description of Lattice Boltzmann models. Since Frisch, Hasslacher and Pomeau have shown that particles moving on a hexagonal lattice with very simple collision rules in its nodes lead to the Navier Stokes equation at the macroscopic level [1], the use of lattice gas models [2, 3], a special class of cellular automata, has received considerable interest. In order to reduce the statistical noise which was inherent to these particle models, Lattice Boltzmann models which use distribution functions moving on a lattice [4] were subsequently developed as a mesoscopic approach to the same fluid dynamics problems.

The modeling of the isothermal hydrodynamics of a two phase system was achieved in [5, 6] on a hexagonal lattice with unit vectors $\vec{e}_i = \{\cos[2\pi(i-1)/6], \sin[2\pi(i-1)/6]\}$. The particle distribution functions $f_i(\vec{x}, t)$ evolve in accordance to the discretized Boltzmann equation

$$f_i(\vec{x} + \vec{e}_i, t + 1) - f_i(\vec{x}, t) = \Omega_i(\vec{x}, t) = -\frac{1}{\tau} [f_i(v_{eq}, t) - f_i^{eq}(\vec{x}, t)] \quad (1)$$

where the collision term $\Omega_i(\vec{x}, t)$ was linearized introducing the equilibrium distribution functions f_i^{eq} , $i = 0, 1, \dots, 6$, as well as the relaxation time τ . In the frame of this model, the local fluid density is defined as $n(\vec{x}, t) = \sum_i f_i(\vec{x}, t)$, while the local fluid velocity is $\vec{u}(\vec{x}, t) = n^{-1}(\vec{x}, t) \sum_i \vec{e}_i f_i(\vec{x}, t)$.

The equilibrium distribution functions $f_i \equiv f_i^{eq}(\vec{x}, t)$ were expanded as power series in the local velocity $\vec{u} \equiv \vec{u}(\vec{x}, t)$:

$$\begin{aligned} f_i^{eq} &= A + B e_{i\alpha} u_\alpha + C u^2 + D u_\alpha u_\beta e_{i\alpha} e_{i\beta} + F_\alpha e_{i\alpha} + G_{\alpha\beta} e_{i\alpha} e_{i\beta} + \dots \\ f_0^{eq} &= A_0 + C_0 u^2 \quad (i = 1, \dots, 6 \quad ; \quad \alpha = 1, 2) \end{aligned} \quad (2)$$

and the appropriate coefficients

$$\begin{aligned} A_0 &= n - 2(p_0 - \kappa n \nabla^2 n) & B &= n/3 & C_0 &= -n \\ A &= (p_0 - \kappa n \nabla^2 n)/3 & C &= -n/6 & D &= 2n/3 \\ F_\alpha &= 0 \end{aligned} \quad (3)$$

$$G_{xx} = -G_{yy} = \frac{\kappa}{3} \left\{ \left(\frac{\partial n}{\partial x} \right)^2 - \left(\frac{\partial n}{\partial y} \right)^2 \right\} \quad G_{xy} = 2 \frac{\kappa}{3} \frac{\partial n}{\partial x} \frac{\partial n}{\partial y}$$

were determined using local conservation of mass and momentum, as well as Galilean invariance and isotropy of pressure tensor :

$$P_{\alpha\beta} = p \delta_{\alpha\beta} + \kappa \frac{\partial n}{\partial x_\alpha} \frac{\partial n}{\partial x_\beta} \quad (4)$$

where

$$p = n \frac{\delta \Psi}{\delta n} - \Psi = p_0 - \kappa n \nabla^2 n - \frac{\kappa}{2} |\nabla n|^2 \quad (5)$$

Here

$$\Psi \equiv \Psi(\vec{x}) = \int \left\{ \frac{\kappa}{2} |\nabla n(\vec{x})|^2 + \psi(n(\vec{x})) \right\} d\vec{x} \quad (6)$$

is the free energy functional [7], the constant κ defines the strength of the surface tension and $p_0 = n\psi'(n) - \psi(n)$ is the state equation of the fluid.

In order to have a Van der Waals fluid, the bulk free energy density ψ has the form

$$\psi = nT \ln \left(\frac{n}{1 - nb} \right) - an^2 \quad (7)$$

where T is the system temperature. Current simulations were done with $a = 0$, $b = 0$ (when the ideal gas equation was recovered) as well as with $a = 9/49$, $b = 2/21$ (giving the critical temperature value $T_c = 0.571$).

When introducing a chemical potential $\mu(\vec{x})$ in each lattice node \vec{x} , thermodynamic forces are defined as gradients of this potential [5]. These forces are introduced in accordance with the general momentum equation

$$\sum_i f_i^{eq} e_{i\alpha} = n u_\alpha - \tau n \frac{\partial \mu}{\partial x_\alpha} \quad (8)$$

and therefore the coefficient F_α in the expansion (3) becomes

$$F_\alpha = -\frac{\tau n}{3} \frac{\partial \mu}{\partial x_\alpha} \quad (9)$$

When the potential $\mu(\vec{x})$ vanishes overall the lattice domain except the boundaries, it provides the possibility to incorporate wetting phenomena near the domain walls, as first suggested in [5].

The expression (9) may be extended in order to include also the action of an external force field $\mathcal{F}_\alpha(\vec{x})$ acting on each node \vec{x} of the lattice :

$$F_\alpha = -\frac{\tau n}{3} \left\{ \frac{\partial \mu}{\partial x_\alpha} + \mathcal{F}_\alpha(\vec{x}) \right\}. \quad (10)$$

In particular, the external force field $\mathcal{F}_\alpha(\vec{x})$ may be of gravitational origin

$$\mathcal{F}_\alpha(\vec{x}) = n(\vec{x})\vec{g} \quad (11)$$

where $\vec{g} = \text{const}$ is the gravitational acceleration.

Viscous flow between parallel plates. The suitability of the Lattice Boltzmann model to reproduce physical aspects in fluid dynamics problems was tested in the case of Poiseuille and Couette flows [8]. In the first case, parabolic velocity profiles between the two plates were always recovered after a certain number of automaton steps. These profiles were depending on the value of the relaxation time τ introduced into the linearized Boltzmann equation (1). The differences between the values of the kinematic fluid viscosity ν found after fitting these parabolic profiles and the analytical expression [9]

$$\nu = \frac{2\tau - 1}{8} \quad (12)$$

was found to be less than one percent [8].

Suppose now that the fluid and the two parallel plates are initially at rest state. After the lower plate is suddenly brought to the steady velocity U in its own plane, while the upper one is still maintained at rest, the governing differential equation is

$$\frac{\partial u}{\partial t} = \nu \frac{\partial^2 u}{\partial y^2} \quad (13)$$

with the boundary and initial conditions

$$u(0, t) = U, \quad u(H, t) = 0 \quad \text{for } t > 0 \quad (14)$$

$$u(y, 0) = 0 \quad \text{for } 0 < y \leq H \quad (15)$$

The velocity distribution is given by [10]

$$u(y, t) = U \left(1 - \frac{y}{H} \right) \frac{2U}{\pi} \sum_{i=1}^{\infty} \frac{1}{i} \exp \left(-i^2 \pi^2 \frac{\nu t}{H^2} \right) \sin \left(i \pi \frac{y}{H} \right) \quad (16)$$

The simulation was done on a lattice with 101×100 nodes, where the real distance between plates was $H = 101 \sqrt{3}/2 - \sqrt{3}/4$ [8]. The time evolution of the velocity profile is presented in figure 1, at $t = 300, 1200, 4800$ and 10000 , the kinematic viscosity being $\nu = 0.125$. An excellent agreement is observed between the numerical and analytical results. The

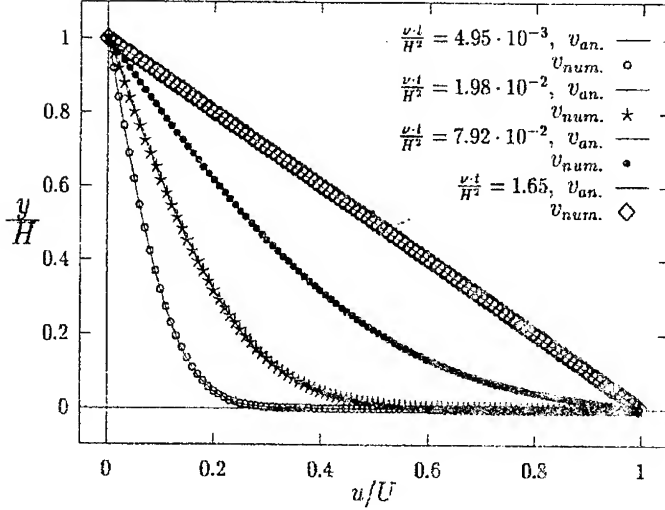


Figure 1: Development of velocity profile between parallel plates in relative motion (dots - Lattice Boltzmann results; solid lines - analytical solution (16)).

linear velocity profile corresponding to the steady Couette flow with no pressure gradient is naturally obtained for $t \rightarrow \infty$.

Equilibrium configuration of a two - phase fluid in a tank. The equilibrium configuration of a fluid contained in a tank subjected to constant gravitational acceleration is a major problem in space technology. Specific criteria [11] allow the determination of the position of a free gas - liquid interface in the absence of gravitation, when the tank geometry is well defined. Here we deal with the equilibrium configuration of a two - phase Van der Waals fluid placed in a 2 - dimensional rectangular container subjected to terrestrial ($g \neq 0$) or space conditions ($g \simeq 0$). Simulations were generally done on a 128×128 lattice at $T = .565$. Because of the scaling factor $\sqrt{3}/2$ on the vertical axis in the triangular lattice [3, 8], the real domain had always a rectangular form. All simulations were done starting from the same initial configuration, which had two subdomains of different mean densities, with 1% random fluctuations. The two possibilities, when the fluid may or may not wet the tank walls were also considered. For this purpose, the chemical potential $\mu(\vec{x})$ had always a null value in the inner lattice nodes, but this value was negative at the boundary nodes when the walls were wetted by the fluid, and positive in the contrary case [5, 12].

Wetting case. Figure 2 shows the initial state (a) and the final state (b) reached after 20,000 automaton steps, when the gravitational acceleration had the value $g = 50$ and the tank walls were wetted by the fluid. Because of the gravitational acceleration oriented downwards, the liquid phase (of greater density) always remains at the bottom of the vessel,

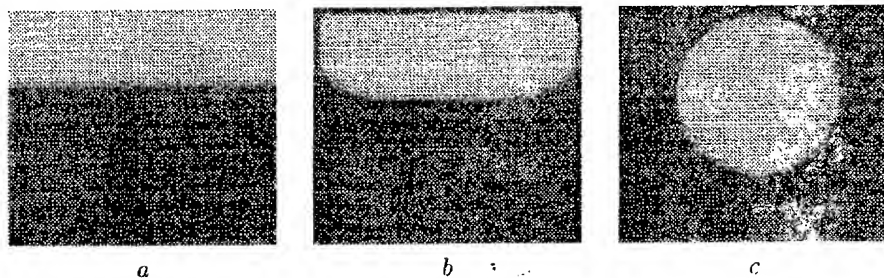


Figure 2: Initial (a) and equilibrium states at $g = 50$ (b) and $g = 0$ (c) of the two - phase fluid, obtained at $T = .565$, $\kappa = 0.01$, $\mu = -0.1$ (wetting case).

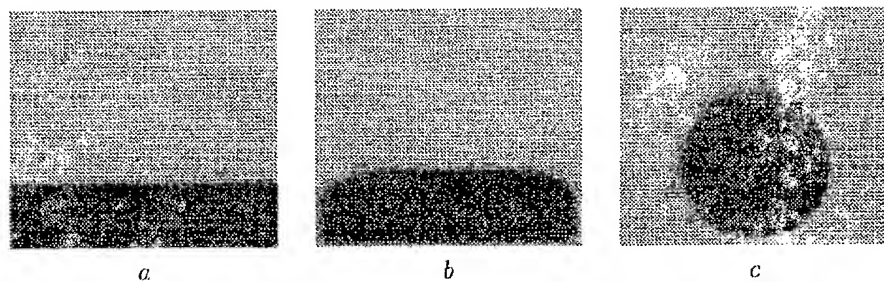


Figure 3: Initial (a) and equilibrium states at $g = 50$ (b) and $g = 0$ (c) of the two - phase fluid, obtained at $T = .565$, $\kappa = 0.01$, $\mu = 0.5$ (non-wetting case).

even a thin film becomes attached to the tank walls. In the absence of gravity, the liquid phase remains all around the walls, while the gas phase is situated at the center of the tank, having a very slow evolution towards a rather circular shape, as shown in figure 2c, which was obtained after 60,000 automaton steps [12].

Non - wetting case. Figure 3 is similar to figure 2, except the fact that the walls are no more wetted by the fluid. One can see that the curvature of the gas - fluid interface is opposite compared to the wetting case. In the absence of gravity (figure 3c), the liquid phase achieves again a circular shape in order to reduce the interfacial energy, as in the wetting case.

Spinodal decomposition. Phase separation into the coexisting liquid and vapor phases occurs after a sudden quench of the homogeneous fluid into the two-phase coexistence region. In order to get detailed information about the kinetics of spatial structures arising during the spinodal decomposition, the lattice system was first initialized with a mean density ρ and 1% random fluctuations of the local density $\rho(\vec{x})$ were allowed around the mean value. Most simulations were done on lattices with 1024×1024 nodes using periodic boundary conditions, different values of the relaxation time τ and a constant value $\kappa = 0.01$ of the surface tension constant, which ensures the width of the interface region between homoge-

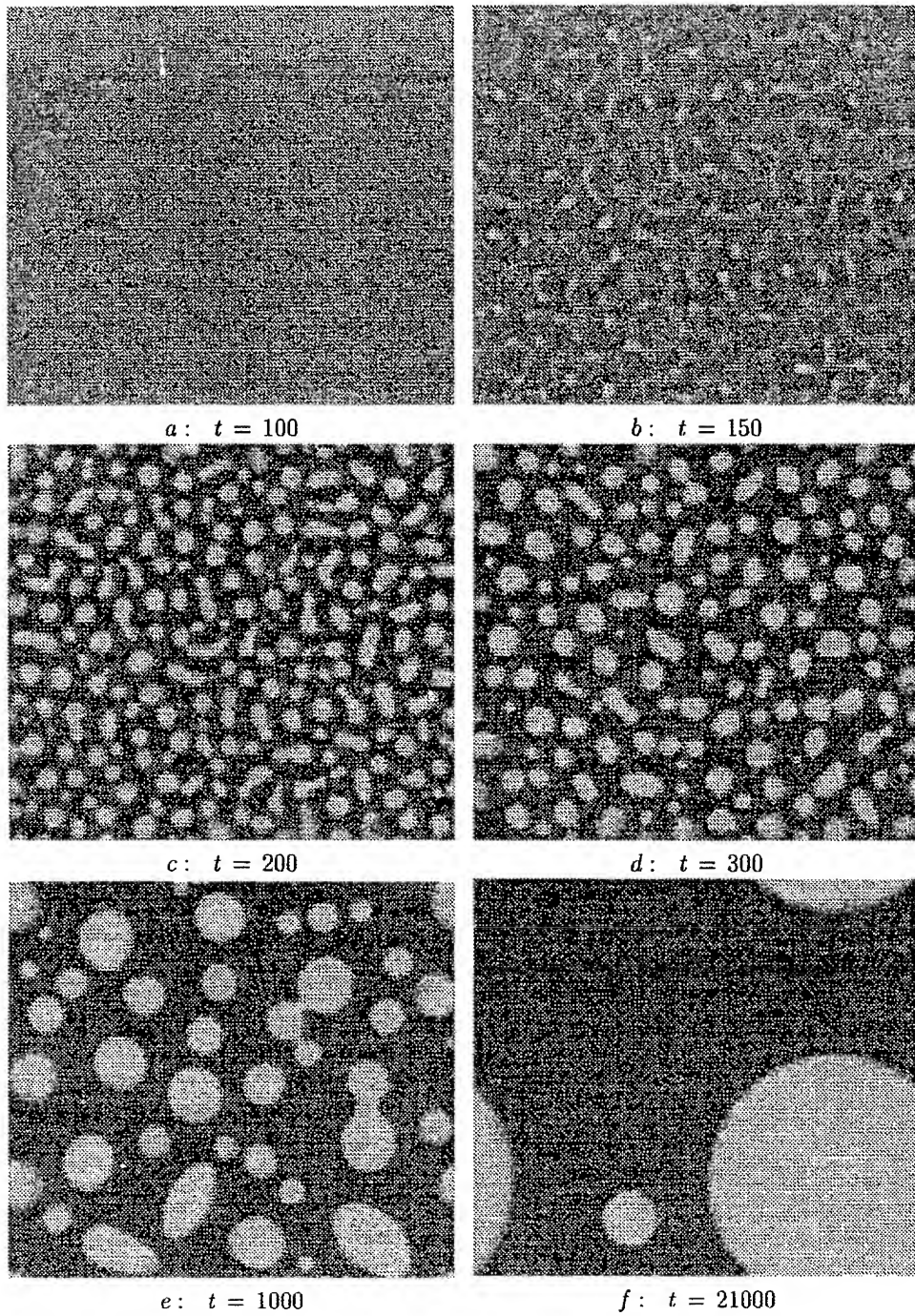


Figure 4: Time evolution of the local density across a 256×256 lattice after the quench at $t = 0$ ($\rho = 3.0$, $\kappa = 0.01$, $\tau = 0.60$).

neous phases to be approximatively 10 lattice units. After each initialisation, the system was released to evolve during 500 preliminary automaton steps at the initial temperature $T_{in} = .580$ above the critical one, then the temperature was suddenly changed to the final value $T_{fin} = .550$. Starting from this moment ($t = 0$), the system was allowed to evolve to its equilibrium state, as seen, e.g., in figure 4, while the patterns were characterized through the values of three morphological measures following a procedure described below.

In a d -dimensional space, morphological measures [13, 14, 15] are generally defined as functionals on homogeneous domains, i.e. on subsets $A \in \mathcal{R}^d$, having three fundamental properties: additivity, motion invariance and continuity. Any morphological measure is a linear combination of the $d + 1$ Minkowski functionals $W_\nu(A)$. In $d = 2$, these Minkowski functionals are related to familiar measures: covered area F , boundary length U and Euler characteristic (connectivity) χ .

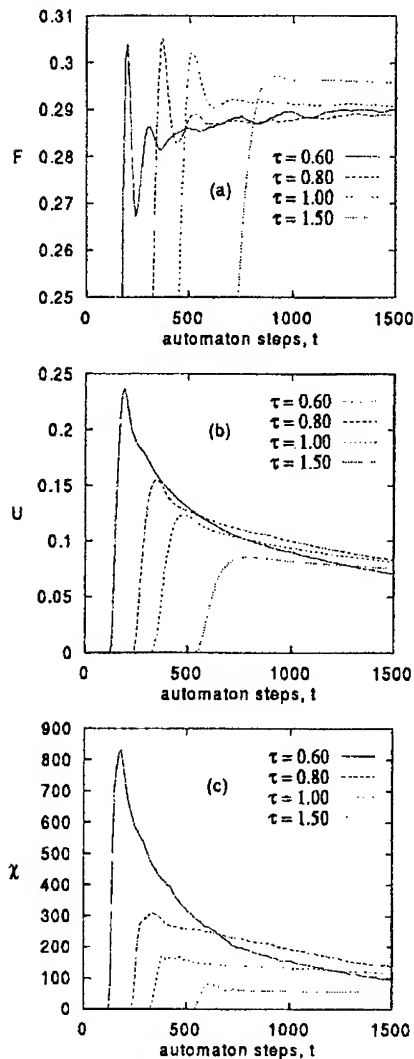


Figure 5: Time evolution of the Minkowski functionals.

In order to compute the values of the Minkowski functionals at a given time during the spinodal decomposition process, a threshold value $\rho_{th} = 3.5$ is introduced and the gray value at each pixel is set to either white or black depending on whether the original local density value $\rho(\vec{x})$ is larger or lower than ρ_{th} , respectively. The first obvious quantity is the relative white area, $F := N_{\rho_{th}}/N$, i.e. the number $N_{\rho_{th}}$ of the pixels in the original image having the corresponding gray level $\rho(\vec{x})$ greater than ρ_{th} , normalized by the total number N of pixels. The second morphological quantity is $U := B/N$ defined as the ratio between the total length B of the boundary lines separating black and white regions, normalized by the total number of pixels. To determine B one has to count the numbers of pairs of neighbored black and white pixels. The third quantity of interest, the Euler characteristics $\chi = N^w - N^b$, defined by the difference of the number of connected components, is not normalized by the total number of pixels in order to keep integer numbers. This quantity describes the connectivity of the domains in the lattice and, e.g., it equals -1 when one has a black drop in a large white lattice and $+1$ vice versa. Despite its global meaning, the Euler characteristics may be calculated in a local way [14, 16].

In figure 5 we show the typical time dependence of the morphological measures $F(t)$, $U(t)$ and $\chi(t)$ obtained for an off-symmetric quench ($\rho = 3.0$), where the fluid phase is the minority phase, using several values of the relaxation time τ . One can clearly distinguish two different time regimes: the early stage of spinodal decomposition kinetics and the late state of domain growth. At early times, the growth of density fluctuations leads to the build up of interfaces between homogeneous domains of the two coexisting phases, as seen in figures 4 a – c. This process is accompanied by an increase of the white area F belonging to the liquid phase, as well as of the boundary length U of the interface. Also the Euler characteristic increases, because many disconnected components of the minority phase arise. In contrast to this early stage, the late stage domain growth (which corresponds to figures 4 d – f) is characterized by a decrease of the quantities U and χ . This is a direct consequence of the increase of the characteristic length scale L . The area of the liquid phase remains quite constant and approaches the final value $F(t \rightarrow \infty) \rightarrow (\rho - \rho_{gas})/(\rho_{liquid} - \rho_{gas})$ which is given by the level rule of the coexistence region. Because of phase demixing, the boundary length U and the Euler characteristic approach their final minimum values $U(t \rightarrow \infty) \rightarrow 8\sqrt{\frac{F}{\pi N}}$ and $\chi(t \rightarrow \infty) \rightarrow 1$, which correspond to a single liquid drop of area F , immersed into the vapor phase.

Since the measures $W_\nu(A)$ are homogenous functions of order $d - \nu$ [13, 15], the following scaling behavior of the Minkowski functionals may be assumed

$$F \sim 1, \quad U \sim L^{-1}, \quad \chi \sim L^{-2} \quad (17)$$

where L is the characteristic domain size. There are other possibilities to define characteristic length scales of spatial patterns, which are based on the calculation of the first zero or the first moment of the radial distribution function. These definitions, although widely used by many authors, are recognized to be computationally expensive and cannot account themselves for the morphology of the rich variety of geometrical shapes of domains, as Minkowski functionals can do. Moreover, the definition (17) of the characteristic length L allows a faster computation algorithm, because it does not involve Fourier transformations, but only pixel counting.

In figure 6 we show the functions $U^{-1}(t)$ and $\chi^{-1/2}(t)$, i.e., the time evolution of the characteristic length $L(t)$, in accordance to the relation (17). We observe the scaling behavior $L(t) \sim t^\alpha$ with three different scaling exponents α being established for various hydrodynamic regimes: $\alpha = 2/3$ for low viscosities ($\tau = 0.54$, kinetic regime), $\alpha = 1/2$ for intermediate values ($\tau = 0.6$), and $\alpha = 1/3$ for high viscosities ($\tau = 1.5$).

Magnetic fluids, also known as ferrofluids, are ultrastable colloidal suspensions of subdomain ferro - or ferrimagnetic particles - e.g., magnetite (Fe_3O_4) - dispersed in various carrier liquids [17]. Many experimental results confirmed that colloidal particles in magnetic fluids coagulate and form chain clusters as a result of their mutual interactions, this process being enhanced in the presence of a magnetic field. The chain formation process, together with the reorientation of individual particles in the presence of a magnetic field, are responsible for the anisotropy of the physical properties of these materials.

Following the general approach in [18], the lattice Boltzmann equation was considered for

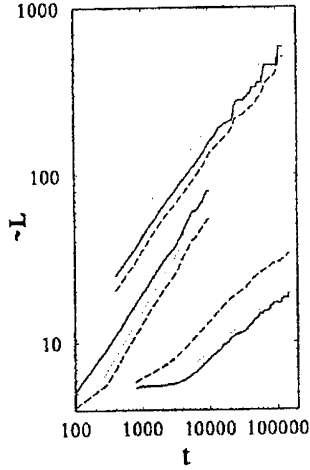


Figure 6:

Time evolution of the boundary length $w_1/U(t)$ (dashed line) and the connectivity $w_2/\chi(t)^{-1/2}$ (thick solid line). The coefficients w_i are chosen to separate the data and the dotted lines show the scaling behavior $L(t) \sim t^\alpha$ with exponents $\alpha = 2/3$ ($\tau = 0.53$, $w_1 = 1$, $w_2 = 400$), $\alpha = 1/2$ ($\tau = 0.60$, $w_1 = 0.5$, $w_2 = 1000$), $\alpha = 2/3$ ($\tau = 1.50$, $w_1 = 0.5$, $w_2 = 80$).

a fluid system with $S + 1$ components moving on the hexagonal lattice [20]:

$$n_a^\sigma(\vec{x} + \hat{e}_a, t + 1) - n_a^\sigma(\vec{x}, t) = -\frac{1}{\tau} [n_a^\sigma(\vec{x}, t) - n_a^{\sigma,eq}(\vec{x}, t)] \quad (18)$$

where $\sigma = 0, 1, \dots, S = 6$, $a = 0, 1, \dots, b = 6$, $n_a^\sigma(\vec{x}, t)$ is the single particle distribution function for the σ -th component having the velocity \hat{e}_a and τ is the mean collision time. Particles with $\sigma = 0$ are "carrier liquid" particles, while "colloidal particles" with $1 \leq \sigma \leq S$ carry a magnetic moment $\vec{m}^\sigma = \hat{e}_\sigma$. The mean fluid density $\bar{\rho}$ and the concentration of the colloidal particles are

$$\bar{\rho} = \langle \rho(\vec{x}, t) \rangle = \langle \sum_{\sigma=0}^S n^\sigma(\vec{x}, t) \rangle, \quad \phi = \frac{1}{\bar{\rho}} \langle \sum_{\sigma=1}^S n^\sigma(\vec{x}, t) \rangle \quad (19)$$

where $n^\sigma(\vec{x}, t) = \sum_{a=0}^b n_a^\sigma(\vec{x}, t)$ and $\langle \dots \rangle$ is the average on the whole lattice. The probability of finding a colloidal particle with the magnetic moment \vec{m}^σ is

$$f^\sigma(\vec{H}, T) = \frac{\exp(\mu_0 \vec{m}^\sigma \cdot \vec{H} / k_B T)}{\sum_{\sigma=1}^S \exp(\mu_0 \vec{m}^\sigma \cdot \vec{H} / k_B T)} \quad (20)$$

where μ_0 is the vacuum permittivity, \vec{H} is the magnetic field vector, k_B is the Boltzmann constant and T is the temperature. We always started our computer runs by assuming that particles are initially quasi-homogeneously distributed over a 128×128 lattice with a small (1%) random perturbation and the fluid is at rest. Consequently, at $t = 0$ we had

$$n^\sigma(\vec{x}) = \rho(\vec{x}) \phi f^\sigma(\vec{H}, T), \quad 1 \leq \sigma \leq S, \quad n^0(\vec{x}) = \rho(\vec{x}) - \sum_{\sigma=1}^S n^\sigma(\vec{x}) \quad (21)$$

$$n_a^\sigma(\vec{x}) = \frac{1-d_0}{b} n^\sigma(\vec{x}), \quad 1 \leq a \leq b, \quad n_0^\sigma(\vec{x}) = d_0 n^\sigma(\vec{x}), \quad 0 \leq \sigma \leq S \quad (22)$$

where $0 \leq d_0 \leq 1$ is a constant [18, 19]; our computer runs were made with $d_0 = 0.5$.

The colloidal particles in magnetic fluids interact themselves via dipole-dipole interactions. Only nearest-neighbours interactions are taken into account and so, the interaction potential energy is [20]:

$$W(\vec{x}, t) = \sum_{\sigma=0}^S n^\sigma(\vec{x}, t) \sum_{\bar{\sigma}=0}^S \sum_{a=1}^b G_{\sigma\bar{\sigma}a} n^{\bar{\sigma}}(\vec{x} + \hat{e}_a) \quad (23)$$

$$G_{\sigma\bar{\sigma}a} = \frac{1}{c^3} \left[\vec{m}^\sigma \cdot \vec{m}^{\bar{\sigma}} - \frac{3(\vec{m}^\sigma \cdot \hat{e}_a)(\vec{m}^{\bar{\sigma}} \cdot \hat{e}_a)}{c^2} \right] \quad (24)$$

where $c = 1$ is the lattice constant and, for convenience, $\vec{m}^0 = 0$.

The interaction process is achieved during the collision phase in the LB automaton. Consequently, the rate of net momentum change induced at each site is also a simple generalisation of an expression in [18, 19]:

$$\frac{1}{\tau} [\vec{u}_{new}^\sigma(\vec{x}, t) - \vec{u}_{old}^\sigma(\vec{x}, t)] = -n^\sigma(\vec{x}, t) \sum_{\bar{\sigma}=1}^S \sum_{a=1}^b G_{\sigma\bar{\sigma}a} n^{\bar{\sigma}}(\vec{x} + \hat{e}_a, t) \hat{e}_a \quad (25)$$

The new values $\vec{u}_{new}^\sigma(\vec{x}, t)$ of the local velocities, established after the interaction determine the local equilibrium distribution functions $n_a^{\sigma,eq}(\vec{x}, t)$ [19] in the lattice Boltzmann equation (18). The continuity equation, as well as the momentum equation are obtained from the Boltzmann equation (18) after a series expansion [20].

Phase transitions. Figure 7 shows the two - dimensional distribution of the x component of the local magnetisation $M_x(\vec{x}, t) = \sum_{\sigma=1}^S (\vec{m}^\sigma)_x n^\sigma(\vec{x}, t)$ after 5000 time steps when the mag-

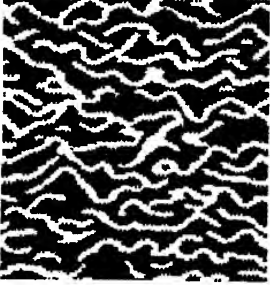


Figure 7: Cluster formation.

netic field is oriented in the x (horizontal) direction ($h = \mu_0 H / k_B T = 0.8$, $\phi = 0.2$, $\bar{\rho} = 0.5$). The white points have $M_x(\vec{x}, t) > 1.01 \cdot \bar{M}_x(t)$, while the black ones have $M_x(\vec{x}, t) \leq \bar{M}_x(t)$, where $\bar{M}_x(t) = \text{const.}$ is the mean value on the whole lattice. The phase separation, i.e., the onset of thread-like clusters orientated along the field direction, is evident. The typical field parameter (h) dependence of the mean magnetisation $\bar{M}_x(t)$, as well as of the mean magnetisations in each phase, $M_x^{high}(t)$ and $M_x^{low}(t)$, is reproduced in Figure 8.

Sound propagation. Let ρ' , \vec{u}' be a weak perturbation of the equilibrium solution $\rho^{eq} = \bar{\rho}$, $\vec{u}^{eq} = 0$ of the LB automaton. The sound propagation equation is:

$$\begin{aligned} \partial_t \rho' - (c_s^1)^2 \nabla^2 \rho' + \frac{(6\tau - 1)c^2}{2(D+2)} \partial_t (\nabla^2 \rho') &= \rho^{eq} \phi \sum_{\sigma} f^\sigma \partial_\alpha \partial_\beta (u'_\alpha u'_\beta) - \\ \rho^{eq} \phi^2 (\partial_\alpha \partial_\beta \rho') \sum_{\sigma, \bar{\sigma}} f^\sigma f^{\bar{\sigma}} (S_{\sigma\bar{\sigma}})_{\alpha\beta} + \phi^2 \partial_\alpha (\rho' \partial_\beta \rho') \sum_{\sigma, \bar{\sigma}} f^\sigma f^{\bar{\sigma}} (M_{\sigma\bar{\sigma}})_{\alpha\beta} \end{aligned} \quad (26)$$

where $(c_s^1)^2$ is the squared sound velocity in the first order approximation

$$(c_s^1)^2 = \frac{c^2}{D} (1 - d_0) + \rho^{eq} \phi^2 \left[\frac{bc^2}{D} - \frac{3bc^4}{D(D+2)} \right] \sum_{\sigma, \bar{\sigma}} f^\sigma f^{\bar{\sigma}} (\vec{m}^\sigma \cdot \vec{m}^{\bar{\sigma}}) \quad (27)$$

Figure 8: Field dependence of the mean (\bullet), high (\diamond) and low (\square) magnetisation values after $t = 5000$ time steps.

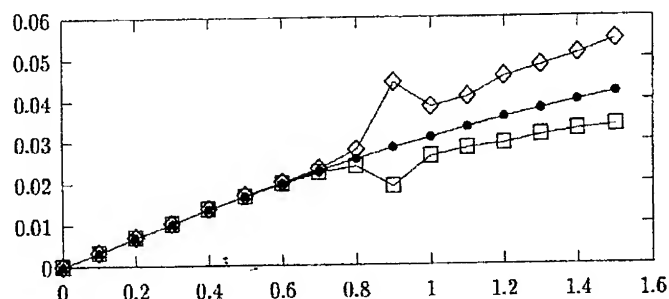
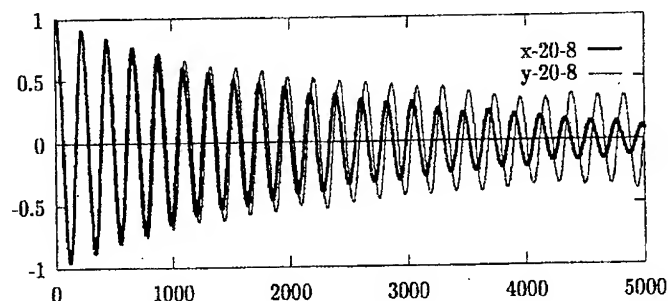


Figure 9: Time evolution of the small amplitude density perturbation $\rho'(0, t)$ during $t = 5000$ steps ($\bar{\rho} = 0.5$, $\varphi = 0.20$, $h = 0.8$) when the magnetic field is oriented along the x and y axes.



Equation (26) reduces to the usual damped sound equation when $\phi = 0$, i.e., no colloidal particles are present.

In order to take advantage of the periodic boundaries in the LB automaton, we considered the problem of standing waves in the x direction, and therefore, the lattice was initialized at $t = 0$ with a cosine perturbation having a small amplitude ($\rho_0 = 0.1 \cdot \bar{\rho}$). The general behaviour of the space and time dependence of the perturbation (after a mediation in the y direction) was found to be close to $\rho'(x, t) = \rho_0 \exp(-\alpha t) \cos(kx) \cos(\omega_s t)$ where $k = 2\pi/L$, $L = 128$ is the wavenumber. Figure 9 shows the time evolution of the perturbation at $x = 0$ during $t = 5000$ steps for $\bar{\rho} = 0.5$, $\phi = 0.20$ and $h = 0.8$, when the field direction was oriented along the x and y axes, respectively. From this figure, as well as from the computed Fourier spectrums, one can see that the sound velocity is greater when the field is oriented along the x direction. The field attenuation coefficient α was found to be dependent not only on the field parameter h , but also on the angle θ between the x axis and the field direction [20].

Conclusions. Lattice Boltzmann methods have several important advantages over other classical numerical methods for fluid flow problems (finite difference schemes, finite element methods, etc.). First, there is no need to solve algebraic equations systems since the distribution functions characterizing the particle system at the mesoscopic level evolve in accordance

with local automaton rules. These automaton updating rules are very simple and may be fully parallelised. Physical interactions at the particle level e.g., interparticle interactions, external forces or the presence of boundaries may be also introduced. Wetting phenomena under terrestrial or space conditions are also well described using this model, whose advantage is the consideration of the microscopic level fluid physics (collisions and long range interactions between particles) instead of the macroscopic level (continuous media) approach.

Acknowledgements. The author acknowledges the financial support from the Romanian Ministry of Research and Technology, supervised through the Romanian Space Agency.

References

- [1] U. Frisch, B. Hasslacher, Y. Pomeau, *Physical Review Letters* **56** (1986) 1505.
- [2] U. Frisch, D. d'Humières, B. Hasslacher, P. Lallemand, Y. Pomeau, J. P. Rivet, *Complex Systems* **1** (1987) 649.
- [3] D. H. Rothman, S. Zaleski, *Reviews of Modern Physics* **66** (1994) 1417.
- [4] R. Benzi, S. Succi, M. Vergassola, *Physics Reports* **222** (1992) 145.
- [5] M. R. Swift, W. R. Osborn, J. M. Yeomans, *Physical Review Letters* **75** (1995) 830.
- [6] M. R. Swift, E. Orlandini, W. R. Osborn, J. M. Yeomans, *Physical Review E* **54** (1996) 5041.
- [7] J. S. Rowlinson, B. Widom, *Molecular Theory of Capillarity*, Clarendon Press, Oxford, 1982.
- [8] B. Szilágyi, R. Susan - Resiga, V. Sofonea, *International Journal of Modern Physics C* **6** (1995) 345.
- [9] H. Chen, S. Chen, W. Matthaeus, *Physical Review A* **45** (1992) 5339.
- [10] G. K. Batchelor, *An Introduction to Fluid Dynamics*, Cambridge University Press, Cambridge, 1967.
- [11] P. Concus, R. Finn (Editors), *Variational Methods for Free Surface Interfaces*, Springer Verlag, New York - Berlin, 1987.
- [12] V. Sofonea, *International Journal of Modern Physics C* **7** (1996) 695.
- [13] H. Hadwiger, *Vorlesungen über Inhalt, Oberfläche und Isoperimetrie* Springer Verlag, Berlin, 1957.
- [14] K. R. Mecke, *Physical Review E* **53** (1996) 4794.
- [15] K. R. Mecke, V. Sofonea, submitted to *Physical Review Letters* (1997).
- [16] V. Sofonea, K. R. Mecke, submitted to *Physical Review E* (1997).
- [17] R. E. Rosensweig, *Ferrohydrodynamics*, Cambridge University Press, Cambridge, 1985.
- [18] X. Shan, H. Chen, *Physical Review E* **47** (1993) 1815.
- [19] X. Shan, H. Chen, *Physical Review E* **49** (1994) 2941.
- [20] V. Sofonea, *Europhysics Letters* **25** (1994) 385.

Some remarks on the Witten laplacian

by

Mircea Puta and Florian Cret

Abstract

We study some geometrical properties of the Witten laplacian and point out some of its applications in geometric quantization.

1 Preliminaries

Let M be a smooth n -dimensional Riemannian manifold, orientable, without boundary and $\mathcal{D}^p(M)$ the space of smooth ($= C^\infty$) exterior p -forms on M with compact support.

For each $\alpha, \beta \in \mathcal{D}^p(M)$ we define their inner product (α, β) by

$$(\alpha, \beta) = \int_M \alpha \wedge * \beta, \quad (1.1)$$

where $*$ is the Hodge star operator. Then $\mathcal{D}^p(M)$ is a pre-Hilbert space and we denote by $L^2 \mathcal{D}^p(M)$ its completion.

DEFINITION 1.1 ([2]) Let $f \in C^\infty(M, \mathbb{R})$ be an C^∞ -smooth function on M and $t \in \mathbb{R}$ a real number. Then we define the differential operators d_t^f, δ_t^f and $W_{t,f}^{(p)}$ respectively by:

- (i) $d_t^f : \alpha \in \mathcal{D}^p(M) \mapsto d_t^f \alpha = (e^{-tf} de^{tf})(\alpha) \in \mathcal{D}^{p+1}(M)$
- (ii) $\delta_t^f : \alpha \in \mathcal{D}^p(M) \mapsto \delta_t^f \alpha = (e^{tf} \delta e^{-tf})(\alpha) \in \mathcal{D}^{p-1}(M)$
- (iii) $W_{t,f}^{(p)} : \alpha \in \mathcal{D}^p(M) \mapsto W_{t,f}^{(p)}(\alpha) = d_t^f \delta_t^f \alpha + \delta_t^f d_t^f \alpha \in \mathcal{D}^p(M).$

The second order differential operator $W_{t,f}^{(p)}$ is usually called p -Witten laplacian or Witten laplacian on p -forms. In all that follows we shall suppose that f is fixed and we shall write $d_t, \delta_t, W_t^{(p)}$ instead of d_t^f, δ_t^f and $W_{t,f}^{(p)}$ respectively.

THEOREM 1.1 ([2]) For each $p \in \mathbb{N}, 0 \leq p \leq n$ we have:

- (i) $d_t \circ W_t^{(p)} = W_t^{(p)} \circ d_t$
- (ii) $\delta_t \circ W_t^{(p)} = W_t^{(p)} \circ \delta_t$
- (iii) δ_t is the adjoint of d_t with respect to the inner product (1.1).
- (iv) $W_t^{(p)}$ is the elliptic, self-adjoint and positive definite operator.

2 Hodge theory for the Witten laplacian

Let us suppose now that M is also a compact manifold.

DEFINITION 2.1 A differential form $\alpha \in L^2\mathcal{D}^p(M)$ will be called a Witten harmonic form if

$$W_t^{(p)}(\alpha) = 0.$$

We shall denote by $\mathcal{H}_t^p(M)$ the space of Witten harmonic p -forms on M . Then as a consequence of the Theorem 1.1 (iv) we have immediately:

THEOREM 2.1 ([2]) For each $p \in \mathbb{N}$, $0 \leq p \leq n$ we have:

- (i) $L^2\mathcal{D}^p(M) = \ker(W_t^{(p)}) \oplus \text{range}(W_t^{(p)})$,
- (ii) $\mathcal{H}_t^p(M) \subset \mathcal{D}^p(M)$,
- (iii) $H^p(M, d_t) \simeq \mathcal{H}_t^p(M) \simeq \mathcal{H}^p(M) \simeq H^p(M, d)$.

Now, using the above result we can prove:

THEOREM 2.2 For each $p \in \mathbb{N}$, $0 \leq p \leq n$, the equation:

$$W_t^{(p)}(\eta) = \lambda \tag{2.1}$$

has always solution if and only if λ is orthogonal to $\mathcal{H}_t^p(M)$ with respect to the inner product (1.1).

PROOF If η is a solution of the equation (2.1) and $\gamma \in \mathcal{H}_t^p(M)$, then we have successively:

$$(\lambda, \gamma) = (W_t^{(p)}(\eta), \gamma) = (\eta, W_t^{(p)}(\gamma)) = 0$$

and so λ is orthogonal to $\mathcal{H}_t^p(M)$.

Conversely, let us suppose that λ is orthogonal to $\mathcal{H}_t^p(M)$. By means of Theorem 1.1 (i) we have

$$\lambda = d_t\alpha + \delta_t\beta + \gamma$$

with

$$W_t^{(p)}(\gamma) = 0.$$

On the other hand,

$$\begin{aligned} 0 &= (\gamma, \lambda) = (\gamma, d_t\alpha) + (\gamma, \delta_t\beta) + (\gamma, \gamma) \\ &= (\delta_t\gamma, \alpha) + (d_t\gamma, \beta) + (\gamma, \gamma) \\ &= (\gamma, \gamma) \end{aligned}$$

and then $\gamma = 0$. It follows that

$$\lambda = d_t\alpha + \delta_t\beta.$$

We shall put now

$$\eta = \mu + \nu$$

and try to solve the equations

$$W_t^{(p)}(\mu) = d_t\alpha$$

and

$$W_t^{(p)}(\nu) = \delta_t \beta.$$

Using again Theorem 1.1 (i) we have:

$$\begin{aligned} \alpha &= d_t \alpha_1 + \delta_t \beta_1 + \gamma_1 \\ d_t \alpha &= d_t \delta_t \beta_1 \\ \beta_1 &= d_t \alpha_2 + \delta_t \beta_2 + \gamma_2 \\ d_t \delta_t \beta_1 &= (d_t \delta_t + \delta_t d_t)(d_t \alpha_2) = W_t^{(p)}(d_t \alpha_2). \end{aligned}$$

It follows that:

$$W_t^{(p)}(\mu) = d_t \alpha, \quad \text{with } \mu = d_t \alpha_2.$$

ν can be obtained in a similar manner.

q.e.d.

COROLLARY 2.1 The equations

$$W_t^{(p)}(\mu) = d_t \lambda$$

and

$$W_t^{(p)}(\nu) = \delta_t \lambda$$

have always solutions.

Using now the induction over m we can prove also

THEOREM 2.3 The equation

$$(W_t^{(p)})^m(\mu) = \lambda$$

has solution if and only if λ is orthogonal to $\mathcal{H}_t^p(M)$ with respect to the inner product (1.1).

3 Continuity properties

Let $\lambda_1^{(p)}(t, g)$ be the first nonzero eigenvalue of the Witten laplacian on p -forms and \mathcal{M} the space of Riemannian metrics on M endowed with the C^∞ -Whitney topology. Then we can define a map

$$\lambda_1^{(p)} : g \in \mathcal{M} \mapsto \lambda_1^{(p)}(g) = \lambda_1^{(p)}(t, g) \in (0, \infty) \quad (3.1)$$

and we can establish the following continuity result:

THEOREM 3.1 For each $p \in \mathbb{N}$, $0 \leq p \leq n$, the map $\lambda_1^{(p)}$ depends continuously on g in \mathcal{M} .

PROOF The proof will be obtained in three steps.

Step 1 The adjoint of $d_t + \delta_t$ is $d_t + \delta_t$. Indeed, we can write successively:

$$\begin{aligned} ((d_t + \delta_t)\alpha, \beta) &= (d_t\alpha, \beta) + (\delta_t\alpha, \beta) \\ &= (\alpha, \delta_t\beta) + (\alpha, d_t\beta) \\ &= (\alpha, (d_t + \delta_t)\beta). \end{aligned}$$

Step 2 $(d_t + \delta_t)^2(\alpha) = W_t^{(p)}(\alpha)$, for each $\alpha \in \mathcal{D}^p(M)$. Indeed,

$$\begin{aligned} (d_t + \delta_t)^2(\alpha) &= d_t^2\alpha + \delta_t^2\alpha + (d_t\delta_t\alpha + \delta_td_t\alpha) \\ &= (d_t\delta_t\alpha + \delta_td_t\alpha) \\ &= W_t^{(p)}(\alpha). \end{aligned}$$

Step 3 Let

$$\lambda(t) = \inf_{\substack{\alpha \in \mathcal{D}^p(M) \\ \alpha \neq 0}} \left\{ \frac{\|d_t\alpha + \delta_t\alpha\|^2}{\|\alpha\|^2} \right\}.$$

Then the equation:

$$W_t^{(p)}(\alpha) = \lambda(t)\alpha$$

has always a nonzero solution α . Since $\|d_t\alpha + \delta_t\alpha\|^2$, $\|\alpha\|^2$ depend continuously on g in \mathcal{M} and the infimum depends also continuously on α , we obtain the desired result.

q.e.d.

4 Witten laplacian and geometric quatization

Let (Q, g) be a geodesially complete Riemannian manifold, $M = T^*Q$ its cotangent bundle, $\bar{\tau}$ the vertical polarization on M and $\omega = d\theta$ its canonical symplectic structure.

Let h be the generator of geodesics on M , i.e.

$$h = \frac{1}{2} g^{ij} p_i p_j.$$

Then the classical quantum operator which is canonically associated to h is given by

$$(\delta_{\bar{\tau}})_h = -\frac{\hbar}{2} \left(\Delta - \frac{R}{6} \right),$$

where Δ is the Laplace operator and

$$R = g^{ij} R_{ij}$$

is the scalar curvature on M , [3, p. 179].

Let f be an C^∞ -function on M and t a real number such that the following relation holds:

$$t^2 \sum_{i,j=1}^n g^{ij} \frac{\partial f}{\partial x^j} \frac{\partial f}{\partial x^i} + t \sum_{i,j=1}^n \frac{\partial^2 f}{\partial x^i \partial x^j} [a^i, a^j] = \frac{\hbar}{12} \sum_{i,j=1}^n g^{ij} R_{ij}, \quad (4.1)$$

where

$$x^i = \begin{cases} q^i & \text{if } i = 1, \dots, n \\ p^i & \text{if } i = n + 1, \dots, 2n \end{cases}$$

and a^i [resp. a^{i*}] is the interior [resp. exterior] multiplication, [1].

Using now the local expression of the Witten laplacian on functions we have:

THEOREM 4.1 Under the restriction (4.1) the following equality holds:

$$(\delta_{\bar{r}})_h = -\frac{\hbar}{2} W_t^{(0)}.$$

Let us finish with the observation that it is an open and very tempting problem to decide if there exist other concrete situations where the quantum operator given by geometric quantization can be regarded as a Witten laplacian.

References

- [1] E. COMBET, Les inégalités des Morse d'après E. Witten, *Publ. Dept. Math. Lyon 1, Seminaire de Geometrie*, 1983-1984.
- [2] E. WITTEN, Supersymmetry and Morse theory, *J. Diff. Geometry*, 17 (1982), 661-691.
- [3] N. WOODHOUSE, *Geometric quantization*, Clarendon Press - Oxford (1980).

West University of Timișoara Seminarul de
Geometrie-Topologie B-dul V. Pârvan 4
1900 Timișoara, Romania

Universitatea de Științe Agricole și Medicină
Veterinară a Banatului din Timișoara, Cate-
dra de Matematică, Calea Aradului 119,
1900 Timișoara, Romania

SAMPLING EXPANSIONS FOR A CLASS OF BAND-PASS SIGNALS

Aldo De Sabata

"Politehnica" University of Timișoara

Dept. of Telecommunications

Bd. V. Pârvan nr. 2, 1900 Timișoara, România

Abstract

In this paper a sampling scheme for a class of complex valued, finite energy, multiband signals is presented, based on the Papoulis sampling procedure. An example of "bunch sampling" which leads to a closed form expansion is derived. The sampling densities are kept to a minimum in the Shannon-Landau sense, and the expansions are stable in the Cheung-Marks sense.

1. Sampling Procedure

Let I be a closed interval on the (angular) frequency axis, of length l , and let K be a finite set of positive integers. The class of signals we will consider, denoted B_S , consists of complex-valued, finite energy signals, whose spectrums are concentrated on:

$$S = \bigcup_{k \in K} (I + kI). \quad (1)$$

An example is shown in fig. 1, for $I = [-5\Omega/2; -3\Omega/2]$, and $K = \{1, 2, 4, 5\}$.

In order to derive a sampling expansion for such a signal we will use the multichannel sampling scheme (MSS) approach introduced by Papoulis [4]. Note that the Shannon-Landau sampling density of a signal from the class we deal with is $2\pi/N\Omega$, where:

$$N = \text{card}(K). \quad (2)$$

According to the MSS the signal $x(t)$ is, on one hand, input to a single filter with frequency response $H(\omega)$, and, on the other hand, it is the input of N filters with frequency responses $H_k(\omega)$, $k=0..(N-1)$ (fig. 2). The single filter output $y(t)$ will be expressed in terms of the sampled outputs of the other filters $y_k(nT)$, taken at a rate $T=2\pi/\Omega$, and some functions to be obtained:

$$y(t) = \sum_{k=0}^{N-1} \sum_n y_k(nT) f_k(t-nT). \quad (3)$$

We shall denote, as usual, by $X(\omega)$, $Y(\omega)$ and $Y_k(\omega)$ the Fourier transforms of $x(t)$, $y(t)$ and $y_k(t)$ respectively.

The derivation of (3) includes some standard steps. First we have:

$$y(t) = \frac{1}{2\pi} \int_S X(\omega) H(\omega) e^{j\omega t} d\omega. \quad (4)$$

Let $\phi_l(\omega, t)$ be some Ω -periodic functions in ω such that, for every t :

$$H(\omega) e^{j\omega t} = \sum_{l=0}^{N-1} H_l(\omega) \Phi_l(\omega, t), \quad \omega \in S. \quad (5)$$

The existence of Φ_l is ensured under a certain independence condition on H_k to be derived now. (5) can be written as a system:

$$H(\omega + k\Omega) e^{j(\omega + k\Omega)t} = \sum_{l=0}^{N-1} H_l(\omega + k\Omega) \Phi_l(\omega, t), \quad \omega \in I. \quad (6)$$

If the determinant of this system of equations is non-zero a. e. on I , then the $\phi_l(\omega, t)$ are uniquely determined on I and, implicitly, on the whole frequency axis through Ω -periodicity. The condition:

$$\Delta(\omega) = \det \|a_{kl}\| = \det \|H_l(\omega + k\Omega)\| \neq 0, \quad k \in K, \quad l = 0..N-1, \quad \omega \in I \quad (7)$$

is known as "the independence condition" on H_k [4].

Now, $\Phi_l(\omega, t)$ can be developed in a Fourier series for every t :

$$\Phi_l(\omega, t) = \sum_n b_l(n, t) e^{jn2\pi\omega/\Omega}. \quad (8)$$

Let:

$$T = \frac{2\pi}{\Omega}. \quad (9)$$

The substitution of (8) and (5) into (4) yields:

$$y(t) = \frac{1}{2\pi} \int_S X(\omega) \sum_{l=0}^{N-1} H_l(\omega) \sum_n b_l(n, t) e^{jn\omega T} = \quad (10)$$

$$= \sum_{l=0}^{N-1} \sum_n b_l(n, t) \frac{1}{2\pi} \int_S X(\omega) H_l(\omega) e^{jn\omega t} d\omega = \sum_{l=0}^{N-1} \sum_n y_l(nT) b_l(n, t).$$

Now we will prove that:

$$b_l(n, t) = b_l(0, t - nT). \quad (11)$$

The substitution of t with $t - mT$ in (5) yields, by taking into account (8):

$$H(\omega) e^{j\omega(t-mT)} = \sum_{l=0}^{N-1} \sum_n b_l(n, t - mT) e^{jn\omega T},$$

which implies:

$$H(\omega) e^{j\omega t} = \sum_{l=0}^{N-1} H_l(\omega) \sum_n b_l(n, t - mT) e^{j(n+m)\omega T}, \quad \omega \in I.$$

As both the solution of (6) and the expansions of Φ_l are unique, there results:

$$b_l(n+m, t) = b_l(n, t - mT).$$

For $n=0$ we obtain (11) with n replaced by m . We will summarize this procedure in the following:

Proposition. For every signal from B_S the equation (3) holds in connection with the systems in fig. 2 if the frequency responses H_k satisfy the independence condition (7). The functions f_l are the continuous components (zero frequency terms) of the developments in Fourier series of the Ω -periodic functions defined on I in (6).

Note that until now the MSS has been applied to signals whose spectrum support has been an interval, which is not the case here.

2. Example

As an example we will derive a sampling expansion for a signal with the spectrum as in fig. 1. We will put $N=4$, and we will take all the systems in fig. 2 as pure delays:

$$H(\omega) = e^{j\omega\tau}, \quad H_l(\omega) = e^{j\omega\tau_l}, \quad l=0..3. \quad (12)$$

We need the following simple algebraic identity:

$$\Delta(a,b,c,d) = \begin{vmatrix} 1 & 1 & 1 & 1 \\ a & b & c & d \\ a^3 & b^3 & c^3 & d^3 \\ a^4 & b^4 & c^4 & d^4 \end{vmatrix} = V_4(a,b,c,d)(ab+ac+ad+bc+bd+cd) \quad (13)$$

where $V_4(a,b,c,d)$ is the fourth order Vandermonde determinant.

Direct application of the MSS and of (13) lead, after some algebraic manipulations to:

$$f_0(t) = \frac{\sin[\frac{\Omega}{2}(t-\tau+\tau_0)]}{\frac{\Omega}{2}(t-\tau+\tau_0)} \times \frac{\sin[\frac{\Omega}{2}(t-\tau+\tau_1)]\sin[\frac{\Omega}{2}(t-\tau+\tau_2)]\sin[\frac{\Omega}{2}(t-\tau+\tau_3)]}{\sin[\frac{\Omega}{2}(\tau_1-\tau_0)]\sin[\frac{\Omega}{2}(\tau_2-\tau_0)]\sin[\frac{\Omega}{2}(\tau_3-\tau_0)]} \times$$

$$\times \frac{\cos[\frac{\Omega}{2}(t-\tau-\tau_1+\tau_2+\tau_3)] + \cos[\frac{\Omega}{2}(t-\tau+\tau_1-\tau_2+\tau_3)] + \cos[\frac{\Omega}{2}(t-\tau+\tau_1+\tau_2-\tau_3)]}{\cos[\frac{\Omega}{2}(\tau_0+\tau_1-\tau_2-\tau_3)] + \cos[\frac{\Omega}{2}(\tau_0-\tau_1+\tau_2-\tau_3)] + \cos[\frac{\Omega}{2}(\tau_0-\tau_1-\tau_2+\tau_3)]}. \quad (14)$$

f_1 , f_2 , and f_3 can be obtained from (14) through the circular shift of the set $\{0,1,2,3\}$. These functions are to be substituted into (3) in order to obtain the sampling expansion of $x(t-\tau)$ at the Shannon-Landau density. The delays must be chosen such that the independence condition (7) be observed, but this is not very restrictive. Note that the sampling expansion is in a closed form.

3. Stability considerations

The Cheung-Marks stability of the considered sampling scheme deals with

perturbed values of the samples $y_1(nT)$, which is a more realistic case. If instead of $y_1(nT)$ one disposes of the values $y_1(nT) + X_n$, where X_n are uncorrelated random variables with zero mean and the same variance σ , the sampling expansion is said to be stable if the reconstructed signal tends to $y(t)$ as $\sigma \rightarrow 0$. In the sequel we consider $\tau=0$. In this context the sampling scheme can be viewed as in fig. 3 [1], [2]. The pre- and post-filters, not necessarily realizable, are related in the frequency domain through [1], [2]:

$$\|a_k\| \|b_{mq}\| = \frac{1}{T} I, \quad (15)$$

where I is the N 'th order identity matrix, the matrix $\|a_k\|$ is defined in (7), and:

$$\|b_{mq}\| = \|G_m(\omega + q\Omega)\|, \quad q \in K, m=0..M-1. \quad (16)$$

In order to apply the theory from the above cited literature we must view B_S as a subclass of the class of finite energy signals defined on the smallest interval which contain S . Then, if the H_i are bounded, square-integrable functions, it is known that the sampling scheme is stable if and only if the G_i are square integrable on I . Furthermore, a sufficient condition for stability is that the determinant $\Delta(\omega)$ must be bounded away from zero on I :

$$|\Delta(\omega)| > \delta > 0, \quad \omega \in I. \quad (17)$$

In the given example we have:

$$\Delta(\omega) = \prod_{l \geq 0}^3 |e^{j\Omega\tau_l} - e^{j\Omega\tau_k}| \times \left| \sum_{k \geq 0}^3 e^{j\Omega(\tau_l + \tau_k)} \right| > 0$$

if the independence condition is met for every $\omega \in I$.

Conclusions

We have shown in this paper that the Papoulis sampling scheme is more flexible than presented until now, in the sense that it can be applied to signals whose spectrums contain gaps. The bands in the spectrum can be closer together than allowed by other sampling techniques [3]. As an example, we have presented a stable "bunch sampling" of a signal, which seems to be new. The sampling scheme we have presented in the 1-D

case can be extended to higher dimensions, provided that the spectrum of the signal results from integer translations of a connected set in which a Fourier series is defined, such as a hypercube.

References

- [1] J. L. Brown Jr., S. D. Cabrera, *Multi-Channel Signal Reconstruction Using Noisy Samples*, Proc. 1990 Int. Conf. IEEE-ASSP, Albuquerque, NM, pp. 1233-1236, Apr. 1990.
- [2] ----- *On Well-Posedness of the Papoulis Generalized Sampling Expansion*, IEEE Tr. Circ. & Syst, vol. 38, No. 5, pp. 554-556, May 1991.
- [3] J. R. Higgins, *Some Gap Sampling Series for Multiband Signals*, Signal Processing, North Holland Pub., No. 12, pp. 313-319, 1987.
- [4] A. Papoulis, *Systems and Transforms with Applications in Optics*, Malabar, FL, Krieger Pub., 1981.

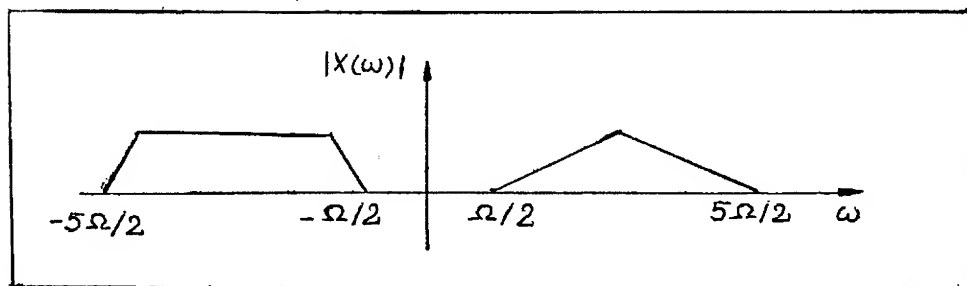


Fig. 1. Example for the Fourier spectrum.

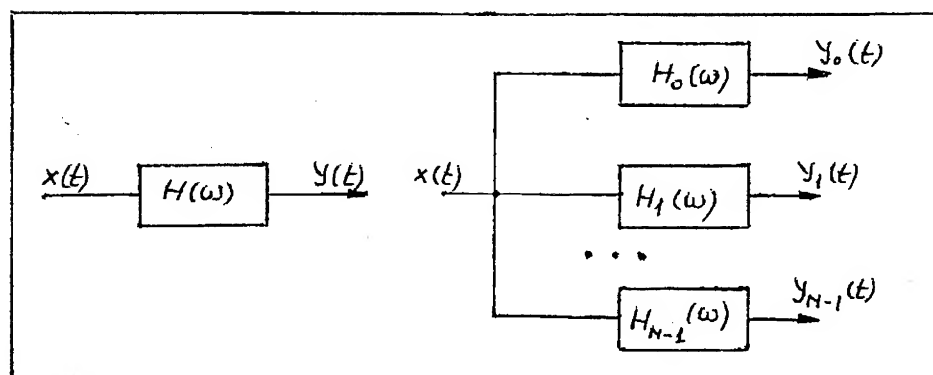


Fig. 2. The multi-channel sampling scheme.

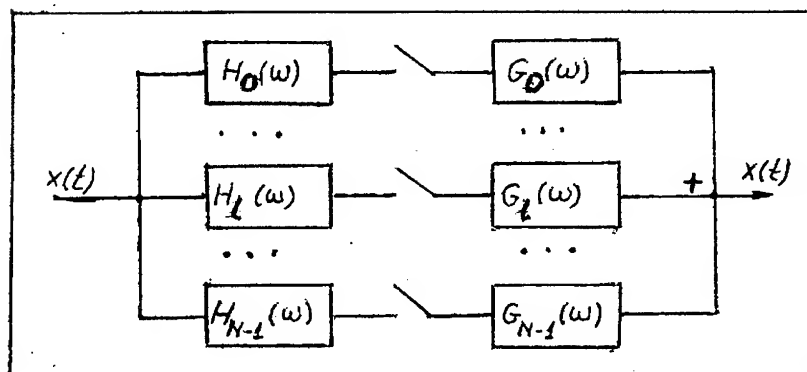


Fig. 3. The sampling scheme in the context of pre- and post-filters.

Cascade of creation-annihilation of symmetric periodic orbits in a reversible flow

Emilia Petrişor

"Politehnica" University of Timişoara

Department of Mathematics

Str. M. Viteazul nr.1

e-mail emilia@utt.ro

Abstract

We investigate numerically the dynamics of a reversible laser flow simulating a Poincaré map associated to the vector field defining the system. Using shooting method we locate some symmetric periodic orbits of the chosen Poincaré map, and their type. A cascade of creation-annihilation of periodic orbits is put into evidence, and bifurcation of a 1:3 resonant elliptic fixed point.

Introduction

The growing interest for laser systems led to the investigation of some models for such systems. According to the relation among the three damping rates for polarization, population inversion and field amplitude the lasers can be classified into three classes, called class *A*, *B*, respectively *C*.

A class-*B* laser system is modelled [Politi, 1986] by a three dimensional reversible nonlinear dynamical system. In cylindrical coordinates an approximation of this class laser with injected signal is given

by:

$$\begin{aligned}\dot{r} &= zr + A \cos \theta \\ \dot{\theta} &= -1 - (A/r) \sin \theta \\ \dot{z} &= D - \alpha r^2,\end{aligned}$$

where r is the field amplitude, z the population inversion, θ the field phase, D the pump parameter and A the amplitude of the external signal.

The Poincaré map associated with a transversal section to the above vector field is the first known example of nonarea-preserving reversible diffeomorphism exhibiting both conservative and dissipative behaviour, and symmetry breaking bifurcation (Rimmer bifurcation) [Post,1990] of a fixed point.

We introduced a slight modification of the third component of the vector field describing the dynamics of the class- B laser, namely a third parameter of control of the amplitude of z , $\alpha > 0$, so that $\dot{z} = D - \alpha r^2$. This modification generated a wealth of intricate and unknown behaviours, as far as we know, in a reversible system.

Numerical simulations of a Poincaré map associated to the modified system suggested the theoretical approach of the dynamics of reversible diffeomorphisms of an open annulus $(a, \infty) \times S^1$, $a > 0$, that are perturbations of an integrable one, whose closed orbits have rotation numbers decreasing from ∞ to 0 as the radius of invariant circles increases from 0 to ∞ [Petrişor, 1997].

Because the main feature of the systems to be investigated next is the reversibility, recall some results concerning this class of dynamical systems.

Let R be an involution (reversor) of \mathbf{R}^n , that is a C^1 diffeomorphism satisfying $R \circ R = id$. A complete C^1 -vector field $V : D \subseteq \mathbf{R}^n \rightarrow \mathbf{R}^n$ is called R -reversible vector field if

$$dR \circ V = -V \circ R, \quad (1)$$

Denoting by Φ_t the flow of the vector field V condition (1) implies:

$$R\Phi_t = \Phi_{-t}R, \quad \forall t \in \mathbf{R} \quad (2)$$

This means that along with $x(t) = \Phi_t x_0$, $Rx(-t) = R\Phi_{-t}x_0$ is also a solution of the system defined by the vector field V . The orbit

$\Phi_t x_0$ of the point $x_0 \in \mathbf{R}^n$ is called symmetric with respect to R if $\Phi_t x_0 = R \Phi_{-t} x_0$. Taking $t = 0$ we get $R x_0 = x_0$, i.e. a symmetric orbit is the orbit of a point in the set $\text{Fix}(R)$. If the orbit of $x_0 \in \text{Fix}(R)$ is periodic then it reintersects $\text{Fix}(R)$. Such an orbit is called symmetric cycle.

Let R be a fixed C^∞ involution of the smooth manifold M_{2n} , with $\dim(\text{Fix}(R)) = n$. A $C^r, r \geq 1$ diffeomorphism f of M is called R -reversible diffeomorphism if $I = f \circ R$ is also an involution. So $f = I \circ R$, and $f^{-1} = R \circ f \circ R$.

The conjugation of f to f^{-1} by R ensures that $f^k = R \circ f^{-k} \circ R$, $\forall k \in \mathbf{Z}$, that is f^k is also an R -reversible diffeomorphism. It is clear that the diffeomorphisms $I_j = f^j \circ R$ are also involutions for every $j \in \mathbf{Z}$. Denote by $\Gamma_j = \text{Fix}(I_j)$. Γ_j is called the j th symmetry submanifold of f . Γ_0 is the fixed point set for R , while Γ_1 for I . It is known [Devaney, 1976] that a point $x \in \Gamma_j \cap \Gamma_k$ is a periodic point of the R -reversible diffeomorphism f , whose period divide $|j - k|$. Conversely, if $x \in \Gamma_j$ is a periodic point for f , then there is a $k \in \mathbf{Z}$ such that $x \in \Gamma_k$. Hence some periodic points lie on a symmetry submanifold. Such periodic points are called symmetric periodic points. But obviously the diffeomorphism can also have asymmetric periodic points. For more information on discrete reversible dynamical systems see [Roberts, 1992].

A large interest there is in the study of persistence/breaking up of invariant circles (so called KAM circles) of a reversible diffeomorphism of the plane, cylinder or annulus that is a perturbation of an integrable system, whose integrals are circles. The reversible KAM theory is presented in [Sevryuk, 1986].

The persistence of KAM curves has an important implication for the stability of dynamics of the system. These invariant curves are boundaries for strips on the phase space. The orbit of a point in such a strip has a confined dynamics and therefore cannot wander arbitrarily far in the phase space. The breakup of the KAM curves corresponds to the loss of stability and confinement.

Analysis of the model

In cartesian coordinates the vector field describing the dynamics of our system is:

$$V(x, y, z) = (xz + y + A, yz - x, D - \alpha(x^2 + y^2)).$$

It is nonconservative because $\text{div}(V) = 2z$. It is reversible with respect to the involution $R: \mathbf{R}^3 \rightarrow \mathbf{R}^3$, $R(x, y, z) = (-x, y, -z)$, having fixed point set $\text{Fix}(R) = \{(x, y, z) \in \mathbf{R}^3 \mid x = 0, z = 0\}$.

For $A^2 \geq \frac{D}{\alpha}$ the vector field has two assymetric equilibrium points, one stable and another unstable.

We are interested in the case $A^2 < \frac{D}{\alpha}$. For fixed D , and α ($D = 4/3$ a choice made in [Politi, 1986] according to realistic conditions, and $\alpha = 4/9$) we study the bifurcation of periodic points and Kolmogorov tori as A increases from zero to $\sqrt{\frac{D}{\alpha}}$.

Subjecting the unperturbed system ($A = 0$) given in cylindrical coordinates to the transformation $(r, \theta, z) \rightarrow (s = \ln r, \theta, z)$ it becomes:

$$\begin{aligned}\dot{s} &= z \\ \dot{\theta} &= -1 \\ \dot{z} &= D - \alpha e^{2s}\end{aligned}\tag{3}$$

It is clear that the system (3) may be embedded in a Hamiltonian system with two degrees of freedom, generated by the Hamilton function $H(u, s, \theta, z)$

$$= \frac{z^2}{2} - Ds + \frac{1}{2}\alpha e^{2s} + u, \text{ i.e.}$$

$$\begin{aligned}\dot{u} &= \frac{\partial H}{\partial \theta} = 0 \\ \dot{s} &= \frac{\partial H}{\partial z} = z \\ \dot{\theta} &= -\frac{\partial H}{\partial u} = -1 \\ \dot{z} &= -\frac{\partial H}{\partial s} = D - \alpha e^{2s}\end{aligned}$$

The phase space is foliated by the two-dimensional surfaces

$$\begin{aligned} u &= C \\ \frac{z^2}{2} - Ds + \frac{1}{2}\alpha e^{2s} &= K \end{aligned}$$

These submanifolds are compact surfaces and by the theory of integrable Hamiltonian systems they are diffeomorphically tori.

In original cylindrical coordinates the tori in \mathbf{R}^3 are:

$$T_k : \quad \frac{z^2}{2} + \alpha \frac{r^2}{2} - D \ln r = K.$$

They are symmetric under the reflection in the plane $z = 0$. Their intersection to the plane $z = 0$ is defined by the set of intersections of the parabolas $q = \frac{\alpha}{2}r^2 - K$ to the logarithmic graph $q = D \ln r$.

The two graphs have tangential contact for $K_0 = \frac{D}{2} \left(1 - \ln \frac{D}{\alpha} \right)$ at $r = \sqrt{\frac{D}{\alpha}}$, and two points of intersection (r_m, q_m) , (r_M, q_M) , $r_m < \sqrt{\frac{D}{\alpha}} < r_M$, for $K > K_0$. Therefore the phase space of the unperturbed system is foliated by the tori

$$\alpha \frac{x^2 + y^2}{2} + \frac{z^2}{2} - D \ln(x^2 + y^2) = K, \quad K \geq K_0$$

surrounding the symmetric cycle $\Gamma : x^2 + y^2 = D/\alpha, z = 0$.

Obviously, after the change of coordinates defined by $s = \ln(x^2 + y^2)$ the motion of these tori is no longer conservative, because the flow of the vector field in cartesian coordinates does not preserve the volumes ($\text{div} V \neq 0$).

Hence the unperturbed system in cartesian coordinates is derived by a non-symplectic change of coordinates from an integrable Hamiltonian system. Excepting the points of the circle $x^2 + y^2 = D/\alpha$ the plane $z = 0$ is transversal to the unperturbed vector field. Denote $\Sigma = \{(x, y, z) | z = 0, x^2 + y^2 > D/\alpha\}$ and define the Poincaré map $P : \Sigma \rightarrow \Sigma$, $P(M_0) = \Phi_{t(M_0)} M_0$, where Φ_t is the flow of the vector field, and $t(M_0)$ is the first time of the reintersection of the orbit of M_0 to Σ . Obviously P is an integrable reversible diffeomorphism. The reversor is the reflection denoted also R , $R(x, y) = (-x, y)$. Its

invariant curves are the circles $\gamma_\rho : z = 0, x^2 + y^2 = \rho, \rho > D/\alpha$, i.e. the circles $z = 0, r = r_M$ of intersection of invariant tori of the vector field V to Σ . As $\rho \rightarrow D/\alpha$ the rotation numbers of the orbits of points on the circles γ_ρ tend to ∞ , while for $\rho \rightarrow \infty$, the rotation numbers tend to 0. If one denotes by ω_1, ω_2 the frequencies of motion on a torus in the direction of parallels, respectively in the direction of meridians, then the frequencies on the symmetric cycle are $(\omega_1, 0)$, that explains the above limits for rotation numbers.

Our chosen Poincaré map P in conjugated to another one $\tilde{P} : \tilde{\Sigma} \rightarrow \tilde{\Sigma}$, where $\tilde{\Sigma} = \left\{ (x, y, z) \mid z = 0, 0 < x^2 + y^2 < \frac{D}{\alpha} \right\}$, and the conjugation is the semi-Poincaré map $\pi : \Sigma \rightarrow \tilde{\Sigma}$, i.e. $\pi(M_0)$ is the first reintersection of the orbit of M_0 to the plane $z = 0$, or more precisely to $\tilde{\Sigma}$.

For the perturbed system choose the transversal section in the same way, namely the surface at which the orbits attain (in cylindrical coordinates) their extremal amplitudes r_{\max} and r_{\min} , i.e. $\dot{r} = 0$.

Thus the surface of section is

$$\Sigma = \{(r, \theta, z) \mid zr + A \cos \theta = 0\} = \left\{ (x, y, z) \mid z = -\frac{Ax}{x^2 + y^2} \right\}.$$

Consider the Poincaré map

$$P : \Sigma \rightarrow \Sigma$$

that associates to a point $M_0 \in \Sigma$ the point $\Phi_t(M_0) \in \Sigma$, where $t > 0$ is the smallest such that $\Phi_t M_0$ is a point of maximum for r along the orbit of M_0 .

In numerical simulations in order to plot the points of Σ at which r is max we retain the point of intersection to Σ when orbit crosses Σ from the region Σ_+ to the region Σ_- , where

$$\Sigma_{\pm} = \left\{ (x, y, z) \mid z \gtrless -\frac{Ax}{x^2 + y^2} \right\}.$$

As in the unperturbed case the intersection of a trajectory of the vector field from Σ_- to Σ_+ generates a point of the orbit under a conjugated to P , Poincaré map.

Observe that the fixed point set of the reversor of the vector field V minus the origin lies on the surface Σ . Hence the Poincaré map is a reversible diffeomorphism with respect to the involution $R : \Sigma \rightarrow$

Σ , $R(x, y, z) = (-x, y, -z)$. Obviously P is not area-preserving and as a consequence, the second involution $I = P \circ R|_{\Sigma}$ in the decomposition of P is not area-preserving.

Numerical results

We simulated the Poincaré map for different values of $A \in [0, 0.26]$, and D, α fixed at the values $4/3$, respectively $4/9$. We started with a very small perturbation, $A = 10^{-3}$. The corresponding mapping P has three fixed points: a pair of Birkhoff fixed points, one elliptic and another saddle, and a third elliptic point above the saddle one on the symmetry line Γ_0 . This fact reveals that the symmetry line $\Gamma_1 = \text{Fix}(I)$ intersects Γ_0 at three distinct points. The stable and unstable manifolds associated to the saddle point define two homoclinic loops intersecting Γ_0 at two points, and between them is located an elliptic point (Fig. 1).

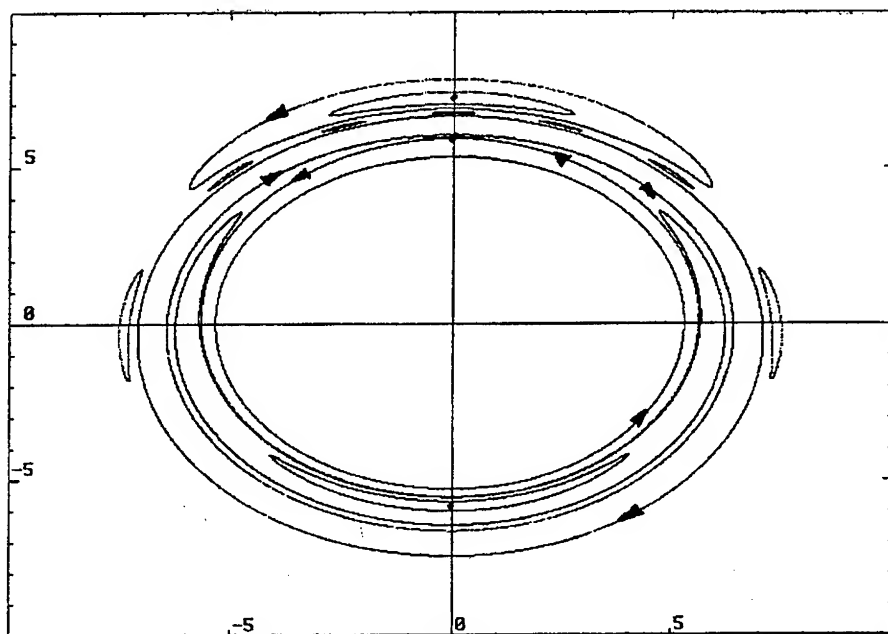


FIG. 1. Homoclinic loops to the saddle point. $A = 0.001$.

Since the orbit of a fixed point has zero rotation number, and persisting KAM curves are ordered by their rotation numbers, it follows

that the homoclinic loops separate the phase surface into two regions, one in which persisting KAM circles have negative rotation numbers and another where the rotation numbers are positive. This implies opposite directions of motion on the two different kinds of persisting KAM curves. Namely, the motion of the inner invariant circles is anticlockwise (positive rotation numbers) as well as on the innermost homoclinic loop, while on the outermost homoclinic loop and surrounding it persisting KAM curves the motion is clockwise. The third fixed point (of elliptic type) is surrounded by invariant curves (born at the same time with the fixed point) and the motion here is anticlockwise.

The direction of motion on the invariant circles around just born elliptic fixed points depends on the angle of intersection of the symmetry lines Γ_0, Γ_1 [Petrişor, 1997].

In this special situation when the reversible diffeomorphism has a pair of Birkhoff fixed points, and a third elliptic fixed point, there exist two centers of rotation on the phase surface: one at the origin and the second is the upper elliptic fixed point (Fig. 2).

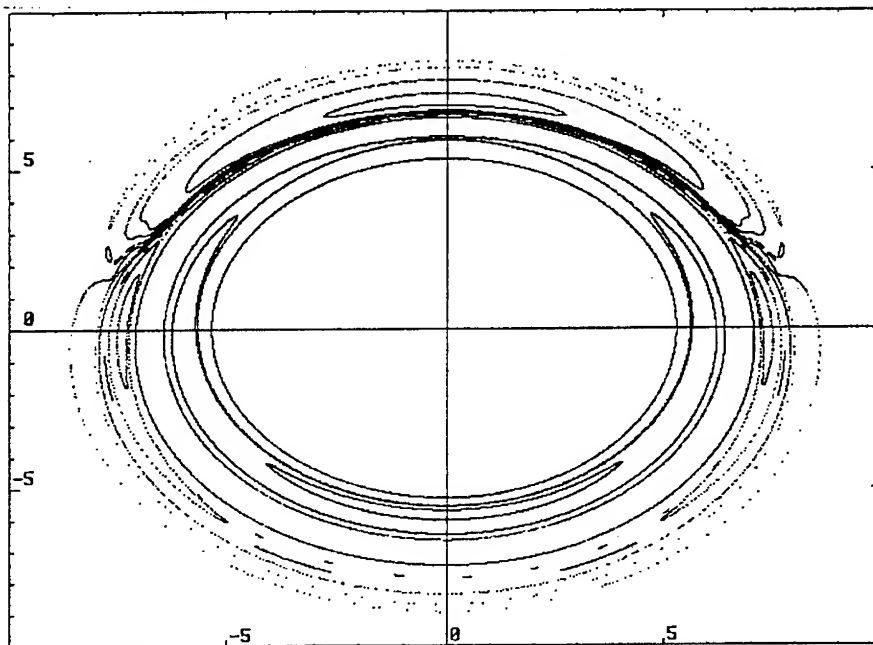


FIG. 2. Orbits rotating around the origin, and upper elliptic point.

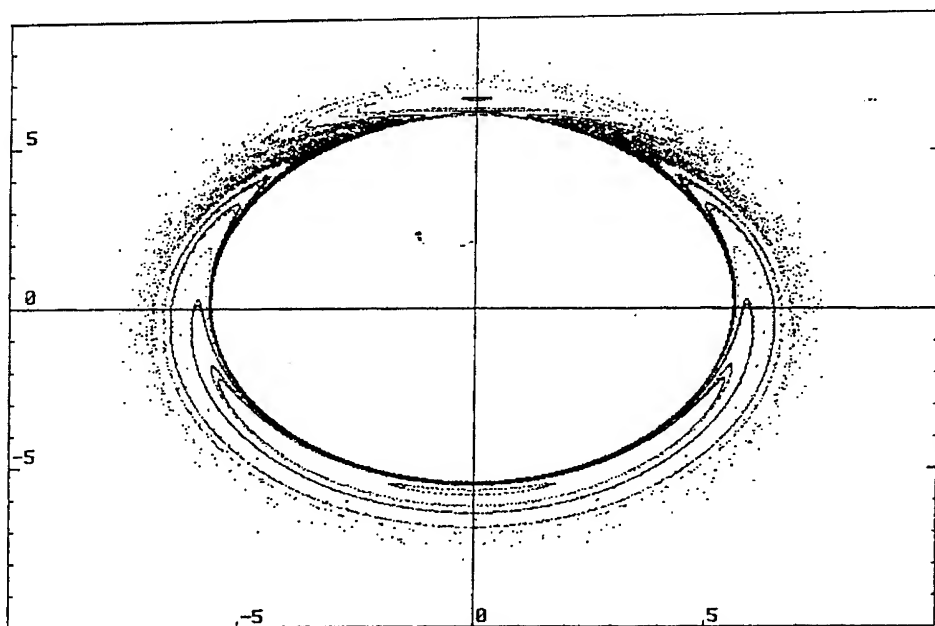


FIG. 3. Chaotic orbits at $A = 0.002$.

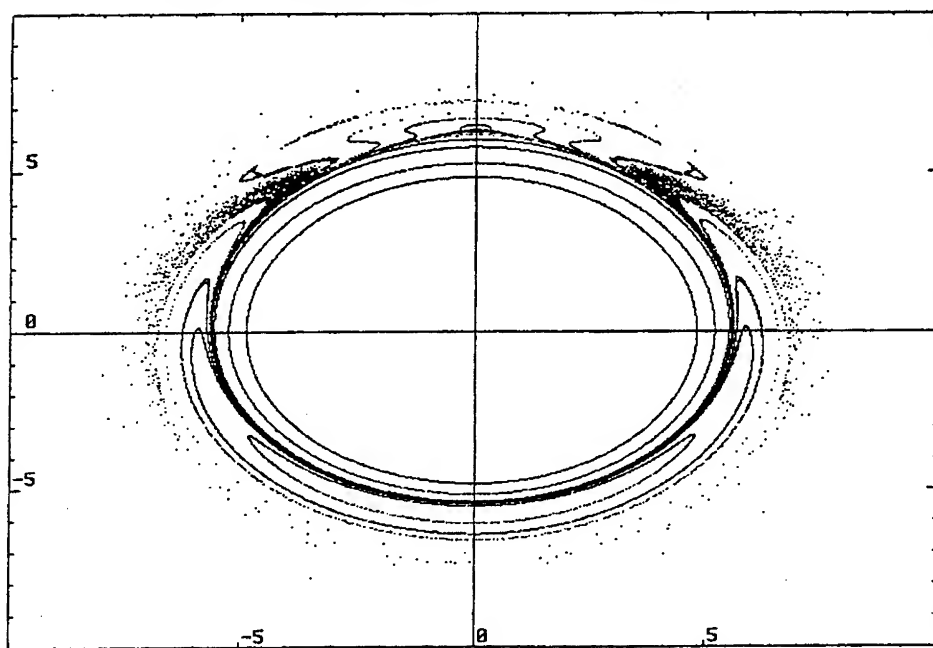


FIG. 4. Common invariant curves; $A = 0.022$.

The elliptic fixed points correspond to two symmetric cycles of the reversible vector field, and KAM circles surrounding them to deformed invariant tori. Unlike the deformed original symmetric cycle, these two cycles born after the perturbation connect an elliptic point of P to the corresponding elliptic fixed point of the conjugated to P Poincaré map, mentioned above.

As A increases to 0.002 the upper elliptic point moves downwards on the symmetry line Γ_0 to the saddle point, and KAM curves around the homoclinic loops, and the upper elliptic point breaks up giving rise to a chaotic layer (Fig. 3).

As the two fixed points become closer and closer, invariant curves surrounding both upper and central configuration appear (Fig. 4).

The two fixed points collide at 0.0023 when the symmetry line becomes tangent at a parabolic fixed point of P . By approximating Γ_1 by its osculating parabola at the point of tangency to Γ_0 it is explained [Petrişor, 1997] the collision and disappearance of two symmetric fixed points. After the disappearance of two symmetric fixed points chaotic motion persists around the remaining elliptic point (Fig. 5).

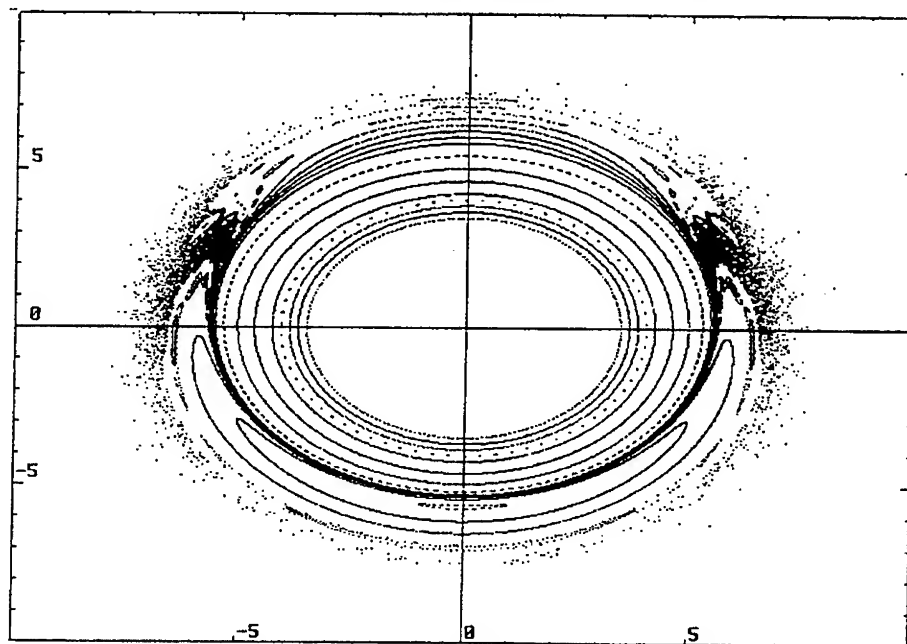


FIG. 5. Phase portrait for $A = 0.035$.

Note that the same scenario of the disappearance of the two sym-

metric fixed points exhibits the Politi's system too (corresponding to $\alpha = 1$), but it was not revealed.

Beginning with $A = 0.1$ a pair of three periodic orbits, one elliptic and another hyperbolic, is identified in the central annulus. Increasing more and more the parameter A no unusual behaviour for a reversible system is present up to A close to 0.23. As A increases over 0.2 the KAM curves surrounding three periodic orbits exhibit two points of inflection (symmetric with respect to Γ_0). These are due to an inflection point on the symmetric line Γ_1 [Petrîşor, 1997].

Near the value $A = 0.23$ the surrounding KAM circles of the elliptic fixed points also have two symmetric inflection points and the outermost ones break up and chaotic trajectories left behind interact to chaotic trajectories generated by disintegration of KAM curves surrounding the central annulus (Fig. 6).

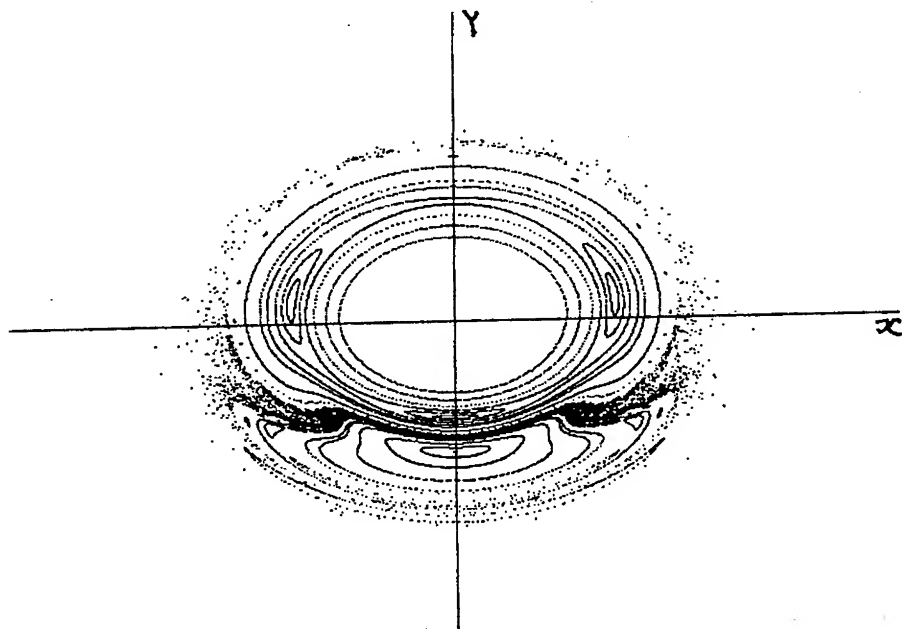


FIG. 6. Chaotic orbits surrounding both configurations; $A = 0.23$.

The elliptic fixed point passes through a strong 1:3 resonance for $A = 0.23624$, that is the linear part of the Poincaré map at this point has eigenvalues $\lambda_{1,2} = e^{\pm i \frac{2\pi}{3}}$.

Here takes place the birth of a pair of three periodic orbits, one of saddle type and another of elliptic type.

The three points of the saddle cycle are connected by a heteroclinic cycle around the persisting elliptic fixed point, and the points of the elliptic orbit are surrounded by a homoclinic loop to a corresponding saddle (Fig. 7a). Note that this configuration is stable and common invariant curves surround it up to A close to 0.2375 (Fig. 7b). As far as we know bifurcation of an elliptic point at 1:3 strong resonance for a general system gives birth to an unstable period three saddle [Kuznetsov, 1995], while for a reversible system Sevryuk [1986] gave an example of reversible diffeomorphism that also has an unstable elliptic fixed point after a bifurcation at a 1:3 resonance. Hence our system seems to be an exception. It remains as an open problem to derive the normal form of a reversible diffeomorphism on the annulus (as in [Petrisor, 1997]) around a 1:3 resonant elliptic fixed point, and to describe the bifurcations that can occur.

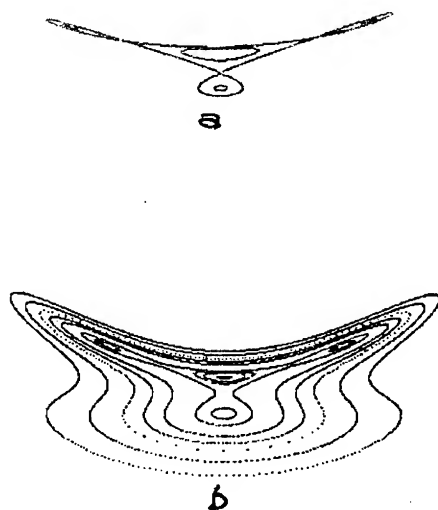


FIG. 7. a) Heteroclinic cycle, and homoclinic loops; $A = 0.2364$.
b) Invariant circles surrounding the structure a).

Increasing the parameter A , the points of the saddle cycle get closer and closer to the elliptic fixed point. The homoclinic loops break up following an

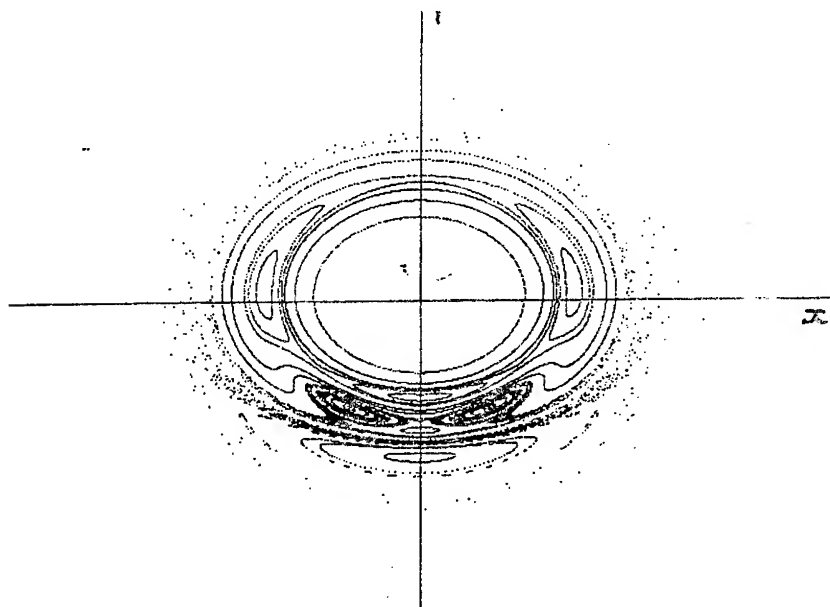


FIG. 8. Unstable lower three period orbits; $A = 2.43$
 unidentified scenario and the period three orbits turn out unstable
 (Fig. 8).

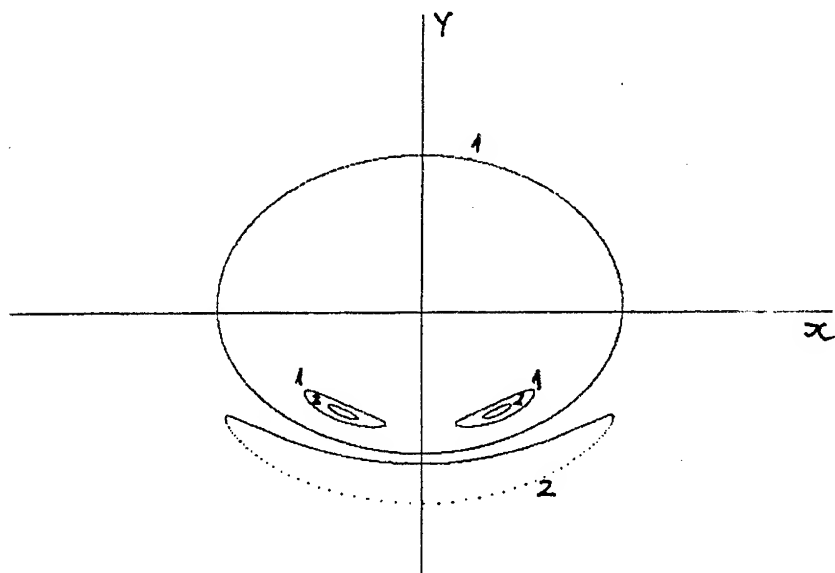


FIG. 9. Unstable orbit around lower three period elliptic orbit; $A = 0.2485$

The instability of lower three periodic orbits is more evident if one looks at the orbit in Fig. 9 denoted 1 in comparison to that denoted 2. The 1-orbit runs only around two of the three points of the period three elliptic orbit. The point belonging to the symmetry line Γ_0 is repulsive for some orbits.

The points of each saddle type orbit generate a family of six heteroclinic arcs (Fig. 10). The heteroclinic cycles of this structure, excepting two, namely the cycles surrounding two of the three period lower elliptic points, are stable. The mentioned two heteroclinic cycles are unstable only from interior.

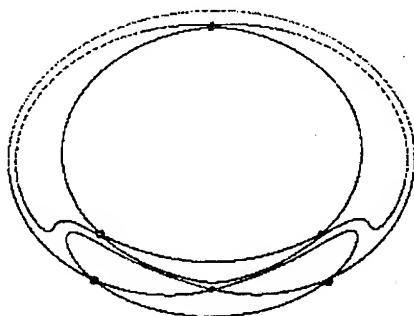


FIG. 10. The heteroclinic structure associated to the pair of saddle type three period orbits; $A = .25$.

After crossing the value 0.25 of the parameter A , the points of the central elliptic three period orbit move downwards (their y coordinate decreases), collide to the corresponding saddle points and disappear. This happens because the symmetry line Γ_1 had an inflection point and its arcs on the two sides of the inflection point were strongly folded, having each an intersection to the symmetry line Γ_4 . As the parameter increases to the value 0.259 the curvature of one of the arcs decreases, the arc passing through a tangential contact to Γ_4 and moving apart from Γ_4 . So disappears one of the two three period orbits. At the same time Γ_1 rotates around the origin and reintersects the symmetry line Γ_0 giving rise to a saddle fixed point.(Fig. 12).

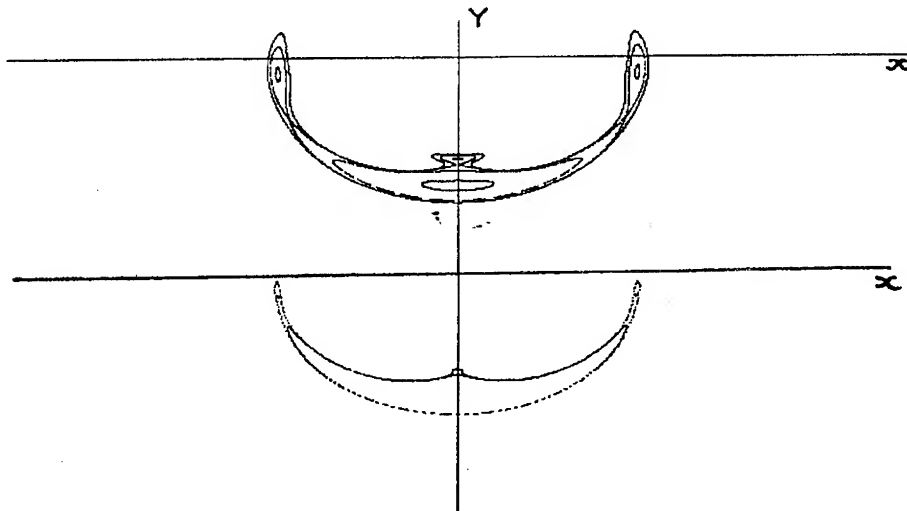


FIG. 11. Disappearance of a three period orbit; $A = .258, A = .2595$

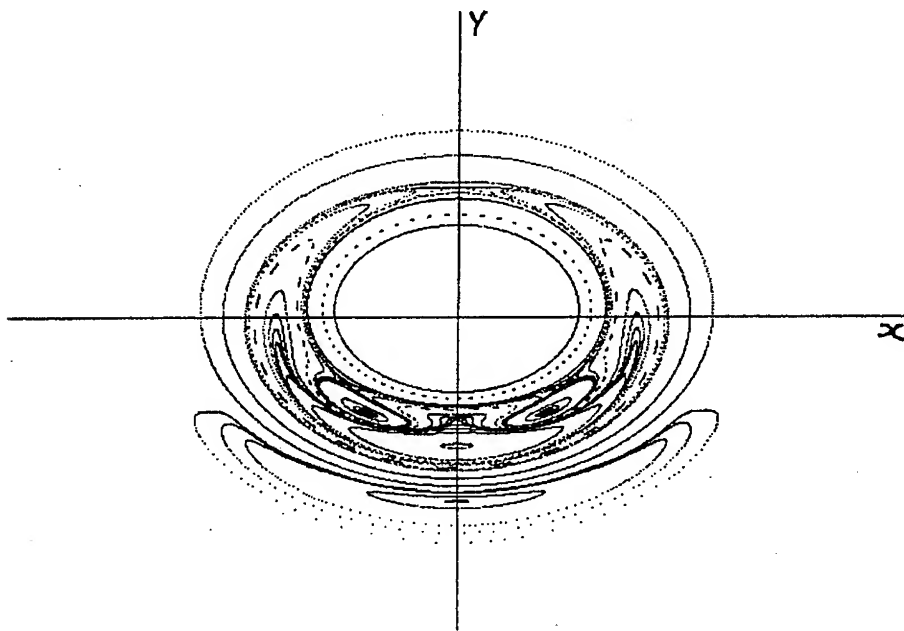


FIG. 12 The phase portrait after the reappearance of the saddle fixed point; $A = 0.26$.

Conclusions. The system we have investigated exhibits a wealth of unknown phenomena in the dynamics of two-dimensional reversible discrete systems (see the survey [Roberts, 1992]). As far as we know there are not reported until now examples of reversible systems whose

periodic (fixed points) disappear, and 1:3 resonant bifurcation leaving behind a stable behaviour in some range of the parameter of the system (see [Post, 1990] for a study of bifurcation of periodic points in planar reversible systems).

The main causes of this odd behaviour is rotation number decreasing order of invariant circles in the unperturbed map, that it is preserved in the perturbed system, and the successive foldings and rotation about the origin of the symmetry line Γ_1 . Similar bifurcations occur for values of $0.26 < A < \sqrt{D/\alpha}$.

References

- [1] **R.L. Devaney** Reversible diffeomorphisms and flows, *Trans. Am. Math. Soc.*, 218 (1976), 89–113.
- [2] **Y. A. Kuznetsov** Elements of applied bifurcation theory, Springer-Verlag, New-York, 1995.
- [3] **E. Petrişor** Creation and annihilation of symmetric periodic orbits in a class of reversible dynamical systems on the annulus, to appear.
- [4] **A. Politi, G.L. Oppo, R. Badii** Coexistence of conservative and dissipative behaviour in reversible dynamical systems, *Phys. Rev. A*, **33** (1986), 4055–4060.
- [5] **T. Post, H.W. Capel, G.R.W. Quispel, J.P. Van der Weele** Bifurcation in two dimensional reversible maps, *Physica A* 164 (1990), 635–662.
- [6] **J.A.G. Roberts, G.R.W. Quispel** Chaos and time reversal symmetry. Order and chaos in reversible dynamical systems, *Phys. Rep.* 216 (1992), 63–177.
- [7] **M. B. Sevryuk** Reversible systems, *Lect. Notes in Math.*, Vol. 1211, Springer-Verlag, Berlin, 1986.

A NUMERICAL SOLUTION OF EQUATIONS DESCRIBING THE THREE PHOTONS INTERACTION IN NONLINEAR OPTICAL MATERIALS

Dan G. Sipoșean,

Military Technical Academy, George Coșbuc Av.32-34, Bucharest, Romania

Ion Lăncrănjan

Solid State Laser TECHNOLOGIES S.R.L., Țîncăni St.10, Bucharest 77349, Romania

An analysis of spatial and temporal modulated waves parametric amplification on the picosecond time scale is presented. The three photons interaction in nonlinear KDP, LiJO_3 , LiNbO_3 nonlinear optical crystals is analysed regarding the definition of a mathematical model describing parametric amplification phenomenon.

The most important item of this mathematical model consists of the cvasi-optical equations describing the parametric interaction of spatial and temporal modulated waves propagating along the z axis. The contribution magnitudes of the terms entering into these differential equations is analysed. The analysed terms are related to phenomena of importance on picosecond and subpicosecond time scale such as:

- the group velocities dispersion of the waves with different frequencies propagating in dispersive media,
- the aperture effect,
- the transverse spatial extension of the waves - beam diffraction.

This term contribution analysis is done in order to obtain a more accurate numerical solution of the differential equations system describing the parametric optical amplification.

The main purpose of this more accurate numerical solution consists of obtaining enlarged possibilities for the design of Optical Parametric Oscillators and related nonlinear optical components used for manufacturing such a system. For example: necessary nonlinear crystal length evaluation, the optimum operation wavelength and the necessary pump radiation intensity become possible.

COMPUTER SIMULATION OF PASSIVE OPTICAL Q-SWITCHES LASER OPERATION THERMAL LOADING

Ion Lăncrăjan,

Solid State Laser TECHNOLOGIES S.R.L., Țincani St.10, Bucharest 77349, Romania

Dan G. Sipoșean,

Military Technical Academy, George Coșbuț Av.32-34, Bucharest, Romania

For an enlarged series of small volume high power solid state lasers scientific, technological applications the passive optical Q-switching represents a constructive solution because of its relative low costs and ease of construction, especially in comparison with electro-optical and acousto-optical Q-switching. It is attractive for designing special solid state laser configurations, such as those using Nd:YAG tube and slab active media geometries. The high power solid state laser oscillators design has an important part consisting in evaluation of passive Q-switches thermal loading during laser operation.

The purpose of this work is to present a numerical analysis performed for passive optical Q-switches designed for rod, tube and slab high power Nd:YAG laser oscillators. This analysis is developed specifically for use of lithium fluoride crystals with F_2^- color centers (LiF:F $_2^-$ crystals) passive Q-switches. A comparison with experimental data is performed. This analysis is based on numerical solving the thermal conductivity equation (Θ -temperature) for initial conditions resembling the specific laser configuration:

$$\frac{2(1 - e^{-\alpha_p l})}{\pi C_p \rho w^2} \frac{P_0}{1 - R} e^{-\frac{2r^2}{w^2}} + \frac{K}{C_p \rho} \left(\frac{\partial^2 \Theta}{\partial r^2} + \frac{1}{r} \frac{\partial \Theta}{\partial r} \right) = 0$$

with r as a radial coordinate versus laser beam axis, C_p the LiF specific heat ($C_p = 1615.3 \text{ Jkg}^{-1}\text{K}^{-1}$), ρ as the LiF density ($\rho = 2640 \text{ Kgm}^{-3}$), K the thermal conductivity ($K = 11 \text{ Wm}^{-1}\text{K}^{-1}$), α_p the LiF:F $_2^-$ parasitic absorption coefficient for the laser radiation circulating inside laser resonator, P_0 as the axial value of laser radiation intensity, w as the waist of the laser beam intensity distribution, l is the LiF:F $_2^-$ crystal length and R as the laser output mirror.

MODELAREA FENOMENELOR TERMICE ÎN ARDEREA DIFUZIVĂ A COMBUSTIBILILOR GAZOȘI

Ing. KARINA DUMITRU*

Preparator Ing. AMADO ȘTEFAN**

REZUMAT

Se prezintă particularitățile fenomenelor de schimb de masă și de căldură în procesul de ardere difuziv. Din ecuațiile de difuzie și ecuația de transport de căldură în ipoteza unui sistem adiabatic și a unei camere de ardere cilindrice se determină distribuția concentrației și ecuația suprafeței de ardere.

În marea majoritate a instalațiilor de ardere care folosesc combustibili gazoși este utilizată flacăra difuzivă, caracterizată prin formarea amestecului gaz-aer chiar în spațiul de ardere, componentele care reacționează fiind introduse separat.

1. STRUCTURA FLĂCĂRII DIFUZIVE

Timpul total necesar desfășurării procesului de ardere este format din doi termeni t_a și t_r , unde primul se referă la perioada necesară realizării contactului fizic dintre carburant și comburant, pentru aducerea sistemului la o temperatură care să permită propagarea frontului de flăcăre, iar al doilea termen reprezintă timpul necesar desfășurării reacției chimice.

În cazul flăcării difuzive se admite că viteza de reacție chimică este infinit de mare, ceea ce corepunde situației când concentrația combustibilului sau a oxigenului la suprafața de reacție este nulă.

* UNIVERSITATEA TEHNICĂ DE CONSTRUCȚII BUCUREȘTI

** ACADEMIA TEHNICĂ MILITARĂ

Către suprafața de reacție difuzează carburantul și comburantul conform legii lui Fick, iar la suprafața de reacție acestea difuzează complet în proporție stoichiometrică ($\alpha = 1$).

Se consideră o cameră de ardere cilindrică de rază R prin care circulă un curent de aer și un ajutaj central, de rază r ($r < R$) prin care trec gaze combustibile (Fig.1), în care este reprezentat frontul flăcării difuzive pentru coeficientul de exces de aer $\alpha > 1$. Mărimile care se referă la gazul combustibil se notează cu indicele 1, oxidantul cu indicele 2, iar mărimile inițiale cu indicele 0.

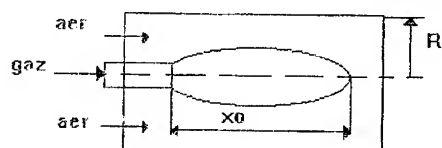


Fig.1

2. ECUAȚIILE DE DIFUZIE ȘI ECUAȚIA DE TRANSPORT DE CĂLDURĂ

Ecuatiile de difuzie, fără a considera efectul Soret, în coordonate cilindrice pentru cele două fluide sunt :

$$u \frac{\partial C_1}{\partial x} = D \left[\frac{\partial^2 C_1}{\partial x^2} + \frac{1}{y} \frac{\partial}{\partial y} \left(y \frac{\partial C_1}{\partial y} \right) \right] - W_1 \quad (1)$$

$$u \frac{\partial C_2}{\partial x} = D \left[\frac{\partial^2 C_2}{\partial x^2} + \frac{1}{y} \frac{\partial}{\partial y} \left(y \frac{\partial C_2}{\partial y} \right) \right] - W_2 \quad (2)$$

respectiv:

$$u \frac{\partial T}{\partial x} = a \left[\frac{\partial^2 T}{\partial x^2} + \frac{1}{y} \frac{\partial}{\partial y} \left(y \frac{\partial T}{\partial y} \right) \right] + \frac{q_1}{c_p} + W \frac{q_0}{c_p} \quad (3)$$

unde C_1 , C_2 sunt concentrațiile; D - coeficientul de difuzie moleculară ; W - cantitatea de fluid în moli care reacționează în unitatea de timp (viteza de reacție chimică); T - temperatura; a - coeficientul de difuzie a temperaturii ($a = \frac{\lambda}{\rho c_p}$, iar în cazul gazelor

ideale $D=a$); u - viteza axială; q_0 - căldura de reacție pentru un mol de amestec stoechiometric din fluidele 1 și 2; q_r - fluxul de căldură cedat de unitatea de volum în spațiul de ardere către mediul exterior.

Condițiile la limită ale sistemului de ecuații (1), (2), (3) sunt:

a) la intrarea în camera de ardere ($x=0$):

$$\begin{aligned} 0 \leq y \leq r, C_1 = C_{10}, C_2 = 0, T = T_{10} \\ r \leq y \leq R, C_1 = 0, C_2 = C_{20}, T = T_{20} \end{aligned} \quad (4)$$

b) la pereții camerei de ardere ($y = R$):

$$\frac{\partial C_1}{\partial y} = 0, \frac{\partial C_2}{\partial y} = 0, -\lambda \text{grad} T + q_r = -\lambda_p \text{grad} T_p \quad (5)$$

care exprimă condițiile de izolare masică și condițiile de schimb de căldură. Condiția schimbului de căldură este determinată de egalitatea dintre suma fluxurilor de căldură prin conductibilitate în stratul limită la pereți ($-\lambda \text{grad} T$) prin radiația q_r și fluxul de căldură transmis prin pereți către exterior ($-\lambda_p \text{grad} T_p$). În cazul izolării adiabactice a sistemului, $q_r = 0$, $\lambda_p \text{grad} T_p = 0$, de unde rezultă condiția $\frac{\partial T}{\partial y} = 0$;

c) pe axul camerei ($y = 0$), din condițiile de simetrie ale sistemului

$$\frac{\partial C_1}{\partial y} = 0, \frac{\partial C_2}{\partial y} = 0, \frac{\partial T}{\partial y} = 0 \quad (6)$$

Pentru a determina câmpurile de concentrații și de temperaturi în flacără se integrează sistemul de ecuații (1), (2), (3) cu condițiile la limită (4), (5), (6).

3. IPOTEZA SISTEMULUI IZOLAT ADIABATIC

În ipoteza menționată ($q_r = 0$) cele trei ecuații (1), (2), (3) au o formă analoagă, ceea ce permite eliminarea termenului neliniar (W) și obținerea unei relații între concentrațiile C_1, C_2 . Dacă se notează cu φ_0 cantitatea în moli de oxigen care reacționează cu un mol de gaze combustibile, cantitatea totală de amestec care reacționează în unitatea de timp și unitatea de volum va fi:

$$W = W_1 + W_2 = W_1(1 + \varphi_0) = W_2 \frac{1 + \varphi_0}{\varphi_0} \quad (7)$$

Se înmulțește ecuația (1) cu mărimea $\frac{1}{\varphi_0}$ și se scade din (2) obținându-se o ecuație din care dispare termenul vitezei de reacție :

$$u \frac{\partial C}{\partial x} = D \left[\frac{\partial^2 C}{\partial x^2} + \frac{1}{y} \frac{\partial}{\partial y} \left(y \frac{\partial C}{\partial y} \right) \right] \quad (8)$$

în care variabila $C = C_1 - C_2 / \varphi_0$, condițiile la limită fiind:

$$\begin{aligned} & \text{- pentru } x = 0 ; 0 \leq y \leq r ; C = C_1 ; r \leq y \leq R ; C = -\frac{C_2}{\varphi_0} \\ & \text{- pentru } y = 0 \text{ și } y = R ; \frac{\partial C}{\partial y} = 0 \end{aligned} \quad (9)$$

Din conservarea entalpiei totale în orice punct al spațiului flăcării și ecuațiile (1), (2), (3) se obține o relație între concentrații și temperatură T de forma :

$$\frac{C_1}{C_{10}} + \frac{C_2}{C_{20}} = \frac{T_f - T}{T_f - T_0} \quad (10)$$

unde T_f, T_0 reprezintă temperatura teoretică de ardere respectiv, temperatura inițială a gazelor care reacționează ($T_{10} = T_{20} = T_0$).

În cazul arderii difuzive, când viteza de reacție chimică se consideră infinit de mare, spațiul de ardere este împărțit de frontul de flacără în două zone : una în care concentrația de combustibil este nulă ($C_1 = 0$) și a doua în care concentrația de oxidant este nulă ($C_2 = 0$). La suprafața frontului de flacără, de grosime nulă, se justifică condiția $C_1 = C_2 = 0$. În acest caz din relația (10), pentru fiecare din zone rezultă :

$$\frac{T_f - T}{T_f - T_0} = \frac{C_1}{C_{10}}, \frac{T_f - T}{T_f - T_0} = \frac{C_2}{C_{20}} \quad (11)$$

câmpurile de temperaturi și concentrații fiind asemenea.

Ecuația suprafeței de reacție în flacăra difuzivă, pentru sistemul izolat adiabatic, se obține din ecuația (8) cu condițiile la limită (9) în care se adoptă $C = 0$ ($C_1 = C_2 = 0$).

În ipoteza neglijării fluxului de masă în direcția axei Ox în raport cu fluxul difuziv transversal, situație valabilă la camerele de ardere de lungime mare în raport cu diametrul camerei, ecuația (8) devine :

$$u \frac{\partial \alpha'}{\partial x} = \frac{D}{y} \frac{\partial}{\partial y} \left(y \frac{\partial \alpha'}{\partial y} \right) \quad (12)$$

Notând $\xi = \frac{xD}{uR^2}$, $\eta = \frac{y}{R}$ (R - raza camerei de ardere) ecuația (12) ia forma :

$$\frac{\partial \alpha'}{\partial \xi} = \frac{1}{\eta} \frac{\partial}{\partial \eta} \left(\eta \frac{\partial \alpha'}{\partial \eta} \right) \quad (13)$$

cu condițiile:

$$\xi = 0; 0 \leq \eta \leq \frac{r}{R}, C = C_1$$

$$\frac{r}{R} \leq \eta \leq 1, C = -\frac{C_2}{\varphi_0} \quad (14)$$

$$\eta = 0, \eta = 1; \frac{\partial \alpha'}{\partial \eta} = 0$$

4. CONCLUZII

Din soluția ecuației (13) cu condițiile la limită (14) se obține distribuția concentrației C în spațiul camerei de ardere.

Ecuația suprafeței de ardere rezultă din funcția de distribuție a concentrației în care se adoptă $C = 0$.

În funcție de cantitatea de oxidant, mai mare sau mai mică decât proporția stoechiometrică sunt posibile două tipuri de flacără pentru oxidant în exces ($\alpha > 1$) frontul de flacără se va curba spre interior, flacăra terminându-se pe axul jetului, iar în cazul insuficienței de oxidant ($\alpha < 1$) suprafața de reacție se va deplasa spre periferie, mărginându-se la peretele exterior ($\eta = 1$)

BIBLIOGRAFIE

1. D.GRECOV, I.IORDACHE, N.ANTONESCU - Arderea combustibililor gazoși. Flăcările difuziv turbulente. Editura Academiei, București, 1969
2. W.M.THRING, P.M.NEWBY, Combustion length enclosed turbulent jet flames., Fourth Symposium on Combustion, Baltimore, 1953

3. D.P.SUNAVALA, C.HULSE, W.M.THRING, Mixing and Combustion in free and enclosed turbulent jet diffusion flames, Combustion and Flame, 2, 1957

4. I.IORDACHE, Schimbul de masă în cazul a două jeturi coaxiale în echicurent mărginite de pereți, St. cerc. energ. electr., 1, 1968.

5. E.H.HUBBARD, Recirculation in cold Models of Furnaces, Journal of the Institute of Fuel, 255 april., 1962.

6. A.STAMBULEANU, Flacăra industrială, București, Ed.Tehnică, 1971

7. N.LEMNEANU, E.CRISTEA, C.JIANU, Instalații de ardere cu combustibili gazoși, Ed. Tehnică, București, 1982

8. L.MIHĂIESCU, T.PRISECARU, A.S.ENE, C.NEAGA, Arderea cu pulsații de presiune în focarele generatoarelor de abur energetice. Variația distribuției de presiune a gazelor de ardere la modificarea excesului de aer, Conferința Internațională, Turbo, 1996.

UNELE CONSIDERAȚII PRIVIND MODELUL DE PROBABILITATE EULERIANO-LAGRANGEIANĂ (PEL)

Prof.dr. ing. Sterie Ștefan *
Ing. Iuliu-Adrian Goleanu **
Dr. ing. Petre Poradici **

REZUMAT

În lucrare se prezintă modelul PEL cu luarea în considerație a efectului arderii asupra aerodinamicii și turbulenței. Cuplajul aerodinamică ardere descris prin ratele medii de produși și prin masa volumică permit elaborarea unei organigrame generale a modelului PEL bazat pe calculul vitezelor și al compozițiilor în procesul de ardere.

Modelul PEL se bazează pe cuplajul unei metode euleriene pentru calculul vitezelor și o metodă stohastică lagrangeiană pentru calculul compozițiilor.

1. Cuplajul aerodinamică - ardere

Cu cât structurile turbulenței sunt mai mari în raport cu întinderea frontului de flacără laminară, cu atât aceasta își conservă structura, care va fi supusă la întindere și deformare de către turbulență. Acesta este regimul de flăcărăuie.

Pe măsură ce structurile turbulenței devin mai mici (de ordinul întinderii frontului de flacără, deci $D_a = \Gamma_t / \Gamma_c < 1$), structura flăcării laminare este afectată, arderea devenind volumică.

Trebuie văzut în ce mod, acest cuplaj este luat în calcul în modelul PEL.

Densitatea probabilistică poziție/compoziție se poate reprezenta printr-un ansamblu de N particule a căror evoluție satisface sistemul de ecuații [1]:

$$\frac{d}{dt} \left(\frac{\overline{B}^{**}}{\overline{x}^{**}} \right) = \left(\frac{\overline{B}^{**}}{\overline{U}^{**}} \right) \quad [1]$$

* Academia Tehnică Militară

** ROMAVIA

unde U - spațiul vitezelor și \bar{B} reprezintă vectorul rată de variație a compoziției pentru o particulă stohastică.

Pentru simplificare, în cele ce urmează, se va renunța la exponentul (**) pentru cantitățile stohastice.

Influența aerodinamicii asupra arderii și a compoziției se va manifesta la nivelul mărimilor \bar{B} și \bar{U} , care vor fi exprimate astfel:

\bar{U} se descompune într-o viteză medie \vec{U} corespunzătoare convecției și o fluctuație U'' corespunzătoare efectului structurilor turbulente de mărime superioară sau egală cu mărimea particulei în discuție :

$$\frac{d\bar{x}}{dt} = \vec{U} + U'' \quad [2]$$

În ceea ce privește turbulența, pentru a putea construi un model pentru acest termen este utilă relația (3) pentru k și ecuația (4) care dă energia cinetică turbulentă și tensorul lui Reynolds.

$$\frac{\partial \bar{\rho}k}{\partial t} + \frac{\partial}{\partial x_\alpha} (\bar{\rho} u_\alpha k) = \frac{\partial}{\partial x_\alpha} \left(\frac{\mu_l + \mu_t}{\sigma_k} \frac{\partial k}{\partial x_\alpha} \right) + p_k - \bar{\rho} \varepsilon \quad [3]$$

unde μ_t este vâscozitatea turbulentă;

$$\bar{\rho} u''_\alpha u''_\beta = -\mu_t \left(\frac{\partial \bar{u}_\alpha}{\partial x_\beta} + \frac{\partial \bar{u}_\beta}{\partial x_\alpha} \right) + \frac{2}{3} \delta_{\alpha\beta} \left(\bar{\rho} k + \mu_t \frac{\partial \bar{u}_\gamma}{\partial x_\gamma} \right) \quad [4]$$

unde $\bar{\rho} u''_\alpha u''_\beta$ reprezintă tensorul lui Reynolds; $k = (1/2) u''_\alpha u''_\alpha$ energia cinetică a turbulenței.

Pentru o particulă fluidă,

$$\rho B_\alpha(\bar{x}, t) = -\frac{\partial J^\alpha i}{\partial x_\alpha} + \rho \omega_\alpha \quad [5]$$

în care se pot recunoaște un termen de difuzie și un termen sursă chimică.

Termenul amestec apare sub forma unei necunoscute și necesită o modelare.

Sistemul de ecuații (1) poate fi rescris în funcție de acestea sub forma:

$$\frac{d}{dt} \left(\frac{\bar{Y}}{\bar{x}} \right) = \left(\frac{D(\bar{Y}i) + \omega_i}{\bar{U} + \bar{U}'} \right) \quad [6]$$

unde $D(Y_i)$ este termenul de amestec turbulent la scară mică.

2. Cuplajul ardere - aerodinamică

Arderea influențează aerodinamica în mod esențial, prin degajarea de căldură, pe care o provoacă. Aceasta va antrena o încălzire a amestecului gazos și o accelerare a acestuia, urmată de variația densității sale.

Este de așteptat ca accelerarea să provoace o creștere a curgerii medii și deci să fie o sursă de turbulență. În mod contrar, încălzirea gazului duce la creșterea vâscozității laminare. La numere Reynolds mari, vâscozitatea laminară devine neglijabilă în raport cu vâscozitatea turbulentă astfel încât, efectul acesteia se poate neglija.

La nivelul modelului PEL, efectul arderii asupra aerodinamicii și turbulenței va trebui considerat prin introducerea termenilor sursă medii de entalpie și de produși (dați de metoda probabilistică) în ecuațiile euleriene ale metodei momentelor. Această tehnică obligă la folosirea unei descrieri simplificate a spațiului fazelor în partea euleriană, ceea ce presupune o ecuație de bilanț pentru entalpia medie și alte două pentru câmpul produșilor majoritari (de exemplu, un produs reactiv și un produs inert). O primă schemă de cuplaj este reprezentată în figura 1.

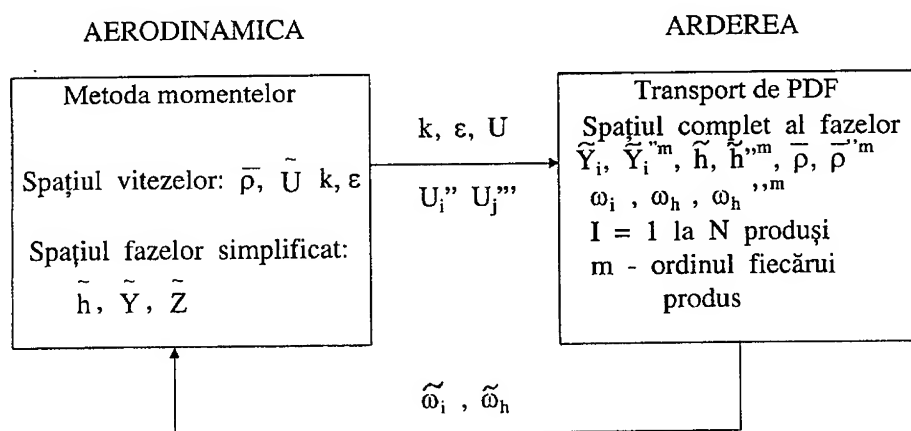


Fig. 1 Cuplaj aerodinamică - ardere prin ratele medii de producere / consum produși și de degajare de căldură

Se pot efectua și alte cuplaje. Astfel este posibil ca în calculul eulerian să se introducă densitatea medie, evaluată prin calcul lagrangeian (figura 2),

soluția fiind utilizată de Varvish (1). Această tehnică permite o descriere simplificată a spațiului fazelor în partea aerodinamică.

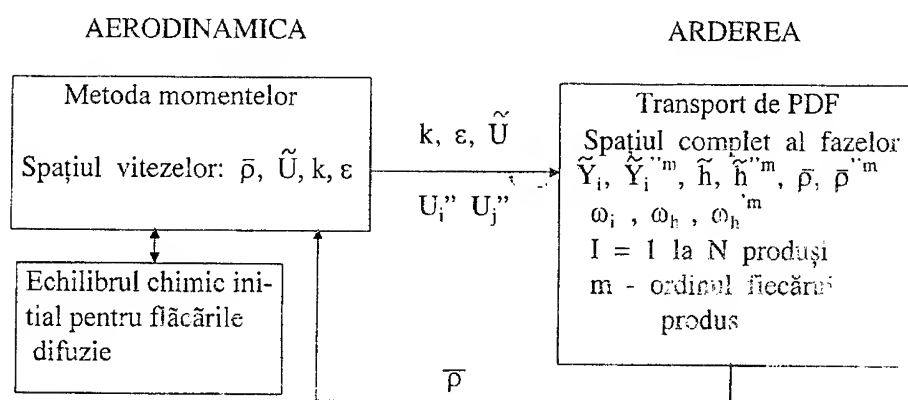


Fig.2 Cuplaj aerodinamică-ardere prin masa volumică

3. Procesul iterativ

Modul cel mai simplu de abordat constă în cuplajul nestaționar al aerodinamicii și arderii. Această tehnică presupune ca la fiecare pas de timp de integrare a ecuațiilor euleriene, să se efectueze un pas de timp lagrangeian în spațiul fizic și în spațiul fazelor. Termenii de cuplaj $\bar{\omega}_i$ și $\bar{\omega}_h$ sunt introduși în ecuațiile euleriene care se integrează cu un nou pas de timp și așa mai departe.

Această metodă impune ca, la fiecare pas de timp, să se lanseze noi particule în intrările domeniului în așa fel încât să fie suficiente la toate momentele și în toate punctele pentru a calcula mediile și momentele de ordin superior.

Alternativa adoptată de Gilbank [2], pentru o curgere medie staționară, constă din posibilitatea de a face convergent calculul eulerian (plecând de la modelul simplificat al arderii turbulente), pentru ca apoi să se "lanseze" particule a căror traiectorie se integrează în spațiul fizic și în spațiul fazelor, până când toate vor ieși din configurație. Termenii de cuplaj lagrangeian medii (degajarea de căldură, rată de producere/consum de produși) se reîntorc în calculul eulerian, care va fi din nou făcut convergent. Sunt necesare 4-5 iterații euleriene-lagrangeiene, până ce procesul va converge. Totodată procesul fiind staționar este de așteptat ca timpul de calcul să fie diminuat față de calculul proceselor nestaționare.

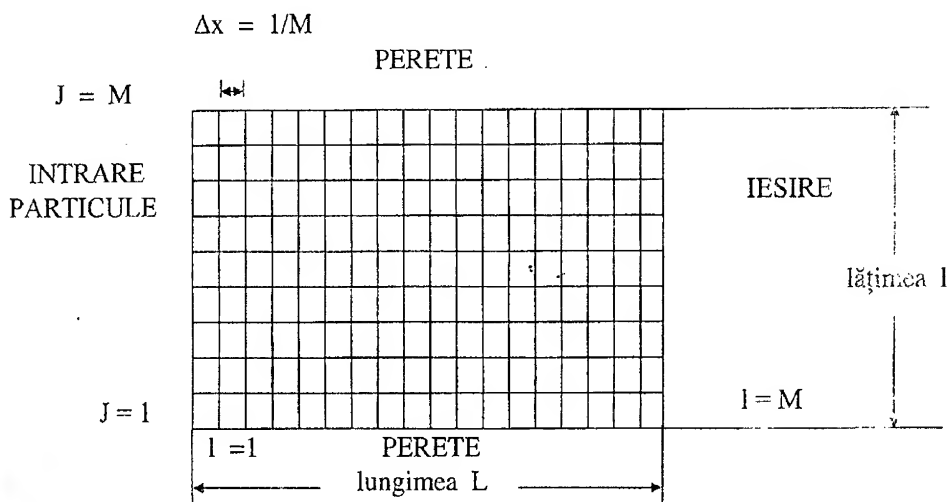


Fig.3 Configuraţie bidimensională simplă

Este utilă comparaţia numărului de particule ce trebuie lansate prin aceste două metode pentru o configuraţie bidimensională rectangulară de lungime L (M ochiuri) şi lăţimea l (N ochiuri) reprezentată în figura 3.

Pentru simplificare, se presupune viteza constantă în tot domeniul şi se notează V_0 .

Fie K_0 numărul de particule ce vor trece printr-un ochi (sau prezente la un moment dat în cazul nepermanent) pentru a putea realiza statistici precise.

Metoda staţionară. Este suficient ca la t_0 să se lanseze K_0 particule în fiecare ochi de intrare ($N K_0$ particule) pentru ca la sfârşitul timpului $t=1/V_0$ toate particulele să fie ieşite şi prin fiecare ochi să fi trecut K_0 particule.

Metoda nestaţionară. Timpul de integrare $t=1/V_0$; la t_0 se introduc NK_0 particule; la $t_0 + \Delta x/V_0$, aceste particule au părăsit primul rând de ochiuri ($L=1$) şi au trebuit reintroduse NK_0 particule şi așa mai departe.

În total au fost introduse de n ori câte NK_0 particule cu :

$$n = (1/V_0)(V_0/\Delta x) = (L/V_0)(V_0/L)M, \text{ deci } n = M$$

Numărul de particule este : MNK_0 , iar raportul numărului de particule introduse prin cele două metode este de ordinul lui M .

Metoda staționară necesită unele comentarii. Pentru primul calcul eulerian nu se dispune de $\bar{\omega}_i$ și $\bar{\omega}_h$ date de calculul lagrangeian.

Inițializarea acestui prim calcul eulerian se face cu ajutorul modelelor simple de ardere turbulentă ca Eddy Break Up, Crammer sau Magnusen (3).

Prin această tehnică nu pot fi structurate regimuri nestaționare, iar numărul cuplajelor euleriene-lagrangeiene succesive necesare pentru obținerea convergenței va depinde de exactitatea câmpului aerodinamic inițial obținut cu modelul simplu.

În cazul limită când $\bar{\omega}_i$ și $\bar{\omega}_h$ dați de modelul simplu nu diferă de ratele medii date de modelul PEL nu este necesar să se introducă acestea în calculul eulerian. Este de ajuns o lansare de particule, iar în acest caz, modelul PEL permite o descriere detaliată a spațiului compozițiilor medii.

Toate aceste considerații permit în final elaborarea unei organigrame generale a modelului PEL (figura 4).

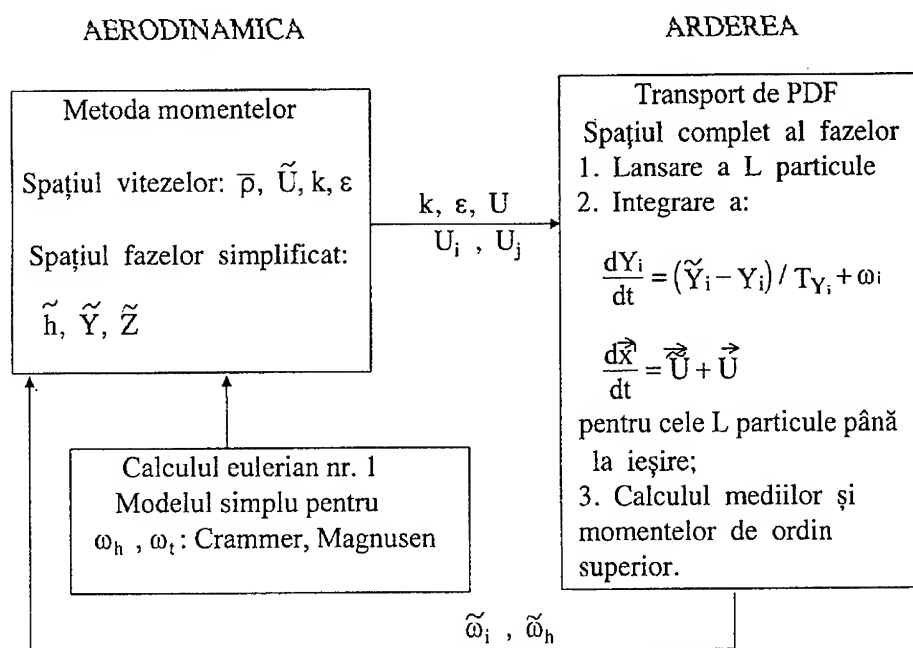


Fig.4 Organigrama modelului PEL

Totodată, unele aspecte ale calcului cantităților medii, condițiile inițiale și la limită, trebuie precizate.

4. Calculul mediei

În cazul apropierei nestaționare media de ansamblu a unei mărimi termochimice oarecare din mulțimea $\{Y_i, \omega_i, h, \omega_h\}$ este dată la un moment dat, în ochiul respectiv, în funcție de starea particulelor prezente în acel moment în acel ochi :

$$\bar{\Psi} = \frac{1}{N} \sum_{n=1}^N \Psi^{(n)} \quad [7]$$

În metoda descrisă în paragraful anterior se rezolvă problema staționară în care cantitățile medii nu depind de timp. În acest caz media se poate exprima prin media temporală a contribuțiilor particulelor care au trecut prin acel ochi și care sunt în acel moment acolo.

Media temporală se definește prin:

$$\bar{\Psi} = \lim_{T \rightarrow \infty} \frac{1}{T} \int_0^T \Psi(t) dt \quad [8]$$

Scrierea sub formă discretă ține cont de faptul că o particulă n poate rămâne k_n pași de timp în ochiul considerat:

$$\bar{\Psi} = \frac{\sum_{n=1}^N \left(\sum_{k=1}^{k_n} \Psi^{(n,k)} \delta t^{(n,k)} \right)}{\sum_{n=1}^N \left(\sum_{k=1}^{k_n} \delta t^{(n,k)} \right)} \quad [9]$$

În [4], Pope arată că cele două medii definite (media discretă de ansamblu și cea temporală (8) și (9)) sunt medii ale lui Favre (ponderate prin masa volumică), atunci când particulele au aceeași masă Δm . Aceasta este o consecință a faptului că densitatea ρ este direct proporțională cu numărul de particule din ochi. Se obține această condiție prin introducerea în intrările domeniului a unui număr de particule proporțional cu debitul masic.

Bibliografie

1. VERVISCH L. - Prise en compte d'effets cinétique chimique dans les flammes de diffusion turbulentes par l'approche fonction densité de probabilité. Thèse de Doctorat de l'Université de Rouen, 1991.
2. GILBANK P. - Contribution à la modélisation de la combustion turbulente dans cas d'une stabilisation par accroche-flammes. Thèse de Doctorat de l'Université Paris VI, 1989.
3. CAILOT PH. - La modélisation de la combustion turbulente - R.T. ONERA 1994.
4. POPE S.B. - PDF methods for turbulent reactive flows. Progress in Energy and Combustible Science, vol. 11, pag. 119-192, 1985.

UNELE CONSIDERATII PRIVIND MODELAREA DIFUZIEI MOLECULARE IN GAZE

Prof.  r. ing. Stefan Sterie*
Cpt. asist. univ. ing. Calin Curea**
Lt. col. ing. Constantin Avadanei**

Rezumat :

In lucrare se prezinta un program de calcul pentru determinarea concentratiei in difuzia moleculara unidimensionala . Rezultatele numerice permit analiza fenomenelor de poluare produsa in timp si spatiu de mijloacele de transport .

Difuzia pura sau moleculara se caracterizeaza prin diminuarea gragientilor de concentratie existenti in limitele unei faze oarecare si se produce prin migrarea atomilor sau moleculelor in lipsa curentilor de convecție .

Difuzia in regim stationar are loc in cazul in care intre doua puncte se mentine o diferent  constanta de concentratie, fenomenul fiind descris de prima lege a lui Fick :

$$J = \frac{\partial C}{\partial \tau} = -D \frac{\partial C}{\partial x} \quad [\text{kmoli/m}^2\text{s}] \quad (1)$$

unde J este fluxul de difuzie , D [m²/s] - coeficientul de difuzie , C - concentratia substantei care difuzeaza , $\frac{\partial C}{\partial x}$ - gradientul de concentratie .

Difuzia in regim nestationar se caracterizeaza prin variatia in timp a fluxului de difuzie si este descrisa de legea a doua a lui Fick

$$J = \frac{\partial C}{\partial \tau} = D \frac{\partial^2 C}{\partial x^2} \quad (2)$$

Pe baza teoriei cinetice a gazelor se deduce relatia :

$$D_{AB} = \frac{2}{3} \left(\frac{K_B}{\pi} \right)^3 \frac{T^{3/2}}{p_1 d_{AB}^2} \sqrt{\frac{1}{2M_A} + \frac{1}{2M_B}} \quad [\text{m}^2/\text{s}] \quad (3)$$

unde D_{AB} - coeficientul de difuzie a gazelor A si B care difuzeaza , K_B este constanta lui Boltzmann (K_B = 1,38 10⁻⁹) [J/molec*K], d_{AB} - diametrul mediu al

* - Academia Tehnica Militara

** - Comisia Militara de Coordonare Reprezentanti Militari Cugir

moleculelor ($d_{AB} = (d_A + d_B)/2$ [m]), M_A, M_B - masa moleculara [Kg/molec], p_t - presiunea totala [N/m²], T - temperatura [K].

1. Modelarea difuziei unidimensionale

Ecuatiei (2) i se atasaza urmatoarea problema Cauchy :

$$c(x, t)|_{t=0} = \begin{cases} c_0 & \text{daca } x_1 < x < x_2 \\ 0 & \text{daca } x < x_1 \text{ si } x > x_2 \end{cases} \quad (4)$$

Solutia ecuatiei (2) cu conditia (4) are forma :

$$c(x, t) = \frac{C_0}{2D\sqrt{\pi t}} \int_{x_1}^{x_2} e^{-\frac{(u-x)^2}{4D^2 t}} du \quad (5)$$

care devine :

$$c(x, t) = \frac{C_0}{2} \left[F\left(\frac{x-x_1}{2D\sqrt{t}}\right) - F\left(\frac{x-x_2}{2D\sqrt{t}}\right) \right] \quad (6)$$

unde

$$F(z) = \frac{2}{\sqrt{\pi}} \int_0^z e^{-y^2} dy, \quad (7)$$

este functia lui Laplace (erfz)

2. Program difuzie moleculara unidimensionala

Se adopta $x_1 = -x_0$, $x_2 = x_0$, $D = a$, $t \in (3600, 7200)$

```
#include <math.h>
#include <stdio.h>
#include <sys\stat.h>
#include <string.h>
#include <fcntl.h>
#include <io.h>
#include <stdlib.h>
```

```
float
```

```
    a/*coeficient de difuzie*/,
    x0/*jumătate din latimea norului*/,
    c0/*concentratia initiala a norului*/;
```

```
double erf(float z){
double f;
if(z<1.51)
```

```

f=2*(z/sqrt(M_PI))*(1-pow(z,2)/3+pow(z,4)/10-pow(z,6)/42+pow(z,8)/(24*9)-
pow(z,10)/(120*11));
else
f=1-(exp(-z*z)/(z*sqrt(M_PI)))*(1-1/(2*pow(z,2))+3/(4*pow(z,4))-
15/(8*pow(z,6))+ 15*7/(16*pow(z,8))-15*7*9/(32*pow(z,10)) );
return f;
}

```

```

double conc(float x,int t){
double f;
f=(c0/2)*(erf( (x+x0)/(2*a*sqrt(t)) )-erf((x-x0)/(2*a*sqrt(t))) );
return f;
}

```

```

void main(){
int i,file,t;
char timp[6],cc[24],line[30],init[20];
float c,dist;

```

```

clrscr();
printf("a=");
scanf("%e",&a);
printf("x0=");
scanf("%e",&x0);
printf("c0=");
scanf("%e",&c0);
printf("distanta=");
scanf("%e",&dist);

```

```

file=creat("rez.dat",S_IWRITE|S_IREAD);
sprintf(init,"a=%e\n",a);
write(file,init,strlen(init));
sprintf(init,"x0=%e\n",x0);
write(file,init,strlen(init));
sprintf(init,"c0=%e\n",c0);
write(file,init,strlen(init));

```

```

t=3300;
for(i=0;i<24;i++){
printf("t=%d conc=%e\n",3600+i*300,conc(dist,3600+i*300));
t+=300;
c=conc(dist,3600+i*300);
itoa(t,timp,10);

```

```

        sprintf(cc,"  %e\n",c);
        strcpy(line,timp);
        strcat(line,cc);
        write(file,line,strlen(line));
    }
    close(file);
    getch();
}

```

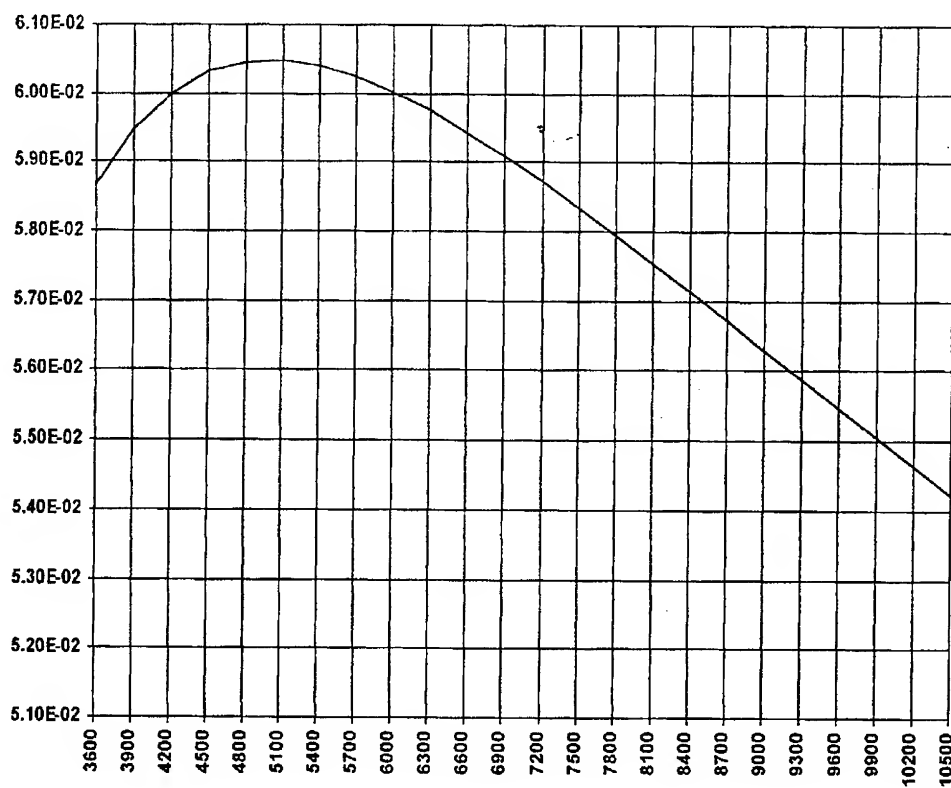
3. Date numerice

```

a=2.000000e-01      Date introduce
x0=5.000000e-01
c0=5.000000e+00

```

Timp [s]	Concentratie [miligrame/m³]
3600	5.867995e-02
3900	5.947733e-02
4200	6.000221e-02
4500	6.031575e-02
4800	6.046469e-02
5100	6.048486e-02
5400	6.040380e-02
5700	6.024296e-02
6000	6.001949e-02
6300	5.974688e-02
6600	5.943561e-02
6900	5.909444e-02
7200	5.873021e-02
7500	5.834827e-02
7800	5.795356e-02
8100	5.754916e-02
8400	5.713860e-02
8700	5.672403e-02
9000	5.630727e-02
9300	5.589027e-02
9600	5.547414e-02
9900	5.505994e-02
10200	5.464851e-02
10500	5.424071e-02



Variatia concentratiei in timp
intr-un punct la distanta de 20 m de centrul
de difuzie

4. Concluzii

Algoritmul, programul si datele numerice prezentate permit studiul variatiei concentratiei in spatiu si timp in functie de valoarea coeficientului de difuzie moleculara, concentratia initiala si latimea norului poluant .

Fenomenul poluarii chimice are loc prin emisii de oxid de carbon si hidrocarburi diverse nearse .

Caile de actiune pentru combaterea poluarii vor avea in vedere procesul de elaborare a combustibilului, cunoasterea si perfectionare procesului de ardere, perfectionarea concepiei si tehnologiei camerelor de ardere .

Bibliografie :

1. Stefan Sterie - Ecuatiile mecanicii fluidelor , Ed. ATM, 1996 .
2. L.Landau, E. Lifchitz - Mecanique des fluides , Ed. MIR, 1989.
3. D. Stefanescu si a. - Transfer de caldura si masa, Ed. D.P., 1983.
4. N. Cioranescu - Tratat de matematici speciale, Ed. D.P. , 1963.
5. C. Plavitiu , s.a. - Fizica moleculara , Ed. D.P. , Buc., 1977.

INVARIANTI ALGEBRICI UTILIZATI IN MODELAREA FENOMENELOR EXPLOZIVE

Prof.dr.ing. Ștefan Sterie*

Cpt.ing.fiz. Dan VasIU*

Lt.col.ing. Nicolae Marin**

Lt.col.ing. Marian Bunea*

REZUMAT

Studiul fenomenelor explozive se bazează pe ecuațiile fundamentale ale mecanicii fluidelor scrise sub forma adimensională. Utilizând ipoteza miscării autosimilare se introduc invarianti algebrici care permit determinarea unor relații între parametrii caracteristici fenomenului exploziv.

Integralele algebrice ale unui sistem de ecuații diferențiale ordinare pot fi stabilite independent de condițiile inițiale sau sau condițiile particulare pe frontieră, folosind analiza dimensională pentru mișcările autosimilare. În cazul general, ordinul sistemului de ecuații diferențiale ordinare poate fi redus.

Considerăm cazul mișcării unidimensionale adiabatică și nestationară a unui gaz perfect cu simetrie sferică, unde atracția newtoniană este luată în considerare. În acest caz avem următorul sistem de ecuații:

* Academia Tehnică Militară.

** Institutul de Cercetări și Proiectări Electromecanice Ploiești.

$$\begin{aligned}
\frac{\partial \rho}{\partial t} + \frac{\partial \rho v}{\partial r} + \frac{(v-1)\rho v}{r} &= 0 \\
\frac{\partial M}{\partial r} &= \sigma_v \rho r^{v-1} \\
\frac{\partial v}{\partial t} + v \frac{\partial v}{\partial r} + \frac{1}{\rho} \frac{\partial p}{\partial r} + \frac{GM}{r^{v-1}} &= 0 \\
\frac{\partial S}{\partial t} + v \frac{\partial S}{\partial r} &= 0
\end{aligned}
\tag{1}$$

unde $\sigma_v = 2(v-1)\pi + (1/2)(v-2)(v-3)$, G este constanta gravitacionala $[G] = M^{-1}L^3T^{-2}$, M este masa continuta intre suprafata fixa si suprafata luata in discutie $[M] = M L^{v-3}$ iar S este entropia sau o functie data de entropie. Pentru cazul sferic avem $v=3$, la fel se poate considera cazul cilindric pentru $v=2$ (caz in care forta gravitacionala deasemenea poate fi luata in considerare) si cazul undelor plane $v=1$ cand $G=0$.

Sa consideram miscarea autosimilara definita de doua constante dimensionale a si b :

$$\begin{aligned}
[a] &= M L^k T^s \\
[b] &= L^m T^n
\end{aligned}$$

Expresia entropiei in termenii ρ si p nu trebuie sa contina constante dimensionale independente de a si b . Constantele multiplicative si aditive sunt nesemnificative. Pentru $m \neq 0$, putem pune fara a pierde generalitatea ca $m=1$, $n=-\delta$ si $k=-3$. Pentru aceasta este suficient sa luam:

$$a_1 = a b^{(-k-3)/m}, \quad b_1 = b^{1/m}$$

Este necesar sa consideram ca $[a] = [1/G]$ pentru $k=-3$ cand atractia newtoniana este luata in considerare. Ca urmare $s=2$ iar δ va fi singurul parametru caracteristic. Exponentul s poate fi arbitrar pentru $G=0$. In cazul general al miscarilor autosimilare cand $m \neq 0$ putem scrie:

$$\begin{aligned}
\lambda &= \frac{r}{b_1 t^\delta} & v &= \frac{r}{t} V(\lambda) & \rho &= \frac{a}{r^{k+3} t^s} R(\lambda) \\
p &= \frac{a r^2}{r^{k+3} t^{s+2}} P(\lambda) & M &= \frac{a r^v}{r^{k+3} t^s} M(\lambda)
\end{aligned}
\tag{2}$$

Substituind marimile (2) in (1) se obtine un sistem cu patru ecuatii diferentiale ordinare pentru $V(\lambda)$, $R(\lambda)$, $P(\lambda)$ si $M(\lambda)$. Invariantii algebrici sunt relatii analitice intre marimile adimensionale V , R , P , M si λ .

1. Invariantul masei

Din a doua expresie a sistemului (1) se obtine:

$$\frac{\partial M}{\partial r} = \sigma_v \rho r^{v-1}$$

$$M'' - M' = \int_{M'}^{M''} dM = \sigma_v \int_{r'}^{r''} \rho r^{v-1} dr$$

unde suprafetele mobile $r'(t)$ si $r''(t)$ corespund cazului in care parametrul λ ia valori constante, respectiv λ' si λ'' .

Se va utiliza formula de derivare totala pe un volum variabil:

$$\frac{d}{dt} \int_{r'}^{r''} F \sigma_v \rho r^{v-1} dr = \frac{\tilde{d}}{dt} \int_{r'}^{r''} F \sigma_v \rho r^{v-1} dr + \left[F \sigma_v \rho r^{v-1} \left(\frac{dr}{dt} - v \right) \right]_{r'}^{r''}$$

unde $\frac{\tilde{d}}{dt}$ este derivata in raport cu timpul pentru un volum mobil de integrare compus din aceleasi particule, iar F este o functie arbitrara in r si t .

Deoarece:

$$M'' - M' = \frac{a b_1^{v-k-3}}{t^{s+\delta(k+3-v)}} [\lambda'^{v-k-3} M(\lambda'') - \lambda''^{v-k-3} M(\lambda')]$$

rezulta

$$\left. \frac{d(M'' - M')}{dt} \right|_{\lambda', \lambda'' = \text{const.}} = - \frac{s + \delta(k+3-v)}{t} (M'' - M')$$

Din legea de conservare a masei: $\frac{\tilde{d}(M'' - M')}{dt} = 0$

Ca urmare daca in formula generala facem $F = 1$ obtinem:

$$- \frac{s + \delta(k+3-v)}{t} (M'' - M') = \sigma_v \left[\rho r^{v-1} \left(\frac{dr}{dt} - v \right) \right]_{r'}^{r''}$$

Utilizand relatiile (2) si marimile

$$dr' / dt = \delta (r'/t)$$

$$dr'' / dt = \delta (r''/t)$$

se obtine invariantul:

$$\lambda^{v-k-3} \{ [s + \delta(k+3-v)] M - \sigma_v R(V - \delta) \} = C = \text{const.} \quad (3)$$

care este corolar cu legea de conservare a masei.

2. Invariantul entropiei

In miscarea reversibila adiabatica se obtine o integrala derivata ca un corolar a legii de conservare a entropiei pe traiectoriile particulelor.

Fie $\Phi(p, \rho) = f(S)$ o functie data a entropiei.

Conditia data de ultima ecuatie din sistemul (1) respectiv de conservare a entropiei pe traiectoriile particulelor este echivalenta cu o relatie de forma:

$$\Phi(p, \rho) = F(M^*, a, b, \alpha_1, \alpha_2, \alpha_3, \dots)$$

unde $\alpha_1, \alpha_2, \alpha_3$ sunt constante abstracte, si M^* este coordonata Lagrangeiana. Se considera formula dimensionala pentru Φ , $[\Phi] = M^{\omega} L^{\mu} T^{\tau}$.

Daca nu exista nici o valoare pentru χ care sa satisfaca $[a b_1^{\chi}] = [M^*]$, atunci este imposibil sa formam o combinatie a celor trei parametri a, b_1 si M^* . Singura valoare pentru care se obtine o combinatie adimensionala a celor trei parametrii este $\chi = \nu - k - 3$.

Ca urmare rezulta urmatoarea ecuatie:

$$\Phi(p, \rho) = M^{*\omega} \left(\frac{ab_1^{\frac{1}{\delta}}}{M^*} \right)^{\frac{[\mu - \omega(\nu - 3)]\delta}{s + \delta(k + 3 - \nu)}} \times \left(\frac{ab_1^{\nu - k - 3}}{M^*} \right)^{\frac{\tau}{s + \delta(k + 3 - \nu)}} f(\alpha_1, \alpha_2, \dots) \quad (4)$$

Prin inlocuirea marimilor p, ρ si M^* in (4) cu ajutorul formulelor adimensionale, se obtine o relatie finala intre V, R, P si λ . Daca exista o combinatie ab_1^{χ}/M^* , cum s-a mentionat anterior, functia f poate sa depinda de ab_1^{χ}/M^* . Ca urmare in cazul general ecuatia entropiei nu se poate reduce la un invariant.

Exista invarioant al entropiei daca gazul este perfect, caz in care $\Phi = p / \rho^{\nu}$ si $\omega = 1 - \gamma$ $\mu = 3\gamma - 1$ $\tau = -2$.

Invariantul entropiei se obtine sub forma:

$$\frac{P}{R^{\gamma}} = [R\lambda^{\nu}(V - \delta)]^{\frac{2 - (\nu - 1)s + \delta[K + 1 - \nu(K + 3)]}{s + \delta(K + 3 - \nu)}} \times \lambda^{\frac{[2 + \nu(\nu - 1)]s + 2(K + 3 - \nu)}{s + \delta(K + 3 - \nu)}} f(\alpha_1, \alpha_2, \dots) \quad (5)$$

Luand in considerare invariantii rezultati din conditiile de conservare a masei si entropiei, ordinul sistemului de ecuatii diferentiale este redus de la patru la doi.

3. Invariantul energiei

Vom arata ca acest invariant exista daca o constanta cu dimensiunile $ML^{\nu-2}T^{-2}$ (egala cu dimensiunile energiei in cazul sferic, cu energia calculata pe unitatea de lungime sau suprafata in cazul cilindric respectiv plan) poate fi formata cu ajutorul constantelor caracteristice a si b_1 .

Consideram cazul cand atractia gravitationala lipseste, iar ν ia valorile 1, 2 si 3.

Energia totala intre doua suprafete mobile $r'(t)$ si $r''(t)$ este data de:

$$E = \int_{r'}^{\infty} \left(\frac{v^2}{2} + e \right) \sigma_v \rho r'^{\gamma-1} dr'$$

unde e este energia internă pe unitatea de masă. Variația energiei particulelor continute între suprafețele $r'' = \text{const.}$ și $r' = \text{const.}$ la un moment de timp este dată de lucrul mecanic al forței de presiune pe această suprafață; ca urmare:

$$\frac{dE}{dt} = -\sigma_v (p'' v' r'^{\gamma-1} - p' v' r'^{\gamma-1})$$

Mai mult rezulta din considerațiile adimensionale aplicate mișcărilor autosimilare ($m \neq 0$) că mărimea E ale cărei dimensiuni sunt $M L^{\gamma-1} T^{-2}$ este dată de relația:

$$E = a b_1 v^{-k} t^{\delta(\gamma-1-k)-2-s} f(\lambda'', \lambda', \alpha_1, \alpha_2, \dots)$$

unde $f(\lambda'', \lambda', \alpha_1, \alpha_2, \dots)$ este o funcție arbitrară. Să considerăm acum că r' și r'' sunt determinate de condițiile $\lambda', \lambda'' = \text{const.}$ Atunci în cazul general:

$$\frac{dE}{dt} = [\delta(\gamma-1-k)-2-s] \frac{E}{t}$$

Acum folosind formula de derivare totală pe un volum variabil și înlocuind funcția $F(r, t)$ cu $v^2/2 + p/(\gamma-1)\rho$ (am luat $e = p/(\gamma-1)\rho$) se obține ușor următoarea relație care este valabilă pentru unele mișcări autosimilare.

$$[s+2-\delta(\gamma-1-k)] f(\lambda', \lambda'', \alpha_1, \alpha_2, \dots) = \sigma_v \left\{ \lambda'^{\gamma-1-k} \left[PV + (V-\delta) \left(\frac{RV^2}{2} + \frac{P}{\gamma-1} \right) \right] \right\}$$

Funcția necunoscută $f(\lambda', \lambda'', \alpha_1, \alpha_2, \dots)$ din relația anterioară este eliminată dacă:

$$s - \delta(\gamma-1-k) = -2$$

În acest caz obținem alt invariant esențial:

$$\lambda'^{\gamma-1-k} \left[PV + (V-\delta) \left(\frac{RV^2}{2} + \frac{P}{\gamma-1} \right) \right] = \text{const} \quad (6)$$

corolar cu legea de conservare a energiei.

4. Concluzii

Invariantul (3) poate fi considerat independent de ecuațiile de mișcare în absența atracției gravitaționale, ca expresie a lui $M(\lambda)$ în termenii λ , R și V în formă finită.

În cazul când se ia în considerare atracția gravitațională funcția $M(\lambda)$ intra în ecuația diferențială de mișcare. În acest caz $M(\lambda)$ poate fi eliminată folosind invariantul (3)

Daca $M=0$ (cand folosim M intelegem cantitatea de masa cuprinsa intre suprafata fixa si suprafata in considerare, iar cand folosim $M(\lambda)$ intelegem marimea adimensionala corespunzatoare lui M) sau $M = \text{const.}$ pentru solutia ce se studiaza la $\lambda = 0$, rezulta ca in centrul de simetrie nu exista o sursa de masa, iar din formula (3.3.3.) sau din derivata acestei expresii se poate obtine constanta C din partea dreapta a expresiei care va fi egala cu zero in acest caz.

Daca $C = 0$ variabilele M si M^* difera numai printr-un factor numeric.

Cazul $V = \delta$ corespunde solutiei particulare cu distributia de viteze $v = \delta r/t$ liniara in r ; in acest caz $\lambda = \text{const.}$ pentru miscarea particulelor si variabila λ este de asemenea o coordonata lagrangeiana.

Existenta invariantului energiei este echivalenta cu conditia ca marimea ab_1^{V-1-k} sa aiba dimensiunile unei energii E ; miscarea autosimilara poate fi determinata de constanta E si constanta b_1 , $[b_1] = L T^{-\delta}$ unde exponentul δ poate fi oarecare.

Rezultatul nu depinde de folosirea relatiei:

$$e = p/(\gamma-1)\rho$$

In cazul miscarii unidimensionale nestationare a undelor plane, daca cu marimile caracteristice a si b se poate forma o combinatie a b^χ avand dimensiunea $c = M L^{-1} T^{-1}$ (moment pe unitatea de arie) cu $\chi = \text{constant}$, atunci se deduce si invariantul momentului:

$$P - (V - \delta) RV = \text{const.} \quad (7)$$

Bibliografie.

- 1 Carafoli, E., Constantinescu, V. N., Dinamica fluidelor compresibile, Editura Academiei Române, 1981, 1984.
- 2 Batchelor C.K., An introduction to fluid dynamics, Cambridge, 1970.
- 3 Sedov, L.I., Metode de similitudine folosite în mecanică, Moscova, 1975.
- 4 Landau L., Lifchitz E., Physique theorique, tome 6, Mecanique des fluides, Moscow, 1989.
- 5 Stefan, S., Ecuatiile mecanicii fluidelor, Ed. A.T.M., 1996.

Advection in chaotically time-dependent open flows

ZOLTAN NEUFELD

Department of Atomic Physics, Eötvös University,
4-1088 Budapest, Puskin.u. 5-7, Hungary

Abstract

The passive advection of tracer particles in open two-dimensional incompressible flow is considered, in case of chaotic time-dependence of the velocity field.

This is realised by the chaotic motion of four ideal point vortices. The advection problem can be seen as a chaotic scattering process in a chaotically driven Hamiltonian system.

Studying the motion of tracer ensembles, we present numerical evidence for the existence of a **bounded chaotic set** containing trajectories never leaving the mixing region of the flow. We investigate fractal properties of this set using time-delay functions telling us how the time spent in the mixing region depends on the tracer's initial conditions.

We propose different random baker maps as simple models of the phenomenon.

Advection in chaotically time-dependent open flows

Z. Neufeld

Department for Atomic Physics

Eötvös University,

Puskin u. 5-7, H-1088 Budapest, Hungary

T. Tél

Institute for Theoretical Physics, Eötvös University,

Puskin u. 5-7, H-1088 Budapest, Hungary

The passive advection of tracer particles in two-dimensional incompressible flows is a chaotic phenomenon [1]. In such cases, the tracer dynamics turns out to be area preserving in the phase space which coincides with the plane of the flow and is thus directly observable. The advection in non-steady flows is described by a driven Hamiltonian dynamics. In the last decade, a comprehensive knowledge has accumulated in the case of strict *time-periodicity* both for flows in closed containers [2]-[6] and for open flows with asymptotic simplicity [7]-[15], where the velocity field in the far up and downstream region is uniform. A unique feature of such open flows is the pronounced and stable *fractal feature* associated with chaotic tracer dynamics [10]-[15]. This is clearly measurable in laboratory experiments [16]. The central object governing the tracer dynamics is a nonattracting chaotic saddle [17] containing an infinite number of periodic and nonperiodic bounded tracer orbits which never reach the far up or downstream region. The saddle has an unstable manifold which leads tracers ever approached the saddle in the far downstream region. Both the saddle and its unstable manifold are fractal objects. Since the asymptotic dynamics is simple, the tracer motion can be considered as a scattering process with all the characteristics of a periodically driven one-dimensional *chaotic scattering* [18].

Our aim in this paper is to study how this picture changes when the velocity field has a *chaotic* time-dependence. We restrict ourselves to flows of asymptotic simplicity further on, which implies that the time dependence is relevant in a finite region of the plane only, in the so-called mixing region. Note that this does not mean at all that the flow would be turbulent here. In fact, we shall consider four-vortex problems as illustrative examples. Nevertheless, we do hope that by understanding such cases, we come a step closer to the understanding of what passive transport looks like in flows exhibiting two-dimensional turbulence [19, 20] in regimes of finite extents. In the language of point mechanics, such tracer motions correspond to chaotic scattering processes generated by chaotic temporal driving.

Studying the motion of tracer ensembles, we present numerical evidence for the existence of a *bounded chaotic set* containing trajectories never going out to the far up or downstream region. Although periodic orbits are atypical, an infinite number of bounded orbits belong to this set which seems thus to be a direct generalization of a chaotic saddle. Local Lyapunov exponents around it are found to be strictly positive.

Tracer droplets rapidly evolve interwoven, *filamental* patterns which cannot be distinguished by naked eye from the fractal filaments of the periodic flows. A closer observation, however, reveals that these need not follow exact fractal scaling. In other words, if a local fractal dimension of such filaments can be defined at all, it might depend on the length scale of observation. The recently coined concept of *indecomposable continua* [14] seems to be an appropriate tool for describing the filamental patterns observed in chaotic flows.

The equation of motion of interacting ideal point vortices in incompressible two-dimensional flows can be written in the canonical form [22]

$$\Gamma_i \dot{x}_i = \frac{\partial H}{\partial y_i}, \quad \Gamma_i \dot{y}_i = -\frac{\partial H}{\partial x_i}, \quad i = 1, 2, \dots, N. \quad (1)$$

where $\{x_i, y_i\}$ are the coordinates of the vortex i of strength Γ_i and the Hamiltonian appears in the form

$$H(\{x_i, y_i\}) = -\frac{1}{\pi} \sum_{i < j} \Gamma_i \Gamma_j \ln r_{i,j}, \quad (2)$$

$r_{i,j}$ being the distance between vortices i and j .

Our aim now, as explained above, is to investigate advection in a velocity field produced by point vortices moving chaotically. It can be easily shown that the minimal number of vortices necessary for chaotic dynamics is four [22, 21].

We are interested in advection in open flows where distant tracer particles can come close to the point vortex system along a simple path, exhibit complicated motion around them, and then leave this system along a simple trajectory again. The condition for such open flow is, that the sum of the vortex strengths has to be zero ($\sum_{i=1}^4 \Gamma_i = 0$). In this case the streamlines far from the vortices are straight lines along which the vortices can be approached. (Otherwise the streamlines far from the vortices are closed curves.)

The above conditions are also satisfied by the so-called *leapfrogging* motion of two identical point-vortex pairs [12]. However, due to the special symmetry of the initial positions ($x_1 = x_4$, $x_2 = x_3$, $y_1 = -y_4$, and $y_2 = -y_3$, i.e., vortices 1 and 2 are mirror images of vortices 3 and 4) which is preserved by the dynamics, the motion of the vortices is non-chaotic, but periodic. By considering a four-vortex system with the same set of vortex strengths $\Gamma_1 = \Gamma_2 = 1$, $\Gamma_3 = \Gamma_4 = -1$, but without restricting the initial conditions to a symmetric one, we obtain a locally chaotic and asymptotically steady open flow. The only disadvantage is the fact that this system is unstable in the sense that can disintegrate into two vortex pairs moving away in different directions. In other words the chaotic vortex motion itself is transient. This has been studied in great detail as a chaotic scattering process of vortex pairs. The time on which the system breaks up in two pairs strongly depends, however, on the initial conditions. Thus one can choose appropriate initial conditions to make this time long enough to investigate the advection for an arbitrarily long time.

One can prevent this break up by changing the vortex strengths to keep the vortices close to each other forever. The condition is that the system should not be decomposable into subsystems having the sum of the vortex strengths zero. The simplest case which satisfies this condition is the following: $\Gamma_1 = \Gamma_2 = \Gamma_3 = 1$ and $\Gamma_4 = -3$.

We shall consider both vortex systems as illustrative examples of chaotically time-dependent open flows. Typical vortex trajectories are shown on figure 1. The common feature of both dynamics is that the four vortices move chaotically, do not depart from each other, but move together along a

line. (The latter is true only for a finite but long period of time in the first case.) Thus the motion of the vortices can be seen as a superposition of a straight translating motion along a line and a chaotic relative motion which produce a chaotic velocity field confined to a region of finite average linear extent, the mixing region.

The dynamics of passively advected particles is determined by the underlying velocity field generated, in our case, by the point vortex systems described above, and is given by the superposition of circular velocity fields of single vortices. The streamfunction ψ for a point vortex system can be written as

$$\psi(x, y, t) = - \sum_i \frac{\Gamma_i}{\pi} \ln r_i(t), \quad (3)$$

where $r_i(t)$ stands for the distance of point (x, y) from vortex i . The tracer equations of motion can be expressed by the streamfunction ψ as

$$\dot{x} = \frac{\partial \psi(x, y, t)}{\partial y}, \quad \dot{y} = - \frac{\partial \psi(x, y, t)}{\partial x}. \quad (4)$$

Note the Hamiltonian character of the dynamical system (4).

Vortex systems chosen in the preceding Section translate as a whole along a line with an average velocity. By introducing a co-moving reference frame, we can make the translation of the vortices to disappear. In this *comoving* frame the velocity field ensures that particles are advected towards the mixing region and then leave it by moving away on asymptotically straight lines. Thus, the condition for an open flow with asymptotic simplicity is fulfilled.

Similarly to periodic open flows, the advection of passive tracers is a chaotic scattering process. Typical trajectories of tracer particles are shown in Figure 2. As usual, the time spent in the mixing region, and the chaotic part of the trajectory itself is sensitively dependent on the initial coordinates of the tracers.

Lyapunov exponent measured along long time orbits are clearly positive. Measurements were carried out by starting a test-particle with an initial condition close to the one of the reference orbit (the initial distance is $\delta = 10^{-5}$). The test-particle departs from the reference orbit and as their distance becomes larger than a threshold (10δ) value, we shift it close to the orbit again to a distance δ along the line connecting the test and reference particle. We represented the number of such replacements used up to time t along the

reference trajectory (in fact, this number is proportional to the logarithm of the total stretching rate) as a function of t on Figure 3. The average slope corresponding to the chaotic part of the plot gives an estimate of the Lyapunov exponent.

We can now investigate the evolution of an *ensemble* of tracer particles simulating the evolution of a droplet of dye injected into the mixing region. Snapshots taken at different times (Fig. 4) show that the ensemble tends to produce a complicated *filamental* structure characteristic to chaotic mixing and reminiscent to the ones observed in the case of periodic open flows. The latter was identified as the unstable manifold of the chaotic saddle existing in the mixing region [10, 12]. An important difference is, however, that in contrast to the periodic generation of identical lobes, here the emerging patterns continuously change their form and size due to the chaotic motion of the vortices driving the flow.

Using these tracer trajectories we can represent the time spent in the mixing region for each initial condition (Fig. 5). The tracers were distributed on a two-dimensional grid in these simulations. We are particularly interested in the singularities of the escape times, which means trapping for a large, theoretically infinite, time in the mixing region. The latter was chosen for numerical purposes as a box centered initially to $x = y = 0$ and moving with the average velocity of the vortex system in the x direction. The dimensions of this box was $l_x = l_y = 4$ which is large enough to fulfill the condition that particles leaving this box will never return to the mixing region again.

Figure 5. shows that there are two qualitatively different sets formed by initial conditions leading to long escape times. One of them has a compact ellipsis shaped structure and is situated around the vortices. The particles in this set are trapped forever in these *vortex cores*, and their trajectories cannot be approached by particles coming from outside the cores. This kind of vortex cores are a generic feature of point vortex dynamics as it was pointed out in different papers [21]. The motion of the tracers is a regular motion around the chaotically moving vortex centers, being just a slaved chaotic motion with zero relative Lyapunov exponent. In conclusion, these cores are irrelevant for the chaotic scattering process we are interested in.

The other set of initial conditions with large escape times, in contrary, has a complex filamentary structure reminiscent to the fractal stable manifolds of the chaotic saddles observed in the case of time-periodic flows. The motion of the particles in this set is chaotic and is restricted to the mixing region, in

the forward dynamics. We shall call it the (forward) *nonescaping foliation*.

One can also construct a similar set corresponding to the time-reversed tracer dynamics starting with the same set of initial conditions. This *backward nonescaping foliation* will exhibit similar patterns. The intersection of these two foliations has the property that trajectories starting from it never leave the mixing region either in the forward or in the backward dynamics. It is thus a natural generalization of the chaotic saddle introduced in the periodic case, and we call it the *chaotic set*. The most important difference is that this chaotic set *cannot* contain periodic orbits since the driving flow has an inherently nonperiodic character.

For a quantitative characterization one can measure the decay of tracer particles in the mixing region by starting with an ensemble of particles and monitoring the number $N(t)$ of particles staying still inside after time t . In case of periodic flows there is an exponential decay $N(t) \sim \exp(-\kappa t)$ characterized by the escape rate κ . In our case the decay is found to be nonuniform which means that the escape rate is time dependent. This is a natural consequence of the fact that the advection is driven by a flow with chaotic time dependence.

The variation in escape rates also implies a non-uniform scaling of the geometry as well. The fractal properties of the singularities of the time delay function were investigated by the box counting method.

We claim that the escaping process and the tracer foliations in chaotically driven flows are of similar character as in open random (Hamiltonian) maps. This explains the fluctuations of the time decay and fractal dimensions, as they appear as statistical averages with $1/n$ type of convergence in random baker maps.

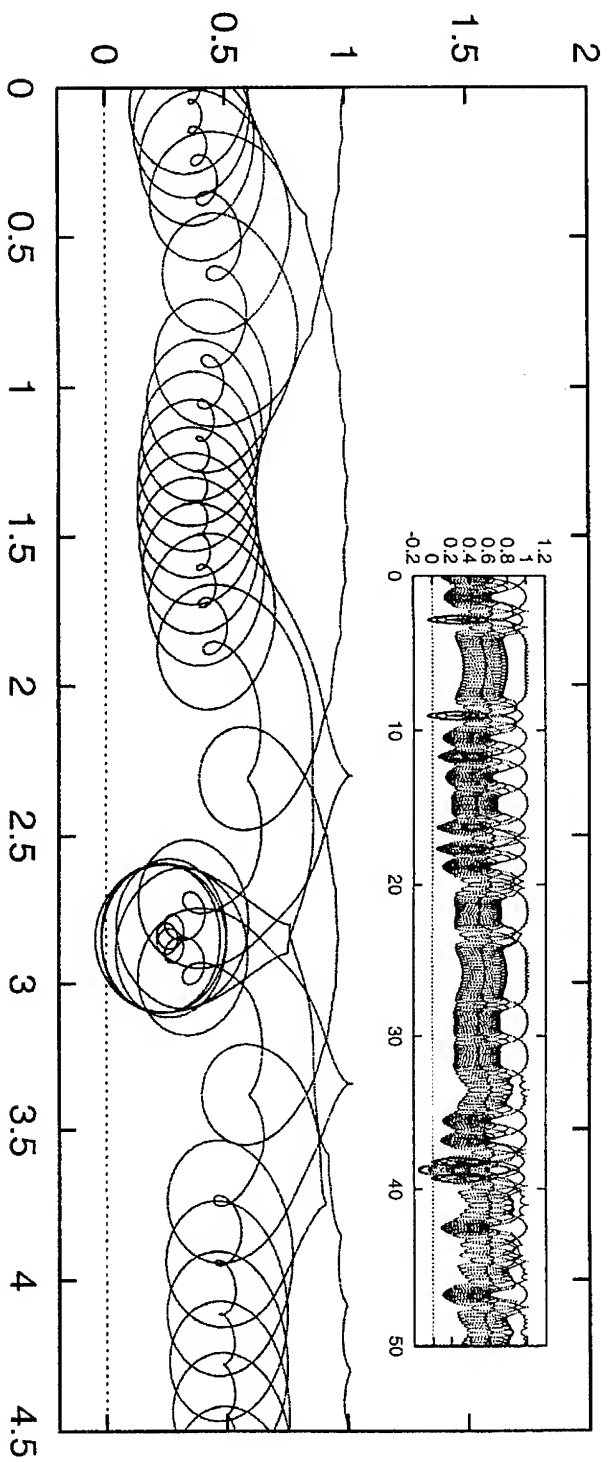
A central assumption is of course the stationarity of the random process. Since the mixing region is finite, we can assume that such a stationary distribution of the chaotic driving exists and sets in after a finite time. In a particular observation, unfortunately, we cannot be sure that the stationarity has already reached. If this is not the case, no well defined characteristics can exist, not even in the weak sense of random averages.

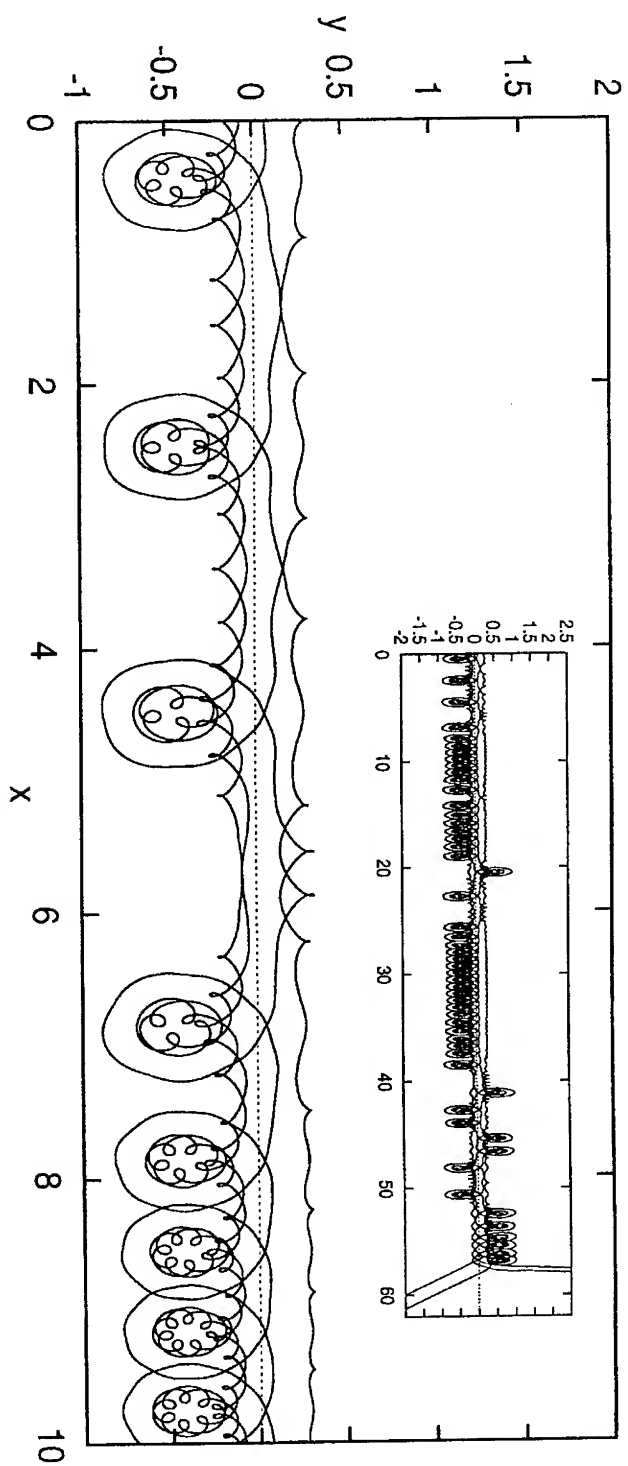
References

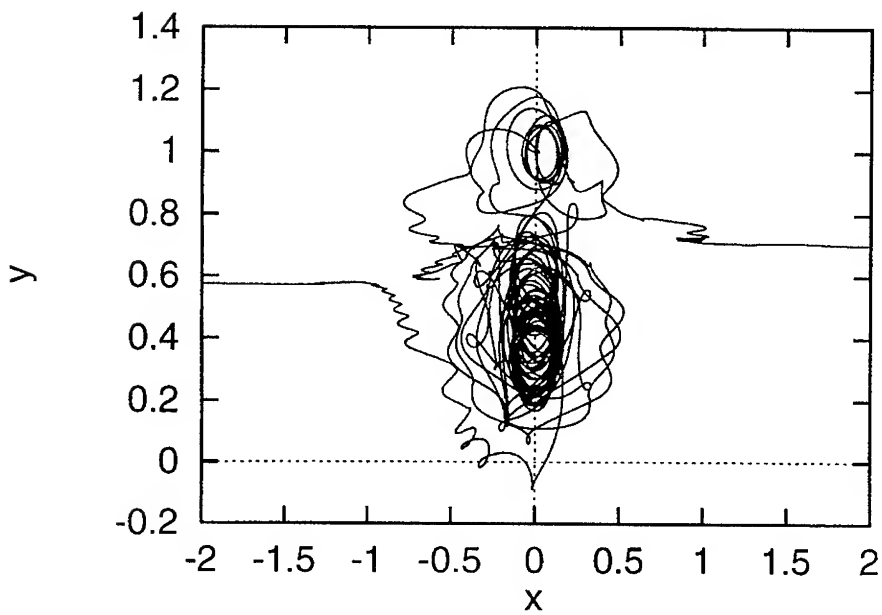
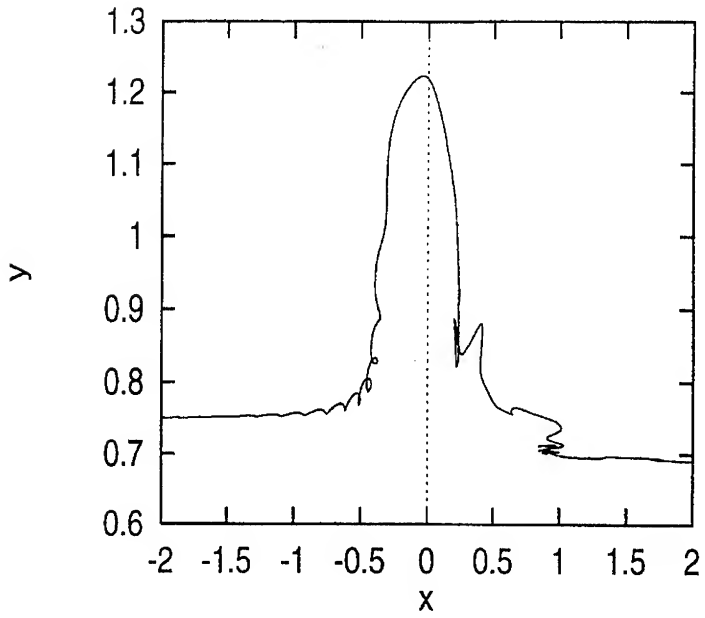
- [1] J. M. Ottino, *The kinematics of mixing: stretching, chaos and transport*,

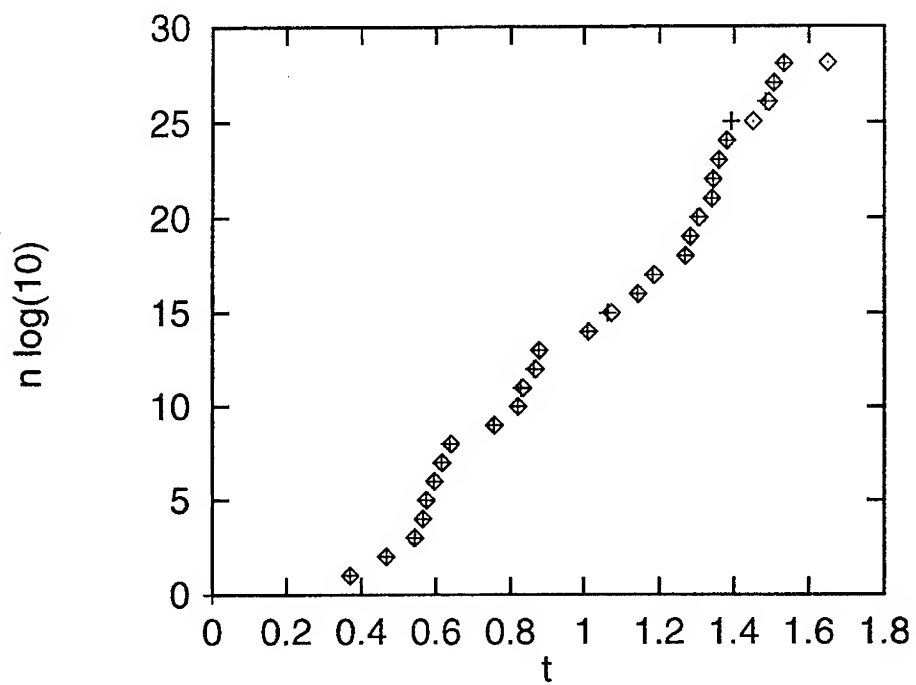
- (Cambridge University Press, Cambridge, 1989); J. M. Ottino, *Ann. Rev. Fluid Mech.* **22**, 207 (1990); S. C. Jana, G. Metcalfe and J. M. Ottino, *J. Fluid Mech.* **269**, 199 (1994).
- [2] H. Aref, *J. Fluid Mech.* **143** (1984) 1; D. V. Khakhar, H. Rising, and J. M. Ottino, *J. Fluid Mech.* **172** (1987) 419.
 - [3] H. Aref and S. Balachandar, *Phys. Fluids* **29**, 3515 (1986).
 - [4] A. Crisanti et al., *Riv. Nuov. Cim.* **14**, 1 (1991).
 - [5] J. C. Sommerer and E. Ott, *Science* **259**, 281 (1993); J. C. Sommerer, *Physica D* **76**, 85 (1994).
 - [6] R. T. Pierrehumbert, *Chaos Sol. Fract.* **4**, 1091 (1994).
 - [7] K. Shariff, A. Leonard, N. J. Zabusky and J. H. Ferziger, *Fluid. Dyn. Res.* **3**, 337 (1988).
 - [8] H. Aref, S. W. Jones, S. Mofina, and I. Zawadski, *Physica D* **37** (1989) 423.
 - [9] K. Shariff, A. Leonard, *Ann. Rev. Fluid. Mech.* **24**, 235 (1992).
 - [10] C. Jung, T. Tél and E. Ziemniak, *Chaos* **3**, 555 (1993); E. Ziemniak, C. Jung and T. Tél, *Physica D* **76**, 123 (1994).
 - [11] D. Beigie, A. Leonard, and S. Wiggins, *Chaos Sol. Fract.* **4**, 749 (1994).
 - [12] Á. Péntek, T. Tél, and Z. Toroczkai, *J. Phys. A* **28**, 2191 (1995); *Fractals* **3**, 33 (1995).
 - [13] Á. Péntek, Z. Toroczkai, T. Tél, C. Grebogi, and J. A. Yorke, *Phys. Rev. E* **51**, 4076 (1995).
 - [14] M. A. Sanjuan et al, Indecomposable continua in dynamical systems with noise: fluid past an array of cylinders, preprint (1996)
 - [15] Z. Toroczkai, G. Károlyi, Á. Péntek, T. Tél, C. Grebogi and J. A. Yorke, Wada dye boundaries in open hydrodynamical flows, preprint, (1996).

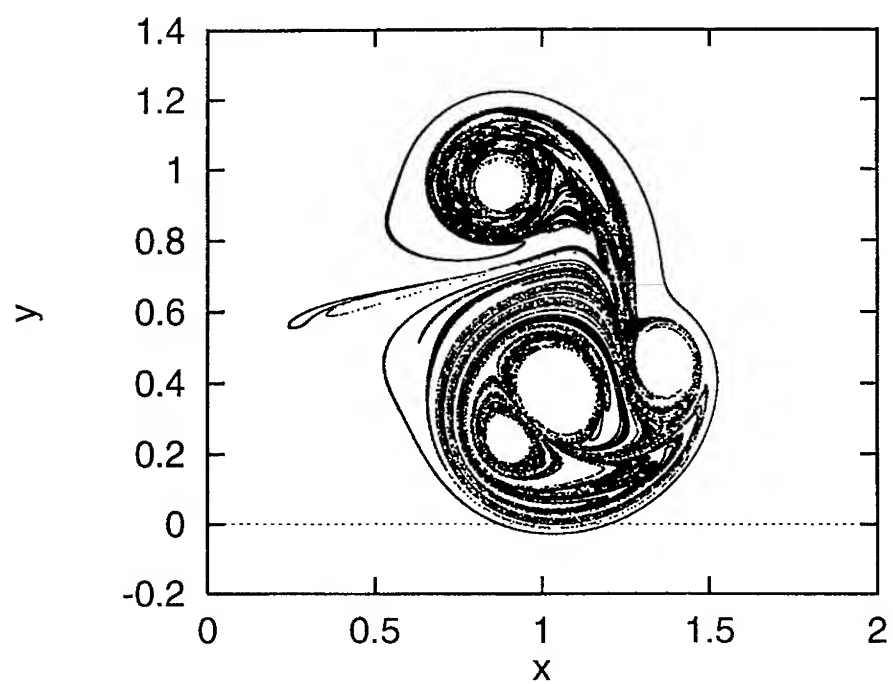
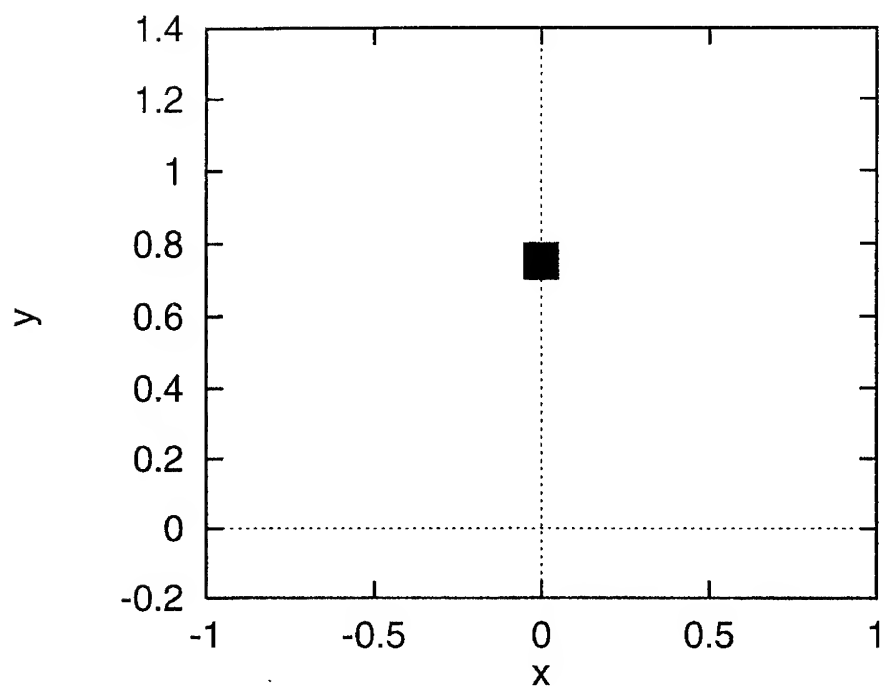
-
- [16] J. C. Sommerer, H.-C. Ku, and H. E. Gilreath, Phys. Rev. Lett. **77**, 5055 (1996)
- [17] T. Tél, in: *Directions in Chaos*, vol. 3, Ed.: Hao Bai-Lin, (World Scientific, Singapore, 1990) pp. 149-221; T. Tél, in *STATPHYS'19* ed.: Hao Bailin (World Scientific, Singapore, 1996) pp. 346-362
- [18] U. Smilansky, in *Chaos and Quantum Physics*, Eds.: M. J. Giannoni et al., (Elsevier, NY, 1992); C. Jung, Acta Phys. Pol. **23**, 323 (1992); E. Ott and T. Tél, Chaos **3**, 417 (1993); Z. Kovács and L. Wiesenfeld, Phys. Rev. E **51**, 5476 (1995).
- [19] D. Elhmaidi D, A. Provenzale and A. Babiano, J. Fluid Mech. **257** 533 (1993); A. Provenzale, A. Babiano and B. Villone Chaos Solitons and Fractals **5** 2055 (1995)
- [20] A. Babiano, G. Boffetta, A. Provenzale and A. Vulpiani, Phys. Fluids **6** 2465 (1994)
- [21] Z. Neufeld and T. Tél T, J. Phys. A **29** (1997)
- [22] P. G. Saffman, *Vortex Dynamics* (Cambridge University Press, Cambridge, 1992))

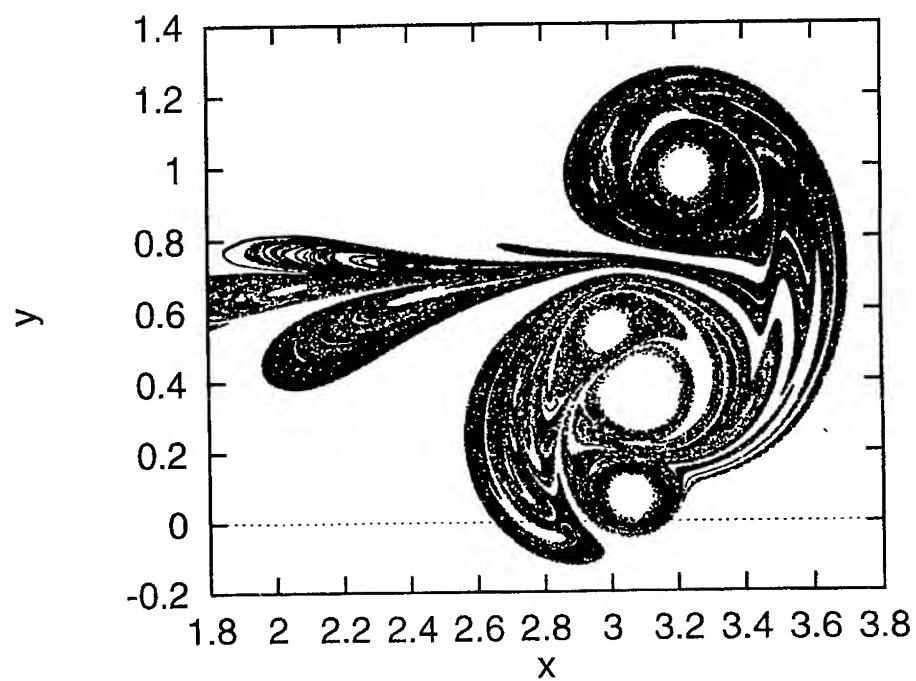
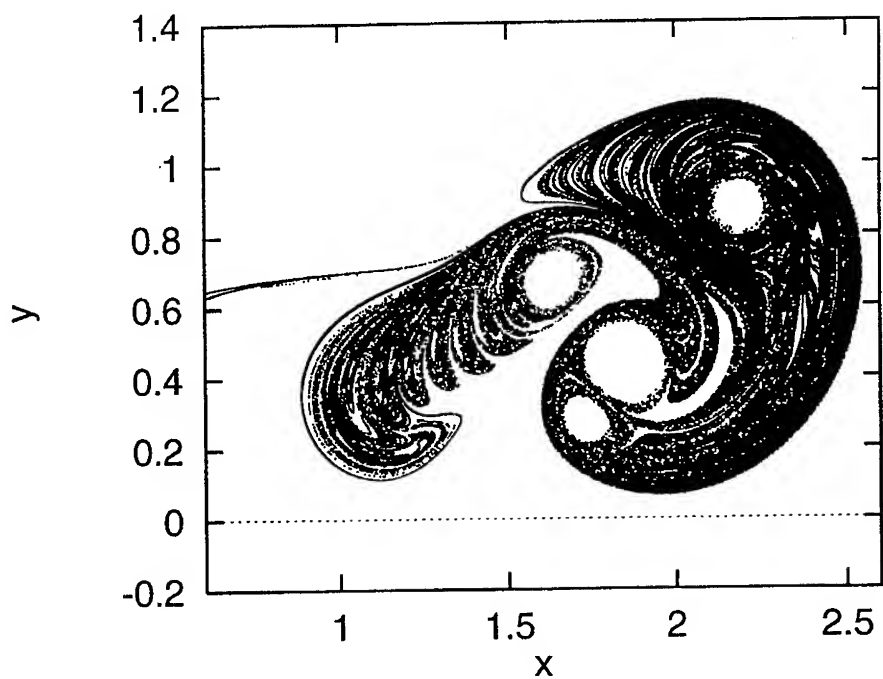


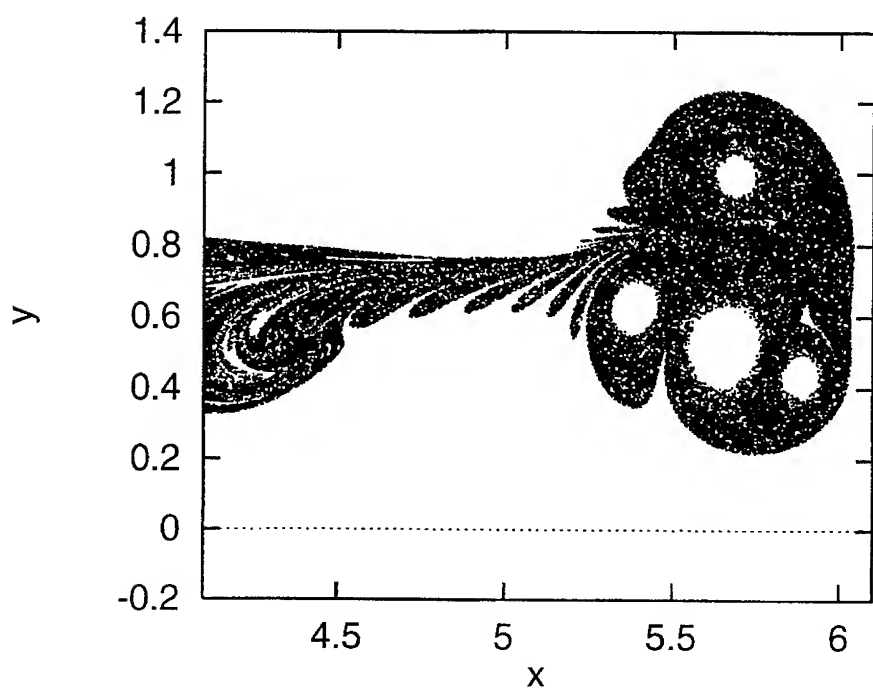
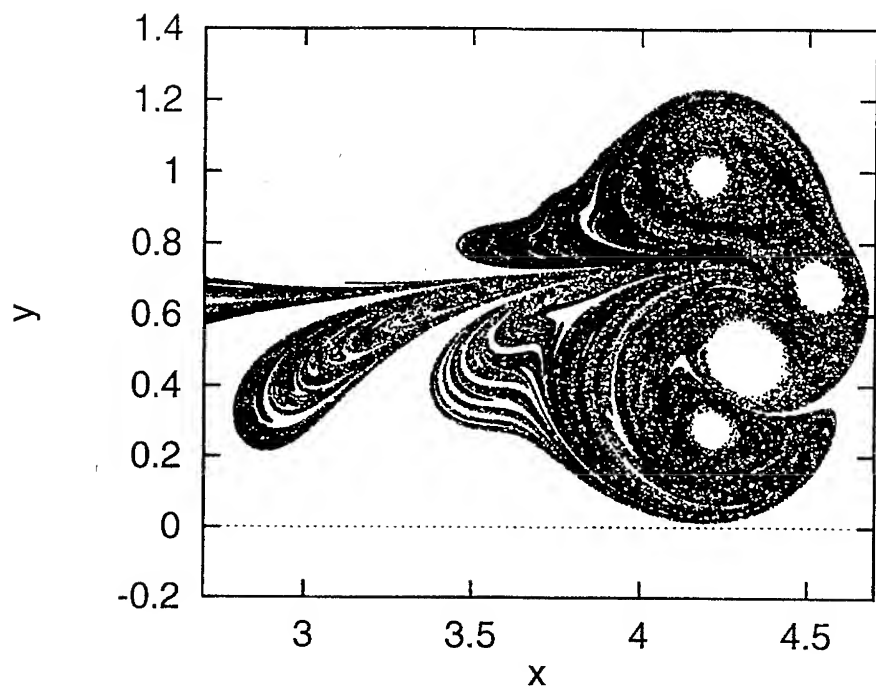


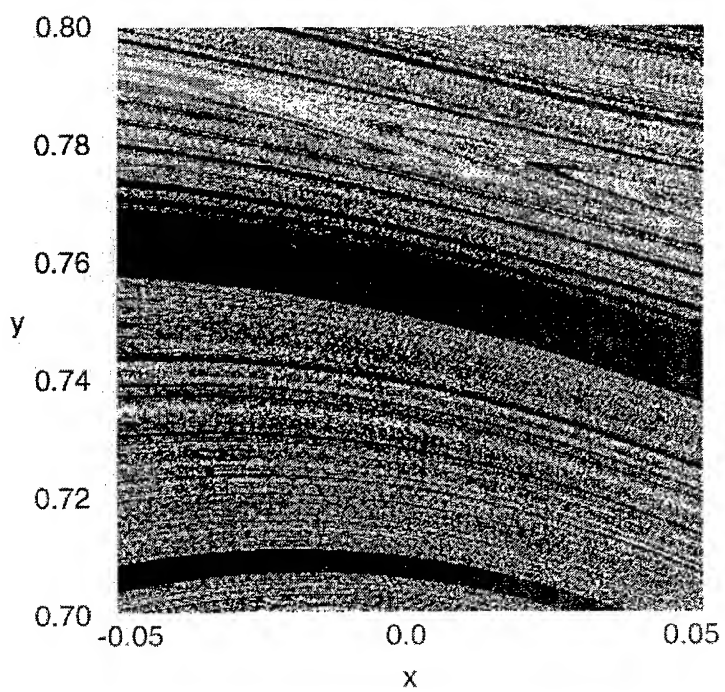
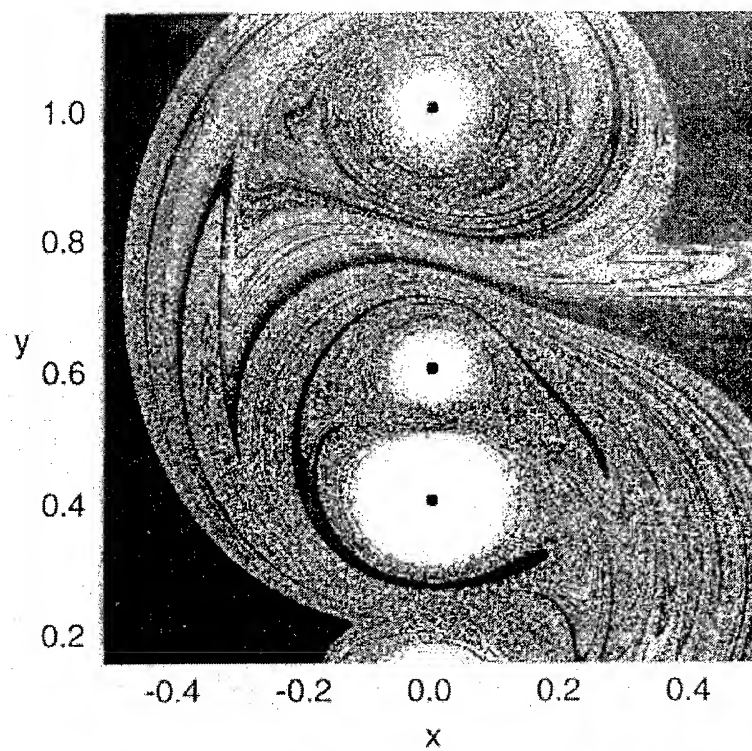












Global Heat Transfer Modelling on Bridgman Crystal Growth

F. Barvinschi*, I. Nicoară **, O. Bunoiu **, D. Nicoară**

* Dept. of Physics, Technical University of Timisoara, P-ta. Horatiu, No.1, 1900,
Timisoara, Romania

**Dept. of Physics, West University of Timisoara, B-dul. V.Parvan, No.4, 1900,
Timisoara, Romania

Abstract

The temperature distribution in fluoride-type crystal growth furnace have been studied by modelling the vertical Bridgman growth equipment. The steady-state heat transfer equation with boundary conditions have been solved using the finite element method. The influence of the thermal conductivity of the two phases on the solid-liquid interface shape have been also investigated. The calculated interface shape was found in good agreement with the quenched interface of the BaF_2 crystals.

1. Introduction

Over the last years a major effort has been made for studying the crystallization process taking into account the global thermal behaviour of the crystal growth equipments. Generally, a Bridgman furnace consists of a heating system and a number of screens. One may easily understand that control strategies for generating desired temperature distributions during growth are difficult to obtain. The numerical simulation of heat transfer in such a complex furnace may be extremely useful.

The temperature distribution in the solid and in the melt during the growth process affects the crystal quality. Particularly, the solid-melt interface shape has specific interest for the understanding of the defects formation. The modelling of the Bridgman method has been the subject of several papers [1-3], but most of the analyses do not take into account the radiative heat transfer within the crystalline and the melt phases.

It has been pointed out [4-11] that the role of internal radiation transfer of energy during crystal growth process of semitransparent materials cannot be neglected. Brandon and Derby [10,11] were the first to develop a model in which the internal radiative transport in solid phase was included rigorously. In their model the melt is assumed to be opaque and consequently radiation through the melt is not considered. There are semitransparent materials [12,13] (such as LiF , CaF_2 , BaF_2 , etc) whose optical absorption coefficient is not so high as to consider the molten phase opaque.

In the present paper we have studied the temperature distribution in the furnace and the crystal by modelling the vertical Bridgman growth equipment [14,16] built by the Crystal Research Laboratory of West University of Timisoara (CryT). We have tried to study the growth equipment as a system where the growth of the crystal can be simulated on the basis

of a reduced number of controllable parameters, such as the power input, the coolant temperature, the pulling rate, the geometrical size of the crystal (i.e. its length and diameter) and some physical properties of the material (thermal conductivity, transparency, etc.). Our heat transfer model takes into account both radiative and conductive heat exchange in furnace, crystal and melt. The interface shape dependence upon the thermal conductivity and transparency of the solid and molten phase were of special interest. The temperature distribution in the system and the interface shape has been obtained by solving the heat transfer equation using the FIDAP software [17] offered for use by DEM/SPCM/LPSI CEA-CEN Grenoble, France. The interface shape obtained by the modelling was then compared with the quenched interface of the BaF_2 crystals.

2. Global modelling of heat transfer

A schematic diagram of the CryT vertical Bridgman growth system is shown in fig. 1.a., where a graphite crucible, containing a BaF_2 charge is slowly lowered through a shaped, cylindrical graphite-heater [14,15]. The two-dimensional section of our mathematical representation of this system is presented in fig. 1.b. The ampoule is moved down the furnace at pulling rates small enough for a quasi-steady-state assumption for heat transfer through the system to be valid. The latent heat released at the solidification interface is small and assumed to be negligible. The crystal growth process takes place in a vacuum of 10^{-3} - 10^{-4} torr. We suppose that convection in the melt does not have a significant influence on heat transfer in this system.

Our main interest was to calculate the shape of the liquid-solid interface and the temperature distribution within the crystal at various stages of its growth. We have also studied the influence of the melt and crystal thermal conductivities on the crystallization interface shape for opaque and fully transparent cases.

Because the temperature distribution in crystal and melt depends strongly upon the boundary conditions on their outer surface, which are a priori unknown, a global calculation of the heat transfer throughout the whole furnace is indicated. Our numerical calculations employ the commercial software package FIDAP [17] which is a finite element analysis software which solves the equations for incompressible and compressible flow, heat and mass transfer.

In order to obtain the temperature distribution we have divided the whole system in subdomains. Heat transfer in all the subdomains of our model is described by the steady-state equation:

$$\nabla(k(T, r, z)\nabla T) + H(r, z) = 0 \quad (1)$$

where $k(T, r, z)$ is the thermal conductivity of the considered domain and $H(r, z)$ is the heat source term in the heating domain. When equation (1) describes the heat transfer in the heater, $k(T, r, z)$ is the temperature dependent thermal conductivity of the graphite. $H(r, z)$ vanishes in all the subdomains, except the heater.

The following boundary conditions are used:

The temperature and heat flux between adjoining subdomains is continuous:

$$T_i = T_j \quad (2)$$

and on the boundary between the subdomains i and j :

$$-(k_i \nabla T)_i \cdot \vec{N}_{ij} = -(k_j \nabla T)_j \cdot \vec{N}_{ij} \quad (3)$$

where N_{ij} is the unitary normal to the boundary between subdomains.

External boundaries lose heat via convection and radiation to the ambient temperature, T_∞ :

$$k_i (\bar{N}_i \nabla T) = h_i (T - T_\infty) + \epsilon \sigma (T^4 - T_\infty^4) \quad (4)$$

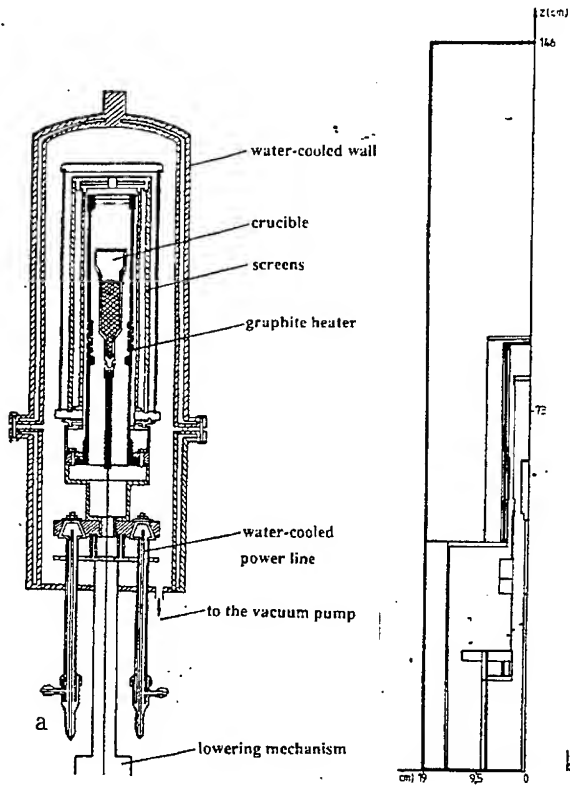


Fig. 1. (a) Vertical section showing the major features of the growth system;
(b) Two-dimensional mathematical model for the global calculation.

where h_i is the heat transfer coefficient on the boundary i , σ is the Stefan-Boltzmann constant.

At the boundary where the radiative heat transfer is taken into account the following boundary condition is used:

$$-k_i \left(\frac{\partial T}{\partial N} \right)_i = q_r^i \quad (5)$$

where q_r^i is the radiative flux at the boundary of the i -th subdomain.

As usual, the heat exchange relationship between the radiating boundaries is written as follows [18]:

$$\sum_{j=1}^N \left(\frac{\delta_{ij}}{\epsilon_j} - F_{ij} \frac{1-\epsilon_j}{\epsilon_j} \right) q_r^j = \sum_{j=1}^N (\delta_{ij} - F_{ij}) \sigma T_j^4 \quad (6)$$

where ϵ_j is the emissivity of the surface A_j , and F_{ij} is a view factor which represents the fraction of diffuse radiant energy leaving a surface A_i and directly falling upon a surface A_j .

The heat transfer equation (1) with the boundary conditions subjected to the considered subdomain has been solved using the finite element package (FIDAP). The computational domains are discretized with quadrilateral elements as is shown in fig. 1.b.

2.1. Influence of the charge position in the furnace on the interface shape

In order to verify the correctness of our model we have calculated the axial temperature distribution along the furnace centerline and we have compared it with the measured temperature (see fig.2). We can observe that computed and measured values are in good agreement.

In order to study the dependence of the interface shape on the charge position in the furnace we have solved the heat transfer equation with the boundary conditions which correspond to three ampoule positions in the furnace, noted as positions (-2), (0), (+2) and also shown in fig.3. on the right. We can observe that the interface curvature depends on the position of the ampoule in the furnace and on the thermal conductivity of the melt and solid. As it is known, when the ratio between the thermal conductivity of the melt and solid phase $k_L/k_S < 1$, the interface is convex towards the melt.

Fig. 4. shows the interface shape for the transparent case for the position (-2) of the ampoule and for three k_L/k_S values. We observe that the interface curvature is approximately 2 times smaller than that of the opaque case.

2.2. Interface shape dependence on the thermal conductivity of the opaque and transparent crystals

One of the purposes of this paper is to study the influence of the radiative heat transfer in the charge (i.e. the heat transfer in transparent crystals) on the interface shape. We have also taken into account the effect of the different thermal conductivity values of the melt and the solid. There are some crystals such as YAG, sapphire, CaF_2 , etc. which are relatively transparent to the infrared spectrum at high temperature and which have the k_L/k_S ratio smaller than the unity. For BaF_2 crystals a melt thermal conductivity about ten times smaller than that of the solid phase has been reported [13] as well as a melt absorption coefficient also about ten times higher than that of the crystal. Figure 5 shows the influence of the k_L/k_S ratio on the crystallization interface shape for the opaque and transparent cases for (-2) position. We can observe that the value of the k_L/k_S ratio changes the interface

curvature sign, from convex to concave, but in all cases the interface deflection is smaller for the transparent case than for the opaque case.

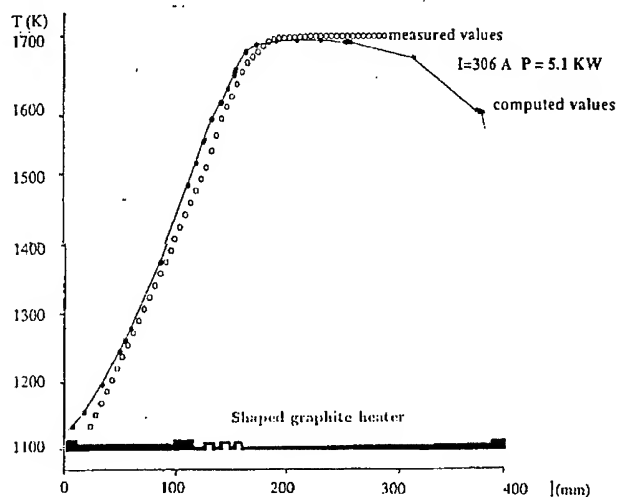


Fig.2. Computed and measured axial temperatures at the centerline of the furnace; the bottom is the section of the shaped graphite heater.

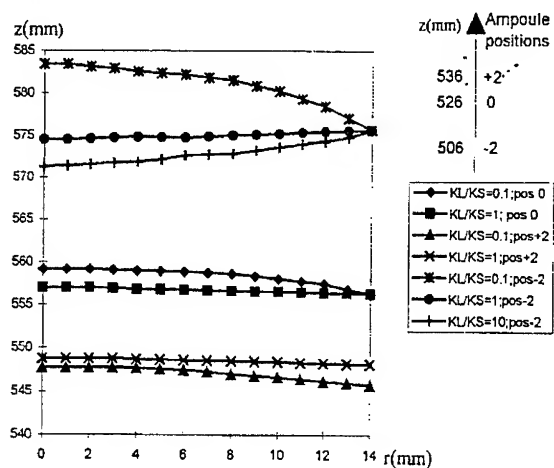


Fig.3. Interface shape of opaque crystal and melt for various k_L/k_S values and various ampoule positions.

All these results can be understood if we take into account the effects of the internal radiative transport in the crystal. For the transparent crystal the axial temperature gradient becomes smaller than that for the opaque case because the total heat flux is increased by the radiative flux and this leads to a decreased interface curvature [16].

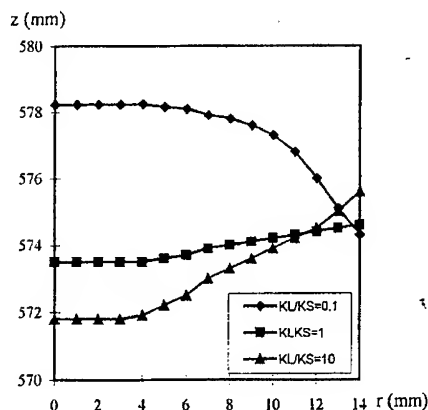


Fig.4. Interface shape of transparent crystal and melt for various k_L/k_S values for the (-2) position of the ampoule in the furnace.

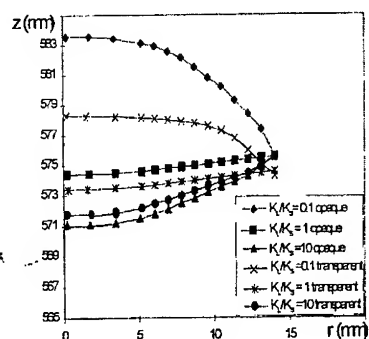


Fig.5. Interface shape for the (-2) position of the ampoule for various thermal conductivity values of the opaque and transparent charges

As we will show in section 3, for BaF_2 crystals, the quenched experiments confirm the reported $k_L/k_S = 0.1$ value (the interface is convex towards the melt) and the fact that in this crystal we must take into account the radiative heat transfer within the charge because the measured interface deflection value corresponds to the fully transparent case.

3. Experimental results

BaF_2 crystals were grown in a shaped graphite heater [14,15] using the conventional Bridgman-Stockbarger method. The temperature distribution within the furnace is measured by means of a Pt-Rh-Pt thermocouple which is moved along the furnace axis. During the crystal growth process the temperature is also measured by placing the thermocouple within the lower part of the crucible. In figure 2 we show the computed (the global modeling using FIDAP software) and the measured axial temperature distribution along the furnace. We can observe a good agreement between computed and measured values and this is important in order to compare the computed and measured interface deflection, δ . The solidification interface is located at $z = h(r)$. The interface deflection (δ) has been defined as the difference between the axial location at the centre and at the edge of the charge, i.e. $\delta = h(0) - h(R)$, where R is the crystal radius.

The crucible is made of a spectral pure graphite with a 1.5 mm wall thickness. In order to verify the correctness of the computed interface deflection values ($\delta_{\text{calculated}}$ by FIDAP software) we have grown several BaF_2 crystals. For the melt/solid interface shape demarcation the melt was doped with CoF_2 (0.5 % weight). To accomplish the demarcation, when the grown crystal had a length of a few centimeters, the power of the furnace was interrupted for five minutes and then the power and the standard growth translation rate were restored.

In the fig. 6. we can see the quenched interface. We can observe that the interface is convex towards to the melt and this means that $k_L/k_S < 1$, as confirmed by the reported values [13]. The computed interface deflection value and the measured δ value are in good agreement.

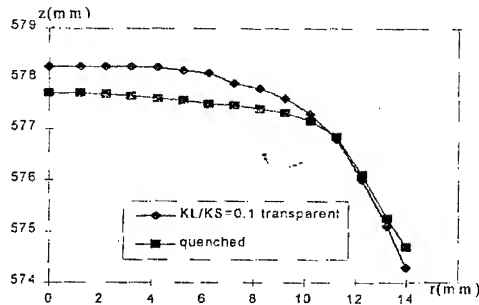


Fig.6. The melt-solid interface shape revealed by quenching experiments and the calculated interface for the transparent case ($k_L/k_S \leq 0.1$)

$$\delta_{\text{exp}} = 3 \text{ mm}, \delta_{\text{calculated}} = 3.7 \text{ mm}$$

Using the global modelling of the heat transfer we have obtained the interface curvature for transparent and opaque cases (see fig. 5). The concordance between the computed and experimental values corresponds to the fully transparent approximation rather than to an opaque melt and solid. The obtained results show that the mathematical model of the heat transfer used is correct enough to describe the heat transfer in such a crystal.

4. Conclusions

It is known that control strategies for generating a desired temperature distribution during the crystal growth process are difficult to obtain only by experimental attempts. The numerical simulation of the heat transfer in such a complex system may be extremely useful in the design of the real growth configuration. It is also important to know if the mathematical model of the physical phenomena is correct; this can be verified by comparing experimental and computed values.

Using the FIDAP software we performed a steady state simulation of the global Bridgman furnace in order to obtain the temperature distribution and to compare this with that measured in the CryT apparatus. The influence of various k_L/k_S ratio values and of the radiative heat transfer on the interface shape have also been studied. The temperature distribution obtained by this simulation and that measured are in good agreement. We have compared the S-L calculated interface shape deflection with that obtained using the quenching method for the revelation of the solid-liquid interface. The good agreement between the calculated and experimental δ values shows that the model is correct and can be used for the design of a furnace and of other aspects of the growth process which make it possible to obtain good optical quality crystals.

Acknowledgments

This work was supported in part by the CEA, French Atomic Commission and in part by the Ministry of Education, Romania, through grant Nr. 5032 /17.1/1996.

References

- [1] J.J.Derby and R.A.Brown, J.Crystal Growth **87**(1988), 251.
- [2] M.J.Crochet, F.Dupret and Y.Ryckmans, J. Crystal Growth, **97**(1989), 173.
- [3] S.Brandon, J.J.Derby, L.J.Atherton, D.H.Roberts and R.L.Vital, J.Crystal Growth, **132**(1993), 261.
- [4] B.Cockayne, M.Chesswas and D.B.Gasson, J.Mater.Sci., **4** (1969), 450.
- [5] Ji.Kvapil, Jo.Kvapil, B.Manek, B.Perner, R.Autrata and R.Schauer, J.Crystal Growth, **52** (1981), 542.
- [6] T.I.Butaeva, A.V.Gevorkyan, A.S.Kuzanyan and A.G.Petrosyan, Dokl. Akad.Nauk Arm. SSSR, **84** (1987), 38.
- [7] V.S.Yuferev, Zh.Prikl.Mat.Tekh.Fiz., **4** (1979), 31.
- [8] P.I.Antonov, S.I.Baholdin, E.A.Tropp and V.S.Yuferev, J.Crystal Growth, **50** (1980), 62.
- [9] V.S.Yuferev and M.G.Vasiliev, J.Crystal Growth, **82** (1987), 31.
- [10] S.Brandon and J.J.Derby, J.Crystal Growth, **110** (1991), 481.
- [11] S.Brandon and J.J.Derby, J.Crystal Growth, **121** (1992), 473.
- [12] P.I.Antonov, S.I.Baholdin, M.G.Vasiliev, V.M.Krimov and V.S.Yuferev, Izv.Akad.Nauk SSSR Ser.Fiz., **52** (1988), 1997.
- [13] V.D.Golishev and M.A.Gonik, Izv.Akad.Nauk SSSR Ser.Fiz., **52** (1988), 1896.
- [14] I.Nicoara, D.Nicoara and O. Aczel, Cryst. Res. Technol., **22** (1987), 1139.
- [15] D.Nicoara and I.Nicoara, Mat.Sci.Eng., **A102** (1988), L1,
- [16] D.Vizman, I.Nicoara and D.Nicoara, J. Crystal Growth, **169** (1996), 161.
- [17] FIDAP Users Manual (Revision 7.0), Evanston, USA.
- [18] R.Siegel and J.R.Howell, Thermal Heat Transfer, McGraw-Hill, N.Y. 1972.
- [19] I.Nicoara, A.Pusztai and M.Nicolov, Cryst. Res. Technol., **32** (1997), submitted.

On the Solidification Particularities of the Opaque and Semi-transparent Crystals obtained by Bridgman Method

Irina Nicoară^{a,1}, Mirela Nicolov^b, Artur Pusztai^a, Daniel Vizman^a

^aDepartment of Physics, West University of Timisoara

Bd. V. Pârvan 4, 1900 Timișoara, România

^bDepartment of Physics, "A.Vlaicu" University of Arad

Bb.Republicii 81, 2900 Arad, România

Abstract

The effect of the pulling rate and of the furnace configuration on the interface shape and its position in semitransparent and opaque crystals grown by the vertical Bridgman method are studied using the finite-element analysis.

Keywords: Crystal growth, Heat transfer modeling, Transparent materials

1 Introduction

Single crystals are the basic material for the production of many devices for microelectronics, optoelectronics and other industries. The original Bridgman [1] technique together with the wide variety of this method, is one of the most common technique

for single crystal growth from melt. The temperature distribution in crystal during the growth process, which is a solidification phenomenon, has a great influence on the crystal quality. Particularly, the solid-melt interface shape - the solidification isotherm - determines the formation of a part of the structural defects. At the same time, the temperature distribution in the grown crystal influences the defect formation due to thermal stresses.

The factors that affect isotherm shape are not always obvious, especially in the complex geometries of real growth systems. A realistic numerical simulation of the heat transfer phenomena in these systems can effectively support the developments for improved crystal growth processes. The modeling of Bridgman method has been the subject of several papers [2-4].

In the growth process of the optically transparent materials, at high temperatures, the energy transport via radiation within the solid and melt phases becomes important [5-8], but difficult to model [9-11].

In the present paper we have studied some particularities of the solidification process of the semitransparent materials by modeling a vertical Bridgman configuration using the finite - element method in order to solve the heat transfer equation. In particular, we have focused our investigation on the influence of some growth parameters - such as pulling rate and furnace type - on the crystallization interface shape. The use of the numerical simulation for process evolution allows important decisions to be made for crystal growth system design.

2 Thermal model of the crystallization process

We consider the solidification of the melt in an idealised vertical Bridgman system [1] with a three - zone furnace [see fig.1.a]. The gradient zone, which assures the crystallization condition by extraction of the latent heat released at the solidification

Table 1.

Characteristics of various furnace types

Furnance type	l_g (cm)	Temperature gradient $G(K \cdot cm^{-1})$			$T_c(K)$	$T_h(K)$
		G_h	G_g	G_c		
A	4	6	40	30	1593	1753
B	4	6	40	30	1553	1713
C	4	6	20	10	1593	1673
D	2	6	40	30	1593	1673
E	2	6	20	40	1633	1673

heat transfer coefficient: $h = 5 \cdot 10^{-4} W/cm^2 K$.

Table 2.

Charge properties

$T_m = 1653 K$	$c_M = 0.88 Jg^{-1} K^{-1}$
$\Delta H = 380 Jg^{-1}$	$c_c = 0.88 Jg^{-1} K^{-1}$
$\rho_{M,c} = 3.2 g cm^{-3}$	$a_M = 3 cm^{-1}$
$k_M^{mol} = 0.6 Wm^{-1} K^{-1}$	$a_c = 0.3 cm^{-1}$
$k_c^{mol} = 6 Wm^{-1} K^{-1}$	$n = 1.44$

Table 3.

Crucible Characteristics

$k_a = 45 Wm^{-1} K^{-1}$	$w = 1 mm$
$c_a = 1.44 Jg^{-1} K^{-1}$	$D = 10; 18; 40 mm$
$\rho_a = 2.1 g cm^{-3}$	$L = 100 mm$
$\epsilon_a = 0.81$	$\alpha = \frac{D}{L} = 0.1; 0.18; 0.4$

Table 1.

Characteristics of various furnace types

Furnance type	l_g (cm)	Temperature gradient $G(K \cdot cm^{-1})$			$T_c(K)$	$T_h(K)$
		G_h	G_g	G_c		
A	4	6	40	30	1593	1753
B	4	6	40	30	1553	1713
C	4	6	20	10	1593	1673
D	2	6	40	30	1593	1673
E	2	6	20	40	1633	1673

heat transfer coefficient: $h = 5 \cdot 10^{-4} W/cm^2 K$.

Table 2.

Charge properties

$T_m = 1653 K$	$c_M = 0.88 Jg^{-1} K^{-1}$
$\Delta H = 380 Jg^{-1}$	$c_c = 0.88 Jg^{-1} K^{-1}$
$\rho_{M,c} = 3.2 g cm^{-3}$	$a_M = 3 cm^{-1}$
$k_M^{mol} = 0.6 Wm^{-1} K^{-1}$	$a_c = 0.3 cm^{-1}$
$k_c^{mol} = 6 Wm^{-1} K^{-1}$	$n = 1.44$

Table 3.

Crucible Characteristics

$k_a = 45 Wm^{-1} K^{-1}$	$w = 1 mm$
$c_a = 1.44 Jg^{-1} K^{-1}$	$D = 10; 18; 40 mm$
$\rho_a = 2.1 g cm^{-3}$	$L = 100 mm$
$\varepsilon_a = 0.81$	$\alpha = \frac{D}{L} = 0.1; 0.18; 0.4$

to obtain the various growth configurations, listed in table 1 we have used a shaped graphite furnace [12]. The crystallization process takes place by a controlled solidification of the melt contained in the crucible which is lowered through the furnace at a velocity $v = 1 \div 7$ mm/h. Because the pull rate is small, the quasi-steady state assumption is justified [4] and the axial crystal growth rate (v_g) is approximated to be equal to the ampoule pull rate ($v_p = v_g = v$).

The heat transfer model takes into account both radiative and conductive heat exchange in furnace and charge. The influence of the ambient temperature distribution (the furnace type), of the pulling rate and of the charge properties on the shape of the solid-melt interface and on the temperature distribution in semi-transparent and opaque crystal is studied. We take into account two particularities of the CaF_2 crystals, namely (1) the thermal conductivity of the crystal (k_c) is greater than that of the melt (k_M) and (2) these crystals are semi-transparent, the absorption coefficient of the melt (a_M) being greater than that of the crystal (a_c). The optical absorption coefficient for many materials is very high and in consequence the internal radiation within the solid and the melt phases during the crystal growth process can be neglected. We have also studied the behavior of these materials (denoted as pure opaque) in growth conditions identical with those used for semitransparent materials. In order to write the energy equation for heat transfer in charge we use the diffusion approximation [5]. In this model the medium behaves like a material that has a thermal conductivity dependent on temperature (for both phases), and we can write that:

$$k = k^{mol} + k^{rad} = k^{mol} + \frac{16n^2\sigma T^3}{3a} \quad (1)$$

where k^{mol} and k^{rad} are the molecular and the radiative heat conductivity, respectively, n is the refractive index, σ is the Stefan-Boltzmann constant and a is the Rosseland mean absorption coefficient. In the case when the crystal and the melt are opaque, we have considered that $k = k^{mol}$.

Although this approximation is not so accurate (especially near the boundaries) as that used by Brandon and Derby [9,10] in order to account for the internal radiation transfer of energy during the crystal growth process, our results are in concordance with their conclusions and with our experimental observations on CaF_2 and BaF_2 crystal growth and their interface shape [13-15].

The thermal model of crucible, charge and furnace is shown in fig.1. The cylindrical coordinate system (r, z, θ) has its origin at the centre of the bottom of the crucible. The solidification interface is located at $z = h(r)$. In the numerical simulations we made the following assumptions: (1) the system is in a pseudo-steady state and (2) is radially symmetric (the system properties do not depend on θ), (3) the natural convection in the melt is negligible, (4) the crystal is isotropic. With the above assumptions, the governing energy equation is:

$$k_i \left[\frac{\partial^2 T}{\partial r^2} + \frac{1}{r} \frac{\partial T}{\partial r} + \frac{\partial^2 T}{\partial z^2} \right] = v \rho_i c_i (\vec{e}_z \cdot \nabla T) \quad (2)$$

where $i = M, C$ and M, C denote the melt and crystal, k is the thermal conductivity defined by equation (1), ρ is the density, c is the specific heat, v is the pulling rate, \vec{e}_z is the unit vector of the Oz axis. The heat transfer equation was solved using the finite element method with the following boundary conditions:

1. Along the outside wall of the crucible we have:

$$k_a (\vec{N} \cdot \nabla T_a) = h[T_a - T_A(z)] + \varepsilon_a \sigma [T_a^4 - T_A^4(z)] \quad \text{on } \Gamma_i, i = 1, 2, 3, 4 \quad (3)$$

where k_a is the thermal conductivity of the ampoule, h is the heat transfer coefficient, ε_a is the emissivity, \vec{N} is the outward normal vector to each boundary. The ambient temperature distribution of each furnace configuration is described by $T_A(z)$ and is specified in table 1.

2. The midplan ($r = 0$) of the rod crystal is assumed to be a plan of reflective symmetry in the temperature profile, so that:

$$k_i \frac{\partial T_i}{\partial r} = 0 \quad (i = M, C) \quad \text{on} \quad \Gamma_7, \Gamma_8 \quad (4)$$

3. Along the inner wall of the crucible we have:

$$k_i \frac{\partial T_i}{\partial r} = k_a \frac{\partial T_a}{\partial r} \quad (i = M, C) \quad \text{on} \quad \Gamma_5, \Gamma_6 \quad (5)$$

4. At the solid-melt interface (Γ_9) we took into account the latent heat released:

$$k_C(\vec{N} \cdot \nabla T_C) - k_M(\vec{N} \cdot \nabla T_M) = v\rho\Delta H(\vec{e}_z \cdot \vec{N}) \quad (6)$$

5. The solid-liquid interface corresponds to the melting-point isotherm, T_m :

$$T_m = T_M = T_C \quad (7)$$

The shape of the crystallization interface is set by the condition for the equilibrium temperature (7) and by the interfacial energy balance (6). The equations are three conditions on temperature at the solidification interface. Two of these are needed as boundary conditions for the energy balance equation (2) applied for both the melt and the solid phases. The third is distinguished for calculating the shape $h(r)$. The thermo-physical properties of the materials used - charge and crucible - are given in tables 2 and 3. We do not take into account temperature or frequency dependencies of optical or of thermal properties of the materials. The temperature distribution and shape of the crystallization interface for different growth conditions is calculated by finite element analysis [11].

3 Results and discussions

In order to analyze the influence of the growth conditions on the crystallization process we have studied the interface shape, its position with respect to the gradient zone and the temperature gradient near the solidification isotherm, both for semi-transparent and opaque cases.

For these we have solved the energy equation (2) with the boundary conditions (3-7) for many furnace types (we present here the results for only five types) and for the pulling rate with values between 1-7 mm/h. It is known that the temperature distribution in the crystal during the growth process influences the crystal quality. Particularly, the solid-liquid (S-L) interface shape is an important factor, because it influences the stress, incidence of poly-crystallinity and the optical quality of the transparent crystals. The shape of the crystallization interface can vary from concave to convex, depending on its axial location within the furnace. A convex isotherm (towards to the solid) will often lead to the best crystallinity, but if the segregation is important, a flat isotherm is desirable. Besides, if the thermal conductivities of the melt and the crystal have unequal values and at the growth interface the latent heat of solidification is released, the so called "interface effect" will be important. This also causes a nonplanar interface shape. The variations of the temperature distribution (in the obtained crystal) during the solidification process can lead to the appearance of thermal stresses and in consequence, to the formation of the dislocations. Thus knowledge of the temperature distribution is important in order to obtain good quality crystals. In all cases, an interface as flat as possible is needed.

The shape of the crystallization interface is characterized by its curvature. We define the interface deflection (δ) as the difference between the axial-interface location $h(r)$ at the centre and at the edge of the charge, i.e:

$$\delta = h(0) - h(R)$$

where R is the crystal radius. The interface deflection is a measure of the crystallization interface curvature, and a positive sign of δ means that the S-L interface is convex towards the melt.

We define the aspect ratio, α , as the ratio between the crystal diameter ($D = 2R$) and the crystal length (L), $\alpha = D/L$. This is one of the geometrical parameters of the study. The solidified fraction, f , is defined as the ratio between the grown

crystal length (l_c) at various stages of the growth process and the final crystal length (L), $f = l_c/L = 0 \div 1$.

3.1 The crystallization interface shape

In order to study the influence of the growth conditions - the furnace type and pulling rate - on the shape of the solidification interface we have solved the energy equation (2) with the boundary conditions corresponding to each furnace type, both for the semitransparent and for the opaque case. The influence of the various stages (characterized by the "f" factor) of the growth process on the interface shape has been obtained by setting various crucible positions in the selected furnace profile. We have started by setting the bottom of the ampoule in the gradient zone at 1 cm or 2 cm above the turning point (T_c); this corresponds to a certain solidified part of the charge, defined by a value of the solidified fraction (f). The process is assumed to be finished when all of the melt has been solidified. In our calculations we have taken five or six such crucible positions. In each case at the bottom of the crucible there is a certain temperature $T_A(z)$ value determined by the furnace type.

Influence of the pulling rate

In figures 2 and 3 we can see the interface position and shape for two furnace types (A and C), for two selected pulling rate values, both for the semitransparent (ST) and for the opaque case (O). For the selected crucible position, the bottom of the crucible is at the following ambient temperature: 1563 K for the A - type furnace and 1613 K for the C - type.

If we take into account both radiative and conductive heat transfer within the solid and molten phase, our calculations indicate that within limits of the used pulling rate values, this parameter of the growth process has no remarkable influence on the position (f is a measure of this parameter) or on the shape of the solid-liquid interface (the δ values) (see figures 2a,2b,3a,3c). If only conduction is considered for the two phases (i.e. pure opaque material) the influence of the pulling rate is not

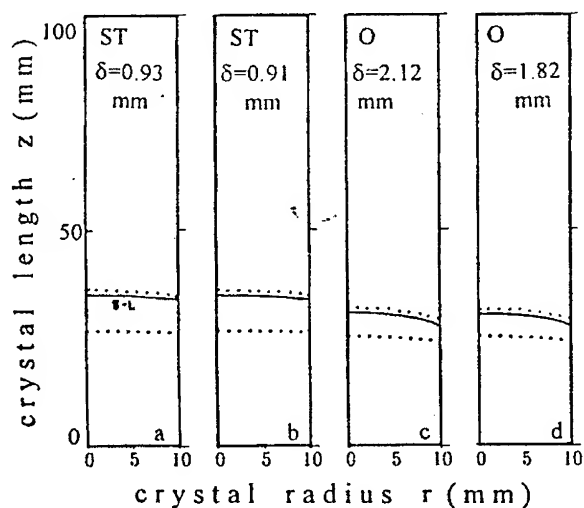


Fig.2. Interface shape and position (continue line) for a A-type furnace at various pulling rates for a semi-transparent crystal and melt (ST) and for the pure opaque case (O). The temperature difference between the three isotherms is $\Delta T = 10K$; (a,c) for $v = 3mm/h$ and (b,d) for $v = 7mm/h$, (a,b) $f = 0.34$ and (c,d) $f = 0.29$, $\alpha = 0.18$.

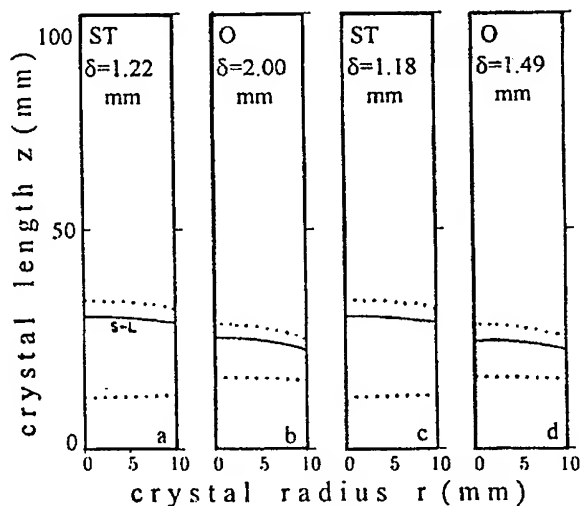


Fig.3. Interface shape and position for a C-type furnace at various pulling rates for a semi-transparent crystal and melt (ST) and for the pure opaque case (O). The temperature difference between the three isotherms is $\Delta T = 10K$; (a,b) for

$v = 3mm/h$ and (c,d) for $v = 7mm/h$, (a,c) $f = 0.29$, (b) $f = 0.25$, (d) $f = 0.21$, $\alpha = 0.18$.

negligible. These behaviours can be observed in figs. 2c,2d,3b,3d). In order to compare the solidification processes, we have taken the same crucible position in the selected furnace. We observe two main characteristics. For the same ampoule position in furnace, the solidification interface shifts upwards, toward the hot zone, if the material is transparent to radiation (compare figs.2a and 2c,3a and 3b). This behaviour of the interface position in the case of a partially transparent melt and solid, can be explained by the fact that the total heat flux through the medium is augmented by the radiative flux (by an increased k value) and this determines a shift of the interface to a higher position in the crucible toward the hot zone. The other characteristic refers to the value of the interface deflection (δ): the curvature of the crystallization interface for the opaque melt and opaque solid is greater than for the semitransparent case and depends on the pulling rate. Because the pulling rates employed are sufficiently small, the influence of this growth parameter on the interface shape is negligible for semitransparent materials, as we can see in the above mentioned figures. The radiative heat transfer in semitransparent crystals reduces the interface deflection and increases the interface location in comparison to opaque crystals, reducing the interface effect due to the difference in the thermal conductivities of the melt and crystal.

In order to observe the influence of the heat transfer type on the solidification interface in the figure 4 we have plotted two isotherms near the S-L interface, both for the pure opaque (fig.4a) and semitransparent cases (fig.4b), and for a semitransparent solid and opaque melt (fig.4c). We can observe that the S-L interface shifts to a higher position in the crucible for a semi-transparent solid (see figs. 4b and 4c), but

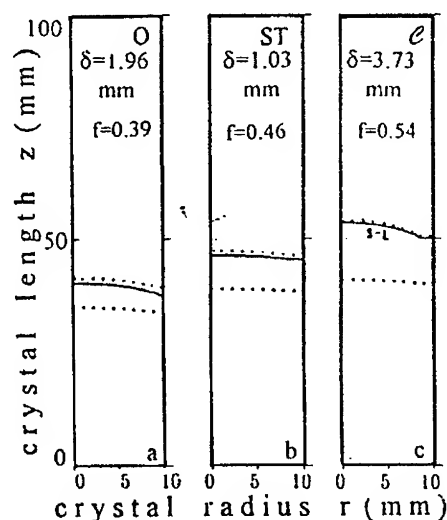


Fig.4. Influence of the heat transfer type on the S-L interface: a) heat transfer by conduction (pure opaque case), b) heat transfer by conduction and radiation (semi-transparent material), c) semitransparent solid and opaque melt. In all cases the ampoule is in the same position in furnace, the temperature of the bottom is 1533 K, with several corresponding f values. The difference between the isotherms is $\Delta T = 7$ K. $\alpha = 0.18$, $v = 5$ mm/h, A-type furnace.

this effect is greater if the melt is opaque (fig.4c). The temperature gradient in solid phase decreases progressively from the case shown in fig.4a to fig.4c, but the temperature gradient near the interface in the melt phase has the highest value for the situation depicted in fig.4c, i.e. when the melt is opaque and the solid phase is semitransparent. The interface deflection has the lowest value when both the melt and the solid are semitransparent (see fig.4b).

As the melt and crystal become transparent, the axial heat transfer is augmented by radiation and this leads to a higher axial heat flux than in the pure opaque case and this can explain all the particularities of the solidification process of the semitransparent materials.

The influence of the furnace type

The influence of the furnace type - especially the temperature gradient (G_y) in the gradient zone (see table 1) - on the interface shape is shown in fig.5. We can observe that the pulling rate (V) does not have a considerable effect on the δ value for semitransparent materials (fig.5a), unlike the pure opaque case or an opaque melt and a semitransparent solid. This last situation is specified by the letter C (a combined case) in the figure. We observe that the interface curvature depends on the furnace type in all cases, but the δ value is always greater for the opaque materials than for the transparent ones. In order to obtain a good quality crystal we have to choose a furnace type which determines the smallest δ value.

It is known that the first stage of the solidification process has an important influence on the crystal quality (the defect structure). Consequently, in this stage a low interface deflection value is needed. Fig.6 shows the influence of the furnace type on the interface shape (δ values) at the beginning of the solidification process. We observe that the lowest δ value is for the A type furnace for semitransparent case. Although, the temperature gradient in solid phase has a lower value for the C furnace than for the A one, the change in the sign of the isotherm curvature (for the C furnace), leads to the formation of thermal stress and then to the generation of dislocations. We also observe that, in the opaque case, all the above mentioned parameters have higher values than in the semitransparent material (compare fig.6.a,b with 6c,d).

If we study the influence of the geometrical factor - i.e. the aspect ratio, α , - on the interface curvature for the various furnace types we obtain figure 7. We can see that the aspect ratio is an important factor that has to be taken into account in the choice of the furnace type. We can say that for good quality crystal it is necessary to maintain a certain proportion between the crystal length and diameter; for α a value not higher than 0.2 is recommended.

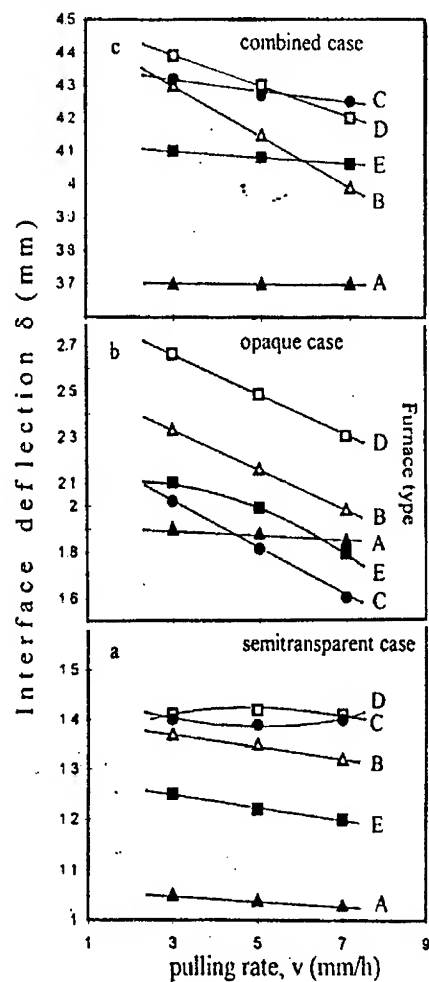


Fig.5. The interface deflection (δ) dependence on the pulling rate (v) for various furnace types, for the semi-transparent (ST), pure opaque case (O) and semi-transparent solid-opaque melt (); $\alpha = 0.18$ and $f = 0.5$.

▲: A-type furnace, △: B-type furnace, ●: C-type furnace, □: D-type furnace, ■: E-type furnace.

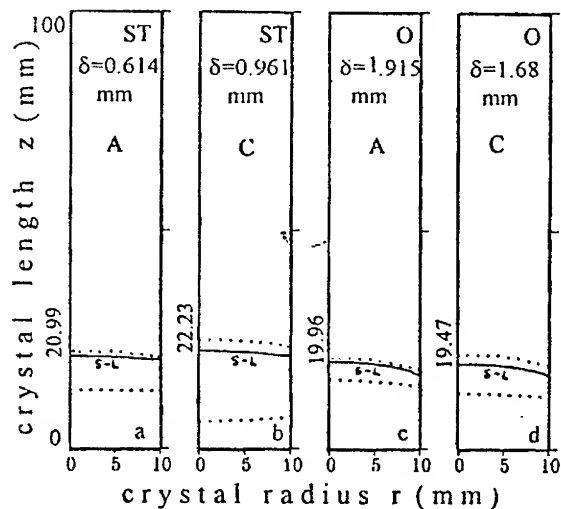


Fig.6. Influence of the furnace types on the interface shapes at the beginning of the solidification process ($f = 0.2$). (a) for A-type furnace, ST case, (b) C-type furnace, ST case, (c) A-type furnace, opaque case, (d) C-type furnace, opaque case. The temperature difference between the isotherms is $\Delta T = 7K$, pulling rate 5 mm/h, $\alpha = 0.18$.

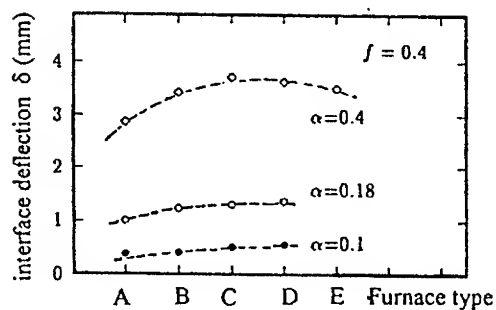


Fig.7. Interface deflection for several furnace types and for various aspect ratios; the solidified fraction is $f = 0.4$ and the pulling rate $v = 5mm/h$.

3.2 Interface position in the furnace

In order to obtain a low interface deflection value (δ) it is necessary to maintain the interface position in the gradient zone (see fig.1) during the solidification process. This means that for all "f" values the interface has to be located under the upper part of the gradient zone. In figs.8 we have plotted the interface position with respect to the gradient zone for the five furnace studied here for the beginning ($f = 0.2$) and for the end ($f = 0.7$) of the solidification process. If we analyze the interface location for the mentioned furnaces, we observe that for the A and B type furnace the interface is maintained in the gradient zone, but $\delta_A < \delta_B$ (see figs.5). We can also say that for the C-type furnace the T_h - temperature (see table and fig.1) is too low in order to compensate for the heat losses by radiation. If the material is opaque we see that for all "f" values the interface is located in the gradient zone (fig.8b), for all furnaces, but the interface curvature (δ) is higher for the opaque case than for the semitransparent one (see also figures 5). As the solidification fraction value increases the interface shifts towards the hot zone, indicating the contribution of the heat transfer by radiation within the solid phase. In order to show the influence of the geometrical factor, α , upon the location of the interface in the furnace, we have also plotted the interface position for $\alpha = 0.4$ and $f = 0.7$. We can observe that for this value of the aspect ratio, the interface for semitransparent materials leaves the gradient zone.

For D and E furnaces the interface is located out of the gradient zone. This means that such a furnace design is not recommended because it is known that in this case all of the isotherms are disturbed and will lead to a high value of the thermal stresses in crystals.

If we take into account all aspects of the solidification process described above we can say that in order to obtain good quality crystal a careful choice of the furnace type is necessary, depending of the optical properties of the charge (opaque or semitransparent). But in all cases an aspect ratio smaller than 0.2 is necessary. For

opaque crystals a C-type furnace is reasonable, but for a semitransparent charge an A-type is recommended.

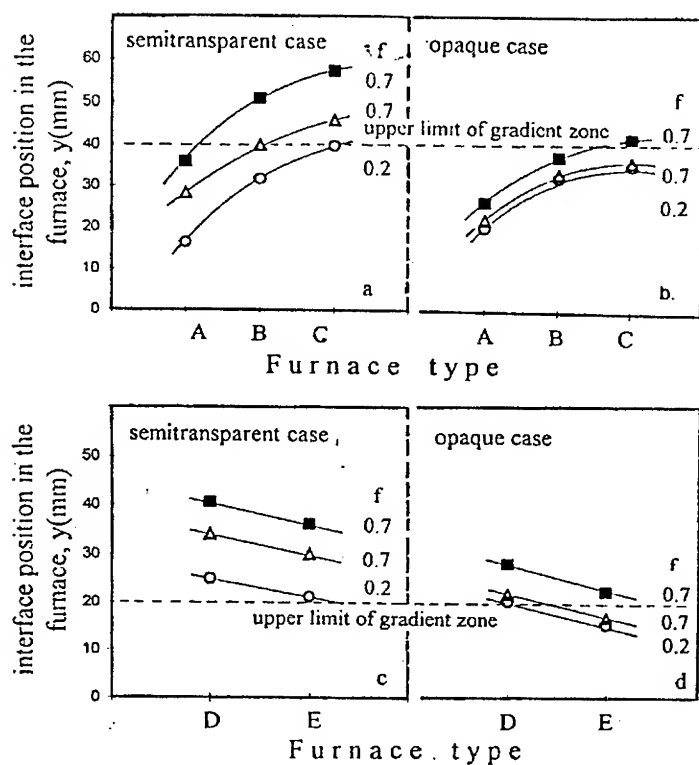


Fig.8. Interface position with respect to the gradient zone: (a,b) for A,B,C furnace type, (c,d) for D,E furnace type; $\alpha = 0.18$, $v = 5\text{mm/h}$. o - at the beginning of the solidification process ($f = 0.2$), Δ for $f = 0.7$ and \blacksquare for $\alpha = 0.4$ and $f = 0.7$.

4 Conclusions

A numerical modeling of the heat transfer in semi-transparent and in pure opaque materials during the crystallization process has been developed, using a three zone vertical Bridgman method. Factors affecting the solidification interface shape - such as furnace temperature profile, pulling rate and geometrical aspect of the charge - have been taken into account. We have presented results of a model that uses the diffusion approximation in order to take into account the internal radiative transport of energy both in the solid and molten phase. We have found that for semitransparent materials the pulling rate with values between 1-7 mm/h has no significant influence on the interface deflection or the interface position in the gradient zone. But the shape and position of the solidification interface strongly depends on the furnace type, aspect ratio and solidification fraction, both for opaque and semitransparent material. A careful furnace design has a great importance on crystal perfection. From our simulation several strategies arise for flattening the interface shape (small δ value). First, we have to take into account the optical properties of the charge and second, for a good quality crystal the aspect ratio (α) does not exceed 0.2. From the studied furnace types, the A-type is recommended if we can build a furnace with a large gradient zone length that has a high temperature gradient value (G_g). If we have a short gradient zone length (l_g) and low temperature gradient in this zone, an E-type furnace can be used with a high T_c temperature value. Opaque materials can be successfully crystallized in a C-type furnace, with low temperature gradient in a large gradient zone length. These characteristics of the furnaces can be adjusted using appropriate heat shields and furnace design, thus obtaining the desired thermal field. Therefore, the application of numerical simulations to the crystal growth process becomes an important tool for the improvement of the crystal quality.

References

- [1] P.W.Bridgman, Proc. Am. Acad. Arts. Sci. 60(1925)305.
- [2] T.W.Fu and W.R.Wilcox, J.Crystal Growth 481(1980)416.
- [3] R.J.Nauman, J.Crystal Growth 58(1982)554,569.
- [4] J.J. Derby and R.A.Brown, J.Crystal Growth 87(1988)251.
- [5] R.Siegel and J.R.Howell, Thermal Radiation Heat Transfer, (McGraw-Hill,N.Y.1972).
- [6] B.Cockayne, M.Chesswas and D.B.Gasson, J.Mater.Sci 4 (1969) 450.
- [7] T.I.Butaeva, A.V.Gevorkyan, A.S.Kuzanyan and A.G.Petrosyan, Dokl.Akad.Nauk Arm. SSR 84 (1987) 38.
- [8] V.S.Yuferev, Zh. Prikl. Mater. Tehk. Fiz. 4 (1979) 31.
- [9] S.Brandon and J.J.Derby, J.Crystal Growth 110 (1991) 481.
- [10] S.Brandon and J.J.Derby, J.Crystal Growth 121 (1992) 473.
- [11] D.Vizman,I.Nicoara and D.Nicoara, J. Crystal Growth, 169 (1996) 161.
- [12] D.Nicoara and I.Nicoara, Mater. Sci. Eng., A102(1988)L1.
- [13] I.Nicoara, D.Nicoara and O. Aczel, Cryst. Res. Technol. 22(1987)1139.
- [14] I.Nicoara, A.Pusztai and M.Nicolov, Cryst. Res. Technol., 32 (1997)37.
- [15] F.Barvinschi, O.Bunoiu, I.Nicoara, J.L.Santailier, T.Duffar, 2nd International Workshop on Modelling in Crystal Growth, Durbuy-Belgium, 13-16 October,1996.

Fourier Approach To Numerical Laser Resonator Calculations

Slobodan Petričević and Jovan Elazar

Faculty of Electrical Engineering, University of Belgrade
11000 Belgrade Yugoslavia, Bulevar Revolucije 73

ABSTRACT:

Paper presents a method for numerical calculation of the transverse modes of the laser resonator with finite rectangular strip mirrors employing Fourier analysis approach in wave optics theory. Physical model and algorithm were developed. Computer program was written. Results of transversal field amplitude and phase distribution for various values of Fresnel number N and various geometrical configurations are presented in the form of diagrams. Results are found to be in agreement with resonator theory.

1. INTRODUCTION

Laser resonator together with the gain medium determines the overall power efficiency, number of wavelengths that constitute and degree of spatial and temporal coherence as well as the geometrical properties of the beam, i.e. divergence and waist or spot size. Since these are the basic elements that make laser such a unique light source it follows that the design of a laser resonator is very important step in the design of the laser. If resonator configuration is not tractable analytically results are obtained by numerical methods. This paper presents a numerical method for laser resonator calculation employing Fourier analysis approach.

2. PHYSICAL MODEL OF THE LASER RESONATOR

To study resonator modes for an arbitrary cavity configuration one can take in account wave nature of the beam through Fresnel-Kirchhoff scalar formulation of the Huygen's principle [4]. This is accomplished by assuming that the dimensions of the resonator are large compared to the wavelength and the field in the resonator is dominantly transverse electromagnetic (TEM) [1]. Solution of the scalar equation yields resonator modes uniformly polarised in one direction. Thus it is possible to invoke first Rayleigh-Sommerfeld solution to the diffraction problem in the shape of the following scalar integral formula [2]:

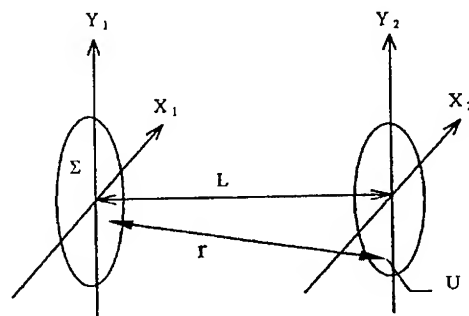


Fig. 1. Diffraction geometry

$$U(x_2, y_2) = \frac{L}{j\lambda} \cdot \iint_{\Sigma} U(x_1, y_1) \cdot \frac{e^{jkr}}{r^2} \cdot dx_1 dy_1 \quad (1)$$

where wave number k is given by $k = \frac{2\pi}{\lambda}$ and the distance r by:

$$r = \sqrt{L^2 + (x_1 - x_2)^2 + (y_1 - y_2)^2} \quad (2).$$

If the mirror separation (L) is large compared to mirror dimensions and the mirrors are lightly curved it is possible to introduce a further simplification. Namely, the two Cartesian components of the vector field can be treated as mutually uncoupled which allows for treating the problem in one dimension instead of the two dimensional integral equation (1). Separate scalar equation can be written for each component [1]. This eases and speeds up the implementation. Resonator structure is represented in Fig. 2. Two opposing

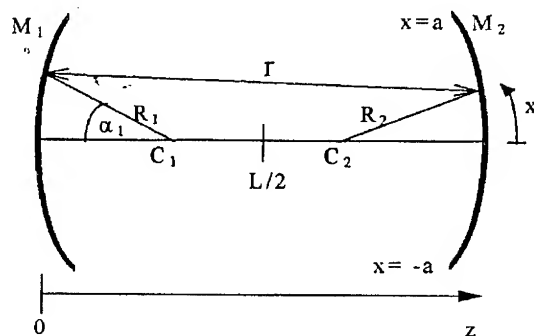


Fig. 2. Resonator geometry

mirrors are separated by distance L . Each mirror is curved with radius R at centre C . Distance r between points on opposing mirrors can be expressed in terms of arc co-ordinate x , radius R and distance L . Applying the assumption that L is large relative to other dimensions it is possible to use approximate expression for (2):

$$r \cong L + \frac{g_1 x_1^2}{2L} + \frac{g_2 x_2^2}{2L} - \frac{x_1 x_2}{L} \quad (3)$$

where confocal parameters g are defined as:

$$g_1 = 1 - \frac{L}{R_1}, g_2 = 1 - \frac{L}{R_2} \quad (4)$$

Importing (3) and (4) into (1) one gets:

$$u(x_1) = \frac{e^{jkL}}{j\lambda L} \cdot \int_{-a}^{+a} u(x_2) \cdot e^{\frac{jk}{2L} \cdot (g_1 x_1^2 + g_2 x_2^2 - 2x_1 x_2)} \cdot dx_2 \quad (5)$$

The equations (5) is known as the Fresnel diffraction integral. It is to be noted that r in (1) has been approximated with (3) in the exponent while r in denominator has been substituted only with L , because r in exponent is critical for determination of the field phase. Integral is calculated along the mirrors, from one end ($-a$) to the other (a). Thus, it is possible to relate the fields on the opposing mirrors by an equation (5) which expresses the field at each mirror in terms of the reflected and diffracted field at the other. This allows for an iterative algorithm capable of solving equation (5) by simulating transient process inside cavity [1]. Algorithm begins with an arbitrary field distribution at one mirror which is reflected back and forth inside cavity, a process governed by equation (5), a one dimensional scalar equation.

3. FOURIER ANALYSIS APPROACH

Alternatively, it is possible to rewrite (5) in the following manner [2]:

$$u(x_1) = \frac{e^{jkl}}{j\lambda L} \cdot e^{\frac{jkg_1 x_1^2}{2L}} \cdot \int_{-a}^{+a} u(x_2) \cdot e^{\frac{jkg_2 x_2^2}{2L}} \cdot e^{-\frac{j\kappa x_1 x_2}{L}} dx_2 \quad (6)$$

Scalar field component $u(x_1)$ can be expressed as a Fourier transform of the field $u(x_2)$ previously multiplied by:

$$m(x) = e^{\frac{jkg_2 x_2^2}{2L}} \quad (7)$$

This is convenient because Fourier transform is easily implemented on a computer. Field $u(x_1)$ can be expressed as a beam of planar waves propagating at different angles and phases with regard to optical axis, that is by its angular spectrum. Each constituent planar wave is represented by its spatial frequency [2]:

$$\omega_x = \frac{kx}{L} = \frac{2\pi\alpha}{L} \quad (8)$$

Thus, the beam inside the cavity is represented by its angular spectrum calculated across the mirror surface.

Finite mirror dimensions serve as boundary conditions, since wave component propagating beyond mirror scope is rejected (not reflected back). This is possible because there is no inverse Fourier transform in the process. Frequency range is set by upper and lower frequency limit given by:

$$f_{a+} = \frac{a}{\lambda L} \quad (9a)$$

$$f_{a-} = \frac{-a}{\lambda L} \quad (9b)$$

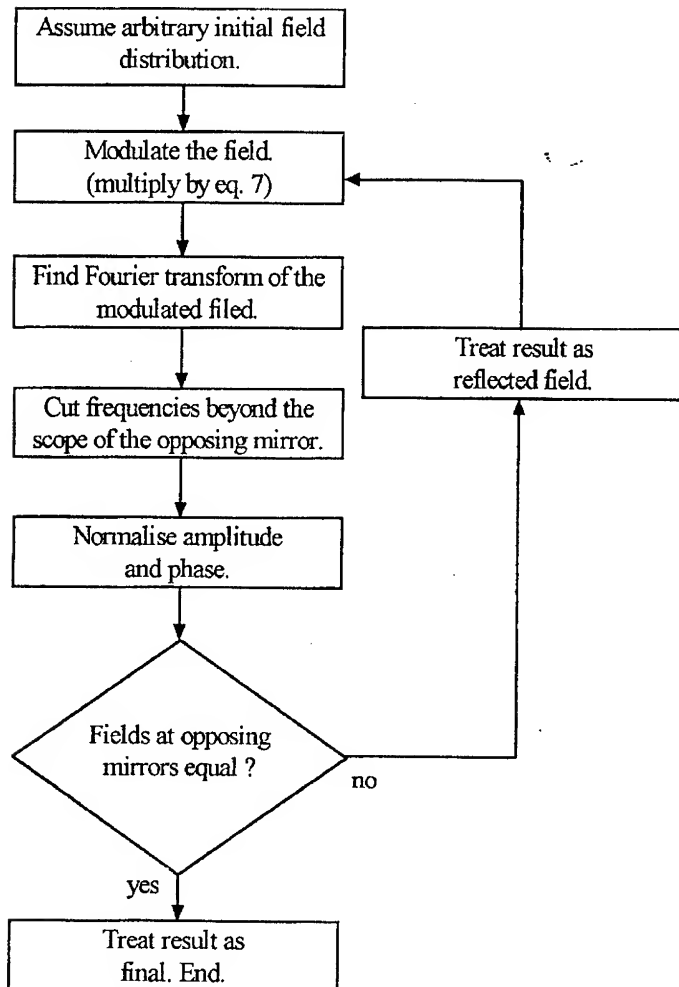
Thus reflection can be treated as low pass filter from the frequency domain point of view. Integral (6) is calculated in the Fresnel diffraction zone where a useful quantity known as the Fresnel number N is defined [3] by:

$$N = \frac{a^2}{\lambda L} \quad (10)$$

Fresnel number presents number of diffraction fringes that appear across the mirror and is directly related to the resonator modes [1]. Namely, higher order modes are visible with higher Fresnel number N . That resonator geometry can be expressed by defining values for Fresnel number N , distance between mirrors L , wavelength λ and confocal parameter g . Half mirror width a is calculated from eq. (10). This is convenient since resonator structures can be grouped according to Fresnel number N which is the most important determinant of the system.

4. NUMERICAL CALCULATION

Algorithm can be summarised by following flow chart.



Initial field distribution can be arbitrary, but best results are obtained by using random initial field distribution. Modulation of the field can be performed in place. In order to compensate for the absence of the active medium in model, it is necessary to normalize the field amplitude after each round trip [3] by setting the maximum field amplitude value to unity. Convergence of the algorithm is assured by normalisation of the field phase after each round trip [3], achieved by shifting entire phase over the mirror by an amount necessary to set phase at the center of the mirror to zero. Simulation ends when distributions on opposing mirror differ to a predefined amount, usually 1%.

Program was written to algorithm in programming language C on a personal computer. In order to increase the speed it was necessary to tabulate trigonometric functions needed to calculate the field

and direct discrete Fourier transform is used. Direct application of the FFT is not possible due to the fact that the spatial frequencies constituting the beam cover only small part of the spectrum. Namely, sampling frequency is given by

$$f_s = \frac{M}{a}, \quad (11)$$

where M is the number of points across half-width of the mirror. For typical values of a , L , λ and M , f_s is large compared to f_c , thus eliminating possible use of direct FFT. M is dependable on the Fresnel number N because in order to resolve the fine field structure M should be at least several times Fresnel number N .

5. RESULTS AND DISCUSSION

Simulation results are presented on the following six diagrams where field phase and normalised intensity are shown with either fixed Fresnel number N and varied confocal parameter g , or fixed confocal parameter g and varied Fresnel number N .

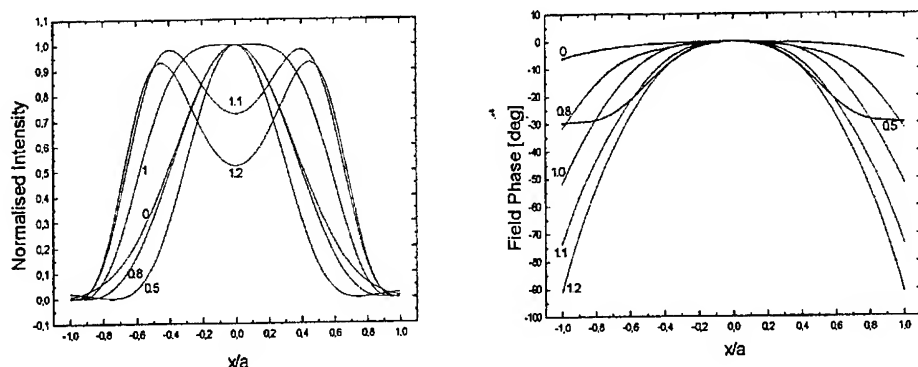


Fig. 3. Normalised field intensity and phase as a function of position on the mirror with fixed Fresnel number $N=1.0$ and confocal parameter g taking values of: 0, 0.5, 0.8, 1, 1.1 and 1.2.

Presence of the TEM_{00} mode with Gaussian distribution for concave stable resonator (confocal parameter g of 0.5 and 0.8) is visible on Fig. 3 confirming the expected behaviour of the laser resonator for Fresnel number $N=1$. For higher values of g (1.1 and 1.2), indicating an unstable resonator, field distribution is determined by geometry of the structure. Change in value of confocal parameter g from 0 to 1.2 indicates a change from marginal stable concentric resonator ($g=0$), via plan parallel Fabry-Perot ($g=1.0$), towards the convex unstable types with g higher than 1. Phase diagrams for stable resonators in Fig. 3 stays close to 0 degrees, meaning that TEM_{00} mode couples with the structure. For $g=1.0$ there exists a significant phase shift at mirror edges because wave front of TEM_{00} mode with finite radius of front curvature cannot couple with infinite radius of curvature of marginally stable Fabry-Perot resonator mirrors.

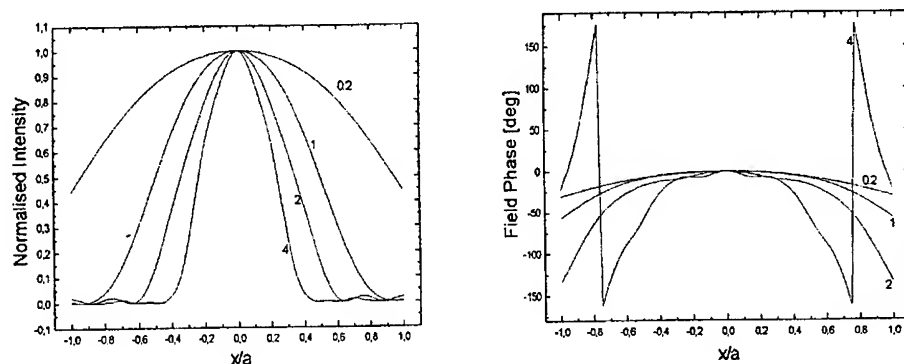


Fig. 4. Normalised field intensity and phase as a function of position on the mirror with fixed confocal parameter $g=1.0$ (Fabry-Perot resonator) and Fresnel number N taking values of: 0.2, 1, 2, and 4.0.

For fixed confocal parameter g , that is for fixed geometry of the resonator, with value of Fresnel number $N=0.2$ only one mode oscillates, TEM_{00} , as on Fig. 4. It is cropped, since part of the mode extends beyond the scope of the mirror. Increasing the N shows presence of higher order modes that is indicated by wiggles in intensity distribution. This can also be observed on the phase diagram since phase distributions for $N=2$ and $N=4$ take value of $\pm 90^\circ$, for $N=2$ once, for $N=4$ twice. Number of these 90° passes is related to number of changes in polarisation of the electric wave field, that is, higher order modes exhibit polarisation changes.

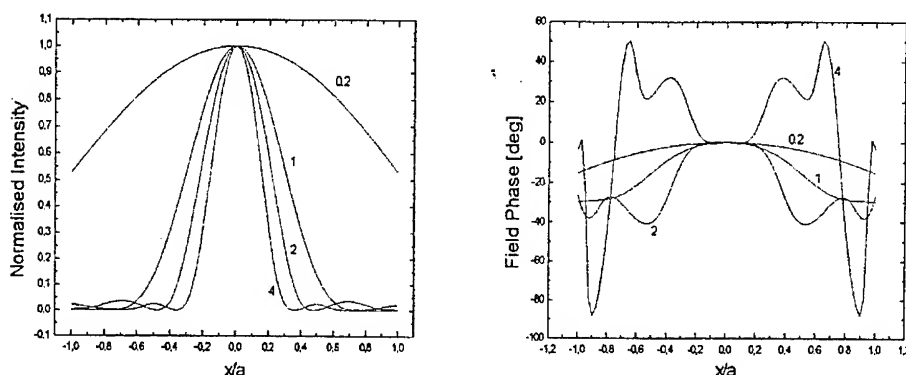


Fig. 5. Normalised field intensity and phase as a function of position on the mirror with fixed confocal parameter $g=0.5$ (confocal stable resonator) and Fresnel number N taking values of: 0.2, 1, 2 and 4.

In the case of the confocal stable resonator results for various values of Fresnel number N are visible on the Figure 5. For $N=1.0$ transverse mode TEM_{00} is clearly visible. Differences in phase diagrams for Fresnel number N up to 1.0 and higher N exists because only TEM_{00} couples with the resonator, and thus with gain medium, for N up to 1.0, not being the case for higher N where higher modes appear across the mirrors. It is visible that the beam exhibits two minima for $N=2$ and four minima for $N=4$ across the extent of the mirror, indicating the presence of higher order modes.

It is to be noted that diagrams for higher Fresnel number are obtained by increasing the transverse dimension of the mirrors. Figures 3, 4 and 5 are drawn with relative position x/a on the mirror, not in absolute values. This means that higher order modes extend further away from the resonator axes, a fact in agreement with resonator mode theory. All results have been obtained with $M=40$ points across half mirror width, that is each diagram is drawn with 81 points across entire mirror.

6. REFERENCES

- [1] H. Kogelnik and T. Li, "Laser Beams and Resonators", Proceedings of the IEEE, vol. 54, no. 10, Pp. 1312-1329, Oct. 1966.
- [2] J. W. Goodman, "Introduction to Fourier Optics", second edition, McGraw-Hill, New York, 1966.
- [3] D. R. Hall, P. E. Jackson et al., "The Physics and Technology of Laser resonators", Adam Hilger, 1989.
- [4] E. Hecht, "Optics", Addison-Wesley, 1990.

UNIVERSITY OF THE WEST. International Conference (1; 1997; Timișoara)

Proceedings of the International Conference:
19-21 May 1997, Timișoara / University of the West; ed. by
Ștefan Balint. - Timișoara:

Universitatea de Vest, 1997

595p.; 25 cm

Bibliogr.

ISBN 973-578-267-7

I. Balint, Ștefan (ed.)

Tiparul executat la
Imprimeria MIRTON Timișoara
Str. Samuil Micu nr. 7
tel. 209469 tel./fax. 208924